

THE LIFTING PADDLEWHEEL

A NON-BUOYANT WHEEL ENABLING A HIGH SPEED WHEELED
AMPHIBIOUS CRAFT TO RUN ON THE WATER SURFACE

A thesis presented for the Degree of Doctor
of Philosophy in Mechanical Engineering at
the University of Canterbury,
Christchurch,
New Zealand

by

K.V. ALEXANDER, B.SC., B.E.(Honours)

Department of Mechanical Engineering,
University of Canterbury,
Christchurch,
NEW ZEALAND.

JULY, 1983

SUMMARY

The lifting paddlewheel, (LPW), is a non-buoyant, bladed wheel similar to the paddlewheels used on riverboats, but is arranged to produce both propulsive and lift forces. Four suitable LPW's used on a high powered, amphibious vehicle would enable it to drive on land as well as water, where it could lift itself up to drive over the water surface at speed, supported only on its blade tips.

Experimental testing tank work with over 40 LPW forms was undertaken, covering force measurements, power measurements and flow visualisation. A wake regime was identified, comprising displacement, transition and planing type wakes, as exhibited by other water craft. A stall-like phenomenon, denoted cavity intrusion, was found to occur when each descending blade begins to encounter the cavity left by the previous blade.

A theory was developed to describe the lift and propulsive forces in the relatively simple case of a flat-bladed LPW in the planing condition. These forces were shown to be predominantly impulsive in nature and to occur at blade entry.

A semi-empirical scheme, based on the above theory, was developed for designing LPW craft.

A 4 kg four-wheel-drive, radio controlled model LPW vehicle successfully demonstrated the LPW concept, and speeds of 32 kph were attained. Practical experience with this type of craft was gained while using this model as a testbed for over 25 different LPW types.

Outline design for a full-sized prototype craft indicated that a performance, in terms of power requirements and speed capability, equalling that of high powered hydrojet boats could be expected.

It was concluded that with the development of combination road and water LPW's from the present successful designs, the LPW craft could be a unique amphibian with its high water speed and all-terrain capabilities.

ACKNOWLEDGEMENTS

I would like to thank Professor D.C. Stevenson who acted as supervisor over the final stages of this project and read the drafts of the thesis. I would also like to thank Dr R.J. Astley for his unobtrusive supervision in the early part of the work, and Dr G.J. Parker for supervision and discussions in the absence of the other supervisors.

I would especially like to thank Mr Peter Giddens for much practical advice, and the staff of the Civil Engineering Department's Fluids Laboratory for their assistance and facilities during the early part of the project.

I am grateful to the Ministry of Works and Development Hydrological Survey Section at Kainga for making their testing tank available, and showing great patience with the peculiarities of my requirements. I should like to thank Mr Dave Gibb as technician at the tank for his generous assistance, enthusiasm and photographic skills. Without his keen interest tank testing would have been greatly limited.

I am indebted to the Department of Mechanical Engineering Workshop for the construction of the force balance and model chassis, and to both Mechanical and Civil Engineering electronics technicians for advice and guidance during my construction and commissioning of the data logging equipment; I am grateful for the use of the Department of Civil Engineering's Solartrons in this respect.

For financial assistance I am indebted to the public of New Zealand through the bursary system, Todd Motors, and the Mercer Scholarship; also to Radio Avon for providing two financially attractive walk-on-water contests.

There are a number of people who by providing encouragement and support at critical stages have helped immensely in this project. Mr Keith Fairweather was consistently enthusiastic and supportive, provided financial help, made numerous model LPW's and produced extensive photographic records of the model craft tests. His help was particularly

valuable. I am grateful also to Hamilton C.W.F. Marine Ltd. for discussions; Ensoc, who organise the Templin Scroll competition, and Pham Doc Truong who encouraged me to take the idea to a higher degree.

I am very thankful that my parents have provided constant encouragement and support.

The willing co-operation, skill and spelling corrections of Jean Percival in typing this thesis to a high standard is gratefully appreciated. The assistance of Jill Ritchie in handling a large quantity of the diagrammatic and photographic material is specially acknowledged, and the efforts of the photographic department of the main library was of much assistance.

No work of this magnitude can take place in a social vacuum, and I would therefore like to thank my fellow postgraduate students, an array of interested flatmates, and in particular Jenny, Janet and Rima who each showed a variety of patience, love and concern while this project progressed.

CONTENTS

	Page
ABSTRACT	(iii)
ACKNOWLEDGEMENTS	(v)
CONTENTS	(vii)
LIST OF FIGURES AND TABLES	(xxvii)
GLOSSARY OF TERMS	(xxxiv)
LIST OF SYMBOLS	(xxxv)

CHAPTER

1. <u>INTRODUCTION</u>	3
1.1 The lifting paddlewheel concept	3
1.1.1 The lifting paddlewheel vehicle	3
1.2 Advantages of the LPW concept	4
1.2.1 Some disadvantages of the LPW vehicle	7
1.3 Rationale for this lifting paddlewheel study	7
1.4 Basic lifting paddlewheel operation	9
1.4.1 The velocity conditions of operation	9
1.4.2 Blade effectiveness, ϵ	15
1.4.3 Effects of blade angle, ϕ	17
1.4.4 The effects of immersion depth, d	17

CHAPTER

	Page
1.4.5 The effect of blade span, s	17
1.4.6 The effect of blade chord, c	19
1.4.7 The effects of the number of blades, B	19
1.4.8 The effect of blade shape	20
1.5 Conclusion	20
2. <u>LITERATURE SURVEY AND BACKGROUND</u>	21
2.1 Introduction	21
2.2 Paddlewheels: wheels for propulsion only	21
2.2.1 Paddlewheel history	21
2.2.2 Gebers, 1952	22
2.2.3 Volpich and Bridge, 1955 to 1957	23
2.2.4 Helm, 1967	29
2.2.5 Wray and Starrett, 1970	33
2.2.6 Beardsley, 1973	38
2.3 Wheels providing buoyant support	45
2.3.1 The Bazin roller ship, 1896	45
2.3.2 The Rollercraft, Kearsley, 1971	45

CHAPTER

	Page
2.3.3 Balloon tyre amphibians	49
2.3.4 The Knapp roller, 1898	49
2.4 Wheels gaining support from dynamic forces	51
2.4.1 The hydroler, 1948	51
2.4.2 Bouncing bombs	53
2.4.3 The Soviet cylinder vehicle, 1967	53
2.4.4 The spinning wheel, 1957	55
2.5 Dynamic water surface lift in nature	57
2.6 Amphibious vehicles	59
2.6.1 LVTP7	61
2.6.2 LVHX-1	61
2.7 Uffa Fox's patent, 1919	63
2.8 Conclusion	65
3. <u>PREVIOUS RESEARCH AND AIMS FOR THIS PROJECT</u>	66
3.1 Close approaches to the LPW concept	66
3.2 The origin of the LPW concept	66
3.3 The Templin Scroll paper, 1976	69
3.4 Third year project, 1977	71

CHAPTER

	Page	
3.5	The first prototype model LPW craft	79
3.6	Aims for this project	80
3.6.1	The research programme in relation to these aims	85
3.6.2	Conclusion	86
4.	<u>THEORIES OF LIFTING PADDLEWHEEL OPERATION</u>	87
4.1	Introduction	87
PART A		
4.2	Dimensional analysis	87
4.2.1	Force coefficients relating to ship propellor theory	89
4.3	A first order momentum theory of LPW operation	90
4.3.1	Thrust force equations	91
4.3.2	Lift force equations	95
4.4	Flat plate drag and the forces on LPW blades	97
4.5	Induced mass and symmetrical impact on a water surface	98
4.6	LPW blade flow geometry and maximum blade-water velocities	101

CHAPTER

	Page
4.6.1 Blade motion relative to the water	103
4.6.2 Blade tip velocity relative to the water	103
4.6.3 Angle of attack through a blade passage	107
4.6.4 Blade angle of attack at entry	111
4.6.5 Maximum blade to water velocities	113
4.6.6 Maximum perpendicular velocity	115
4.6.7 Vertical and horizontal components of perpendicular velocity	117
4.7 The impulse theory of LPW forces	118
4.7.1 The impulse theory after surface cavity intrusion	119
4.7.2 Dimensional analysis and the impulse theory	120
4.8 Other theoretical approaches and the development of mass flow coefficients	120
4.9 Real flow around LPW blades	123
4.9.1 Bowsplash	123
4.9.2 Free streamline theory and LPW blades	124
4.9.3 Estimating surface cavity intrusion conditions	132
4.10 Three results from the impulse theory	137

CHAPTER

	Page
4.10.1 Immersion depth as defined by the lift to thrust ratio	137
4.10.2 Thrust and the angle β	139
4.10.3 Blade angle and the force relations	140
4.11 Power allocation in the impulse theory	140
4.11.1 Thrust power and thrust losses in the impulse theory	140
4.11.2 Water mass flow rate and power per unit thrust	143
4.11.3 Optimisation of incoming mass flow	143
4.11.4 Ways of increasing incoming mass flow	145
4.11.5 Increasing mass flow after cavity intrusion	146
4.12 Lift power in the impulse theory	146
4.12.1 Lift power and depth angle, θ	147
4.13 Other power losses	149
4.13.1 Spray throwing	149
4.13.2 Power to overcome rotational air drag of LPW's	150
4.13.3 Power lost as rotational KE left in the water	151
4.14 Total power, propulsive efficiency and effectiveness	151

<u>CHAPTER</u>	Page
4.14.1 A note on the presentation of efficiency curves	155
4.14.2 LPW propulsive effectiveness	155
4.14.3 Effectiveness decline at high velocity ratios	156
 PART B	
4.15 LPW wakes	157
4.15.1 Blade passage and wake formation	158
4.15.2 The transition zone	158
4.16 Testing paddlewheels in channels of flowing water	167
4.16.1 Waves and flow in channels	167
4.16.2 Modelling wakes in flowing water	168
4.17 Conclusion	172
5. <u>EXPERIMENTAL APPROACH: THE FORCE BALANCE, TEST LPW's AND THE TESTING TANKS</u>	175
5.1 Introduction	175
5.2 The measuring system requirements	175
5.3 The force balance	181
5.4 Force balance operation	181
5.4.1 The lift force section	181

CHAPTER

	Page	
5.4.2	The thrust force section	183
5.4.3	The LPW motive power	183
5.4.4	The torque sensing section	184
5.4.5	Cantilever force sensing elements	184
5.4.6	Damping	189
5.4.7	Immersion setting	189
5.5	Force sensor calibration	191
5.5.1	The original alignment calibrations	191
5.5.2	The in-practice calibration	192
5.6	Force sensor zeroing	192
5.7	Force balance problems	193
5.7.1	Thrust calibration error	193
5.7.2	Minor design faults	194
5.7.3	Running faults	197
5.7.4	Conclusion for the force balance	197
5.8	The tested lifting paddlewheels	197
5.8.1	The wheel size	197
5.8.2	The standard test wheel	199
5.8.3	Other wheels tested	201

<u>CHAPTER</u>	Page
5.9 Testing tanks	201
5.9.1 The flowing-water tank	201
5.9.2 The abortive 1978 tests	205
5.9.3 The fluids laboratory static tank, 1979	209
5.9.4 The MWD rating tank at Kainga	209
5.10 The force balance at the Kainga tank	213
6. <u>INSTRUMENTATION, DATA ACQUISITION AND EXPERIMENTAL PROCEDURES</u>	217
6.1 Introduction	217
6.2 Instrumentation	217
6.2.1 The strain gauge units	217
6.2.2 Immersion depth gauges	221
6.2.3 The tachometer	225
6.2.4 Speed of advance indicator	225
6.3 The data acquisition system	229
6.3.1 The buffer and control unit	232
6.3.2 The Solarton data logger	243
6.3.3 The interface for the papertape punch	243
6.4 The experimental procedure	245

<u>CHAPTER</u>	Page
6.4.1 Setting up	245
6.4.2 The testing procedures	245
7. <u>DATA PROCESSING, PLOTTING AND PRESENTATION</u>	249
7.1 Introduction	249
7.2 Papertape processing	251
7.3 Visual checking of data	251
7.4 Processing the data	251
7.4.1 Zero errors	251
7.4.2 Force calibration errors	252
7.4.3 Speed of advance	252
7.4.4 Constant data standardisation	253
7.4.5 Data acquisition system errors	253
7.4.6 Conclusion for data processing	253
7.5 Data storage	255
7.6 Plotting procedures	255
7.6.1 Multiple plotting	259
7.7 Presentation of multiple plots	259
7.8 Accuracy of the data plots	261
7.9 Conclusion	263

<u>CHAPTER</u>	Page
8. <u>PHOTOGRAPHIC STUDIES</u>	265
8.1 Introduction	265
8.2 The Kainga tank open water studies	266
8.2.1 The photography rig	266
8.2.2 The spray cover	266
8.2.3 Cameras and lighting	269
8.2.4 Outcome of the open water studies	271
8.3 Close-up stroboscopic studies	272
8.3.1 Equipment arrangement	272
8.3.2 Lighting for photography	283
8.3.3 Limitations and scope of this study	283
8.4 Video taperecorder studies	285
8.5 Other photographs	289
8.6 Conclusions	289
9. <u>ANALYSIS OF RESULTS FOR THE LPW WITH FLAT BLADES</u>	290
9.1 Introduction	290
9.2 Results from the tank tests	290
9.2.1 Measured results for the standard wheel	290
9.2.1.1 LPW forces in the plotted data	294

CHAPTER

	Page
9.2.1.2 LPW efficiency in the data	296
9.2.1.3 Other results for the standard wheel	299
9.2.2 Photographic records of the standard wheel	299
9.2.2.1 Stroboscopic records	313
9.3 The impulse theory, former theories and experiment	315
9.3.1 Entry forces compared with forces throughout the passage	315
9.3.2 Induced mass and flat plate drag in experiment	321
9.4 The effects of the variables on performance	324
9.4.1 The use of dimensionless coefficients for comparison purposes	324
9.4.2 Effects of speed of advance, V_o	329
9.4.2.1 The displacement to planing transition	331
9.4.3 Effects of wheel rotational speed, V_t, n	335
9.4.3.1 Surface cavity intrusion	341
9.4.3.2 Bowsplash in observational data	345
9.4.4 Effects of wheel size, D	351
9.4.5 Effects of blade span and end plates, s	353
9.4.6 Effects of blade chord, c	357

<u>CHAPTER</u>		Page	
	9.4.7	Effects of the number of blades, B	363
	9.4.8	Effects of blade angle, ϕ , and immersion depth, d , θ	368
		9.4.8.1 Propulsive efficiency with immersion depth	373
		9.4.8.2 Propulsive efficiency and blade angle	374
	9.5	The thrust to lift ratio in experiment	375
	9.6	Windage losses with LPW's	377
	9.7	Spray forces and losses	380
	9.8	Power estimates and measurements	380
	9.9	The coefficient equations	384
		9.9.1 Limited chord at small immersion depths	386
		9.9.2 The variable functions of the coefficient equations	395
		9.9.3 Computer-aided development of the coefficient equations	399
	9.10	Conclusion	401
10.	<u>RESULTS FOR ROTORS WITH CURVED BLADES</u>		403
	10.1	Introduction	403
	10.2	Analytical approaches to flow past shaped blades	403
	10.3	Shaped blades in the paddlewheel literature	405

CHAPTER

	Page
10.4 Generalised findings for curved-bladed wheels	407
10.5 Convex blades: wheel 6.75, $\phi = 45^\circ$	410
10.6 Slightly concave with small toes: wheel 1.75, $\phi = 90^\circ$	414
10.7 Equal size toe and heel: wheel 1.25, $\phi = 105^\circ$	418
10.7.1 Variation in blade angle with these concave blades	423
10.8 Perforated concave blades: wheel 7.75, $\phi = 90^\circ$	423
10.9 Right-angled concave blades: wheel 7.5, $\phi = 90^\circ$	423
10.10 Semi-circular concave blades: wheel 11, $\phi = 135^\circ$	426
10.11 Differing angles on alternate flat-blades: wheel 1	433
10.12 Conclusion	434
11. <u>RESULTS FOR CONTINUOUS SURFACE ROTORS USED AS LPW's</u>	438
11.1 Introduction	438
11.2 Generalised findings for continuous surface wheels	438
11.3 The smooth cylinder: wheel 0	440
11.3.1 Force balance tests	440
11.3.2 Photographic records	455
11.3.3 Conclusion for wheel 0	459

CHAPTER

	Page	
11.4	Rollercraft inflatable wheel tests: wheel 5	459
11.4.1	The tested wheel	459
11.4.2	The test procedure	461
11.4.3	Results for wheel 5, the rollercraft wheel	463
11.4.4	Observations	473
11.4.5	Comparison with a sample of Kearsey's results	474
11.4.6	Conclusions for wheel 5	474
11.5	The hard rollercraft wheel: wheel 5.5, $\phi = 105^\circ$	475
11.5.1	Results for wheel 5.5	475
11.6	Tractor tyre tests: wheel 7, $\phi = 90^\circ$, and wheel 4.75, $\phi = 90^\circ$	482
11.6.1	Conclusions for tyre tests	502
11.7	Conclusions	502
12.	<u>THE MODEL PROTOTYPE LPW CRAFT</u>	504
12.1	Introduction	504
12.2	Background	505
12.3	The radio-controlled model	505
12.4	Recording craft performance	511

CHAPTER

	Page
12.5 Model preparation and experimental procedure	512
12.6 Problems and characteristics of this craft	517
12.6.1 Motive power and power requirements	517
12.6.2 Achieving lift-off	522
12.6.2.1 Hull drag measurement	527
12.6.2.2 Early methods for achieving lift-off	529
12.6.3 Stability	530
12.6.3.1 Buoyant stability	533
12.6.3.2 Stability in the hull displacement and transition modes	533
12.6.3.3 Stability in the hull planing mode	537
12.6.3.4 Stability after lift-off	540
12.6.4 Steering	543
12.6.5 Land performance	545
12.7 The model craft as a testbed for LPW's	545
12.8 Performance of the craft with purpose-designed LPW's	551
12.9 Performance compared with conventional craft	559
12.10 Conclusion	560

	Page
13. <u>CONSIDERATIONS IN THE DESIGN OF A PROPOSED FULL-SIZED CRAFT</u>	561
13.1 Introduction	561
13.2 General features of LPW craft operation	561
13.2.1 The craft hull	561
13.2.2 The hull with LPW's	562
13.2.3 The thrust to lift ratio	562
13.2.4 Scaling with the thrust to lift ratio	564
13.2.5 The theoretical speed limit	564
13.2.6 The craft slowing down	567
13.2.7 The thrust to lift ratio at lift-off	567
13.2.8 LPW's with variable blade angle	569
13.2.9 Blade angle for a fixed flat-bladed LPW	570
13.2.10 Shaped blades	570
13.2.11 Choice of velocity ratio for cruising operation	571
13.2.12 Span, chord and the number of blades	572
13.2.13 Large spans and high velocity ratios	575
13.2.14 Selection of wheel diameter	575

CHAPTER

	Page
13.3 Design up to lift-off	577
13.3.1 LPW design before lift-off	578
13.3.2 LPW design at lift-off	579
13.3.3 Craft stability up to lift-off	581
13.4 Hull design	585
13.5 Design for flying operation	588
13.5.1 Stability considerations for flying operation	588
13.5.2 Design procedure for flying operation	589
13.6 Computer programme used in this design scheme	591
13.6.1 Assumptions and limitations of this programme	595
13.6.2 Design optimisation using this programme	597
13.6.3 Operational power curves and flying conditions	602
13.7 Outline for the design & testing of a full-sized prototype	608
13.7.1 Design of practical LPW's	611
13.8 Tentative performance predictions	613
13.9 Conclusions	613

CHAPTER

	Page
14. <u>CONCLUSIONS</u>	616
14.1 Introduction	616
14.2 Summary of findings universal to all types of paddlewheels	616
14.3 Summary of findings relating specifically to LPW's	618
14.4 Summary of findings for the LPW craft	618
14.5 Capabilities and limitations of the LPW craft	620
14.6 Applications for the LPW craft	621
14.7 Other uses and developments for the LPW craft	622
14.8 Recommendations for future work	623
14.9 Conclusion	624
 <u>REFERENCES</u>	 626
 APPENDIX 1 Instrumentation circuitry	 A1.1
APPENDIX 2 Estimation of uncertainty in the data	A2.1
APPENDIX 3 Derivation of V_h and V_v	A3.1
APPENDIX 4 Plotted tank test results	A4.1
APPENDIX 5 Derivation of surface cavity intrusion conditions	A5.1
APPENDIX 6 Example of LPW force calculations	A6.1

CHAPTER

Page

APPENDIX 7 Programme 'LPWCRAFT' to calculate forces
and power of the LPW craft A7.1

APPENDIX 8 Programme 'BLADED DRAG' to calculate blade
forces on the basis of flat plate drag A8.1

LIST OF FIGURES AND TABLES

<u>FIGURE</u>		<u>PAGE</u>
1.1	The lifting paddlewheel concept	2
1.2	The lifting paddlewheel	2
1.3	The model lifting paddlewheel craft	5
Table 1.4	List of main variables	8
1.5	The typical wake regime	10
1.6	The force-rps plot	12
1.7	Cavity intrusion	14
1.8	Efficiency cannot be greater than velocity ratio	16
1.9	The usual shape of the efficiency and effectiveness curves	18
1.10	The effects of blade chord	18
2.1	Volpich and Bridge's paddlewheel	24
Table 2.2	Volpich and Bridge's tests	26
2.3	Helm's paddlewheel	28
Table 2.4	Helm's tests	30
2.5	Wray and Starrett's proposal for a high speed amphibian	32
2.6	Wray and Starrett's paddlewheel	32
Table 2.7	Wray and Starrett's tests	34
2.8	A sample of Wray and Starrett's plotted results	36
2.9	Beardsley's paddlewheel and blade shapes	40
Table 2.10	Beardsley's tests	42
2.11	The Bazin roller-ship	44
2.12	The rollercraft wheel and its hydrofoil	46
2.13	The Rollercraft	46
2.14	Amphibious tricycle	50
2.15	The Knapp roller	52
2.16	The hydroler	52
2.17	The Russian cylinder vehicle	54
2.18	The spinning wheel	56
2.19	Ducklings run on the water surface	58
2.20	The lizard which runs on the water surface	58
2.21	The swan grebe running on the water surface	58
2.22	Amphibious personnel carrier, LVTP7	60
Table 2.23	Specifications for the LVTP7	60
2.24	The amphibious hydrofoil vehicle, LVHX-1	62

<u>FIGURE</u>	<u>PAGE</u>
Table 2.25 Specifications for the LVHX-1	62
2.26 Uffa Fox's patent	64
3.1 The original LPW	67
3.2 The preliminary experiments, 1976	67
3.3 Schematic of the apparatus of the preliminary experiments	70
3.4 Results of the preliminary experiments	70
3.5 The 1977 rig	72
3.6 Schematic of the 1977 rig showing forces	72
3.7 The 1977 rig in the flowing water tank	73
3.8 The model LPW craft in mid-1977	77
3.9 The final layout of the Mk I model LPW craft, 1978	81
3.10 Scheme of aims for the project	74
4.1 Actuator rectangle model for momentum analysis	82
4.2 Vertical components of V_t at blade entry and exit	94
4.3 Volpich and Bridge's results compared with flat plate drag calculations: feathering blades	96
4.4 As above for radial blades	96
4.5 General LPW geometry	102
4.6 Locus of a single blade tip. $V_o/V_t = 0.5$	102
4.7 Locus of blade tip and heel	102
4.8 Locus of the tips of a 6-bladed wheel	104
4.9 Blade tip velocity relative to the water vs α	105
4.10 Four cases to determine γ , the angle of attack	106
4.11 Angle of attack, γ , through the blade passage	108
4.12 Variation of angles and velocities along the blade chord	109
4.13 Derivation of ΔV_p and β	112
4.15 Perpendicular velocity, V_p , against α	114
4.16 Vertical velocity V_v against α , for $\phi = 60^\circ$	116
4.17 Spray sheet thrown ahead of a planing plate	122
4.18 Wave formation after entry in flat bottom slamming experiments	122
4.19 Bowsplash in a variety of situations	129 ff
4.20 Flat plate with ambient cavity at 45° to flow	131
4.21 Construction for estimating surface cavity intrusion	134

<u>FIGURE</u>	<u>PAGE</u>
4.22 For small immersions it is difficult to estimate when surface cavity intrusion occurs	136
4.23 The analytical model at surface cavity intrusion	136
4.24 Lift and thrust entry forces with blade angle	138
4.25 Before surface cavity intrusion the LPW does not act on all the entrained flow	142
4.26 Maximum use is made of the entrained flow at surface cavity intrusion	142
4.27 Induced mass variation with blade chord	144
4.28 Point of application of lift force should be at a small angle α to reduce shaft torque	148
4.29 The instantaneous thrust force as a component of the instantaneous tangential force	152
4.30 One of Helm's results covering the transition zone	154
4.31 Blade tip paths at high velocity ratio	154
4.32 (A-D) LPW wakes up to transition zone	159ff
4.33 The oblique wake of the planing mode	163
4.34 The solid cylinder in the planing mode	183
4.35 The wave speed of varying wavelength on water of uniform depth	169
4.36 The LPW in supercritical flow in a glass-sided channel	169
5.1 The data path from the LPW to the plotted form	174
5.2 A general view of the force balance	177
Table 5.3 Force balance specifications	176
5.4 Main components of the force balance	179
5.5 The lift force sensing section	180
5.6 The lift sensing cantilever element and yoke	180
5.7 The thrust sensing section	182
5.8 The torque sensing section	182
5.9 The torque beam bearing arrangement	185
5.10 The torque cantilever element	185
5.11 The cantilever sensing element for lift and thrust	187
5.12 Arrangement of dashpots on the force balance	188
5.13 Calibration thread and weight for the in-practice calibration	190
5.14 Thrust calibration	190
5.15 Negative torque, positive lift calibration	190

<u>FIGURE</u>	<u>PAGE</u>	
5.16	Spray from the wheel striking the force balance	195
5.17	The standard LPW	195
5.18	The working drawings of the LPW	198
5.19	The jig for setting blade angles	200
Table 5.20	Summary of flat-bladed wheel tests	202
Table 5.21	Tests of other types of wheels	203
5.23	Torque sensing section of the 1978 force balance	204
5.24	The water channel for high speed flow	206
5.25	LPW tests in the static flume in the fluids laboratory	207
5.26	Two views of the testing tank at Kainga	210
5.27	The Rating Car with the force balance mounted on it	211
5.28	Some of the instrumentation and data logging equipment on the rating car	211
5.29	Another view of the force balance showing the spray cover	215
6.1	Force sensor wiring to the strain gauge amplifier	218
6.2	The capacitive depth gauge	219
6.3	The displacement transducer as a depth indicator	223
6.4	Mechanical components of the tachometer	226
6.5	Closeup of the tachometer window	227
6.6	The speed of advance meter	227
6.7	Schematic of data acquisition system	230
6.8	Buffer and control unit front panel	233
6.9	Buffer and control unit back panel	233
6.10	Inside the buffer and control unit	235
6.11	The main circuit board and the filter board	235
Table 6.12	Sequence of events caused by activation of the sampling button	238
6.13	Solartron data logging system	240
Table 6.14	Procedure in setting up for a day's testing	242
Table 6.15	Block diagram of testing procedures	244
Table 7.1	The data path from the papertape to the plots	248
7.2	Printout of the voltages read by the Solartron and printed on to paper tape as read by 'TRANSLATE'	250

<u>FIGURE</u>	<u>PAGE</u>
7.3 Fully processed data printed out by 'VIZCHECK'	250
7.4 Plotted output from 'LPWPLOT' with associated data	254
Table 7.5 Programme sequence for 'LPWPLOT'	256
7.6 Flow chart for multiple plotting routine 'ALTOGETHER'	258
7.7 Assemblage arrangement for the description of a single LPW	260
Table 7.8 Uncertainties in the recorded data	262
8.1 The photography rig on the rating car	267
8.2 The spray cover for the photographic rig	267
8.3 Lighting circuit, and camera and lighting arrangement, for the open water studies	270
8.4 Wheel 9.5 in the hump condition in this photography series	273
8.6 The cylinder operating under similar conditions	275
8.7 Photography rig and equipment at the glass-sided tank	277
8.8 The planing condition with a single flash	279
8.9 The planing condition with strobe lighting from behind	279
8.10 Single flash from the front and 20 strobe flashes from the rear	281
8.11 Transition mode photograph	281
8.12 The lighting circuit and the camera and lighting arrangement for the stroboscopic studies	284
Table 8.13 The conditions of operation recorded in photographs or video	286
8.14 Two photos from the 1978 series showing splash effects as the blades enter the water	287
9.1 Force measurements for the standard wheel at 0m/s	291
9.2 Force measurements in the displacement and transition conditions	292
9.3 Force measurements in the planing mode	293
9.4 Beardsley's results showing the effects of immersion depth on efficiency	298
9.5 The static mode, standard wheel at 30 mm immersion	301
9.6 Displacement mode, 0.4 m/s and 30 mm immersion	303
9.7 Transition zone, 0.76 m/s and 20 mm immersion	305
9.8 Low planing speed, 1.72 m/s, 20 mm immersion	307

<u>FIGURE</u>		<u>PAGE</u>
9.9	Planing speed, 2.36 m/s, 20 mm immersion	309
9.10	Stroboscopic series showing the passage of a blade	312
9.11	Calculation of LPW forces using a flat plate drag model	316
9.12	Standard wheel results on the same scale	318
9.13	Calculation of LPW forces using Beardesley's approach	320
9.14	Calculation of LPW forces using the impulse theory	322
9.15	Water moving away from the pressure face of the blade after entry	325
Table 9.16	The force coefficients	327
9.17	Thrust coefficient K_T vs Froude number for paddlewheels and LPWS	328
9.18	Lift coefficient, K_L , vs waterline length Froude number F_x	330
9.19	K_L vs depth Froude number, F_d	332
9.20	Plot of Wray and Starrett's thrust results against rps	334
9.21	Wray and Starrett's results in thrust coefficient form, K_T , vs rps	336
9.22	Lift coefficient, C_L , vs rps before surface cavity intrusion	338
9.23	C_L vs rps after surface cavity intrusion	340
9.24	Surface cavity intrusion in measured lift and thrust results	342
9.25	Comparison between experimental and analytical cavity intrusion predictions	343
9.26	Lift coefficient, K_L , vs rps	344
9.27	Closeup stroboscopic views from below of the onset of bowsplash	347
9.28	Bowsplash in experiment compared to the onset of surface cavity intrusion	349
9.29	Beardesley's results showing efficiency with wheel diameter	350
9.30	Lift coefficient, K_L , showing no variation with wheel diameter	352
9.31	Variation of efficiency with diameter	352
9.32	The effect of blade span, s , on the lift coefficient, K_L	354
9.33	The effect of blade span on efficiency, η	356
9.34	The effect of blade chord, c , on K_L vs velocity ratio	358

<u>FIGURE</u>	<u>PAGE</u>	
9.35	Lift coefficient, K_L , vs chord, c , at a fixed velocity ratio	358
9.36	The effect of blade chord on propulsive efficiency, η	360
9.37	The effect of the number of blades, B , on K_L vs velocity ratio	362
9.38	Lift coefficient, K_L , vs number of blades, B , at a fixed velocity ratio	362
9.39	Beardsley's results showing the effect of the number of blades, B , on efficiency, η	364
9.40	The LPW results showing the effect of B on η	366
9.41	The effect of the blade angle, ϕ , on K_L and K_T	370
9.42	The effects on efficiency, η , of the blade angle, ϕ , and the immersion angle, θ	372
9.43	The thrust to lift ratio in experiment	376
9.44	Windage power losses coefficient, K_{P_w} , under a variety of conditions	378
9.45	LPW power coefficient, C_p , vs velocity ratio	382
Table 9.46	(A) Coefficient equations (B) Variable functions	387ff
9.47	(A) - (Q) Plots of the variable functions	390ff
9.48	θ_c , the immersion angle at which the effective chord, C_{lim} is measured	394
9.49	θ_c with blade angle, ϕ , and immersion	396
Table 9.50	Steps in the programme 'ADDEDMASS' used to determine the coefficient equations	398
9.51	Lift and thrust force-rps plots for the standard wheel produced by the impulse theory and coefficient equations	400
10.1	Differences in flow with curved and flat blades	404
10.2	Edge to edge blade angle	406
10.3	Curved blades examined in this chapter	408
10.4	Wheel 6.75, $\phi = 45^\circ$, static conditions results	411
10.5	Wheel 6.75, $\phi = 45^\circ$, displacement and transition conditions	412
10.6	Wheel 6.75, $\phi = 45^\circ$, planing mode results	413
10.7	Wheel 1.75, $\phi = 90^\circ$, static condition results	415
10.8	Wheel 1.75, $\phi = 90^\circ$, displacement and transition conditions	416

<u>FIGURE</u>	<u>PAGE</u>	
10.9	Wheel 1.75, $\phi = 90^\circ$, planing operation results	417
10.10	Wheel 1.25, $\phi = 105^\circ$, static mode results	419
10.11	Wheel 1.25, $\phi = 105^\circ$, displacement and transition conditions	420
10.12	Wheel 1.25, $\phi = 105^\circ$, planing operation results	421
10.13	Wheel 7.5, $\phi = 90^\circ$, planing operation results	427
10.14	Wheel 11 with cupped blades in operation	427
10.15	Wheel 11, $\phi = 135^\circ$, static mode results	429
10.16	Wheel 11, $\phi = 135^\circ$, displacement and transition conditions	430
10.17	Wheel 11, $\phi = 135^\circ$, planing operation results	431
10.18	Wheel 1, $\phi = 90^\circ$ and 45° alternating. Static operation	435
10.19	Wheel 1, displacement and transition conditions	436
10.20	Wheel 1, planing operation results	437
11.1	Wheel 0, the solid cylinder, static mode results	441
11.2	Wheel 0, displacement and transition conditions	442
11.3	Wheel 0, planing operation results	443
11.4	The cylinder in the static mode	447
11.5	Showing that more water sticks to the wheel in displacement and transition than in planing conditions	449
11.6	The cylinder at different speeds of advance with velocity ratio close to 1	451
11.7	Showing the difference in bowsplash for the cylinder in the planing condition with and without rotation	453
11.8	A suggested origin of bowsplash in LPWs	456
11.10	The dimensions of the tested rollercraft wheel	458
Table 11.11	Comparison between Kearsy's rollercraft wheel, and the rollercraft wheel of this project	460
Table 11.12	The two interpretations of immersion depth	460
11.13	The arrangement for the air supply to the wheel	462

<u>FIGURE</u>		<u>PAGE</u>
11.14	Wheel 5, inflatable rollercraft wheel, static condition	465
11.15	Wheel 5, displacement and transition conditions	466
11.16	Wheel 5, planing operation	467
11.17	The rollercraft wheel of this project rotating at 6 rps in the static mode	469
11.18	Kearsey's results for the rollercraft wheel in the early planing condition	472
11.19	The dimensions and construction of wheel 5.5, the hard rollercraft wheel	476
11.20	Wheel 5.5, $\phi = 105^\circ$, static operation	478
11.21	Wheel 5.5, $\phi = 105^\circ$, displacement and transition conditions	480
11.22	Wheel 5.5, $\phi = 105^\circ$, planing operation	481
11.23	Dimensions of the small tractor tyre	484
11.24	Wheel 7, $\phi = 90^\circ$, the tractor tyre rotating in the normal direction, in the static condition	487
11.25	Wheel 7, $\phi = 90^\circ$, displacement and transition conditions	488
11.26	Wheel 7, $\phi = 90^\circ$, planing operation	489
11.27	Wheel 4.75, $\phi = 90^\circ$, the tractor tyre turned around, static operation	491
11.28	Wheel 4.75, $\phi = 90^\circ$, displacement and transition conditions	492
11.29	Wheel 4.75, $\phi = 90^\circ$, planing operation	493
11.30	Wheel 7, in the transition mode showing the pick up of water	495
11.31	Wheel 4.75, in the transition mode showing less pick up of water	497
11.32	Wheel 7 in the planing mode as revolutions increase	499
Table 12.1	Final specifications for the original model	506
Table 12.2	Original specifications for the second model	506
12.3	Chassis assembly drawings for the second model LPW craft	508
12.4	The model ready for its first runs	509
12.5	The model at a later stage	509
12.6	The model on its stand showing mid-section plates and test identity chart	513

<u>FIGURE</u>	<u>PAGE</u>	
Table 12.7	Procedures before a test series	515
Table 12.8	Procedures at the lakeside	516
12.9	Schematic of the model's chassis dynamometer	518
12.10	The dynamometer in preparation for tests	518
12.11	Results of chassis dynamometer tests	520
12.12	The model in the planing-planing condition	525
12.13	Arrangement for the hull drag towing tests	525
12.14	Results of towing tests	528
12.15	The model at its speed limit just beyond the transition-displacement condition	531
12.16	The model with the same wheels, in the planing-flying condition	531
12.17	The fountain effect causing submergence of the model	534
12.18	The bouncing motion	536
12.19	Excessive bouncing caused the model to leave the water completely	536
12.20	The model with the best wheel design, in the planing-flying condition at 9 m/s	541
12.21	A & B: Details of shaped blades on LPWs tested on the model	546
Table 12.22	Test conditions and results for LPWs tested on the model	547
Table 12.23	Actual and predicted model performance	554
Table 12.24	Model boat performance figures compared to those of the model LPW craft	556
12.25	Modelboat, LPW craft and full sized craft performances	558
13.1	A scheme for the design of flat-bladed LPWs for lift-off	580
13.2	The model LPW craft float dimensions	582
13.3	The mid-section and rear plates used on the model	584
13.4	Drag curves for a broad shallow hull, EMB series 50	586
Table 13.5	The LPW design process after lift-off	590
Table 13.6	Results for prototype 1 tonne LPW vehicle	592
13.7	The 1 tonne craft power vs speed curve	598
13.8	Effects of the variables on the power vs speed curve	600
13.9	Estimated operating conditions for a prototype craft	604

<u>FIGURE</u>		<u>PAGE</u>
13.10	Calculated operating conditions for a prototype craft	605
13.11	Proposed hybrid LPW design for high lift and small immersions after lift-off	607
Table 13.12	Comparisons between the model dimensions scaled up and the suggested prototype dimensions	609
13.13	Suggested rubber tyre for a combination road and water LPW	612
13.14	The predicted performance of the 1 tonne prototype on a power-to-weight ratio plot	614
Table A2.1	Bilateral uncertainty in the measurement of each variable	A2.4
Table A2.2	Example: determination of lift force uncertainty using contributions from all sources	A2.5
A3.1	Construction for vertical and horizontal components of perpendicular velocity	A3.0
A5.1	Derivation and use of ψ'	A5.2
Table 5.2	Iterative subroutine used to find the wheel revolutions when surface cavity intrusion occurs	A5.6

GLOSSARY OF TERMS

	<u>Section</u>
alignment calibration, original alignment calibration: bench calibration of the force balance before tank tests.	5.5.1
aspect ratio: blade span/chord	Fig.1.2
blade angle, (ϕ): angle between blade and tangent	Fig.1.2
blade cavity: hole left in the water after the rapid passage of one blade	Fig.9.10
blade chord, chord (C): blade dimension perpendicular to wheel axis	Fig.1.2
blade passage: transit of the blade through the water	
blade tip speed, tip speed, (V_t): speed of wheel rim relative to its axis	Fig.4.2
bouncing, porpoising: vertical motion of the model LPW craft	12.6.3.3
bow splash: bow wave, or mound pushed ahead of the LPW	4.9.1
buffer and control unit: part of the data logging system	6.3.1
'C' coefficients: impulse theory force coefficients	9.4.1
cavity, wheel cavity: the hole in the water scraped out by the wheel	
cavity intrusion, (C.I.): the condition where the incoming blade breaks through into the blade cavity left by the previous blade (sometimes means surface C.I.)	4.9.3 Fig.1.7

	<u>Section</u>
cavity pounding: drumming sound made by the LPW at high rps during low speed operation	9.2.2
coefficient equation: equation defining the impulse theory coefficient	9.9
concave blade: a blade straight spanwise but curved chordwise to be concave on the pressure face	10.6
constant data: the fixed conditions during tank tests, such as blade angle, date, immersion depth	7.4.4
convex blades: (see concave blades above)	
depth, immersion depth, (d): the distance to the wheel rim below the water surface.	Fig.1.2
depth angle, immersion angle, (θ): angle between the vertical and the wheel radius intersecting the water surface	Fig.4.5
depth Froude Number, (Fd): $V_0\sqrt{gd}$	4.2
diametral Froude Number (Fr): V_0/\sqrt{gD}	4.2
displacement mode, operation, condition: operation at speeds where wavelength is less than wheel diameter $F_x < 0.65$	4.15.2
displacement-displacement: both LPW's and craft hull are in their displacement conditions	12.6.2
displacement length ratio: $\Delta/(\ell'/100)^3$	Fig.13.4
draught: hull immersion	
edge-to-edge blade angle:	Fig.10.3

	<u>Section</u>
effectiveness, blade effectiveness, (ϵ): fraction of maximum theoretical efficiency achieved by a wheel	4.14
efficiency, propulsive efficiency, (η): TV_0/P	4.14
F.B: flat blade	10.4
flying: the condition of the LPW craft where its hull is clear of the water.	Fig.12.20
force balance: the device used for measuring LPW forces	5.3
force-rps plot:	Fig.1.6
fountain, fountain effect: the large quantity of water sometimes thrown up at the rear of a wheel in water	11.3.2
heel: inner edge of LPW blade	Ch.10
hump, hump condition: the second part of the transition zone where the wheel climbs its bow wave	Fig.1.5
immersion angle, (θ): see depth angle	
immersion depth, (d): see depth	
immersion ratio, (d/D): depth/diameter	4.2
impulse theory: analysis assuming the forces are generated by impulsive action at blade entry	4.7
in-practice calibration: calibration of force balance at the testing tank	5.5.2
induced mass: added mass, virtual mass; a construct used to aid force calculations in unsteady flow	4.5
intersection region, zone: the region of the force-rps plot where the curves change from parabolic to linear	Fig.1.6

	<u>Section</u>
'K' coefficients: coefficients derived from dimensional analysis	9.4.1
lift: the force in the vertical direction	
lift augmentation: any lift force additional to that generated by the LPW blades	
lift-off: the action of the LPW craft in raising its hull clear of the water surface	12.6.2
linear section, region: straight line section of force-rps plot	Fig.1.6
LPW: lifting paddlewheel	Fig.1.2
mid-section plates: plates between front and rear wheels on the LPW craft	Fig.13.3
MWD: Ministry of Works and Development	5.9.4
parabolic section: curved section of the force-rps plot	Fig.1.6
perpendicular velocity, (V_p): component of the velocity of the blade tip, perpendicular to the blade	4.6.6
planing operation, condition: wheel operation when $F_x > 0.85$, at a velocity which produces a planing type wake	4.15.2
planing-(displacement, transition, planing, flying): conditions of operation of the LPW craft with LPW's planing	12.6.2
porpoising: see bouncing	
power coefficient, (C_p): impulse theory power coefficient	9.8

	<u>Section</u>
power budget: summation of all power losses	9.8
propulsive efficiency, efficiency, (η): TV_O/P	4.14
Rating Car: trolley used to carry equipment along the testing tank	5.9.4
rating rank: MWD testing tank at Kainga	5.9.4
rear plates: plates behind rear wheels on LPW craft	Fig.13.3
SCI: surface cavity intrusion	Fig.1.7
Solartron: automatic channel reading digital voltmeter, part of the data logging system	6.3.2
span, blade span, (s): dimension of blade parallel to wheel axis	Fig.1.2
speed of advance, (V_O): velocity of LPW over the water	Fig.1.2
standard wheel: the wheel examined most thoroughly in the tank tests	5.8.2
static condition, operation, mode: wheel operation with no speed of advance	Fig.1.5
surface cavity intrusion, (S.C.I.): condition where the entering blade encounters the edge of the cavity left by the previous blade at the water surface	Fig.1.7
test identity chart:	Fig.12.6
thrust: propulsive or horizontal force created by LPW's	
tip: outer edge of LPW blade	Ch.10
tip speed, (V_t): see blade tip speed	

	<u>Section</u>
toe: outer portion of LPW blade	Ch.10
transition zone, operation, condition: operation at the speed of advance between displacement and planing; $0.64 < F_x < 0.85$	4.5.2
trough condition: first part of the transition zone where the wheel sits in the trough of its bow and stern waves	Fig.1.5
variable function: an equation used to adjust the impulse theory estimation of a force, in its relation to one variable, to the force found in reality.	9.9.2
velocity ratio, (V_o/V_t): ratio between the speed of advance and the tip speed	
wheel cavity: see cavity	
waterline length Froude Number: $F_r = V_o/\sqrt{g\ell'}$ for boats. $F_x = V_o/\sqrt{gdsin\theta}$ for wheels.	4.15.2

LIST OF SYMBOLS

		<u>Section</u>
A	cross-sectional area of the LPW craft above water	13.2.5
a_1	distance between the cavity edge and the point of entry of the heel of the incoming blade	4.9.3
B	number of blades on the LPW	
C	any impulse theory coefficient	
c	blade chord; dimension perpendicular to wheel axle	Fig.1.2
C_β	combination of the 'C' coefficients for the T/L ratio	13.2.5
C_D	air drag coefficient of LPW craft	13.2.5
c_{eff}	chosen effective blade chord at small immersions	9.9.1
C_f	general force coefficient from dimensional analysis	4.2
C.I.	short for cavity intrusion	
C_L	impulse theory lift coefficient	9.9
C_P	power coefficient from dimensional analysis	4.2
C_P	power coefficient from experiment	9.8
C_T	impulse theory thrust coefficient	9.9
c_1	projected blade chord $c_1 = c \sin \phi$	4.13.2
C_{1L}	C1L impulse theory lift coefficient before C.I.	9.9
C_{2L}	C2L impulse theory lift coefficient after C.I.	9.9
D	wheel diameter to blade tips	Fig.1.2
d	immersion depth of wheel	Fig.1.2
d_t	horizontal distance between successive blade entries	Fig.4.21
F	generalised force	
FB	flat blade	
F_d	depth Froude number (after Beardsley)	4.15.2
F_r	diametral Froude number of LPW (or waterline length Froude number of hull)	4.2
F_t	tangential force at blade tip	4.14
F_x	waterline length Froude number of paddlewheel	4.15.2

g	acceleration caused by gravity	
h	water depth to bottom	4.16.1
K_L	Beardsley's lift coefficient derived from dimensional analysis	4.2
K_{L1}	lift coefficient based on momentum derivation	4.2
KP_w	coefficient of windage losses from rotation	4.13.2
K_T	Beardsley's thrust coefficient derived from dimensional analysis	4.2
K_t	thrust coefficient derived from dimensional analysis	4.2
K_{T1}	thrust coefficient based on momentum derivation	4.2
L	lift force	
ℓ	half waterline length of LPW	4.15.2
ℓ'	boat hull waterline length	4.15.2
L_{expt}	measured lift force	9.8
L_{theory}	theoretically derived lift force	9.8
\dot{M}	entrained water mass per second	4.3.1
\dot{m}	induced mass per second; induced mass flow rate	4.5
m'	induced mass per blade	4.5
N	revolutions per minute	
n	revolutions per second	4.5
P	power	4.14
P_i	power consumed by paddlewheel	4.14
P_L	power used in providing lift	4.12
P_{lost}	power lost as kinetic energy of the wake in providing the thrust force	4.11.1
P_{rot}	power lost as kinetic energy of rotation in the wake	4.13.3
P_{spray}	power lost in generating spray and overcoming spray-induced drag	4.13.1
P_T	power used in providing the thrust force = $V_o \cdot T$	4.11.1
P_w	power used to overcome rotational air drag in LPW's	4.13.2

		<u>Section</u>
R	radius of LPW = $D/2$	Fig.4.5
R_e	Reynold's number	4.2
s	blade span; length of blade in direction of wheel axis	Fig.1.2
S	slip: $(1 - V_o/V_t) \times 100\%$	
S.C.I.	surface cavity intrusion	Fig.1.7
SD	standard deviation; uncertainties are in terms of $\pm 1SD$	App 2
T	thrust or propulsive force	
t	time	
V	general symbol for velocity	
	velocity of blade tip relative to the water	4.6.2
v	velocity of a wave	4.15
V_c	critical flow velocity of a stream of water	4.16.1
V_h	horizontal component of the perpendicular velocity	4.6.7
V_j	velocity of flow discharge from a propeller	4.3
V_{max}	theoretical maximum speed of a flying LPW craft	13.2.5
V_o	speed of advance of the LPW over the water	
V_p	perpendicular velocity; the component of the velocity of the blade tip perpendicular to the blade	4.6.6
V_t	velocity of blade tip relative to the wheel axis	
V_v	vertical component of the perpendicular velocity	4.6.7
x	displacement in x direction	
y	displacement in y direction	
y_1	cavity parabola approximation half width	Fig.4.21
y_2	horizontal component of y_1	Fig.4.21
α	angular position of blade in its passage	Fig.4.5
β	angle between blade and water surface $\beta = (\phi - \theta)$	Fig.4.14
γ	angle of attack between blade and water	4.6.3

		<u>Section</u>
Δ	'change in'	4.3.1
Δ	displacement of hull in tonnes	Fig.13.4
δ	an angle used in the calculation of γ	Fig.4.10
ε	blade effectiveness; $\varepsilon = \eta \cdot V_t / V_o$	4.14
η	propulsive efficiency; $\eta = T \cdot V_o / P$	4.14
θ	immersion angle	Fig.4.5
θ_c	angular position in blade passage at which the effective blade chord c_{eff} is determined	9.9.1
λ	wavelength	4.15
μ	absolute viscosity of water	4.2
π	3.14159	
ρ	density of water	
ρ_a	density of air	4.13.2
τ	planing angle of craft hull	Fig.4.17
ϕ	blade angle; angle between flat blade surface and the tangent to the wheel	Fig.1.2
ψ	angle used in the calculation of γ	Fig.4.10
ψ'	angle between direction of blade motion at entry and tangent	Fig.A5.1
ω	angular velocity of the LPW (radians per sec.)	4.6.2

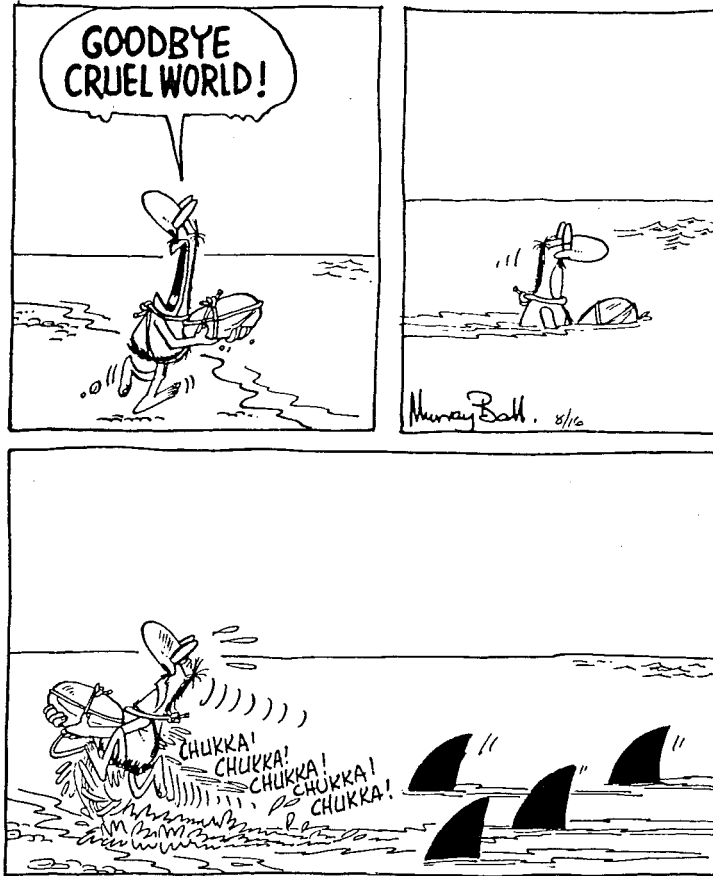


FIGURE 1-1: THE LIFTING PADDLEWHEEL CONCEPT

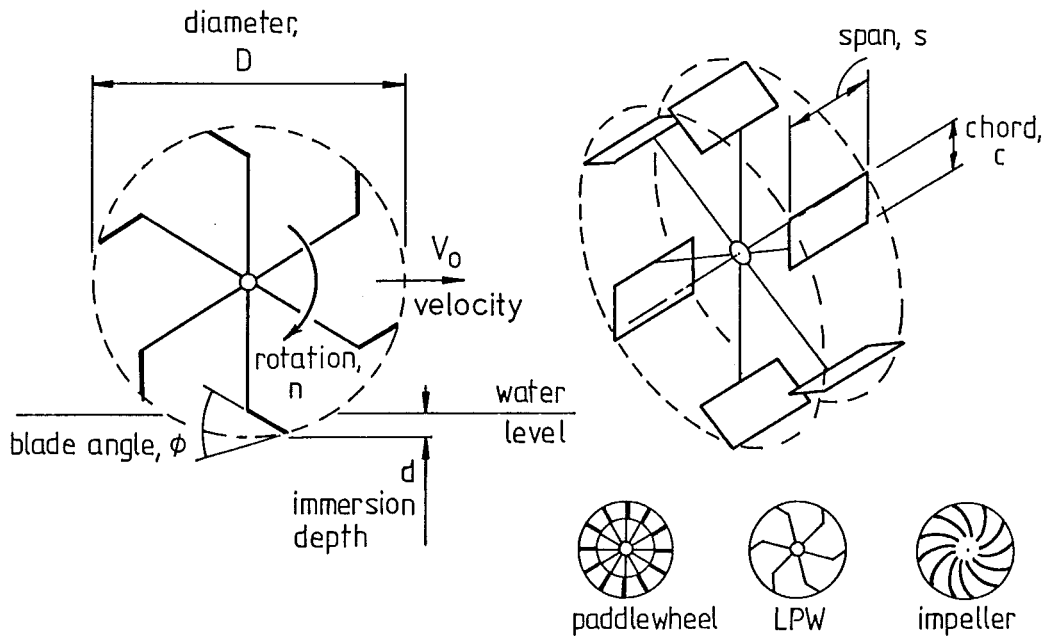


FIGURE 1-2: THE FLAT-BLADED LIFTING PADDLEWHEEL

CHAPTER 1

INTRODUCTION1.1 THE LIFTING PADDLEWHEEL CONCEPT

"If a horse could stamp his feet hard enough and fast enough, he could walk across the surface of the water."

Lord Kelvin (1)

The Lifting Paddlewheel (LPW) is a wheel which attempts to mechanically stamp on the water surface, to produce sufficient lift and thrust to both support and propel a vehicle over the water surface (Fig.1.1). In its present form the LPW is not unlike the paddlewheels used for the propulsion of ships during the last century. The differences are that the blades need not be flat, and instead of being radial they may be fixed at a chosen angle to the radius or tangent, as shown in Fig.1.2.

The LPW is rotated relatively fast in the same direction as the paddlewheel was for propulsion, so that greater forces are generated. As a result, the LPW, as well as exerting a propulsive force caused by the blades passing through the water, also exerts a useful vertical lifting force, sufficient to help support a vehicle.

The LPW as examined in this project, is seen as a new direction in paddlewheel evolution, and because of its unique properties, may find application in a variety of areas, for example it may be used on high speed planing craft, for hovercraft propulsion, on swamp skimmers, on military vehicles or other specialist applications.

1.1.1 The Lifting Paddlewheel Vehicle

The main application imagined for LPW's in this project is for their use as the wheels of a high speed amphibious craft. It is envisaged that such a vehicle could have four LPW's in place of its wheels, arranged in the configuration of those of a road vehicle.

In the water it would be able to float or churn along slowly, or else pick up speed and lift its body clear of the water surface like a hydrofoil craft, and run over the surface at speed. See Fig.1.3. On arriving near the shore it could slow down, perhaps settling back in the water before driving up the beach on its unique wheels, to continue on down the nearest road.

Such a vehicle, while holding a certain appeal, might well fulfil special needs if it could be made to perform as imagined.

1.2 ADVANTAGES OF THE LPW CONCEPT

Apart from the amphibious capability mentioned above, the LPW has a number of special advantages as a propulsive device:

1. The LPW depends only on pressure increases for the development of its forces. Because it operates through the water surface, air entry effectively prevents large pressure reductions from occurring. Cavitation, therefore, is not a limiting factor in LPW operation.

2. LPW's being in the form of wheels will tend to roll over obstacles in the water. They would seem to lend themselves well to operation in obstacle or weed-ridden waters or shoal conditions.

3. An advantage over hovercraft is the positive traction afforded by the LPW's both on land and water.

4. The LPW craft has low drag. Once * flying its main drag sources are much the same as those of a hovercraft, namely air drag and spray drag. Any drag the LPW blades experience as they move through the water only serves to increase the propulsive force.

5. The same steering mechanism may be used for both land and water.

6. Propulsive efficiency does not have a theoretical maximum limit so that it depends on physical and design limitations as to what efficiency may be achieved.

7. As the speed of the LPW craft increases it lifts higher in the water. This not only gives more hull clearance but also improves propulsive efficiency.

* Terms with special meanings are underlined at their first appearance and explained in the Glossary of Terms at the front of the thesis.



FIGURE 1.3:

THE MODEL LPW CRAFT

1.2.1 Some Disadvantages of the LPW Vehicle

Noted here are the most apparent disadvantages to the operation of the LPW concept. It is clear also that some of these might be dealt with effectively by appropriate design in a practical craft.

1. Like aircraft, hovercraft and hydrofoils, the LPW requires power to make it fly. This power is constant once lift-off has occurred and while it is a major proportion of the power requirements at low speeds, it becomes a less significant proportion at higher speeds.

2. Being a water surface craft, like a planing boat the LPW vehicle is sensitive to waves. It would be expected to employ its overwater and amphibious advantages in relatively sheltered waters.

3. LPW blades are required to enter and leave the water rapidly during operation. This action inevitably involves vibration and losses.

4. Spray is produced by the action of the blades. This not only causes energy losses but may be a nuisance in a real craft (see for example Fig.1.3). Fortunately it is not difficult to devise guards which can redirect the spray to advantage, increasing both lift and stability of the craft (see section 12.6.3 discussing this). Model prototype tests indicate also that spray is less of a problem at high speeds.

5. LPW's designed to grip the water also grip the air, especially as the blades move forward at speed over the top of the wheels. Guards would be required to reduce the air drag of the wheels so as to avoid these unnecessary losses.

1.3 RATIONALE FOR THIS LIFTING PADDLEWHEEL STUDY

It used to be thought that the hovercraft would replace the car on the road and so provide its driver with an "Everyman's amphibious vehicle". However, hovercraft do not have the positive traction required of road vehicles so this has never occurred, though the hovercraft has proved itself to be a useful, high speed, all-terrain vehicle where there is plenty of space.

There is still no high speed amphibious road vehicle commercially available which does not have severe disadvantages of one form or another, such as very low water speed, limited road speed, or considerable preparation time for the land to water transition.

TABLE 1.4

VARIABLE	DIMENSIONLESS FORMS	DESCRIPTION
D		Wheel diameter
B		Number of blades
Blade Shape		
s		Blade span
c		Blade chord
A		Blade area $A = sxc$
	s/c	Blade aspect ratio
d		Immersion depth
	d/D	Immersion ratio
ϕ		Blade angle to the tangent
V_o		Speed of advance
V_t		Blade tip speed rel. to wheel axis
	V_o/V_t	Velocity ratio
	S	Slip $S = (1 - V_o/V_t) \times 100\%$
	F_r	Froude Number based on diameter
	F_x	Froude number based on water line length.
L		Lift force
	K_L	Lift coefficient corrected for span
T		Thrust or propulsive force
	K_T	Thrust coefficient corrected for span
F		Total force $F = \sqrt{T^2 + L^2}$
T_o		Wheel torque
P		Wheel power
	η	Propulsive efficiency
	ϵ	Blade effectiveness

As noted above the LPW vehicle in its final form was imagined as being capable of high speeds on both land and water as well as having an all-terrain capability (being a four-wheel drive vehicle) and being capable of moving slowly and providing a useful towing capability in the water.

As long as it appeared possible for the LPW vehicle to perform in these ways, it seemed worth investigating both the vehicle concept, and the LPW itself.

1.4 BASIC LIFTING PADDLEWHEEL OPERATION

Since the LPW concept is new this section is intended to cover its operation in outline and to introduce some of the basic ideas involved before covering them in depth in later chapters. Some of the effects are unavoidably oversimplified, but since the number of variables is large, it is helpful to see how they interrelate before they are tackled individually later. (See Table 1.4).

Forces generated by the rotating LPW are controlled in magnitude by five main factors. These are :

- (1) The mass supply to the wheel in the form of fluid flow into the path of the blades.
- (2) The speed at which the blade encounters this fluid mass.
- (3) The area of the blade acting on the fluid.
- (4) The effectiveness with which the blade acts on the fluid.
- (5) The angle at which the blade is set and the angle at which the flow approaches it.

The following effects are all related to these five factors.

It is convenient to describe the operation of the LPW first by examining how the forces vary with respect to the velocity conditions, with the other variables remaining constant.

1.4.1 The Velocity Conditions of Operation

There are two velocities to be considered, the speed of advance V_o , and the blade tip speed relative to the LPW axis, V_t (Fig.1.5).

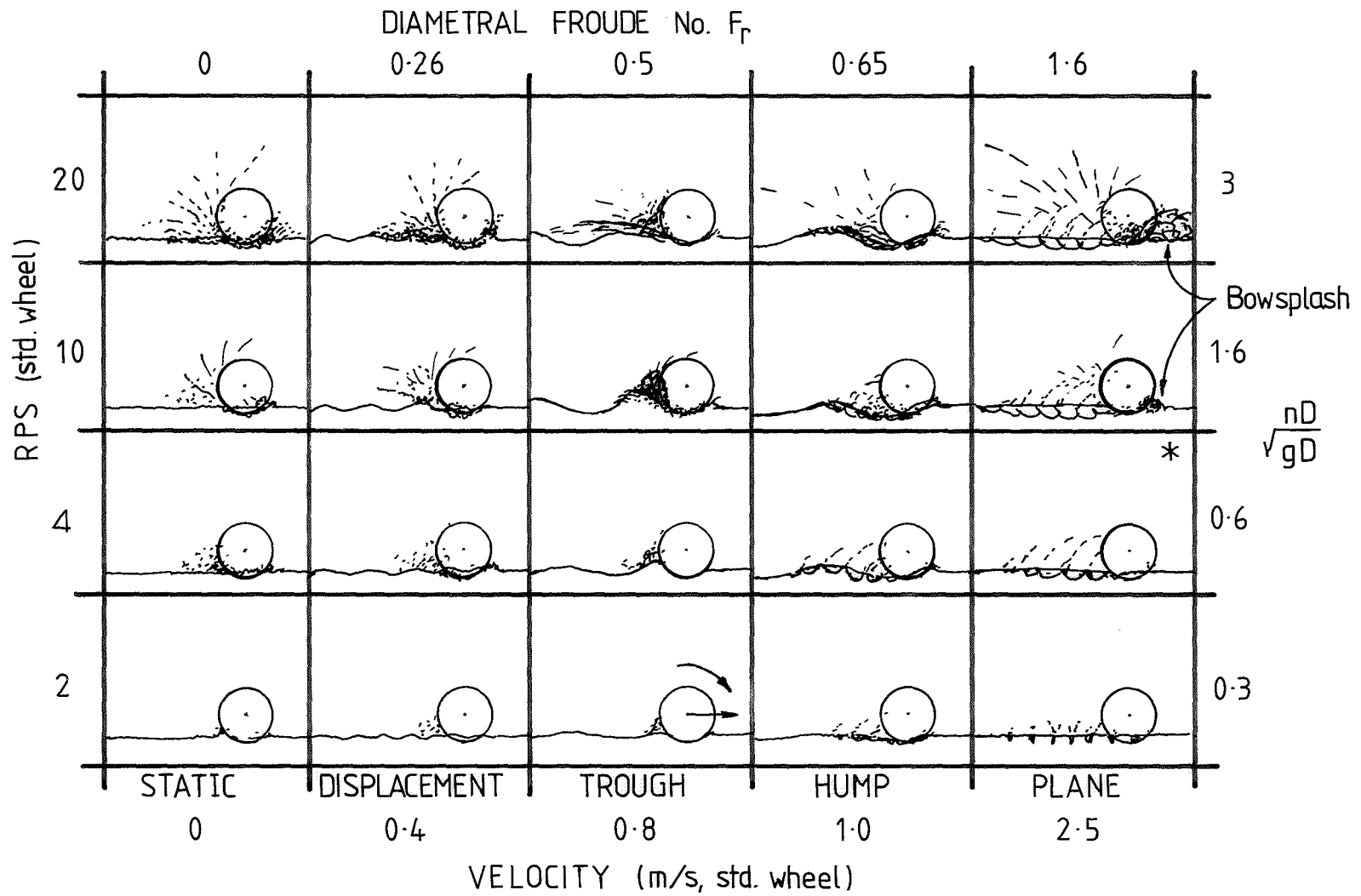


FIGURE 1-5: SKETCHES OF THE WAKE REGIME FOR PADDLEWHEELS. NORMAL FLYING OPERATION IS IN THE CONDITION MARKED * ($d/D \doteq 0.15$)

When the speed of advance is zero, and the wheel is standing in one spot spinning, we have what has been called the static condition. In this case fluid is supplied to the wheel through the bottom and sides of the wheel cavity scraped out by the blades. In addition to this basic fluid supply, a flow is created through the wheel cavity by its rotation. The forces generated depend on this mass supply of fluid, and the amount it is accelerated. As the blade tip speed, V_t , increases, generally both lift and thrust increase. When the wheel revolutions are high ($nD/\sqrt{gD} \doteq 1.6$), the wheel cavity starts to oscillate in and out. This has been termed cavity pounding.

Beyond this static condition, the LPW has two main modes of forward-moving operation, with a transition between them. These are :

- (1) A displacement-type of operation, referred to as the displacement mode, and
- (2) a high speed type of operation called the planing mode.

These are so named because the wakes formed by the wheel in these conditions are closely analogous to the wakes formed by displacement, and planing hulls at similar speeds (based on waterline length Froude numbers).

In the displacement mode water supply is through the sides and bottom of the wheel cavity, but comes increasingly from the front, as the speed of advance, V_o , is increased. The wheel builds up a wave train as if its immersed part was a tubby hull. As long as the speed of advance remains low, this wake is almost unaffected by increase in wheel revolutions, while the forces behave, with increased revolutions, as they did in the static condition, so that cavity pounding occurs at high revolutions as before. A wake like this has an inherent wave drag which reduces the thrust available from the wheel.

As the wheel's speed of advance is increased further, it arrives at a condition where it is sitting in the trough between the bow and stern waves it has created. This is the first part of the two part transition zone and is termed the trough condition. The height of the stern wave is exaggerated by the water being lifted up by the wheel. As can be seen in Fig.1.5, the wheel in this position has almost no flow through its circumference to the blades, and this causes the wheel to be ineffectual in supplying lift or thrust forces. At this speed

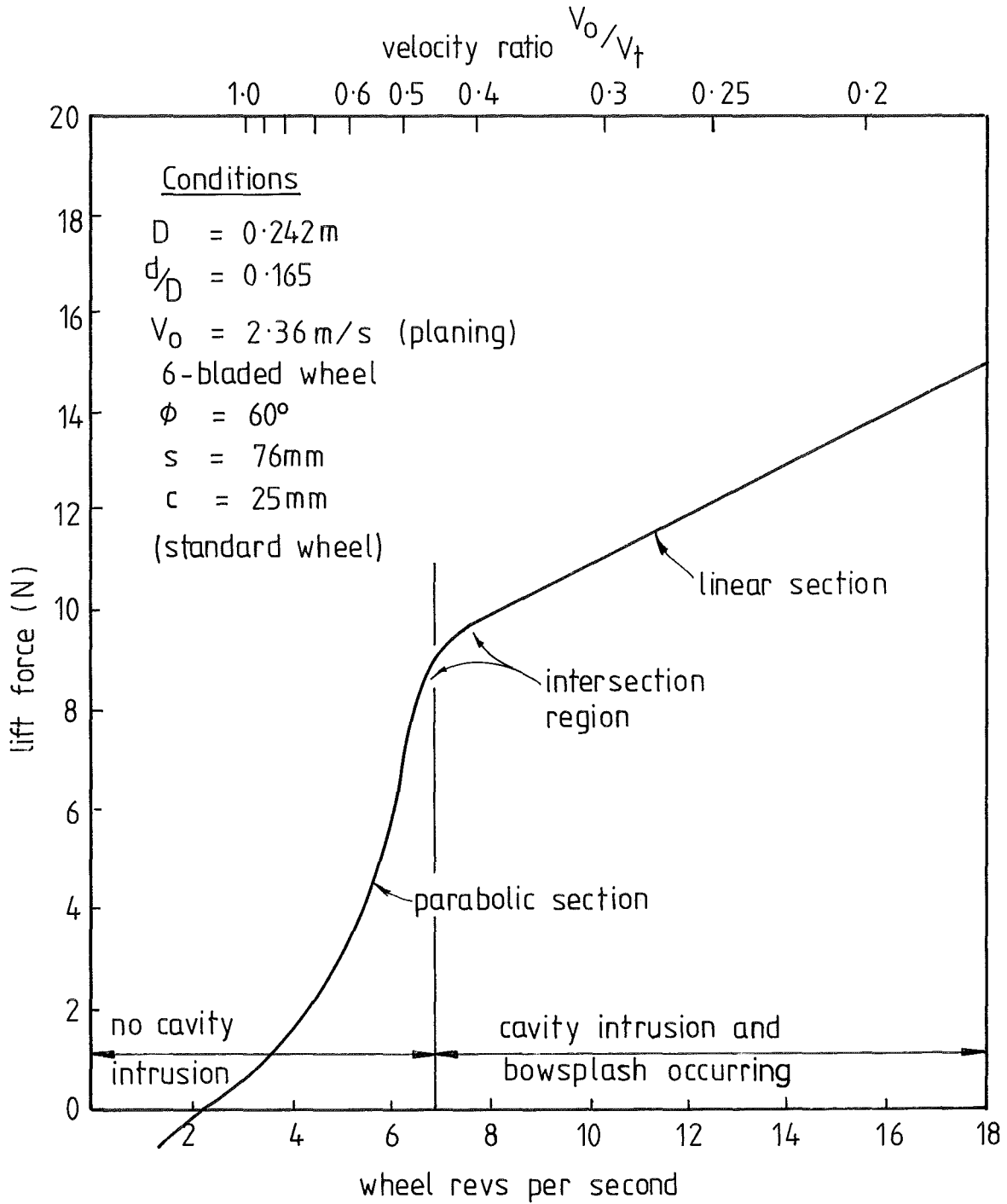


FIGURE 1.6: THE FORCE-RPS PLOT FOR THE LIFT FORCE OF THE STANDARD WHEEL IN THE PLANING MODE.

of advance, then, as revolutions are increased from zero, the forces at first rise as before, until the trough is created, then they remain virtually independent of revolutions from then on. It can be imagined that this trough condition could well put a limit on the speed that a craft, with wheel propulsion, could achieve.

When the speed of advance is increased beyond the trough speed, it enters the second part of the transition zone. The wheel then begins to cut into and climb its own bow wave, leaving the stern wave and trough behind. This is analogous to the hump condition of a boat hull, and this terminology has been adopted. At this stage the relationship between the forces begins to alter.

Once the speed of advance has increased beyond that of the two part transition zone, the wake forms like that of a planing craft with small oblique waves predominating. The Froude Number of the wheel, based on its waterline length is close to that of a planing craft under a similar planing condition. For these reasons this is called the planing mode and is the condition where the LPW would normally operate. In this condition virtually all of the water supplied to the wheel is entrained through the front of the wheel cavity. This causes the forces to occur in a somewhat different way from that of the displacement or static conditions. Forces are found now to be generated only at the moment of blade entry and are largely impulsive in nature. At this speed of advance, as the revolutions of the wheel increase, the lift and thrust forces, at first negative, increase parabolically from zero as shown in the force-rps plot for lift in Fig.1.6. This has been called the parabolic section of the force-rps plot. As wheel revolutions are increased further the descending blade, which had until now been meeting an undisturbed water surface begins to encounter the splash, and the scraped out cavity left by the last blade. This is called cavity intrusion of which two types are distinguished and shown in Fig.1.7, A, B and C. Under almost the same condition as those when surface cavity intrusion occurs (see Fig.1.7) the wheel begins to throw spray and froth forward in the direction of its motion. At high wheel revolutions this can build up into a large wave. This has been termed bowsplash and is shown to the top right of Fig.1.5.

At the point where surface cavity intrusion and bowsplash begin to take place a stall-like effect occurs in the magnitude of the forces generated: the force on the force-rps plot (Fig.1.6) ceases to rise

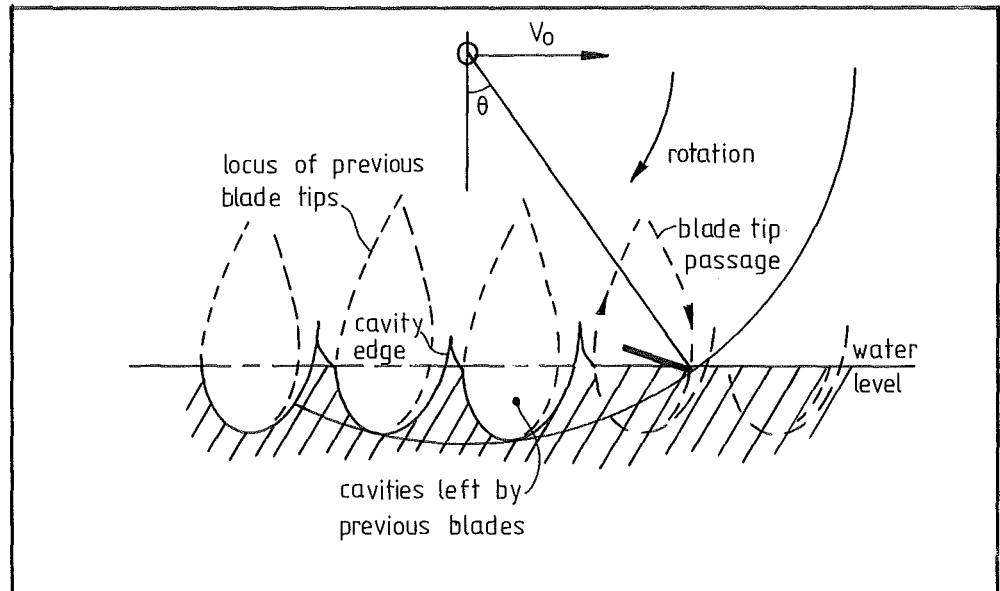


FIGURE 1·7(a) NO CAVITY INTRUSION

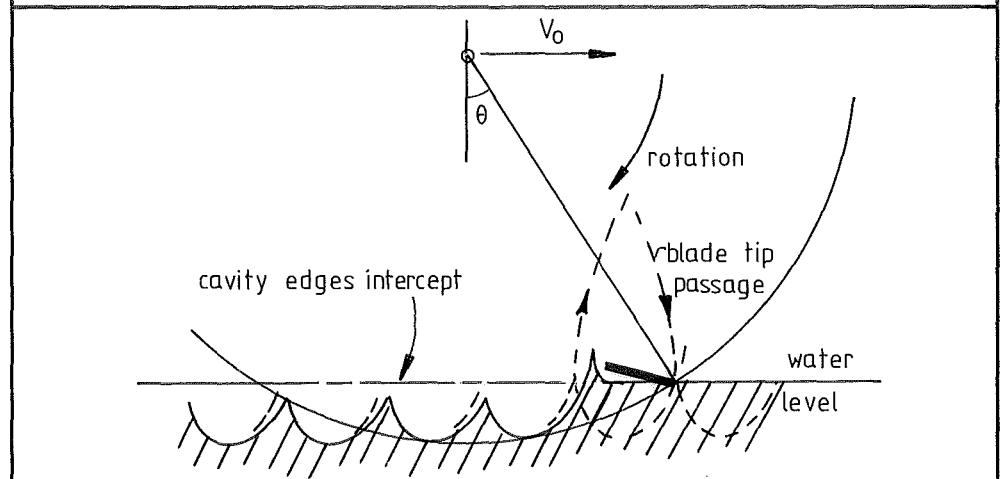


FIGURE 1·7(b) THE BLADE BREAKS INTO THE CAVITY LEFT BY THE PREVIOUS BLADE. THIS IS THE FIRST PART OF CAVITY INTRUSION.

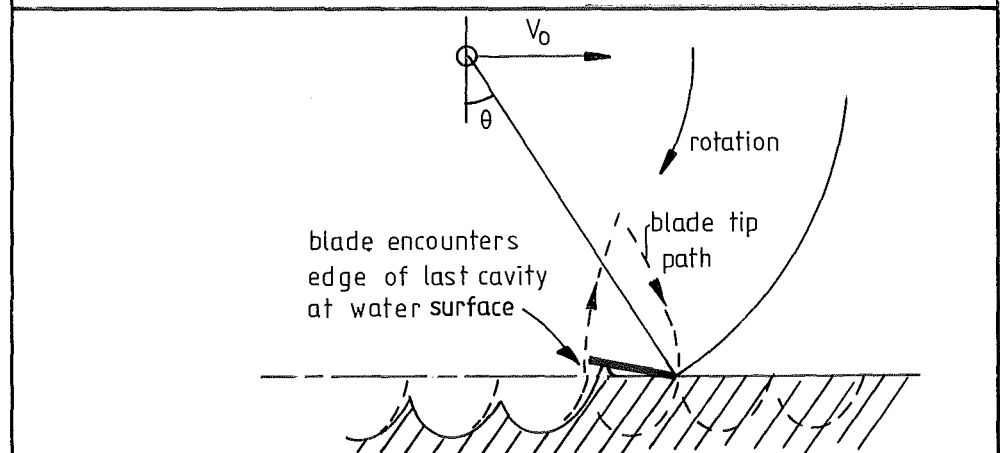


FIGURE 1·7(c) SURFACE CAVITY INTRUSION OCCURRING. (THIS TERM IS OFTEN SHORTENED TO CAVITY INTRUSION)

parabolically and begins to flatten out. This has been termed the intersection region of the plot. With a further increase in wheel revolutions the forces generally continue to increase but not as rapidly, and now in a linear fashion. This has been termed the linear section of the force-rps plot as shown in Fig.1.6. This linear section of the force-rps plot, then, represents the forces generated while surface cavity intrusion and bowsplash are both taking place.

Once in the planing mode, further increase in the speed of advance, V_o , of the wheel simply increases the magnitude of the forces in proportion to the square of the speed as would be expected, as long as the velocity ratio (see below) remains constant. The force-rps plots at different speeds of advance, in the planing mode, have the same general shape as they had for lower planing speeds, each with a parabolic section, an intersection region, and a linear section; only the magnitudes of the forces vary. The velocity ratio at which surface cavity intrusion and bowsplash occur (where the intersection region occurs on the force-rps plot) remains unchanged with changes in speed of advance.

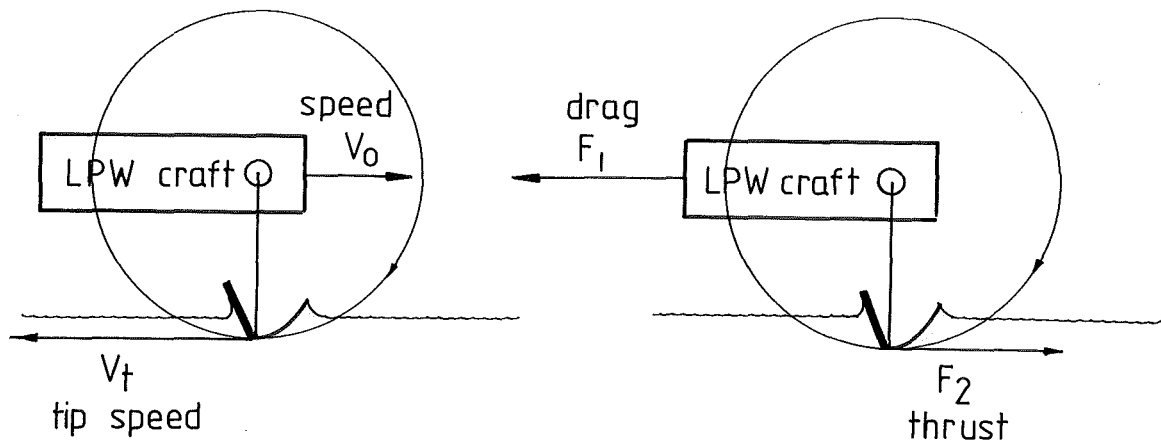
The way the wheel forces vary with the wake, and the effects of cavity intrusion and bowsplash do not seem to have been fully appreciated in the literature.

The two velocities, V_o the speed of advance, and V_t the blade tip speed relative to the wheel axis, are generally combined into the dimensionless velocity ratio, V_o/V_t . This ratio needs to be kept constant for geometric similarity of flow on scaling. For normal operation it is less than unity and when it is one, the blade tips just dip into and out of water so that little or no force is generated. The propulsive efficiency, η , theoretically cannot be greater than this velocity ratio, as indicated in Figs. 1.8 and 1.9, since kinetic energy must be left in the wake if useful forces are to be generated.

Having examined the effects of velocity on LPW operation, the effects of the other variables will be discussed.

1.4.2 Blade Effectiveness, ϵ

As can also be seen in Fig.1.9 the curve of efficiency rises close to the theoretical maximum value, then begins to fall away at



Velocity diagram

Force diagram

For the simple case of steady motion where only the horizontal part of the wheel force is considered, the force on the blades is the drag force of the craft:

$$F_1 = F_2$$

The craft's useful power: $P_{\text{craft}} = F_1 \times V_0$

The power used to drive the wheel:

$$P_{\text{wheel}} = F_2 \times V_t$$

Propulsive efficiency: $\eta = \frac{P_{\text{craft}}}{P_{\text{wheel}}} = \frac{F_1 V_0}{F_2 V_t}$

$$\therefore \eta = \frac{V_0}{V_t} \text{ when } F_1 = F_2$$

Normally, however, F_2 is only part of the resultant force of the blades so that P_{wheel} is greater than shown, and $\eta < \frac{V_0}{V_t}$

FIGURE 1.8: EFFICIENCY, η CANNOT BE GREATER THAN THE VELOCITY RATIO, V_0/V_t .

velocity ratio of about 0.5. Blade effectiveness is defined at a given velocity ratio (say 0.5). Hence at this velocity ratio in Fig.1.9 the blade effectiveness, ϵ is about 0.9 and the propulsive efficiency is 0.45 while the maximum efficiency that could have been achieved is 0.5.

1.4.3 Effects of Blade Angle, ϕ

For flat blades, a good estimate of the forces generated may be made by considering the vector diagrams of the flow velocities created by the blades as they pass through the water. Since the forces can only be normal to the surfaces of the blades, changes in blade angle will alter the directions of the resultant forces, and hence the proportions of their lift and thrust components. Changes in blade angle, then, change the thrust to lift ratio.

1.4.4 The Effect of Immersion Depth, d

(Fig.1.2 shows immersion depth, d , span, s , and chord, c)

An increase in the immersion depth at low speeds, during displacement operation, increases the fluid flow into the wheel cavity. This causes an increase in the forces. During planing operation, on the other hand, when the forces are generated at the point of blade entry, an increase in immersion depth changes the position in the wheel's rotation where the blade encounters the water. It has been found that this has a similar effect as that of changing the blade angle, namely in effecting a change in the relative proportions of the lift and thrust forces generated.

A simple relationship has been found to describe these effects in the thrust to lift ratio expression.

In general efficiency decreases with increase in immersion depth.

1.4.5 The Effect of Blade Span, s

As the blade span is increased the cavity width increases and hence the fluid supplied to each blade increases. The forces generally increase in direct proportion to an increase in blade span both in displacement operation and in planing operation.

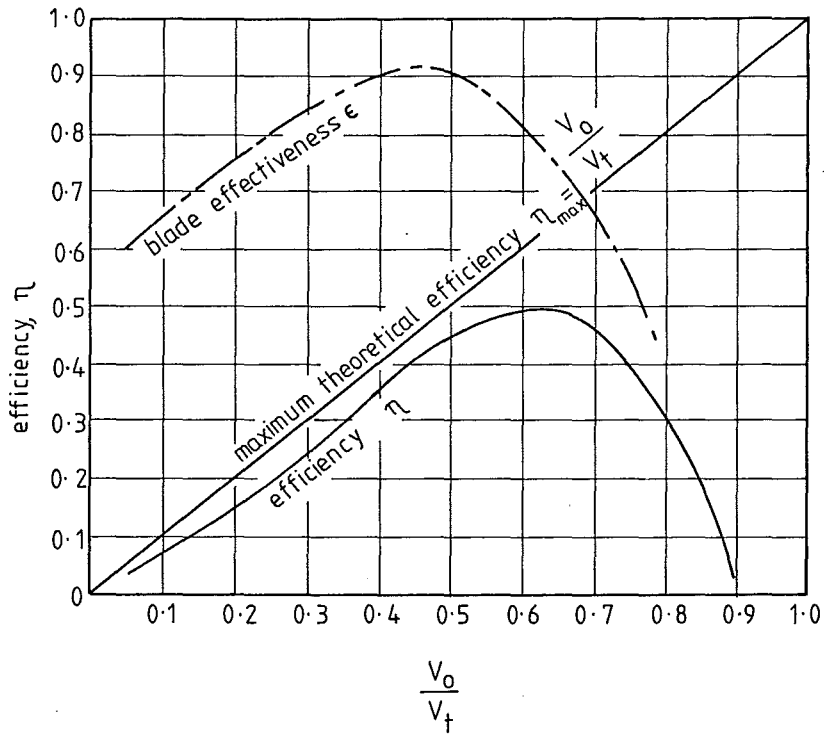


FIGURE 1.9: THE USUAL SHAPE OF THE EFFICIENCY & EFFECTIVENESS CURVES AGAINST VELOCITY RATIO.

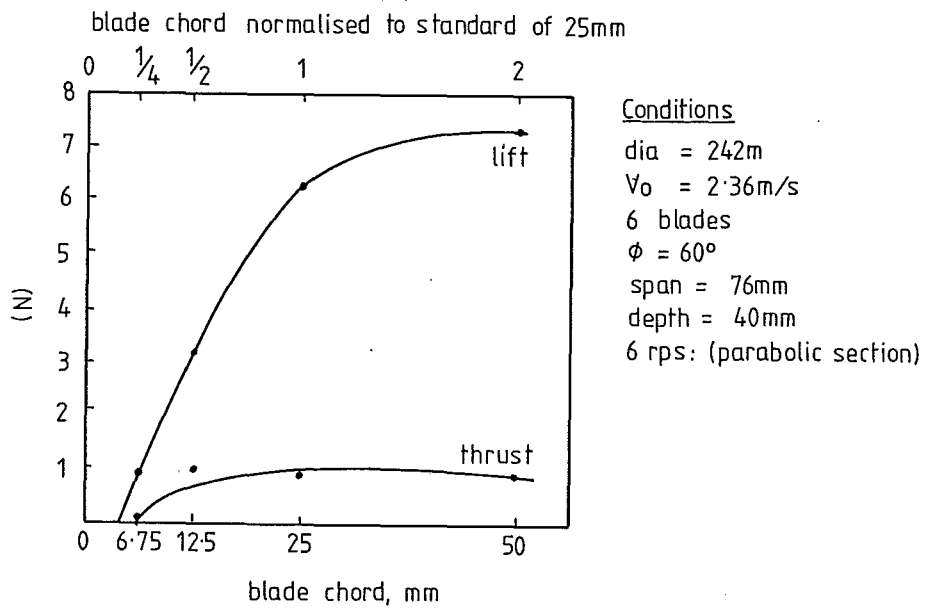


FIGURE 1.10: PLOT OF EXPERIMENTAL RESULTS OF THE BLADE CHORD EFFECT. BEFORE CAVITY INTRUSION IS OCCURRING.

1.4.6 The Effect of Blade Chord, c

The blade chord affects the forces for two reasons:

- (i) The outer edge of the blade is moving at tip velocity V_t relative to the wheel axis, and the inner edge, being on a smaller radius is moving more slowly. Consequently the outer edge of the blade normally generates a greater proportion of the force for a fully immersed blade.
- (ii) At high wheel revolutions the outer edge only, of the blade encounters the water, since cavity intrusion is occurring (see Fig.1.7c).

The result of these two effects is that for a wheel of fixed diameter the increase of chord increases blade area and therefore increases blade forces, but this increase in blade force becomes smaller as the increased area is placed nearer the wheel axis, and has little or no effect after cavity intrusion is occurring. An example is shown in Fig.1.10, for the case before cavity intrusion. A relatively minor additional effect is that the increased wetted area of the wheel means more water is carried around, with a consequent, slight efficiency reduction.

1.4.7 The Effects of the Number of Blades, B

For four reasons an increase in the number of blades is similar to an increase in blade chord when other factors are kept constant :

- (i) Forces are increased approximately in proportion to the increase in total blade area.
- (ii) In the planing mode the intersection region on the force-rps plot occurs at a lower value of wheel revolutions because, with the blade cavities closer together, cavity intrusion starts earlier (see Fig.1.7).
- (iii) The larger wetted area tends to cause a decrease in efficiency as before.

Two further factors also come into play :

- (i) When the number of blades gets below four, the impacts of individual blades cause excessive vibration. A larger number of blades produces a steadier force.

(ii) It is easier to manufacture fewer blades.

A balance between all these factors decides the number of blades to be used. Six blades seems to be a good compromise.

1.4.8 The Effect of Blade Shape

Although this area is not well understood it seems clear that the blade shape can be made to control the flow in the required way, so as to increase momentum exchange, reduce splashing and determine the proportions of lift and thrust in the resultant force. It therefore has an influence on the blade effectiveness.

A specialised blade profile can readily be designed for one set of flow conditions, but changes in depth, velocity ratio and wake type can negate the value of such design. In spite of this, slightly concave blades (concave on the pressure side, curved chordwise but straight spanwise) have been found to be a reasonable compromise and, set at an appropriate angle, can reduce the effects of the trough condition, as well as providing adequate lift and thrust forces throughout their range of operation.

Blade shape design, then, is a compromise and future work is needed to find the optimum shapes.

1.5 CONCLUSION

The LPW concept has, seemingly, not been explored before. It is a new area and therefore does not derive much assistance from the literature. Consequently the project has been initially an experimental one in which information about the LPW has been gathered. Most paddlewheel researchers, with the exception of Beardsley, have gone this far with their research and stopped. This project, however, has continued on from the data collection stage and developed a coherent theory to explain why certain behaviour is exhibited in the data. Much of the basic understanding of LPW operation (and therefore, also paddlewheel operation) outlined in section 1.4 above has therefore been brought to light only during the course of this project.

CHAPTER 2

LITERATURE SURVEY AND BACKGROUND2.1 INTRODUCTION

The idea of using the wheel as the element of support and propulsion on water has attracted attention for many decades. Records of both successful and unsuccessful attempts to use wheels on water contain a considerable number of extravagant claims, most of which were never tried in practice. Although patent literature contains a large number of such claims, untenable and untried ideas are still regularly put forward.

This chapter reviews the more useful and relevant literature dealing with wheels on water. It also reports briefly on some of the unproven claims since they may yet have value, and they help to put some perspective on more promising ideas.

The chapter is in four main sections:

- (i) Wheels for propulsion only, such as the paddlewheels of last century;
- (ii) Wheels providing support from their buoyancy;
- (iii) Wheels providing support from dynamic forces;
- (iv) Amphibious vehicles at present in use.

2.2 PADDLEWHEELS : WHEELS FOR PROPULSION ONLY

The paddlewheel literature provides the most useful basis for the Lifting Paddlewheel, (LPW) concept and is directly relevant to the propulsion aspect of LPW operation.

2.2.1 Paddlewheel History (1)

In ancient times the Egyptians and the Romans were aware of the potential of the paddlewheel as a propulsion device for water craft. It wasn't until 1776, however, that steam power was applied to paddlewheels. From about 1790 on, the paddlewheel gained in favour, especially in the rivers of America, and it remained in common use for a century, though the screw propeller gradually replaced it from the

1850's onwards. Even so, the paddlewheel was still used for special applications in the 1950's though its use nowadays is rare.

The major innovation in paddlewheel design during its regular use, was the development of feathering blades which were arranged to remain perpendicular to the water surface as they moved through it.

Volpich and Bridge (1) point out, "When the screw propeller started to come into the forefront of marine propulsion the paddlewheel soon disappeared from sea-going vessels, not so much on account of any inefficiency of propulsion, but more due to its unsuitability for large changes in draught, and its liability to damage."

Barnaby (2) adds that its greater cost was also a factor against the paddlewheel, and Beardsley notes (3) "By the time facilities and techniques were developed for performing systematic model tests and research in the field of propulsion the paddlewheel had been largely replaced by screw propulsion. As a result of the paddlewheel's fall from fashion, few model tests were conducted, and prior to the work of Volpich and Bridge in 1956 there was a dearth of published data produced by systematic model experiments."

2.2.2 Gebers 1952 (4)

The first extensive tests were conducted by Professor Gebers, superintendent of the Vienna Experiment Tank, in the years preceding the second World War, but the majority of the data was lost during the War. However Gebers showed that slip, or velocity ratio was not a complete definition of dynamic similarity for paddlewheels because of wavemaking, so that Froude's law of similarity had also to be taken into account.

Geber's work is contained in two reports dated 1951 and is referred to by Volpich and Bridge.

1. Volpich & Bridges, Pt I, 1955, P.329
2. Barnaby Art 173
3. Beardsley, H & H, June 1973, P.13
4. Volpich & Bridges, Pt I, 1955, P.330

2.2.3 Volpich and Bridge, 1955 to 1957

These authors, in their three papers summarized previous work, set the paddlewheel in its historical perspective and gave their purposes in part as : (1)

- (i) To establish some basic method of plotting results in a non-dimensional form.
- (ii) To test two geometrically similar wheels of different sizes to establish the validity of the laws of similarity with these non-dimensional figures.

Their small wheel was 0.518 m (1.7 ft) in diameter, and their large wheel, twice this size at 1.04 m (3.4 ft) diameter. One of the major variables covered in their tests was the "star centre position" shown in Fig.2.1 which defined the angles of the feathered blades. Their tests covered the Froude Number range up to $F_r = 1.49$ and are summarised in Table 2.2.

Their findings were mainly involved with the measured results, and gave only a little analysis to provide insight into why certain changes occurred when certain variables were altered. This is unfortunate because without such insight it is difficult to predict what will happen when conditions are different from those in the test situation. However their data do provide a basis for comparison.

Results

Their results from Parts I, II and III (2) are summarised here:

1. Efficiencies up to 80% were achieved with non-feathering blades, and up to 88% with feathering blades, though these efficiencies were at high velocity ratios (0.8) and hence for low thrust forces. (2)
2. There were no significant differences between the performances of the two wheel sizes when compared non-dimensionally. (3)
3. There was an unexplained dip in the thrust curves at certain velocity ratios, and this was most pronounced with radial (non-feathering) blades. (4)

1. Volpich & Bridges, Pt I, 1955, P.332 3. Volpich & Bridges, Pt II, P.467
 2. Volpich & Bridges, Pt II, P.482 4. Volpich & Bridges, Pt I, P.348

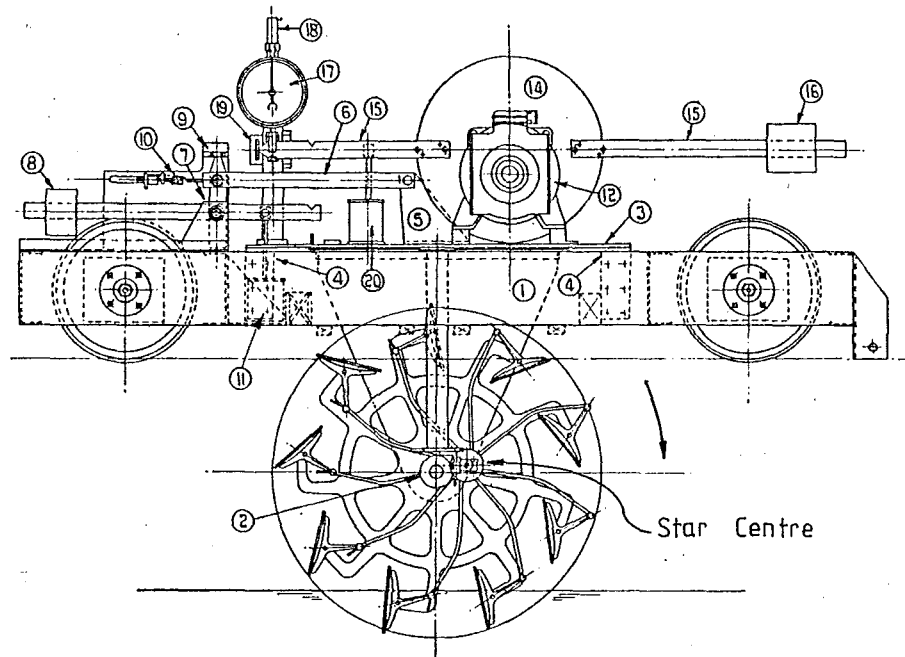


FIGURE 2.1: VOLPICH AND BRIDGE'S LARGE WHEEL
1.04 m (3.4 ft) DIAMETER, ON ITS
TEST CARRIAGE.

4. While there was a complex variation in performance relating to the star-centre position, in general the feathering blades could be arranged to give a 10% improvement in efficiency over the radial blades.
5. Efficiency decreased with increase in immersion: this was a large effect. As an example, under typical conditions, an increase in immersion ratio (immersion depth/wheel diameter) from 0.15 to 0.3 decreased the efficiency from 85% to 62%. (1)
6. Higher efficiencies were possible with fewer blades - 6 blades was the lowest number tested, and this gave peak efficiencies about 15% greater than the 9-bladed wheel, and 12% greater than the 11-bladed wheel. (2)
7. Curved blades gave a 10% increase in efficiency over flat blades in the comparison made, though unfortunately it is not clear which way the blades were curved. (3)
(Apparently standard practice was to have blades concave on the pressure face.) (4)
8. Thrust force was found to increase almost directly in proportion to blade span. (3)
9. Small entry and exit angles for the blades entering and leaving the water were shown to be beneficial. (This was achieved with feathering blades). (5)
10. The results could be plotted on dimensionless plots which contained all the necessary information.
11. The results in many respects merely confirmed the empirical knowledge which had been used before these systematic tests. (5)

1. Volpich & Bridges Pt II, P.474

2. Volpich & Bridges Pt II, P.481

3. Volpich & Bridges Pt II, P.486

4. Taggart P.87 shows concave blades on the wheel of the 'Greater Detroit' 1924.

5. Volpich & Bridges, Pt II, P.489

TABLE 2.2: THE TESTS CONDUCTED BY VOLPICH & BRIDGE

The Test Velocities Gave Froude Numbers up to 1.49

(Ref: Volpich & Bridge, Pt.III, P.507)

Reference letter	Immersion Coeff.	Number of Blades	Shape of Blades	Size of Blades	Star-centre position	
					Forward	Up
A	0.15	9	Curved	30 x 8	0.0551	0.0306
B	0.20	9	Curved	30 x 8	0.0551	0.0306
C	0.25	9	Curved	30 x 8	0.0551	0.0306
D	0.30	9	Curved	30 x 8	0.0551	0.0306
E	0.15	9	Flat	30 x 8	0.0551	0.0306
F	0.30	9	Flat	30 x 8	0.0551	0.0306
G	0.20	9	Curved	30 x 8	0	0
H	0.20	9	Curved	30 x 8	0.0306	0
I	0.20	9	Curved	30 x 8	0.0551	0
J	0.20	9	Curved	30 x 8	0.0766	0
K	0.20	9	Curved	30 x 8	0	0.0306
L	0.20	9	Curved	30 x 8	0.0306	0.0306
M	0.20	9	Curved	30 x 8	0.0766	0.0306
N	0.20	6	Curved	30 x 8	0.0551	0.0306
P	0.20	11	Curved	30 x 8	0.0551	0.0306
Q	0.25	6	Curved	30 x 8	0.0551	0.0306
R	0.25	11	Curved	30 x 8	0.0551	0.0306
S	0.20	9	Curved	22½ x 8	0.0551	0.0306
T	0.25	9	Curved	22½ x 8	0.0551	0.0306
U	0.20	8	Curved	30 x 8	0.0551	0.0306
V	0.25	8	Curved	30 x 8	0.0551	0.0306
W	0.20	9	Curved Wood	30 x 8	0.0551	0.0306
X	0.20	9	Curved	27½ x 8	0.0551	0.0306
Y	0.20	9	Curved wood crescent sect.	30 x 8	0.0551	0.0306

12. The complexity of paddlewheel behaviour precluded a unifying analytical approach. (1)

Part II of their study included a brief geometric study of the blades as they passed through the water. (2) In particular it examined the velocity during the blade passage but did not seem to consider the acceleration of the blade relative to the water, which would have had a significant effect on the forces generated.

Of some note is the fact that efficiencies as high as 88% were achieved. This at first seems remarkable, but the authors noted (3) that since the high efficiency values were at high velocity ratios they could not be attained when the paddlewheels were providing useful thrust. (Calculations carried out during the LPW project indicated that these high efficiencies occurred in the transition zone of Volpich and Bridges' wheels so their results would not be relevant for either the slower displacement mode or the higher planing mode.)

Part III of their work concentrated on gaining ship-model correlations with data collected from operational paddlewheel craft. In this, the high efficiencies found in the testing tank were further examined and the authors concluded : (4)

"It is clear...that under normal working conditions [i.e. providing useful thrust] open wheel efficiencies for the model [wheel in the testing tank] are not likely to exceed 70%. [In the presence of a ship hull the] ...overall propulsive efficiencies are in the order of 40% to 45%. It is therefore apparent that the very high wheel efficiencies obtained in the experiments do not normally lead to correspondingly high propulsive efficiencies in practice."

Part III also included a section of worked examples illustrating the use of the data in paddlewheel design. (This was later summarised by Barnaby (5).)

Comments on Volpich and Bridge's Work

While their project comprised, in the words of Barnaby, (5) "...gallant attempts..to provide adequate design data from experiments..."

- | | |
|------------------------------------|------------------------------------|
| 1. Pt I P.358 | 4. Volpich & Bridges Pt III, P.520 |
| 2. Volpich & Bridges, Pt II, P.498 | 5. Barnaby, Art 174 |
| 3. Volpich & Bridges, Pt II, P.504 | |

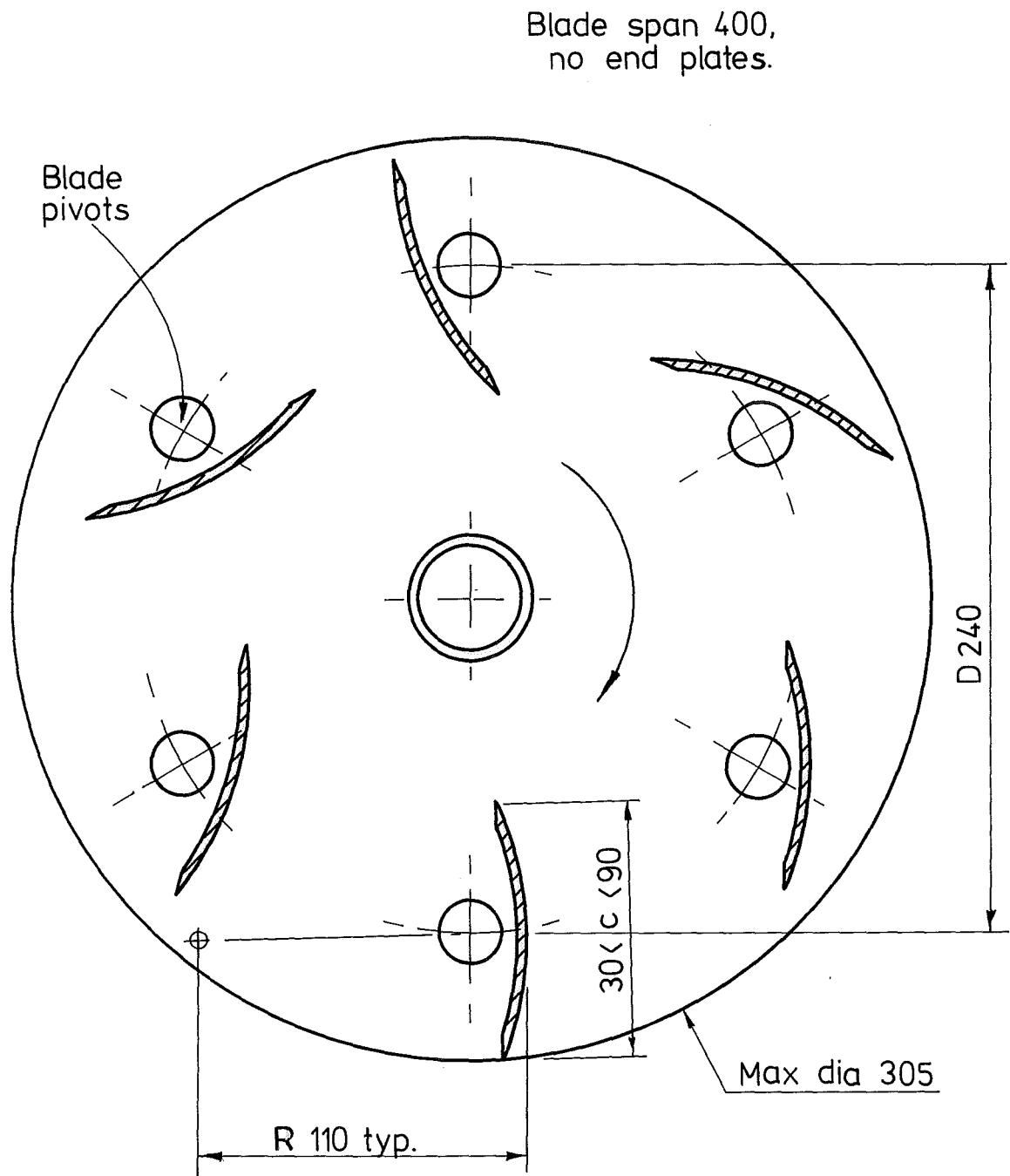


FIGURE 2-3: BLADE ARRANGEMENT FOR HELM'S FEATHERING PADDLEWHEEL. THE FEATHERING MECHANISM WAS CAM OPERATED. A VARIETY OF BLADE TYPES WAS TESTED.

only a little observational and theoretical information was provided to explain certain trends. As an example in the following extract Volpich and Bridge came very close to identifying what this project has called trough speed. They noted in Part II (1)

"...the thrust and torque collapse... which was very marked in the preliminary experiments, persists to a greater or lesser degree throughout the entire field covered...The practical result of this feature is...in that at certain speeds the rpm required for a given thrust or power are abnormally high and in the worst instances become quite impractical."

It seems a pity that they did not observe the wave formation causing this, as this wavemaking is the key to many inconsistencies they observed in their results, such as this dip in the thrust curves, ((3) above).

Their extensive work has unfortunately not been particularly useful for the purposes of the present project as the data presented were only marginally applicable and the theories and observations which could have helped were largely undeveloped.

2.2.4 Helm 1967

Helm, of Germany, tested deeply immersed, six-bladed feathering paddlewheels with the objective of developing a propulsion system for high speed flat bottomed craft for shallow water use. His wheels' feathering mechanism was cam-operated and is shown in Fig.2.3. The immersion ratios were unusually large and ranged from $\frac{d}{D} = 0.5$ to $\frac{d}{D} = 0.72$ so that all tests were conducted with the wheel axis immersed. The wheels were about 0.3 m in diameter, this value varying with the blade chord. The tests covered the Froude Number range up to $F_r = 1.53$. Flat and curved blades were tested, the curved blades being concave on the pressure face. His tests are summarised in Table 2.4.

Results

Helm's results were recorded on dimensionless plots which were less cramped than those of Volpich and Bridge, and used different dimensionless quantities. His main findings were: (2)

1. Volpich & Bridges, Pt II, P.471
2. Most findings are from his plotted data, or his Summary P702 since a full translation was not available.

TABLE 2.4: SUMMARY OF HELM'S TESTS

Wheel diameter: 300 mm (approx...240 mm + blade chord)
 Span , s: 400 mm (no end plates)
 Chord, c: 30, 60, 90 mm
 Number of blades, B: 6
 Blade angle: Feathering blades

Water 900 mm deep:

c (mm)	D (mm)	$\frac{d}{D}$	FLAT BLADES				CURVED BLADES			
			Wheel Revolutions (rps)				Wheel Revolutions (rps)			
			47	59	69	81	47	59	69	81
30	270	0.5	x	x	x	x				
		0.57	x	x	x	x				
		0.65	x	x	x	x				
		0.72	x	x	x	x				
60	300	0.45	x	x	x	x	x	x	x	
		0.52	x	x	x	x	x	x	x	
		0.58	x	x	x		x	x	x	
		0.65	x	x	x		x	x	x	
90	330	0.41	x	x	x		x	x	x	
		0.47	x	x	x		x	x	x	
		0.53	x	x	x		x	x	x	
		0.59	x	x	x		x	x	x	

Shallow water 350 mm deep:

60	300	0.45	x	x	x	x				
		0.65	x	x	x					

1. Although deeply immersed, the wheels produced useful thrusts.
2. Maximum efficiencies were around 40 to 45%.
3. These peak efficiencies occurred at velocity ratios of about 0.46, (suggesting high blade effectiveness).
4. The peak efficiencies occurred at about $F_r = 0.85$ (which would seem to be about trough speed).
5. After the peak efficiencies at about $F_r = 0.85$ the efficiency fell away to zero at about $F_r = 1.5$.
6. The thrust produced at the peak efficiency was about one half to one third of maximum thrust (which is similar to the findings of Volpich and Bridge).
7. Curved blades gave better results for large blade chords, and flat blades were better with small chords. (Blades were concave on the pressure face.)
8. The wheel, with feathering blades, gave efficiencies that were consistently 10% greater than those of a "normal" wheel as tested by F. Süberkrüb in 1949.
9. Tests in shallow water indicated reductions in both torque and thrust with increase in Froude Number (up to $F_r = 0.78$).

Comments on Helm's Work

Helm referred to papers by F. Süberkrüb and O. Krappinger as well as Gebers, which are all published in German. Because of the difficulty in obtaining translations and the fact that these papers are unlikely to shed any more light on the LPW concept, they have not been surveyed for this project.

In relation to 4 above, the data for this project for non-feathering blades also tended to have higher efficiencies at around trough speed, before falling to lower values once the LPW was planing. Beardsley also recorded similar peaks in efficiency at $F_r = 0.3$ to 1, before it settled to apparently steady values for further increase in Froude Number (1). These consistent findings suggest that the presence

1. Beardsley Fig.21, P.22

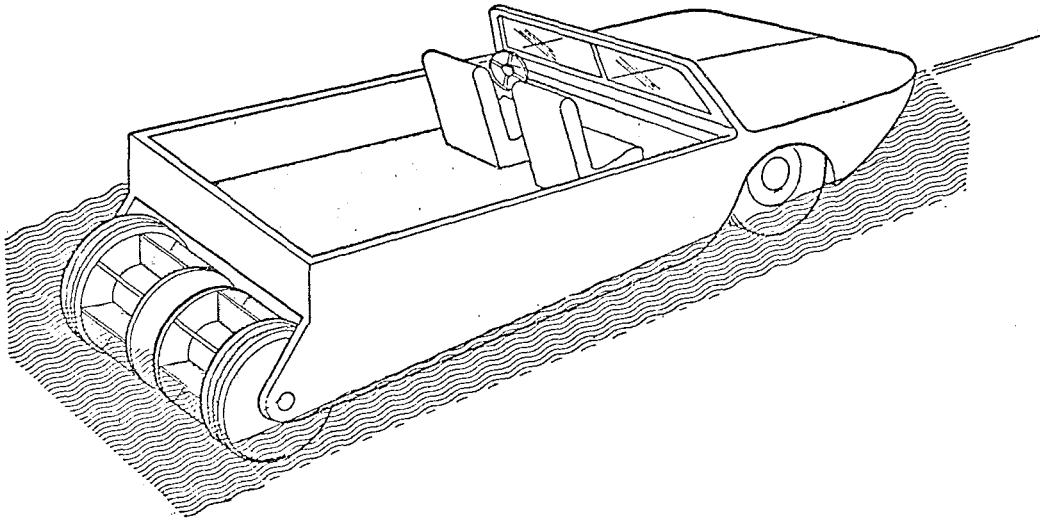


FIGURE 2.5: WRAY AND STARRETT'S CONCEPT DRAWING OF A HIGH SPEED AMPHIBIOUS VEHICLE

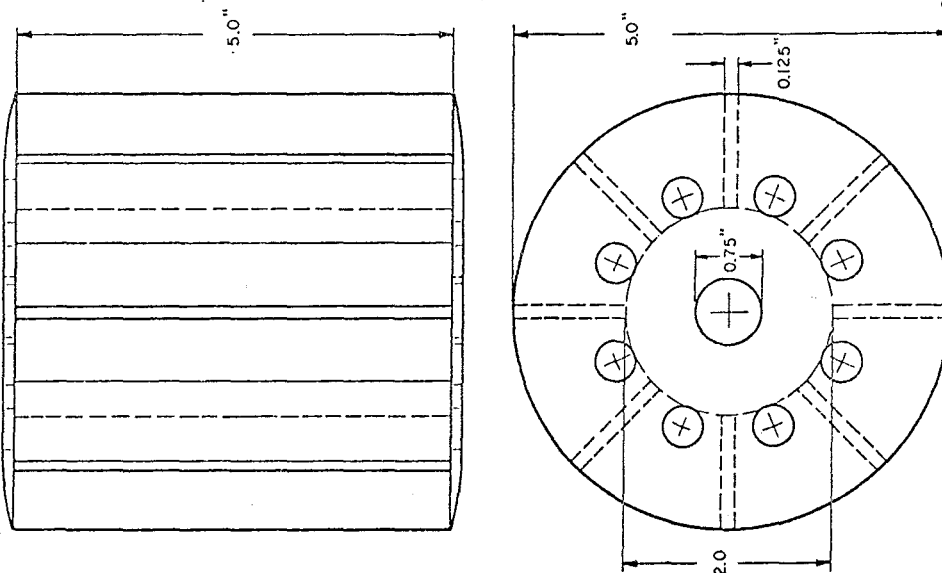


FIGURE 2.6: THE PADDLEWHEEL TESTED BY WRAY AND STARRETT. NOTE VENTILATION HOLES IN THE END PLATES AND THICK BLADES (DIMENSIONS IN INCHES).

of the efficiency peaks is closely related to the wavemaking of the wheel.

Helm apparently did not seem to appreciate that these peak efficiency values were associated only with a wheel in open water, and that the characteristics would be changed by the presence of a hull creating its own wave train. (One of Helm's figures showing peak efficiency in the transition zone is shown in Fig.4.30, section 4.14.1.)

No further records of Helm's work have been found in the literature to date, so it is not known if his wheels were used in practice.

2.2.5 Wray and Starrett 1970

These authors had in mind an idea not unlike that of Helm. They imagined a high speed, flat bottomed hull with the added facility of making the craft amphibious. The craft they envisaged is shown in Fig.2.5. Their stated purposes were:

1. To determine, by means of systematic model experiments, the hydrodynamic characteristics of a series of paddlewheel propulsive devices with fixed radial blades.
2. To determine the feasibility of applying the high-speed paddlewheel to a high-speed planing hull of shallow draft.
3. To develop and extend paddlewheel design parameters for high speed use.

A significant aspect of their concept, in relation to wavemaking, was that they deliberately mounted their test wheel behind the transom of a model flat-bottomed hull where the inflow conditions to the paddlewheel were fixed in the same way that they would be in the full-sized craft.

Because of the limitations of their testing equipment, their wheel was small: 0.127 m (5 inches) in diameter. It is shown in Fig.2.6. Note that the blades were mounted on a central hub, and that there were endplates on the wheel. These features were intended to make the wheel robust, and free from fouling in weed-infested waters. The blade edges were over 3 mm thick which unfortunately would have adversely affected the thrust under some operating conditions.

Their tests were conducted in flowing water in the Davidson Laboratory variable pressure free surface water channel. This was a different arrangement from the other tests cited where the wheels were moved over a still water surface.

TABLE 2.7

WRAY AND STARRETT'S TEST PROGRAMME

Wheel Diameter:	127 mm (5 inches)
Velocities:	1.1, 1.4, 1.65, 2.35 m/s (All planing speeds for the wheel)
	Critical velocity for the channel is 1.32 m/s.
Immersion ratios:	0.06, 0.1, 0.16.
Wheel Revolutions:	0 - 27 rps.
Number of Blades:	12 , 6.

The full set of combinations of these variables was tested.

Table 2.7 summarises their test series. Note that they tested a six and a twelve-bladed wheel, and their Froude Number range was from $Fr = 0.99$ to 2.11.

Their report included performance calculations for a jeep-sized amphibious vehicle as a prototype for their concept. (1) The measured data only allowed for a maximum speed of 26 kph over water using a 70 kW motor, but the authors considered that 50 kph could be attained with only a little extra power.

Results

Wray and Starrett presented their results in a useful variety of ways. By plotting thrust and efficiency against wheel revolutions, they have produced a data form which is easy to comprehend, and the properties of the physical situation are therefore clarified rather than obscured. Their data were also replotted in a dimensionless form which is more useful for design purposes.

Their main findings are summarised:

1. Preliminary tests indicated the need for vent holes in the sideplates, shown in Fig.2.6, to allow the water to enter the space between the blades. (1)
2. Efficiencies in the useful range were low, around 26%, (2) but peak efficiencies were about 40%.
3. Thrust and, contrary to expectation, peak efficiency both increased with immersion. (3) (However a closer look at the data indicates that the sharp efficiency peaks, only, vary in this way and the bulk of the efficiency results decrease consistently with immersion as indicated by earlier reports.)
4. There was a "thrust 'breakdown' occurring at 40% slip [velocity ratio of 0.6] which appeared to occur over a span of 10% slip [velocity ratio of 0.1] after which the thrust again continued to increase with increasing slip".(4) An example from their data is given in Fig.2.8. They noted that similar breakdown were reported by Volpich and Bridge. (This breakdown is cavity intrusion described in section 1.4 and Fig.1.7.)
5. The six-bladed wheel fairly consistently gave more thrust and better efficiencies than the twelve-bladed wheel. (5)

1. Wray and Starrett P.21
2. Wray and Starrett P.26
3. Wray and Starrett P.22
4. Wray and Starrett P.21
5. Wray and Starrett P.21 and 22

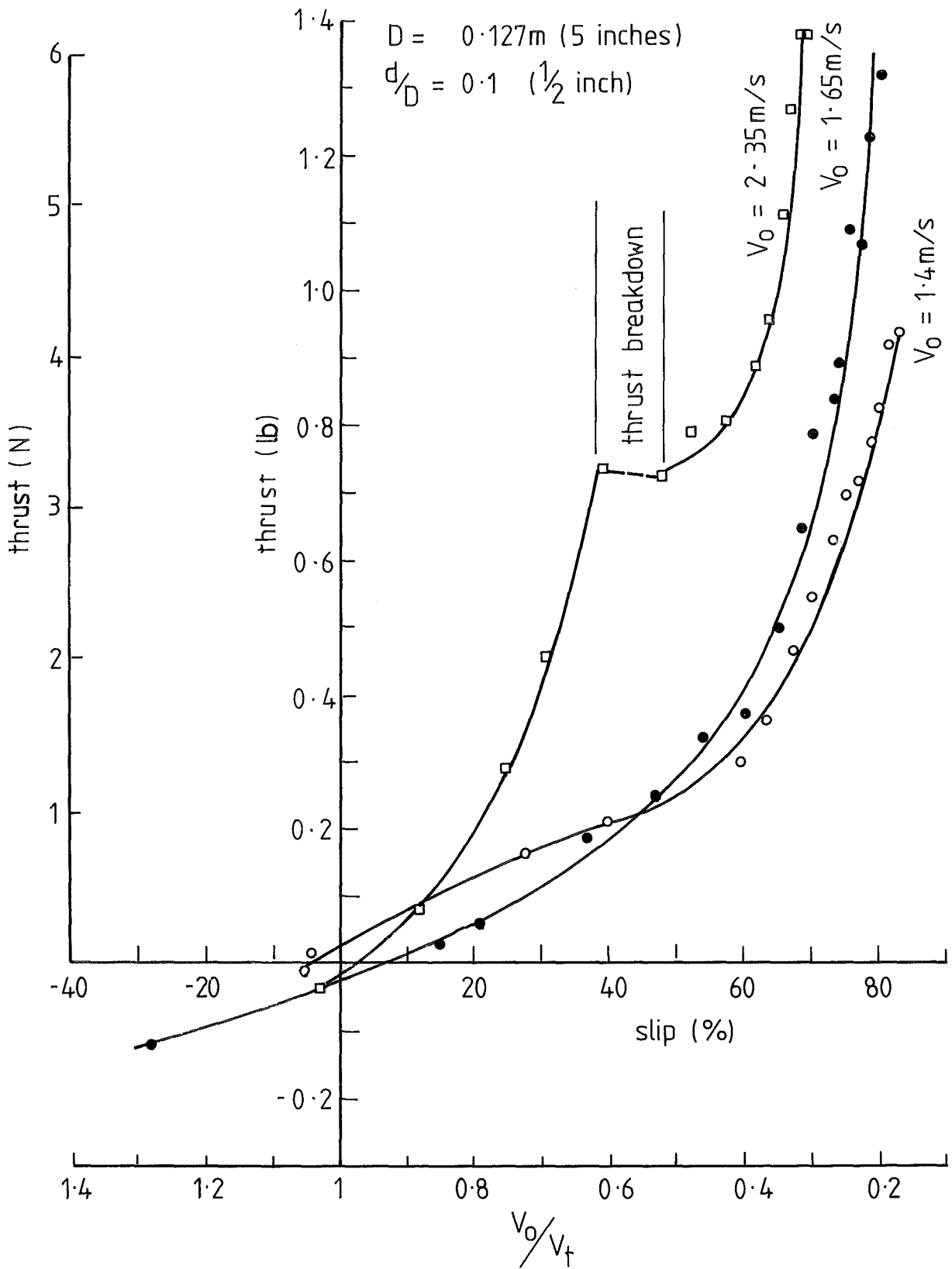


FIGURE 2-8: THRUST vs SLIP FOR VARIOUS ADVANCE VELOCITIES (V_0) FOR WRAY AND STARRET'S 6-BLADED WHEEL

6. They noted the presence of "form" drag of their wheel which prevented the thrust from being zero at a velocity ratio of 1. (1)
7. They proposed that:

"There appeared to be some type of flow phenomenon which more seriously affects a wheel of small diameter than a wheel of large diameter". (2) This was especially noticeable when comparing the efficiency curves with those of other experimenters using larger wheels.

Comments on Wray and Starrett's Work

While it was both wise and innovative of these authors to introduce the craft hull into the test setup there were two factors relating to their test conditions worth comment. Firstly, their channel was relatively confined: the flowing water cross-section was 330 mm wide by 178 mm deep, and into this the wheel, 127 mm wide was immersed up to 20 mm. (3) While blockage effects were likely to have been small they may well have been significant, and the effects of the walls close by may have affected the wavemaking in an unpredictable way. No mention of these factors was made in the report.

Secondly, as noted in section 4.16, flowing water passes through a critical velocity, dependent on its depth, and its wave propagation properties change after it has reached this velocity. For Wray and Starrett's setup this critical velocity can be calculated as 1.32 m/s. From Table 2.7 it is clear that one of their sets of measurements was taken a little below critical velocity and the other three were taken above it. While the presence of the hull in their tests probably limited the influence of the varying flow regime, it would have been cleaner to have excluded this variable.

In 7 above, the authors considered the size of their wheel as being the factor involved in producing low efficiencies in their tests. (Certainly an evaluation of their data indicates low blade effectiveness.) However their conditions were different from those of others in several ways so the following factors should also have been taken into account when comparing results:

1. Wray and Starrett, P.22
2. Wray and Starrett, P.29
3. Wray and Starrett, P.14

1. The presence of endplates.
2. The presence of a hull form altering the inflow conditions (Helm, Volpich and Bridge, Beardsley and this project all give indications that maximum peak efficiency is related to wave formation).
3. The possible influence of the flowing water.
4. The, relatively, very thick blade edges. (Volpich and Bridge had blade edges of the same thickness in their 1.04 m diameter wheel. (1))

With these variables also involved it would be unwise to conclude that the wheel size alone caused the observed performance degradation.

In the light of the LPW concept it is particularly interesting to note the following paragraph in Wray and Starrett's report: (2)

"The entire wheel, drive motor, and tachometer assembly was mounted on a three-component balance system. The balance system was set up to measure the torque, thrust and lift produced by the paddle-wheel. Preliminary data showed the lift component to be negligible and the lift element was therefore removed to reduce vibration and noise in the overall recording system."

Apparently the preliminary data were at the lowest speed, and therefore in the displacement mode, as data for radial blades in this LPW project indicated as much lift as thrust was present in the planing mode once cavity intrusion is occurring.

No reply was received from correspondence with the authors of this concise report.

2.2.6 Beardsley, 1973

In his paper on Surface Impulse Propulsion (SIP) Beardsley presented the most useful reference for this LPW project.

He defined Surface Impulse Propulsion as propulsion by actuation of the surface layer of the water, and he outlined the advantages which

1. V & B Pt I P.341 and 342
2. Wray and Starrett, P.13

this propulsion method may have over other means. Although this SIP concept also relates to surface-piercing propellers, which are exceptionally efficient, in Beardsley's project it was translated into a paddlewheel format, where the wheel was not deeply immersed and had fixed, specially shaped blades. He suggested that the inflow and outflow conditions could be controlled, (like Wray and Starrett's) with surfaces or plates. His wheel concept is shown in Fig.2.9.

As Beardsley felt that his data supported the concept of such high speed amphibious craft as suggested by Wray and Starrett, he made one of his aims to extend the Froude Number of his tests beyond that to which previous tests had been conducted. (1) He achieved a Froude Number of $F_r = 2.6$ with an 0.153 m (6 inch) diameter wheel. (2) Although he did not present a summary of the tests conducted, Table 2.10 covers the range of data he used in his paper.

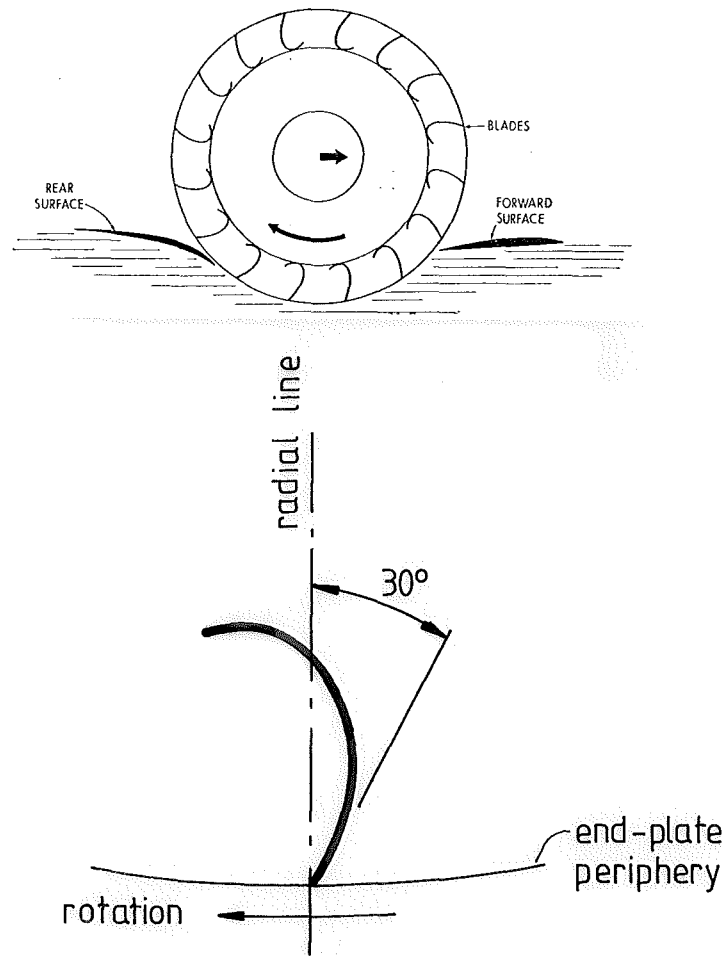
As well as trying to discover the effect of speed (with high Froude Numbers) Beardsley's tests were intended to determine the major effects of size, span, number of blades, blade shape and immersion depth.

Results

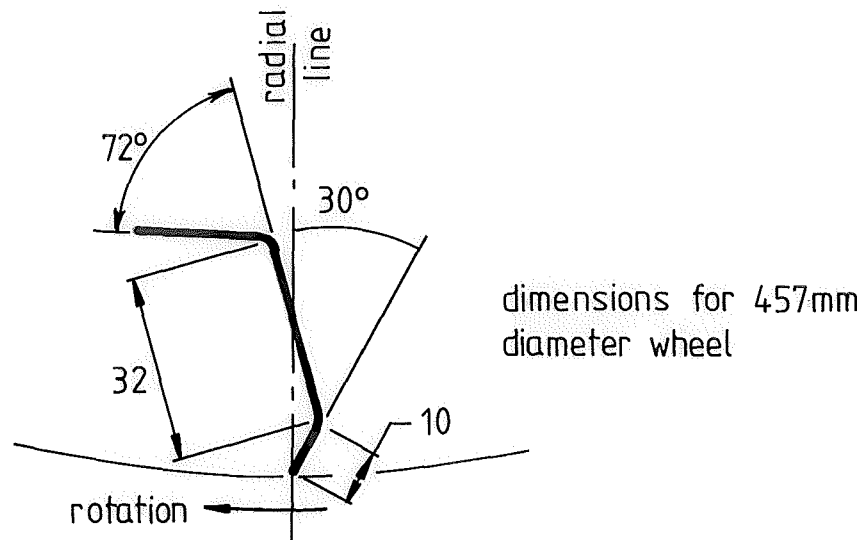
1. From Beardsley's own tests with three wheel sizes, and, notably, from Wray and Starrett's comments he concluded that model rotors should be at least 0.3 m (1 ft) in diameter to assure that test data could be reliably scaled to larger operational sizes. (2) However he admitted that the effect of wheel size did not yet appear to be fully established.
2. The number of blades should be in the range from 6 to 20 but there was a lack of good reason to explain why performance was best in this range. (3)
3. Thrust increased directly with blade span, with no change in efficiency, but with low aspect ratios some degradation possibly occurred.

1. Beardsley P.20
2. Beardsley P.15

3. Beardsley, P.16



(a) original blade shape



(b) typical blade shape

FIGURE 2-9: BEARDSLEY'S SURFACE IMPULSE PROPULSION WHEEL (TOP) AND TWO BLADE SHAPES HE TESTED.

4. There appeared to be little difference between the performance of paddlewheels having blades mounted on a large hub, or with open spaces between the blade roots.
5. Blade shape was seen as important - all previous data and Beardsley's own, pointed to this fact, but since there was little information available on blade flow conditions, this was where he felt future work should be concentrated. (1)
6. The effect of immersion in Beardsley's tests essentially confirmed the results of previous workers: increased immersion produced increased thrust and torque and lower propulsive efficiencies.
7. There was a dip in the thrust curves which was related to speed of advance and depth of immersion. This was termed "transition dip" and was related to the "gravity-induced mass supply to the wheel". (This was the same dip noted by Volpich and Bridge; section 3.2.3, point 3 and this is the transition zone of this project. See Fig.1.5.)
8. As speed was increased beyond the "transition dip", it was believed that Froude or gravity effects should become minor as compared with dynamic effects. It was thought that the thrust coefficient and efficiency would then reach stable values with increasing speed as long as blade effectiveness remained constant.
9. An interesting note was made of the fact that the water flow changed direction relative to the blade as it passed through the water, but the effect of this was not understood. (2)

Comments on Beardsley's Work

Once again the presence of the waves making the trough and hump conditions were overlooked, though Beardsley almost identified the physical situation by graphical handling of the data. He established the "transition dip" which he described "...this dip is considered to occur in the region where the supply of mass flow changes from chiefly

1. Beardsley, P.19
2. Beardsley, P.23

TABLE 2.10: BEARDSLEY'S TESTS

NOTE THAT ALL HIS ROTORS HAD END PLATES OUT TO THE
BLADE TIPS. BLADE SHAPES ARE IN FIG.2.9

D (mm)	B	Blade Shape	$\frac{d}{D}$	V_o m/s	F_r	$\frac{nD}{\sqrt{gD}}$	$\frac{V_o}{V_t}$	$\frac{c}{D}$	$\frac{s}{D}$	Ref.	Test
457	12	Typ.	0.088	0-3.4	0-1.8	0.83	0-0.7	0.088	0.5	Figs. 5 & 6	Diameter
305	"	"	"	"	"	"	"	"	"		
152	"	"	"	"	"	"	"	"	"		
457	12	Curved	0.088	0-3.4	0-1.8	0.58	0-0.8	0.088	0.5	Figs. 7, 8 & 9	No. of Blades
"	15	"	"	"	"	"	"	"	"		
"	30	"	"	"	"	"	"	"	"		
"	60	"	"	"	"	"	"	"	"		
457	12	Curved	0.088	0-3.2	0-1.5	0.75	0-0.7	0.088	0.5	Fig. 10	Central Hub
"	"	On Hub	"	"	"	"	"	"	"		
457	15	Curved	0.088	0-3.4	0-1.8	0.58	0-0.8	0.088	0.5	Fig. 12	Blade Shape
"	"	Flat	"	"	"	"	"	"	"		
"	"	Curved	0.167	"	"	"	"	"	"		
"	"	Flat	"	"	"	"	"	"	"	Fig. 13	
457	12	Curved	0.088	0-3.2	0-1.5	0.72	0-0.7	0.088	0.5	Fig. 15	Blade Shape
"	"	Typ.	"	"	"	"	"	"	"	" "	
457	12	Typ.	0.075	0-3.2	0-1.5	0-0.67	0-0.7	0.088	0.5	Figs. 16,17 18,19	Depth
"	"	"	0.088	"	"	"	"	"	"		
"	"	"	0.117	"	"	"	"	"	"		
"	"	"	0.172	"	"	"	"	"	"		
457	12	Typ.	0.088	0-2.3	0-1.1		0.4	0.088	0.5	Figs. 20 & 21	Froude Number
305	"	"	"	0-2.8	0-1.6		0.4	"	"		
152	"	"	"	0-3.2	0-2.6		0.4	"	"		
457	12	Typ.	0.088	0-2.3	0-1.1		0.5	"	"		
305	"	"	"	0-2.8	0-1.6		0.5	"	"		
152	"	"	"	0-3.2	0-2.6		0.5	"	"		

gravity fed to chiefly horizontally entrained." And further "...at the dip, the speed of advance has become so great that the rotor is running away from the cavity before gravity-induced flow can supply it." (1) This seems like a good description of the wheel making the transition from hump speed to planing speeds.

Beardsley, also, failed to measure lift forces and gave the terse comment: "Unfortunately, vertical forces were not measured" (2) as the only recognition that they probably existed.

His conclusion, while relevant to paddlewheels is equally relevant for the LPW concept; (3)

"The process of SIP depends essentially on the efficiency of a process consisting of three coordinated steps: blade entry, application of change of water momentum, and blade withdrawal. Accomplishment of this process with the required degree of efficiency will require an understanding of flow over the blades for various types of motion relative to the water, and also the development of the mechanical means of accomplishing the type of motion found desirable.

"In view of the significant benefits which may be derived it appears that Surface Impulse Propulsion merits active study and development. It is recommended that efforts be directed to analytical and experimental study of flow and to high speed model tests of impeller rotors having blades designed with the knowledge acquired in the flow studies."

These recommendations were partially carried out by the work described later in this project.

Correspondence with Beardsley proved both instructive and encouraging. (4).

1. Beardsley, P.20
2. Beardsley, P.15
3. Beardsley, P.24
4. Alexander, 1977, Appendix 3

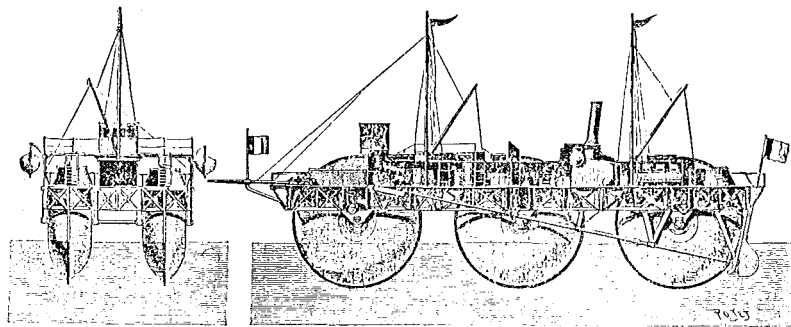
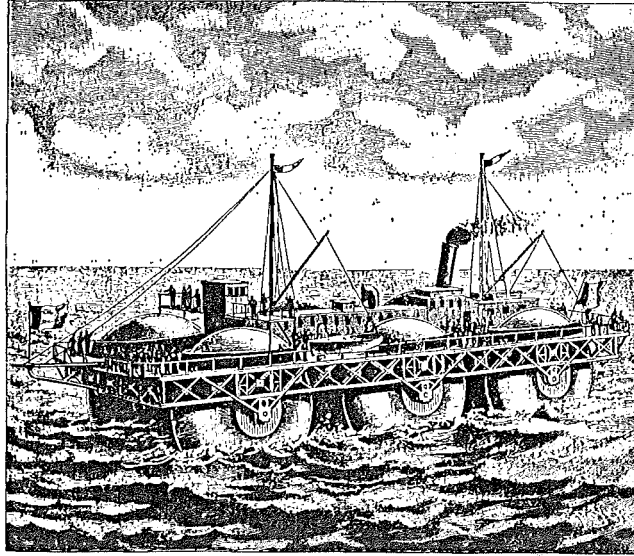


FIGURE 2.11: THE BAZIN ROLLER BOAT. THE ROLLERS PROVIDED BUOYANCY, AND ROTATED TO REDUCE SKIN FRICTION.

2.3 WHEELS PROVIDING BUOYANT SUPPORT

This section considers reports of buoyant wheels which provide most or all of the craft support, if not the thrust as well.

An idea which has surfaced from time to time is that the skin friction of a craft could be reduced to a negligible amount if the craft employed rollers which rotated like wheels as it moved along, making the relative speed between the water and the roller zero somewhere on the roller surface. The significance of wave drag with such tubby buoyant forms as wheels, however, was usually overlooked. In view of some tests done in the testing programme of this project, some of these reports are included briefly here.

2.3.1 The Bazin Roller Ship, 1896

Taggart (1) records the Bazin roller ship shown in Fig.2.11 which was actually constructed, and crossed the English Channel to tour Eastern England in 1869. It displaced 285 tonnes, was 37 m long and was propelled by a 410 kW engine driving a propeller, while the six rollers were turned by three 37 kW engines. The rollers were 12 m in diameter and were immersed about 3 m into the water. Seven knots was claimed as its speed across the English Channel. Twice this speed would normally be expected of a conventional craft of this power, but Bazin felt that the low trial speed of the ship was due to the inability of the motors to drive the rollers at a high enough speed.

This was a case where the rollers were used primarily for buoyancy. There have been a few similar craft constructed and tried, where the rollers were intended to provide propulsion as well as buoyant support. A recent, more serious attempt to come to terms with the idea follows.

2.3.2 The Rollercraft, Kearsy, 1971

In May 1971 Kearsy, from the University of Southampton, published the results of his Ph.D. thesis in which he examined the feasibility of using large, flexible-skinned, inflated rollers as the means of support and propulsion for the Rollercraft. He also saw the possibility of making this craft amphibious.

1. Taggart, P.189

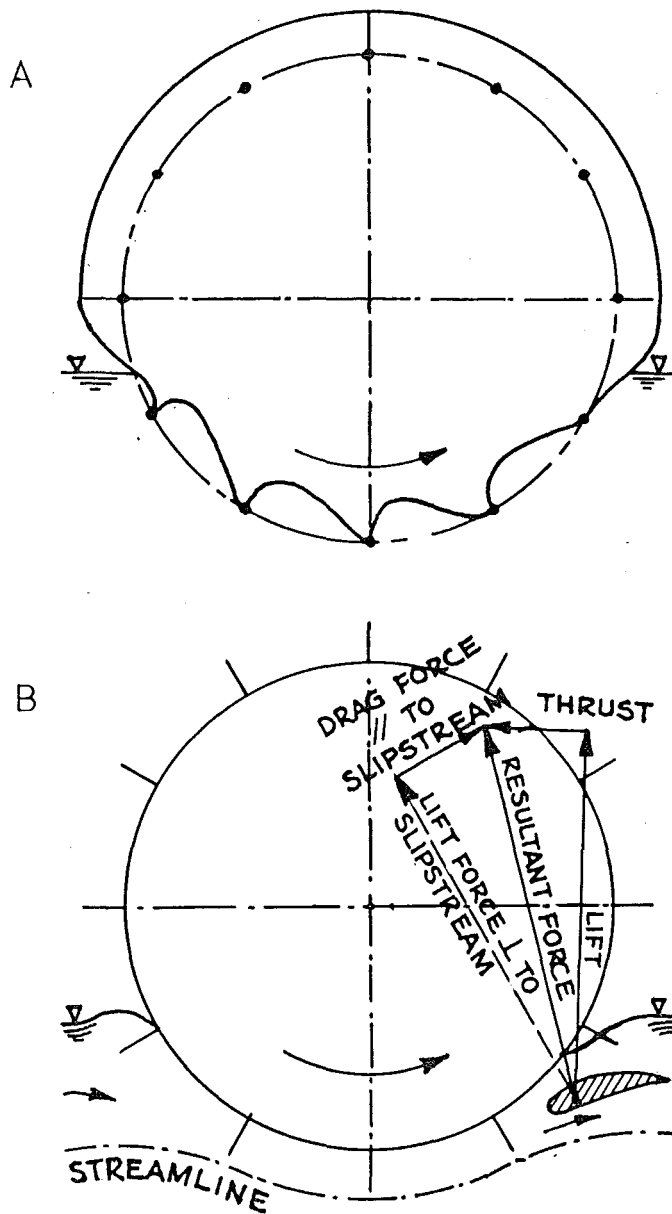
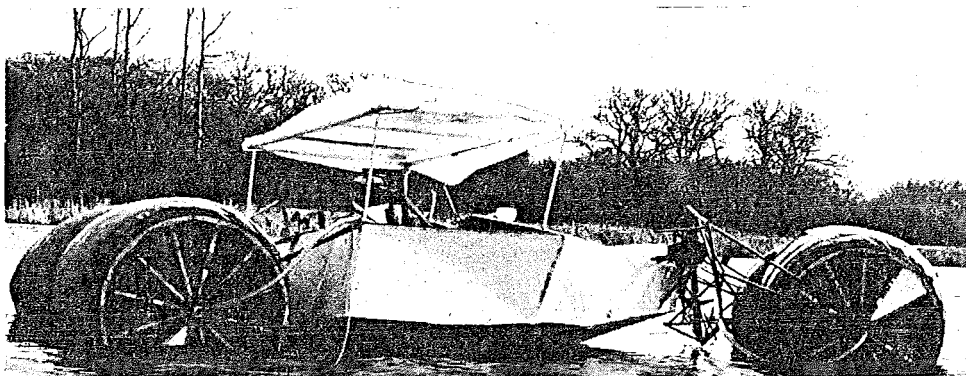


FIGURE 2.12: THE INFLATABLE FLEXIBLE ROLLERCRAFT WHEEL (A), AND A ROLLERCRAFT WHEEL WITH 'HYDROFOIL' (B).



motion

FIGURE 2.13: KEARSEY'S PROTOTYPE ROLLERCRAFT.

The rollers he employed were constructed with rigid circular end plates connected by a number of axial rods spaced around the circumference. Each roller was covered with a flexible loose skin, and the assembly inflated with low pressure air (see Fig.2.12(A)). The blades of the roller were formed when it was partially immersed, by the balance between the internal air pressure and the hydrodynamic and hydrostatic water pressure.

Beardsley described the action: "...during water actuation the plaint surface of the inflated rotor provides a blade shape that continuously adapts to local flow conditions. In addition, the energy absorbed by the inflated rotor during the local surface depression is efficiently converted into propulsive power by the horizontal rearward repulsion of the entrapped water." (1) Kearsey noted that: "...the blades reformed into a smooth cylinder once the hydrostatic and hydrodynamic forces fell below the internal pressure of the rotor and thus were incapable of carrying water up and over the rotor". (2)

Kearsey also tested a rigid roller of dimensions similar to those of the flexible roller, and experimented with a "hydrofoil" placed in the wake of the rollers, shown in Fig.12(B). It was claimed that the flexible rotors in conjunction with the "hydrofoil" were able to "...extend the range of advance ratios and immersion depths for which thrusts [could] be obtained, and to reduce the power requirements by some 50% of the rigid bladed rotor." (3)

It is tempting to think that these rollers would not be required to produce any nett thrust because there is no craft drag to overcome and they can be imagined as simply rolling on the water like a pinion gear on a rack. However the rollers create waves, introducing wave-drag and creating trough and hump conditions which could put an upper limit on the craft's speed unless the rollers are capable of making the transition to a planing-type wake.

Kearsey was aware of the presence of wavedrag (4) through his wheels apparently did not strike the difficulties encountered by the LPW in negotiating the transition zone to planing speeds.

1. Beardsley, P.19

2. Kearsey, Hovercraft and Hydrofoil, P.22

3. Kearsey's Thesis, P.151
No.8

4. Kearsey's Thesis, P.24

He was well aware of the presence of lift forces both from buoyancy and dynamic conditions, and he measured them as a matter of course.

Unfortunately one factor throws doubt on the validity of Kearsey's measured results. The tests from which his data originate were conducted in a flowing stream of water in a restricted channel. His 0.3 m diameter by 0.2 m span test rollers (1) were immersed up to 0.15 m (2) in this channel of dimension 0.46 m wide (3) and 0.29 m deep.(4) Although Kearsey recognised that these were cramped conditions he was unable to assess their effect :

"By taking a datum test at zero rotation an allowance could be made for this; [blockage effects] further tests on the manned model will help clarify the extent of this interference." (5)

Kearsey made no mention of the fact that the velocity of flow for which most of his results were taken (6) was within 10% of the critical velocity of open channel flow (as outlined in section 4.16). Under these conditions the measured results would be affected in such a way as to make it difficult to relate them, with any confidence to conditions of a wheel on open water.

Rollercraft Prototype (7)

Kearsey constructed and tested a man-carrying prototype with three 1.83 m diameter rollers (Fig.2.13). This was claimed to perform as expected and was reported as having attained speeds of 4.6 m/s, (8) with an all up weight of about 720 kg (8) and an installed power of 24 kW (9). While the test programme for the prototype was not complete at the time of his writing it can be noted that:

1. This reported top speed would have been just above the transition zone of 2.62 - 3.35 m/s for this sized wheel.
2. Apparently the expected speed was about 35 kts (17.6 m/s) for the expenditure of about 7.5 kW (9);

- | | |
|------------------------------------|-------------------------------|
| 1. Kearsey's Thesis, Fig.45 | 6. Kearsey's Thesis Fig.51 ff |
| 2. Kearsey's Thesis, P.93 | 7. Kearsey's Thesis, P.95 |
| 3. Kearsey's Thesis, P.43 | 8. Kearsey's Thesis, P.133 |
| 4. Kearsey's Thesis, Fig.35 & P.55 | 9. Kearsey's Thesis, P.113 |
| 5. Kearsey's Thesis, P.37 | |

3. The speed achieved was a little less than half the speed expected of a jet boat of a similar power to weight ratio. (See Fig.12.25).
4. If the expected 35 knots could have been achieved, even with the full installed power of 24 kW, the Rollercraft would have been performing nearly twice as well as any water craft with similar power to weight ratios. This would have conclusively proved its worth as a water craft.

Conclusion

Kearsey's thesis was a useful model for this LPW project which in many ways was following the same course. Kearsey's use of "hydro-foils" and his concept of self-forming blades were of interest in this project, and for this reason a small Rollercraft wheel was built and tested to provide a comparison with LPW data. The unusual results are described in section 11.4.

Apparently Kearsey's work has not been continued as no reports of it have been found over the last 9 years.

2.3.3 Balloon Tyre Amphibians

There are a number of small all terrain vehicles (ATV's) on the market which use balloon tyres for propulsion only, or for both buoyancy and propulsion. A recent one is shown in Fig.2.14 by Honda. These vehicles are primarily land vehicles and their water speeds are usually very limited, most often not achieving trough conditions for the deeply immersed wheels used. Nevertheless they clearly fulfill a function, providing a useful form of transport in rough country, and are really the only present practical application of wheels on water. (For these reasons a small treaded tyre was tested in this project's programme with results in section 11.6.)

2.3.4 The Knapp Roller 1898 (1)

This craft while in fact operating as a buoyant roller was an early attempt at gaining dynamic lift from a wheel on water. As such it provides an introduction to the next section, section 3.4.

The Knapp roller shown in Fig.2.15 was launched on the St. Lawrence about 1898. The complete craft was a 38 m long cylinder, 6 m in diameter, driven by two 37 kW engines. It was intended that it

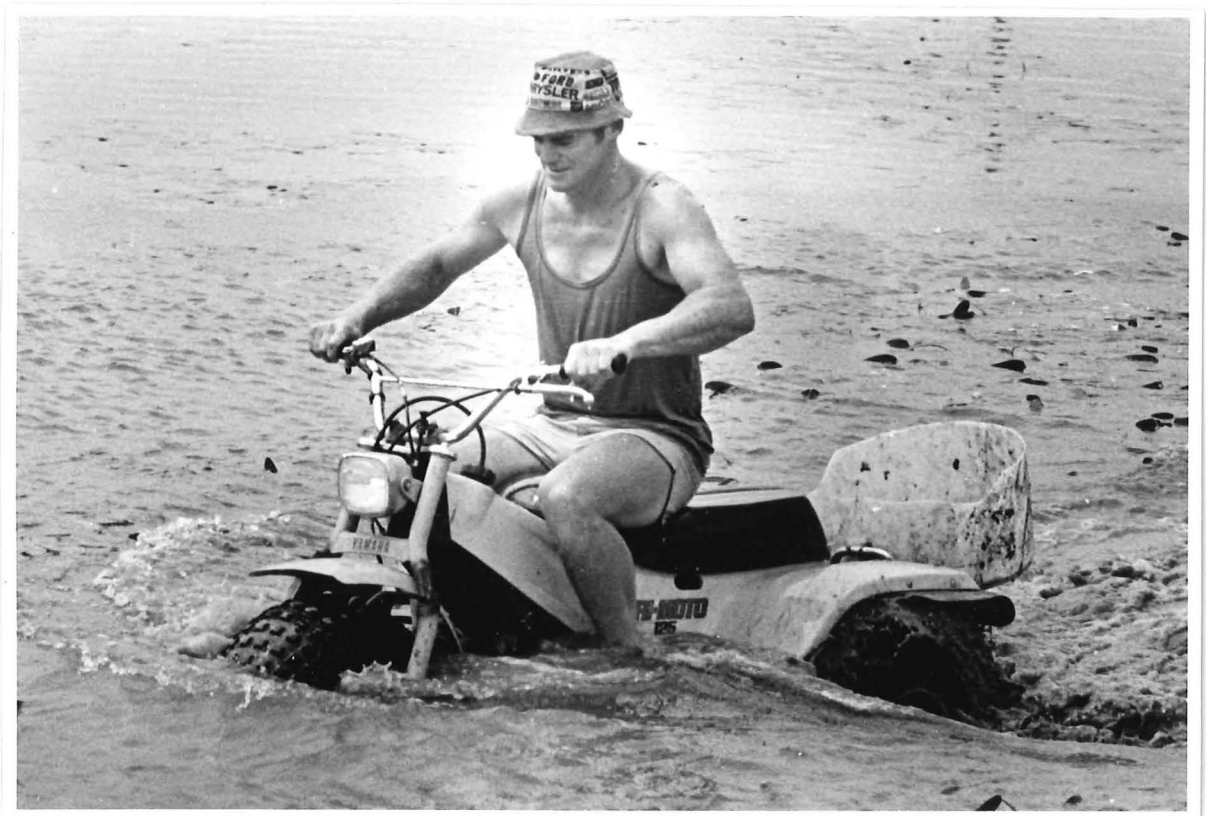


FIGURE 2-14: YAMAHA 125 BALLOON TYRED AMPHIBIOUS THREE WHEELER. (Auckland Star photos)

should travel perpendicularly to its axis on the water surface. Its theory of operation was a rather dubious Archimedes Principle turned through 90°.

"If you cannot displace more water with a body than its weight, how can my boat possibly displace any water when it meets resistance greater than its weight, taken broadside to get the greatest possible resistance? It is this resistance which brings it to the surface."

Needless to say this early attempt to achieve dynamic lift with a rolling cylinder was unsuccessful but nevertheless the belief that a rolling cylinder will lift and skim the water surface is regularly revived.

2.4 WHEELS GAINING SUPPORT FROM DYNAMIC FORCES

This idea has suffered some wild claims but also has achieved some unexpected successes.

2.4.1 The Hydroler 1948

In the Hydroler concept, Fig.2.16, cylindrical rotating rollers were to be used only at high speed to both reduce drag and provide lift. The report was presented by Lombardini & Fidderman in the 7th International Congress of Applied Mechanics (1948) and is a surprisingly confused paper for a respected body.

The operation was described.

"The floats or hull provide buoyancy at zero speed and the necessary lift at forward speeds up to approximately 50 mph. Above this speed rotation of the rollers reduces water drag through centrifugal force and zero relative velocity between the water and the roller face. At the same time since lift varies in relation to the square of the forward velocity, the rollers' mean draught is so reduced as to allow the floats or hull planing bottom to be raised clear of contact with the water." (1)

The report records the results of two tests conducted at NPL (2) and these seem to contradict some of the claims of the authors, who go to

1. Lombardini & Fidderman, P.534
2. Lombardini & Fidderman, P.536 and Fig.11

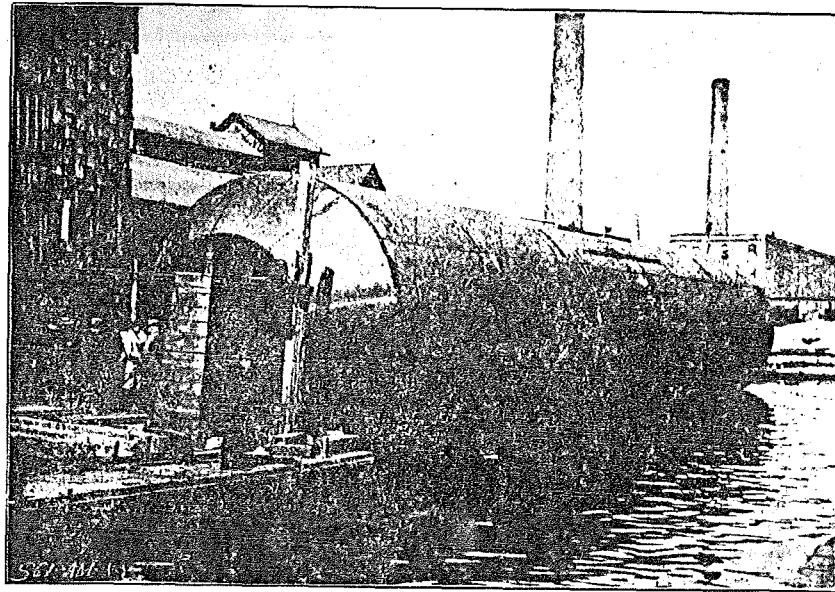


FIGURE 2.15: THE KNAPP ROLLER BOAT. SCALE CAN BE DETERMINED FROM THE MEN AT THE LEFT CENTRE. (REF. TAGGART FIG.6.7.)

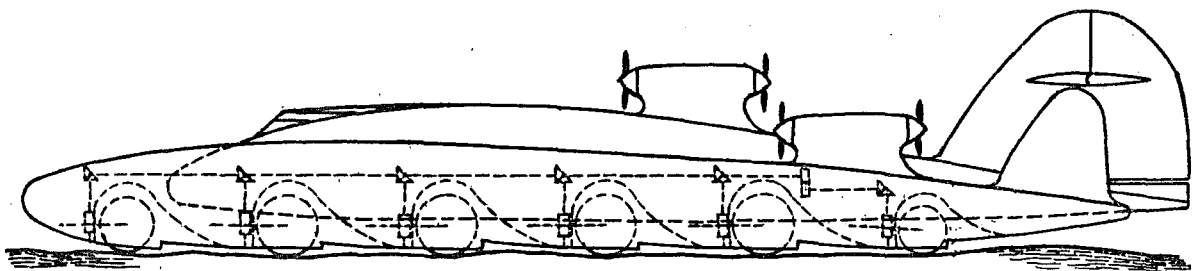


FIGURE 2.16: THE HYDROLER AT HIGH SPEED, LIFTED ON TO ITS ROLLERS.

some lengths to point out that the range of the tests was outside the range where the hydrofoiler concept would work.

Tests conducted in this project (section 11.3) on a rotating cylinder clearly indicate that the idea would not work at low speeds, though a small possibility remains that the claimed lift forces may exist at high speeds.

Once again, no further reports of the concept have surfaced since 1948.

2.4.2 Bouncing Bombs (1)

The performance of the cylindrical British bouncing bombs of the Second World War certainly seems to support the notion that lift can be gained from a cylindrical surface coming into contact with the water at high horizontal speeds. Although these bombs rotated in the opposite sense to the Hydrofoiler cylinders, (2) a number of other recocheting bombs were developed and tried, which had rotation in the forward direction. A non-spinning spherical version called "Baseball" simply ricocheted along the water surface but it was never used operationally. (3)

A German development of the bouncing bomb was called the "...'prism bomb' in which naturally-occurring forward rotation would bring a succession of smooth curved facets down to meet the water surface. Scale models of these bombs were compared with [the British bombs] and the 'prism bomb' was shown to be superior in range and number of ricochets, but the idea was never used in a full-sized weapon." (4)

Such evidence strongly suggests that rotating cylinders might be made to provide lift at high speeds if impacts on the water are involved, and the 'prism bomb' concept indicates the likelihood that unpowered LPW's could provide lift as the free-wheeling rotors of a two-wheel drive, four-wheeled vehicle.

2.4.3 The Soviet Cylinder Vehicle 1967

Hovercraft and Hydrofoil in July 1967 reported a cylinder vehicle which was supposed to operate in a manner somewhat similar to that of the Hydrofoiler. (Fig.2.17.) The developer, Victor Podorvanov, was reported as having conducted tests on partly submerged revolving cylinders to

- | | |
|---|---------------------|
| 1. Hutchings, New Scientist March 2, 1978 | 3. Hutchings, P.564 |
| 2. Hutchings, P.565 | 4. Hutchings, P.565 |

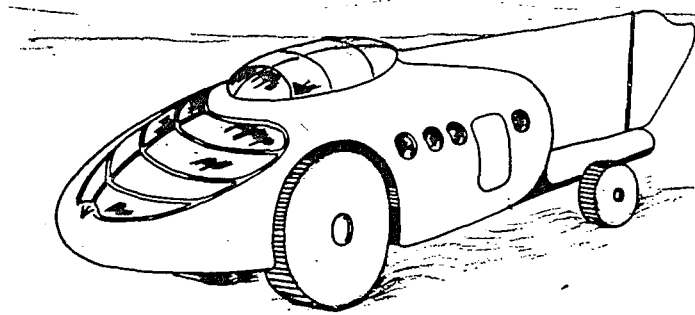
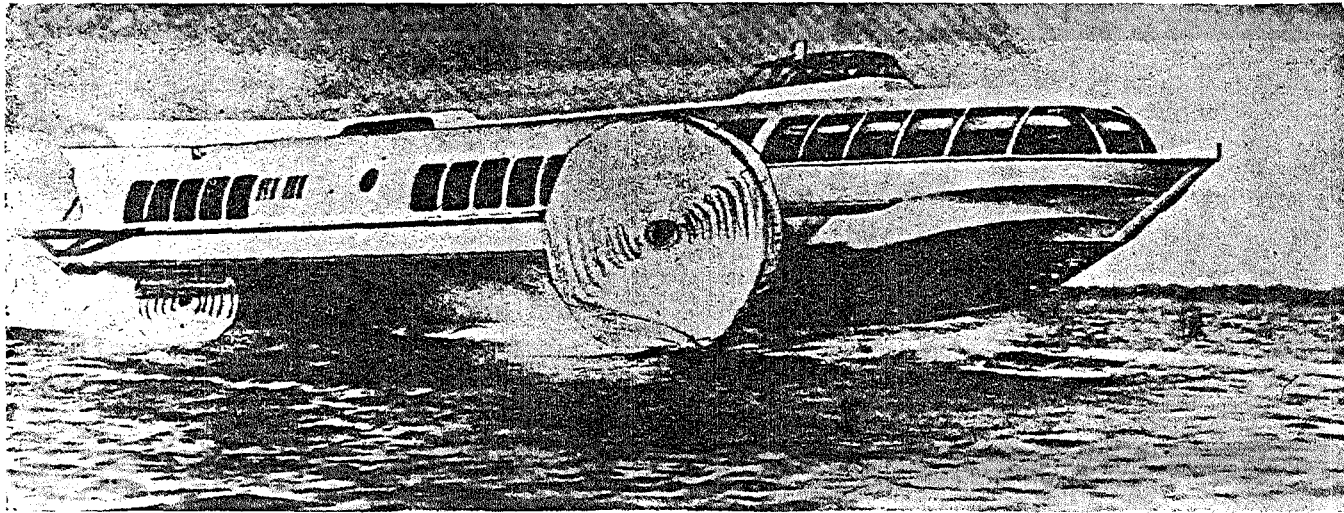


FIGURE 2.17: THE SOVIET 'CYLINDER VEHICLE' CONCEPT.

determine optimal conditions of lift. The article states "...the cylindrical wheels not only do not create a bow wave..[but] by sucking water beneath the hull, they create both additional thrust and vertical lift. He found, moreover, that this vertical lift eventually becomes sufficient to lift the hull completely clear of the water..."

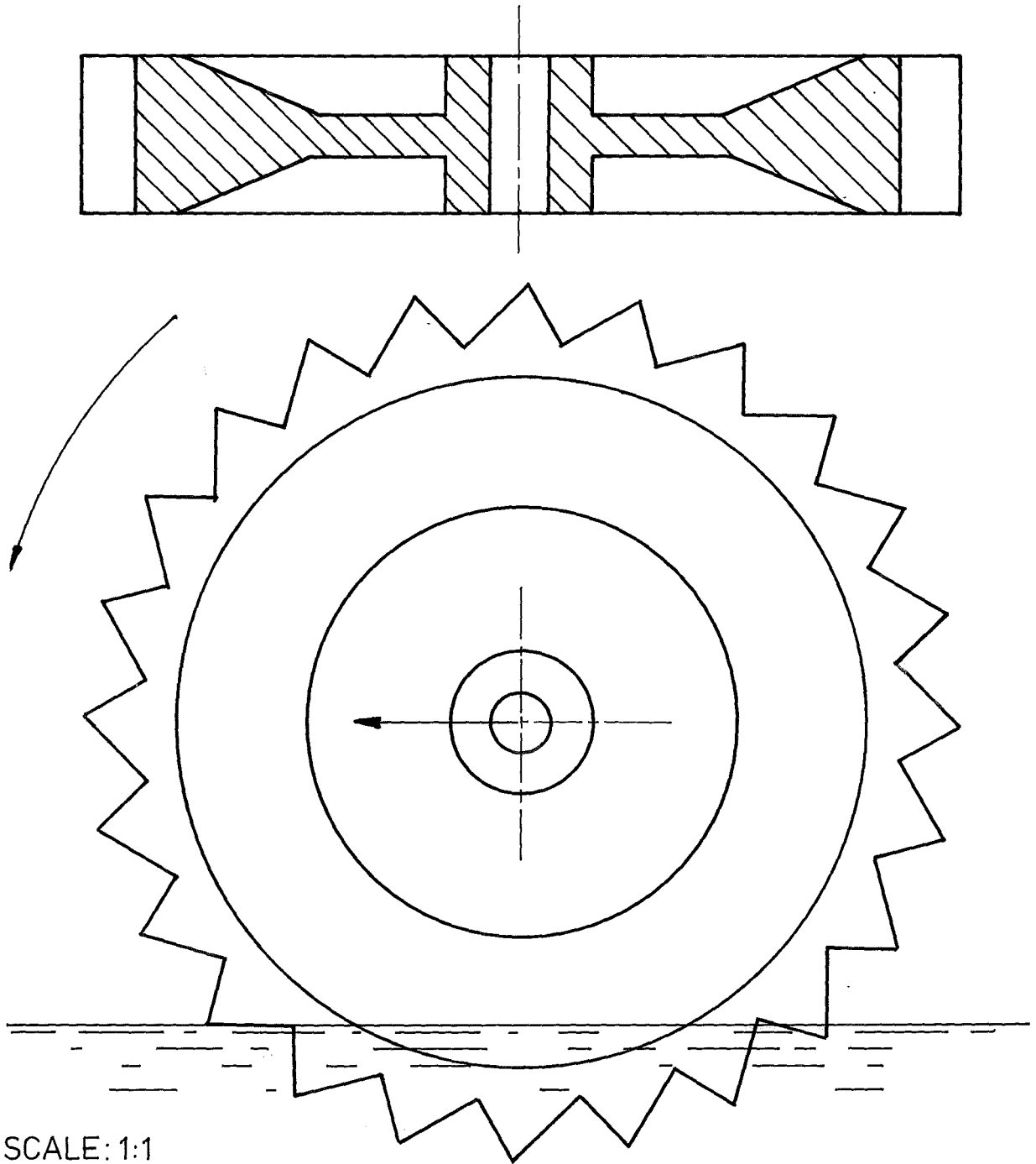
The article indicated that speed trials were being conducted and speeds upwards of 135 kph were expected. Descriptions of the craft's high speed motion are striking in their resemblance to the model LPW craft motion at speed (see Chapter 12), and it is wondered whether the report is a garbled description of Russian priority with the LPW craft.

It is difficult to know how seriously to take such an article which is based on a Soviet News agency report. Since, however, no further reports of the vehicle have been found since 1967 its success is doubtful.

2.4.4 The Spinning Wheel 1957 (1)

One of the closest approaches to LPW operation actually tried, was what was called the Spinning Wheel, Fig.2.18. It was reported in a book by Taggart in 1969. Private communication with Taggart indicates that the information came from a little known Reed Research Report 1288, of 15th July, 1957, which he wrote. The idea originated during World War II when one solution proposed to the problem of getting a line from a landing-craft to the shore was to use the Spinning Wheel. It would house a reel of wire and it would be projected, spinning, from the craft to run across the surface of the water and up the beach, unreeling the wire as it travelled. The wheel and line were then to become entangled in the undergrowth so the vessel could be winched ashore. The idea was taken seriously and tests were begun at the David Taylor Model Basin. However these were soon curtailed by wartime priorities and it wasn't until 1957 that the Hydraulic Lab. of the Newport News Shipbuilding and Drydock Co. began experiments again, with the intention of developing the Spinning Wheel as a high speed propulsion device.

Their experiments evolved the toothed wheel shown in Fig.2.18 which was about 130 mm diameter, 25 mm wide and weighed about 1.6 kg.



SCALE: 1:1

FIGURE 2:18: THE SOLID STEEL SPINNING WHEEL.

(Ref: Taggart, private communication)

Its blade angle (as defined in this project) was about 45° and it had 24 blades. It was spun up to 140 rps and ejected along the water surface at 8 m/s. It retained this speed for the 17 m length of the towing tank, with its periphery barely penetrating the surface of the water, and struck the far end with a force which indicated that it could continue for at least twice that distance. Correspondence with the Newport News Shipbuilding and Drydock Company suggests that no further work was done on this idea.

Taggart discussed the possible application of the Spinning Wheel to water vehicles, and describes what is essentially LPW operation over water:

"These vehicles could be provided with high speed machinery driving the wheels.....starting from a dead start and eventually lifting the vehicle clear of the water."

Neither Taggart nor the author know of anyone who has taken up this suggestion.

2.5 DYNAMIC WATER SURFACE LIFT IN NATURE

In the light of Lord Kelvin's assertion relating to a horse walking across the surface of the water (section 1.1) one is inclined to believe, with Rosen, that: "...there is no horse on earth who could could expend energy at a fast enough rate to maintain himself on the surface of the water by stamping his feet." (1)

There are, however, creatures that do manage this for short bursts. Small ducklings, if panicked come very close to, if not succeed in actually running on the water surface with their large webbed feet (Fig.2.19). Many water birds, notably shags which are relatively heavy, assist their flight take-off by, at first, a series of jumps, then by running with their webbed feet in a similar way to ducklings.

The author has observed at least one variety of long slim fish which, to escape danger, leaps out of the water and with its body sloped upwards at about 45° , zips along the water surface virtually standing on its tail which is rapidly oscillated from side to side.

1. Private communication with Rosen of Newport News Shipbuilding Company: extract from his reason as to why the LPW concept would not work.

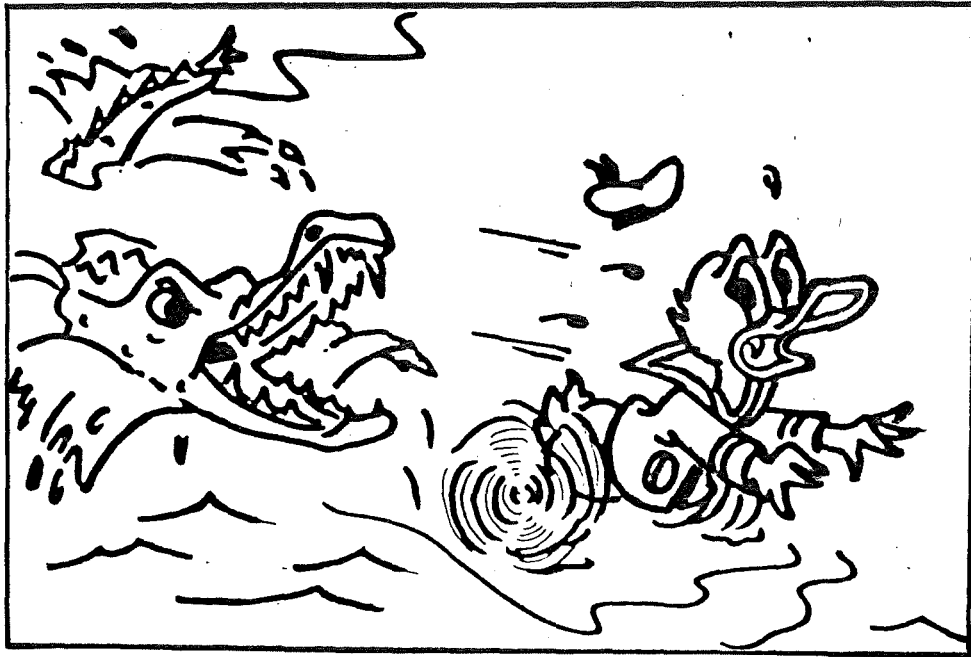


FIGURE 2.19: DUCKLINGS, AND IN WALT DISNEY'S VIEW, DUCKS ALSO CAN RUN ON THE WATER SURFACE.

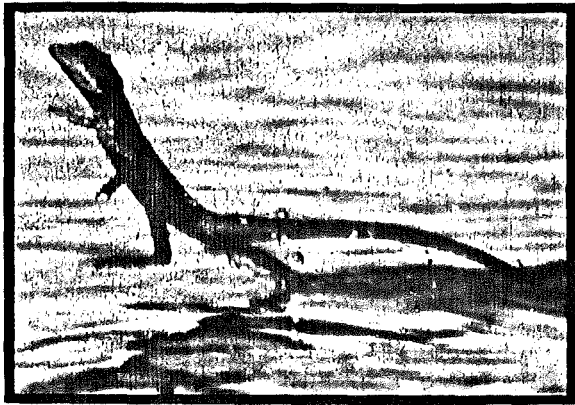


FIGURE 2.20: THE 0.8 m LIZARD, *BASILISCUS BASILISCUS*, USES THIS ABILITY TO ESCAPE PREDATORS OR CAPTURE PREY. (National Geographic Photographs.)



FIGURE 2.21: SWAN GREBE COURTSHIP BEHAVIOUR INVOLVES RUNNING ON THE WATER SURFACE. (Photograph from television screen during 'ANIMAL OLYMPIANS'.)

There is a species of lizard in Central America officially named the Jesus Christ Lizard. (1) This reptile shown in Fig.2.20 can dart from land with its body erect, and use its hind feet for lift and propulsion for a dash of up to 10 meters along the water surface. It does not have webbed feet and from the pictures it is apparent that it gets some dynamic support from its long tail trailing in the water. It is also capable of struggling out on to the water surface from a swimming attitude to make a short run before sinking back and swimming again. (2)

Finally the Swan Grebe of Western America culminates its courtship display with both birds running erect for 10 or 15 m on the water surface as shown in Fig.2.21. Their wings are outstretched behind the birds and are not flapping so they are not used for lift or propulsion, and it is unlikely that much dynamic support is afforded by their short tails. (2)

From these examples it is clear that the LPW principle can be operated with the power to weight ratios available in the small animal range.

It should be mentioned that there are a large number of insects which gain support on the water surface from the surface tension. However this principle only works on a scale where surface tension forces become significant, and since it does not employ dynamic forces, does not come under the LPW concept.

2.6 AMPHIBIOUS VEHICLES

If the LPW was to be used on small amphibious vehicles they would have to take their place among the amphibious vehicles already in use. For this reason information on two of the more recent and well known are included here with some comments about amphibious performance.

The military are likely to have the more advanced and reliable of these vehicles and a brief survey of them was conducted.

1. Hughes, National Geographic Magazine, Jan. 1983, P.50
2. "Animal Olympians "Television programme, BCNZ, November,1980

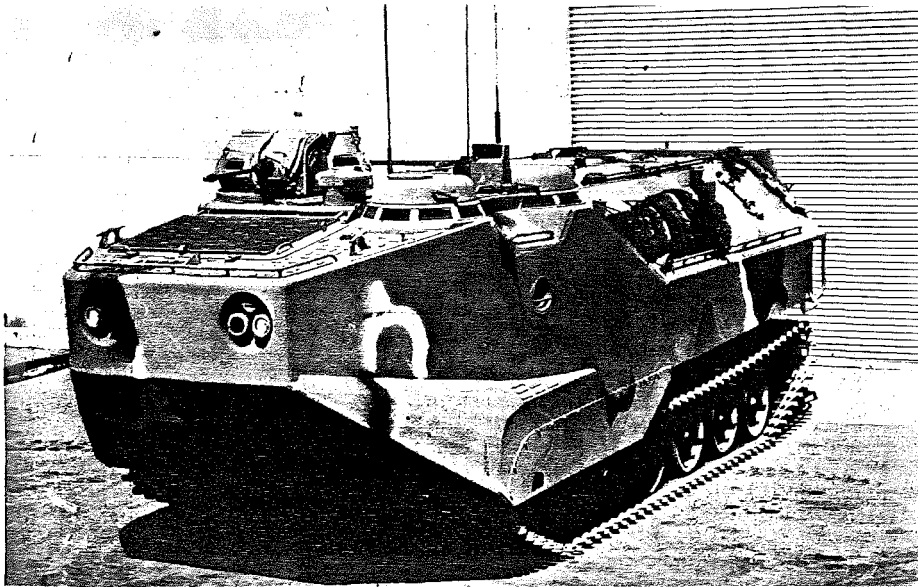


FIGURE 2.22: THE LVTP-7 AMPHIBIOUS VEHICLE.

TABLE 2.23: SPECIFICATIONS FOR THE U.S.
NAVY AMPHIBIOUS VEHICLE
LVTP-7.

CREW:	3 plus 25 infantrymen
WEIGHT:	22.9 tonne (loaded)
PAYLOAD:	4.5 tonne
SIZE:	HEIGHT 3.12 m, LENGTH 7.94 m, WIDTH 3.2 m
SPEED:	LAND 46 kph, WATER 13.5 kph
RANGE:	LAND, 480 km, WATER 90 km
ENGINE:	406 bhp, 6.9 litres.

There are two main types :

- (i) Light tracked vehicles.
- (ii) Wheeled vehicles.

Propulsion takes three forms:

- (i) Hydrojet propulsion, of either vehicle type. Water speed is about 10 kph (2.8 m/s) for one hydrojet unit.
- (ii) Tracked vehicles, using tracks for propulsion. Speeds range from about 4.8 to 5.5 kph (1.3 to 1.5 m/s).
- (iii) Wheeled vehicles, using wheels as propulsion. The speed range in water is 3.9 to 5 kph (1 to 1.4 m/s), with wheels of 1 m to 1.3 m in diameter.

It is worth noting that these speeds for the wheeled type of propulsion are about one third of trough speed for wheels of this size.

2.6.1 LVTP7 (1)

This is a U.S. military tracked amphibious personnel carrier (Fig.2.22). Its specifications are given in Table 2.23. A contract for 942 of these vehicles was awarded in 1970 after five years of extensive testing of 15 prototypes. Delivery of the first 35 vehicles was made in 1972, and they are still in operation at present, though modifications have been regularly taking place in their design.

Note that the maximum water speed is 13.5 kph with the use of two hydrojets, when the vehicle is operating as an ungainly displacement craft. It is, therefore, a little better in its water capability than the fairly large range of amphibious vehicles of this type.

2.6.2 LVHX-1 (2)

This is an experimental, turbine-powered, hydrofoil, amphibious, wheeled vehicle. It is shown in Fig.2.24 and its specifications are given in Table 2.25. It uses two propellers for propulsion, one for normal displacement operation, and another for foilborne operation. The foils retract for boating and land operations, but give the vehicle a high speed rough water capability of about 64 kph in waves of about 1.5m. Control during foilborne operations is accomplished by a special autopilot system.

1. Janes Weapon Systems 1979-1980, P.358
2. Hovercraft and Hydrofoil, November 1964, and February 1965

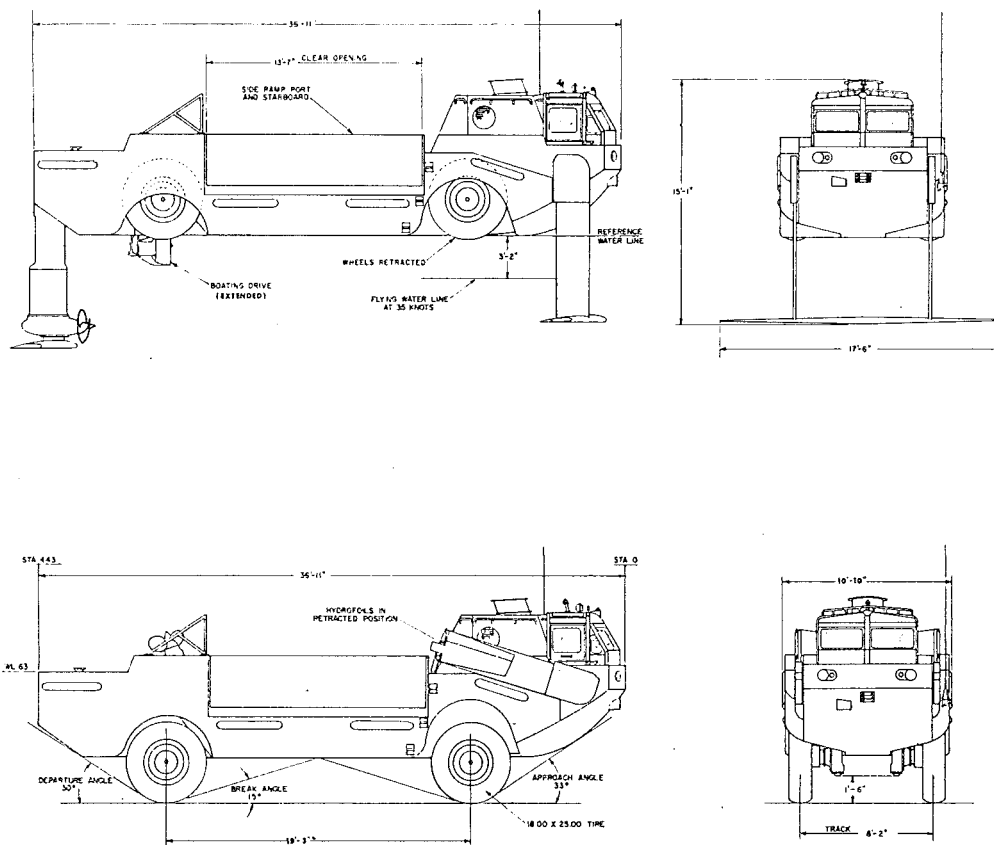


FIGURE 2.24: THE U.S. NAVY EXPERIMENTAL AMPHIBIOUS HYDROFOIL CRAFT LVHX-1.

TABLE 2.25: SPECIFICATIONS FOR THE LVHX-1

WEIGHT:	34 tonne approx. (loaded)
PAYLOAD:	4.5 tonne, approx.
SPEED:	LAND: 65 kph
	BOATING: 12 kts
	FLYING: 35 kts IN WAVES UP TO 1.5 m HIGH
HULL CLEARANCE WHEN FLYING:	0.75 m
RANGE:	25 nautical miles flying
WHEELS:	Individually inflatable, retractable
ENGINE:	1000 shp Lycoming TF14 marine turbine

This vehicle is clearly a very capable water craft but it contains high technology and a high installed power. There are a few similar vehicles in existence, but their functions seem to be limited to research and development and there is no indication that large numbers have ever been ordered.

2.7 UFFA FOX'S PATENT 1919

It seems that Uffa Fox quite independently came up with the following idea recorded in his book "Seamanlike Sense in Powercraft", written in 1969. (1) The vehicle is the closest approach the author has found to the LPW craft concept. Fig.2.26 shows the general arrangement with, details of the wheels, and the following extract conjures up his craft:

"...in 1919 I thought of propelling a boat like a motor-car, by wheels with paddles on the sides of the tyres for low-speed work, and by deep treads on the bottom which acted as small paddles as the boat lifted and ran over the top of the water. At a speed of 100 miles and more an hour, water becomes hard enough to make this possible...

"A glance at the plan will show that here is the form of a motor-car and a planing boat which will be able to run on sea as well as land.

"The tyres are specially designed and moulded with rubber paddles on their sides in the shape of half the blade of an oar. These make theproduction of wheels that much more difficult and expensive. They are needed, however, to drive the vessel as paddle wheels at low speed, since it is not until she lifts out and the blades decrease their depth in the water that the deep crescent-shaped treads in the bottom of the tyres start to propel the vessel by themselves and once the boat is clear out of the water the only resistance is that of air and the wheels themselves. There is no reason why, under such conditions, the boat could not reach a speed of 100 miles an hour.

"Here is a means of future travel over land or sea."

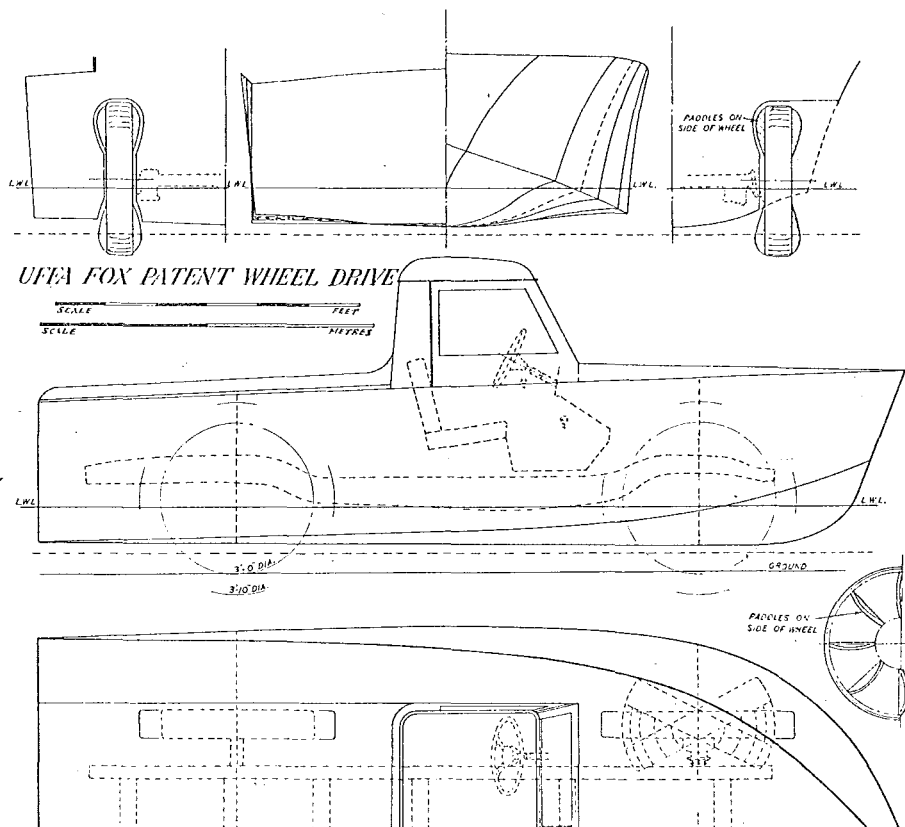


FIGURE 2.26: THE FOX 'WHEEL DRIVE FOR SHIPS'. THIS IS ESSENTIALLY THE LPW CONCEPT. THOUGH NOT CLEAR IN THE DIAGRAM THE TYRES ARE DESIGNED WITH 'DEEP CRESCENT-SHAPED TREADS IN THE BOTTOM' FOR PROPULSION AFTER LIFT-OFF.

Uffa Fox patented both the craft and the wheels in separate patents in 1964 (1) but there is no indication from him or elsewhere that his idea was ever tried.

2.8 CONCLUSION

In spite of the wide range of concepts and claims reviewed in this chapter it is clear that there is only a meagre amount of factual data which relates directly to the LPW concept. However, the little that does relate directly, such as that of the Spinning Wheel, supports the idea that the LPW should work as imagined.

1. British Patent Numbers 1041401 and 1041402.

CHAPTER 3

PREVIOUS RESEARCH AND AIMS FOR THIS PROJECT3.1 CLOSE APPROACHES TO THE LPW CONCEPT

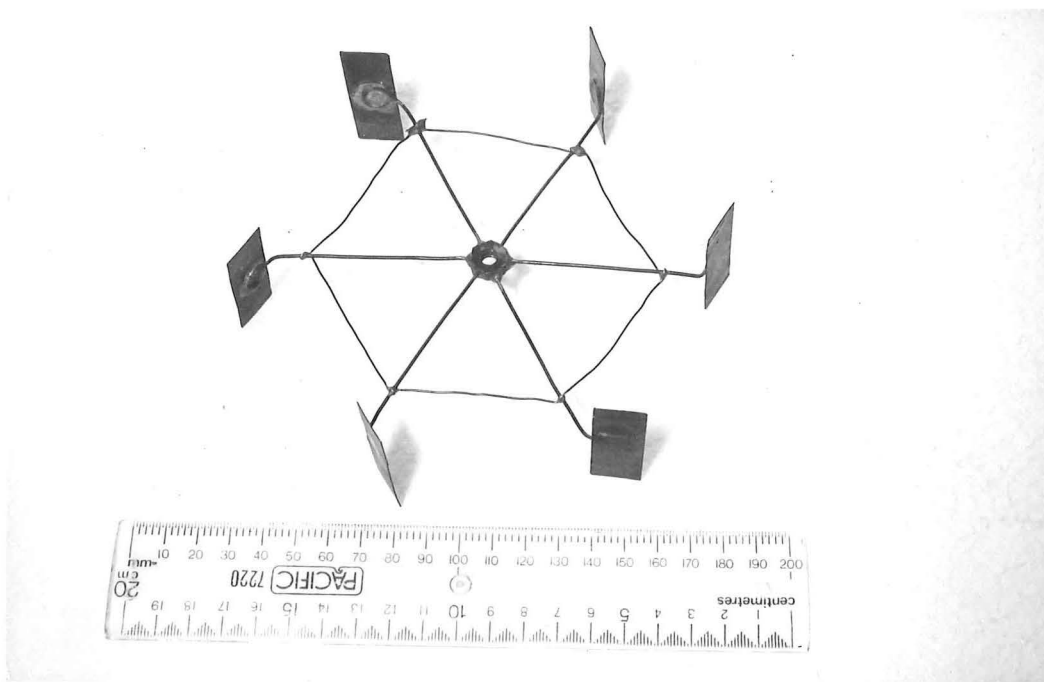
In 1957 Taggart, in writing the report describing the "Spinning Wheel" (covered in section 2.4.4) suggested that a similar wheel could be used to help both support and propel a vehicle on the water surface (1); and in 1959 Uffa Fox patented his boat-car combination vehicle (described in section 2.7) which he imagined would lift up and run on the water surface at "... a speed of 100 miles and more an hour..." (2). Of all the ideas in the literature and outlined in Chapter 2 these two are the closest to the LPW concept, but there is no evidence that either vehicle was actually tried in practice. Nevertheless, the fact that the Spinning Wheel worked at all was encouraging and indicated the probable success of the LPW.

3.2 THE ORIGIN OF THE LPW CONCEPT

The idea of the Lifting Paddlewheel occurred quite independently of these reports, to the author in 1974 while trying to design a new type of all-terrain-vehicle. This ATV was imagined to have large, spoked wheels without rims, and instead of these rims, it was to have a broad flat foot at the end of each spoke. Such a vehicle could possibly be driven so that it would step over obstacles such as fences. The vehicle was mentally put through its paces until it was envisaged approaching water, or a swamp at speed. At this point it became very difficult to foresee intuitively, whether it would plough in, or skip across the surface. This, then, became the fundamental question motivating the first experiments. Can a vehicle be made, as envisaged which would run across the surface of the water on its wheels? From this point interest in this new LPW concept overrode the original ATV idea.

The puzzle was intriguing enough for a model spoked wheel with broad feet, to be made up in early 1976 (Fig.3.1) and it was tried out in the wash-house tubs. It was difficult to simulate the wheel approaching the water at speed, so the different, but related condition

1. Taggart P.198
2. Fox P.195



1280/27

FIGURE 3.1: THE ORIGINAL LPW

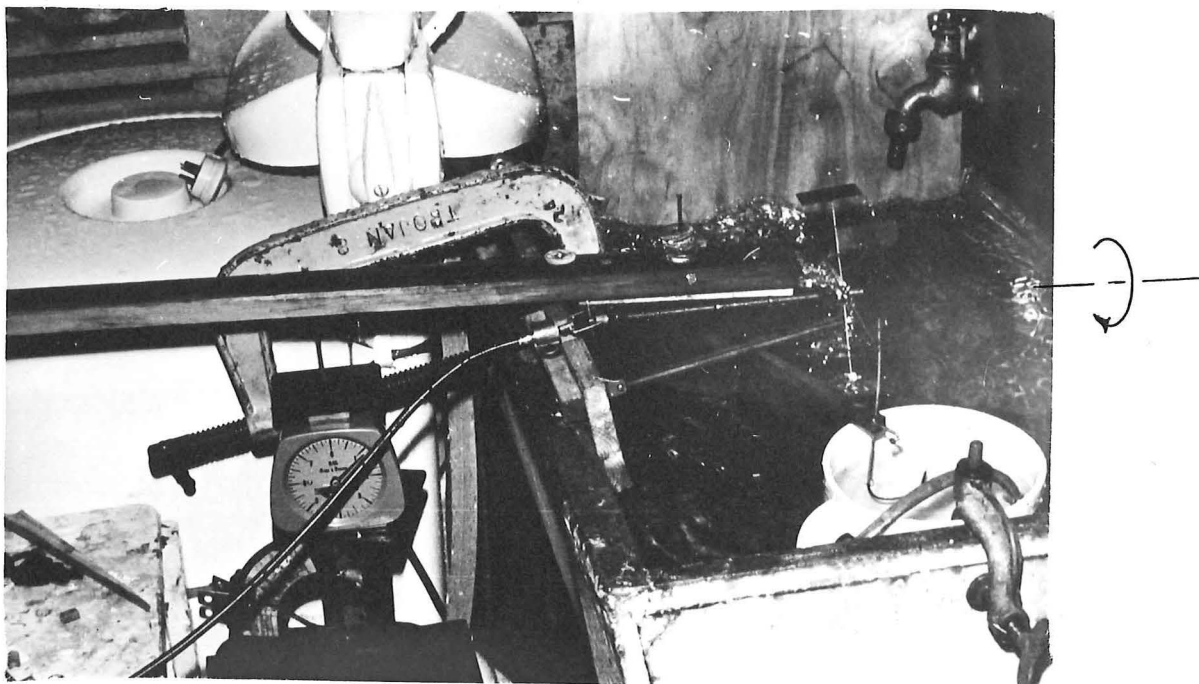


FIGURE 3.2: THE PRELIMINARY EXPERIMENTS 1976

was examined: that of spinning the semi-immersed wheel without allowing any forward movement - the static condition, to see if lift forces were present. The wheel was mounted on a hinged balanced mount and driven by a hand drill through a speedometer cable. Fortunately the blade angles chosen were appropriate and the splashing wheel readily tilted the mount indicating appreciable lift forces.

This provided enough incentive for a minor series of experiments to be conducted, using materials that were to hand, Fig.3.2. In essence the apparatus worked as demonstrated by Fig.3.3. Lift forces were measured using a spring letter balance, and thrust forces were measured by tilting the whole balance arm on its side. Although the equipment was primitive the results were sufficiently self consistent to instill a little confidence and gave a coherent picture of both forces increasing with depth of immersion and revolutions, for the two blade angles tried.

3.3 THE TEMPLIN SCROLL PAPER 1976

Periodically the Templin Scroll Competition is held at the Engineering School for the best student paper offered before a panel of judges. This provided a goal for the experimental findings to be written up as a paper entitled "Preliminary Investigations of the Lifting Paddlewheel" (1). This paper outlined the experiments, included the results shown in Fig.3.4, and speculated, somewhat freely on the possible capabilities of the LPW craft. It concluded in part :

- (i) Lift forces have been shown to be present for the static case.
- (ii) Further tests are necessary to determine what happens to these forces when the LPW is moving over water.
- (iii) Tests also need to examine the power requirements of a moving wheel (2).

As yet there was still no answer to the fundamental question.

1. Alexander 1976
2. Alexander 1976, P.27

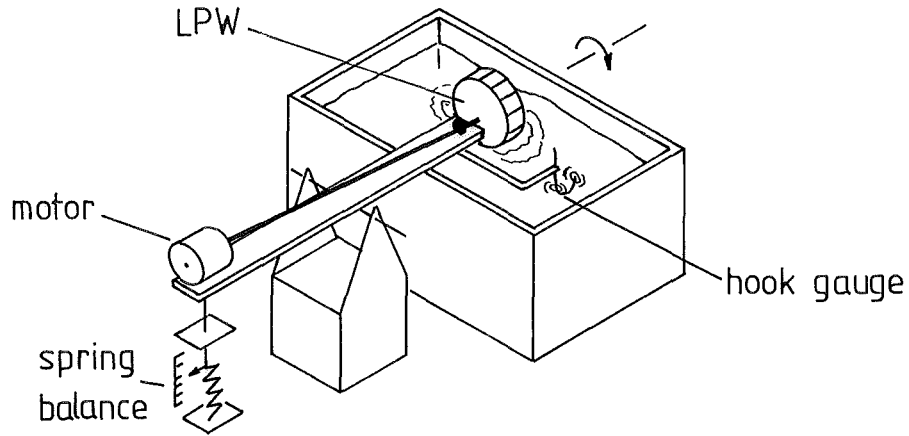
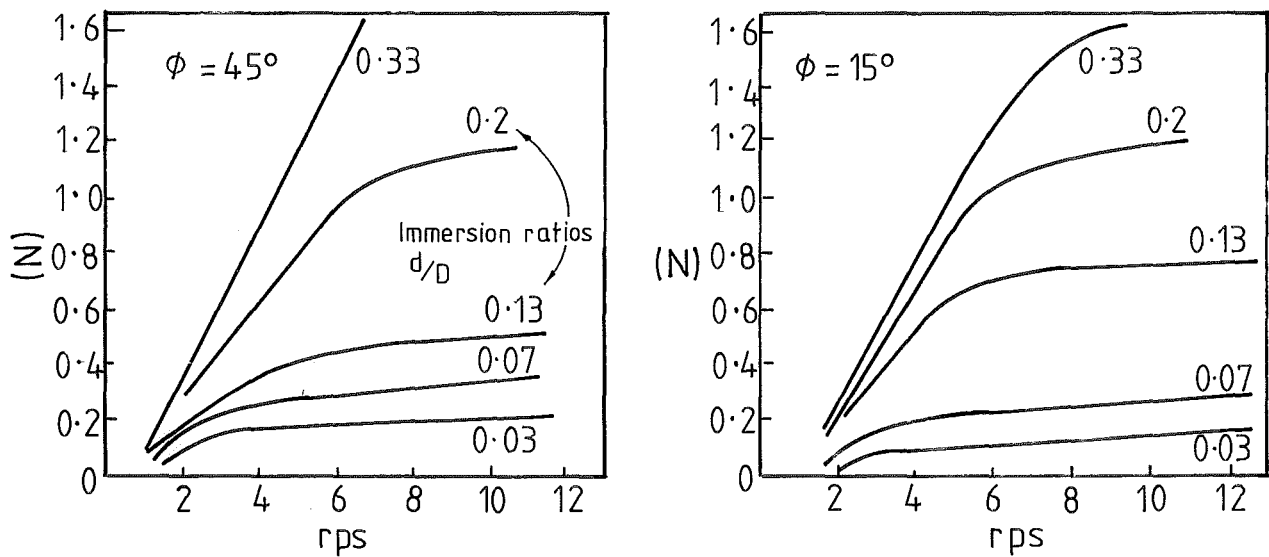


FIGURE 3.3: SCHEMATIC OF THE PRELIMINARY EXPERIMENTAL APPARATUS MEASURING LIFT FORCES



Static lift: variation with rotor speed & immersion depth.

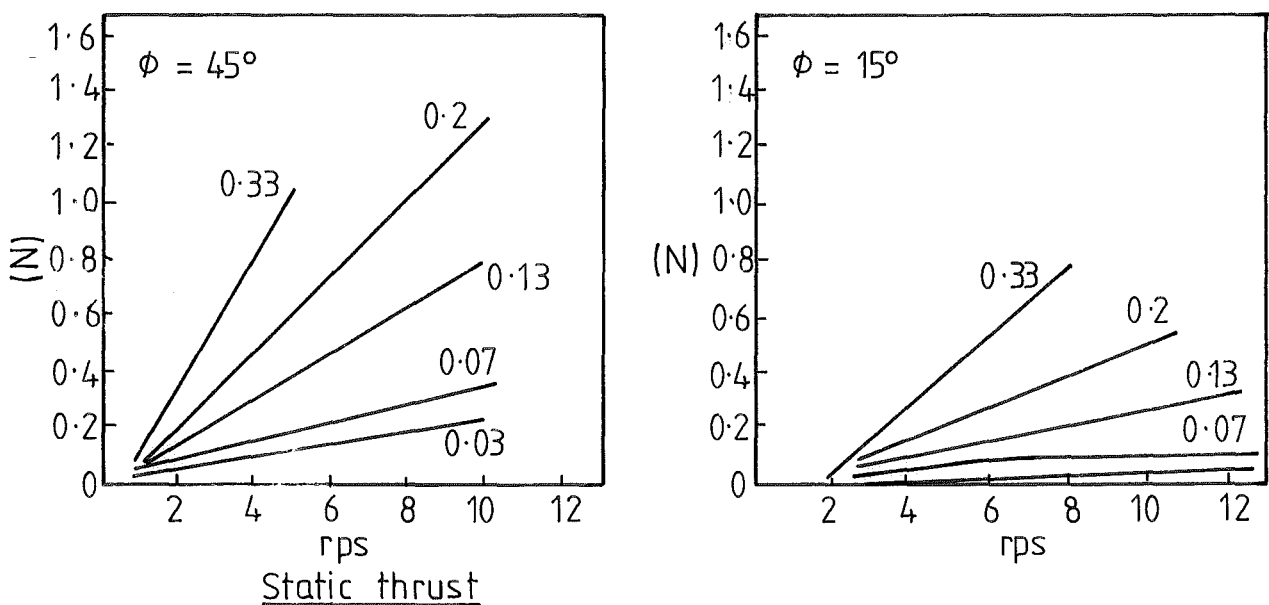


FIGURE 3.4: RESULTS OF THE PRELIMINARY EXPERIMENTS 1976.

3.4 THIRD YEAR PROJECT 1977

In the final year of their undergraduate degree of Mechanical Engineering students undertake an individual project. Because of the case made in the earlier paper for further tests, the author was allowed to continue the LPW study for this project requirement. While the primary aim was to answer the fundamental question, just as it had been for the earlier study, the secondary aims followed on from the earlier study recommendations. These secondary aims were (1);

Aims:

- (1) To re-examine the 1976 static condition tests under more rigorous conditions.
- (2) To examine the lift and thrust forces when the LPW was moving over the water.
- (3) To begin to examine power requirements (if the forces still existed at speed).
- (4) Possibly, to examine some of the effects of the many variables involved in LPW operation.

Project Tasks:

The project involved the following tasks:

- (1) The design of a force balance which could both power the LPW and measure its forces.
- (2) The collection and processing of data using this balance.
- (3) An examination of the literature available.
- (4) A formal report (2) and oral presentation.

A separate but parallel effort was directed towards constructing a small model LPW vehicle powered by a model aircraft engine.

The Force Balance:

The force balance is shown in Fig.3.5 and a schematic of it is in Fig.3.6. It was robust, and the simultaneous measurement of lift and thrust forces was given priority over power measurements (3).

1. Alexander 1977, P.10
2. Alexander 1977
3. Alexander 1977 P.24

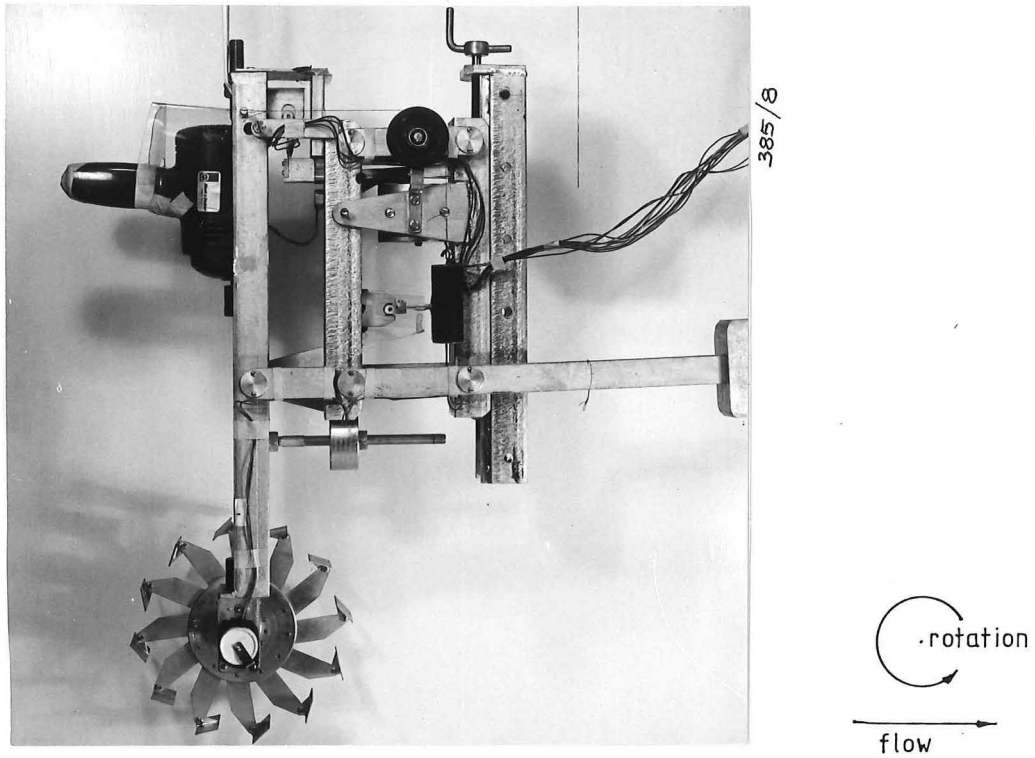


FIGURE 3·5: THE 1977 FORCE BALANCE.

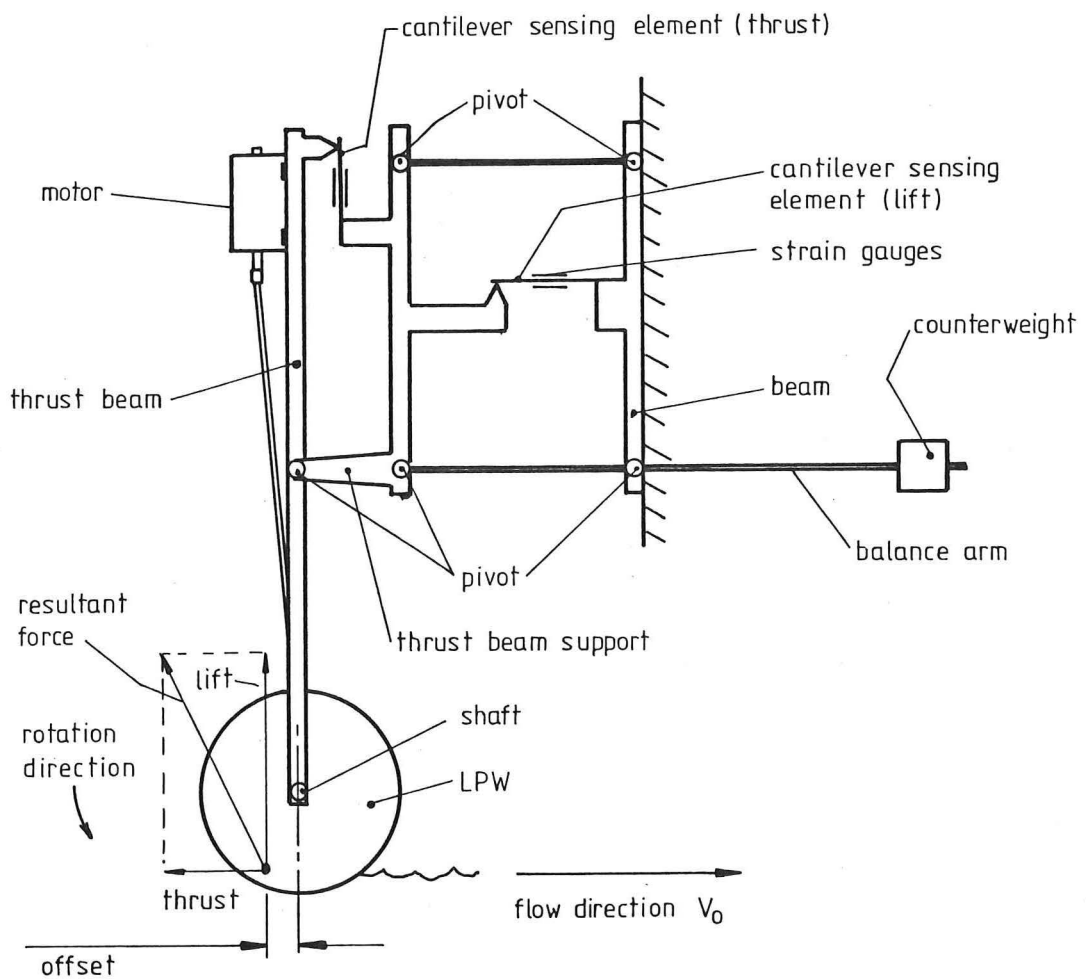
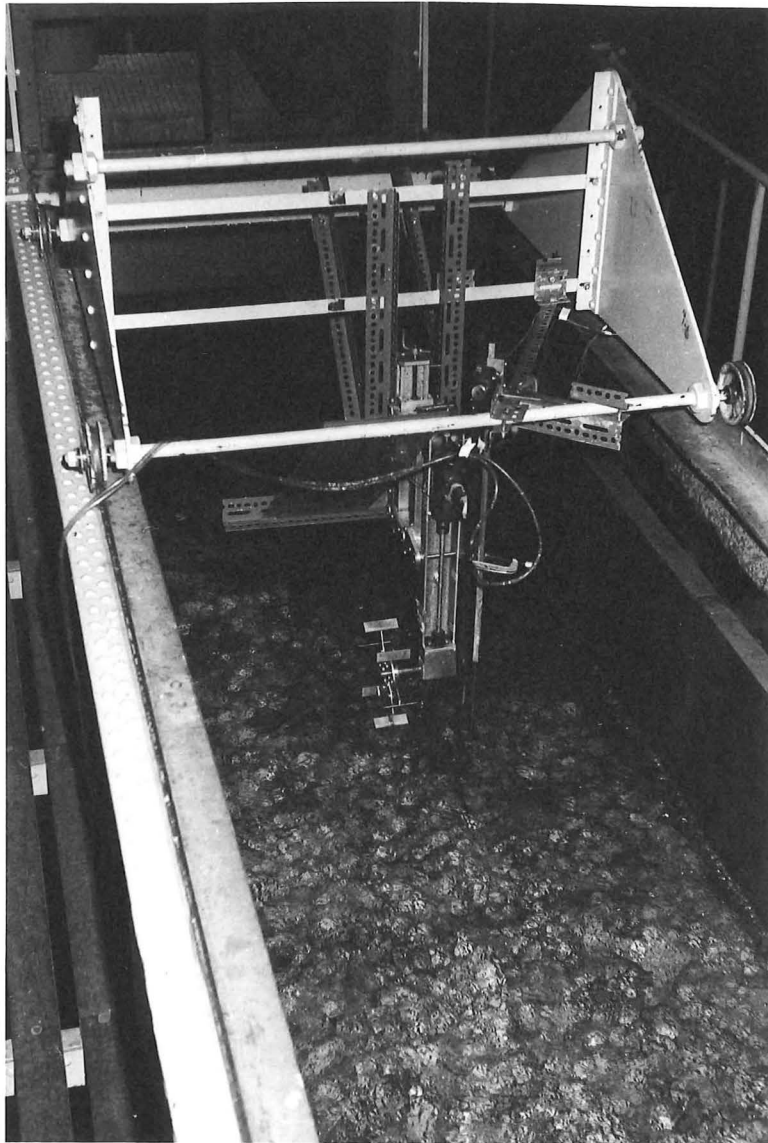


FIGURE 3·6 SCHEMATIC OF 1977 RIG SHOWING FORCES.



/35A

↑
FLOW

FIGURE 3.7: THE 1977 FORCE BALANCE IN THE FLUIDS LABORATORY FLOWING WATER TANK. THE FLOW SHOWN IS SHALLOW (0.1 m) AND SUPERCRITICAL AT APPROXIMATELY 2.5 m/s. THE LPW IS NOT IMMersed; A PITOT TUBE IS BEING USED TO MEASURE FLOW VELOCITY.

Dashpots were necessary to damp out oscillations of the system. Power was measured indirectly by first calibrating the motor power output against voltage input, and then recording voltage input for each set of data (1). This gave large uncertainties, but indicated the power requirements satisfactorily.

The Testing Tank: (2)

The facility available in the Engineering School Fluids Laboratory provided flowing water above which the force balance could be fixed (Fig.3.7). For reasons given in section 4.16 this was not an altogether satisfactory arrangement, but this was not fully appreciated at the time.

Data Processing: (3)

Force measurements were made with strain gauges and the output was recorded on a multichannel Ultra Violet Recorder. While force balance vibration gave a very noisy trace, this could readily be averaged by eye. With the large number of variables involved, and the fairly extensive programme of testing required to cover a sample range of these variables, the processing of this form of data became a task of considerable magnitude. This data was eventually presented in the form of the force-rps plots as shown in Fig.1.6, section 1.4.1. This was found to be a format which could readily be related to the physical situation.

Findings:

The main findings of the project (which concerned only a flat-bladed LPW) were as follows :

- (1) The results of the earlier 1976 tests for the static condition were confirmed.
- (2) Lift and thrust forces certainly still existed for the moving water case, but they were not as large as for the static case, and seemed to vary in a rather confusing way with speed of advance.

1. Alexander 1977 P.27
2. Alexander 1977 P.19
3. Alexander 1977 P.32

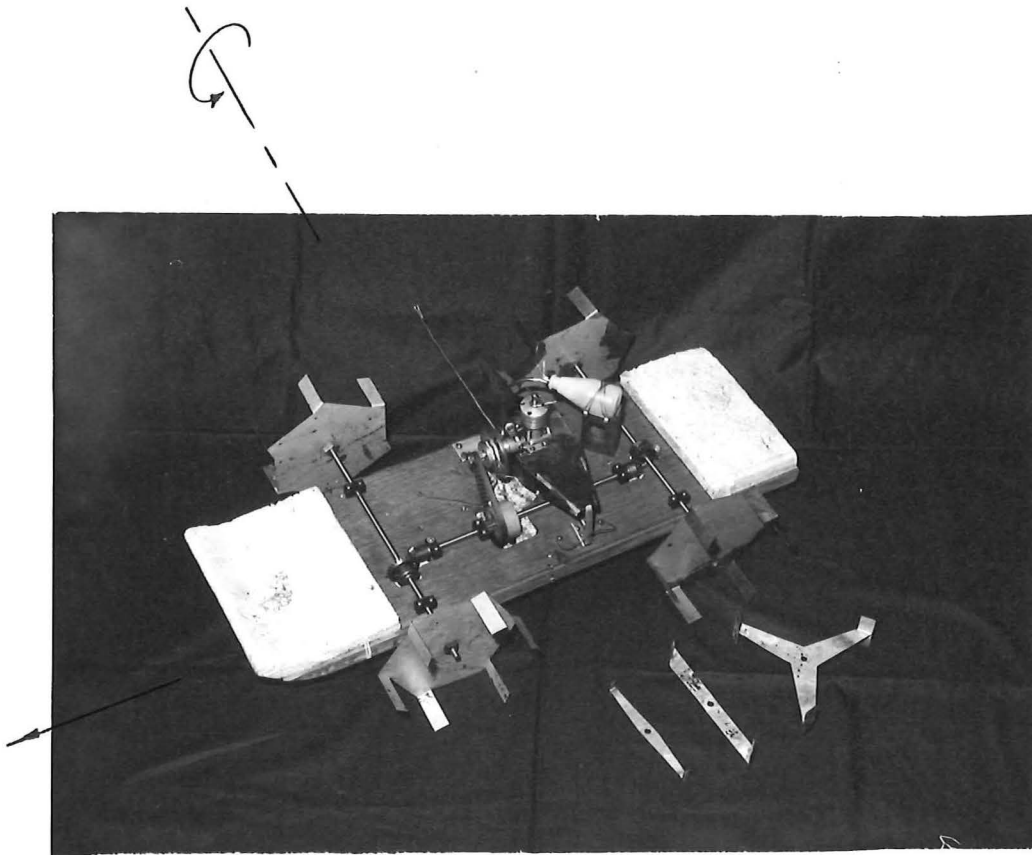
- (3) The somewhat crude measurements of power indicated that a fairly large power would be required for the LPW craft, and propulsive efficiency was generally disappointingly low. (About 30% in operating conditions). (1)
- (4) The large number of variables involved meant that manual data handling methods were not really adequate to cope with these sorts of tests.
- (5) Some understanding of the effects of the variables was gained, though the relationships between them was not altogether clear.
- (6) Theory developed simply followed from dimensional analysis and was tied in to paddlewheel theory by the use of the same propulsive coefficient as used by Beardsley, and a lift coefficient of just the same form as his propulsive coefficient. Attempts at analytic models of the data proved forbiddingly complex. (2)
- (7) An interesting result was that the blade angle seemed to be a strong controlling factor in the balance between the lift and thrust forces. (3)
- (8) Some observations were made of the different wake patterns, and the concepts of the displacement mode and the planing mode were conceived. (4)
- (9) The literature survey produced information on the Spinning Wheel, which helped support the results.

As a result of these findings and the spinning Wheel report, it seemed clear that the answer to the fundamental question was: Yes, a lifting paddlewheel vehicle could be made to run across the surface of the water. (5)

Errata:

The design of the 1977 force balance was, unfortunately, at fault, so that for the following two reasons the thrust force readings were erroneous (see Fig.3.6).

1. Alexander 1977, P.61
2. Alexander 1977 P.13
3. Alexander 1977 P.56
4. Alexander 1977 P.48
5. Alexander 1977 P.64



385/40A

FIGURE 3.8: THE MODEL LPW CRAFT IN MID-1977 FITTED WITH SIX-BLADED, $\phi = 45^\circ$ LPW's. NOTE THE 2 AND 3-BLADED LPW's ALSO TRIED AT THAT TIME

(i) It was assumed that the lift force would act vertically through the LPW shaft. In fact this is rarely the case and consequently some of the lift component of force was normally added to the thrust measurement.

(ii) The fact that the shaft torque would be transmitted into the thrust measurement was not appreciated. Both these errors were caused by the use of a single pivot beam for thrust measurement. As well as this basic design fault the fact that propulsive efficiency, η cannot be greater than the velocity ratio, was not noted so that when plots of efficiency against velocity ratio were produced from the erroneously inflated thrust results, the errors were not noticed.

In spite of these rather basic mistakes, the lift force measurements were unaffected, and the conclusions drawn in the report that ... "the wheel will run on the water surface and carry a load at speed." (1) remained a valid answer to the fundamental question.

3.5 THE FIRST PROTOTYPE MODEL LPW VEHICLE

One way of answering the fundamental question rather dramatically would have been to have constructed a prototype, or model prototype, LPW vehicle and have it work. This was tried during 1977 and repeated attempts gradually developed the craft through a series of disappointing failures. By the end of the 1977 project time no success had been achieved (2). The form of the model at that stage is shown in Fig.3.8.

However, it was realised that the gear ratio was too high for the model motor used, so this was reduced considerably, and the model was tried again with barely enough success to convince a believer that it would work.

The centre of gravity was then shifted well forward to balance the torque reaction and stop the craft from rearing and diving, and LPW's with blade angles of 60° were finally fitted. These tended to provide positive rather than the negative thrust given by the earlier 45° LPW's, at the launch speeds being used.

1. Alexander 1977 Section 12.2, P.67
2. Alexander 1977 Appendix 1

Eventually satisfactory runs of 20 m or so were achieved before the overtaxed motor stalled. In order to prove that the LPW's were providing the support, the buoyancy was removed and the short, unstable runs of about 10 m before the craft sank, were sufficiently convincing to confirm the testing tank results and allow the tattered craft to be retired. Its final form with the motor placed well forward, the large gear reduction, the muffler, and the improved LPW's is shown in Fig.3.9.

(This model is further discussed in section 12.2 and its final specifications are given in Table 12.1.)

3.6 AIMS FOR THIS PROJECT

With this limited success in 1977 showing that the LPW concept worked, the author felt encouraged to continue with a new project to try to establish some fundamental ideas of how the LPW worked and to determine whether its performance could be improved sufficiently to make an economical craft.

The aims of this new project were divided into primary, secondary and tertiary levels. The primary aim set out to answer one fundamental question basic to the LPW concept. The other levels were to provide the framework within which this could be answered.

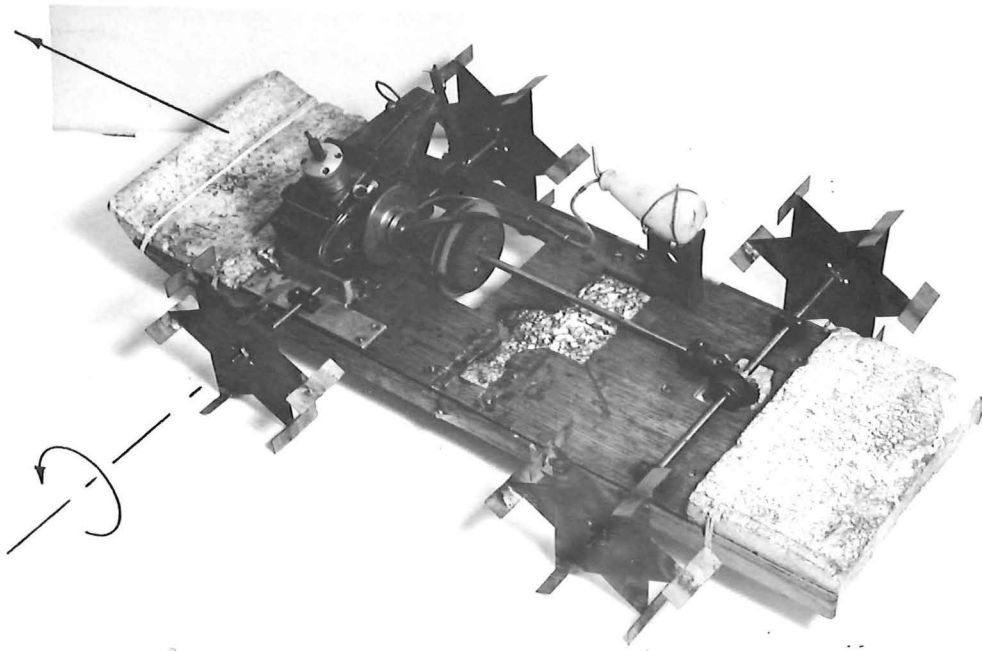
At the beginning of the author's work on the LPW, the primary aim was to answer the fundamental question:

Can a craft be made, as envisaged, which would run across the surface of the water on its wheels?

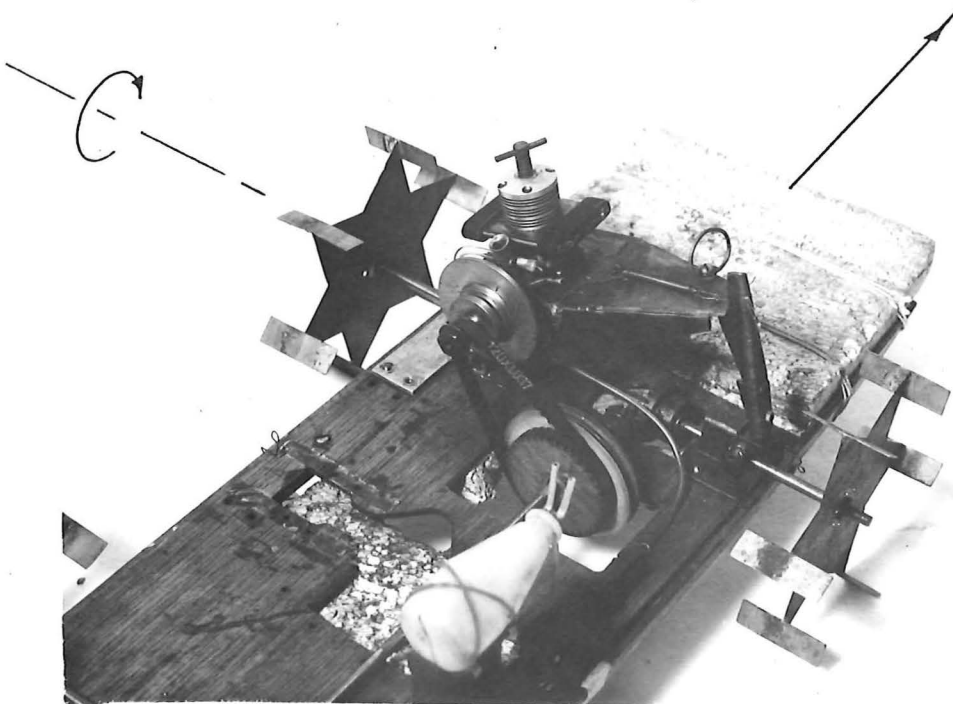
Since then, the earlier investigations, outlined above in sections 3.3 to 3.5, have answered this fundamental question with a simple: Yes. This then lead to the primary aim for this project which posed a new fundamental question as follows :

Primary Aim:

To answer the new fundamental question: How well can a Lifting Paddlewheel craft be made to run across the surface of the water on its wheels? (See Fig.3.10.)



1280/25



1280/24

FIGURE 3.9: THE FINAL LAYOUT OF THE FIRST MODEL LPW CRAFT IN 1978. (WHEELS No.2 IN TABLE 12.22)

This was immediately a much more difficult question to tackle and a full answer will not be available until such a craft has been built and operated on a competitive basis. Nonetheless, this new fundamental question set the direction of the project. Information produced to answer such a question inevitably helped answer many other questions as well, such as: How does the LPW work? How well would it propel a hovercraft? How efficient is it as a propulsive device? And so on.

The secondary aims were in three parts and were intended to provide a framework of information from which the primary aim question could in part, be answered.

Secondary Aims:

(1) To establish theoretical models that indicated the possible capabilities of and limits to the LPW performance. Such models helped answer the question: "How does the LPW work?"

(2) To establish an adequately broad and clear data base of LPW, and LPW craft performance that would make it clear how well the theory was applicable to the real situation.

(3) To use this data base to consolidate the theoretical models.

It can be seen from Fig.3.10 that these secondary aims formed the sort of iterative loop expected in research of a developmental nature.

The tertiary level aims were concerned with the mechanics of fulfilling the secondary level aims, and constituted the groundwork of day to day research. In order to establish the data base for (2) above and the means for (3) above these aims were divided into parts A and B. Part C involved supporting work with the model LPW craft.

Tertiary Aims:

(A) In order to establish a data base, this part of the Tertiary aims was:

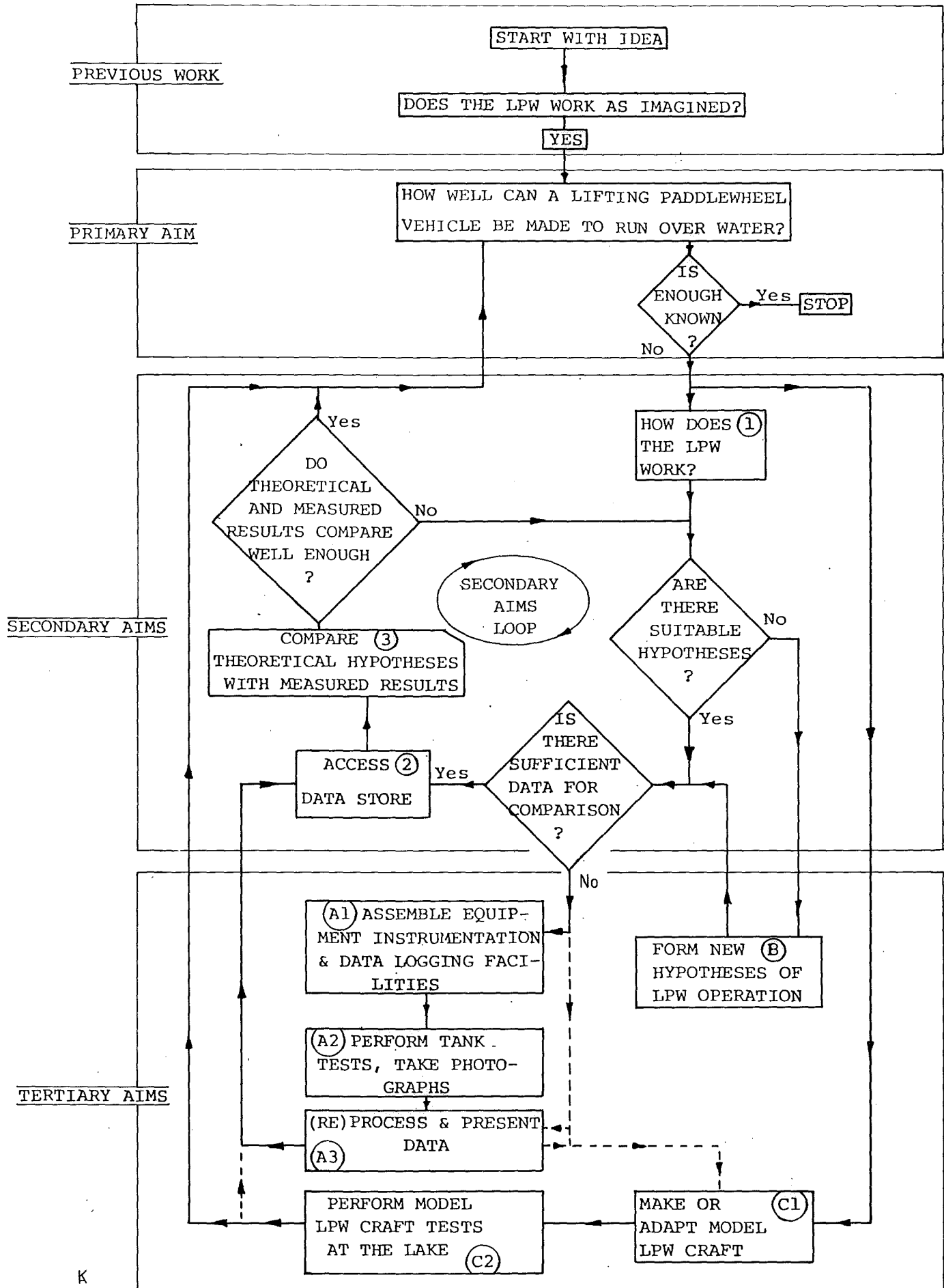


FIGURE 3.10: SCHEME OF AIMS FOR THE PROJECT

- (1) To obtain and/or construct the necessary equipment, instrumentation and data logging facilities.
- (2) To acquire the data with these facilities.
- (3) To establish the methods and software to process and present data in useful forms.

(B) In order to establish how the LPW works, this second part of the Tertiary aims was:

To develop appropriate hypothesis and computer-based models for comparison with the data, to elucidate the mechanism of LPW operation.

(C) To make and test a model LPW craft to assist in answering the fundamental question.

3.6.1 The Research Programme in Relation to These Aims

The search for an analytical description of how the LPW works in the 1977 work (1) was unsuccessful in its attempt to provide a good theoretical description of LPW behaviour. However, neither was it able to establish any compelling reasons why the LPW could not be applicable to a useful amphibious vehicle. For a start then, the first aspect of the secondary aims for this project concerning the theoretical models (part (1)) was held in abeyance until further information was to hand.

The next part of the secondary aims (part (2)) related to the establishment of the data base, and the tertiary aims, part (A) itemised the steps to be taken to acquire this data. There were three main sources of data, and over the course of the project, the work was carried out in fulfilment of the tertiary aims as follows :

(i) The first year concentrated on the development and testing of a new force balance to measure the LPW forces in water, instrumentation of it and development of data-logging facilities, as well as finding a suitable testing tank. Three different tanks were tried. The force balance had to be remodelled during the second year because of the design faults mentioned in section 3.4 above, but finally a large part of the second and third years was spent collecting and processing data from it.

(ii) Stroboscopic, photographic techniques were developed during the second year for observing LPW flow in detail, and throughout the project photographic and video-taped records became a useful part of the data.

(iii) Over the second year the MkII model, prototype, radio-controlled LPW craft was developed, and tests with this till the end of the project continued to provide useful data.

The other part of the secondary aims (part (3)) was concerned with answering the question "How does the LPW work?", and the tertiary aims part (B) spelled out the work as developing hypotheses and computer based models which could assist in answering this question. In the project most of this sort of work took place during the third and fourth years. By then a reasonable data base had been assembled, and so some computer models were developed which attempted to reproduce the plots that had been made of the measured data. These models, using theoretical considerations alone readily tested a number of hypotheses and eventually identified some realistic analytical descriptions of LPW operation.

These analytical descriptions then helped fulfil the theoretical area of the secondary aims which was originally left in abeyance. Finally, using these theoretical models, design predictions could be made and tested with the model LPW craft. This allowed a full-sized craft predicted performance capability to be made as a tentative answer to the fundamental question.

3.6.2 Conclusion

From this outline it can be seen that the project traversed the secondary aims loop in Fig.3.10 and thereby came one step closer to answering the fundamental question: How well can the Lifting Paddle-wheel Craft be made to run across the surface of the water on its wheels?

CHAPTER 4

THEORIES OF LIFTING PADDLEWHEEL OPERATION4.1 INTRODUCTION

This chapter describes work in two areas. First in Part A it examines analytical descriptions of how the LPW forces are developed. Second, in Part B it is concerned with identifying the most appropriate hypotheses to describe the physical environment around the LPW - wake regimes, testing the LPW in flowing water, and so on.

Part A, in dealing with the hypotheses and theories developed to describe the high speed operating performance of the LPW, has discarded a number of theoretical models during the course of the project. Some of these have been based on the work of other authors. The most appropriate analyses have been incorporated into the new theoretical model developed here, the Impulse Theory. This theory at present most closely describes the real high speed situation as outlined in the results in Chapter 9. Some time is spent examining implications of this theory in terms of LPW propulsive efficiency and power consumption. (This part of the chapter fulfils part 1 of the Secondary Aims Loop of Fig.3.10.)

Part B of the chapter contains items not directly related to the generation of LPW forces though defining the limits to the physical situation within which the Impulse Theory applies. It also examines the testing of LPW's in flowing water.

PART A4.2 DIMENSIONAL ANALYSIS

A dimensional analysis carried out for the usual primaries (excluding surface tension) gives the following four recognised dimensionless groups:

Reynolds Number	$R_e = \frac{\rho V D}{\mu}$
Froude Number	$F_r = \frac{V^2}{g D}$
Force Coefficient	$C_f = \frac{F}{\rho V^2 D^2}$

$$\text{Power Coefficient} \quad C_P = \frac{F \cdot V}{P}$$

where: ρ = density of water
 V = general velocity
 D = characteristic dimension
 μ = viscosity
 g = gravitational acceleration
 F = force
 P = power.

In order to retain geometric similarity in flow and LPW blade configurations the following dimensionless groups also need to be satisfied:

$$\begin{aligned} \text{Immersion Ratio} &= \frac{d}{D} \\ \text{Span Ratio} &= \frac{s}{D} \\ \text{Chord Ratio} &= \frac{c}{D} \\ \text{Velocity Ratio} &= \frac{V_o}{V_t} \end{aligned}$$

A further dimensionless group (which is not necessary for geometric similarity if the velocity ratio is constant) is the Rotational Speed Ratio. This is a Froude Number form for the wheel revolutions and is sometimes useful:

$$\text{Rotational Speed Ratio} = \frac{nD}{\sqrt{gD}} = \frac{n\sqrt{D}}{\sqrt{g}}$$

where: d = immersion depth
 s = blade span
 c = blade chord
 V_o = speed of advance
 V_t = blade tip speed relative to wheel axis
 n = wheel rps.

For paddlewheel experiments Volpich and Bridges (1) suggest that it is unlikely that Reynolds Number has any significance, and since its effects are in favour of increase in scale it will be neglected from further consideration here.

1. Volpich & Bridges Pt I, P.333

The other three recognised groups need to be adapted to the LPW situation, and this involves choosing from the three possible velocities which one may be used. These three are V_o , V_t and the velocity difference, $(V_t - V_o)$.

For similarity of wave formation the Froude Number necessarily involves the velocity V_o , which is the speed of the LPW relative to the water, so that the Froude Number then becomes

$$F_r = \frac{V_o}{\sqrt{gD}} \quad \text{where } D = \text{wheel diameter.}$$

If the speed of advance V_o and the propulsive thrust force T are used in the power coefficient, it becomes useful as the propulsive efficiency:

$$\eta = \frac{TV_o}{P_i} \quad \text{where } \eta = \text{propulsive efficiency}$$

$T = \text{thrust force}$

$P_i = \text{power input to LPW.}$

4.2.1 Force Coefficients Relating to Ship Propeller Theory

The force coefficients for the LPW as derived from dimensional analysis present a dilemma with regard to the best choice of velocity. It would seem that the velocity difference $(V_t - V_o)$ should be used as being most closely related to the momentum change and hence the force generation. However, Beardsley has chosen to use V_t since this relates the coefficient to ship propeller coefficients (where V_t represents the blade tip velocity perpendicular to the direction of advance). For this reason, and since it is easier to apply, V_t is chosen for use in this force coefficient relation.

Now V_t may be expressed as $V_t = n\pi D$ which can be truncated to nD for the purposes of coefficient development. Beardsley expresses the standard thrust coefficient for ship propellers in the form:

$$K_t = \frac{T}{\rho n^2 D^4} \quad (4.1)$$

and notes that since both paddlewheel theory and experiment show that thrust increases directly with span, this form may be normalised to include the blade span ratio, so that:

$$K_T = \frac{T}{\rho n^2 D^4} \times \frac{D}{s}$$

This results in the form of the thrust coefficient used by Beardsley:

$$K_T = \frac{T}{\rho n^2 D^3 s} \quad (4.2)$$

Should such a coefficient form be shown to be useful it would be convenient to define the lift force coefficient in the same way:

$$K_L = \frac{L}{\rho n^2 D^3 s} \quad (4.3)$$

where $L =$ lift force.

If LPW operation were analogous to ship propeller operation then these would be the relevant coefficient equations to use. Beardsley (1) has noted however that these equations are based on Bernoulli's equation and therefore require steady flow conditions. The paddlewheel is not strictly a steady flow device so for this reason Beardsley derived a different set of relations, more relevant to paddlewheels, based on the change of momentum of discrete increments of water

4.3 A FIRST ORDER MOMENTUM THEORY OF LPW OPERATION

This section outlines a momentum approach to the problem of how the LPW generates its lift and thrust forces. It is restricted to the high speed planing condition of the LPW only, as this would be the normal operating condition. It relies heavily upon Beardsley's analysis for the SIP concept (1) but here is adapted to the LPW situation.

In developing the theoretical model for the thrust forces on his paddlewheel blades operating at speed Beardsley notes: "the negative pressure on their rear (upstream) face cannot be fully developed because of ventilation at the water-air interface. Thus the water stream flow is interrupted and does not maintain the continuity required for the classical equation...for a propeller in an open stream." (1) This is:

$$T = \rho A_P \left(\frac{V_j + V_o}{2} \right) (V_j - V_o) \quad (4.4)$$

where $\rho =$ fluid density

$A_P =$ swept area of propeller disc

V_j = discharge velocity downstream at
free stream pressure

V_o = free stream fluid velocity.

For the equation in this form the mass flow of the actuated stream tube is represented by the terms

$$\rho A_P \left(\frac{V_j + V_o}{2} \right)$$

This form therefore cannot be used for high speed paddlewheel analysis and a more representative analysis results when the thrust is considered to be produced by the increase in momentum imparted to a differently derived entrained water mass, by a series of impulses generated by the actuation of discrete increments of water encountered by the blades. Since these increments are small, and are actuated at high frequency it is assumed that they merge into a discharge flow of reasonably uniform velocity. (1)

Such reasoning is equally relevant to the LPW situation and an actuator model shown in Fig.4.1 is therefore used for the development of the analysis. In this figure the immersed part of the LPW is represented by an actuator rectangle through which the entrained water passes and where it is given discrete impulses downwards and rearwards as shown. Several assumptions are made:

(i) No water is present below the entering layer that would interfere with its downward exit.

(ii) Gravity effects are ignored: no waves are formed.

(iii) Viscosity is neglected.

4.3.1 Thrust Force Equations

In Fig.4.1 the (horizontal) thrust force may be represented by the equation:

$$T = \dot{m} \Delta V_h \quad (4.5)$$

where \dot{m} = mass per second acted upon by the rectangle

ΔV_h = horizontal velocity change given to the fluid.

In the real case the horizontal discharge velocity is unlikely to be as great as the velocity of the blade tip but if it is assumed to be this great, then:

$$\Delta v_h = v_t - v_o \quad (4.6)$$

Similarly, not all the incoming (or entrained) mass will be acted upon by a real LPW but if it is, then:

$$\dot{M} = \rho d s v_o \quad (4.7)$$

where \dot{M} = entrained mass flow rate

ρ = fluid density

d = immersion depth

s = blade or rectangle span

v_o = speed of advance

(Note that this expression for the mass is less than that in the classical equation (4.4) for a propeller.)

Now the thrust equation (4.5) may be rewritten as:

$$T = \rho d s v_o (v_t - v_o) \quad (4.8)$$

and Beardsley (1) further rearranges it to emphasise the role of velocity ratios:

$$T = \rho d s v_t^2 \left(\frac{v_o}{v_t}\right) \left(1 - \frac{v_o}{v_t}\right) \quad (4.9)$$

and to derive a new expression for the thrust coefficient with span equal to diameter:

$$K_{T1} = \frac{\pi^2 d}{D} \left(\frac{v_o}{v_t}\right) \left(1 - \frac{v_o}{v_t}\right) \quad (4.10)$$

Note that in equation (4.9) the thrust is zero for $\frac{v_o}{v_t} = 1$ and for $\frac{v_o}{v_t} = 0$, and while this is reasonable for $\frac{v_o}{v_t} = 1$ since there has been no change in stream velocity ($v_t - v_o = 0$), it is unreasonable as a slow speed model of the real case when $v_o \rightarrow 0$, since there has been found to be considerable thrust when $v_o = 0$. This serves to emphasise

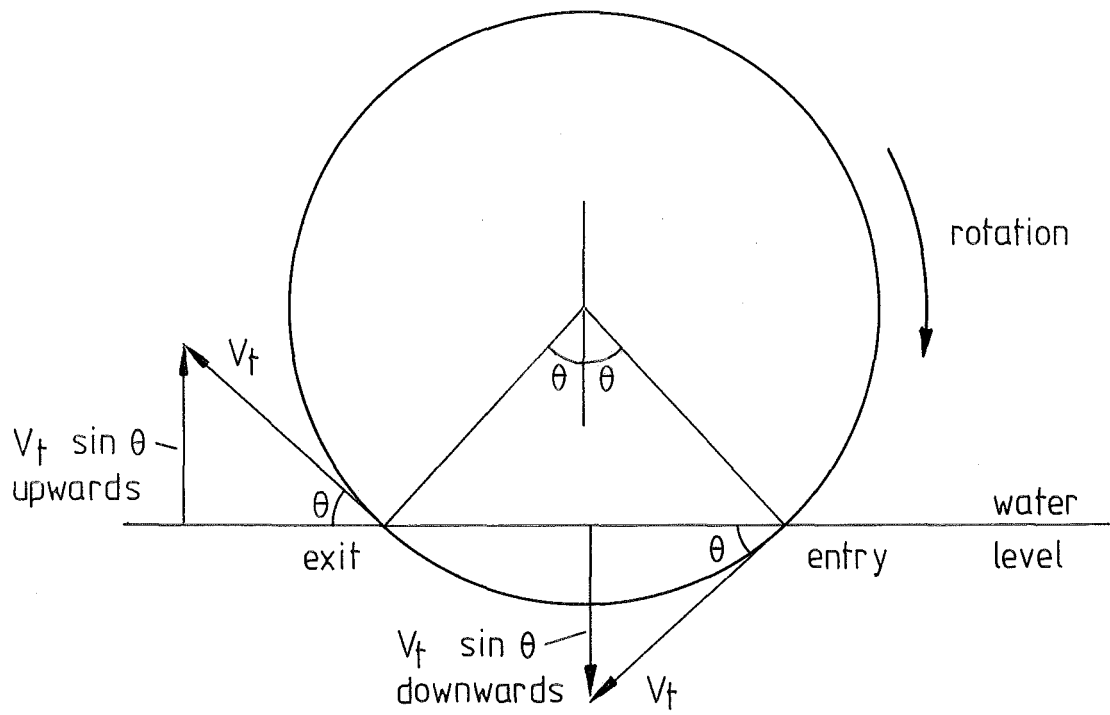


FIGURE 4.2 VERTICAL COMPONENTS OF V_t AT BLADE ENTRY & EXIT.

Beardsley's point that the equations (4.8), (4.9) and (4.10) only apply to the high speed case, (planing conditions) and further equations should be developed to account for the mass supply by gravity-induced flow at low speeds and displacement conditions.

4.3.2 Lift Force Equations

Applying this same approach for the development of the lift force equations is not as straightforward, but using again Fig.4.1 the (vertical) lift force may be represented by the equation

$$L = \dot{m} \Delta V_v \quad (4.11)$$

where L = lift force

\dot{m} = mass per second acted upon by the rectangle

ΔV_v = the vertical velocity change given to the water.

In the thrust force section above the blade tip speed, V_t , was taken as the final horizontal exit velocity of the water. For the lift force situation, the maximum vertical component of the blade tip speed occurs both at entry and exit of the blade. These velocity components are equal and opposite in sign and of magnitude $\pm V_t \sin \theta$ as shown in Fig.4.2. At this point the assumption needs to be made that only the blade entering the water need be considered so that the vertical velocity change may be expressed as:

$$\Delta V_h = V_t \sin \theta \quad (4.12)$$

Substituting the expression (4.7) for the total entrained mass flow rate into (4.11), with the vertical velocity expression (4.12) gives a lift force relation analogous to the thrust force expression (4.8).

$$L = \rho d s V_o V_t \sin \theta$$

$$L = \rho d s \left(\frac{V_o}{V_t}\right) V_t^2 \sin \theta \quad (4.13)$$

A new form for the lift coefficient with span equal to diameter would then be

$$K_{Ll} = \frac{\pi^2 d}{D} \frac{V_o}{V_t} \sin \theta \quad (4.14)$$

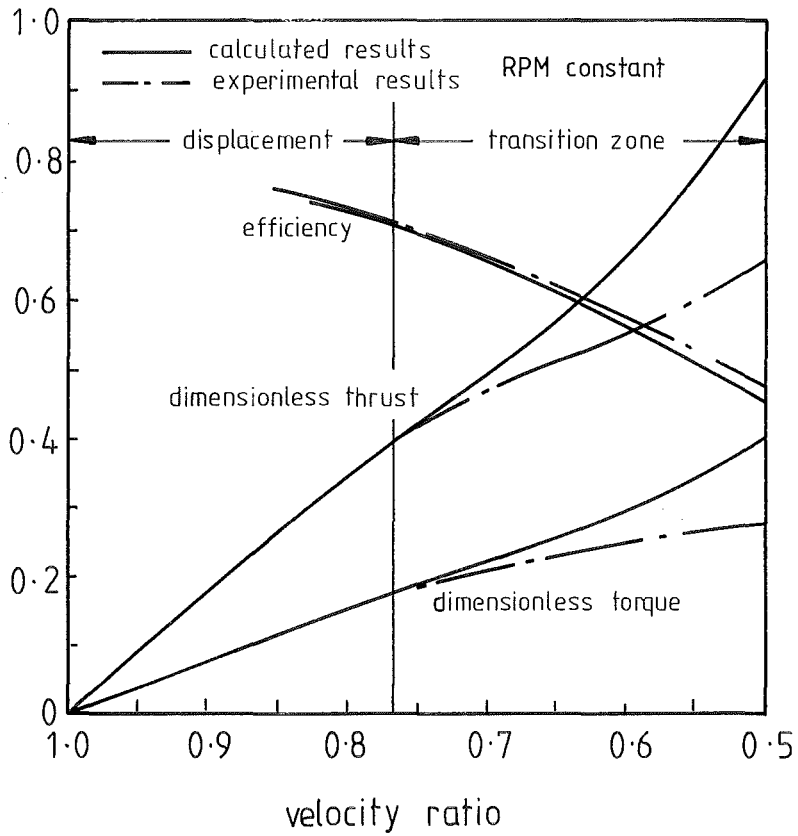


FIGURE 4.3 VOLPICH & BRIDGES RESULTS COMPARED WITH FLAT PLATE DRAG CALCULATIONS: FEATHERING BLADES.

(V & B part II p. 500)

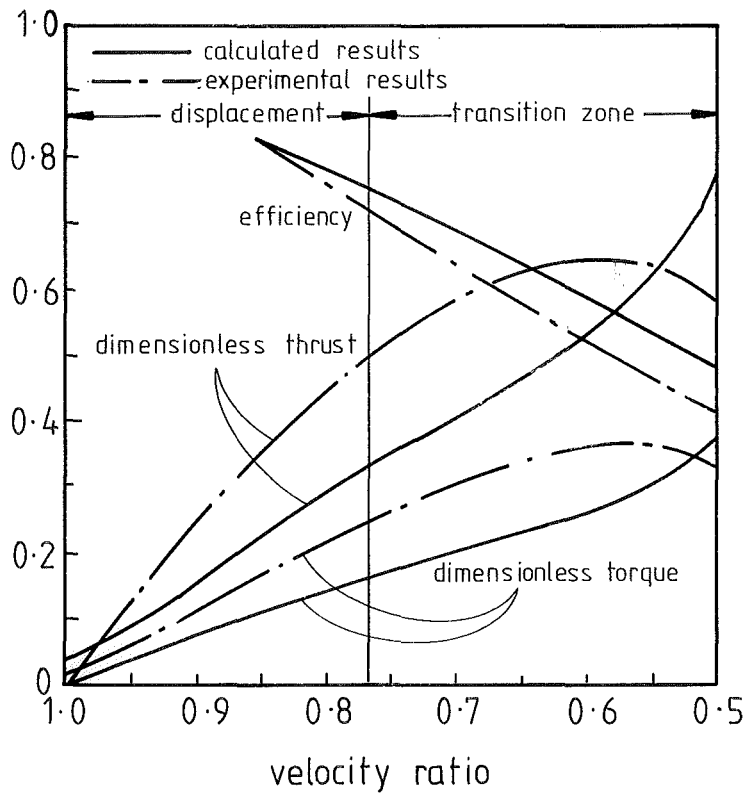


FIGURE 4.4 AS ABOVE FOR RADIAL BLADES FOR BOTH CASES AGREEMENT IS BETTER IN DISPLACEMENT MODE.

In summary then, these two expressions (4.10) and (4.14) for thrust and lift for the LPW differ from the expressions (4.2) and (4.3) derived from the classical propeller equations since they take into account the fact that steady flow is not involved. They assume, however, that all the entrained water mass leaves the LPW at the maximum horizontal and vertical velocities reached by the blade tips. Later sections examine these assumptions more closely in order to refine the theory.

4.4 FLAT PLATE DRAG AND THE FORCES ON LPW BLADES

It would be expected that any consideration of the theory of paddlewheels should model the blade forces in terms of the drag on fully immersed two dimensional flat plates.

Volpich and Bridges with the assistance of McNab (1) carried out such a geometric study of the passage of the feathering paddlewheel blade through the water. From the resulting vector flow velocities they calculated blade forces using lift and drag data for flat plates. Although they did not expect reliable results they found close agreement between calculated values and experimental data for some regions of their curves. This was especially true for forces and efficiencies calculated in the displacement mode, clear of the transition zone and for high velocity ratios ($V_o/V_t > 0.75$). Their results are shown in Figs. 4.3 and 4.4. Their calculations for radial blade forces in Fig.4.4 did not give particularly good agreement though they claimed the discrepancies were probably because of improper extrapolation from their experimental data. (2)

It appears that Volpich and Bridges' success was at least partly because their blade velocities were appreciably lower than the expected wave velocities and gravity-induced flow velocities in the test situation. Under such conditions the paddlewheel blades would be operating near the fully immersed state for which the flat plate data were applicable.

Similar calculations for the LPW blades may also give results which are in fair agreement with experiment at high velocity ratios

1. Volpich and Bridges, Part II P.491. Also this project section 2.2.3.
2. Volpich and Bridges, Part II P.502.

but only in the displacement mode. Such theory, however, has severe limitations when it is applied at the expected high speed operating conditions of the LPW. After the data collection stage of this project considerable effort was spent on a computer programme which attempted to model the high speed data in terms of the flat plate lift and drag forces. (See section 9.3.) The calculations followed procedures similar to those used by Volpich and Bridges, but the results seemed satisfactory only for some conditions of blade angle and never for both lift and thrust forces at once. They could only be made uniformly satisfactory by assuming that all the drag force occurred during the blade entry. Ultimately the constraints required to make the flat plate drag data applicable directed attention to the more promising impulse theory developed later.

These constraints may be itemised:

(1) Since the blades operate with the rear face denuded of water, flat plate data for fully immersed flat plates should not be used. Instead Rayleigh's formula for the front face pressure (1) seems more relevant.

(2) Accelerations are large so that the flow is far from steady. Acceleration forces are of the same order of magnitude as drag forces.

(3) The blades are rotating.

(4) Operation is close to, or through the water surface.

Such constraints effectively limited the application of this theory to the low speed displacement mode of operation, and since high speed LPW operation is of primary interest at this stage, further analysis concentrates on the more relevant theories, leaving this approach to any future analysis of the displacement mode.

(Section 9.3 examines the experimental results in terms of the flat plate drag hypothesis for LPW blade forces.)

4.5 INDUCED MASS AND SYMMETRICAL IMPACT ON A WATER SURFACE

If a body fully immersed in a fluid is accelerated, its kinetic energy is increased. In addition the fluid which it displaces by its

movement is given an increase in kinetic energy. The work done in accelerating the body is therefore greater than if the body alone had to be accelerated, and this increase in work has been shown to occur as if the mass of the body were greater by a fixed amount. This apparent increase in mass is termed the added or induced mass of the body. This artificial mass may be imagined as filling the whole of the surrounding fluid but being concentrated at the body surface and decreasing in density with distance from it. It may be used, however, in momentum or energy exchange calculations as if it were part of the mass of the body itself.

For a fully immersed, two dimensional flat plate moving perpendicularly to the plane of its surface the induced mass is known to be equivalent to the mass of a cylinder of fluid with a diameter equal to the plate width. (1)

This induced mass, however, is not constant under all conditions of motion and its magnitude depends upon the direction of flow relative to the plate, the type of flow, and the presence of boundaries such as a cavity, wall or the water surface.

Normally the total force on an accelerating massless plate would be found by taking the magnitude of the force generated by the change in momentum given to the induced mass, and adding to it the instantaneous flat plate drag of the plate.

For a fully immersed paddlewheel blade any accelerations will generate forces which may be treated by adding the acceleration forces to the flat plate drag forces. For example, had they wanted to, Volpich and Bridges could have used these concepts to estimate their paddlewheel forces more rigorously in Figs. 4.3 and 4.4. For the LPW at high speed, however, the situation is different again from that of a fully immersed plate.

The case of a plate entering through a water surface requires a different treatment than the case of the fully immersed plate. For symmetric impact of a two dimensional flat plate on a smooth water surface the induced mass has been shown to be half the value for the fully immersed plate. (2) It is this value of induced mass which is

1. Streeter, P.13-32
2. Wagner or Batchelor 6.10

more realistic in providing an estimate of the mass used in the high speed LPW impulse theory. The mass of water to be accelerated, then, based on Wagner's result, may be written directly from the dimensions of the LPW blade.

$$m' = \frac{\pi}{2} \left(\frac{c}{2}\right)^2 s \rho \quad (4.15)$$

where m' = induced mass per blade
 c = blade chord
 s = blade span
 ρ = water density.

Now each blade entering the water has this induced mass associated with it so that in the force equations, 4.5 and 4.11, the mass flow rate, \dot{m} , becomes dependent upon the number of blades entering the water per second. It is convenient, therefore, to put the induced mass per blade in the form of a mass flow rate so that equation (4.15) becomes:

$$\dot{m} = \frac{\pi}{8} c^2 s \rho n B \quad (4.16)$$

where n = rps
 B = the number of blades on the LPW.

In the LPW situation the conditions are somewhat divergent from those for which the symmetric impact theory of Wagner is readily applicable. The discrepancies are noted in the following points which must therefore be taken as working assumptions:

- (1) For LPW blades water entry is rarely symmetric but the induced mass will be assumed to be unaffected by this.
- (2) Flow conditions will vary considerably from case to case, and involve rotation and deceleration during entry. Induced mass will be assumed to be unaffected by this, remaining constant in all cases of water entry.
- (3) Although induced mass is known to vary depending upon the alignment of the plate to the flow, this factor will be ignored at this stage, induced mass being assumed constant regardless of the angle of attack of the flow on to the blade.

(4) The water surface is rarely flat, usually containing splash and waves left by the passage of the previous blade (see section 4.9.1). This is assumed to have no effect on the magnitude of the induced mass.

(5) It is very difficult to estimate any flat plate drag contribution to the forces since the action is impulsive and the time duration indeterminate. These forces will therefore be ignored at this stage. (See, however, section 9.3.2 where these drag forces are shown to exist.)

(6) The LPW blades are considered as two-dimensional blades, having no end effects to alter the calculated induced mass.

(7) For the purposes of the theory all the induced mass is assumed to be located at the blade tip. That is, no account is taken of the fact that most of the blade surface is on a smaller radius than the blade tip.

The momentum model described in the earlier section (section 4.3) could now be reassessed using this new limited mass. Firstly, however, the other assumption in that theory regarding the final water velocities will be examined more closely. This involves some preliminary work to investigate the geometry of the flow around the LPW blade.

4.6 LPW BLADE FLOW GEOMETRY AND MAXIMUM BLADE-WATER VELOCITIES

The passage of the LPW blades through the water is a complex motion involving continual changes in flow velocity and direction so that the resulting flow relative to the blades is neither easy to visualise nor to analyse theoretically. Nevertheless the geometry of the blade passage through the water and especially the conditions of blade entry into the water have been found to be the key to the theoretical description of the LPW performance.

The most useful of these geometric concepts are outlined here before they are applied in the later derivation of the maximum velocity expressions.

At this stage the LPW blades are seen simply as flat plates, which provide a basis for the subsequent theory.

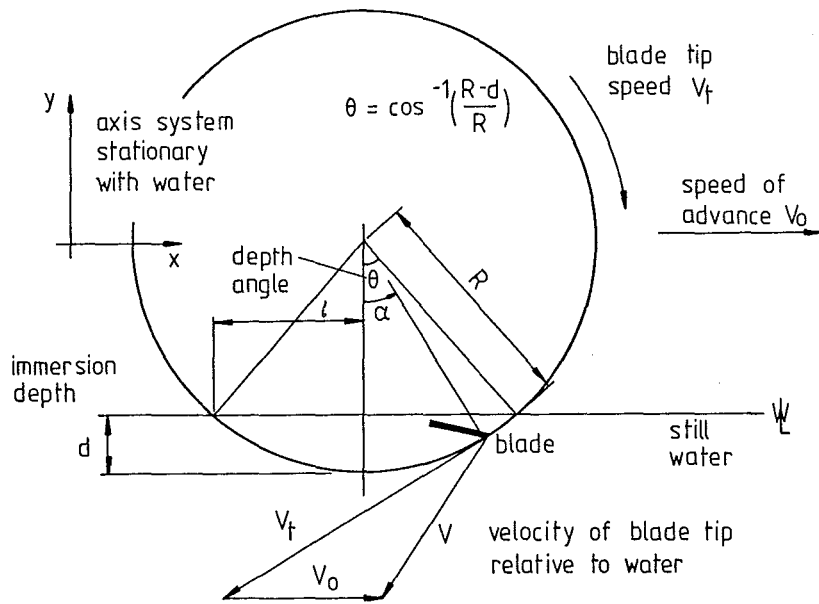


FIGURE 4.5 GENERAL LPW GEOMETRY. NOTE THAT θ DEFINES IMMERSION DEPTH, WHILE α DEFINES ANY POSITION OF THE BLADE IN ITS PASSAGE.

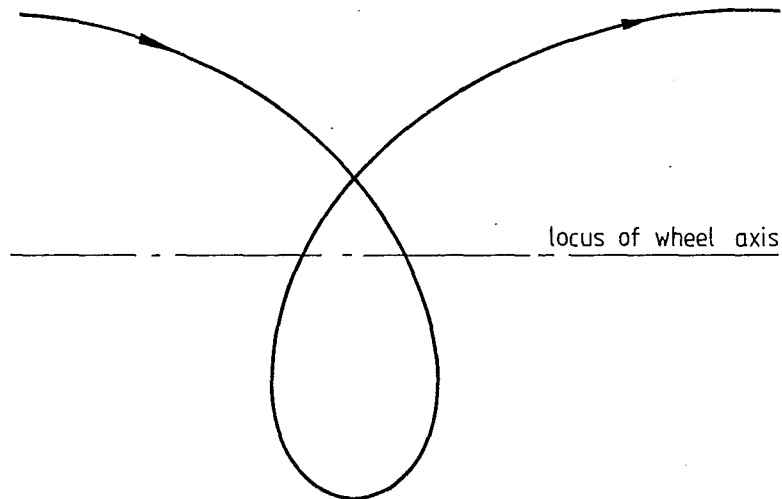


FIGURE 4.6 LOCUS OF A SINGLE BLADE TIP $\frac{V_0}{V_t} = 0.5$

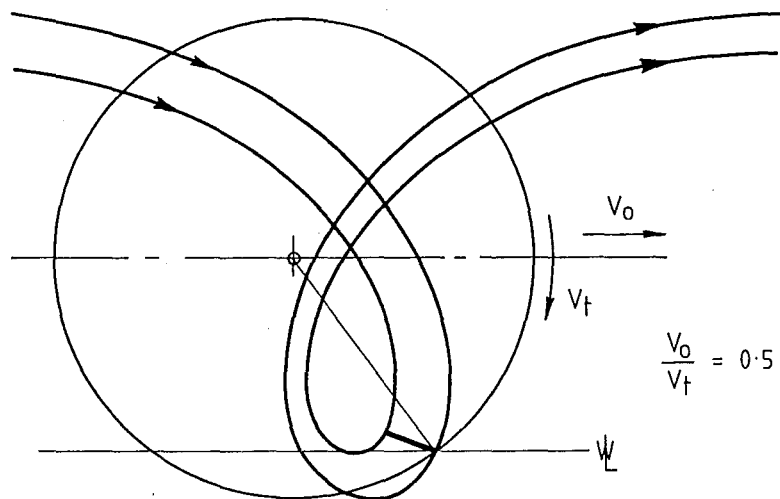


FIGURE 4.7 LOCUS OF BLADE TIP AND HEEL AT $\frac{d}{D} = 0.11$

4.6.1 Blade Motion Relative to the Water

The blade tip may be considered at any instant to be at angle α from the vertical, with tip velocity V_t relative to the wheel axis as shown in Fig.4.5. The wheel axis may then be given a speed of advance V_o so that the parametric equations of the position of the blade tip relative to the x-y axis stationary in the water, are those of a prolate cycloid:

$$x = V_o \cdot t + R \sin \alpha$$

$$y = -R \cos \alpha$$

where t = time

R = LPW radius to blade tip.

When these equations are plotted they give the locus of a single blade tip for the chosen velocity ratio of the wheel as shown in Fig.4.6.

A similar curve, displaced to one side shows the locus of the inside edge (or heel) of a flat LPW blade and both curves are shown together in Fig.4.7.

At a given water depth these curves intercept the water as shown also in Fig.4.7, and when a multibladed wheel is used the loci of the blade tips alone look like Fig.4.8. At the immersion ratio shown ($\frac{d}{D} = 0.125$), for a six-bladed wheel the locus of each blade tip intercepts the locus of the previous blade tip below the water surface. This is a geometric equivalent of cavity intrusion; if the LPW was carving through butter the track left behind would follow these blade loci. In water, cavity intrusion occurs differently since the water spreads away from the blade tip locus, (see section 4.9.2).

4.6.2 Blade Tip Velocity Relative to the Water

Assuming there are no gravity-induced flow velocities in the water, we can differentiate the parametric equations to arrive at an expression for the magnitude of the blade tip velocity relative to the water.

$$\dot{x} = V_o - R\omega \cos \alpha$$

$$\dot{y} = -R\omega \sin \alpha$$

$$V = \sqrt{\dot{x}^2 + \dot{y}^2}$$

$$\therefore V = \sqrt{V_o^2 - 2V_o V_t \cos \alpha + V_t^2} \quad (4.17)$$

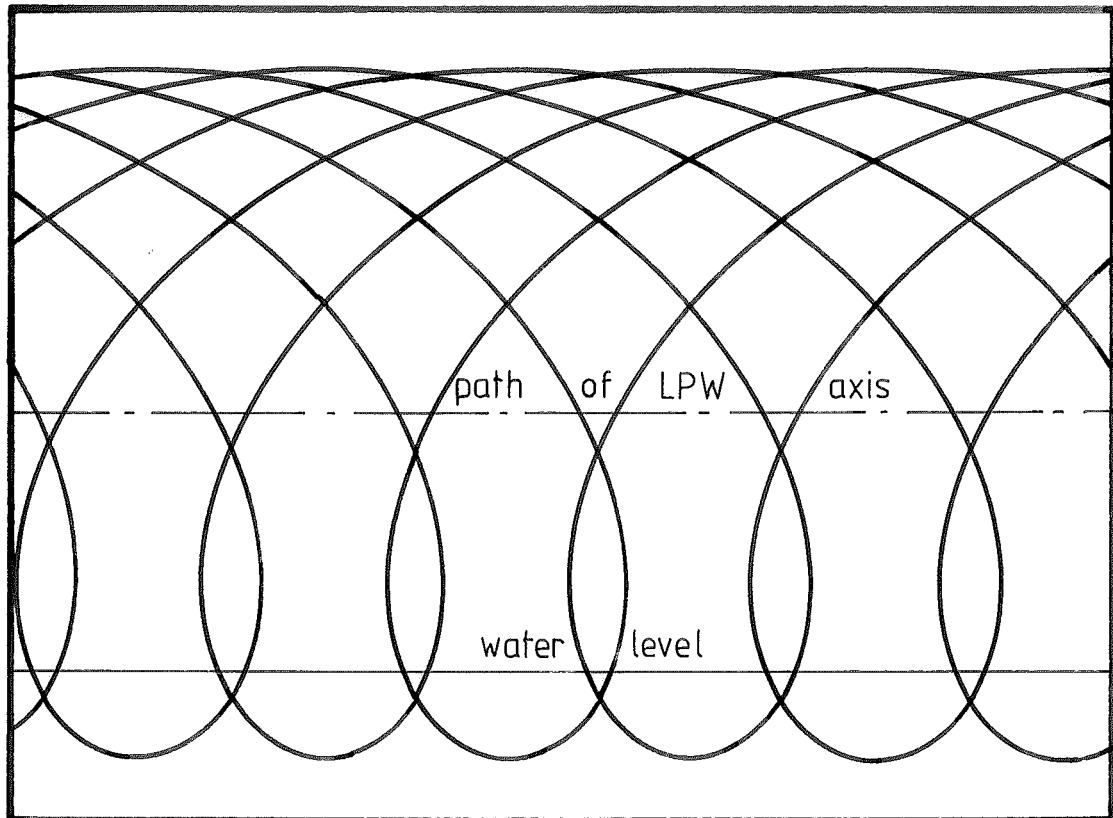


FIGURE 4.8 LOCUS OF THE TIPS OF A 6-BLADED WHEEL $\frac{V_0}{V_f} = 0.5$

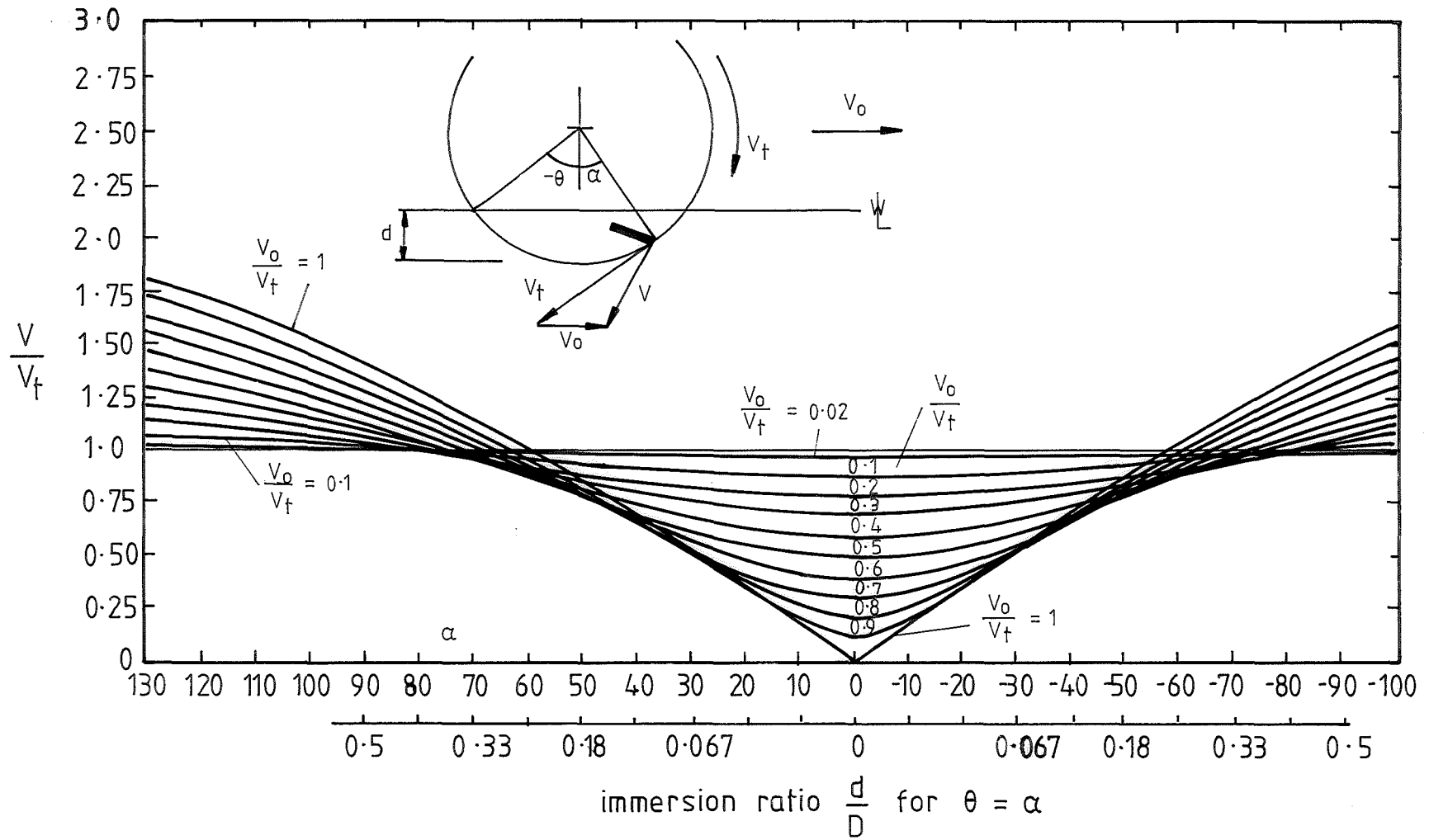


FIGURE 4-9 BLADE TIP VELOCITY RELATIVE TO THE WATER, V vs ANGLE THROUGH PASSAGE α AS A RATIO WITH V_t .

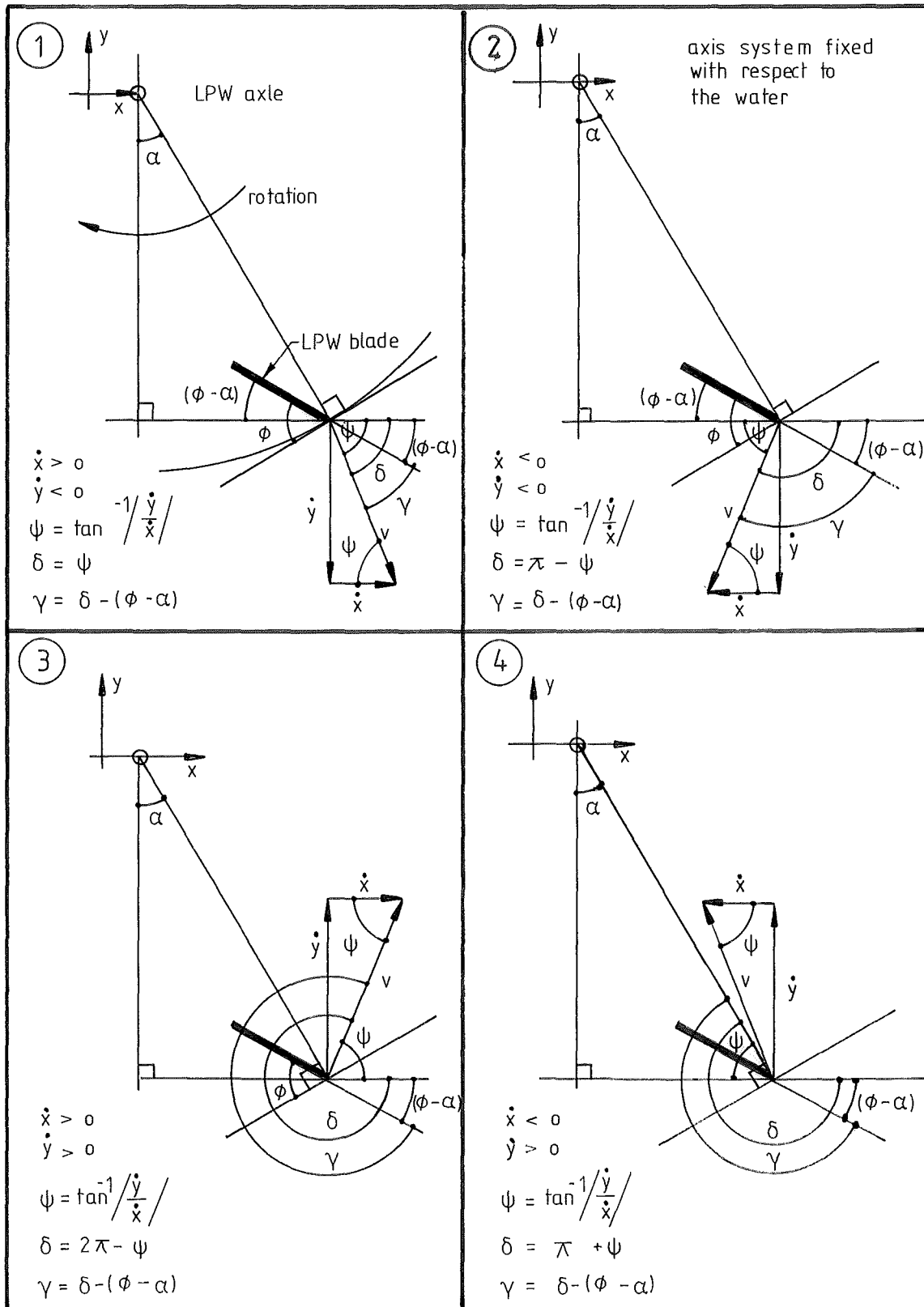


FIGURE 4.10 THE FOUR CASES USED TO DETERMINE γ THE ANGLE OF ATTACK. v IS THE VELOCITY OF THE BLADE RELATIVE TO THE WATER.

where ω = angular speed of LPW
 V = velocity of blade tip relative to the water
 V_t = velocity of blade tip relative to wheel axis
 V_o = speed of advance of wheel axis.

This expression (4.17), is plotted in Fig.4.9 as a ratio with the blade tip speed V_t , for a series of velocity ratios less than 1. Note that the immersion ratios are marked on the horizontal (α) axis, indicating at what angle, α , the blades enter and leave the water for various immersion ratios.

Note also that the blade tip velocity, V , relative to the water decreases from entry to the bottom of the passage and then increases again, so that it is a maximum at blade entry and exit.

4.6.3 Angle of Attack Through a Blade Passage

The direction of motion of the LPW blade tip relative to the water is required in order to estimate the magnitude of the instantaneous force applied by the blade to the water. This depends upon the blade angle, ϕ , for a flat blade. Fig.4.10 shows the four cases of velocity possible at the blade tip, and the derivation of the angle δ for each case. The appropriate case can be chosen for the sense of \dot{x} and \dot{y} from the figure, and the equation for the angle of attack, γ , can be written directly:

$$\gamma = \delta - (\phi - \alpha) \quad (4.18)$$

For normal operation both \dot{x} and \dot{y} are negative so that diagram (2) of Fig.4.10 is most often relevant.

It should be noted that for extremes of blade angle, ϕ , the above equation may produce angles of attack, γ , greater than 2π or less than 0. If this occurs γ is normally readjusted to be within the range $0 < \gamma < 2\pi$.

A subroutine used for calculating γ is given with programme 'BLADED DRAG' as subroutine 'XYWG' in Appendix 8.

If the angle of attack γ , is plotted against α the angular distance through the blade passage, for a series of velocity ratios, the result is as shown in Fig.4.11. This is the case for the blade angle $\phi = 90^\circ$. A simple shift of the vertical axis as shown enables

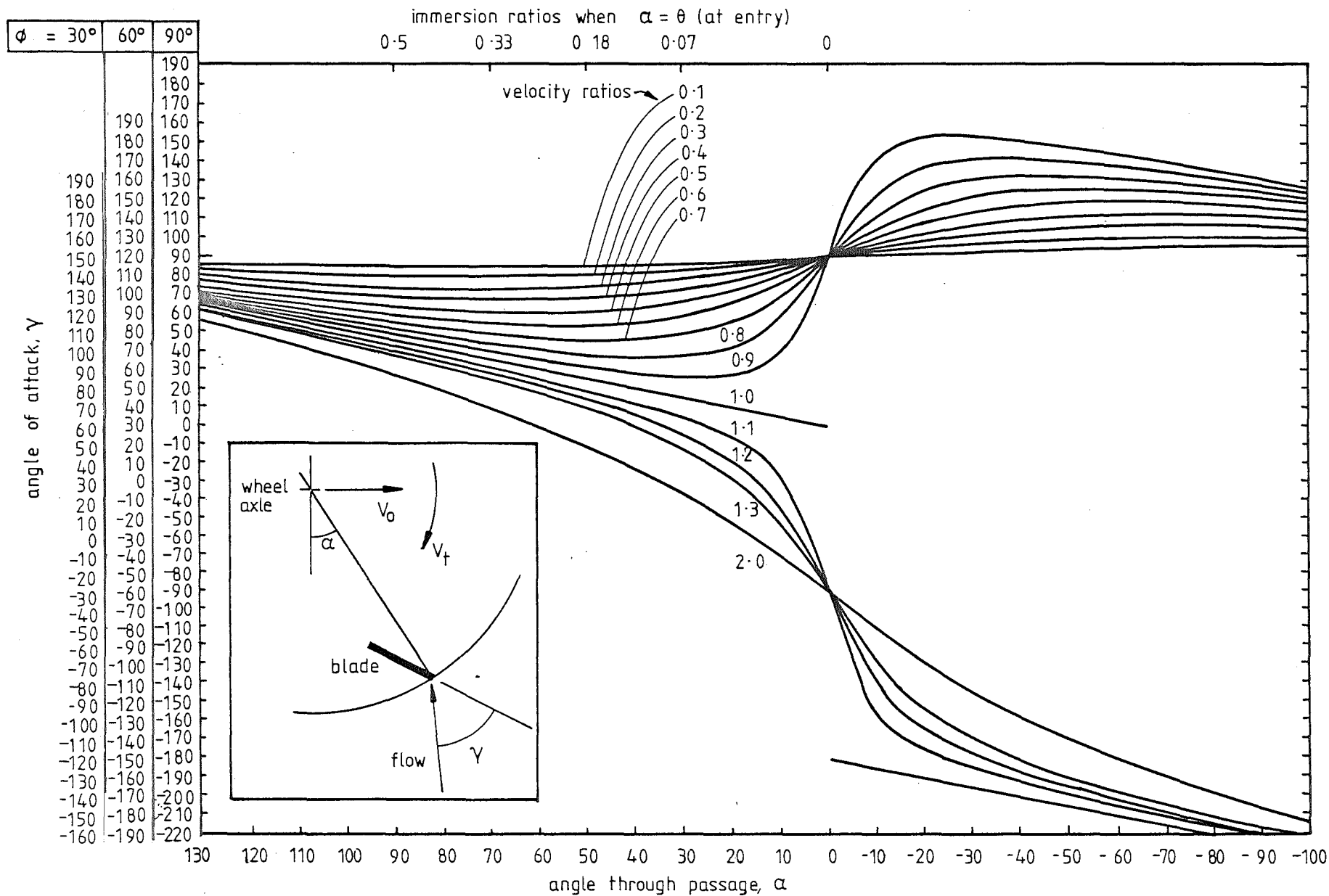


FIGURE 4.11 ANGLE OF ATTACK γ , THROUGH THE BLADE PASSAGE.

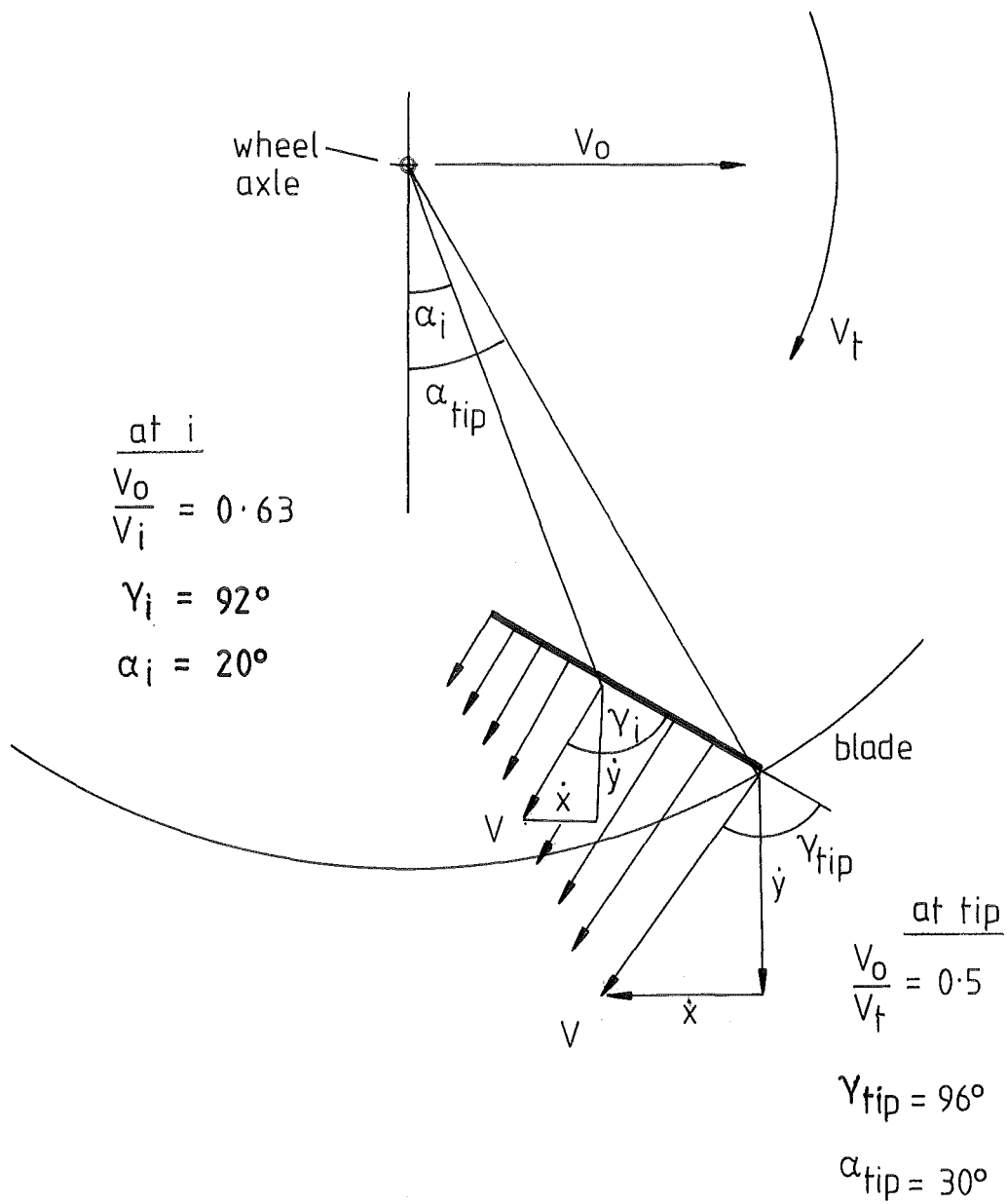


FIGURE 4-12 VARIATION OF ANGLES AND VELOCITIES ALONG THE BLADE CHORD.

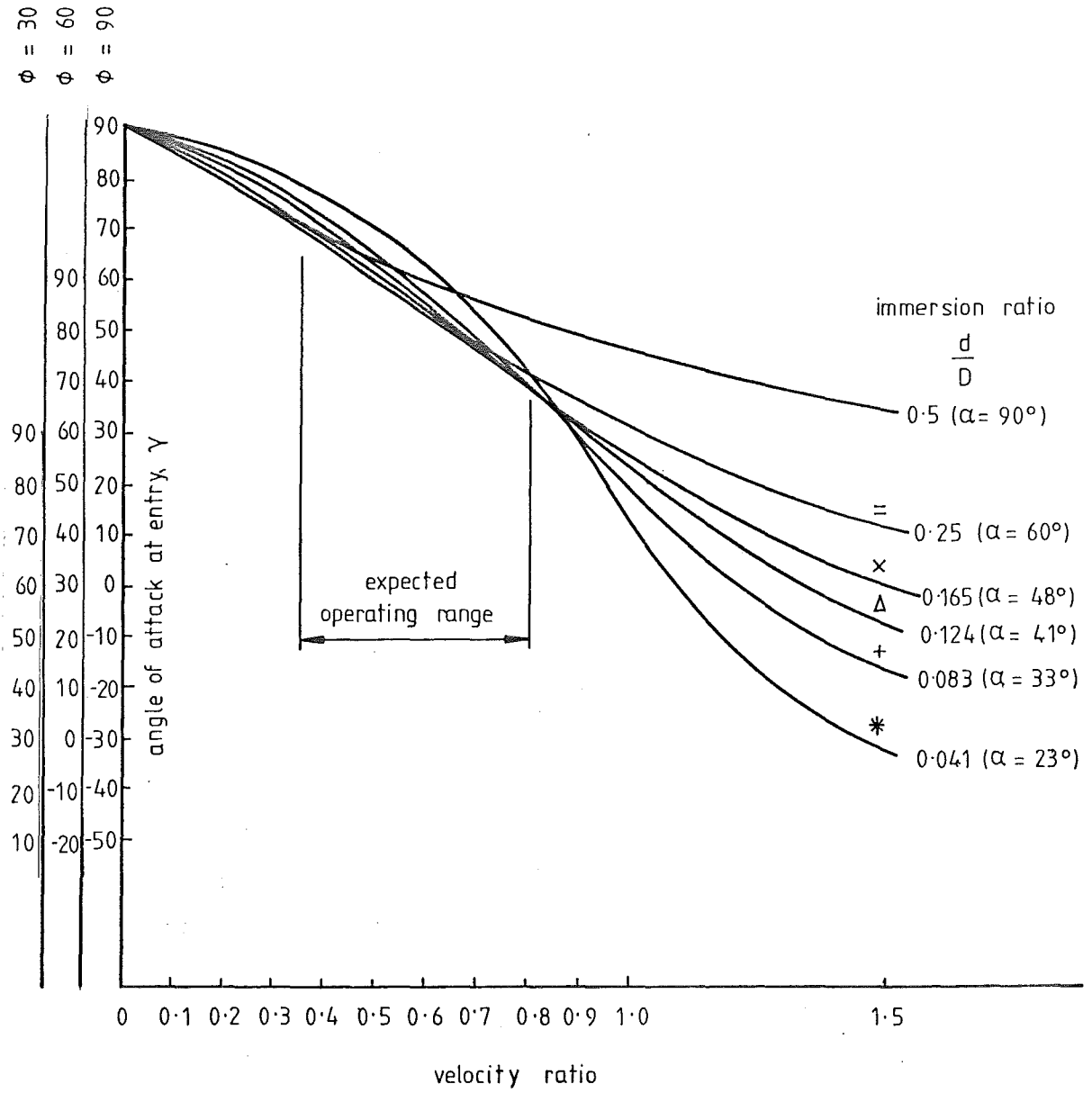


FIGURE 4.13 ANGLE OF ATTACK AT ENTRY AGAINST VELOCITY RATIO

the diagram to apply to other blade angles. Once again depth ratios marked on the horizontal axis indicate the blade entry conditions at these immersions.

The main features of note are:

- (1) As the velocity ratio decreases (rps increases for a given V_0) the angle of attack γ approaches a constant value.
- (2) For a given velocity ratio the angle of attack at entry does not vary greatly over the range of expected immersion depths.

This second point is examined further in the next section (4.6.4).

So far conditions at the blade tip only, have been considered. Any other part of the blade will have a different velocity vector diagram, and a different velocity ratio associated with it, with the consequence that the angle of attack will vary chordwise along the blade. Further, the angle α will be different for different points on the blade surface (unless it is a radial blade with $\phi = 90^\circ$). These effects are sketched in Fig.4.12 and at this stage they are simply noted as complications to the basic concepts.

4.6.4 Blade Angle of Attack at Entry

Since later sections show that most of the water momentum change would normally take place at the instant of blade entry, it is of some value to replot Fig.4.11 as angle of attack at entry against velocity ratio, as shown in Fig.4.13. An expected operating range of velocity ratios is indicated and once again, although the diagram is drawn for a blade angle $\phi = 90^\circ$, a simple shift of the vertical axis enables it to be used for any other blade angle as shown.

Several features are of note:

- (1) For the expected velocity ratio operating range indicated, the angle of attack curves for different immersions are all clustered together. This is specially so for the midrange of immersion ratios ($\frac{d}{D} = 0.08$ to 0.2).
- (2) Angle of attack, γ , for all immersions increases as the tip speed is increased (that is, as velocity ratio is decreased).
- (3) This increase in angle of attack amounts to about 30° over the expected operating range of velocity ratios.

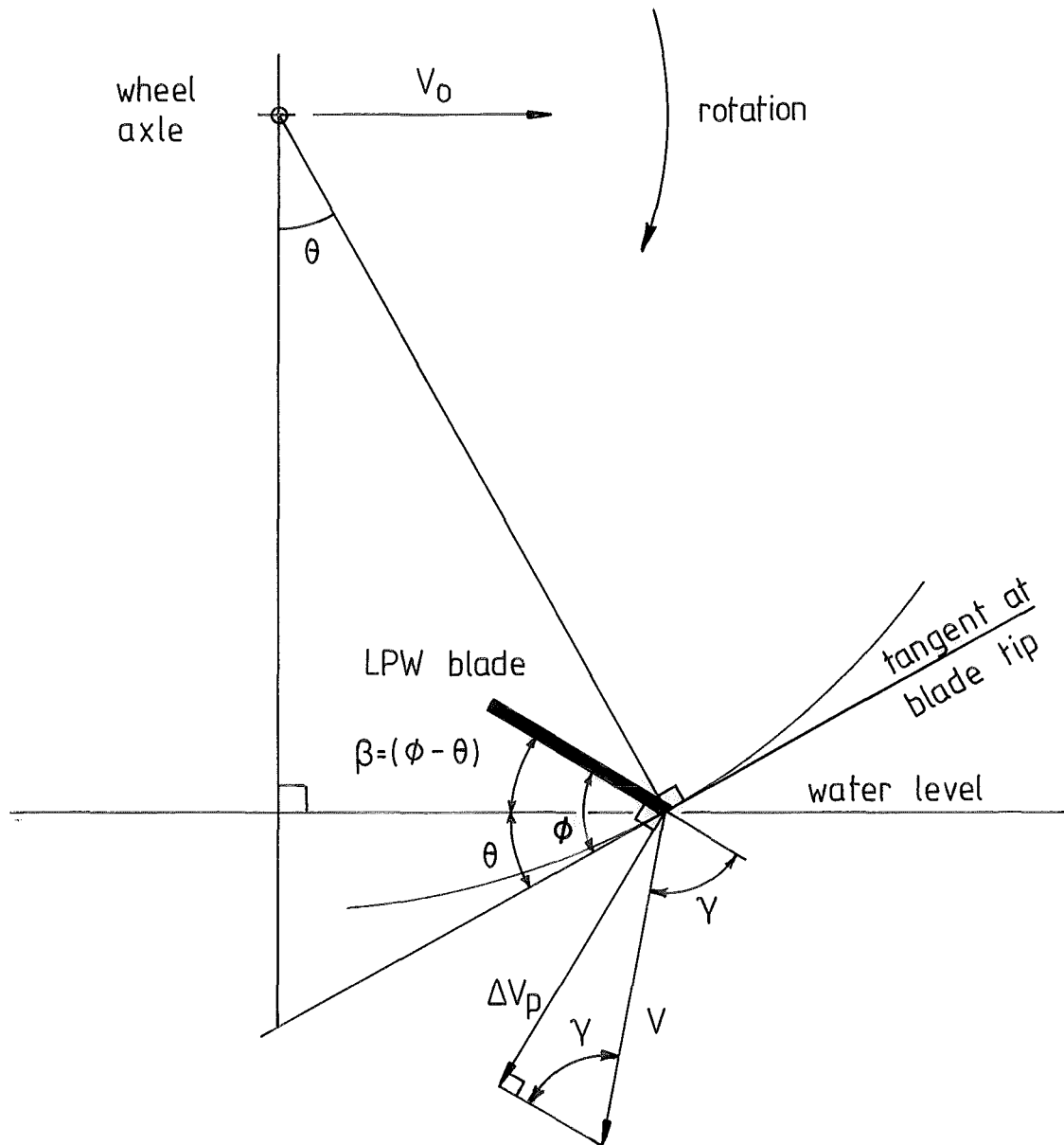


FIGURE 4.14 SHOWING DERIVATION OF ΔV_p AND β

One further point is that for some blades ($\phi > 90^\circ$) it is found that the entry conditions may not be the most significant. Instead, some point after blade entry is where most of the momentum change takes place. (See section 4.6.6 on maximum velocities.) If this is the case, the same diagram may still be used if the family of immersion ratio curves is read instead as a family of curves of α (the angular position in the blade passage where most momentum exchange takes place) as shown in parentheses in Fig.4.13. As noted earlier this diagram still only applies to conditions at the blade tip, and the angle of attack at entry would in fact vary along the blade chord resulting in a more complex picture of blade flow conditions than this analysis presents.

The implications of this diagram are that for a given velocity ratio the flow direction relative to the LPW blade tip at entry is almost independent of fairly large changes in immersion, so that in designing a blade, the angle of attack at entry may be chosen on the basis of velocity ratio, and blade angle alone, with small regard for changes in immersion.

4.6.5 Maximum Blade to Water Velocities

It is apparent from the preceding sections, especially 4.6.2, that the velocity of the LPW blade relative to the water varies considerably during the blade passage. It would therefore be expected that somewhere in the passage the blade would impart a maximum velocity to the water and this would be in some direction determined by the vector geometry of the flow at that point. Once this had occurred, and assuming such a velocity was much greater than any gravity-induced velocity, the blade would slow down relative to the accelerated water. The water would then leave the blade to move away at this maximum velocity, possibly allowing air to move in to take its place. (Since the LPW is operating through the water surface air entry readily occurs.) Once this has happened no more momentum exchange could be caused by the blade unless it caught up again or encountered more water.

From this point it remains to construct vector diagrams to determine the magnitude and direction of these maximum velocities relative to a fixed frame of reference in the water.

While vector diagrams will be used here, it is realised that they do not always accurately predict flow velocities and drag forces (1)

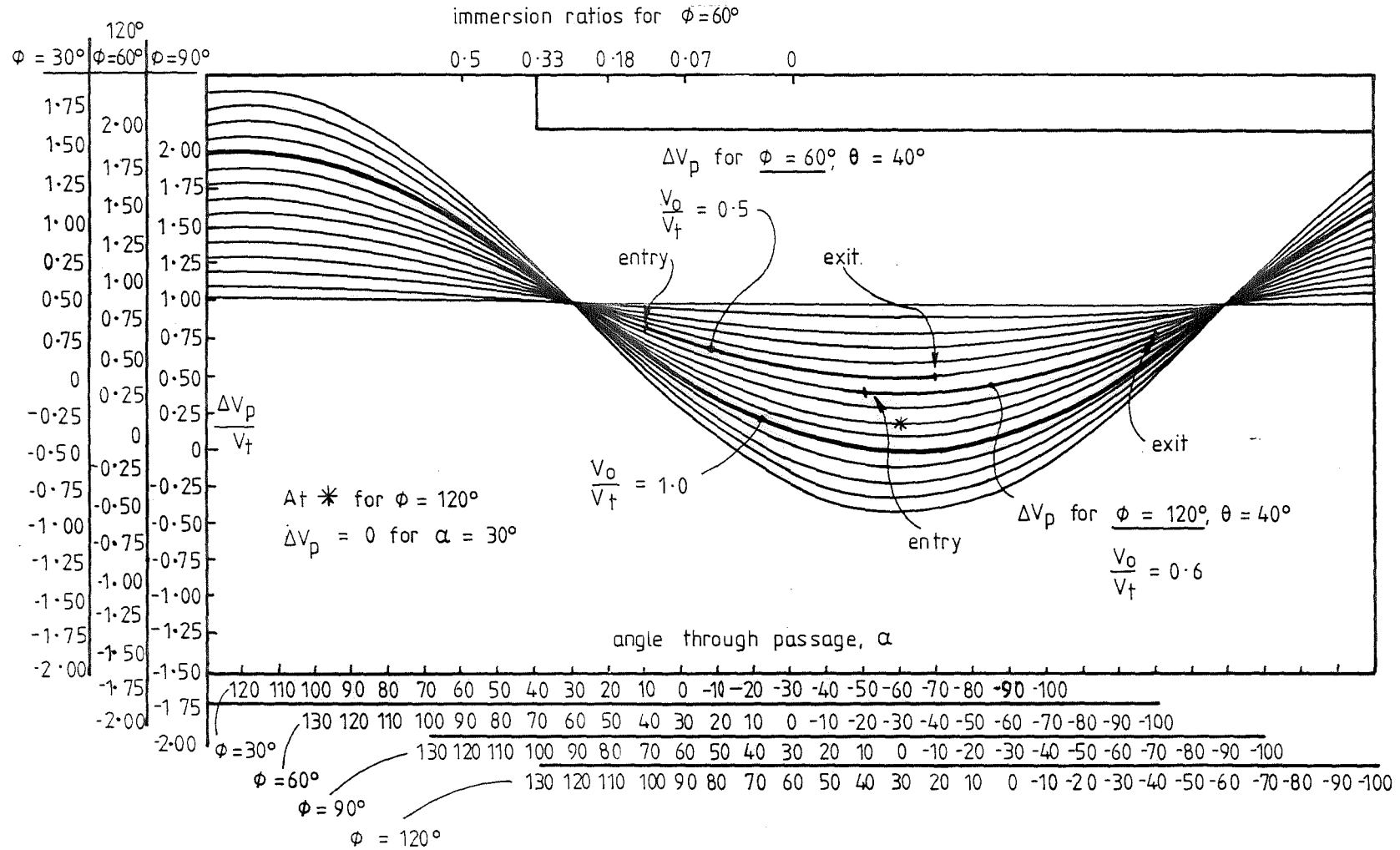


FIGURE 4.15 PERPENDICULAR VELOCITY, V_p , IN A RATIO WITH V_t , AGAINST α .

FOR $\phi < 90^\circ$ V_p MAX OCCURS AT ENTRY.

especially at small angles of attack. Also the assumption is made that velocity changes cannot be transmitted to the water in a direction parallel to a flat plate surface. Thus changes in flow direction are considered to take place vectorially and only in a direction perpendicular to the blade surface.

4.6.6 Maximum Perpendicular Velocity

An expression for the vector velocity change perpendicular to the blade, ΔV_p , may be written directly from Fig.4.14

$$\Delta V_p = V \sin \gamma \quad (4.19)$$

where: V may be found from equation (4.17) and is the velocity of the blade tip relative to the water.

γ may be found from equation (4.18).

It is helpful to examine a plot of this expression to see how the maximum perpendicular velocities may occur. Fig.4.15 is such a plot. The axes may be shifted horizontally and vertically to define the plot for other blade angles as shown. Immersion ratios are marked on the axes for $\phi = 60^\circ$ and a series of curves for different velocity ratios are plotted. Points of note are :

- (i) For blade angles less than 90° ΔV_p is maximum at blade entry. This is most significant.
- (ii) For blade angles greater than 90° ΔV_p is maximum at blade exit.
- (iii) For blade angles greater than 90° , depending on immersion depth, ΔV_p may decrease from its value at entry (which would allow the water to move away from the blade) before increasing again to its maximum at blade exit.
- (iv) It is possible to arrange the blade angle, velocity ratio and immersion depth so that $\Delta V_p = 0$ at entry (as marked in the figure). ΔV_p then increases steadily through the blade passage. (This situation might be expected to provide the smooth application of force normally required with hydrodynamic machinery. This idea, however, is taken no further here since the LPW with the required blade angle generally has very little or no lift force component.)

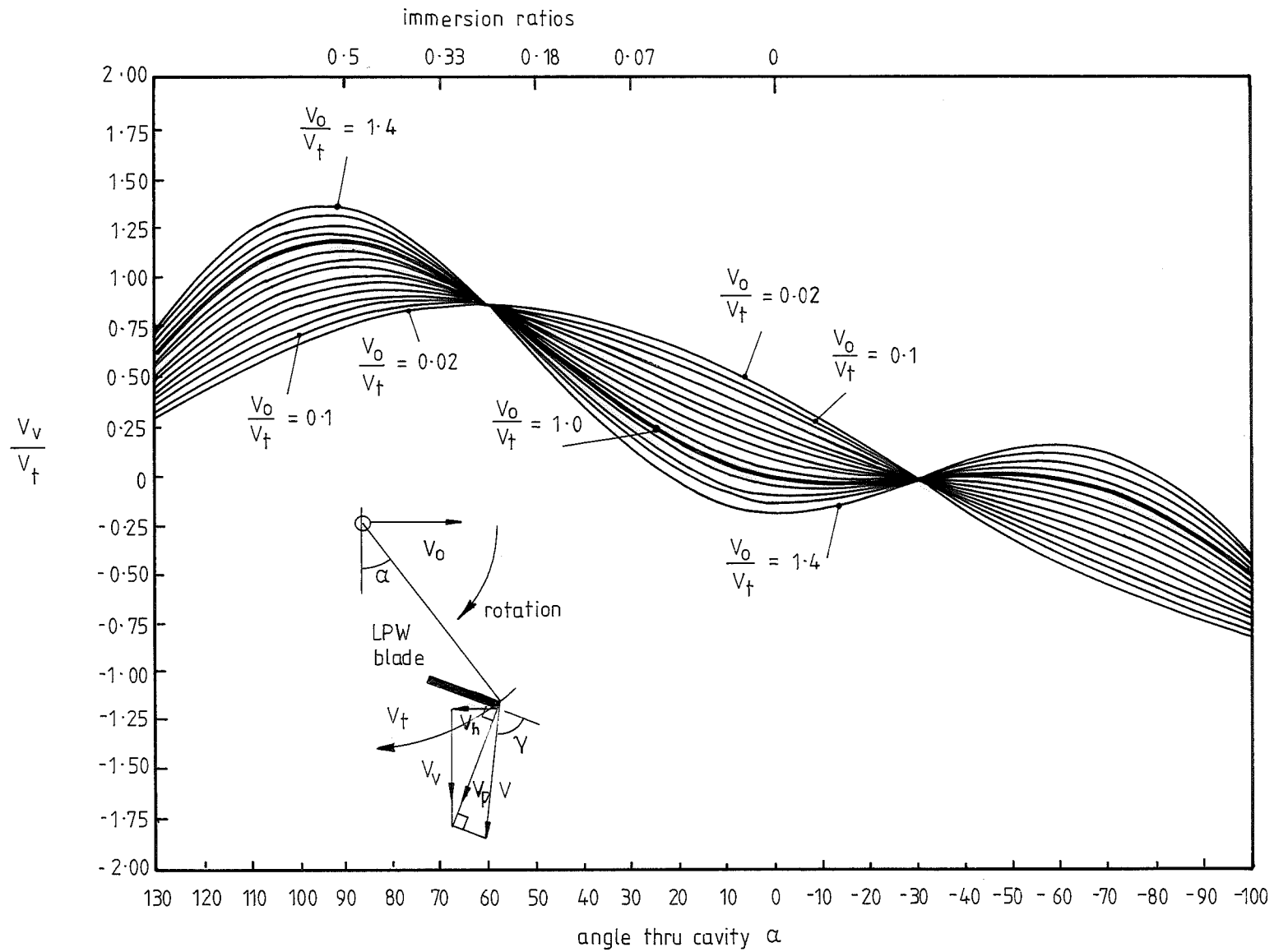


FIGURE 4.16 VERTICAL COMPONENT OF MAX PERPENDICULAR VELOCITY V_v , AS A RATIO WITH BLADE TIP VELOCITY V_t AGAINST α , FOR $\phi = 60^\circ$

- (v) Apart from the case where $\Delta V_p = 0$ at entry, all other entry conditions require a theoretically infinite acceleration to the entry velocity at blade entry. In practice this would be expected to produce shock loadings on the LPW, causing splash and shock losses in the water, and high impulsive forces on the machinery.

From these points the main feature is that maximum perpendicular velocity changes occur at water entry for all blades with angles less than 90° .

4.6.7 Vertical and Horizontal Components of Perpendicular Velocity

This perpendicular velocity change may be resolved into horizontal and vertical components which are required for the estimation of the thrust and lift forces. Relative to the frame of reference fixed in the water these components will also be the horizontal and vertical components of the final water velocity so that Δ is now left out of the relations.

The components of V_p may be derived in two ways. If they come from Fig.4.14 and equation (4.19), they include γ , which is difficult to deal with as shown in Fig.4.10. An alternative derivation which is longer avoids this complication and it is outlined in Appendix 3. The resulting equations are :

$$V_h = \sin(\phi - \alpha)(V_t \sin \phi - V_o \sin(\phi - \alpha)) \quad (4.20)$$

$$V_v = \cos(\phi - \alpha)(V_t \sin \phi - V_o \sin(\phi - \alpha)) \quad (4.21)$$

where V_h = horizontal component of V_p , the perpendicular velocity.

V_v = vertical component of V_p .

Note that α is used for the blade angular position through the cavity. This is because these equations hold for any position in the cavity. For blade entry, however, α may be replaced by θ , the depth angle.

These equations when plotted give results as indicated for V_v in Fig.4.16 (for $\phi = 90^\circ$). However the plot shown cannot be readily

adapted to plots for other blade angles by simple shifts in the axes and in themselves such plots do not indicate much of value.

We are now in a position to reassess the thrust and lift equations (4.5) and (4.11) of section 4.3 in terms of the induced mass of section 4.5 and maximum water velocities between the blade and the water.

4.7 THE IMPULSE THEORY OF LPW FORCES

In this section the induced mass concept of section 4.5 is combined with the maximum velocity expressions (4.20) and (4.21) of section 4.6.7 to modify the momentum model of section 4.3 into a more refined analysis of LPW forces. The conditions of flow are assumed as in previous sections with the LPW in the high speed planing mode. The mass of water now used is considered to be the induced mass rather than the whole of the entrained mass. The velocity to which the wheel accelerates the water is now considered to be the maximum water velocity reached perpendicular to the blade, and this generally occurs at blade entry. The magnitude and direction of this velocity is resolved into horizontal and vertical components in the maximum velocity expressions, and thus the thrust and lift forces may be determined.

From these considerations the simple thrust equation (4.5) $T = \dot{m}V_h$ may be rewritten using equation (4.16) and equation (4.20) as:

$$T = \dot{m} \sin(\phi - \theta) (V_t \sin \phi - V_o \sin(\phi - \theta)) \quad (4.22)$$

$$\text{or } T = \frac{\pi}{8} c^2 s \rho n B \cdot \sin(\phi - \theta) (V_t \sin \phi - V_o \sin(\phi - \theta)) \quad (4.23)$$

Similarly the lift equation (4.11) $L = \dot{m} V_v$ may be rewritten:

$$L = \dot{m} \cos(\phi - \theta) (V_t \sin \phi - V_o \sin(\phi - \theta)) \quad (4.24)$$

$$\text{or } L = \frac{\pi}{8} c^2 s \rho n B \cdot \cos(\phi - \theta) (V_t \sin \phi - V_o \sin(\phi - \theta)) \quad (4.25)$$

where, as usual: L = lift force

T = thrust force

c = blade chord

s = blade span

n = rps

B = number of blades on the wheel

ϕ = blade angle

θ = depth angle

V_t = blade tip speed relative to LPW axis

V_o = wheel speed of advance.

Note that although the depth angle θ is used the relations still hold for any position through the cavity where the maximum perpendicular velocity would be reached. If the angle, α , representing such a position replaces θ then the relations may be used for such unusual circumstances.

Note also that if V_t is replaced by πnD the relations become quadratics in the wheel revolutions, n . Thus force-rps plots would have a parabolic form. The relations correspond to the parabolic section of the force-rps plots (Fig.1.6) since at this point no consideration has been given to the effects of cavity intrusion.

4.7.1 The Impulse Theory After Surface Cavity Intrusion

As was noted in section 4.5 the induced mass flow rate may be increased by an increase in wheel revolutions, n , or in the number of blades, B . It will be apparent that such increases will not increase the induced mass flow rate indefinitely. As wheel revolutions are further increased, cavity intrusion occurs and the cavity left by the previous blade approaches the area of entry of the incoming blade. The induced mass magnitude will be affected by the presence of this new surface as described in section 4.5. Eventually the cavity will be encroaching upon the water surface that would have been encountered by the incoming blade. (See Fig.1.7.) This is surface cavity intrusion.

Under such circumstances it is difficult to estimate theoretically just what the added mass per blade might be, and a number of unsuccessful attempts have been made during the course of this project. The difficulty has been sidestepped by treating the situation as follows:

Once cavity intrusion has advanced so that the width of water surface each blade encounters is less than the chord width of the blade, the mass acted upon is much more like the full entrained mass of section 4.3 as shown in Fig.4.1. So for this situation the mass used in the force expressions 4.22 and 4.24 is allowed to remain as the full entrained mass, \dot{M} (equation 4.7, section 4.3). Thus the expressions for the force after surface cavity intrusion use this mass flow

rate instead of the induced mass per blade, and become:

$$T = \rho V_o \sin(\phi - \theta) (V_t \sin \phi - V_o \sin(\phi - \theta)) \quad (4.26)$$

$$L = \rho V_o \cos(\phi - \theta) (V_t \sin \phi - V_o \sin(\phi - \theta)) \quad (4.27)$$

It will be noted that these expressions, in contrast to (4.23) and (4.25) are linear in V_t (or n) corresponding appropriately to the linear section of the force-rps plots (Fig.1.6).

4.7.2 Dimensional Analysis and the Impulse Theory

It would be expected from Dimensional Analysis that the forces should increase as the square of the velocity or as the square of the characteristic dimension. A check of expressions 4.23, 4.25, 4.26 and 4.27 for the forces both before and after cavity intrusion verifies that this is the case as long as the velocity ratio is kept constant for similarity of flow, and it is noted that the tip velocity, V_t , is related to the wheel revolutions, n , by :

$$V_t = \pi n D$$

where: D = wheel diameter.

4.8 OTHER THEORETICAL APPROACHES AND THE DEVELOPMENT OF MASS FLOW COEFFICIENTS

It has been one of the tasks of the project to develop a comprehensive theory of LPW operation which could both explain how LPW forces are generated and be used to predict forces in untested situations. The development of the present theory is only one of a number of theories tried. Each theory used, and found inadequate has been helpful in that it has suggested that the concepts involved are not instrumental in the generation of LPW forces.

It was found, for example, that the forces before cavity intrusion are in fact considerably larger than those predicted by the impulse theory already described. Some time was spent in trying to discover whether this discrepancy could be accounted for by the concept of cavity induced mass. (1) There were difficulties in that this concept is normally used for deeply immersed cavities and the required case of entry through the surface did not readily comply. Ultimately this line was fruitless, neither proving nor disproving the value of the

concept in this context and therefore not adding to the understanding of LPW forces.

Another approach, which was imagined relevant, was Wagner's wedge entry theory. (1) This theory takes account of boundary migration on sloping surfaces entering the water and while it applies to symmetrical wedges it was felt that it could be adapted to LPW blades. A number of calculations and refinements failed to improve the present impulse theory to a level which would make the combined theories a convincingly better model of the real case, and it is therefore tentatively concluded that the enhancement of entry impact forces as described by Wagner's wedge entry theory do not contribute significantly to LPW forces.

One further discrepancy deserves mention: the impulse theory as it stands predicts, under certain circumstances, that the LPW forces remain positive to velocity ratios well beyond unity. (For example with blade angle $\phi = 60^\circ$ and depth angle $\theta = 60^\circ$ in equation 4.25.) Experimental results do not wholly support this, and it became clear that this is because the impulse theory is only concerned with conditions at water entry and it ignores everything thereafter. Attempts were made to incorporate expressions to take into account the fact that the water catches up with the blades at the bottom of their passage at velocity ratios near or greater than unity, thereby introducing negative components of force. These attempts, however, did not satisfactorily model the real situation and introduced considerable complication to the theory. Once again the attempt was abandoned, but it suggested that the reasons the experimental forces fall to zero just before or after the velocity ratio reaches one, are rather more complex than a simple subtraction of flat plate drag forces at the bottom of the blade passage.

For this project then these extra theoretical models have been tried and abandoned. While the present impulse theory does, in large measure, clarify what is happening between the LPW and the water there are the expected discrepancies between theory and practice which at present may be most usefully dealt with by employing coefficients.

Chapter 9, analysing the experimental results for flat blades, contains a section (section 9.9) where coefficients are developed to adjust the magnitude of the mass flow in the equations to model the

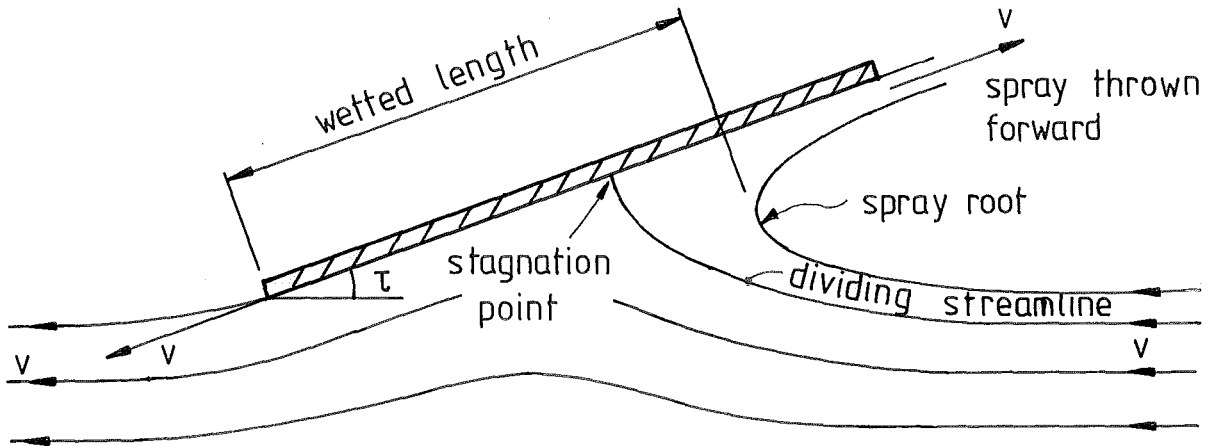


FIGURE 4·17 SPRAY SHEET THROWN AHEAD OF A PLANING PLATE.

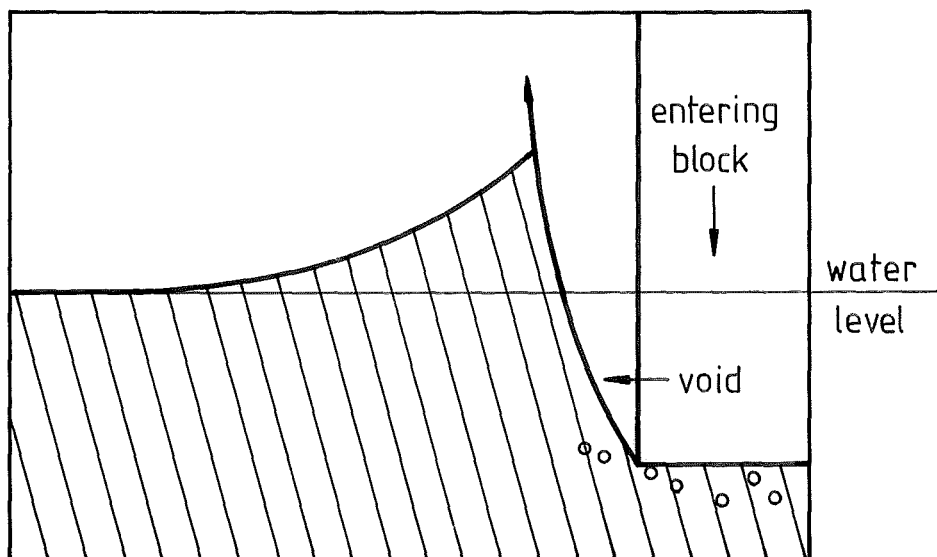


FIGURE 4·18 A SKETCH, TRACED FROM PHOTOGRAPHS, OF WAVE FORMATION AFTER ENTRY IN FLAT BOTTOM SLAMMING EXPERIMENTS.

(Ref: Chuang S.L. p.15)

real situation both before and after surface cavity intrusion, and for lift and thrust forces. These coefficients are used in the normal way, to multiply the mass flow in the appropriate force expressions (4.23, 25, 26, 27). While they have been imagined as coefficients of the mass flow rate only, since this has been seen to incorporate the most gross assumptions (discussed in section 4.5), they clearly also allow for any smaller discrepancies between the maximum velocity expressions, (4.20) and (4.21) and the real situation.

One further step remains to complete the present impulse theory, and that is to predict when surface cavity intrusion occurs, since this defines which of the two sets of relations must be used to calculate LPW forces.

4.9 REAL FLOW AROUND LPW BLADES

In the foregoing sections the effects of blade entry splash have been ignored, and the flow over the LPW blades during water entry and after immersion has been examined simply in terms of the net vector velocity changes occurring. The real flow situation is rather more complex than this and an examination of the actual water flow around the blades helps to explain the causes of bowsplash, and gives reasons for the discrepancies in the maximum velocity expressions, as well as providing a means of calculating the point where surface cavity intrusion begins to occur.

4.9.1 Bowsplash

Splash at blade entry may be examined in two ways. First, the entry of an inclined plane through the water surface is little different in terms of the flow it causes from the case of a planing surface. It is well known (1) that such a surface throws a thin sheet of spray ahead of itself as shown in Fig.4.17. Such a spray formation would also occur when LPW blades enter the water inclined to the surface. This splash formation while present at LPW blade entry is relatively insignificant compared to the other splash type.

The second splash type is more dramatic. It may be seen in terms of "Waves due to Local Impulse" as treated by Lamb. (2) Such theory shows how an impulse on the water surface (such as the sudden entry of the LPW blade) produces short wavelength, large amplitude

1. Wagner, 1932
2. Lamb, Art. 239, P.388

waves. Experiments on flat-bottom slamming (1) show how this occurs in practice so that just after a high speed blade entry the water surface would appear as shown in Fig.4.18. These waves are of some significance to LPW operation and theory for two reasons. Firstly, as the oncoming blade meets this rising surface the velocity between the blade and the water is increased. It may be imagined that under the right conditions this would cause an appreciable increase in the blade force and possibly a change in the depth angle θ at which the maximum perpendicular velocity is reached. At this stage this effect is simply noted as a possible discrepancy in the impulse theory.

Secondly these waves are apparently instrumental in causing bowsplash. While no rigorous confirmation of this has been done experiments show that if, under the right conditions in the planing mode, the oncoming blade encounters such a wave there is a regenerative buildup of water ahead of the wheel. It seems that this occurs since each descending blade encounters the splash, traps air in it and this causes the bowsplash to grow so that the next descending blade encounters the same conditions but higher above the water surface. Ultimately the blades are pushing a mound of water ahead of the wheel. This is shown in Figs. 4.19 (A)-(E) and may be compared with the cylinder in Fig.4.34, ahead. It is pointed out in Chapter 12 that this is apparently a hindrance to lift-off for LPW craft.

No analysis has yet been attempted of the phenomenon, since in practice it ceases to be a problem if the velocity ratio is kept high enough to be clear of surface cavity intrusion.

4.9.2 Free Streamline Theory and LPW Blades

Once the fast moving LPW blade has become immersed it may be compared with the case of a flat plate fully immersed in a flow, with a cavity of ambient pressure. (2) For such a plate the flow divides at the stagnation point, moves in both directions across the plate surface with a velocity relative to the blade surface equal to its incoming velocity, then separates from the edges to form the cavity behind the plate as illustrated in Fig.4.20.

Several points may be noted :

- (1) The stagnation point may be found analytically. (3)
- (2) The centre of pressure may be similarly determined.

1. Chuang, S.L., P.15
2. Batchelor, 6.13, P.498

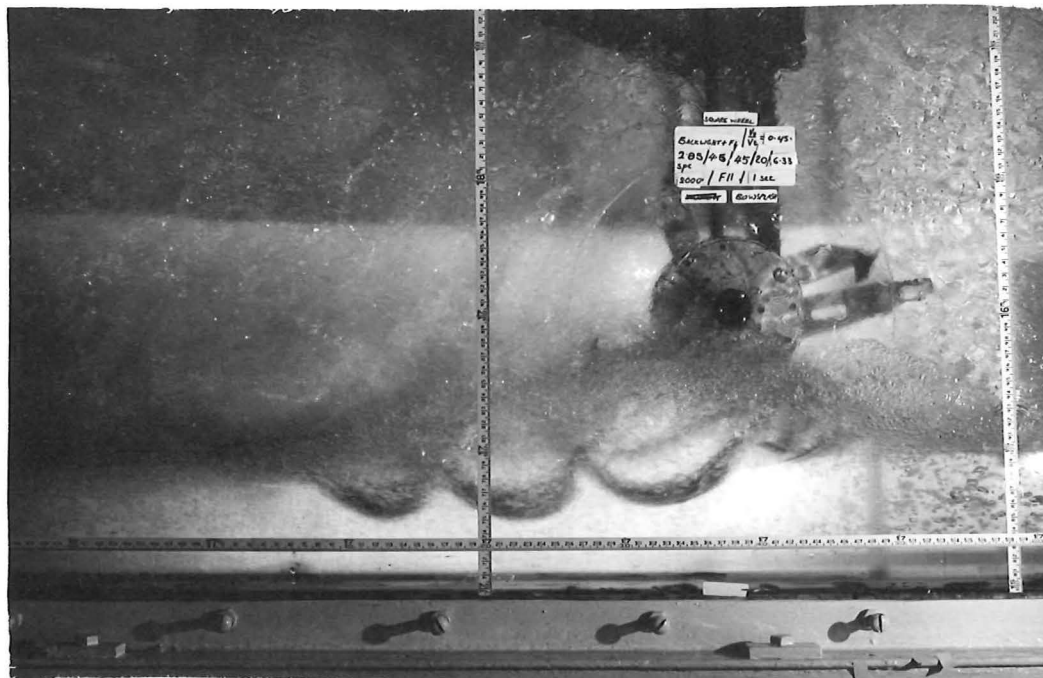
3. Birkhoff & Zarantorello II.2,
P.28.



632/38A

(A) INCIPIENT BOWSPASH $V_o/V_t = 0.45$

CONDITIONS: $D=0.242$ m, $\phi=45^\circ$, $d/D=0.083$, 4 blades, $c=25$, $s=76$
 SUPERCRITICAL FLOW, $V_o=2.85$ m/s, PLANING



632/37A

(B) BOWSPASH $V_o/V_t > 0.45$

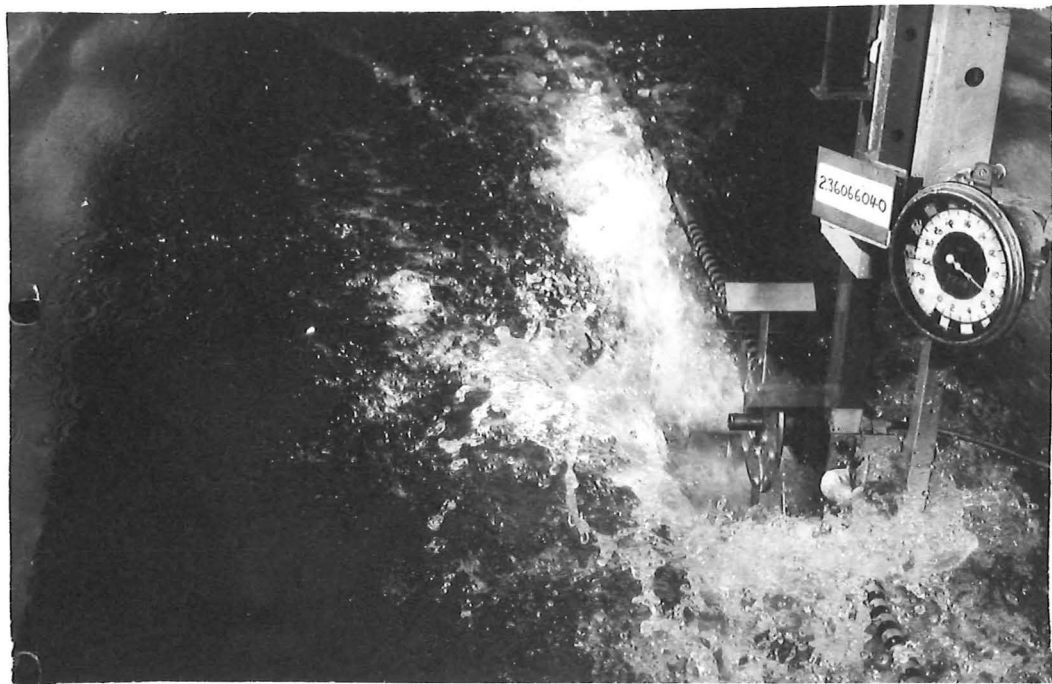
FIGURE 4.19: (A) AND (B) STROBOSCOPIC PHOTOGRAPHS OF BOWSPASH
 IN THE GLASS-SIDED TANK



1300B/33A

(C) INCIPIENT BOWSPASH: $v_o/v_t = 0.62$.
 STD. WHEEL, PLANING, $v_o = 2.36$ m/s,
 $d/D = 0.17$, $n = 5$ rps

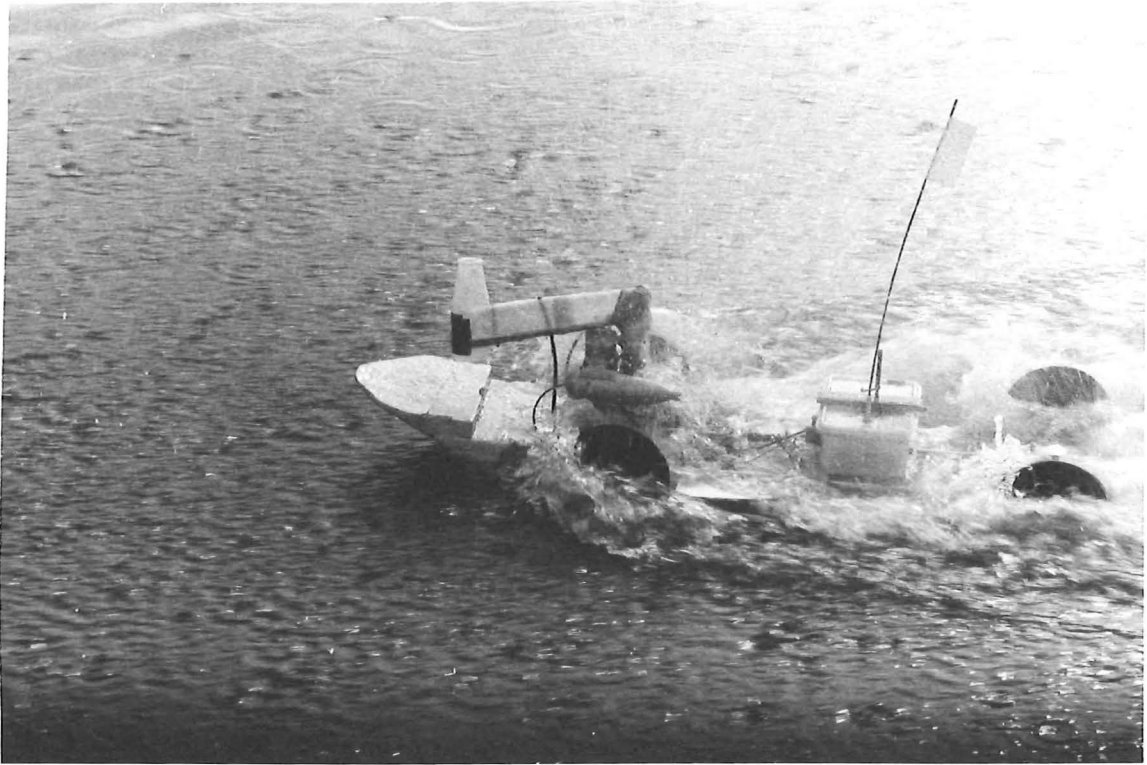
MOTION



1300B/35A

(D) BOWSPASH: $v_o/v_t = 0.41$, $n = 7.6$ rps

FIGURE 4.19: (C) AND (D) BOWSPASH IN OPEN WATER



43390/2

CONDITIONS:

WHEEL 12 (IN FIG.12.12)
 CRAFT FLOATING
 LPW'S PLANING
 LONG WHEELBASE VERSION

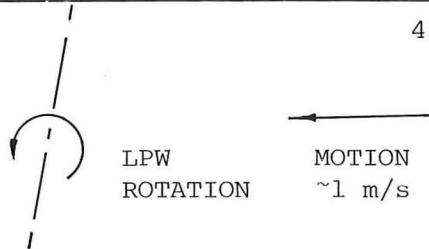


FIGURE 4.19 (E): BOWSPASH IS EVIDENT AT THE FRONT WHEELS OF THE MODEL CRAFT AND IS ENHANCED BY THE HULL'S BOW WAVE.

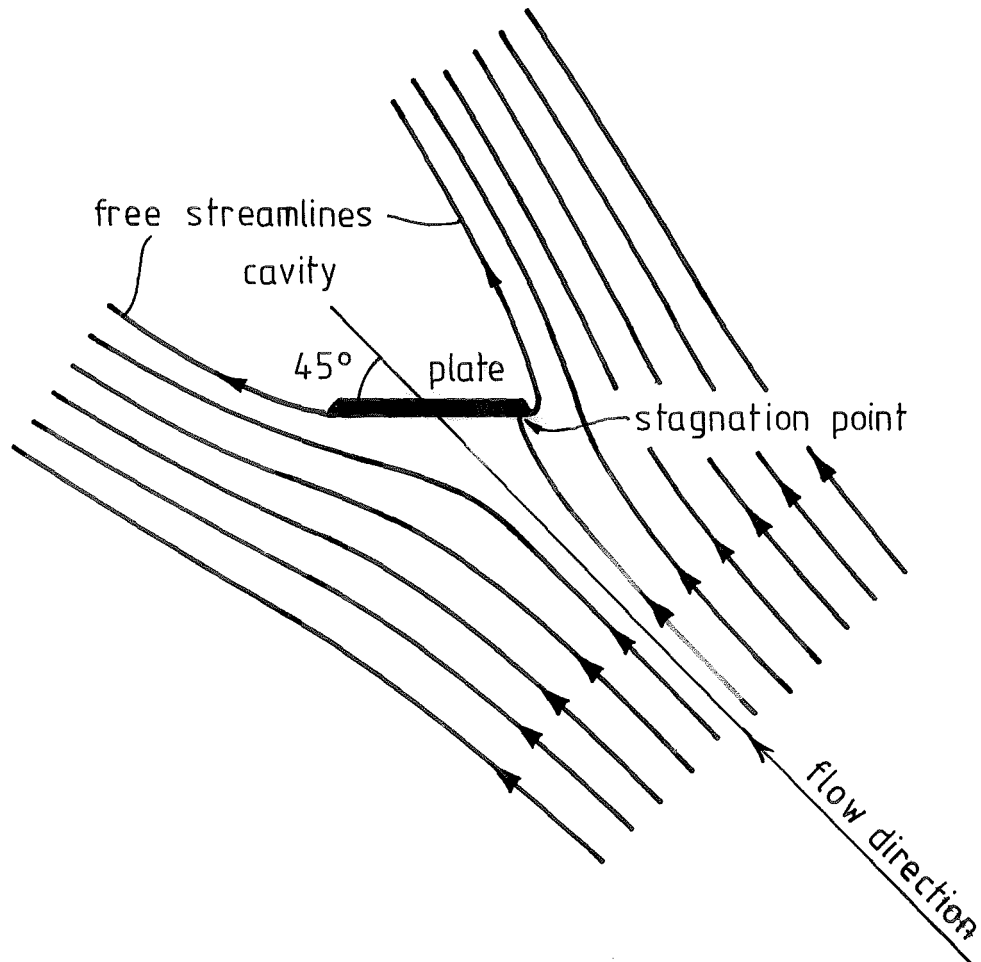


FIGURE 4.20 FLAT PLATE WITH AMBIENT CAVITY AT 45°
TO FLOW; FULLY IMMERSED.
(Ref: Birkhoff & Zarantonello plate 2, p340)

- (3) The velocity over the surface is known so the skin friction may be estimated analytically.
- (4) The shape of the edge of the cavity - the free streamlines - can be calculated. (1)
- (5) The pressure distribution can be calculated.
- (6) All these quantities may be determined for any angle of attack of the plate.

For the LPW in the displacement mode where the blades may be fully immersed and moving steadily with a ventilation cavity these points may be of value. It should be noted especially that point (3) above in relation to Fig.4.9 in section 4.6.2 supports Beardsley's claim (2) that the paddlewheel is likely to have lower frictional losses than the propeller since the relative velocity between the blades and the water is less than for a propeller.

Once again, however, the high speed case is more difficult to deal with.

4.9.3 Estimating Surface Cavity Intrusion Conditions

It would be expected that for the high speed case of LPW operation only the moments of blade entry would be of importance since it has been shown (section 4.6.6) that all the blade-water momentum exchange takes place at this point. Since this occurs essentially in the water surface it is difficult to decide whether any analysis should treat the flow as a symmetric impact on the water surface (3), or the beginning of the formation of a flat plate cavity at ambient pressure. (4) Both treatments require a number of assumptions. It is found, however, that for the purposes of the estimation of the surface cavity intrusion conditions, the cavity formation method is adequate, and it is assumed that there is unlikely to be a large discrepancy between the results of the two methods since the surface splash in the real situation looks not unlike the extension of the cavity of the immersing blades.

In the case of the paddlewheel blade the direction of motion is changing, as it moves in a curved path, and the blade is decelerating as it enters the water. Fortunately the theory of cavity formation

- | | |
|--|---------------------------|
| 1. Birkhoff & Zarantonello, II.2, P.28 | 3. Batchelor, 6.10, P.474 |
| 2. Beardsley, P.12 | 4. Batchelor, 6.13, P.498 |

can accommodate such irregular motion, as the principle of "independent expansion" (1) states that the cross section of the cavity expands relative to the path of the blade centre almost independently of the subsequent or preceding motion. This applies equally well for straight or curved paths.

It is now possible to construct a diagram which contains the essential features for the determination of the position of the cavity edge at a given time after the blade has entered the water. Such a diagram is shown in Fig.4.21.

The derivation of the equations for calculating the wheel revolutions at which surface cavity intrusion occurs is carried out in full in Appendix 5 which uses the Fig.4.21. A number of the equations used have been derived elsewhere in this report and they are simply restated here.

As they stand they require an iterative solution for n , the wheel revolutions. Such an iterative subroutine in Fortran is contained in Appendix 5.

$$V_t = n \pi D$$

$$V = \sqrt{V_o^2 - 2V_o V_t \cos \theta + V_t^2} \quad (\text{Equation 4.17})$$

$$\psi_1 = \sin^{-1} \left(\frac{V_o}{V} \sin \theta \right) \quad (\text{A5.3})$$

γ can be found from section 4.6.3 and equation 4.18

$$t = \frac{1}{Bn} \quad (\text{A5.4})$$

$$y_1 = \sqrt{\frac{4 \sin^2 \gamma V t c}{\pi \sin \gamma + 4}} \quad (\text{A5.1})$$

$$y_2 = \left[\frac{y_1}{\sin(\psi_1 + \theta)} \right] \quad (\text{A5.2})$$

$$n = \frac{V_o}{B(c \cdot \cos(\phi - \theta) + y_2)} \quad (4.28)$$

Notation for these equations is the usual notation and is itemised fully in Appendix 5.

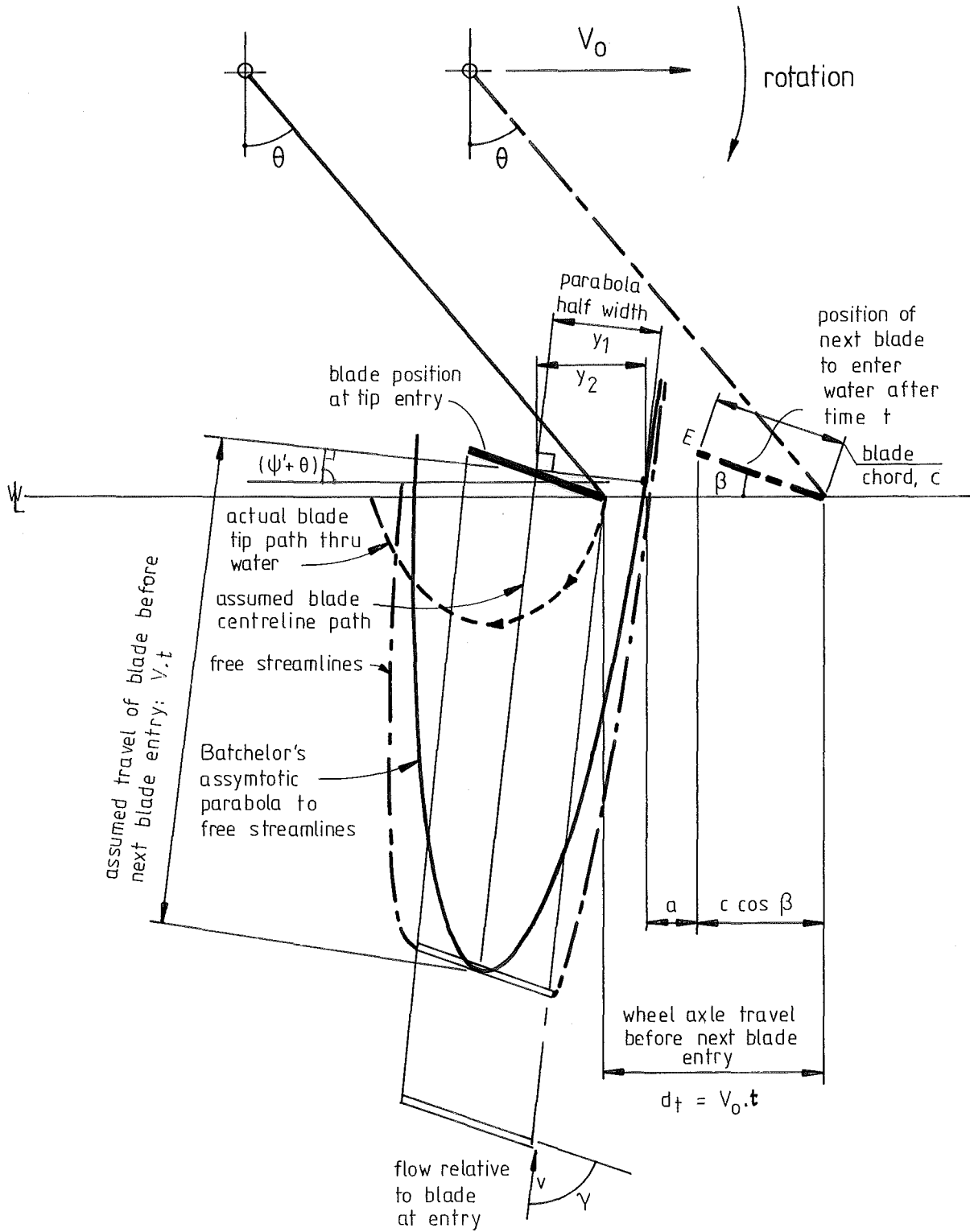


FIGURE 4.21 CONSTRUCTION FOR ESTIMATING SURFACE CAVITY INTRUSION CONDITIONS

It is unnecessary to use the iterative approach if it is required to know whether a given wheel revolutions, n , exists either before or after surface cavity intrusion in order, for example, to decide which coefficients to use. In the following expression a_1 is the distance between the cavity edge and a point near the heel of the incoming blade where the presence of the cavity edge causes cavity intrusion to occur. Thus, if a_1 is negative surface cavity intrusion is occurring.

$$a_1 = \frac{V}{nB} - c \cdot \cos(\phi - \theta) - y_2 \quad (4.29)$$

where a_1 positive: before surface cavity intrusion

a_1 negative: after surface cavity intrusion

n = value of rps with unknown cavity intrusion conditions.

By way of conclusion several general comments will be made about this method.

(1) It should be stated that this method is not rigorous. It contains some minor geometric assumptions as well as the assumptions involved in the theory used and an experimental adjustment. Nevertheless for most cases of LPW flat blade data its results are as close to the experimental results as is possible to estimate with the present set of data. (Exceptions are for very large or very small blade chords: see section 9.4.6)

(2) Once surface cavity intrusion has occurred the LPW blade is no longer acting as an immersed flat plate with a cavity since a free streamline leaves only one side of the blade. Under such circumstances it is likely that any thorough analytical treatment of the blade cavity would be better done by considering the blade as a planing plate.

(3) When the LPW is not immersed deeply the blades themselves may not become fully immersed at any stage during the blade passage. Under such conditions, the blades are acting more like planing plates and it becomes difficult to see just when cavity intrusion occurs. (See Fig.4.22.) Even so, the experimental results still indicate its presence, and a workable approach, has been to use the above equations, taking the blade chord value as no greater than the immersion depth.

(4) It is inevitable that with the use of this estimate of wheel revolutions at surface cavity intrusion, as well as the coefficient-

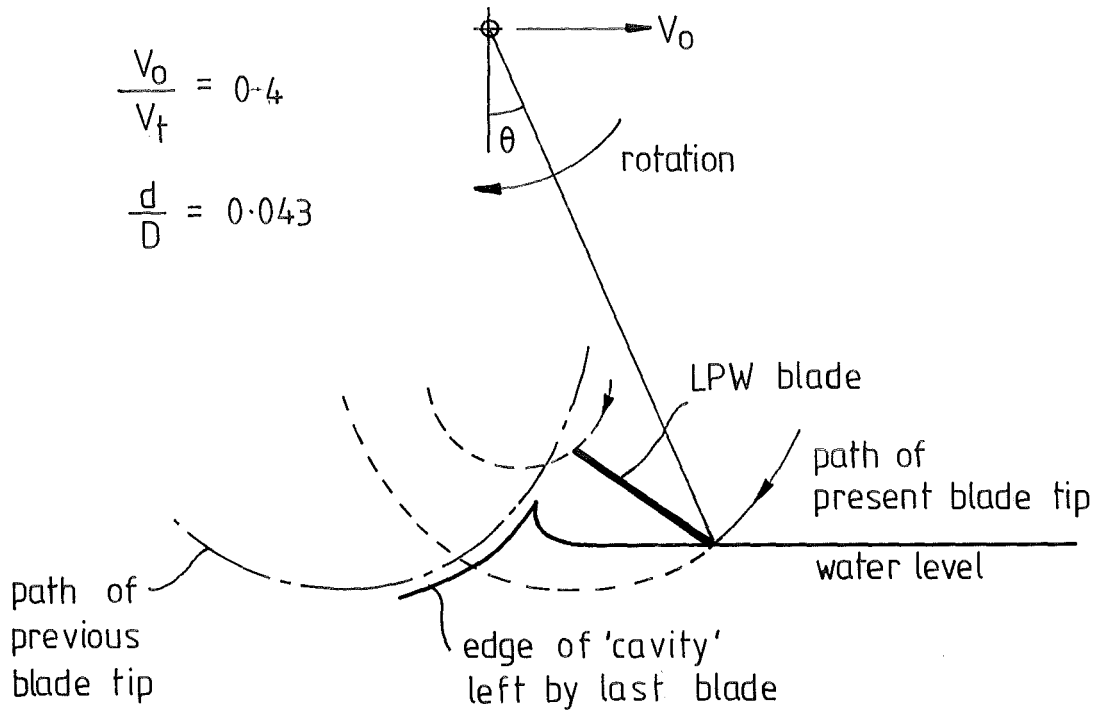


FIGURE 4.22 FOR SMALL IMMERSION DEPTHS IT BECOMES DIFFICULT TO ESTIMATE WHEN SURFACE CAVITY INTRUSION OCCURS. (Compare Figure 4.21.)

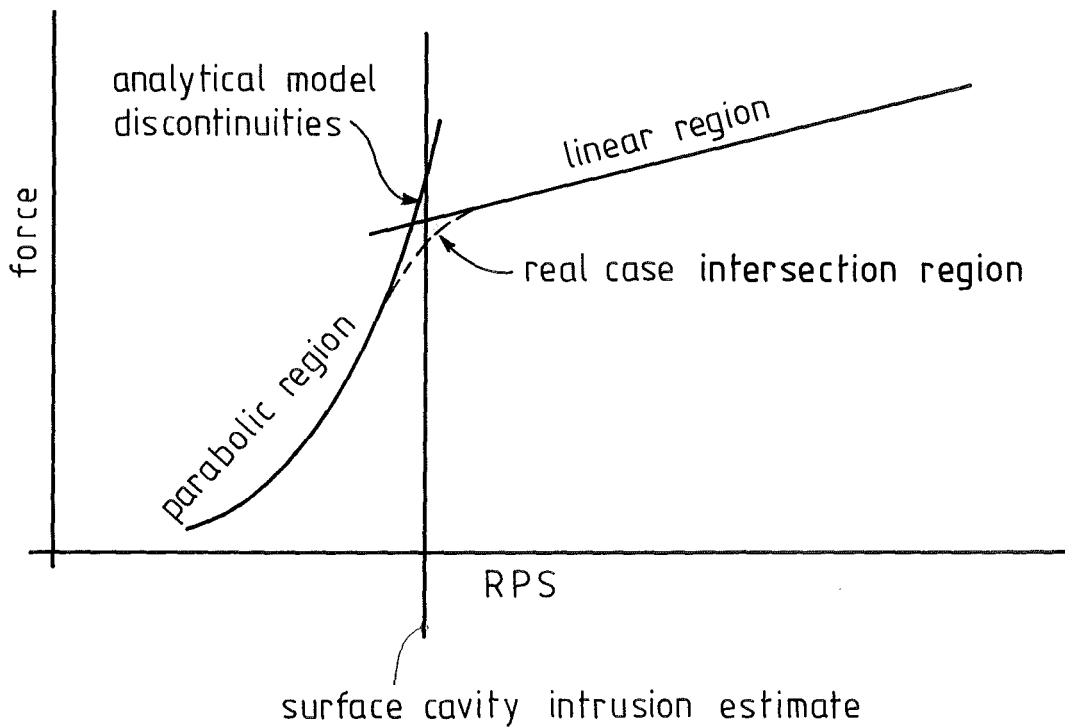


FIGURE 4.23 THE ANALYTICAL MODEL AT SURFACE CAVITY INTRUSION

adjusted theoretical results, there will be discontinuities between the force calculations at cavity intrusion, as sketched in Fig.4.23. This is simply accepted as one of the limitations of the present model, and it is pointed out that in the real case there is a gradual change from one curve to the other across the cavity intrusion point.

(5) Free streamline theory has been developed to such a stage where it can be used to predict the streamlines past a polygonal plate. Such theory could be used to design polygonal or curved LPW blades to control both cavity intrusion and bowsplash (see Chapter 10). Forces on such blades could also be determined using this theory. (1)

(6) In Appendix 6 calculations of LPW forces are undertaken using the impulse theory and the coefficients developed for use with it. When these coefficients are used it is not necessary to calculate where surface cavity intrusion occurs, since the parabolic and linear sections of the force-rps plots can be drawn as shown in Fig.4.23 and their intersection taken as the point where cavity intrusion occurs. Under some circumstances this is an easier method of calculation than that described above.

4.10 THREE RESULTS FROM THE IMPULSE THEORY

Three results of significance derive directly from the impulse theory as it stands, and these are examined before power consumption is considered.

4.10.1 Immersion Depth as Defined by the Lift to Thrust Ratio

If the vertical and horizontal velocity expressions (4.21) and (4.20) can be assumed, and if all the force is considered to occur impulsively at blade entry then a simple expression may be derived which defines the immersion depth angle θ , given only the blade angle ϕ , and the lift to thrust ratio. From (4.21) and (4.20) the lift to thrust ratio is :-

$$\frac{L}{T} = \frac{\cos(\phi-\theta) (V_t \sin \phi - V_o \sin(\phi-\theta)) \dot{m}}{\sin(\phi-\theta) (V_t \sin \phi - V_o \sin(\phi-\theta)) \dot{m}}$$

which reduces to:

$$\frac{L}{T} = \cot(\phi-\theta) \quad (4.30)$$

$$\text{or} \quad \frac{T}{L} = \tan(\phi-\theta) \quad (4.31)$$

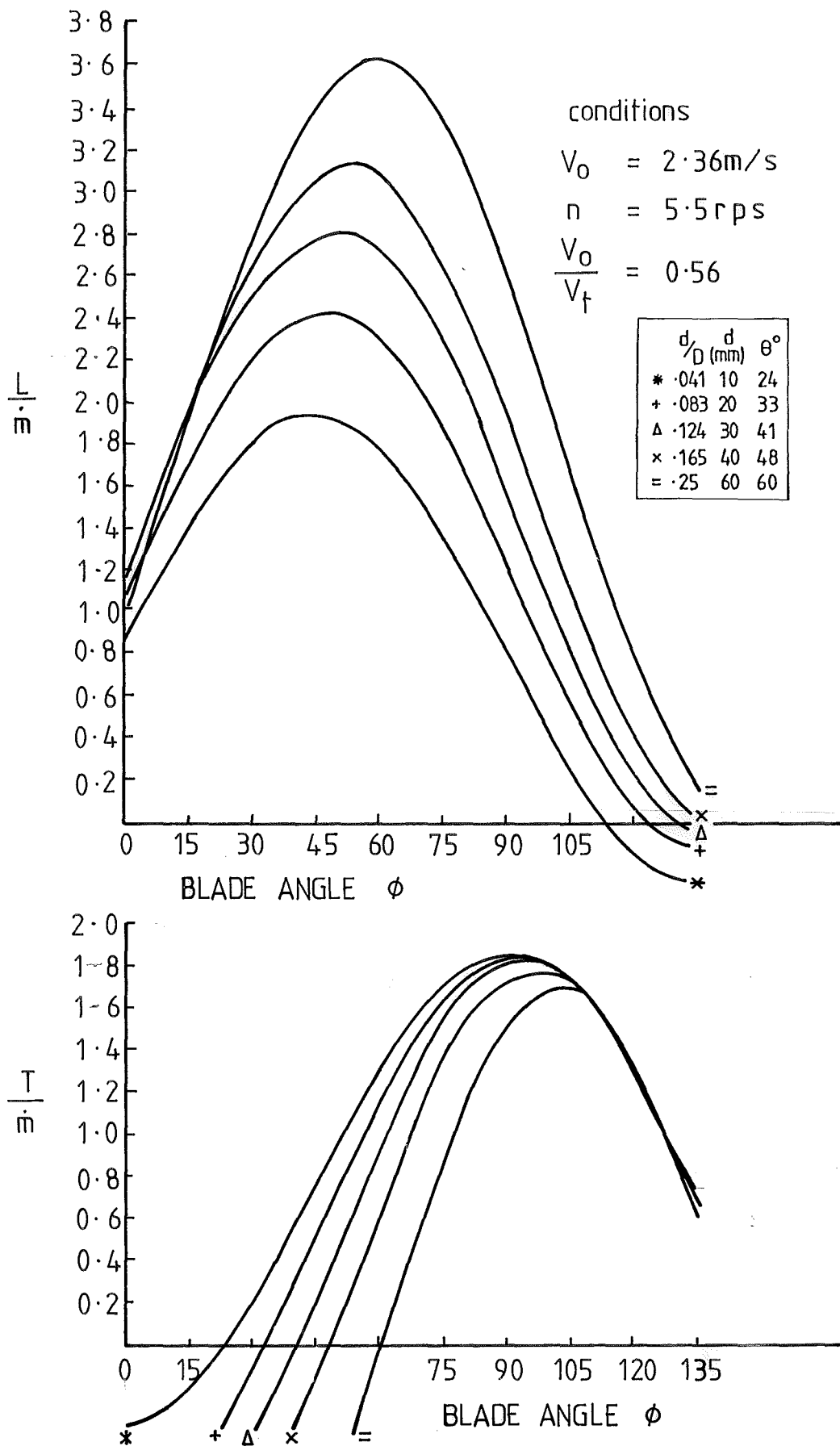


FIGURE 4.24 LIFT AND THRUST ENTRY FORCES WITH BLADE ANGLE BEFORE CAVITY INTRUSION

It is significant that these two expressions are independent of so many of the variables of the LPW, most notably velocity, velocity ratio, mass flow rate, and cavity intrusion, though such variables will be changed by changes in the lift to thrust ratio.

Such a useful expression points to a strong relationship between lift, thrust and immersion depth, and indicates, for example, that as craft drag (or thrust) increases for a given weight of craft the vehicle will rise higher in the water. This is an unexpected relationship which is most significant in clarifying the high speed performance of the LPW craft, the difficulties it experiences at lift-off when there might be a sudden change in drag force, and the bouncing motion of the model LPW craft.

4.10.2 Thrust and the Angle β

The angle $(\phi-\theta)$ occurs throughout the force expressions (4.23 for example) and in the thrust to lift ratio expression (4.31) above. It has been redefined as:

$$\beta = (\phi-\theta)$$

in Fig.4.14 earlier where it will be seen that it is the angle between the entering blade and the undisturbed water surface. If $\beta = 0$ the blade enters the water parallel to the surface, in which case there can be no horizontal component of the maximum perpendicular velocity of the flow relative to the blade, so that the thrust force becomes zero. (See section 4.6.7 on the maximum perpendicular velocity.) The fact that if $\beta = 0$, thrust is zero is also evident from the expressions for thrust, 4.23 and 4.26, where the term $\sin(\phi-\theta)$ must also be zero setting the whole expression to zero. The angle β has no such influence on the lift force in expressions 4.25 and 4.27 where the term $\cos(\phi-\theta)$ replaces the term $\sin(\phi-\theta)$ in the thrust expressions. The angle β therefore has a strong influence on the magnitude of the thrust force and little influence on the lift force, especially as β is often small in normal LPW operation.

If immersion is such that β is negative the thrust force will also be negative. This is a useful result and one which allows a quick appreciation of the thrust force that may be expected from a given set of conditions. Examination of Fig.4.24 in the next section shows the extent of this result in graphical form.

4.10.3 Blade Angle and the Force Relations

It is of value to examine the relationship between the lift and thrust forces with variation in blade angle, ϕ , using the impulse theory force expressions, (4.22) and (4.24). For this purpose V_o , V_t and \dot{m} are fixed and families of curves for different immersion depth ratios (or depth angles, θ) are plotted. The results are shown in Fig.4.24 and the following points may be noted from the figure:

- (1) Maximum lift force occurs for blade angles, ϕ , between 40° and 60° .
- (2) The magnitude of the forces depends upon the immersion, (which is a function of θ); and in general the trend with immersion for lift is opposite that for thrust.
- (3) Thrust force maximum values occur between 90° and 105° which are beyond the angles for which maximum perpendicular velocity occurs at blade entry. (See section 4.6.6 and Fig.4.15.) The most dependable maximum thrust values therefore occur at $\phi = 90^\circ$ since blade angles of greater than 90° are unlikely to be used.
- (4) For different values of LPW revolutions these curves would alter in magnitude and shift slightly, but for midrange conditions (velocity ratios near 0.6) the curves are representative of the trends.

4.11 POWER ALLOCATION IN THE IMPULSE THEORY

This section looks at how the LPW power is shared between the thrust, lift and losses, on the basis of the impulse theory of force generation. Its findings generally uphold the idea that the LPW craft could be a fast economic water craft.

4.11.1 Thrust Power and Thrust Losses in the Impulse Theory

The power absorbed by the LPW for propulsion or thrust may be divided into two parts. First there is that used to overcome the drag forces of the flying LPW craft. This is the useful thrust power denoted P_T . For the LPW craft in the flying condition this power is analogous to the power a road vehicle requires to overcome air drag. Second there is the power which is put into the water in the horizontal momentum exchange. It is lost as kinetic energy of the water after the LPW has passed. This power is denoted P_{lost} .

From expression (4.5) :

$$P_T = T V_o = \dot{m} V_h V_o \quad (4.32)$$

$$\text{and } P_{\text{lost}} = \frac{1}{2} \dot{m} (V_h)^2 \quad (4.33)$$

where T = propulsive or thrust force

V_o = speed of advance

\dot{m} = mass of water acted upon per second

V_h = final rearward component of horizontal velocity given to the water.

Both these expenditures of power are required to be kept to a minimum.

It is useful to examine these as ratios. The useful thrust power per unit thrust derives from (4.32) above and may be given in two forms :

$$\frac{P_T}{T} = \frac{\dot{m} V_h V_o}{\dot{m} V_h} = \frac{T V_o}{\dot{m} V_h} \quad (4.34)$$

and

$$\frac{P_T}{T} = V_o \quad (4.35)$$

Similarly the power lost may be written as a ratio with two results:

$$\frac{P_{\text{lost}}}{T} = \frac{\dot{m} (V_h)^2}{2 \dot{m} V_h} = \frac{V_h}{2} \quad (4.36)$$

and

$$\frac{P_{\text{lost}}}{T} = \frac{T}{2 \dot{m}} \quad (4.37)$$

It is further valuable to note that the ratio of the useful thrust power P_T to the power lost, P_{lost} should be maximised. Thus

$$\frac{P_T}{P_{\text{lost}}} = \frac{2 V_o}{V_h} \quad (4.38)$$

should be maximised.

These expressions provide a number of insights in LPW power:

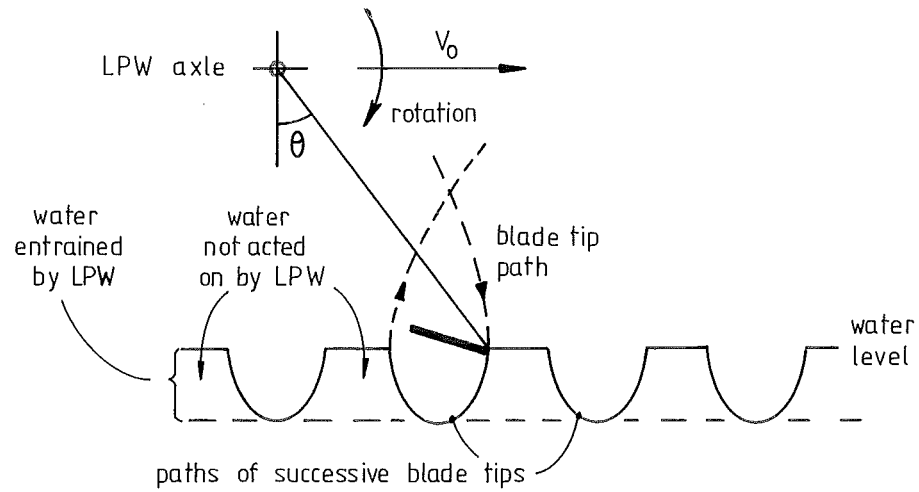


FIGURE 4·25 BEFORE SURFACE CAVITY INTRUSION THE LPW DOES NOT ACT ON ALL ENTRAINED FLOW

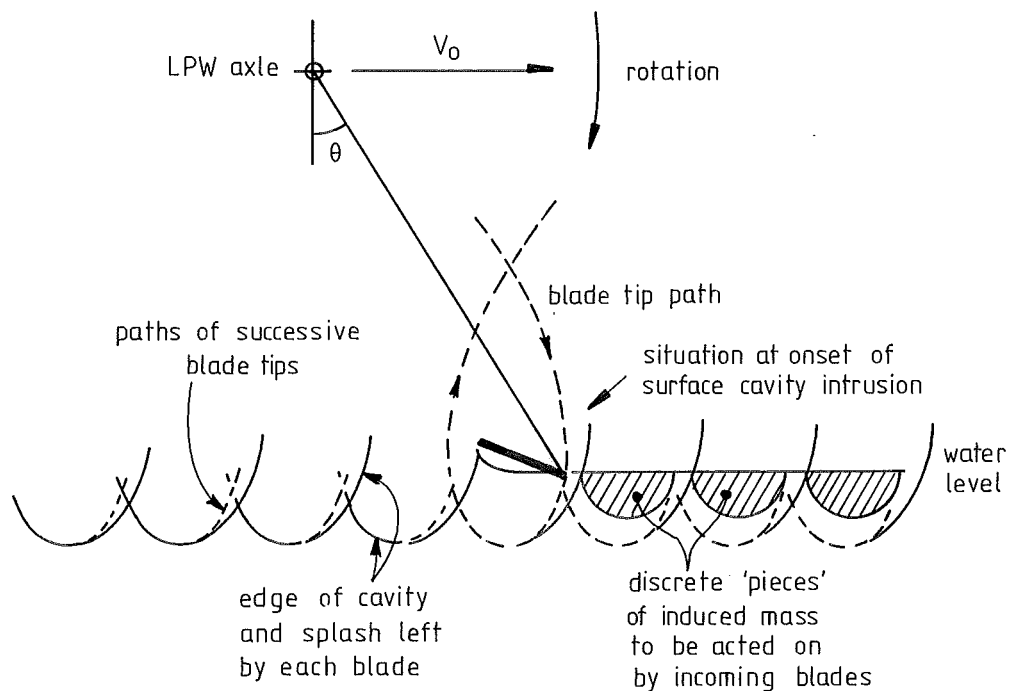


FIGURE 4·26 MAXIMUM USE IS MADE OF THE ENTRAINED FLOW AT ONSET OF SURFACE CAVITY INTRUSION.

(1) From (4.35) it is apparent that the useful power per unit thrust is proportional to craft velocity and is independent of velocity ratio, blade tip speed V_t and mass acted upon. This is as would be expected from (4.32) above and is the same as for a road vehicle.

(2) Expression (4.36) shows that the power lost per unit thrust is dependent upon the final horizontal velocity of the water. To minimise the power lost V_h must be kept as small as possible.

(3) From (4.38) it is again evident that to maximise the useful power to power lost, V_h must be kept to a minimum with respect to V_o .

(4) It can be seen from $T = \dot{m} V_h$ (expression 4.5), that for a given thrust force, T , V_h may only be reduced if \dot{m} is correspondingly increased. And it is further apparent from (4.37) that an increase in \dot{m} will reduce the ratio of power lost to thrust force.

While these are expected results they provide the choices for optimisation of the thrust power which are examined in the next sections where methods are outlined for increasing \dot{m} .

4.11.2 Water Mass Flow Rate and Power Per Unit Thrust

The choices for optimisation of the thrust power by the increase in mass flow rate are divided into two groups. First the use of the mass flowing into the LPW can be optimised, and second the magnitude of the mass flowing into the LPW can be increased.

4.11.3. Optimisation of Incoming Mass Flow

If the LPW is operating before surface cavity intrusion (in the parabolic region of the thrust-rps plot) it is not acting on all the water approaching it, as shown in Fig.4.25. Several options are available to increase the proportion of this incoming flow acted upon, each of course decreasing the power required per unit thrust in equation (4.34).

First it is clear from Fig.4.25 that the maximum possible use of the incoming mass is made at such a velocity ratio that surface cavity intrusion is about to occur and therefore as much as possible of the incoming flow is converted to induced mass as it is acted upon by the blades. This is illustrated in Fig.4.26, and would represent operation in the intersection region of the force-rps plot.

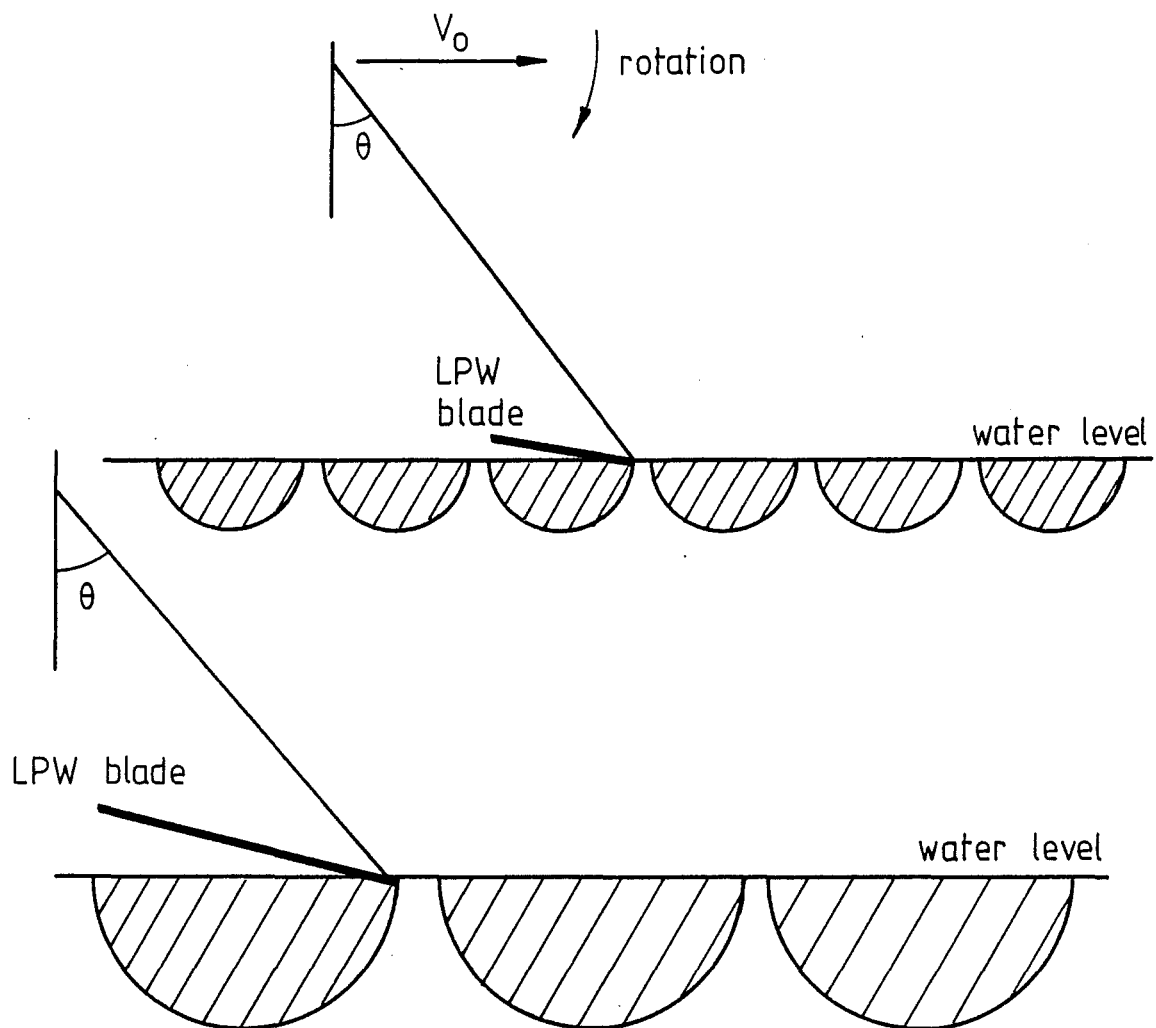


FIGURE 4.27 TRAIN OF INDUCED MASS 'PIECES' FOR SMALL CHORD (TOP) AND LARGE CHORD BLADES, BOTH AT SURFACE CAVITY INTRUSION

For the second point, for high propulsive efficiency it is important that the velocity ratio be kept as high as is practicable (see Fig.1.9). Thus it is required that this optimisation of mass acted upon should occur at as high a velocity ratio as possible. This may be achieved by two methods:

(a) By adding more blades to give the effect shown in Fig.4.26 at lower wheel revolutions (higher velocity ratio).

(b) By increasing the chord as shown in Fig.4.27. This would apparently increase the induced mass more effectively than by adding more blades as indicated by the c^2 term in expression (4.16) for the induced mass flow rate. This however must be considered with caution as an increase in chord also places the centre of the induced mass nearer the wheel axis and therefore reduces the mean velocity to which it is accelerated. This complication will be avoided at this stage simply by noting that the impulse theory indicates that an increase in blade chord will increase the induced mass to some degree.

4.11.4 Ways of Increasing Incoming Mass Flow

This section outlines a second method of increasing the mass acted upon by the LPW as a way of reducing the power per unit thrust. Again the LPW is considered as operating before surface cavity intrusion has occurred, and several options are available in this case to actually increase the incoming flow. All these relate to equation (4.16), $\dot{m} = \frac{\pi}{8} c^2 \rho s n B$.

First, the density of the incoming flow may be increased. While this may seem trivial, observations of the LPW in action show that either an LPW in front of the one in question (as on a craft) or the presence of bowsplash can aerate the water considerably thus reducing the mass supply to the rotor.

Second, the entrained mass may be increased by an increase in blade span. The thrust power to thrust ratio increases linearly with an increase in span for a given velocity ratio.

It is interesting to note that for a given thrust force as the blade span is increased the pressure on the blade must decrease. Thus for a fixed set of conditions blade pressure is an indicator of the power per unit thrust.

4.11.5 Increasing Mass Flow After Cavity Intrusion

After cavity intrusion the impulse theory has not attempted to estimate induced mass. There is therefore no advantage to be gained by speculation beyond the fact that it is clear that an increase in blade span will proportionally increase the induced mass for a fixed velocity ratio.

4.12 LIFT POWER IN THE IMPULSE THEORY

A body supported against gravity by forces generated by dynamic means uses power in the production of these forces. This is also the case for the LPW craft, and since lift is a special property of the craft it is important to examine just how this lift power is used. Since the expressions for propulsive efficiency treat the power used to generate the lift force as a loss, they give little indication of how effectively the lift force is generated, so a separate expression needs to be employed. The lift power to lift ratio, $\frac{P_L}{L}$, is used and the related analysis is to some extent comparable with that of section 4.11.1, where the thrust power to thrust ratio $\frac{P_T}{T}$ was examined.

The power used to generate the lift force may be expressed in terms of the kinetic energy lost to the water in the vertical direction per second.

$$P_L = \frac{1}{2} \dot{m} (V_v)^2 \quad (4.39)$$

The lift power to lift force ratio* then becomes:

$$\frac{P_L}{L} = \frac{\dot{m} (V_v)^2}{2\dot{m}V_v} = \frac{L V_v}{2\dot{m}V_v}$$

which yields the two results:

$$\frac{P_L}{L} = \frac{V_v}{2} \quad (4.40)$$

and

$$\frac{P_L}{L} = \frac{L}{2\dot{m}} \quad (4.41)$$

* It should be pointed out that $\frac{P_L}{L}$ is not the commonly used power to weight ratio, since the power considered in this section is only the power required for lift and not the overall input power, denoted P_i in this report.

where P_L = power used for lift
 \dot{m} = induced mass flow rate
 V_V = final velocity of the water in the vertical direction
 L = lift force.

These expressions indicate the following general ways to minimise the lift power to lift ratio:

(1) From (4.40) $\frac{P_L}{L}$ depends upon V_V , which should be minimised to minimise the lift power per unit lift.

(2) From (4.41) it is apparent, as it was for the thrust power, that the mass acted upon should be made as large as possible, and reference may be made to the above sections regarding induced mass flow rate (4.11.2, 3 and 4) which are equally applicable to the lift and thrust cases.

Of course any decrease in V_V must be accompanied by a proportional increase in \dot{m} and vice versa if the lift force is to remain constant by equation (4.11), ($L = \dot{m}V_V$), as it would for a flying LPW craft, though such a fixed relation between these two quantities is not necessary for changes in the $\frac{P_L}{L}$ ratio.

(In practice the lift force cannot be so simply calculated, as the expression 4.11 then contains a coefficient which itself varies, sometimes considerably, with the conditions. In this case a realistic estimate of how the lift power will change can more properly be determined using expression 4.11 with the coefficient equation for lift as described in section 9.9. The most notable departure from the theory in that case is that $\frac{P_L}{L}$ in fact tends to increase with wheel revolutions in the normal operating state before cavity intrusion.)

4.12.1 Lift Power and Depth Angle, θ

An idea which has often been put forward is that if the point of application of the lift force is moved as close as possible to a position directly below the LPW axis, power required for lift will be reduced. See Fig.4.28.

While the present theory supports this notion it shows that the result is the same as the methods just described for power optimisation.

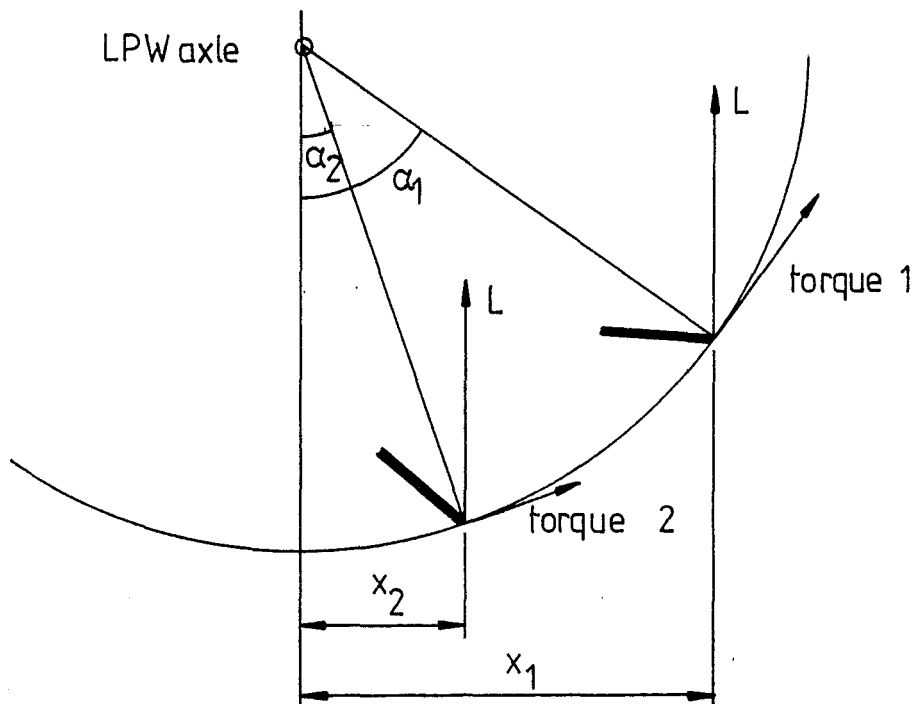


FIGURE 4.28 POINT OF APPLICATION OF LIFT FORCE SHOULD BE AT A SMALL ANGLE, α_2 , TO REDUCE SHAFT TORQUE.

From equation (4.21) for V_v , and its depiction for $\phi = 60^\circ$ in Fig.4.16 it can be seen that for the normal range of immersion depths and blade angles V_v can be reduced by a reduction in immersion ratio, (θ or α). As has been noted above in relation to equation (4.40) for $\frac{P_L}{L}$, the lift power per unit lift is also reduced by a reduction in V_v . Thus the idea is supported by the impulse theory equations.

In order to reduce V_v , however, and still maintain constant lift force required for a flying LPW craft, \dot{m} must be proportionally increased by equation (4.11), ($L = \dot{m}V_v$). This is the same conclusion reached by the above sections 4.12, 4.11.2 and 4.11.3.

The depth angle, θ , and the lift power per unit lift will therefore decrease together as proposed, but only as a consequence of an increase in the mass flow \dot{m} as already described.

4.13 OTHER POWER LOSSES

Three more areas of power loss are evident in LPW operation. Analytical estimates for two of these have been attempted. These three are:

- (1) Power lost to spray.
- (2) Power lost to rotational air drag on the LPW's.
- (3) Power lost as kinetic energy of rotation

given to the water by the rotation of the immersed LPW blades.

4.13.1 Spray Throwing

It is clear that some of the water mass acted upon by the LPW will move upwards as spray. Some of this will be lifted out by the blades while some will constitute impact splash as described in section 4.9.1. All of it however will be kinetic energy lost to the water. Any water actively lifted by the blades would reduce the nett downwards velocity in expressions (4.11) and (4.40), reducing the lift force, and also increasing the $\frac{P_L}{L}$ ratio. Any spray directed against the body of the craft would increase the drag force and hence the thrust power.

In practice, however, a large proportion of the inherent vertical momentum in the spray may be regained by the craft. It has already been pointed out in section 4.9.1 that the impulse

splashes may add to the lift force if encountered by the incoming blades. Also suitable spray deflectors on the body of the craft (as used on the model in Chapter 12) may be used productively to channel the flow back downwards to assist the lift of the wheels. Such deflectors, however, introduce skin friction losses and it would be better if the LPW could be made to operate without throwing a significant amount of spray. As yet no ready method has been attempted for estimating the power lost to a craft in spray.

4.13.2 Power To Overcome Rotational Air Drag of LPW's

LPW's are, unfortunately, decidedly similar in form to large centrifugal fan impellers. With improperly chosen shrouding they may well be made to pump large volumes of air during their operation. While this may be a way of coping with a spray problem, it is also going to absorb considerable power when the wheel speeds are high. Suitably chosen shroudings may be designed to prevent much of this power loss.

A power coefficient suitable for the experimental measurements of LPW windage (based on the relation (4.2)) has been found to be:

$$KP_w = \frac{P_w}{\rho_a n^3 s c_1 B D^3} \quad (4.42)$$

where KP_w = LPW windage power coefficient for rotation

P_w = windage power loss for rotation

ρ_a = air density

n = wheel revolutions per second

s = blade span

c_1 = projected blade chord $c_1 = c \sin \phi$

B = number of blades

D = wheel diameter to blade tips.

This expression contains no term for speed of advance, V_o , which seemed during tests, to have little effect even for unshrouded wheels. (See section 9.6, describing windage tests.) An average value for KP_w is 16 ± 1.5 for the test wheels with no shrouding. (16.7 ± 4 for all wheels tested.)

4.13.3 Power Lost as Rotational KE Left In The Water

It has been imagined that a proportion of the torque applied to the LPW would be expected to simply rotate the water adjacent to the blades and that the power absorbed in this way would be left behind as rotational kinetic energy lost to the water.

As an indication of the real magnitude of this energy loss, estimates were made as follows :

The added mass per blade, as calculated from the impulse theory, was assumed to be of the form of a semicylinder on the LPW blade. Its moment of inertia was then calculated assuming it to rotate about the centreline of the blade. Its final angular velocity was that of the LPW. Each blade's added mass was thus imagined to be left rotating in the LPW exit flow. A summation of the rotational kinetic energy thus left in the water, gave the power lost in this way.

This method indicated that this is a negligible power loss during normal craft operation, usually being less than 1% of the total power consumption. (Results calculated by this method are, however, included in the results of Table 13.6 for full-sized LPW craft power.)

4.14 TOTAL POWER, PROPULSIVE EFFICIENCY AND EFFECTIVENESS

The total power input to the LPW, P_i , could be assessed by summing the known power requirements and losses described in the foregoing sections. Such a method would give:

$$P_i = P_T + P_{\text{lost}} + P_L + P_w + P_{\text{spray}} + P_{\text{rot}} \quad (4.43)$$

where P_i = input power expected
 P_T = power for thrust or propulsion (4.32)
 P_{lost} = power lost in horizontal KE of the water
 P_L = power used for lift
 P_w = windage loss in the LPW's
 P_{spray} = power lost in spray (not yet assessed)
 P_{rot} = power lost as rotational KE in the water.

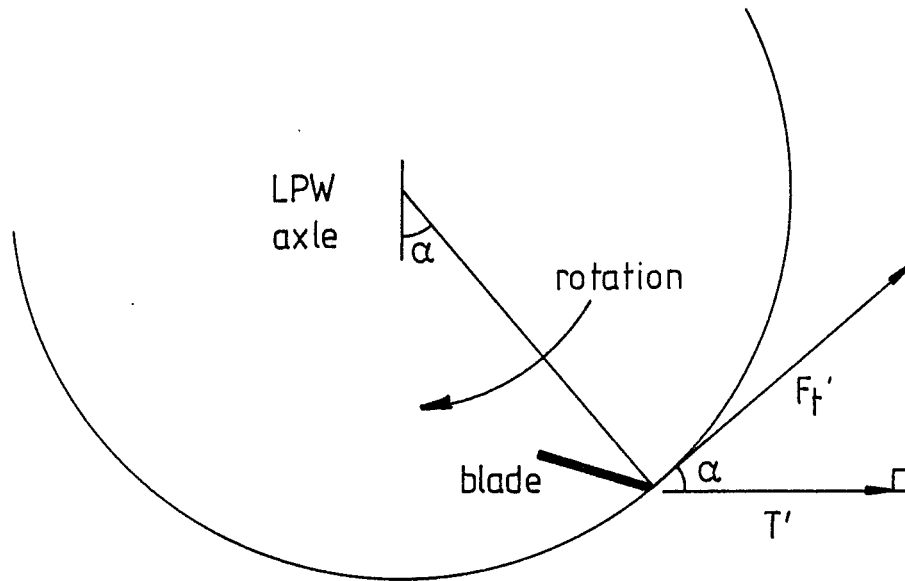


FIGURE 4-29 INSTANTANEOUS THRUST FORCE IS THE HORIZONTAL COMPONENT OF INSTANTANEOUS TANGENTIAL FORCE F_t'

This approach assumes all losses are known. It is used in power calculations in the design procedure of section 13.5.2 and in section 9.8 assessing experimental power measurements.

More conventionally the power input to the LPW may be expressed:

$$P_i = F_t V_t \quad (4.44)$$

where P_i = power to the wheel.

F_t = average tangential force assumed to be acting at the blade tip, calculated from wheel torque = $F_t \times R$

V_t = blade tip velocity relative to wheel axis.

(While it would be more realistic to assume a larger force acting at the smaller radius to the centre of pressure of the blades, the power equations following are unaffected by the above form.)

The useful propulsive, or thrust power used by the LPW may be written (from 4.32):

$$P_T = T V_o$$

where P_T = useful thrust power

T = thrust force

V_o = speed of advance.

And from (4.44) and (4.32) the propulsive efficiency, η , can be expressed:

$$\eta = \frac{P_T}{P_i} = \frac{T V_o}{F_t V_t} \quad (4.45)$$

From this relation it appears possible for η to be greater than the velocity ratio, $\frac{V_o}{V_t}$, as long as T is greater than F_t but since T is the average horizontal component of F_t it would not exceed F_t . (See Figure 4.29.)

If we assume, however, that all the force at the blade tips acts uniformly through the actuator rectangle in the (useful) horizontal direction, as assumed in section 4.3, so that $T = F_t$, then

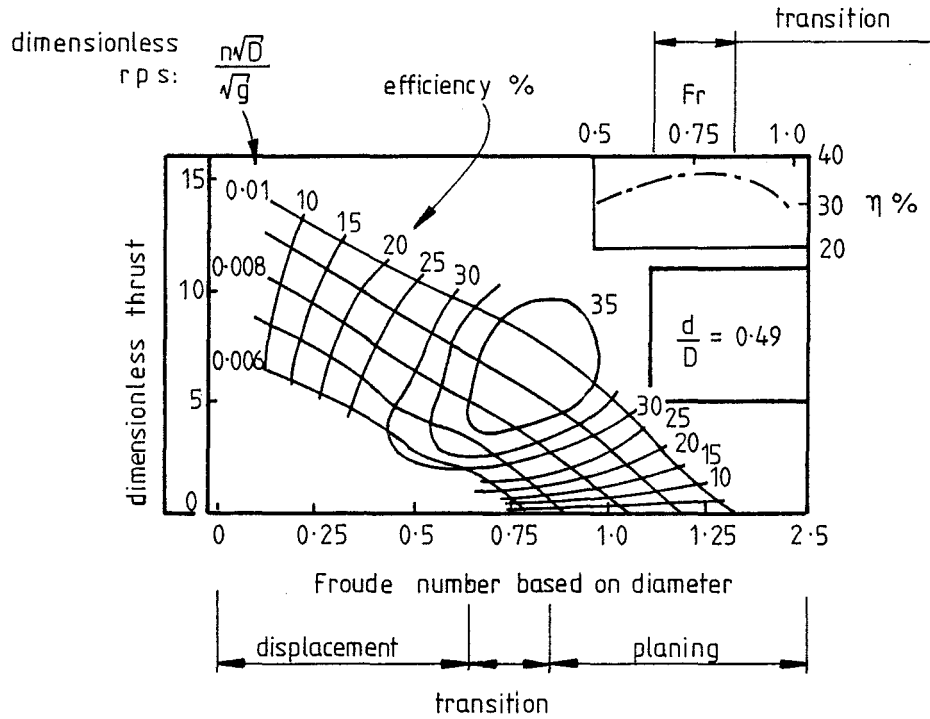


FIGURE 4.30 ONE OF HELM'S RESULTS RELATED TO THE TRANSITION ZONE.

(Ref: Helm Abb 10 p. 692)

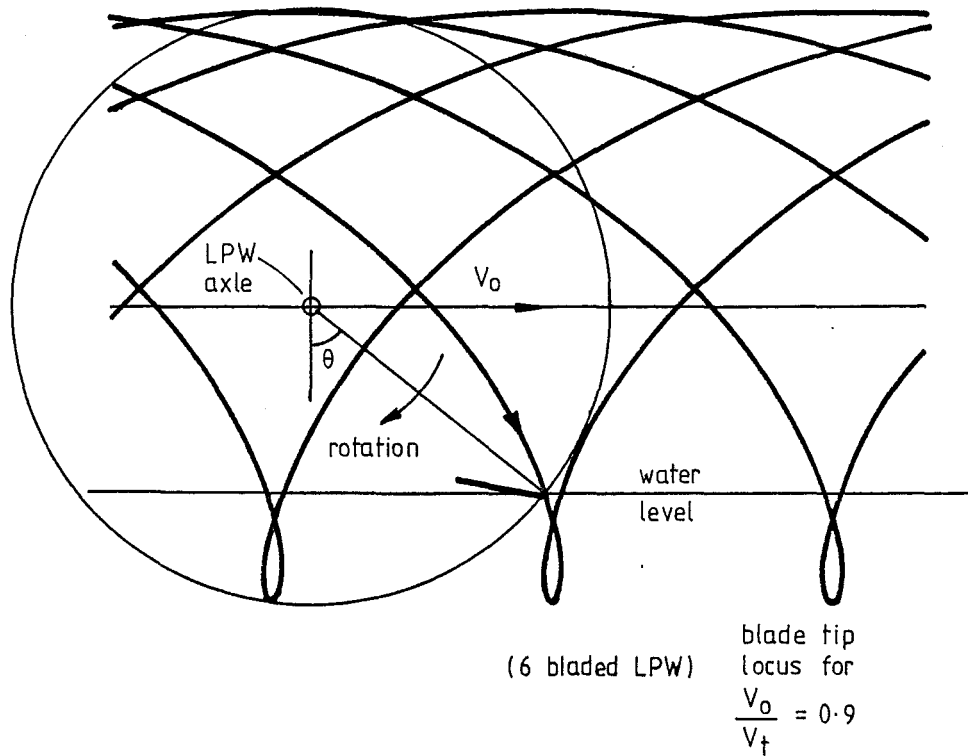


FIGURE 4.31 BLADE TIP PATHS AT HIGH VELOCITY RATIO

from Fig.1.8:

$$\eta \leq \frac{V_o}{V_t} \quad (4.46)$$

This may be taken as an ideal efficiency. This is the most significant limit to LPW operation: the propulsive efficiency cannot be greater than the velocity ratio. Thus the greater this ratio, or the less slip or skidding that exists between the blades and the water, the greater the propulsive efficiency. Wheels should therefore be operated in such a way as to minimise slip, for maximum efficiency. This conclusion is in agreement with the above section 4.11, discussing LPW power allocation.

4.14.1 A Note on the Presentation of Efficiency Curves

Many authors (Helm, Beardsley, Volpich and Bridges), when plotting paddlewheel propulsive efficiency results, have plotted them against a horizontal axis of Froude Number or velocity ratio in a similar manner as has been done in this project. However they have consistently produced their results by keeping the tip speed, V_t , fixed while varying the speed of advance V_o . Such a course of action produces confusing results since the efficiency plot then runs from the displacement mode at low values of velocity ratio (or high values of slip) through the transition zone and sometimes into the planing mode, often producing peak efficiencies at very low values of thrust in the region of the transition zone. (See for example one of Helm's figures in Fig.4.30 related to the probable wake formations occurring.)

Such results are unhelpful and especially confusing when a different tip speed V_t is chosen to define the velocity ratio as it then begins to produce peaks and troughs in the efficiency curves which are caused by the transition zone wave formations, but which cannot be equated directly with plots of different tip speeds or different size wheels, at different velocity ratios.

This project has always presented efficiency results on a velocity ratio axis composed by keeping the speed of advance V_o constant while varying the blade tip speed, V_t .

4.14.2 LPW Propulsive Effectiveness

The first order momentum analysis (section 4.3) and the form for the ideal efficiency (equation 4.46) assumed that the thrust force

T was equal to the blade tip force F_t . Clearly as shown in Fig.4.29 F_t will not always act horizontally so that through most of a blade passage and especially at entry $F_t > T$. However a wheel which has the greater proportion of force on the blade throughout the blade passage as useful thrust will be a more effective propulsor. Beardsley therefore defines the blade effectiveness factor:

$$\epsilon = \frac{T}{F_t} \quad (1) \quad (4.47)$$

which he claimed was "useful....to compare test performance under various operating conditions with the ideal." From (4.45) and (4.47) a further useful form may be derived:

$$\epsilon = \eta \frac{V_t}{V_o} \quad (4.48)$$

After the velocity ratio, wheel effectiveness is the most important factor as the limit to LPW performance. It is valuable, then, to examine a major property of wheel effectiveness.

4.14.3 Effectiveness Decline At High Velocity Ratios

Having stated that the velocity ratio should be as high as possible for a high propulsive efficiency it is worth examining the practical upper limits to which $\frac{V_o}{V_t}$ can be taken.

As velocity ratio is increased and approaches unity the blade path begins to look like Fig.4.31. At entry the blades are moving forward relative to the water, at the bottom of their passage they move rearward, and at exit they are once again moving forward. At some stage the blades will begin to trip on their own cavity edge as they leave the water, thus creating drag. So, as $\frac{V_o}{V_t}$ is increased there will come a point where the drag of the blades leaving the water outweighs the thrust force created by them.

The result of this is that for low velocity ratios the effectiveness will remain high so that the efficiency curve as shown in Fig.1.9 will be a large proportion of the velocity ratio. As the velocity ratio increases, however, the nett thrust in expression (4.47) is reduced by this blade drag as compared with the tangential force, so

that the effectiveness falls, causing the efficiency curve to fall away from the ideal, as shown in the figure, Fig.1.9.

In order, then, to operate the LPW at high efficiencies, ways need to be found to keep the wheel effectiveness high at high velocity ratios.

PART B

4.15 LPW WAKES

LPW operation has been divided into four areas which are related to its forward speed: static, displacement mode, transition zone, and planing mode. The latter three of these are distinguishable by the type of wake formed by the wheel.

As with ship wakes, LPW wakes may be usefully described in terms of the dispersive theory of surface waves in deep water. Here the principal relation is:

$$v = \sqrt{\frac{g\lambda}{2\pi}} \quad (4.49)$$

where v = velocity of the wave
 λ = wavelength of the wave
 g = gravitational acceleration.

A moving ship creates waves of all wavelengths and so, by this relation, all wavespeeds. Waves moving more slowly than the ship reinforce obliquely to the line of motion in the wake. Waves moving faster move away ahead and are of such a small amplitude as to be largely unnoticed. Waves moving at the speed of the ship appear as stationary waves along its hull, such as its bow wave train. This is also true for the lone LPW moving through the water.

Like a ship, the LPW reinforces waves that are of a wavelength in some way related to its action or dimensions. For a ship these are waves of length close to the waterline length of the ship. For the LPW, these favoured waves are related to the immersed waterline length, the shape of the immersed part of the wheel, and appear to be enhanced by bowsplash and the kick up of spray by the blades leaving the water.

As the LPW increases speed from rest in the displacement mode the length and amplitude of the waves travelling with it also increase until a state is reached where the wheel is moving at the wave speed of the waves it generates preferentially. Then the wave amplitudes become large and the LPW sits in the forward part of the trough of the wave it has created. This is shown in Figs. 4.32, (A) - (D), and Fig.1.5. This is the trough condition of the transition zone and because of the small mass supply to the rotor in this condition, forces generated by the blades are small. In passing, it may be pointed out that it should be possible to arrange the wheelbase length of the LPW craft to make the wave train from the front wheels cancel the wave train of the rear wheels under trough conditions in order to retain traction through the transition zone.

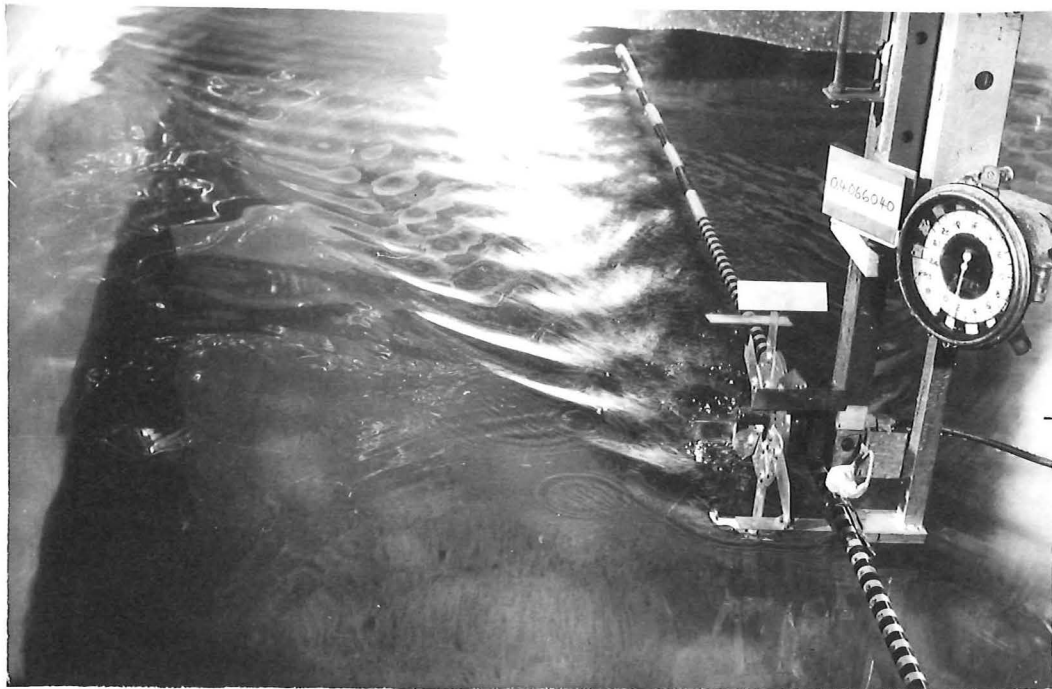
At higher speeds than the transition zone the dimensions, shape and action of the LPW no longer enhance the amplitude of the waves travelling with it, and may even oppose their formation. Now the long wavelength waves, being of relatively small amplitude are barely noticeable, and the wheel wake comprises only shorter wavelength waves travelling obliquely to the path of the wheel. This is shown in Fig.4.33. This, then, is the planing mode of operation, and as noted below is closely analogous to the wake of a planing boat.

4.15.1 Blade Passage and Wake Formation

The wake of the LPW is, of course, formed by the action of the LPW blades and not by the wheel as such. The wake could possibly be analysed as if it were the wave train caused by the rapid action of an endless series of disembodied blades. It has however been found quite satisfactory to consider the wheel itself as a solid body, as long as it is rotating fast enough. This has been confirmed by tests using a solid cylinder of the same dimensions as the LPW (as described in Chapter 10) where it was shown that the wakes formed by the two types of wheel were essentially no different in terms of displacement transition and planing wave trains (see Figs. 4.32 (D) and 4.34).

4.15.2 The Transition Zone

There is a recognised transition parameter used in the design of water craft which is chosen as the point where the planing type of wake begins to predominate over the displacement type, and where dynamic forces become significant as compared with hydrostatic forces.

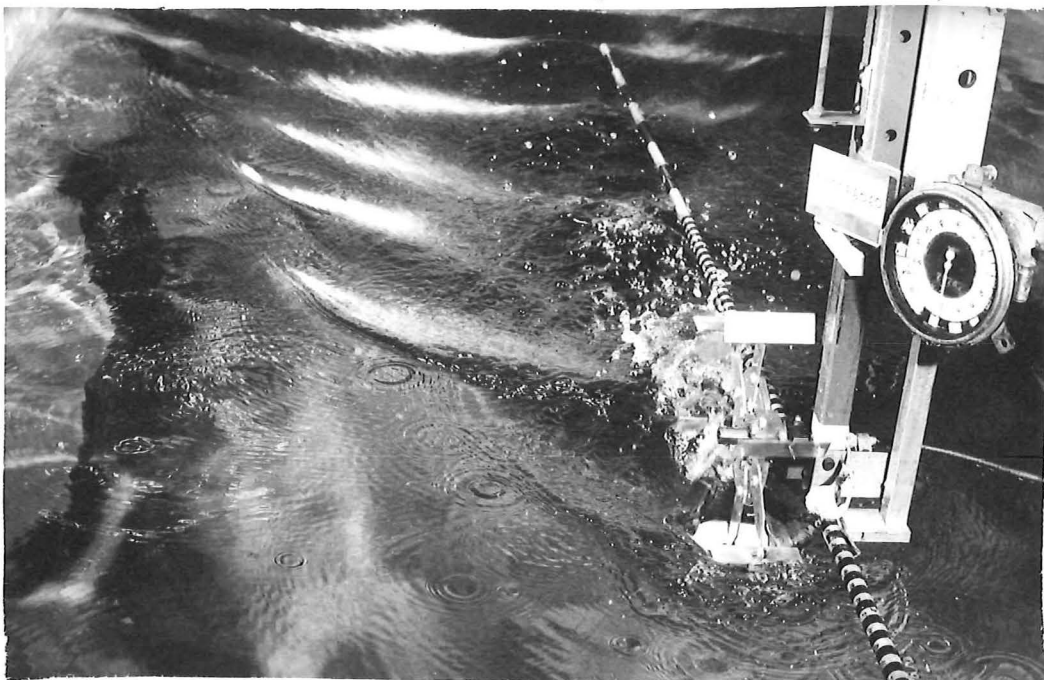


1300B/16A

FIGURE 4.32(A): DISPLACEMENT WAKE, BEFORE TRANSITION ZONE.

STD.WHEEL, $d/D = 0.17$, $V_O = 0.4$ m/s, $F_R = 0.26$,
 $n = 2$ rps

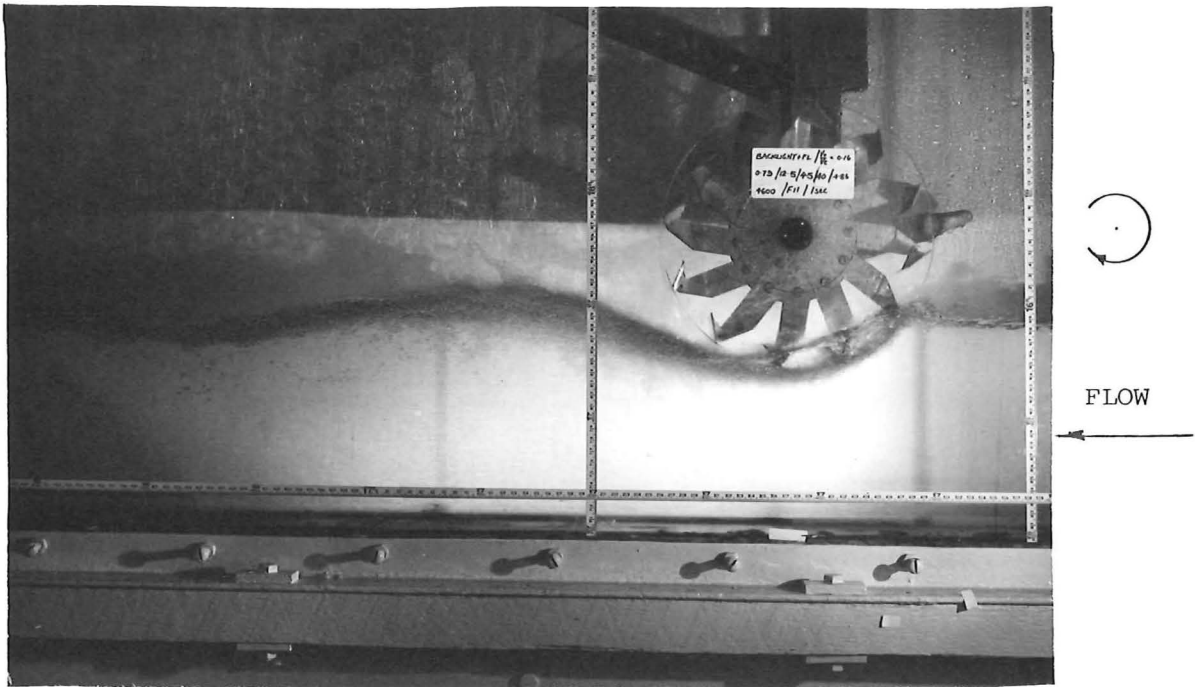
MOTION



1300B/12A

FIGURE 4.32(B): TRANSITION ZONE WAKE; TROUGH CONDITION.

STD.WHEEL, $d/D = 0.25$, $V_O = 0.76$ m/s, $F_R = 0.49$,
 $n = 2$ rps



632/25A

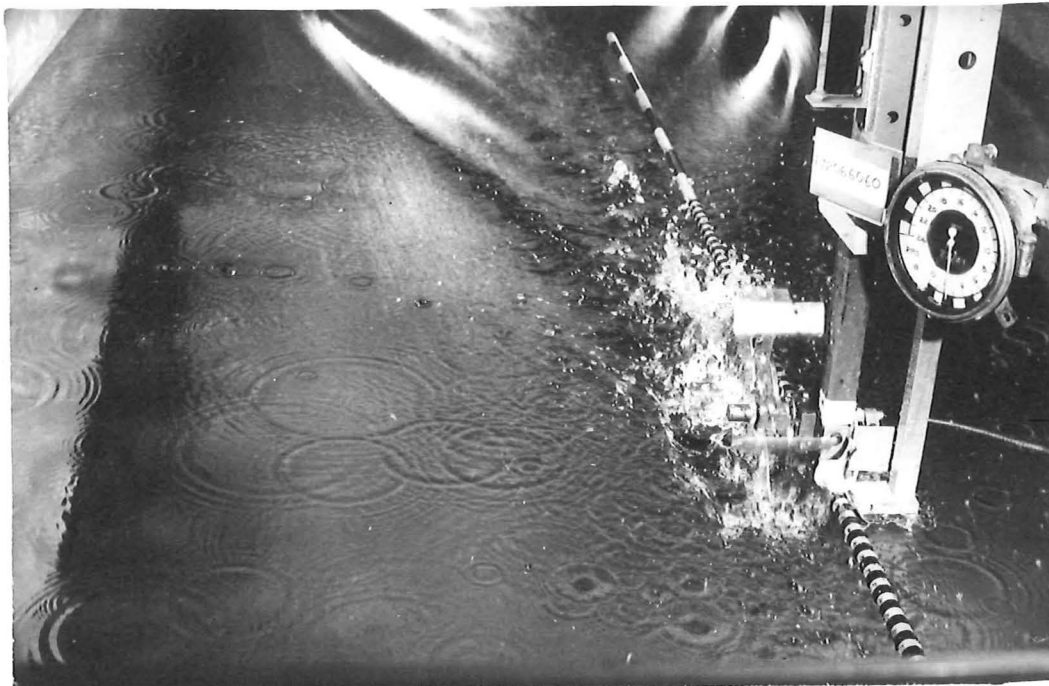
FIGURE 4.32(C): STROBOSCOPIC PHOTOGRAPH: TROUGH CONDITION OF TRANSITION ZONE. $V_O = 0.79$ m/s, $F_r = 0.51$, $F_x = 0.59$, $d/D = 0.17$, STD. BLADE DIMENSIONS, $\phi = 45^\circ$, $n = 6.4$ rps SUBCRITICAL FLOW



1300E/13A

MOTION

FIGURE 4.32(D): LPW SIZED CYLINDER CREATING TRANSITION WAKE. $V_O = 0.76$ m/s, $F_r = 0.49$, $F_x = 0.57$, $d/D = 0.17$, $n = 2$ rps



1300B/2A

FIGURE 4.33: SHOWING THE OBLIQUE WAKE OF THE PLANING MODE BEFORE BOWSPASH. STANDARD WHEEL, $V_o = 1.72$ m/s, $n = 2$ rps, $d/D = 0.25$

MOTION



1300E/18A

FIGURE 4.34: THE SOLID CYLINDER IN THE PLANING MODE, PRODUCING THE OBLIQUE WAVE TRAIN. NOTE THE "BOWSPASH" AND THE EXTRA WAVEFRONT IT PRODUCES. $V_o = 1.72$ m/s, $n = 3.5$ rps, $d/D = 0.17$

This is where the Froude Number for boat waterline length may be given by:

$$\frac{V_o}{\sqrt{g\ell^1}} = 0.75 \quad (4.50)$$

where V_o = speed of boat
 g = gravitational acceleration
 ℓ^1 = boat waterline length.

Boats which are designed to operate with Froude Numbers greater than this are normally planing craft which make use of the dynamic forces present to reduce hull resistance.

Beardsley identified the transition zone for his paddlewheels apparently without relating it to the formation of waves, or to the transition from displacement to planing found in fast water craft. He described it as the speed of advance where "...the supply of mass flow changes from chiefly gravity-fed to chiefly horizontally entrained." (1) He also pointed out that beyond the transition zone "...the speed of advance has become so great that the rotor is running away from the cavity before gravity-induced flow can supply it." (1) He decided upon what he called the Depth Froude Number to specify the transition zone and found its value by experiment:

$$F_d = \frac{V_o}{\sqrt{g d}} = 1.5 \text{ to } 2.0 \quad (4.51)$$

where F_d = depth Froude Number
 V_o = speed of advance
 g = gravitational acceleration
 d = depth of immersion

A difficulty with this relation is that it suggests that wheels of different diameters immersed to the same depth would reach transition at the same velocity.

Since waterline length and not draught is the dimension used to define the transition for boats, a transition Froude Number, F_x

1. Beardsley, P.20

was chosen for this project based on the waterline length of the wheel. It is found that this form seems more consistent in the real situation at larger wheel immersions, though for geometric similarity between wheels of different diameters it is necessary that they be compared only at a common immersion ratio, $\frac{d}{D}$.

This transition Froude Number is given by:

$$F_x = \frac{V_o}{\sqrt{2 g \ell}} \quad (4.52)$$

From the geometry of the wheel (Fig.4.5):

$$\ell = R \sin \theta$$

and $\ell = \sqrt{d(D-d)}$

so that further forms of F_x are:

$$F_x = \frac{V_o}{\sqrt{g D \sin \theta}} \quad (4.53)$$

$$F_x = \sqrt{\frac{V_o}{g D}} \cdot \frac{1}{\sqrt{\sin \theta}}$$

$$\therefore F_x = \frac{F_r}{\sqrt{\sin \theta}} \quad (4.54)$$

and $F_x = \frac{V_o}{\sqrt{2g \sqrt{d(D-d)}}} \quad (4.55)$

where: V_o = speed of advance

d = immersion depth

D = wheel diameter

F_r = Froude Number based on wheel diameter, D

ℓ = half the waterline length of the immersed part of the wheel (Fig.4.5)

θ = immersion angle.

The range of values for F_x corresponding to Beardsley's experimental depth Froude Number values: $F_d = 1.5$ to 2 , is $F_x = 0.64$ to 0.85 . It is interesting to note that Beardsley's results once converted to this new Froude Number form, based on wheel water-line length, neatly span the transition parameter chosen for water craft mentioned above (expression (4.50), where $F_r = 0.75$). It is felt that this helps to confirm the validity of the usage of the terms planing, displacement and transition in this project, terms which would normally be reserved for boat hulls.

4.16 TESTING PADDLEWHEELS IN CHANNELS OF FLOWING WATER

It was mentioned in the literature survey (section 2.3.2) and in the discussion of previous work on the LPW (section 3.4) that some paddlewheel and LPW tests have been carried out in channels of flowing water rather than under the more ideal conditions of the wheel being moved through still water. Such less-than-ideal test conditions have been employed usually because better facilities were not available. It is of some value to re-examine the validity of these flowing water tests in the light of the importance of the wheel wave trains and the transition from displacement to planing as outlined by this project.

4.16.1 Waves and Flow in Channels

The important elements relating waves and channel flow are as follows:

- (i) Wave velocity of deep water surface waves (i.e. waves in water with depths greater than their wavelength) is related to the wavelength by relation (4.49).
- (ii) In shallow water there is an upper limit to wave velocity, and hence also wavelength, which is related to the depth by the relation:

$$v_c = \sqrt{g h} \quad (4.56)$$

where v_c = critical velocity

g = gravitational acceleration

h = still water depth.

- (iii) In shallow water, waves of all wavelengths below this upper limit may exist (above a capillary wave lower limit of 0.23 m/s). Figure 4.35 shows the transition between the linear theories describing shallow and deep water waves.
- (iv) Water flowing in a channel has two regimes of flow:
 - (a) subcritical flow, where the water is moving relatively slowly and is deep enough so that the waves of interest may travel up or downstream from any disturbance;
 - (b) supercritical flow, where the flow is shallow so that its velocity is greater than the wave speed of any wave on its surface. This flow is turbulent in the interior.
- (v) Between these two regimes there is flow of critical velocity where waves of the largest wavelength that can be formed travel at the same speed as the flow, becoming standing waves.
- (vi) Near this critical flow velocity, the amplitude of the standing waves is very sensitive to small disturbances, and even small changes in water depth can cause the flow to become supercritical.

4.16.2 Modelling Wakes in Flowing Water

It can be concluded from Fig.4.35 that if water is deep enough not to affect the velocity of the largest wavelength waves expected, there is little difference between the wheel moving in infinitely deep water, or water as shallow as half the wavelength of the waves. (1) For the LPW the longest waves of interest are generated at transition and their wavelengths may be found from expressions (4.52) and (4.49) and the fact that $F_x = 0.64$ to 0.85 at transition. These depend on the wheel immersion depth, but by way of example for a wheel immersed to its axle expression (4.56) and Fig.4.35 indicate that the water depth should be at least $2.3 D$; at $\frac{d}{D} = 0.1$ water depth may be $1.3 D$.

Similarly if water of these depths is flowing in a channel with a velocity well below critical velocity there will be little difference between the wave train of a stationary tested wheel in the flow, and a wheel moving over still water at the same speed.

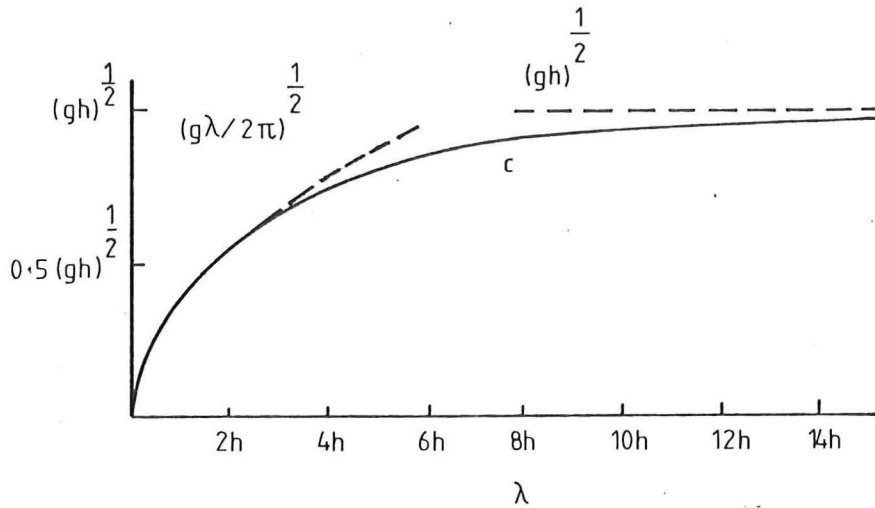


FIGURE 4.35 THE WAVE SPEED c GIVEN BY LINEAR THEORY FOR WAVES OF VARYING LENGTH λ ON WATER OF UNIFORM DEPTH h . NOTE THE TRANSITION BETWEEN THE DEEP WATER VALUE $(g\lambda/2\pi)^{1/2}$ AND THE LONG-WAVE VALUE $(gh)^{1/2}$

(Ref: Lighthill p. 217 Fig. 52)

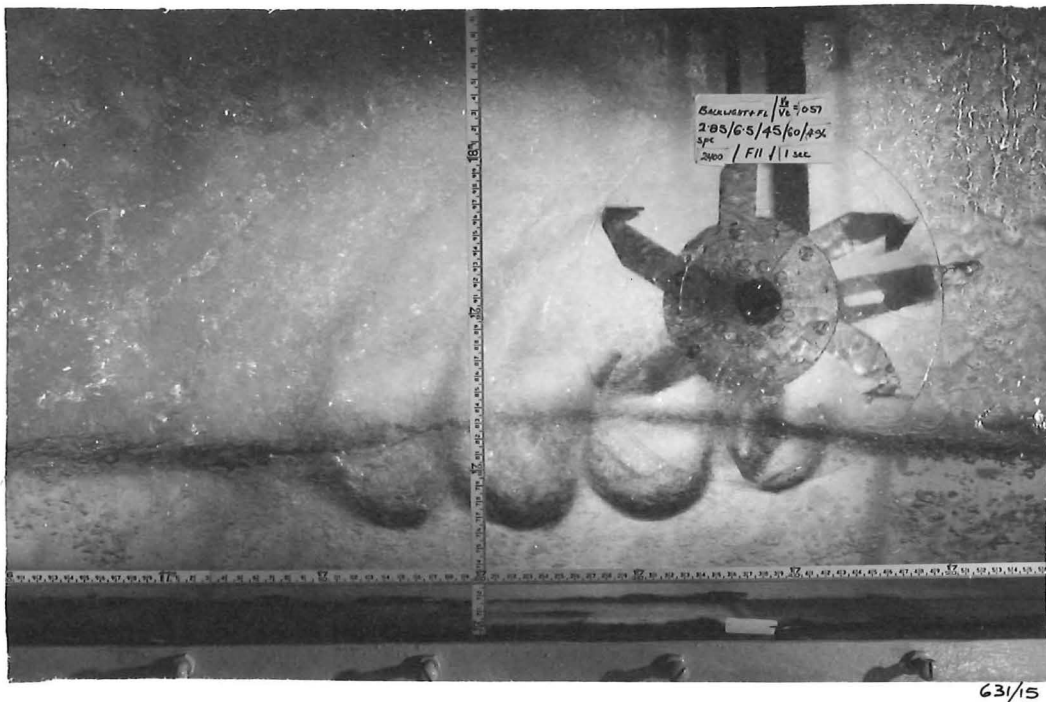


FIGURE 4.36: THE LPW IN SUPERCRITICAL FLOW IN THE GLASS-SIDED TANK. NOTE THE RISE IN THE WATER SURFACE AT THE WHEEL. Std LPW with sideplates, $V_0=2.85\text{m/s}$, $D/d=0.19$, $n=6.6\text{rps}$, $V_0/V_t=0.57$.

If, however, the depth of the water is small with respect to the largest waves in the wave train the flowing water no longer models the situation of the wheel in still water. Certainly displacement, trough and planing wakes may occur but the speed of the flow can no longer be scaled by Froude scaling alone to represent the wheel in open water. Further, different components of the wake will have different velocities with respect to each other because waves of different wavelengths are differently affected by the water depth.

If the flow velocity approaches critical velocity wave amplitudes will be excessive (by (vi) above) and once again this will not model the open water case. The presence of a test wheel in such flow can also induce it to become supercritical.

On the other hand if the depth and velocity of the flow are such that it is supercritical to begin with, it may be used to model the LPW in its planing condition. Several items need to be kept in mind if this is done:

- (1) If the water is shallow it may be moving at a speed lower than the planing speed of the wheel in open water. Tests in such flow would show the wheel to be in the planing mode at a velocity where over still water it would be in the displacement mode or transition zone.
- (2) The depth of such flow should be such that the velocity of the oblique waves expected in the wake is not limited.
- (3) Blockage effects occur in supercritical flow as shown by the rise of the water surface in Fig.4.36 of supercritical flow in a glass-sided flume.
- (4) Since supercritical flow is turbulent, small-scale effects such as flow around blades may not be reproduced as well as they would in still water.

It is clear that as long as the LPW wakes are closely represented in the flowing water tests measurements of its forces will also be representative of those in the open water case.

Tests in flowing water, then, have certain disadvantages when compared with tests in still water. They do however have the advantage of continuous testing and with care, and a proper awareness of wake formations, can give useful test results.

This project began by conducting tests in flowing water, and some of the photographic studies were carried out in narrow channels of flowing water. Fortunately, though, most of the testing and wake studies could be carried out with still water facilities.

4.17 CONCLUSION

This chapter, though long, has introduced new material in both the LPW impulse theory and the maximum velocity expressions, to better describe analytically the generation of forces by high speed paddlewheels or LPW's. These theories are compared with experiment in Chapter 9. It has also related LPW wakes to boat wakes and identified the displacement, transition and planing wakes for LPW's.

It is felt that in these areas it has made a useful contribution to the understanding of both high speed paddlewheels and LPW's.

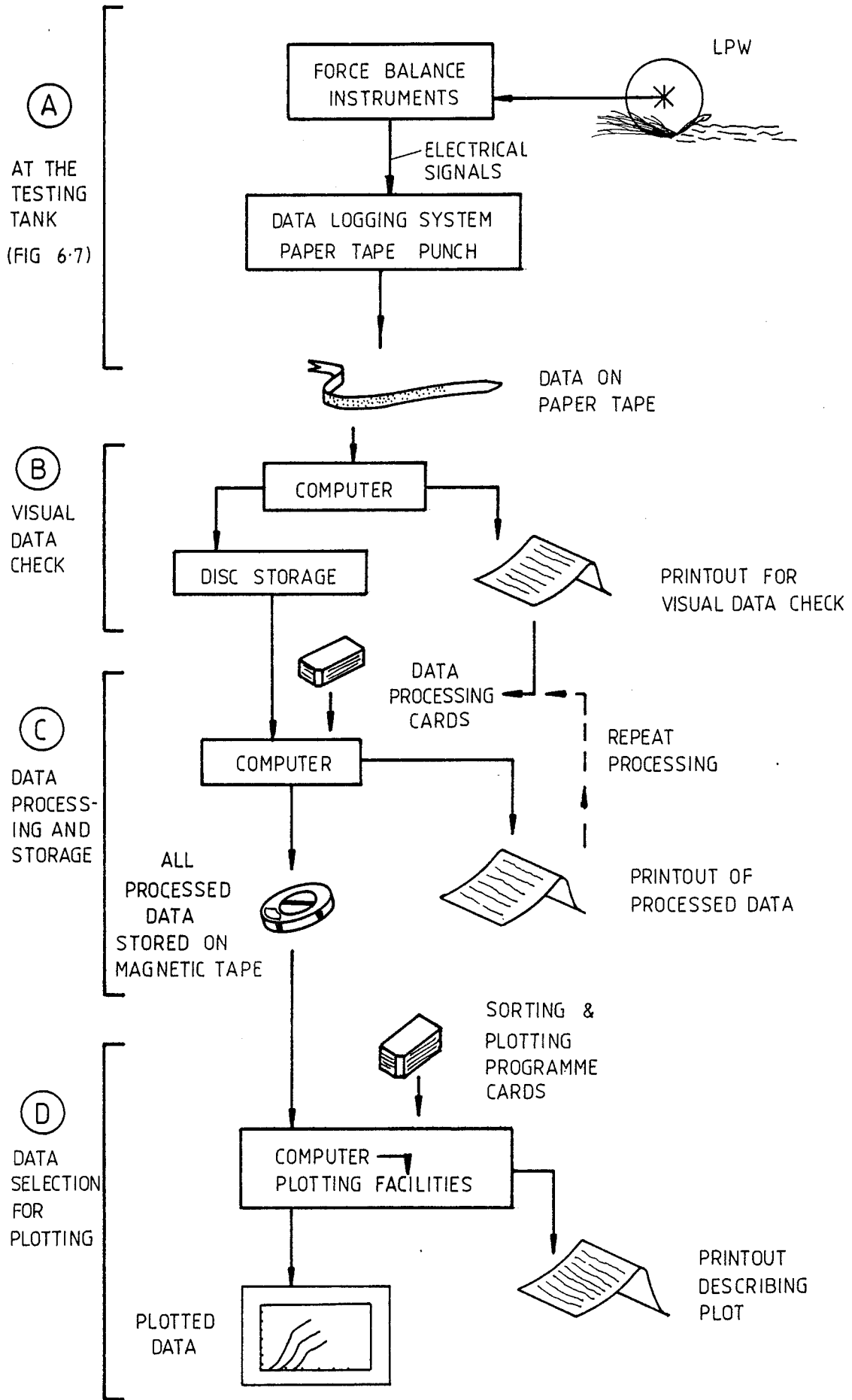


FIGURE 5.1 THE DATA PATH FROM THE LPW TO THE PLOTTED FORM

CHAPTER 5

EXPERIMENTAL APPROACH: THE FORCE BALANCE, TEST LPW'S
AND THE TESTING TANKS

5.1 INTRODUCTION

Since the 1977 and 1978 data were found to be in error in respect of the thrust measurements (1), it was necessary to do the tank tests again. The force balance was therefore redesigned to again fulfil the data acquisition aim as expressed by the secondary and tertiary aims (see section 3.6).

The force balance and tanks were the mechanical parts of the total measuring system and are described in this chapter. The other parts of the measuring system, the instrumentation, data logging, data processing and data plotting are described in Chapters 6 and 7. A line diagram of the path of the data through the measuring system, from the LPW to the plotted presentation of the results, is given in Fig.5.1 and this summarises the information in these three chapters.

The work of this chapter then fulfils the tertiary aims of Fig.3.10, parts A1 and A2.

5.2 THE MEASURING SYSTEM REQUIREMENTS

In tests like these with a large number of variables (as shown in Table 1.4, Chapter 1) it is necessary to fix as many as possible within known narrow limits and measure the variation of the others. Different experimenters select different variables to measure, but in this case it seemed easiest to measure the forces alone, fixing the external conditions of speed of advance, V_o , speed of rotation, V_t , and immersion depth, d ; as well as the conditions of the test wheel itself, such as its diameter D , blade angle ϕ , span and chord s and c , and its number of blades, B .

The ideal measuring system as seen for this project then, was one where the force balance would support the LPW with these selected wheel conditions, at a chosen immersion depth and a fixed rotational speed, and run it over a still water surface at a known speed of advance. At a selected time when conditions were suitably steady,

1. Section 3.4, section 5.9.2 and Alexander 1977

TABLE 5.3: FORCE BALANCE SPECIFICATIONS

DIMENSIONS: HEIGHT: 900 mm LENGTH: 900 mm WIDTH: 260 mm
 WEIGHT: ~ 35 kg
 MOUNTING: HOLES VERTICALLY IN LINE ON 3 INCH CENTRES

POWER AT SHAFT: 110 W max.
 RATED POWER: 340 W
 SHAFT SPEED: 1500 rpm max.
 SHAFT DIAMETER: 15 mm, LENGTH: 78 mm OUTSIDE BALANCE.

FORCE SENSORS:

LIFT: (VERTICAL) RANGE ± 20 N, PROTECTED BY STOPS AT ± 25 N.
 RESONANT FREQUENCY: ~ 5 Hz, DAMPED TO ONE ZERO CROSSING.
 FULLY BALANCED SECTION.
 RANGE OF MOVEMENT: 0.7 mm VERTICALLY BETWEEN STOPS.

THRUST: (HORIZONTAL) RANGE ± 20 N, PROTECTED BY STOPS AT ± 25 N.
 RESONANT FREQUENCY: ~ 10 Hz, DAMPED TO ONE ZERO CROSSING.
 UNBALANCED SECTION, SENSITIVE TO HORIZONTAL ACCELERATIONS.
 RANGE OF MOVEMENT: 0.5 mm HORIZONTALLY BETWEEN STOPS.

TORQUE: RANGE: ± 1.4 Nm PROTECTED BY STOPS AT ± 1.7 Nm.
 RESONANT FREQUENCY: ~ 8 Hz, DAMPED TO ONE ZERO CROSSING.
 UNBALANCED SECTION, SENSITIVE TO VERTICAL AND HORIZONTAL ACCELERATIONS.
 RANGE OF MOVEMENT: 0.5° ROTATION BETWEEN STOPS.

All force sections sense force with strain gauges mounted on both sides of Aluminium cantilever elements.

MAX. STRAINS ALLOWED ~ 750 μ s units.

All force sections can be locked for transport.

MAX. RANGE OF SHAFT MOVEMENT ALLOWED BY FORCE SENSORS: 0.9 mm.

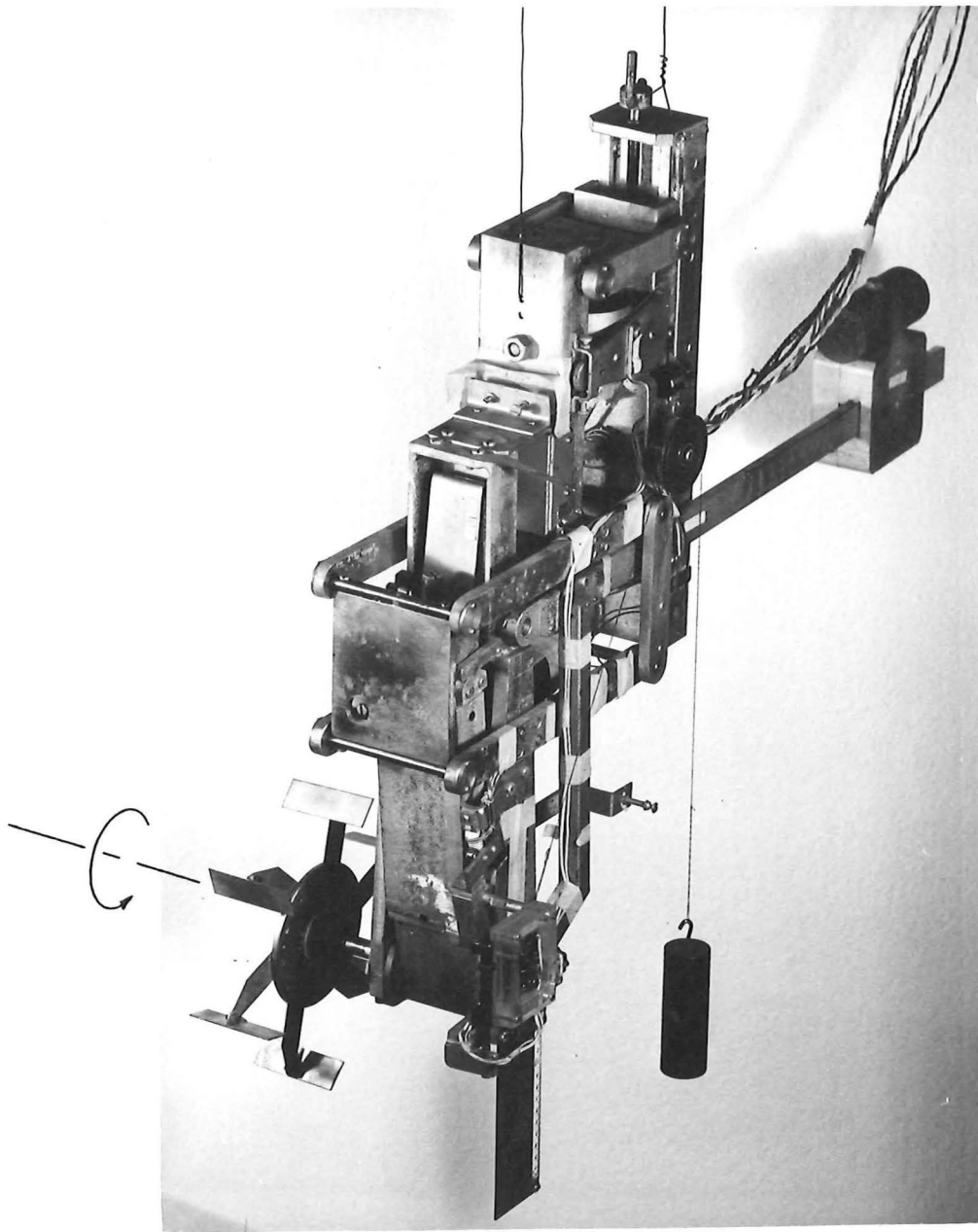
FORCE CALIBRATION: BY WEIGHT ON THREAD FROM CALIBRATION ATTACHMENT POINTS, AND OVER CALIBRATION PULLEY.

IMMERSION SETTING: RANGE 120 mm
 ADJUSTED WITH HEIGHT ADJUSTMENT SCREW
 LOCKED WITH LOCKING SCREW.

TACHOMETER: MAKE AND BREAK CONTACTOR ON LPW SHAFT.
 19 MAKE-BREAK CYCLES PER SHAFT REVOLUTION.

IMMERSION DISPLACEMENT TRANSDUCER: TEN-TURN POTENTIOMETER OF 20 k Ω RESISTANCE GIVING ~ 50 μ /mm DISPLACEMENT BETWEEN MOUNTING BEAM AND IMMERSION BEAM.
 LINEARITY: WITHIN 0.5 mm.

DEPTH GAUGE: MOUNTED ON ARM ON LIFT BEAM.
 CAPACITANCE TYPE (See section 6.2.2).



859/36

FIGURE 5.2: THE FORCE BALANCE

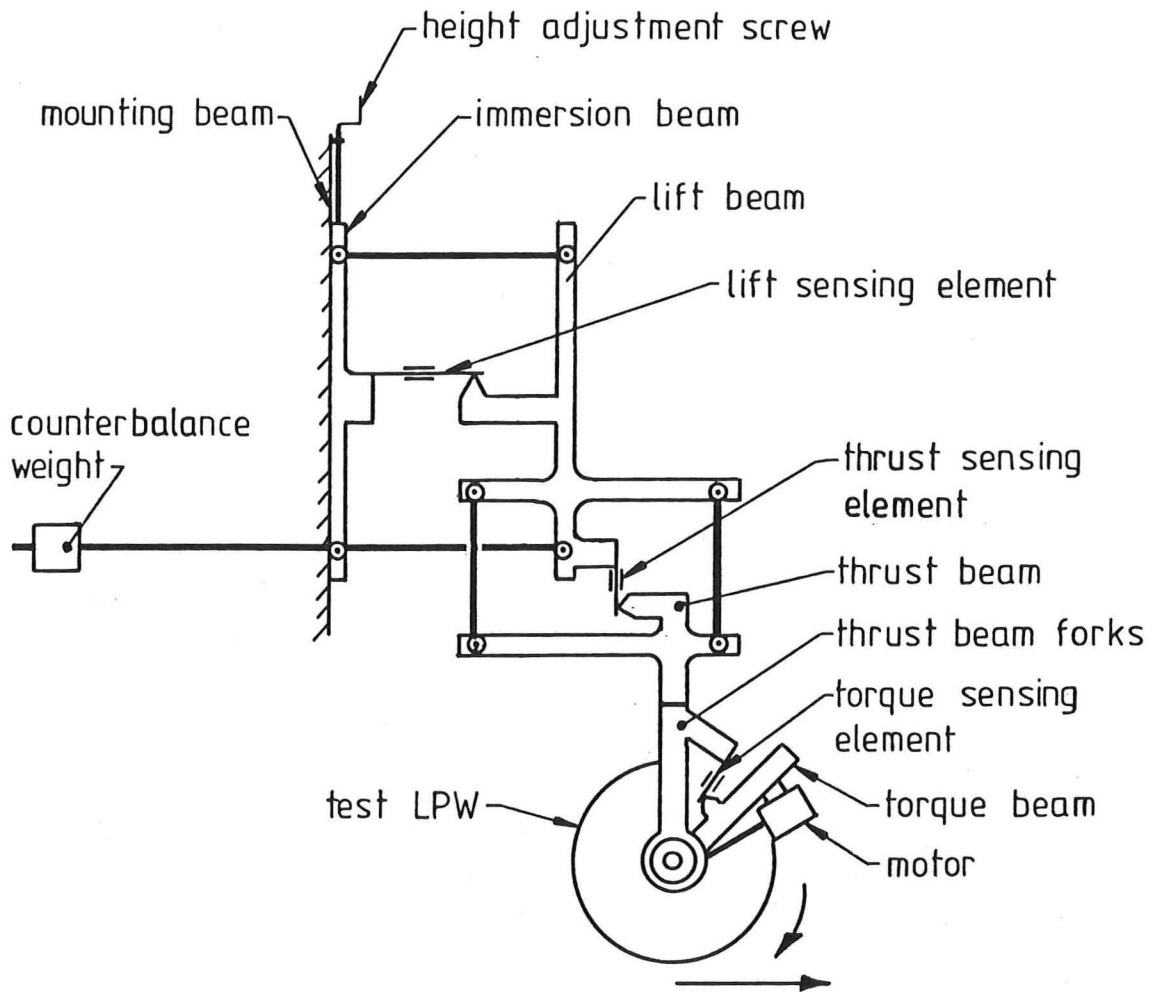
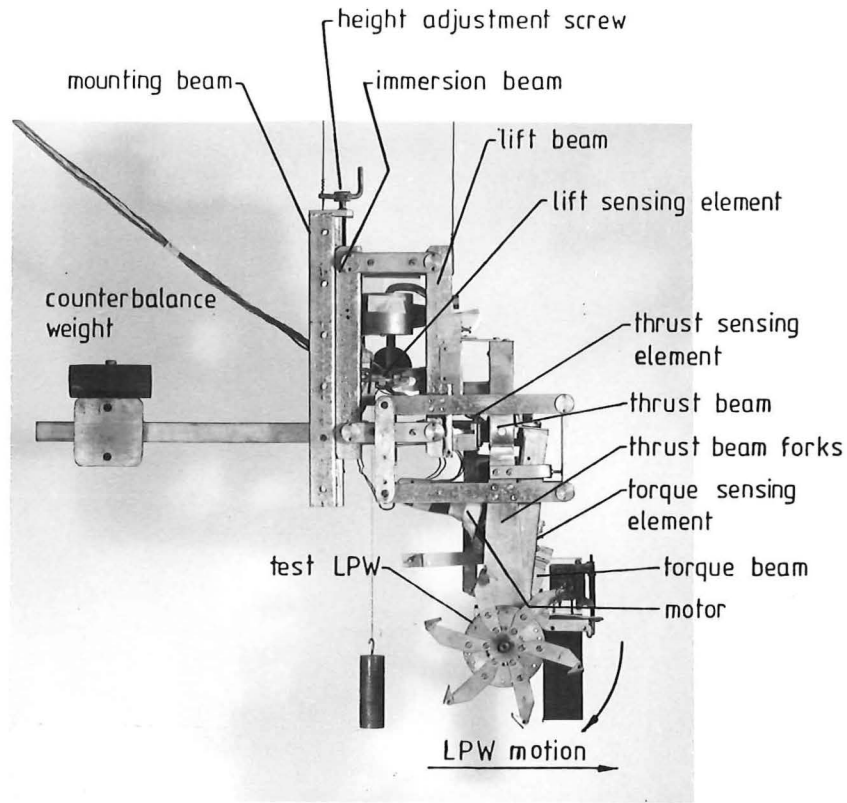


FIGURE 5·4: MAIN COMPONENTS OF THE FORCE BALANCE

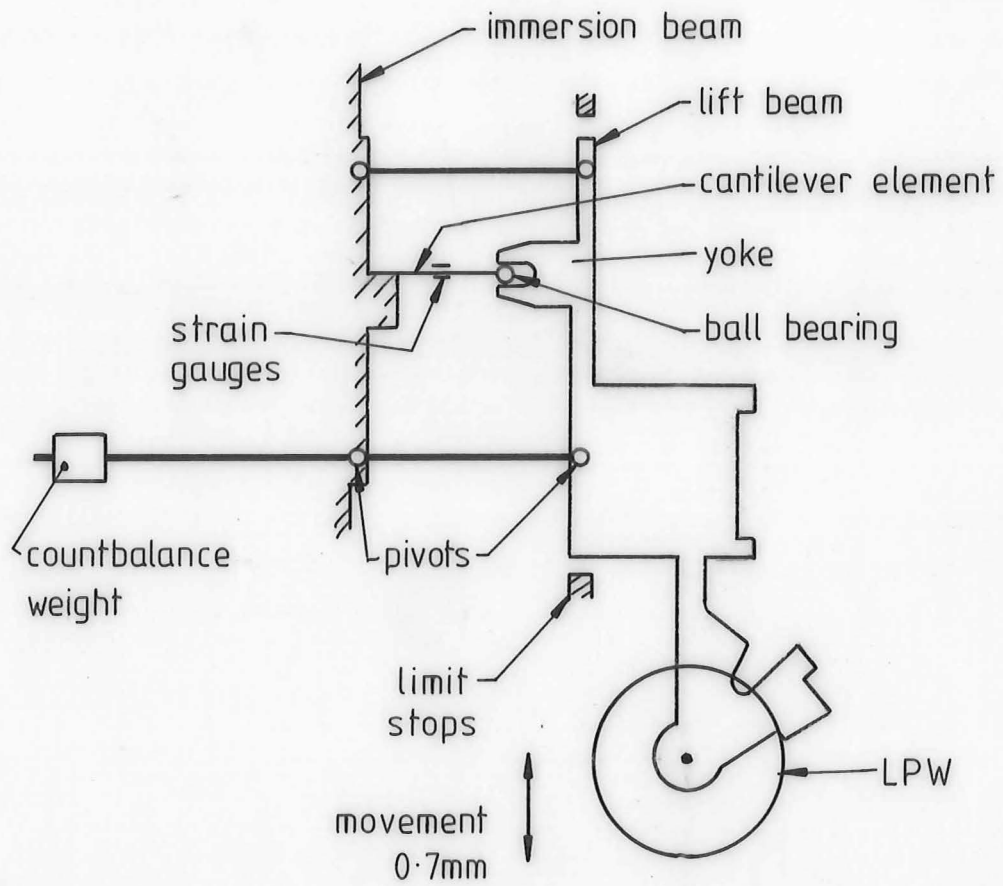
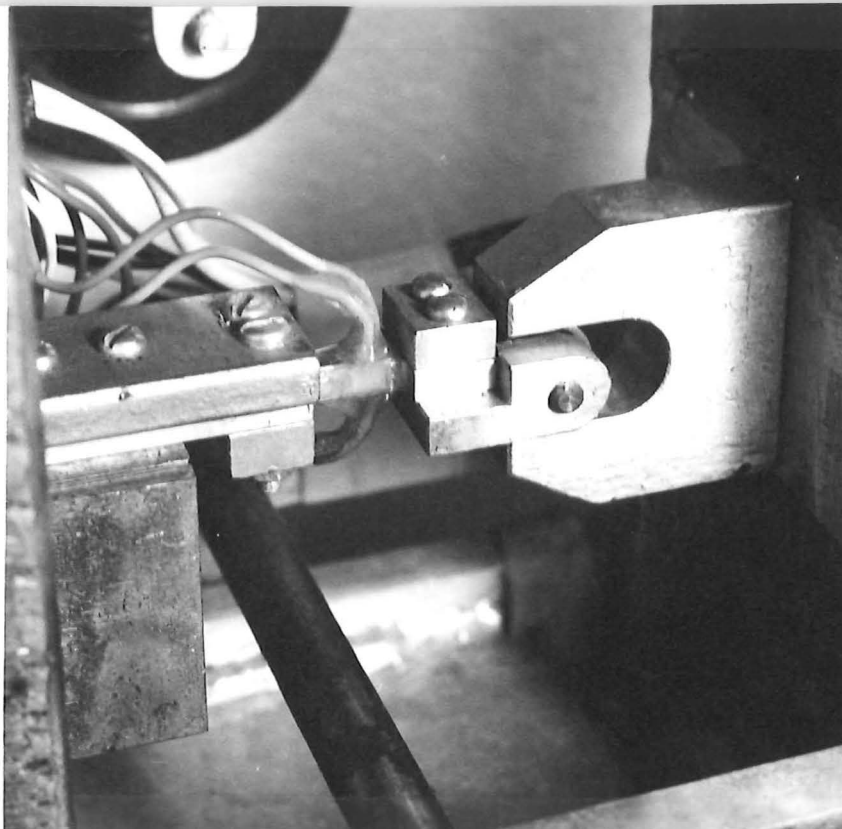


FIGURE 5.5 THE LIFT FORCE SENSING SECTION



1280/32

FIGURE 5.6: THE LIFT SENSING CANTILEVER ELEMENT AND YOKE (SEE ALSO FIGURE 5.11)

simultaneous measurements would be made of the lift and thrust forces and the torque of the wheel. From such measurements the ideal data record would be a short list of quantities which would be comprised of both the values of the preset conditions and the values of the measured forces. The total performance picture for steady conditions could be built up by plotting the data from repeated runs over the water each with one of the preset conditions altered.

5.3 THE FORCE BALANCE

The force balance used in this project evolved from the one used in the 1977 and 1978 work and inevitably carried some redundant fittings from its past. In its final form, shown in Fig.5.2 it was the major component of the measuring system which compared well in practice with the ideal outlined above. The major deviation from this ideal was that the wheel rotational speed could not be preset, so this also had to be measured as a variable, along with the torque and forces.

Operating specifications for the force balance are given in Table 5.3.

5.4 FORCE BALANCE OPERATION

Since the force balance developed into a complex-looking piece of equipment its functions are described separately. A simplified schematic of its overall operation is shown with Fig.5.4.

5.4.1 The Lift Force Section

The lift sensing section of the apparatus is outlined in Fig.5.5. The lift beam was attached to the immersion beam by a four-bar link system. This allowed the lift beam, and all that was attached to it, to move vertically, parallel to the immersion beam. The weight of the lift beam and its attachments was balanced by the counterbalance weight.

The vertical movement of the lift beam caused deflection of the small cantilever element, which was fitted with strain gauges to indicate its strain, and hence the vertical lift force. This element is shown in detail in Fig.5.6, and described later in section 5.4.5.

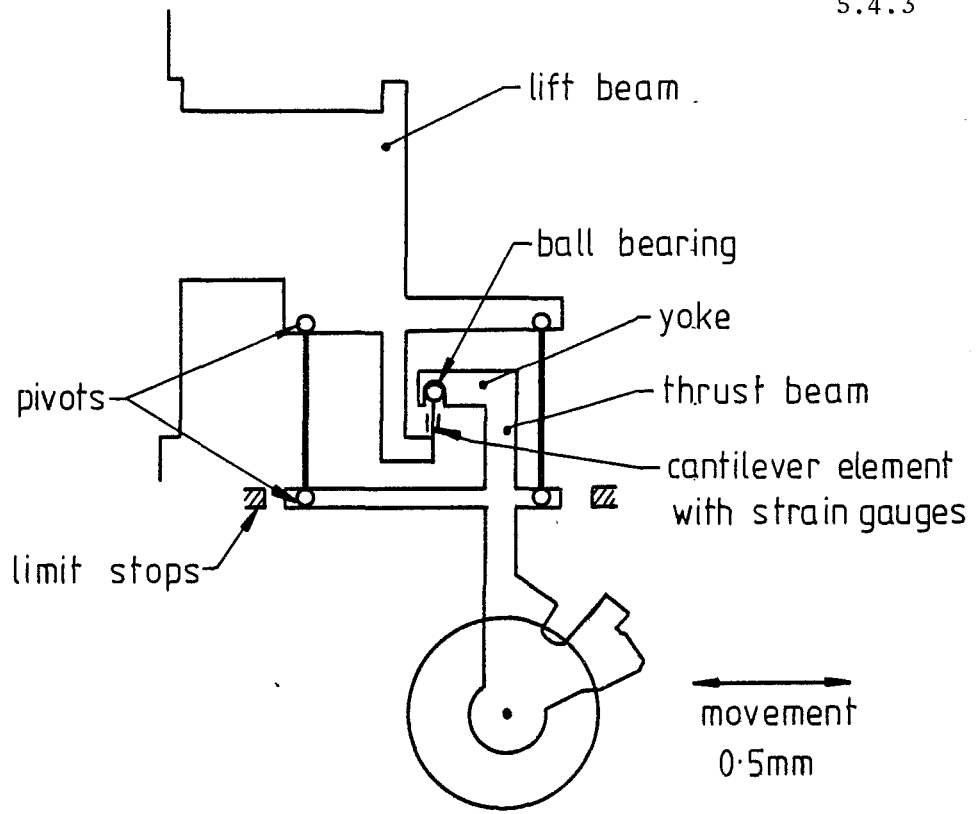


FIGURE 5.7 THE THRUST SENSING SECTION

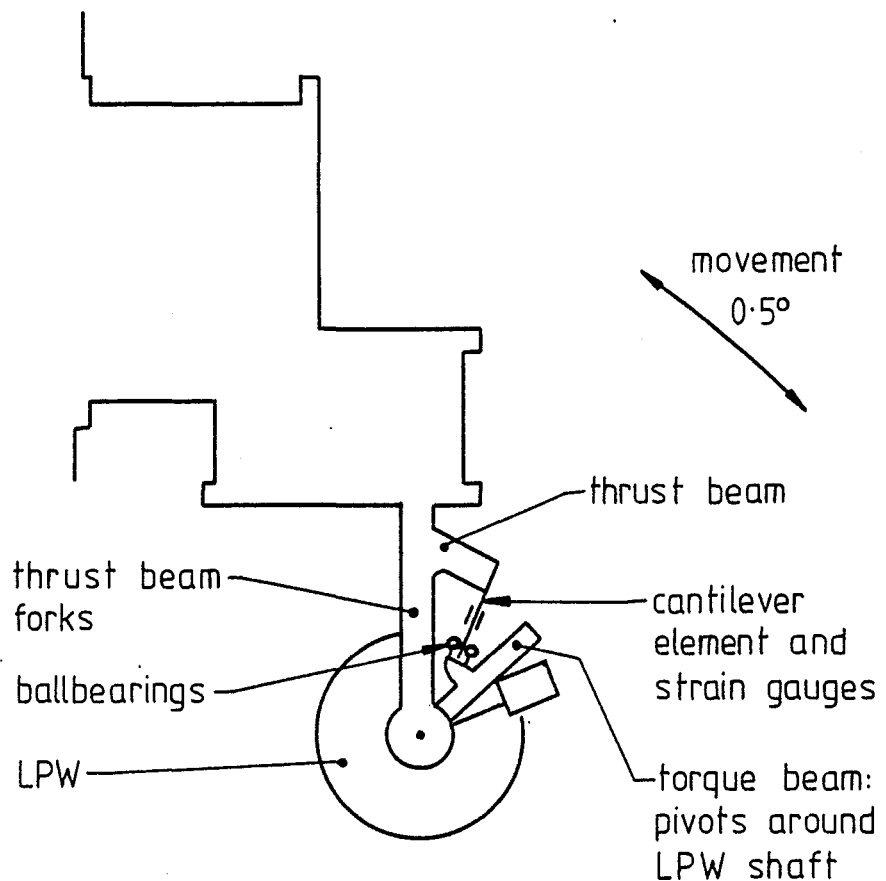


FIGURE 5.8 THE TORQUE SENSING SECTION

No end loads could be transmitted to this cantilever element as it had a ball bearing fitted to its free end which could move freely in the yoke on the lift beam. The total range of vertical movement of the lift beam was 0.7 mm and limited by stops. This range of movement represented forces from -25 N to +25 N with the particular lift sensing element used.

5.4.2 The Thrust Force Section

The thrust or propulsion force sensing section of the apparatus is shown in Fig.5.7. It was a four-bar link arrangement similar to the lift sensing section but at right angles to it to measure the horizontal component of the wheel force. No counterbalance weight was used as the weight of the thrust beam and its attachments was hanging on the links. However this meant that the thrust sensing section was sensitive to horizontal accelerations.

The cantilever force sensing element, fitted with strain gauges and a ball bearing on its free end, was of the same design as the one used for the lift sensing section. It was attached to the lift beam and the yoke engaging the ball bearing on its free end was attached to the thrust beam. Total horizontal movement of the thrust beam and its attachments was limited to 0.5 mm, and again this represented a force range from -25 N to +25 N.

5.4.3 The LPW Motive Power

The test wheel was mounted on a horizontal shaft which was driven through an enclosed right-angle drive of 2:1 reduction by a 340 W Black and Decker electric drill. The drill was incorporated into the torque beam as noted in Fig.5.4, and the standard drill power cable was replaced by more flexible, light wiring which was fixed to the balance in such a way as to have a minimal influence on the force sensing sections. Once this wiring left the force balance it was kept remote from the instrumentation wiring, to reduce interference.

The electric drill was powered from a Variac which can be seen on the Rating Car floor in Figs.5.28 and 5.29, and this allowed the operator to vary the LPW speed at will.

5.4.4 The Torque Sensing Section

The torque sensing section of the apparatus is shown in Fig.5.8. The torque beam was pivoted about the LPW shaft centre on a large ball bearing in the thrust beam fork, as shown in Fig.5.9. It was considered important that the bearings for the torque beam should not be mounted on the shaft itself since this would add the LPW shaft bearing friction to the measured torque. The torque beam was held almost upright by the torque sensing element (Fig.5.8). No practical counter balance weight was possible, so this section was sensitive to horizontal and vertical accelerations. The sensing element was originally intended to be a direct tension or compression element but the cantilever arrangement shown in Figs.5.8 and 5.10 was finally adopted as being more reliable and sensitive in practice. It was fixed to the thrust beam, and its free end moved between a pair of ball bearings on the torque beam so that no end loads could be transmitted to it. The total range of movement of the torque beam was 0.5° and this represented a torque range from -1.7 Nm to $+1.7 \text{ Nm}$.

5.4.5 Cantilever Force Sensing Elements

The cantilever elements, as shown in Fig.5.11 and photographed in Fig.5.6, were designed to give the optimum balance between the following three requirements:

- (i) minimum possible apparatus deflection on the application of the measured force,
- (ii) maximum possible strain in the cantilever element without permanent distortion,
- (iii) highest possible natural frequency for the apparatus.

Minimum deflection meant that small changes in the apparatus geometry, which resulted from the application of a force at the wheel, would not significantly effect the wheel's position nor introduce noticeable non-linearities or mutual interference between the sensors.

Maximum strains meant that the sensors would have a good sensitivity, producing large signals in the strain gauges for the application of small forces. Also for this reason the strain gauges were attached to both sides of the cantilever elements, and wired

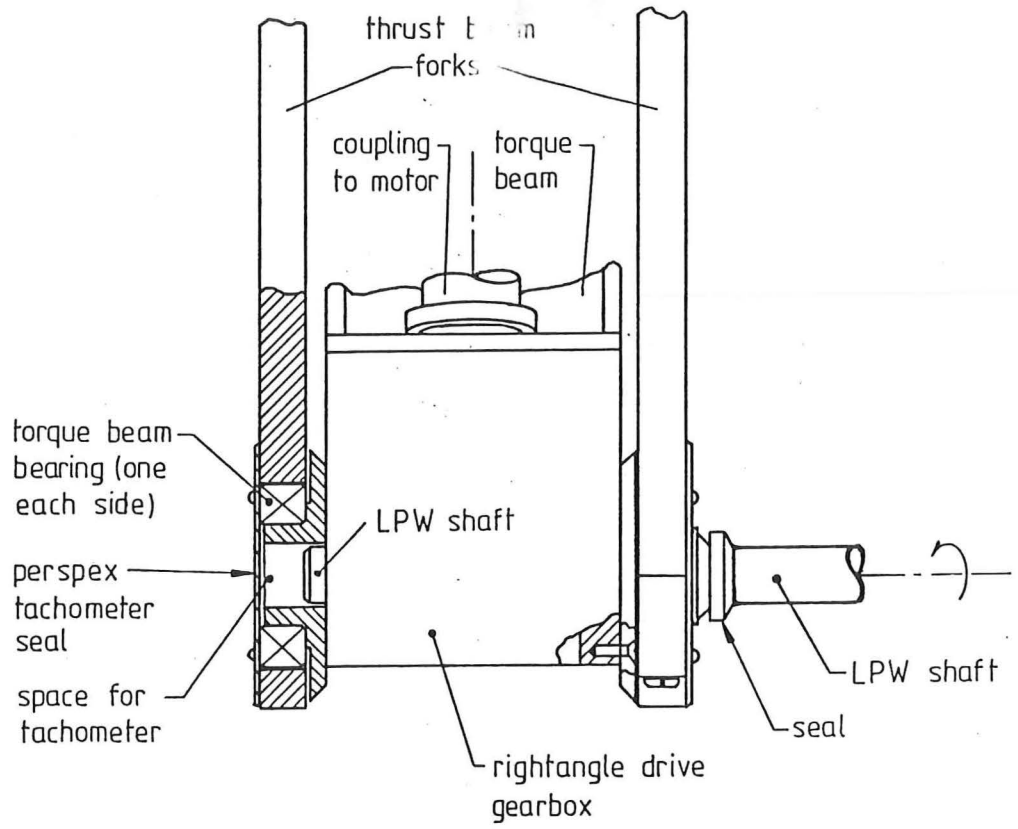
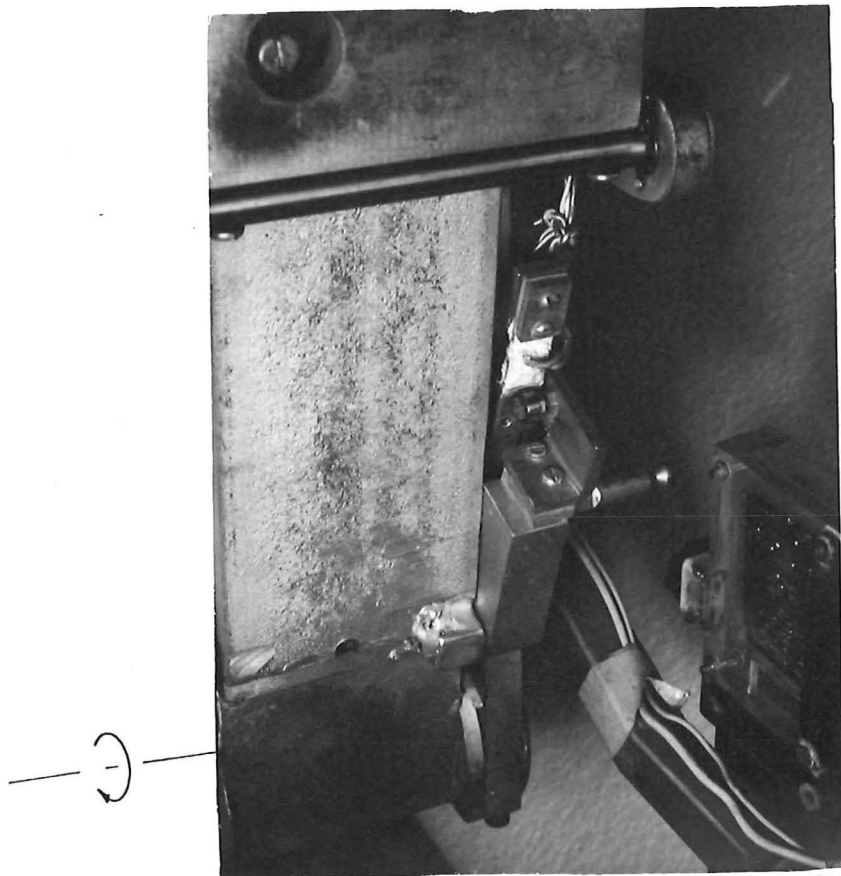


FIGURE 5.9 ASSEMBLY DRAWING SHOWING TORQUE BEAM BEARING ARRANGEMENT, LOOKING UPSTREAM.



1280/31

FIGURE 5.10: THE TORQUE CANTILEVER ELEMENT ATTACHED TO THE THRUST BEAM FORKS (LOOKING DOWNSTREAM)

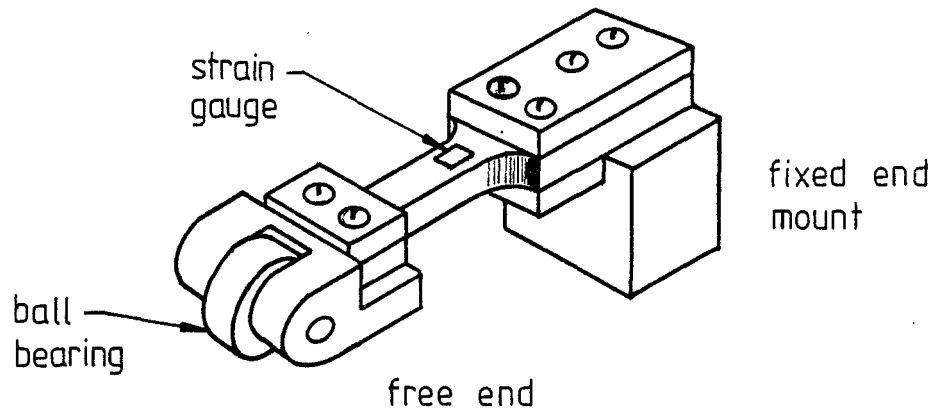
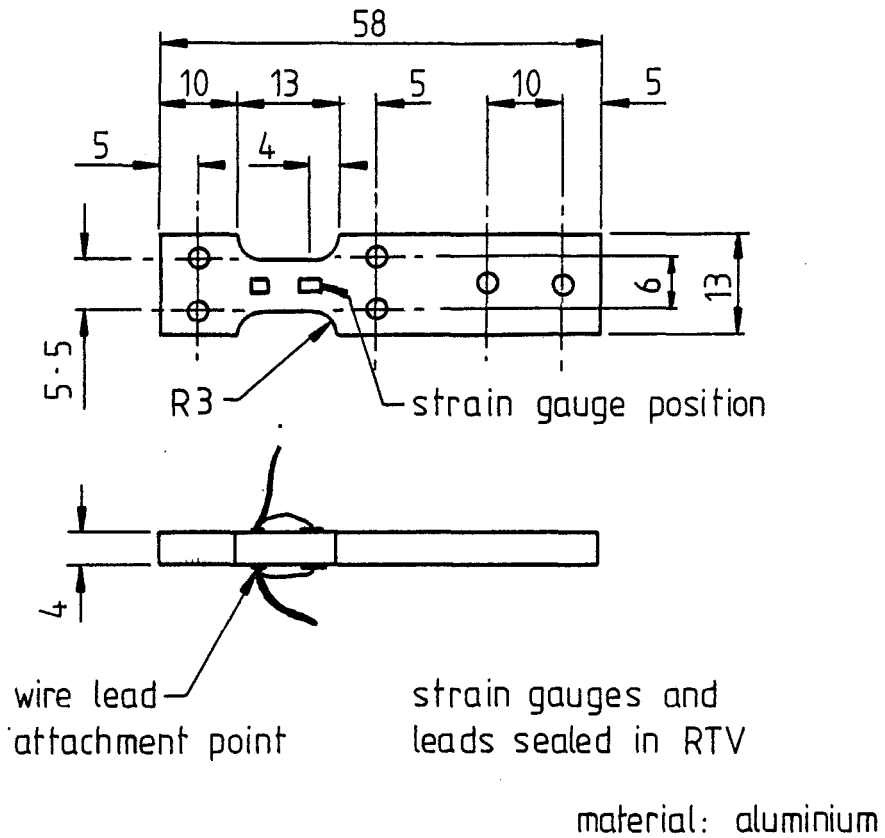


FIGURE 5.11 THE CANTILEVER SENSING ELEMENT FOR LIFT OR THRUST

Strain Gauge Specifications:

Kyowa type KFL-2-C1-23
 temperature compensated for aluminium
 gauge length - 2mm
 resistance - $120.0 \pm 0.3 \Omega$
 gauge factor - $2.11 \pm 1\%$

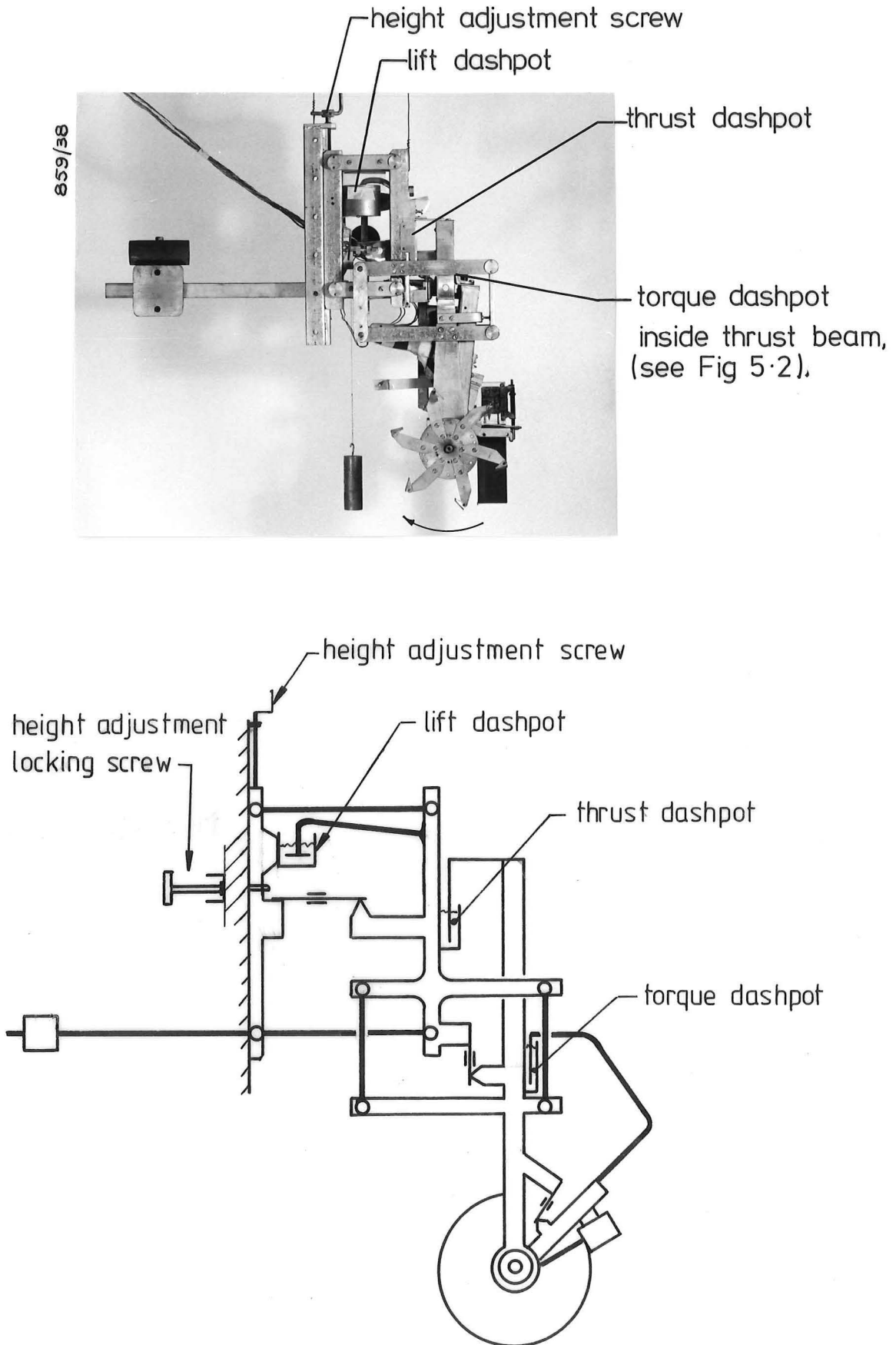


FIGURE 5.12 ARRANGEMENT OF DASHPOTS ON THE FORCE BALANCE

into the strain gauge bridges to make signals additive.

A high natural frequency for the apparatus meant that resonances in the apparatus could be filtered electrically from the signals produced, while the filters still allowed the system a reasonably fast response time. For example, the lift sensing section was calculated to have a mechanical resonant frequency of about 5 Hz with the final cantilever element design. With sharp cut-off filters (see section 6.3.1) resonances at this frequency in the signals could be reduced to negligible proportions (-26 dB) while the system response time remained at about 0.5 sec.

Aluminium was used for the cantilever element material as it gave larger strains for the limited space and forces being measured. Dimensions are given in Fig.5.11.

5.4.6 Damping

Small needle roller bearings were used on the link pivots and these were found to be very satisfactory low friction bearings, especially with the vibration caused by the wheel and the motor. However, this vibration and mechanical noise meant that the apparatus required mechanical damping to stop long term oscillations occurring. For this reason dashpots were incorporated into the balance, as shown schematically in Fig.5.12. The thrust and torque dashpots were of the side-to-side type. All three dashpots had oil as the working fluid, and the viscosity of oil in each one was adjusted so that the response of each section was a little less than critical damping. (Damping is further elaborated in section 6.3.1).

5.4.7 Immersion Setting

Vertical height adjustment of 120 mm was provided by means of the height-adjustment screw on the mounting beam (see Fig.5.12). This raised or lowered the immersion beam and the rest of the apparatus attached to it. Once the wheel immersion was set, the immersion beam was locked to the mounting beam by a locking screw also shown in Fig.5.12.

Greater height adjustment than this could be accomplished by remounting the whole apparatus on the next holes provided in the mounting beam.

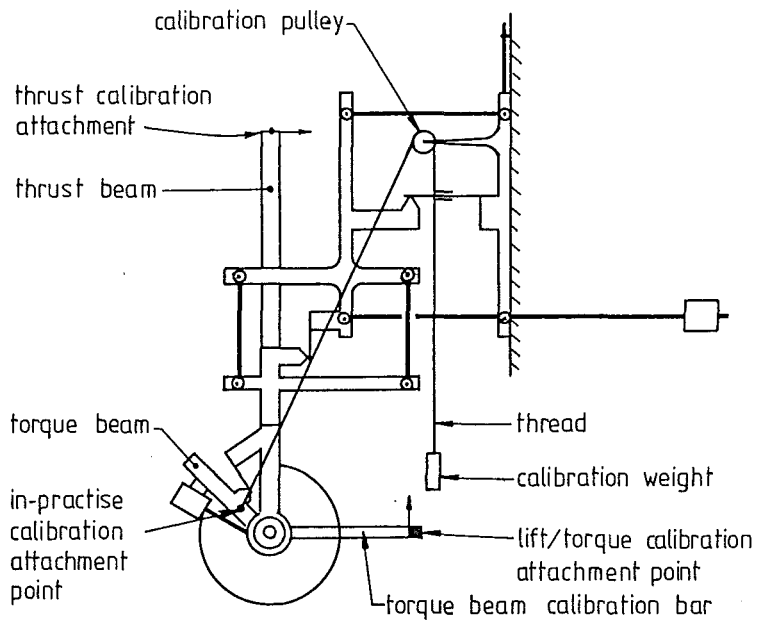


FIGURE 5-13 CALIBRATION THREAD AND WEIGHT ATTACHMENT POINTS WITH THE IN-PRACTICE CALIBRATION BEING PERFORMED.

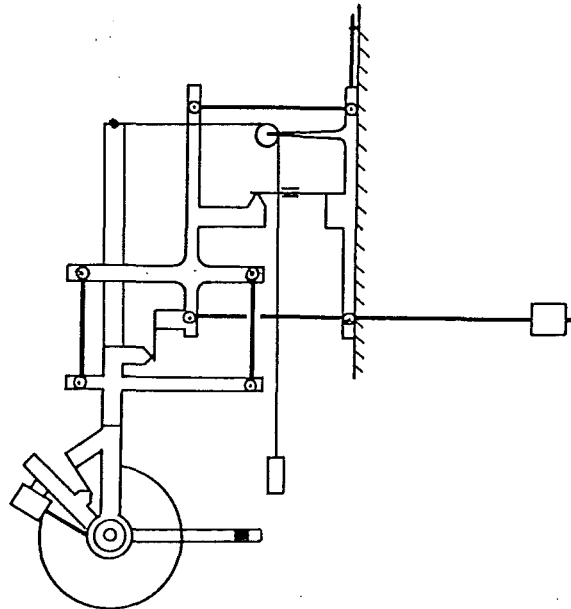


FIGURE 5-14 THRUST CALIBRATION

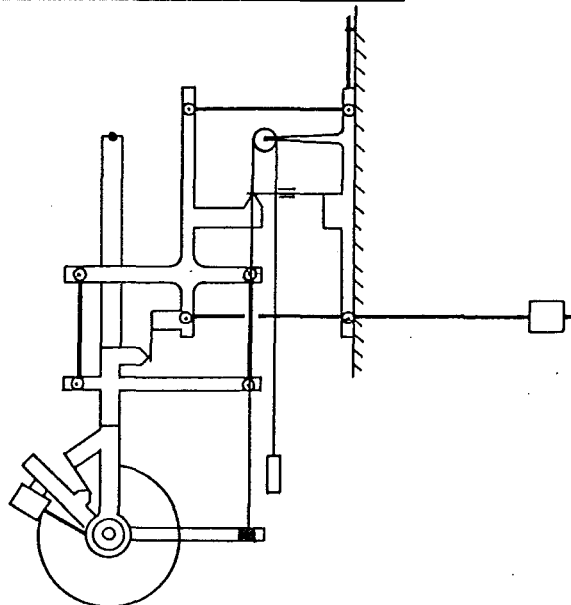


FIGURE 5-15 NEGATIVE TORQUE, POSITIVE LIFT CALIBRATION

5.5 FORCE SENSOR CALIBRATION

The electrical sections of the measurement system (discussed fully in section 6.2.1), namely the strain gauges, the strain gauge bridges, amplifiers and filters were subject to small scale temperature and time drift as well as being susceptible to unpredictable breakdowns in the wet environment around the LPW. In addition to this the cantilever sensing elements themselves could be overstrained under some extreme circumstances. For these reasons it was necessary to recalibrate the force sensors at regular intervals during the testing programme.

Two levels of calibration were used:

1. The original alignment calibrations.
2. The in-practice calibration.

5.5.1 The Original Alignment Calibrations

These involved balancing the strain gauge bridges, and applying a known force to each sensor in turn, first in one direction then the other. This process was carried out to determine the calibration factor to be used to multiply the value of the output voltage from the strain gauge amplifiers to arrive at the known applied force. This was a relatively long-winded task and originally involved checking the linearity of each sensor over the whole operating range as well.

(See Appendix 2.)

Thrust: For the original alignment thrust calibration the thrust beam incorporated a calibration attachment point noted in Fig.5.13 horizontally in line with the top of the calibration pulley. Positive thrust calibration involved hanging a known weight on a thread over an external pulley in line with this attachment point; and negative thrust calibration used the calibration pulley on the balance in a similar way (Fig.5.14). Note that the calibration pulley was attached to the immersion beam so that for calibration purposes it could be considered as external to the balance.

Torque and Lift: The torque beam incorporated a calibration bar with an attachment point vertically below the edge of the calibration pulley groove, as also shown in Fig.5.13. By passing a thread from this

attachment point and over the pulley to a known weight, both a known negative torque and a known positive lift force could be produced. (See Fig.5.15). Measurement of the moment arm of the calibration bar was required before the torque sensor could be calibrated.

To calibrate for positive torque and negative lift the weight was simply hung on the calibration bar attachment point.

These alignment calibrations were undertaken with considerable care both before and after the major series of tank tests. This briefing and debriefing procedure not only produced a set of appropriately accurate calibration factors, but also brought to light any significant peculiarities of the force balance system. (See Appendix 2.)

5.5.2 The In-Practice Calibration

The in-practice calibration was simpler and quicker to perform. It involved zeroing each sensor's output, then hanging the calibration weight over the calibration pulley on a thread attached to the other calibration attachment point on the torque beam as shown in Fig.5.13. This method applied midrange loads to all three sensors simultaneously. The actual forces applied were calculated after measuring the angle of the thread to the vertical, and the moment arm length to the shaft centre.

The advantage of this method was that it provided a quick check on the functioning of all the sensors, gave their calibration factors, and one data record could contain the calibration data for all three sensors at once. The disadvantage was that it was a little less accurate than the original alignment calibrations, though tests showed the two methods to give calibration factors within $\pm 0.5\%$ of each other. This was adequate for the purposes of these tests.

During tank tests the in-practice calibration was performed at the beginning and end of each day's testing, and any discrepancies between the two calibrations were dealt with during the subsequent data processing, (Part C, Fig.5.1 and section 7.4.2.)

5.6 FORCE SENSOR ZEROING

The force sensors, being strain gauges, needed to be rebalanced regularly to allow for the small scale amplifier drift and temperature

effects. As well as this, the amount of water clinging to and splashed on to the force balance affected zero readings, as did changes made to the test wheel, or extreme loads applied to the apparatus. For these reasons, as well as those affecting the force calibrations, it was necessary to keep a regular check on zero force readings.

During the tank tests the force zeros were registered at the beginning of each group of runs by balancing the strain gauge bridges then recording the close-to-zero values produced. At the end of the runs, or at any time it was felt necessary, a recording of what should still have been zero values was made, and the bridges rebalanced. Any significant discrepancies between a pair of zero force recordings was dealt with by linear interpolation in the subsequent processing of the data recordings (Part C on Fig.5.1 and section 7.4.1).

In practice it was found necessary to regularly check on the zero values and when this was done zero shift could readily be kept to insignificant proportions - about 0.5% of the rated force range, or within ± 0.1 N.

5.7 FORCE BALANCE PROBLEMS

Any complex system will have its running problems, so the most important ones encountered with the force balance are outlined here, while a thorough examination of sources of error is contained in Appendix 2 and a summary of sensor errors is contained in Table 7.9.

5.7.1 Thrust Calibration Error

This error meant that for most of the duration of the project recorded values of thrust force were 6.1% too great. The error was caused by the gain adjustment on the strain gauge amplifier. This introduced a discrepancy between the original alignment calibration and the original calculation of the in-practice calibration factor during the early bench testing of the apparatus. The error was perpetuated until the final, thorough debriefing calibration procedures brought it to light. Some concern was felt that this sensitive gain adjustment may have introduced intermittent errors during the tank tests but a careful examination of the in-practice calibration factors gave no indication that this had occurred. This error is discussed more fully in the introduction to Appendix 4, and at the end of Appendix 2.

5.7.2 Minor Design Faults

Six design difficulties caused minor problems during the life of the force balance:

- 1) The thrust and torque sensing sections, unlike the lift sensing section of the apparatus, were not balanced units, with the result that accelerations or bumps given to the force balance during operation caused erroneous readings to be recorded. In practice this ceased to be a problem when the Kainga tank was used, as long as velocity conditions were kept steady.
- 2) Aluminium was used for the cantilever sensing elements. Since this material does not have a linear stress-strain relationship the aluminium remained slightly strained after the application of large forces. This meant that the sensor would not quite return to indicating a zero force after such an application. Errors however were small, and became negligible with proper management, as discussed under Experimental Procedures, section 6.4.
- 3) The gearbox and shaft bearings were necessarily close to the LPW. This meant that during tests, especially at deep immersions, spray was thrown against this portion of the apparatus from the LPW as shown in Fig.5.16. While measurements suggested the effect on the measured forces to be negligible, a better design might have avoided the situation.
- 4) The dashpots were designed with small internal clearances and sideplay in the force balance bearings occasionally allowed the parts to touch. This was normally immediately apparent as force readings would not return to zero, and then the apparatus could be readjusted for free play.
- 5) The electric drill used to power the LPW was found to be inadequate for tests with the large, 383 mm diameter wheel and overheating limited the data that could be collected in such tests.
- 6) The sliding faces between the immersion beam and the mounting beam were not machined flat during construction. This meant that the apparatus tilted slightly (about 0.05°) for different immersion settings, and because of the unbalanced nature of the torque and thrust sensors, caused small zero force errors in these sensors. These force

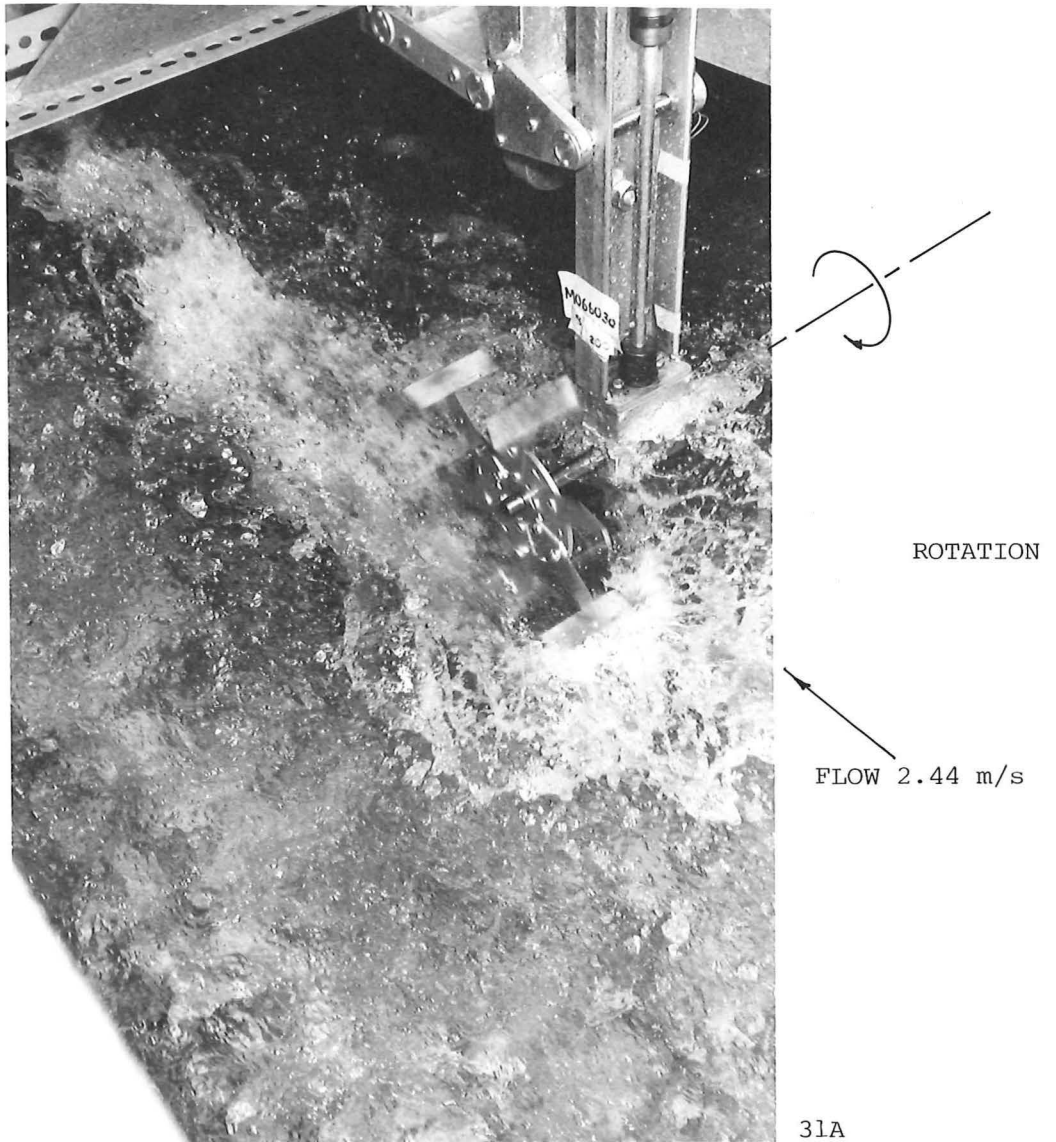
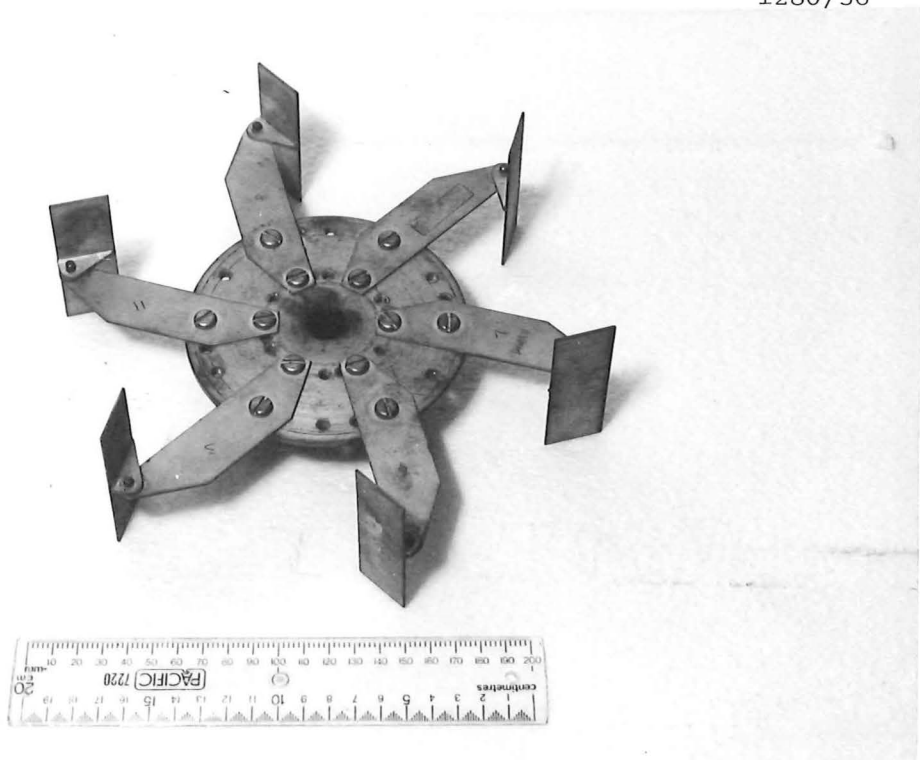


FIGURE 5.16: SPRAY FROM THE STANDARD WHEEL STRIKING THE 1977 VERSION OF THE FORCE BALANCE. $d/D = 0.17$, $n = 15$ rps

FIGURE 5.17: THE STANDARD LPW

1280/36



errors amounted to about 0.15 N and 0.01Nm and were normally negligible.

5.7.3 Running Faults

During the course of the tests some breakdowns occurred. The most significant of these were:

- 1) The perspex spray cover used over the LPW, occasionally jammed the thrust force sensor, if it was not properly in place. It is shown in Fig.5.29.
- 2) A thrust sensor strain gauge came loose from the cantilever element, and a tachometer wire broke inside the tachometer housing. These were readily fixed, but each caused the loss of a day's testing.
- 3) The torque beam bearings (Fig.5.9) showed a tendency to stiffen with time, causing some concern but very little actual error.

5.7.4 Conclusion For The Force Balance

The force balance was a complex piece of apparatus and therefore susceptible to some minor faults. While a simple system might have been devised the system used adequately fulfilled its intended function.

5.8 THE TESTED LIFTING PADDLEWHEELS

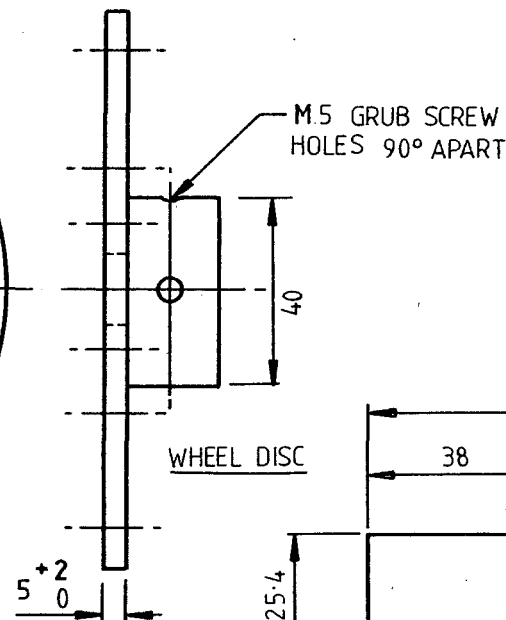
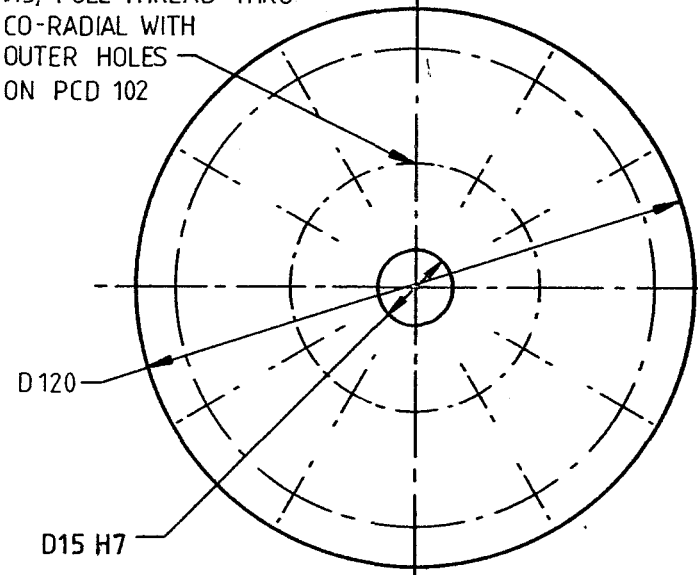
5.8.1 The Wheel Size

The wheel used for most of the tests in this project was close to 0.242 m in diameter (see Figs. 5.17 and 5.18). This wheel size was chosen mainly because the force balance and wheel were available from the 1977 tests and had been designed to fit the university flowing water tank (see section 5.9.1) which was to be used for this project's tests as well.

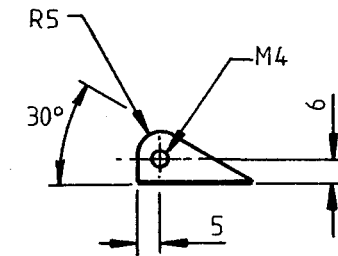
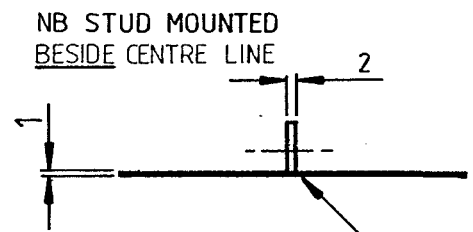
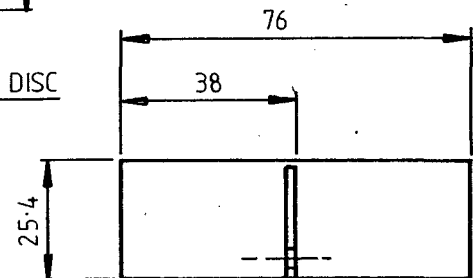
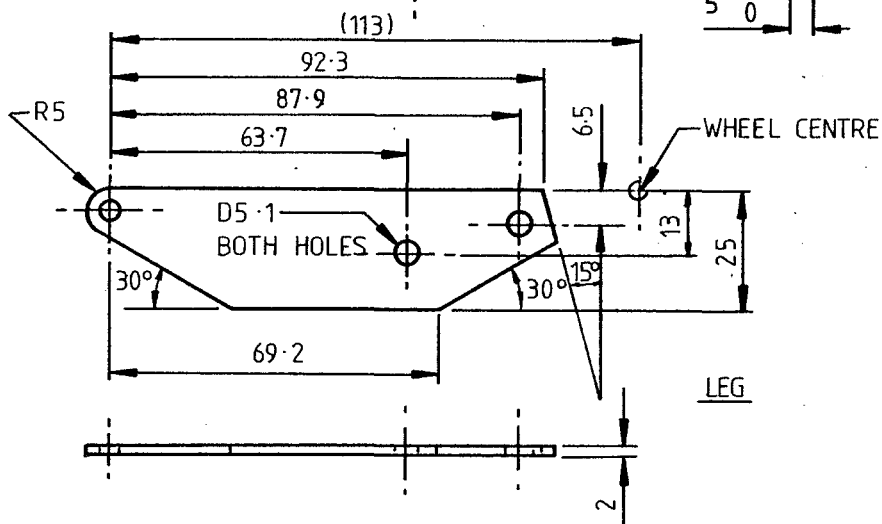
Beardsley recommended, however, that test paddlewheels should be a minimum of 0.3 m in diameter. (1) This is about 20% larger than this project's test wheel. Beardsley's recommendation was based in part on his own tests with a small diameter wheel and in part on the results of Wray and Starrett's tests with a 0.127 m wheel. (2) Beardsley, however, regarded his own results with small wheels as

1. Beardsley, P.15
2. Wray and Starrett, P.29

12 HOLES EQUI-SPACED, PCD 52,
M5, FULL THREAD THRU'
CO-RADIAL WITH
OUTER HOLES
ON PCD 102



BLADE ANGLE	WHEEL DIAMETER
0°	245mm
15°	242
30	243
45	243
60	242
75	239
90	236
105	239
120	242



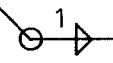
NOTE: BLADES MUST BE FLAT AFTER BRAZING
 'EASY FLO' BRAZING

FIGURE 5:18 THE WORKING DRAWINGS OF THE LPW AND TABLE OF DIAMETER CHANGES WITH BLADE ANGLE.

inaccurate because of the small forces involved and while in Wray and Starrett's results degradation of performance was recorded, there are a number of reasons other than its small size as to why their wheel demonstrated a poorer performance than others (these were noted in section 2.2.5).

With this uncertainty surrounding the effects of wheel diameter the alternatives were to build a wheel sufficiently large to avoid scale effects or to retain the available equipment, and investigate the effects of size in a test series. The only indication of how large wheels had to be to avoid scale effects came from the work of Volpich and Bridge (1) who found no discernable difference in the performance of wheels 0.518 m and 1.04 m in diameter, so that a wheel of 0.5 m in diameter would be required. This was too large for the testing tank it was intended to use, and it also would have made tests at high Froude Numbers difficult. It was decided therefore to develop the equipment from the 1977 tests, retain the wheel size of 0.242 m and examine the effects of wheel diameter. The test series examining these effects is discussed in section 9.4.4.

5.8.2 The Standard Test Wheel

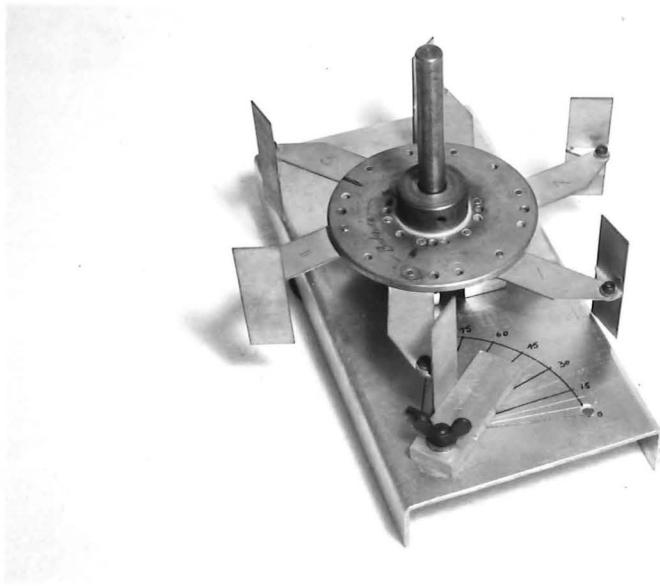
The lifting paddlewheel used for the tests was generally 242 mm in diameter with a blade span of 76 mm and chord of 25 mm. It is shown in Figs. 5.17 and 5.18. This was the same wheel as used in the 1977 project (2) and was geometrically similar to the 153 mm diameter wheel tested in the 1976 preliminary investigations (3) (Fig.3.1).

The wheel disc was designed so that it could be used with 2, 3, 4, 6, 8 or 12 evenly spaced blades. Each blade was attached to its leg by a single screw which could be loosened to allow adjustment of the blade angle, and tightened sufficiently to hold the setting while the wheel was operating.

The jig used in 1977 for setting the blade angles (Fig.5.19) was retained and continued to give a blade-setting accuracy of better than $\pm 1^\circ$ whenever it was checked.

The geometry of the wheel was arranged to minimise diameter changes with changes in blade angle, but for a practical design some

1. Volpich and Bridge, Part II, P.467
2. Alexander, 1977, P:22
3. Alexander, 1976 P.4



1280/28

FIGURE 5.19: THE JIG FOR SETTING BLADE ANGLES

diameter variation was inevitable. The wheel diameter for each blade angle is tabulated in Fig.5.18 and whereas the range of variation is only 0.75% of the total diameter this error is increased to 3% in coefficient calculations, so must be kept in mind.

This standard wheel was used for all the tests, with flat blades of all chords and spans, and with blade angles from 0° to 90° . The wheel was reversed to test for flat blades with blade angles between 90° and 120° .

A summary of the wheels tested with flat blades is contained in Table 5.20 and the results for wheels with flat blades are discussed in Chapter 9.

5.8.3 Other Wheels Tested

While the majority of tests undertaken were with flat bladed wheels, and the theory in Chapter 4 concerns only flat bladed wheels, a number of tests were conducted examining the effects of shaped blades, as well as some examining a variety of wheel variants. For most of these tests part of the standard wheel structure was used. The curved blades simply replaced the flat blades on the standard wheel spokes; the wheel disc was used with the cylinder, tractor tyre, Rollercraft wheels and the large diameter, 363 mm LPW. Perspex sideplates were readily mounted on the shaft itself, on small hubs for tests using sideplates, and the small, 153 mm diameter wheel had its own hub.

A summary of these other wheels tested is given in Table 5.21 and the results for wheels with other than flat blades are contained in Chapters 10 and 11.

5.9 TESTING TANKS

The LPW force balance was used to take measurements in three different tank systems during the course of the project. Although the final reliable results were obtained, eventually only from the Ministry of Works and Development (MWD) instrument calibration tank, the others are described as the difficulties encountered were instructive.

5.9.1 The Flowing-Water Tank

The 1977 and 1978 work used the large concrete flume in the Civil Engineering Department's Fluids Laboratory (earlier Figures

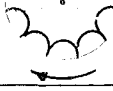
TABLE 5.20: SUMMARY OF FLAT-BLADED WHEEL TESTS

(Standard wheel dimensions: D=242, s=76, c=25; Fig. 5.18)

WHEEL CODE	NO. BLADES	DESCRIPTION	ANGLES	FULL OR SHORT TEST
<u>(A) THE REFERENCE SERIES OF TESTS:</u>				
6	6	STANDARD WHEEL 242 mm	60°	FULL + EXTRA
6	6	" " "	45°, 75°, 90°	FULL
6	6	" " "	0°, 15°, 30°, 120°	SHORT
<u>(B) THE WHEEL SIZE SERIES:</u>				
6.25	6	SMALL 153 mm	60°	SHORT
10	6	LARGE 383 mm	60°	SHORT
<u>(C) THE NUMBER OF BLADES SERIES:</u>				
3	3		60°	FULL
4	4		60°	SHORT
8	8		60°	SHORT
12	12		60°	FULL
<u>(D) THE CHORD AND SPAN SERIES:</u>				
9	6	SPAN = $\frac{1}{2}$ CHORD = $\frac{1}{2}$	60°	SHORT
2.75	6	" 1	60°	SHORT
7.25	6	" 2	60°	SHORT
8.5	6	SPAN = 1 CHORD = $\frac{1}{4}$	60°	FULL
2.25	6	" $\frac{1}{2}$	60°	FULL
5.25	6	" 2	60°	FULL
9.25	6	SPAN = 2 CHORD = $\frac{1}{2}$	60°	SHORT
9.5	6	" 1	60°	FULL
5.75	6	" 2	60°	SHORT
<u>(E) THE 3-BLADED CHORD & SPAN SERIES:</u>				
3.75	3	SPAN = 1 CHORD = $\frac{1}{2}$	60°	SHORT
3.25	3	SPAN = 1 CHORD = 2	60°	SHORT
<u>(F) THE MISCELLANEOUS SERIES:</u>				
6.5	6	SIDEPLATES ON STD. WHEEL	60°	FULL
1	6	3 BLADES @ 45°, 3 BLADES @ 90°	45/90°	SHORT

TABLE 5.21: TESTS OF OTHER TYPES OF WHEELS

(Full dimensions given in Figs.10.3,11.10,11.19,11.23)

WHEEL CODE	NO. BLADES	DESCRIPTION	ANGLES	FULL OR SHORT TEST
<u>(A) THE CHORDWISE-SHAPED BLADE SERIES</u>				
1.25	6		75°, 105°	SHORT
7.75	6	 Same as 1.25 but with holes.	90°	SHORT
1.25	6		90°	FULL
1.75	6		90°, 105°	SHORT
6.75	6		45°	SHORT
7.5	6		90°	SHORT
11	6	 semicircle	135°	FULL
<u>(B) THE TRACTOR TYRE SERIES</u>				
7	15	TRACTOR TYRE FORWARDS 	90°	FULL
4.75	15	TRACTOR TYRE BACKWARDS	90°	FULL
<u>(C) THE ROLLERCRAFT SERIES</u>				
5	12	KEARSEY'S ROLLERCRAFT WHEEL $\phi = 215$ mm	-	SHORT
5.5	12	METAL IMMITATION OF ROLLERCRAFT 	90°	SHORT
<u>(D) THE SOLID CYLINDER SERIES</u>				
0	-	SOLID CYLINDER, STANDARD DIMENSIONS	-	FULL

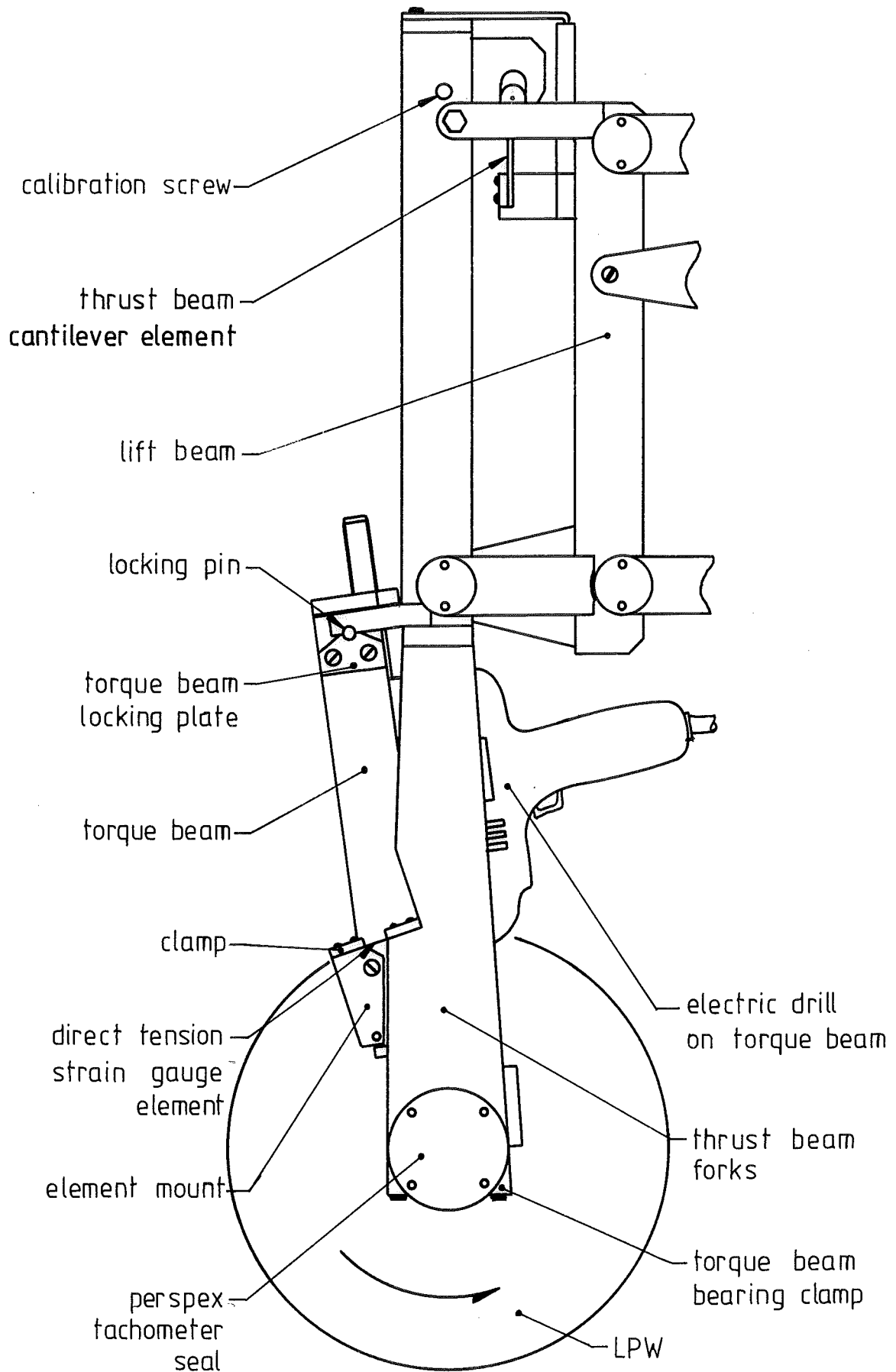


FIGURE 5-23 THE TORQUE SENSING SECTION OF THE 1978 FORCE BALANCE.

3.7 and 5.16). This measured 9 m long by 0.86 m deep and 1.1 m wide. It could be made to pass the full flow of the Fluids Laboratory pumps which amounted to almost 0.425 cumecs (15 cusec). The speed of flow was limited to about 5.7 m/s by the 2 m height of the header tower at the tank inlet. Below this speed, the water depth, velocity and type of flow could be controlled by gates at either end of the tank, as well as by the inlet valve, and constrictions placed in the flow.

The 1977 project used subcritical deep flow up to 1.7 m/s and supercritical, shallow (0.1 m) flow at 2.36 m/s. This flow can be seen in the tank during the 1977 tests in Fig.3.7.

5.9.2 The Abortive 1978 Tests

Two of the main recommendations forwarded by the 1977 project were that: (1)

- (1) Reliable power measurements were necessary, and
- (2) it would be advantageous to find out if efficiency improved with speed as seemed to be the case from the 1977 tests.

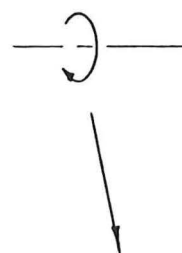
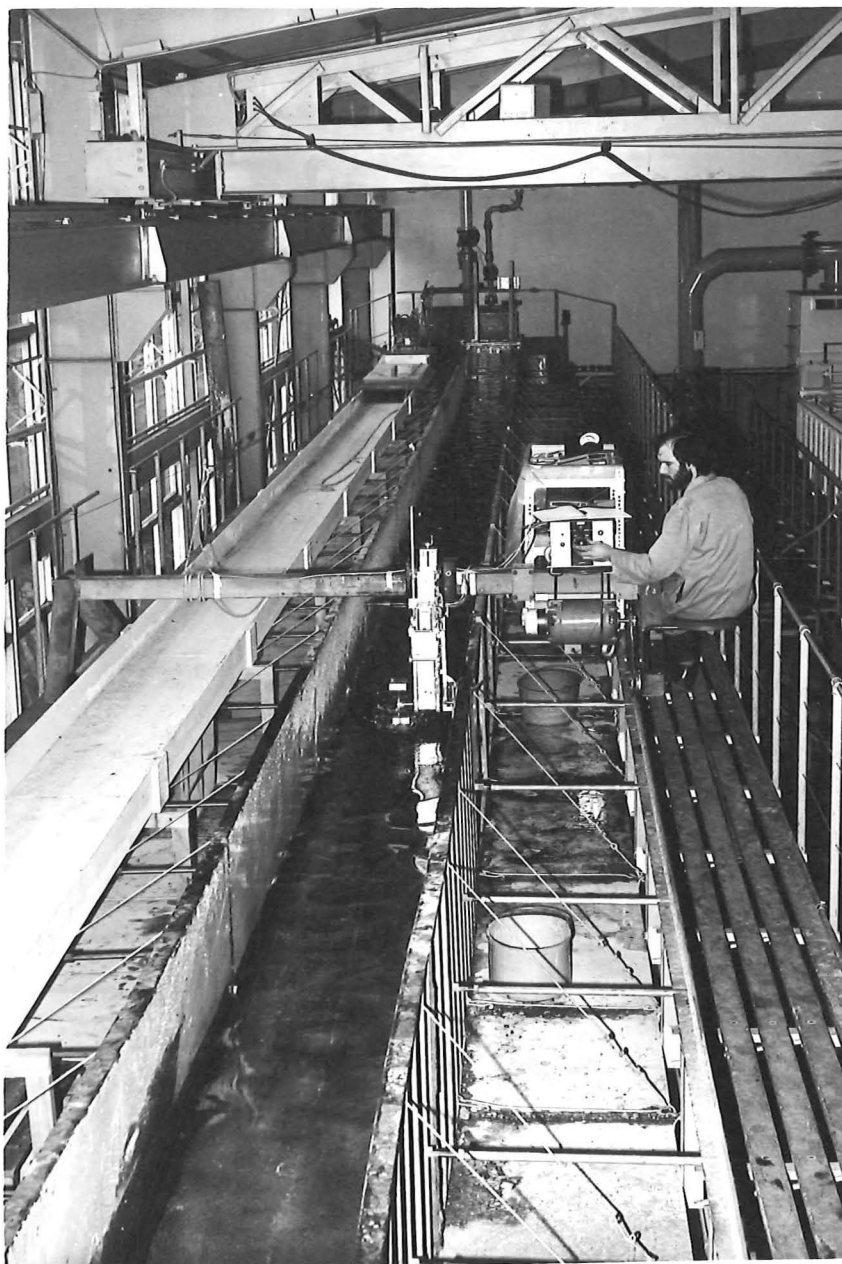
For these reasons the 1977 force balance was considerably altered during 1978 so that it could now measure the LPW torque as well as lift and thrust forces (Fig.5.23). Also attention was given to obtaining the highest practicable water speeds for a test series.

The MWD stated that its facility was limited to speeds of 3.7 m/s. The Fluids Laboratory flowing water tank gave 5 m/s at a depth of about 70 mm. In order to get an adequate depth of flow a 300 mm wide channel was designed by the author (Fig.5.24) to fit into this tank, and after the eventual addition of curved entry plates speeds of 5 m/s of supercritical flow with depths of 230 mm were achieved.

However there were a number of disadvantages with this arrangement, the main ones being that the oblique standing waves on the water surface, while only about 20 mm in height, were significant for the LPW tests, and as well as this, any high speed tests necessitated a complete take-over of the Fluids Laboratory in terms of pump power, water supply, noise and mess.



FIGURE 5.24: THE HIGH SPEED, FLOWING WATER CHANNEL FOR THE CONCRETE FLUME BEFORE INSTALLATION.



664/25

FIGURE 5.25: LPW TESTS IN THE LONG STATIC FLUME IN THE FLUIDS LABORATORY. THE TROLLEY IS MOVING OUT OF THE PAGE

The initial runs at this full capacity produced a set of consistent results, but analysis produced efficiencies of up to 130% which necessitated a careful examination of the fundamental design of the force balance. It was at this stage that the basic design fault mentioned in section 3.4 was brought to light. This meant that the thrust results for these high speed tests as well as for all the 1977 tests were erroneous.

In theory these earlier results could have been retrieved from the recorded data, but after some considerable effort it was found that in practice the accumulated errors of the measured forces rendered the calculated thrust values irretrievable. The force balance was again redesigned, and the subsequent test programme necessarily repeated the 1977 tests.

5.9.3 The Fluids Laboratory Static Tank 1979

Since it was now necessary to repeat all the LPW tests it was decided to try to avoid the uncertainties of flowing water and aim to use still water tanks for all tests. As the redesigned force balance system was intended for use with an expensive Solartron data logger it was seen as important to keep the equipment within the university if possible. For these two reasons an attempt was made to use another tank system available in the Fluids Laboratory.

The tank considered was the long flume normally used with flowing water for sediment transport studies. This tank had a useable length of 20 m, was 0.8 m deep and 0.6 m wide, and was spanned by a crude trolley which ran on rails along the length of the tank. The tank was levelled, filled with water, and the trolley was motorised with a variable speed electric motor. The equipment and force balance were mounted on it and a power supply cord was arranged. (See Fig.5.25.) A week was spent ironing out the usual problems and attempting to obtain sensible results. Only a few consistent results could be acquired. The trolley rails had never been intended for this purpose; they were not flat or smooth and the consequent jolting of the force balance rendered the torque results meaningless.

These tests also had to be abandoned.

5.9.4 The MWD Rating Tank at Kainga

The presence of this excellent facility 20 kilometres from the university was one very fortunate aspect of the project. Such a tank

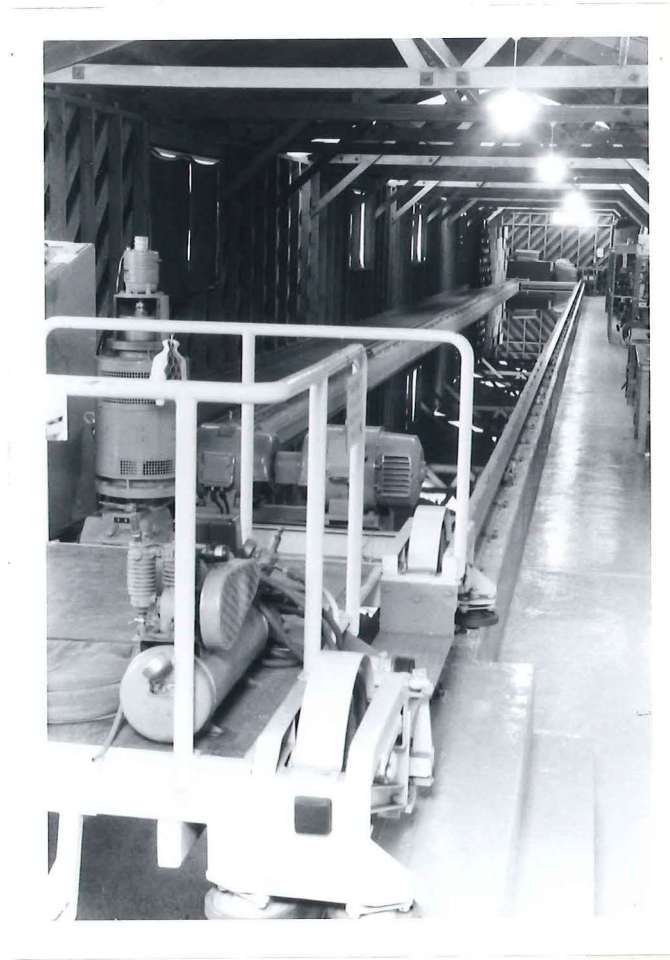
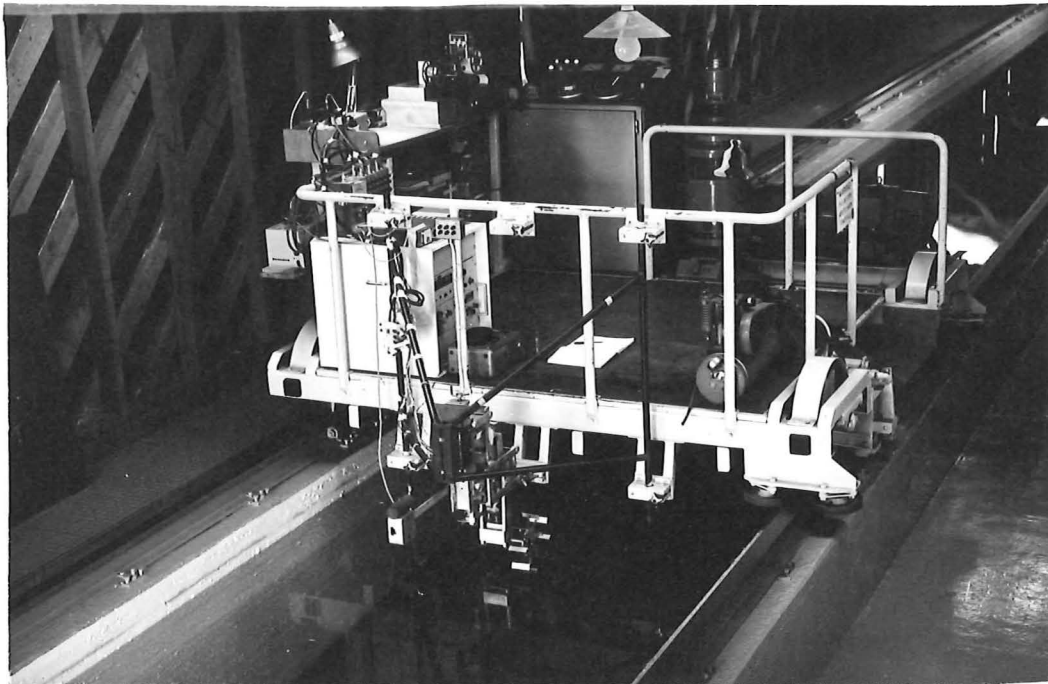
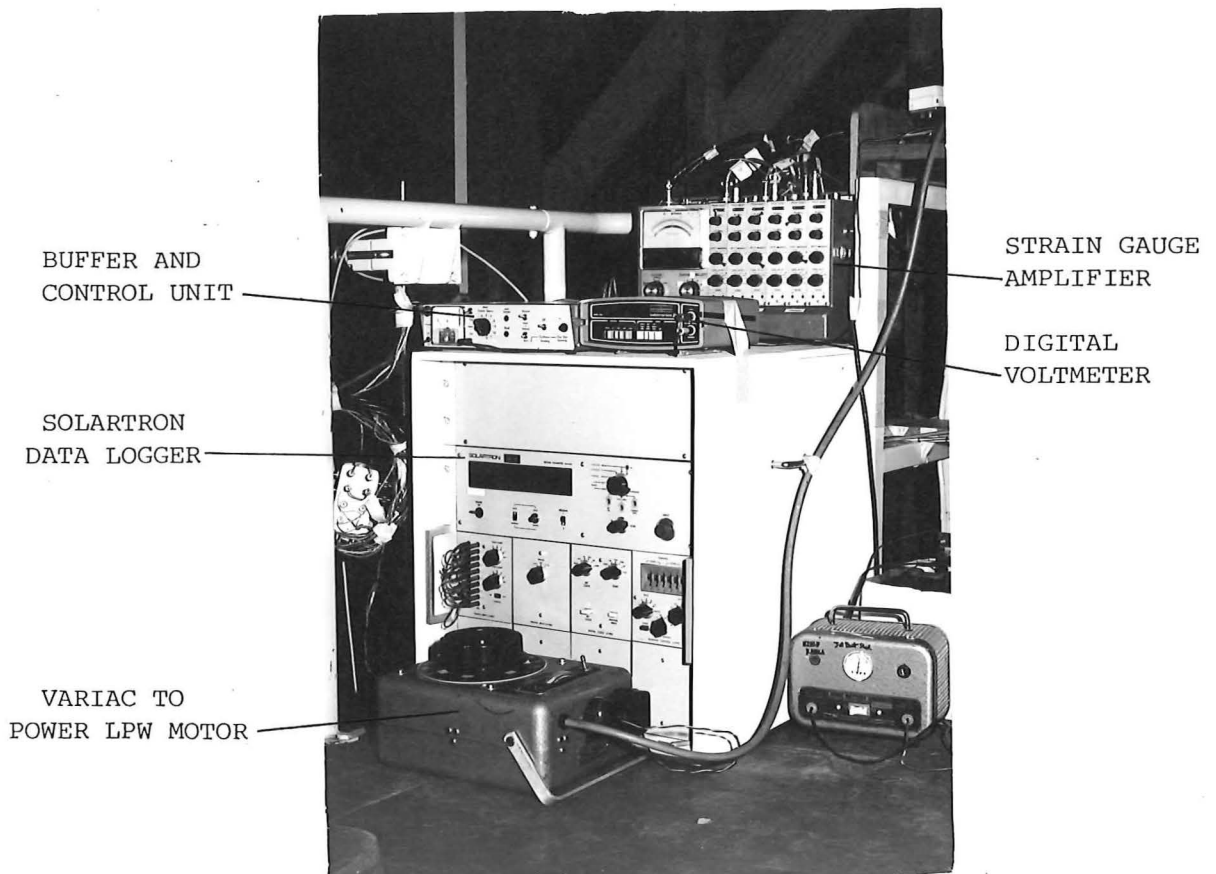


FIGURE 5.26: TWO VIEWS OF THE TESTING TANK AT KAINGA; TOP, FROM BESIDE THE RATING CAR, AND BOTTOM FROM THE OTHER END OF THE TANK. THE RATING CAR CAN BE SEEN STRADDLING THE TANK IN THE BOTTOM VIEW.



762/30A

FIGURE 5.27: THE RATING CAR AT THE KAINGA TANK WITH THE FORCE BALANCE MOUNTED ON THE BACK



717/23A

FIGURE 5.28: SOME OF THE INSTRUMENTATION AND DATA LOGGING EQUIPMENT ON THE RATING CAR

could hardly have been more ideal.

The indoor tank itself is close to 50 m in length, 1.83 m wide and 1.83 m deep (Fig.5.26). It is used by the Ministry of Works and Development for calibrating river flow meters. For this purpose an electrically driven "Rating Car" (Fig.5.27) spans the tank and runs on rails along its sides. The Rating Car was originally designed to travel at speeds up to about 7.3 m/s but this speed cannot be reached safely since the tank is only half its original design length of 100 m. Nevertheless speeds of 5 m/s can usefully be achieved within the present tank length, (which is contrary to the original information that the maximum speed was 3.7 m/s).

The speed of the car can generally be controlled to within very narrow limits, and an accurate measuring device gives a papertape output which can be used to calculate the car speed to an accuracy of within 3 mm/sec. Unfortunately, because of a fault in the Rating Car control system at the time of the tests, the speed of the Rating Car could not be predetermined to better than $\pm 5\%$ of a selected speed, although once set, the speed remained constant within narrow limits. This meant that some variation from the five selected speeds chosen for the tests had to be tolerated.

The Rating Tank building also houses a well equipped workshop where the staff repair and maintain the instruments.

Formal permission for use of the facility was arranged in June 1979 and tests were conducted intermittently for over a year as and when the tank became available from its routine work.

5.10 THE FORCE BALANCE AT THE KAINGA TANK

The equipment for the LPW tests had to be mounted on the Rating Car in such a way that it could readily be removed at the end of each day's testing, so the tank could be used for its normal purposes. The electrical equipment was stored on the Rating Car itself and presented no problem, Fig.5.28.

The force balance required a specially built frame to allow it to be mounted on the standard fittings at the rear of the Rating Car (Fig.5.27). Its attachment and removal were brief tasks, and storage space was provided for the balance, still attached to the frame, beside the tank.

It was stipulated that spray should be kept off the tank rails to prevent their rusting, so a perspex guard was constructed to cover the LPW, as shown in Fig.5.29. Some concern was felt that spray might rebound from this guard and interfere with the LPW action, but observations of it at high wheel revolutions indicated that the spray spread over the inside of the guard and left it at the sides and rear. Clearly, though, the guard prevented air drag effects which were examined separately with the wheel out of the water.

Tests in this tank at speeds of 5 m/s and 3.71 m/s were difficult to perform since the steady speed could only be maintained for a few seconds in which time one or possibly two data recordings could be made. (Each recording took 2.75 sec.) This necessitated a large number of runs for very little data. However, because of minor problems with the car control unit, the Officer-in-Charge limited test speeds to 2.5 m/s after the first few days of testing. Fortunately a representative set of high speed data had been obtained at this stage, and the lower speed limit was sufficiently high for the test wheels to be well into their planing mode of operation.

One of the conditions of use of the facility was that operation of the car could only be performed by MWD staff, and it was much to the advantage of the project that the technicians concerned were entirely helpful, interested and encouraging.

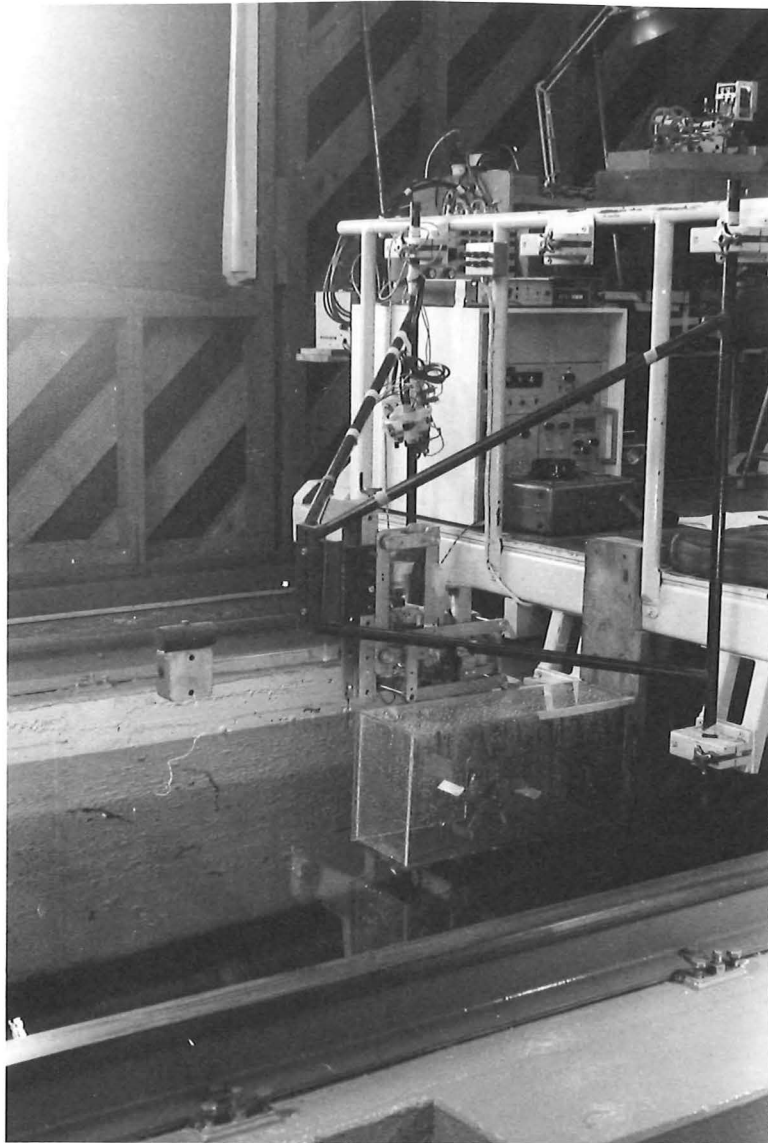


FIGURE 5.29: ANOTHER VIEW OF THE FORCE BALANCE MOUNTED ON THE RATING CAR. THE PERSPEX SPRAY COVER ENCLOSSES THE LPW

CHAPTER 6

INSTRUMENTATION, DATA ACQUISITION AND
EXPERIMENTAL PROCEDURES6.1 INTRODUCTION

This chapter covers three areas. The first describes the instrumentation, the electromechanical devices other than the force balance itself, which were developed and used as parts of the measuring system. The second describes the data acquisition equipment forming the train from the instruments to the punched papertape record, and the third describes the procedures used at the testing tank in taking measurements and getting them on to this record.

This chapter completes the description of the equipment and procedures used at the testing tank. The next chapter, Chapter 7, outlines the data handling process from the papertape record produced at the testing tank to the data plotted in graphical form.

This process fulfils the tertiary aims of Fig.3.10, part A2.

6.2 INSTRUMENTATION

Since the Solartron data logging unit was used and this was set up to read analogue rather than digital signals, all instrumentation was designed to produce analogue signals of either -10V to +10V or 0V to 10V.

6.2.1 The Strain Gauge Units

As noted in section 5.4.5 and Fig.5.11, the force sensing cantilever elements were each fitted with a temperature compensated strain gauge of 2 mm gauge length on each side. The pair of strain gauges was wired into the terminal box in the quarter-bridge configuration so that the two signals were additive, making a more sensitive instrument. The wiring from each cantilever element was arranged on the force balance so as to have as little influence as possible on the movement of the sensing sections, and it was securely fastened to the immersion beam at its exit point so that no movement of the wiring leading from the apparatus could influence the force readings.

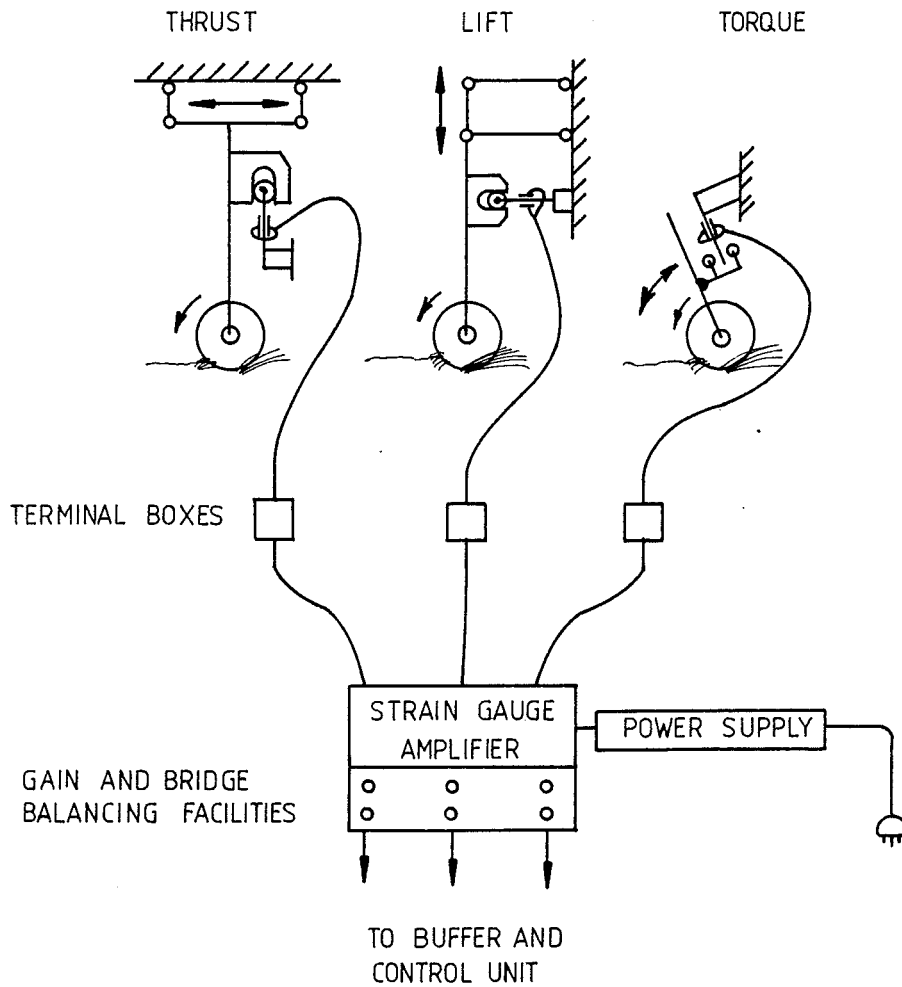
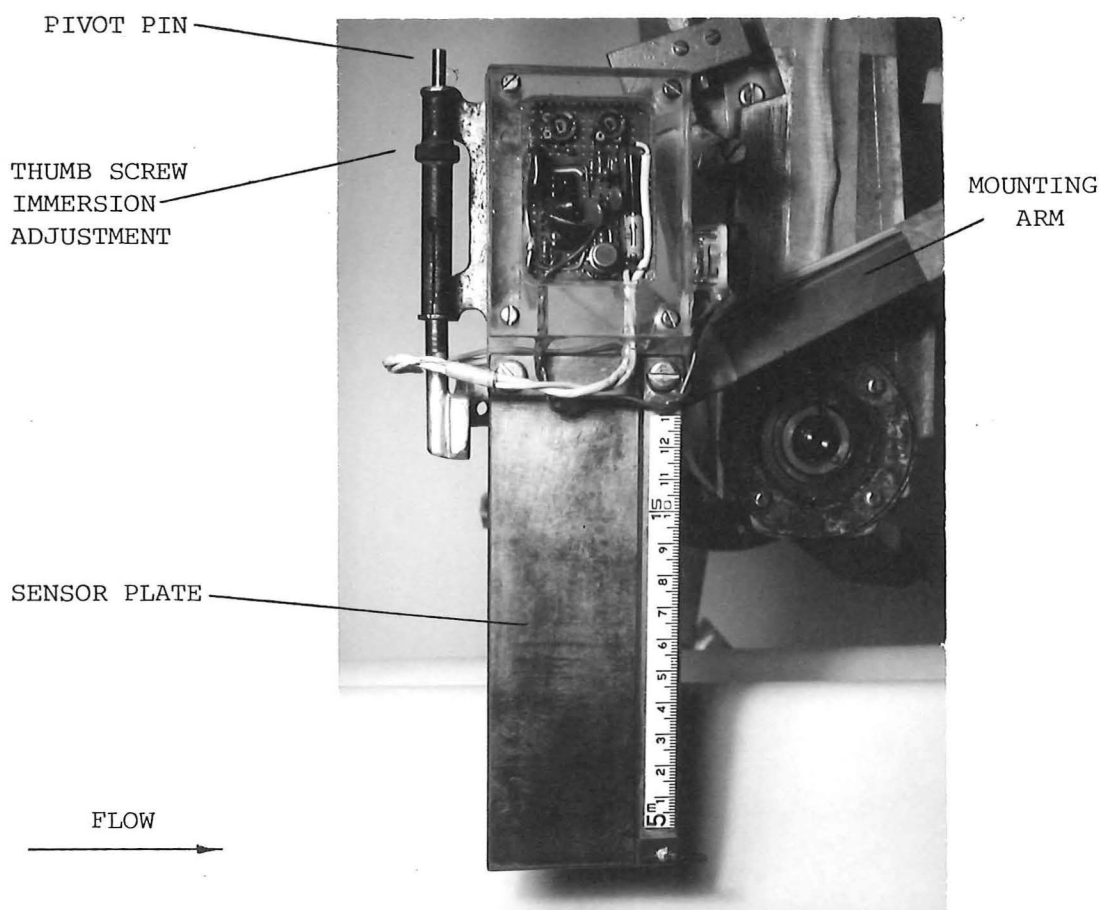


FIGURE 6.1 FORCE SENSOR WIRING TO THE KYOWA STRAIN GAUGE AMPLIFIER



1280/37

FIGURE 6.2: THE CAPACITANCE DEPTH GAUGE

As shown in Fig.6.1 the terminal boxes lead to the Kyowa six-channel strain gauge amplifier where the bridges could be balanced (thereby zeroing the force balance sensors), and the calibration factors set, using the gain controls. In practice, there was no need to adjust the gain of each amplifier as the calibration factors varied little from test to test, and the in-practice calibration procedure determined the exact calibration factors for each day's testing.

The Kyowa amplifiers offered a constant voltage or constant current output and the constant current varying voltage option was chosen and these signals fed into the Buffer and Control Unit.

6.2.2 Immersion Depth Gauges

Two depth indicators were used during the tests. One is shown in Fig.6.2 and the other can be seen in Fig.6.3. The first was developed by the author as a water depth measuring instrument for use with the LPW in water with a relatively unstable surface, such as the high speed flowing water channel, described in section 5.9.2, where it would be necessary to get an immersion depth reading at the moment of force measurement.

It worked as a capacitance meter, with the water acting as one capacitor plate, and gave a linear voltage output for a linear change in immersion. The circuitry for this unit is contained in Appendix 1, Fig.A1.1. Since the changes in immersion of the sensor plate gave changes in capacitance of only picofarad magnitudes it was not possible to run long leads from the sensor capacitor plate to the circuitry without introducing spurious capacitance effects in them on the way. For this reason the circuitry was mounted as close as possible to the plate itself and it can be seen in Fig.6.2 mounted on the plate in a sealed perspex box.

The capacitance probe itself was made of standard p.c. board with copper on one side only. The copper was used as one plate of the capacitor and water as the other. The copper was insulated from the water by a thin sheet of mylar. The plate was protected from splashes from the wheel as the copper surface was on the side of the p.c. board away from the LPW, as shown in Fig.6.2.

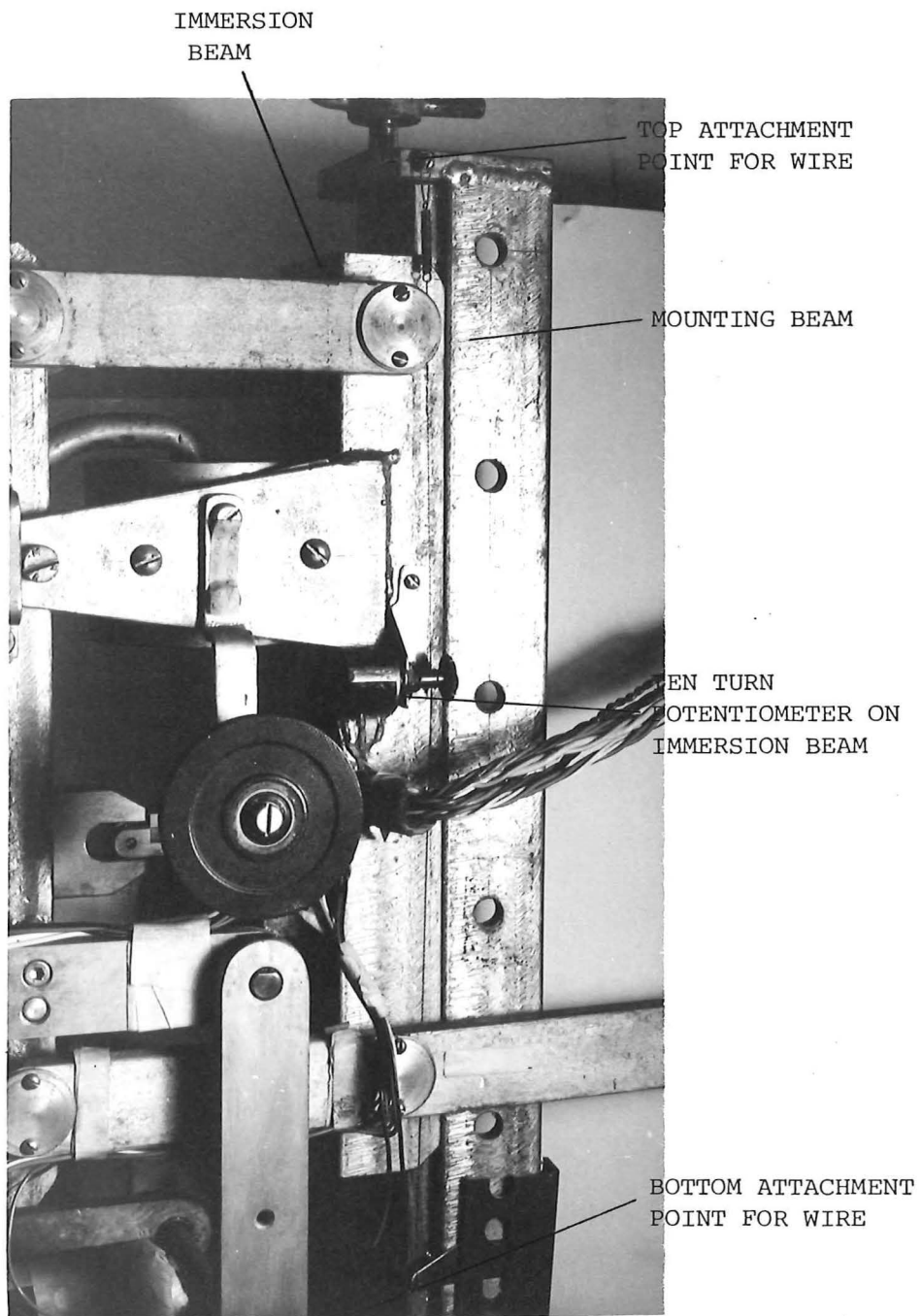
The unit pivoted on its mounting pin so it could trail in the water, and its immersion could be adjusted to suit each test wheel zero immersion level, using the thumbscrew between its upper and lower mounting points.

Its mounting arm was attached to the lift beam. This meant that its drag would not be recorded by the thrust sensor, but changes in immersion of the gauge would cause its buoyancy force to be added to the lift force. This was tolerable as it amounted to 0.06 N maximum.

While this gauge worked well under static conditions its response time to a step reduction in immersion was long (2 sec.) for large changes in immersion (60 mm) instead of the 0.5 sec. required, since a water film tended to cling to its surface. In flowing water it set up its own small wave train which caused a slight variation in the immersion reading depending on the velocity of the flow. As well as this, it was noted in the flowing water tests (see section 5.9.1) that the surface level at the gauge, which was placed 20 cm to one side of the LPW itself, could be different than the level at the wheel, by up to 10 mm.

For these reasons it could only be used with caution and although it was kept as a back-up throughout the Kaianga tank tests and was used to estimate wave heights in the tank, it was not normally used during the actual testing.

The other indicator shown in Fig.6.3 did not measure water immersion. It was simply a displacement transducer in the form of a ten-turn potentiometer, attached to the immersion beam, with its shaft rotated by a fine wire which was looped around it and connected to the mounting beam. In practice, the force balance zero immersion position was set by the height-adjustment screw (Fig.5.12) so that the wheel was just touching the water surface, and then the potentiometer was turned by hand, its shaft slipping in the wire loop, until the voltage reading it gave at the Buffer and Control Unit represented zero immersion. Any subsequent changes in immersion of the wheel, as set by the height-adjustment screw, rotated this potentiometer giving an immersion depth reading representative of the change. Checks of linearity and repeatability with this gauge indicated that in use



1280/34

FIGURE 6.3: THE 'DISPLACEMENT TRANSDUCER' (TEN TURN POTENTIOMETER) USED TO INDICATE IMMERSION DEPTH

depth settings were normally made to within ± 0.7 mm of the required setting. This was considered satisfactory.

Clearly, readings from this gauge were not always representative of the actual immersion of the wheel, such as when waves or seiches were present in the tank. These proved to be a potential, if not actual source of large errors during the tests, since a difference in water level of 10 mm between the ends of the 50 m tank could cause force measurements to vary up to 25%. Normally, however, such errors were avoided by allowing the tank water to settle between runs, and then this gauge was an adequate indicator of the wheel immersion depth.

6.2.3 The Tachometer

As noted in section 5.3 it was necessary to measure the wheel revolutions since circuitry to control the wheel revolutions at fixed settings was not made in time for the project. A sketch of the mechanical components of the tachometer is given in Fig.6.4. It was essentially a rotating on-off switch which changed its state 19 times per wheel revolution. The rotating part was machined by the author from a Meccano gear which had had its teeth filled with Araldite, and it was attached centrally to a perspex mount on the end of the LPW shaft. One pair of phosphor-bronze wipers contacted the teeth and another pair contacted the gear hub. The whole assembly was sealed behind a perspex window as shown in Fig.6.5 where its condition could be readily observed.

The circuitry which converted this switching into an analogue voltage was contained in the Buffer and Control Unit and was built round a frequency-to-voltage converter integrated circuit, with its associated components. The actual circuit is shown in Appendix 1, Fig.A1.2.

The instrument was checked for linearity and found to be within $\pm 0.4\%$; it was adjusted to give an output of 10 V for the maximum expected wheel speed of 26 rps. It performed well, though one lead broke, and it once needed cleaning when water penetrated the seal during the period of testing.

6.2.4 Speed Of Advance Indicator

A speed measuring device was necessary for use in the Fluids Laboratory tanks, especially for the large static tank described in section 5.9.3, where the trolley speed would not otherwise have been

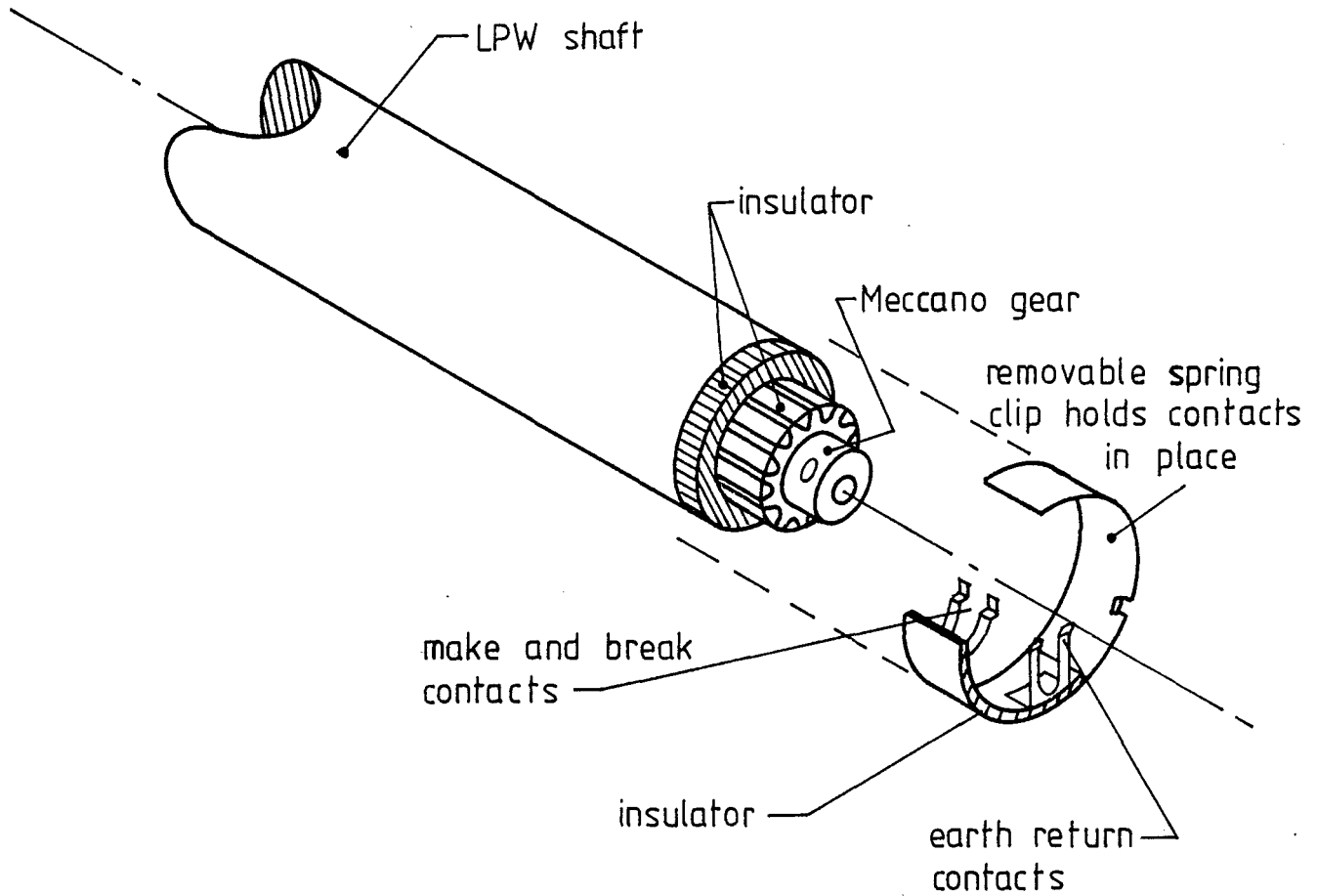


FIGURE 6.4 THE MECHANICAL COMPONENTS OF THE TACHOMETER

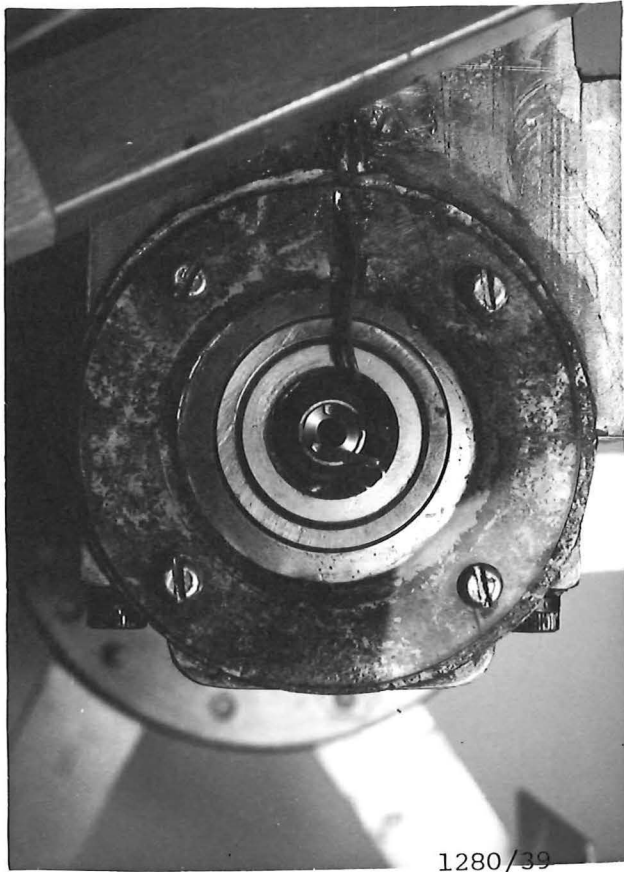


FIGURE 6.5: CLOSE-UP OF TACHOMETER WINDOW

578/22A

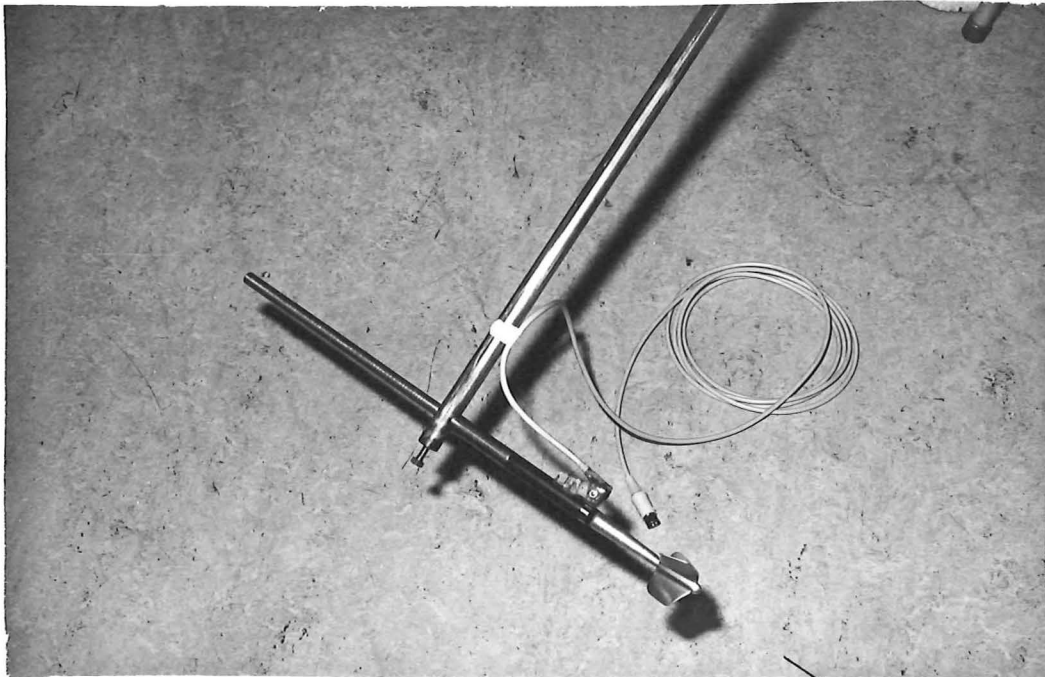
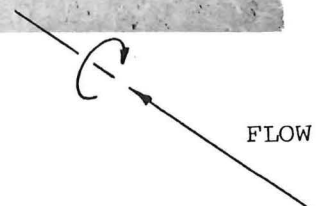


FIGURE 6.6: THE SPEED OF ADVANCE METER
WITH THE OPTOELECTRIC ARRAY:
TEXAS INSTRUMENTS TYPE TIL139,
INFRA RED EMITTER AND SENSOR



known. For this purpose the instrument shown in Fig.6.6 was developed.

This device was composed of the shaft and bearing section of one of the Department's propeller anemometers, combined with a suitable propeller from a small "Ott" river flow meter, borrowed from the workshop at the Kaianga Rating Tank. A black and white grid pattern was accurately transferred on to a rotating portion of the propeller shaft and this was scanned by a sealed optoelectronic, infrared, source and sensor module which gave a high-low signal output corresponding to the passing of the dark and light bands. This signal was processed by frequency-to-voltage circuitry similar to that of the tachometer, giving an output of 0 - 10 V for the range of expected water speeds. The actual circuitry is shown in Appendix 1, Fig.A1.2.

The instrument was calibrated on the Rating Car at the Kainga tank in the same manner that the river flow meters are normally calibrated.

It was mounted horizontally on a 19 mm diameter vertical tube which allowed it to be attached somewhere near the LPW operating point. At the Kainga tank it was connected to the force balance mounting frame which positioned it about 0.5 m to one side of the LPW and 0.4 m below the water surface. Its mounting rod can just be seen to the left in Fig.5.27.

Although it worked consistently in the Fluids Laboratory tests, and for a time at the Kaianga tank its calibration eventually began to vary, possibly with water getting into the scanning unit. Little attempt was made to get this working properly again as it served to indicate the approximate test speeds on the papertape records, and since these speeds were set, and accurately measured by the Rating Car's normal measuring device as a matter of course, and recorded in the test notebook, the instrument was simply retained as an often-necessary check on the written notebook records. The more accurate Rating Car speed measurements were written into the data records at the later data checking stage.

6.3 THE DATA ACQUISITION SYSTEM

The ideal data acquisition system was seen as one fulfilling the function described in The Measuring System Requirements (section 5.2) which noted that at a selected time simultaneous readings would

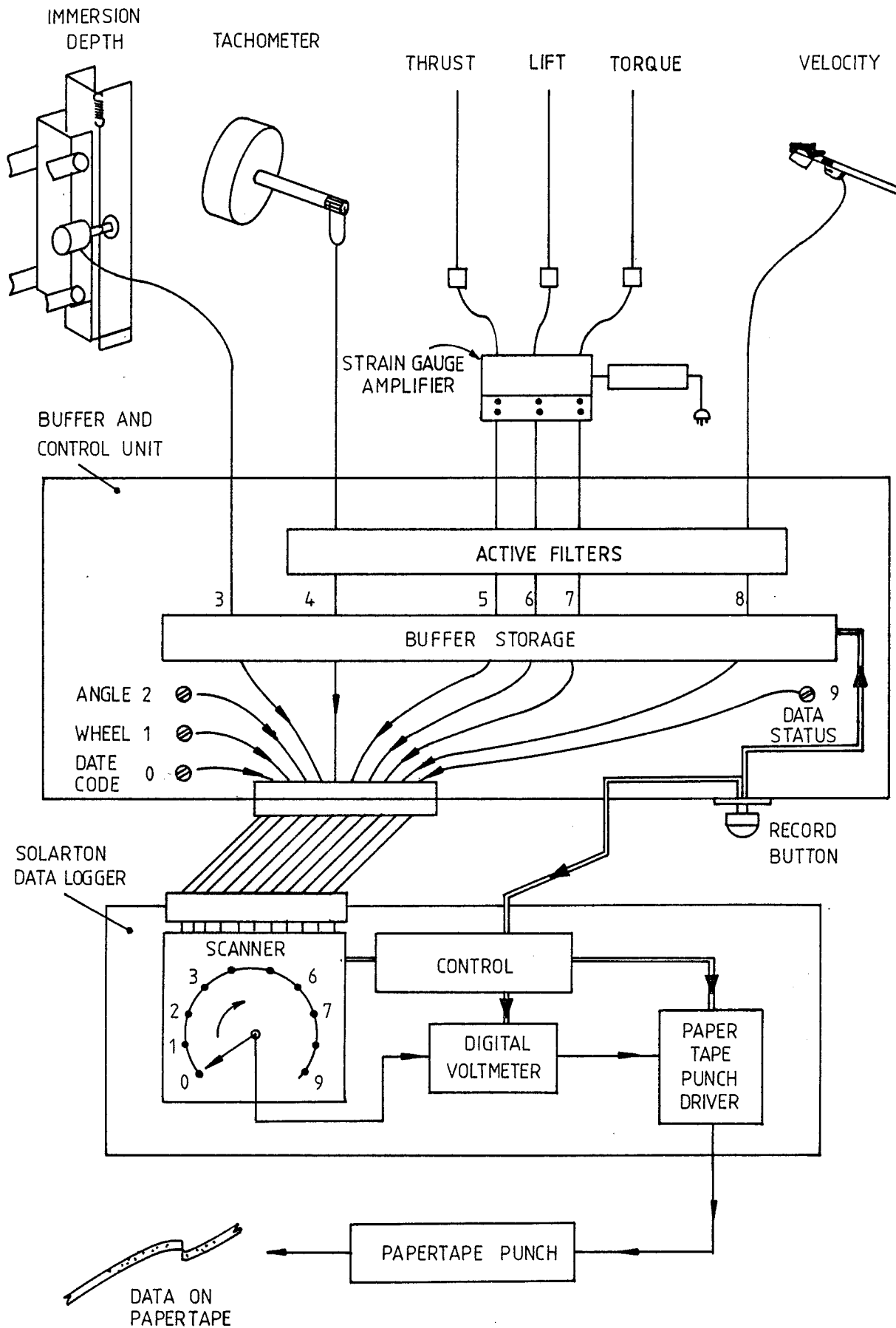


FIGURE 6.7 SCHEMATIC OF DATA AQUISITION SYSTEM

be obtained from all the sensors and a record created in the system which would contain all the information relevant to the conditions of the LPW at that time. In practice such a record would contain the following ten items (numbered according to the channel assignments in the system):

- 0) the date of the test;
- 1) a code number for the wheel type under test;
- 2) the blade angle;
- 3) immersion depth;
- 4) wheel rotational speed;
- 5) thrust force;
- 6) lift force;
- 7) torque;
- 8) speed of advance;
- 9) a code number indicating whether the record was of zero values, calibration values, or was an ordinary data record.

All this information needed to be stored in some form so it could be processed later.

In order to build up such a data acquisition system a survey was made of the existing data logging facilities available in the University. The Civil Engineering Department's Solartron Compact-33 Data Logger was found to be operational and available during the anticipated period of testing, and almost compatible with the requirements outlined above.

This logger could drive a papertape punch and record the required ten channels of information on to papertape in 2.5 seconds. Such a period was seen as a suitably long time between recordings since, for example, if a change in wheel revolutions had been made, since the last recording, it allowed the force balance system to settle to the new conditions before the next recording was taken.

However this meant that the measurements were not simultaneous and so the Solartron required the addition of a buffer in order that data could be stored at a much faster rate, and then be recorded at the speed of the papertape punch. Enquiries indicated that a Solartron buffer would be very expensive and would involve a long wait for delivery. The author therefore designed and built the Buffer and

Control Unit which, on the "Hold" signal, stored the ten channels of data and initiated the Solartron scan and papertape recording. This unit completed the practical data logging system from the sensors to the papertape record. A schematic of the system is given in Fig.6.7.

This system was used for the flowing water experiments of 1978 but this Solartron was unavailable from then on. There was however an older malfunctioning Solartron, Compact Series 2 Logger available. It was without a suitable case, needed aligning and drove an unacceptably slow papertape punch (12 seconds for 10 channels of data). Since by this stage the data acquisition system was designed around the Solartron functions, and the force-balance was ready to be used, the author built a suitable case, checked calibration and alignment of the instrument and designed and built a suitable interface which allowed it to drive the original, fast Facit papertape punch.

The final data acquisition system was similar to that shown in Fig.6.7 but used the Solartron Compact Series 2 Logger and employed an interface unit between the Solartron and the papertape punch.

6.3.1 The Buffer and Control Unit

This unit, designed and built by the author was a multifunctional unit. Its basic functions are outlined in Fig.6.7 and its actual circuitry is given in Appendix 1, Fig.A1.2 to A1.9. Its most important features are described below and the unit is pictured in Figs. 6.8 to 6.11.

Buffer Storage The buffer modules employed were sample-and-hold integrated circuits (National LF398H). These devices operate in one of two modes. In the sample mode their output signal is the same as the input signal while in the hold mode the output signal remains fixed at the voltage value the input had, at the instant the hold signal was given. They normally operate at megahertz speeds but in this case were required to sample and hold signals for periods in the order of seconds.

The associated circuitry was arranged to give them a (slow) response time of $\frac{1}{20}$ sec. which filtered out any spurious high frequency noise, and on the sample signal they were allowed $\frac{1}{10}$ sec. to acquire the analogue data voltage level from the instruments before being given the hold signal. The Solartron scanner could then read



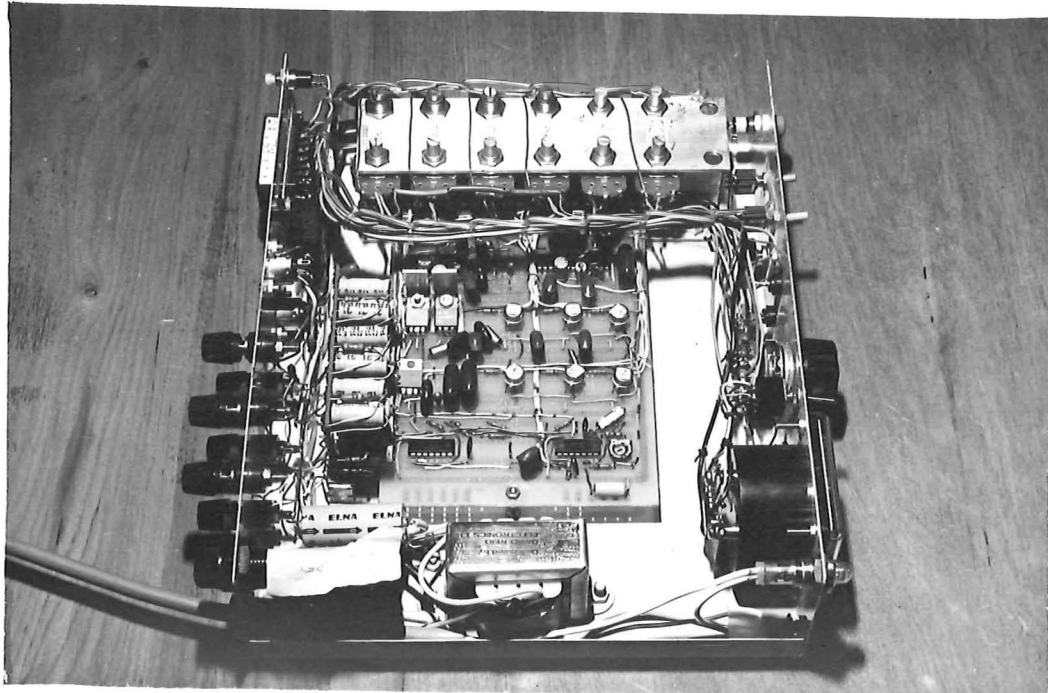
578/26A

FIGURE 6.8: THE BUFFER AND CONTROL UNIT FRONT PANEL



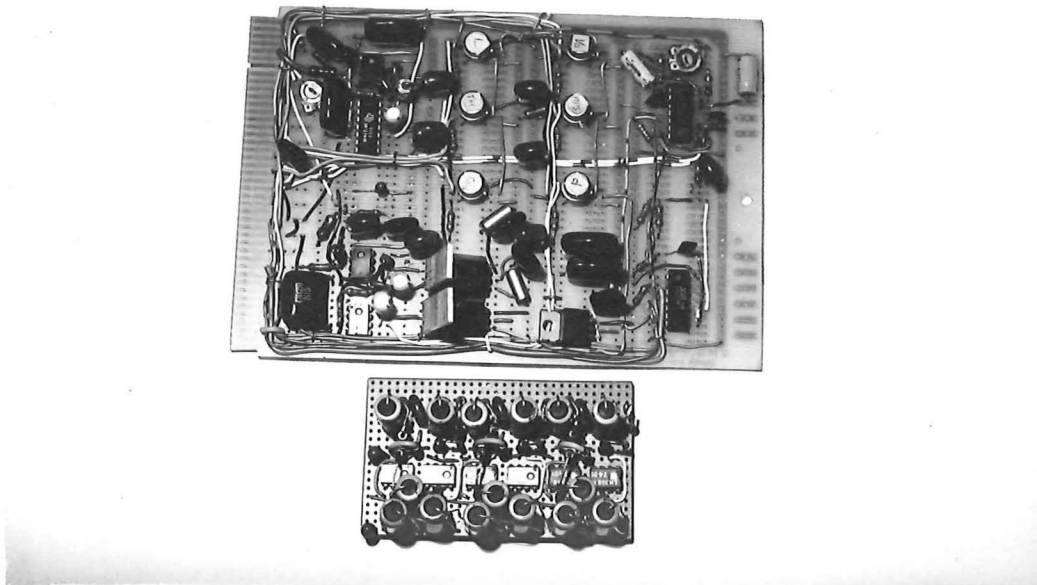
578/25A

FIGURE 6.9: THE BUFFER AND CONTROL UNIT BACK PANEL



578/24A

FIGURE 6.10: INSIDE THE BUFFER AND CONTROL UNIT. THE FRONT IS TO THE RIGHT



578/23A

FIGURE 6.11: THE MAIN CIRCUIT BOARD WITH 6 SAMPLE-AND-HOLD MODULES, TOP, AND THE FORCE SENSOR ACTIVE FILTER BOARD

the voltage level in each module in turn. This took about 2.7 sec., in which time the signal levels in the modules were observed to have drifted about 2 mV; an acceptable amount in a range of 0 to 10 V.

Six of these modules were used, three for the force and torque signals, and one each for the tachometer, depth gauge, and velocity meter. They can be seen on the circuit board in Figs. 6.10 and 6.11 and their wiring is given in Appendix 1, Fig.A1.9.

The other data channels had non varying signals (constant data) and did not, therefore need sample and hold modules.

Constant Data Potentiometers There were twelve potentiometers in all. Four pairs were used for the coarse and fine adjustments that set the voltage levels on the four channels which contained the constant data for the test run. These were: (0) the date, (1) the code number for the wheel type, (2) the blade angle, and (9) the record status (data, calibration or zero). For example, wheel number six was the standard flat-bladed test wheel, so the constant data value chosen for this wheel was 6 Volts on the "wheel" channel, channel (1).

The potentiometers can be seen in Fig.6.10 mounted on the aluminium mount at the rear of the figure.

The remaining four potentiometers were used to control the automatic timer function, depth calibration, and tachometer and water speed sensor calibrations. All these potentiometers could be accessed with a small screwdriver through holes in the top of the box, which can be seen in Fig.6.8.

After some use it was found convenient to convert the coarse adjustment for the constant data potentiometers to multistop switches which made adjustment quicker.

The Control Functions The front panel of the unit displaying its control functions is shown in Fig.6.8.

There were two modes of operation of the unit manual and automatic and one of these was selected by the "Manual-Auto" switch.

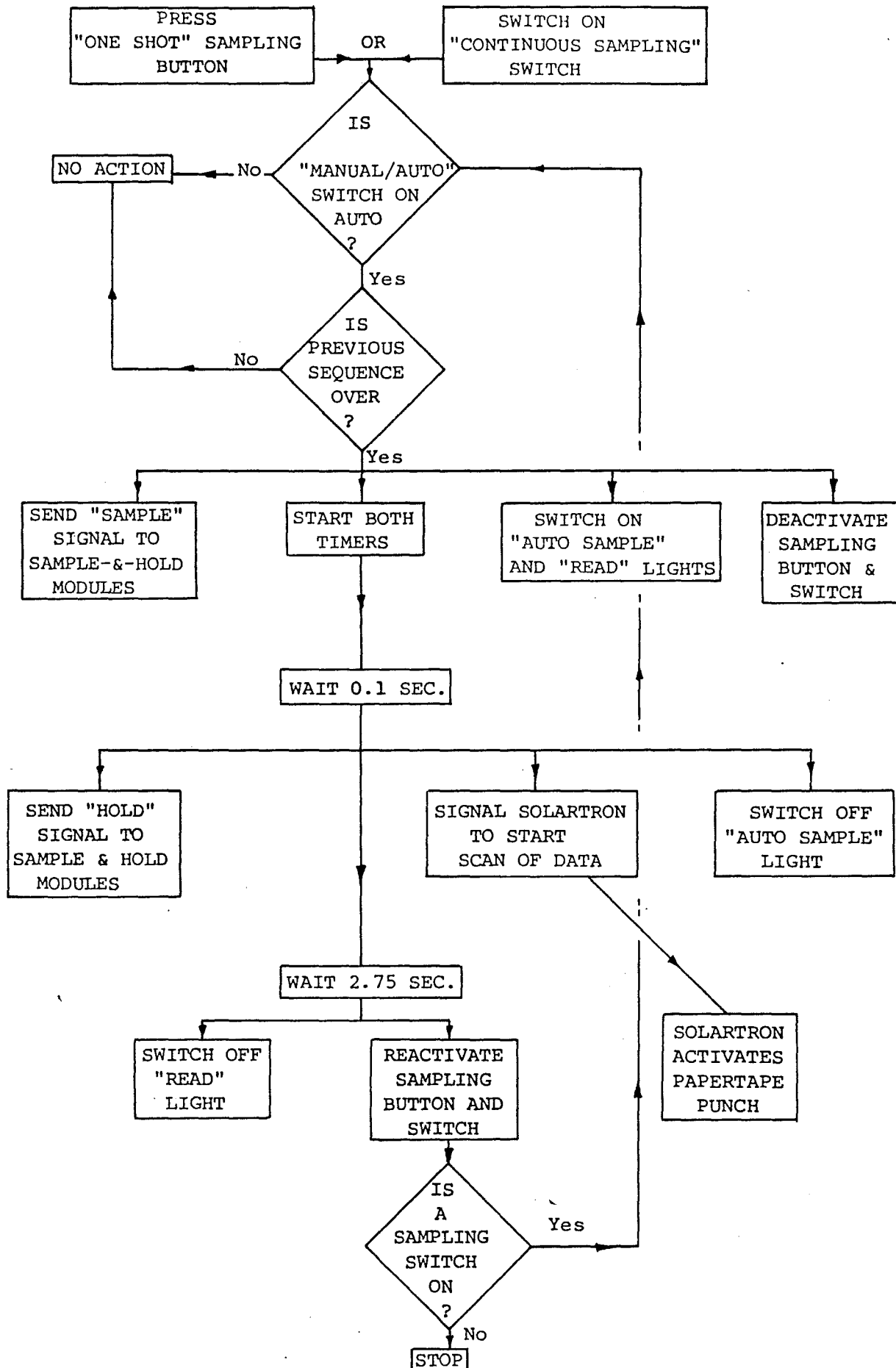


FIGURE 6.12: SEQUENCE OF EVENTS CAUSED BY ACTIVATION OF THE "ONE SHOT SAMPLING" BUTTON ON THE BUFFER AND CONTROL UNIT.

In the "Manual" mode the sample-and-hold modules were manually made to sample or hold their signal by the "Sample-Hold" switch. In either mode the "Channel Selector" switch could select a channel for display on the front panel meter (or it could be fed to a digital volt meter from the "O/p" socket). In the hold mode the signal levels in each of the sample-and-hold units could be recorded by pencil and paper by reading each channel in turn, using the "Channel Selector" switch.

This method was often used to check operation of the channels, and to display the force sensor strain gauge output signals when zeroing the strain gauge bridges.

In the "Auto" mode the "Sample-Hold" switch became de-activated, and the "Continuous Sampling" switch and "One Shot Sampling" button could be used. Pressing of this button began an extended train of events shown in Fig.6.12. The timed period of the second timer was about 2.75 sec. which was sufficient for the papertape to complete the punching of the ten-channel record.

In practice, then, when the operator felt conditions were right to make a data record, he simply pressed the button and in 2.75 seconds the data was recorded on the papertape. At this stage any one of the values recorded could be observed on the front panel meter by selecting the appropriate channel with the "Channel Selector Switch", since the sample-and-hold modules remained in the hold mode until the button was pressed again.

The logic diagram, and circuitry controlling these functions, is given in Appendix 1, Figs.A1.6, 7, 8 and 9.

Electric Filters Filters were needed in the force sensor and instrument circuits to both eliminate electrical noise from the signals, and to ensure that all transducers had approximately the same response times. Similar response times were necessary to make certain that any transients recorded would be treated equally by all transducers, to give a valid record.

The force sensor signals required sharp cut-off, low pass, active filters, (as noted in section 5.4.6) and the chosen design was a fourth order, multiple feedback, 0.1 dB, Chebyshev, active filter

Printer drive LU1963
Scanner & Controller LU1975
Punch drive LU1967
DVM LM1426

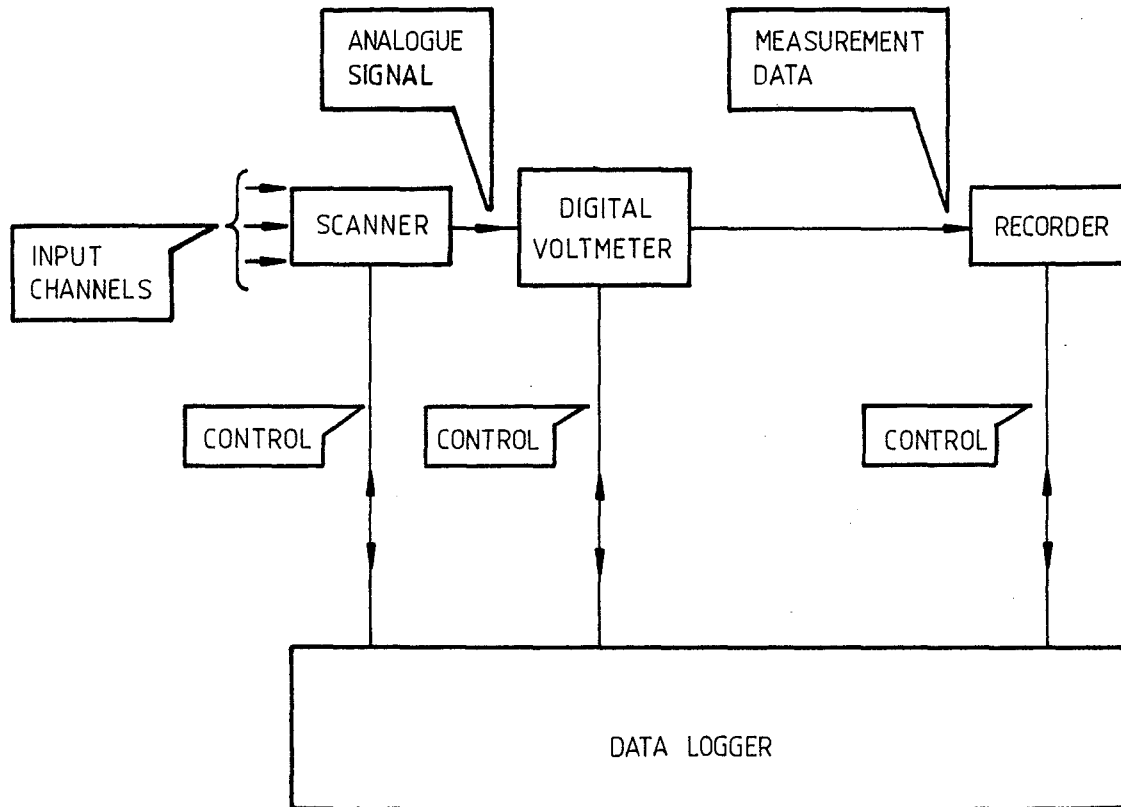


FIGURE 6.13 SOLARTRON DATA LOGGING SYSTEM

with a gain of 10. This was constructed from an active filter design handbook.(1) Since the required response time at the signal output was 0.5 sec., each filter had to be matched to one of the force sensing sections of the force balance since each section had a different mechanical response time and resonant frequency and already contained a mechanical dashpot damper (section 5.4.6). This matching was accomplished by a process of trial and error in adjusting the filter resistor values until each sensor output gave a smooth, 0.5 sec. response to a step change in force at the LPW shaft. The sharp cut-off property allowed this 0.5 sec. response, while at the same time reducing any noise above 5 Hz by at least 26 dB. This meant that the majority of the resonances, mechanical noise and vibration from the force balance was effectively eliminated from the force sensor signals.

The filter circuitry is given in Appendix 1, Fig.A1.3.

The tachometer and speed of advance instruments did not experience the vibration and noise as severely as did the force sensors so the filtering did not need to be so sharp. However to give the required response times and to reduce any electrical noise, 3rd order multiple feedback Chebyshev active filters were used. These are shown in Appendix 1, Fig.A1.4.

The capacitance depth gauge required only a passive filter circuit to give it the required response to a step increase in immersion. Although the filter was bypassed for a step decrease in immersion the response time could not be reduced below 2 sec. as the water left a film on the sensor surface, which only slowly shrank away. (This was noted above in section 6.2.2.)

Unit Layout Fig.6.10 shows the inside of the Buffer and Control Unit. The front panel is to the right. The main circuit board with the six sample-and-hold modules is central and the board containing the three active filters for the force sensor inputs stands vertically to the left. The power supply section is at the front and the code and calibration potentiometers are mounted on the frame at the rear of the figure.

1. Johnson and Hilburn, P.16, Table 2.9, P.31

TABLE 6.14: PROCEDURE IN SETTING UP AND DISMANTLING
EQUIPMENT FOR EACH DAY'S TESTING

1. 8:00 am TURN ELECTRICAL EQUIPMENT ON TO WARM UP.
 2. MOUNT FORCE BALANCE ON RATING CAR AND CONNECT UP ELECTRICAL LINES.
 3. PREPARE TEST LPW AND MOUNT ON FORCE BALANCE.
 4. 8:30 am SET CONSTANT DATA POTENTIOMETERS.
 5. ZERO EQUIPMENT AND RECORD 6 ZEROES.
 6. SET DATA STATUS POTENTIOMETER TO INDICATE CALIBRATION.
 7. CALIBRATE FORCE SENSORS AND MAKE 6 RECORDS.
 8. REMOVE CALIBRATION WEIGHT AND MAKE 6 ZERO RECORDINGS.
 9. SET DATA STATUS POTENTIOMETER TO INDICATE DATA
-
10. PERFORM TESTS (SEE FIG.6.15)
-
11. 3:45 pm REPEAT CALIBRATION SEQUENCE, 5-8 ABOVE
 12. TURN OFF EQUIPMENT AND DISCONNECT.
 13. REMOVE FORCE BALANCE FROM RATING CAR AND STORE IT.
 14. TAKE PAPERTAPE FROM PUNCH.

The main circuit board and the filter board could readily be removed for servicing, and these are shown in Fig.6.11.

The rear panel, in Fig.6.9 shows the input sockets at the right and output socket to the Solartron at the left. The "Manual Bypass" button, at the upper left, allowed a papertape record to be initiated to record data already stored in the sample-and-hold modules by the manual "Sample-Hold" switch. This bypass was necessary under such circumstances since normal pressing of the "One Shot Sampling" button would cause the unit to take a new sample. However, this option was rarely used. (Circuitry for this, Appendix 1 Fig.A1.6.)

6.3.2 The Solartron Data Logger

A block diagram of the Solartron data logger function and the units used is shown in Fig.6.13. Because this instrument is so versatile it can be difficult to understand, but once mastered it proved adequate for its task, the main malfunctions being operator errors. For high accuracy in voltage recording it needs to be calibrated, but for this project the accuracy was more than sufficient and the in-practice calibrations of the force balance were all that was necessary.

All recordings fed to the papertape from it were base ten four-digit numbers representing the voltages scanned by the scanner, and these were in integer form, the decimal points being left out to save punching time.

6.3.3 The Interface for the Papertape Punch

The Solartron (Compact Series 2 Logger) papertape punch driver unit (LU1967) was not compatible with the fast Facit papertape punch and drove instead a slow punch, recording the 10 channels of data in 12 seconds. This length of time was seen as unacceptably long since it would mean that a large number of runs down the tank would be required to record sufficient data; this sort of tedious repetition was to be avoided when the tests required the services of MWD personnel to drive the Rating Car.

An interface unit was designed and built by the author under pressure of time. Its functions were mainly to:

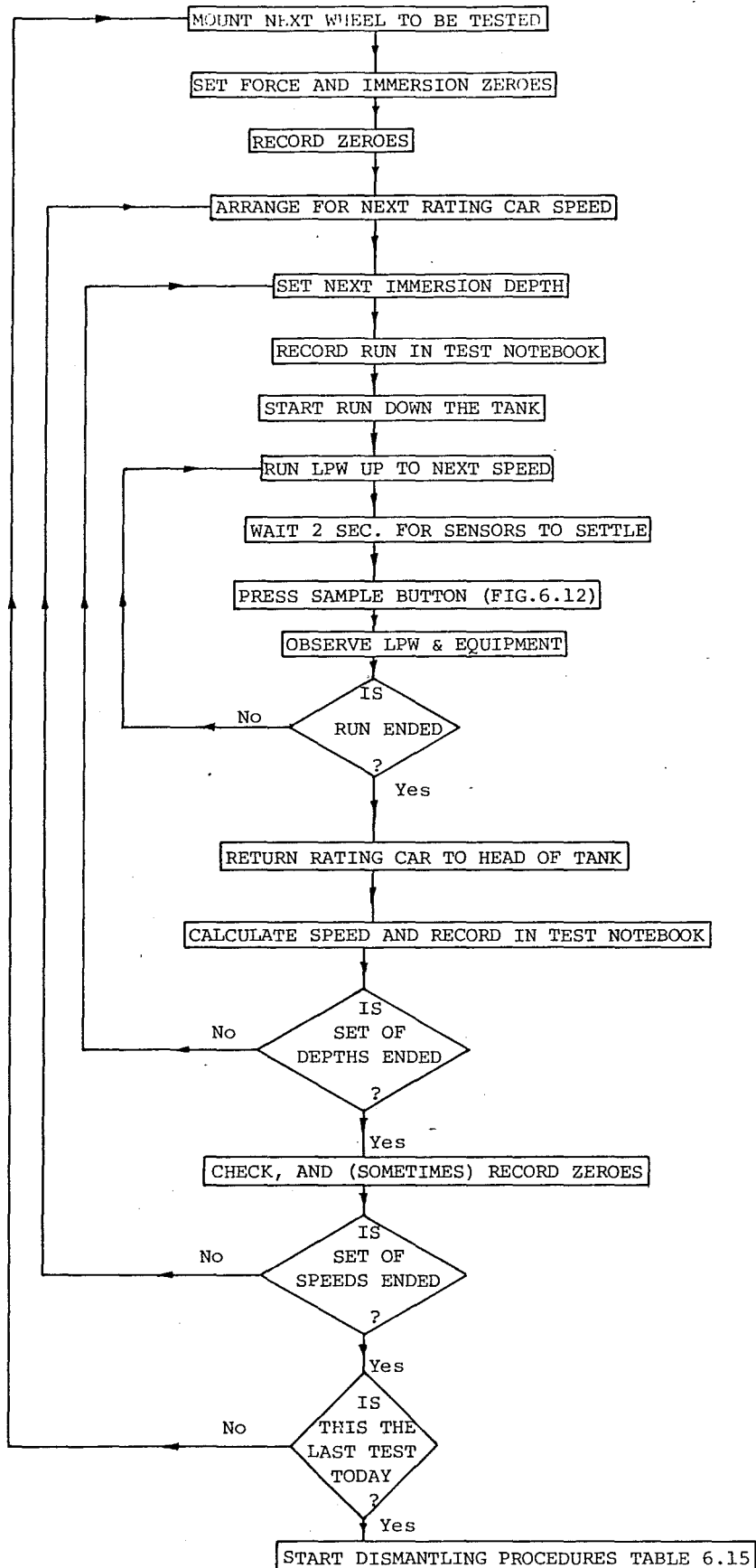


FIGURE 6.15: BLOCK DIAGRAM OF TESTING PROCEDURES.

1. Convert the data from a BCD form to ASCII.
2. Alter voltage levels of data and control signals.
3. Invert the polarities of data and control signals.
4. Create some necessary control signals between the two units.

Once this interface was operational it gave trouble-free service throughout the series of tests, allowing the recording of 10 channels of data in 2.85 seconds.

The Facit papertape punch also operated without problems throughout the test series.

6.4 THE EXPERIMENTAL PROCEDURE

All the equipment and instrumentation used in the measuring and data logging system between the LPW and the papertape recording have been described. This section describes the procedure evolved for obtaining reliable data recordings.

6.4.1 Setting Up

Normally, testing at the Kainga tank involved the use of the facilities for a whole day. Table 6.14 shows the setting-up and dismantling procedure. Of note is the fact that the warm-up time for the electrical equipment needed to be about 30 minutes to ensure stability of the instrumentation between the time of calibration and data recording. Also note that recordings of zeros were made before and after the calibration procedures to indicate the presence of any hysteresis or jamming present in the sensing sections.

6.4.2 The Testing Procedures

The procedure used in undertaking test runs is given in Fig.6.15. Note that it incorporated the use of a written record in the test notebook for each run down the tank. This record noted the speed of the Rating Car for the run once it had been calculated from the car's measuring device. This actual speed was slotted into the appropriate data records at the later data checking stage (section 7.4.3).

This written record also included any observations made during the run, as well as notes on equipment conditions.

For each wheel tested a standard set of tests was carried out. This involved testing at five fixed immersion depths, and five fixed speeds of advance covering the range from the static condition, through the transition zone to planing speeds. Each run, at a fixed immersion depth and fixed speed of advance, also tested at a number of different wheel rotational speeds usually more than five.

If a particular wheel was considered less important the test set covered only two immersion depths, instead of five, at the three intermediate speeds of advance.

In a normal day's testing three wheels could be tested if a reasonable amount of time was allowed for the water to settle between runs. Sixteen to twenty runs were required for the full set of tests for each wheel, but this could be reduced to about ten for a shortened set.

Over 1979 and 1980 twenty-five full days of testing were carried out at the Kainga tank, and over 40 different wheel configurations were tested.

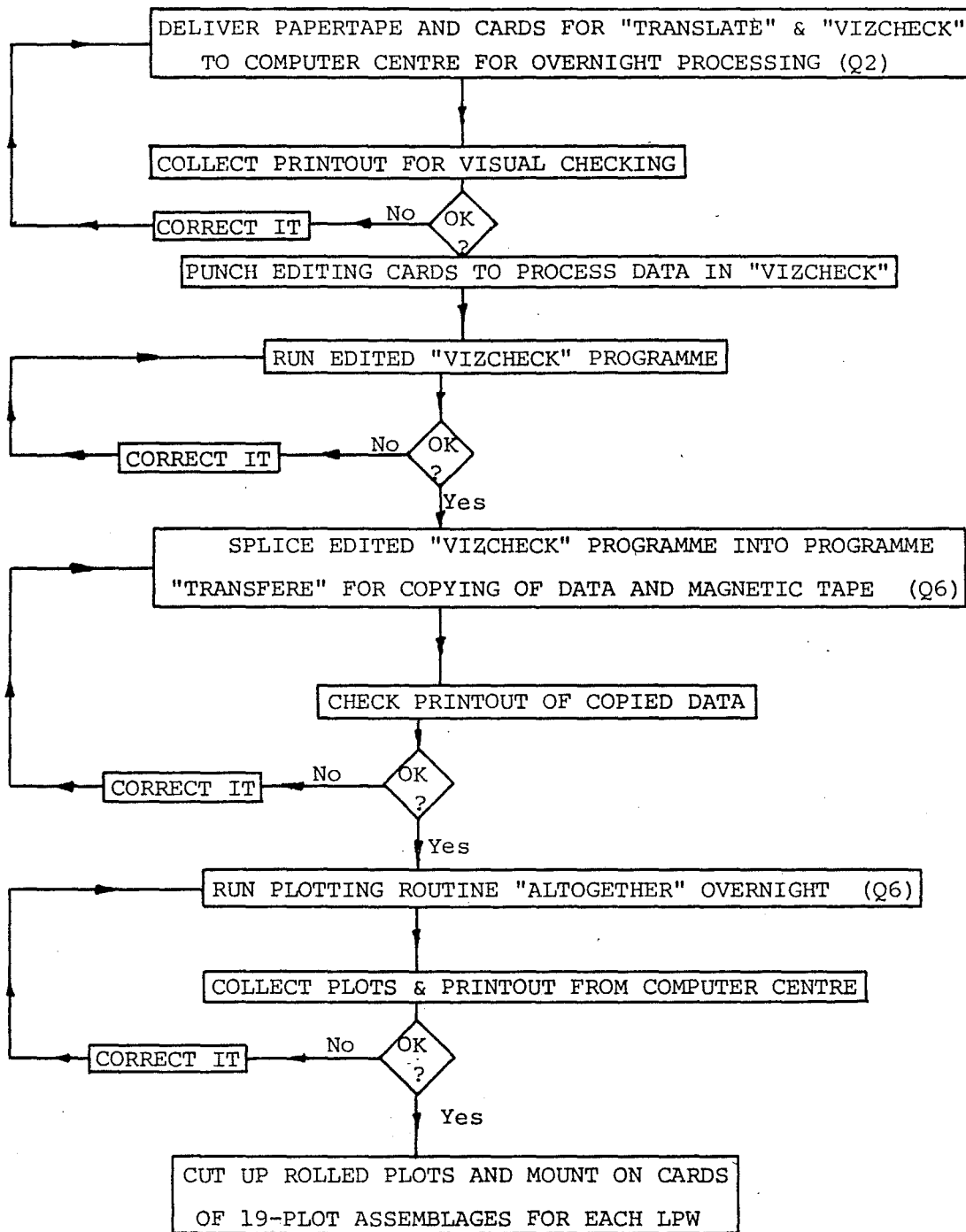


FIGURE 7.1: THE DATA PATH FROM THE PAPERTAPE, PRODUCED AT THE TESTING TANK, TO THE COMPUTER-GENERATED PLOTS.

CHAPTER 7

DATA PROCESSING, PLOTTING AND PRESENTATION7.1 INTRODUCTION

Since the LPW tests involved many variables it was found necessary to use a large number of plots of the test data to adequately describe each wheel's performance. The data from the 1977 tests had been processed and plotted by hand and the experience made it clear that computer processing and plotting would be almost essential for an extended series of tests.

This chapter describes the computer-assisted data processing. It outlines the path of the data through a number of computer programmes, from the papertape record produced at the testing tank to the final form where the data for each LPW is plotted on an assemblage of graphs which give a visual picture of the LPW performance. Fig.7.1 shows this data path in block diagram form. (This is really an amplification of parts B, C and D of Fig.5.1 which showed the overall data path.) In this process the following 5 computer programmes were used:

- (1) 'TRANSLATE': which converted the data on papertape from ASCII to EBCDC and stored it for later processing.
- (2) 'VIZCHECK': which printed out, or processed and printed out the stored data from 'TRANSLATE'.
- (3) 'TRANSFERE': which transferred the processed data into the permanent magnetic tape storage.
- (4) 'LPWPLOT': which sorted through the stored data, selected and plotted the requested graph.
- (5) 'ALTOGETHER': which plotted the full assemblage of 19 graphs to describe a selected LPW's performance.

All programmes were in FORTRAN except the first.

1	+2137	+5974	+5983	+3469	+0006	-0020	-0009	+0019	+0011	+0008
2	+2138	+5973	+5984	+3469	+0007	-0020	-0009	+0018	+0011	+0009
3	+2138	+5975	+5984	+3469	+0007	-0018	-0005	+0023	+0011	+0009
4	+2138	+5975	+5985	+3470	+0007	-0019	-0006	+0024	+0011	+0010
5	+2139	+5974	+5984	+3470	+0007	-0018	-0004	+0024	+0011	+0009
6	+2139	+5975	+5985	+3470	+0007	-1103	+1980	+2222	+0010	+9986
7	+2139	+5975	+5984	+3469	+0007	-1106	+1990	+2232	+0011	+9987
8	+2139	+5974	+5984	+3470	+0007	-1106	+1983	+2233	+0010	+9986
9	+2138	+5975	+5985	+3470	+0008	-1109	+1987	+2234	+0010	+9986
10	+2140	+5975	+5985	+3470	+0007	-1108	+1988	+2231	+0010	+9986
11	+2139	+5976	+5985	+3470	+0007	-1107	+1991	+2232	+0010	+9986
12	+2139	+5974	+5985	+3470	+0007	-1109	+1990	+2231	+0010	+9986
13	+2140	+5975	+5986	+3470	+0008	-0023	+0002	+0022	+0012	+0010
14	+2139	+5976	+5985	+3470	+0006	-0021	-0003	+0014	+0011	+0009
15	+2139	+5976	+5986	+3470	+0006	-0020	-0005	-0005	+0005	+0003
16	+2137	+5975	+5984	+3470	+0006	-0020	-0002	-0001	+0005	+0003
17	+2138	+5976	+5985	+3470	+0006	-0021	-0007	+0017	+0011	+0010
18	+2143	+5972	+5984	+8406	+0455	+0292	+0234	+0618	+0007	+1001
19	+2145	+5972	+5984	+8408	+0594	+0449	+0361	+0922	+0006	+1000
20	+2145	+5972	+5985	+8407	+0840	+0799	+0633	+1579	+0007	+1000
21	+2144	+5970	+5984	+8406	+1301	+1544	+1076	+2852	+0005	+0998
22	+2145	+5971	+5985	+8407	+1723	+2242	+1572	+4208	+0005	+0999
23	+2142	+5968	+5982	+8405	+1971	+3206	+2125	+5622	+0003	+0999
24	+2143	+5971	+5985	+8407	+2380	+4358	+2842	+6628	+0004	+1000
25	+2144	+5972	+5985	+8407	+2862	+5416	+3747	+6844	+0004	+1000
26	+2142	+5972	+5983	+8406	+3117	+5898	+4134	+6802	+0003	+0998
27	+2142	+5971	+5984	+8406	+3021	+5869	+4030	+6802	+0004	+0999
28	+2137	+5975	+5982	+6990	+0445	+0239	+0198	+0466	+0007	+0992
29	+2139	+5976	+5982	+6991	+0637	+0377	+0324	+0709	+0006	+0993
30	+2139	+5975	+5982	+6991	+0976	+0795	+0594	+1391	+0006	+0993
31	+2139	+5975	+5982	+6991	+1395	+1262	+0920	+2248	+0006	+0992
32	+2139	+5975	+5982	+6990	+1792	+1948	+1294	+3255	+0005	+0994
33	+2139	+5975	+5982	+6991	+2290	+3000	+2002	+5000	+0005	+0993
34	+2139	+5975	+5982	+6991	+2997	+3722	+2481	+6038	+0004	+0992
35	+2139	+5975	+5983	+6990	+3268	+5000	+3128	+6602	+0004	+0991
36	+2139	+5976	+5982	+6991	+3888	+5637	+3498	+6533	+0004	+0993

FIGURE 7.2: 10 CHANNELS OF INTEGER VOLTAGES AS READ BY PROGRAMME 'TRANSLATE' FROM THE PAPER TAPE. THE RIGHT HAND COLUMN (IN BOTH FIGURES) SHOWS THAT ROWS 1-5 AND 7-17 ARE ZERO RECORDINGS, 6-12 ARE CALIBRATIONS, AND THE REST ARE DATA RECORDINGS

LINE NO.	DATE	WHEEL NO.	ANGLE	DEPTH	RPS	THRUST	LIFT	TOOXLO	VO	SPARE
1	21.380	6.000	60.000	20.000	0.000	-0.088	-0.036	0.064	0.014	0.000
2	21.380	6.000	60.000	20.000	0.000	-0.088	-0.036	0.061	0.014	0.000
3	21.380	6.000	60.000	20.000	0.000	-0.079	-0.020	0.077	0.014	0.000
4	21.380	6.000	60.000	20.000	0.000	-0.083	-0.024	0.081	0.014	0.000
5	21.380	6.000	60.000	20.000	0.000	-0.079	-0.016	0.081	0.014	0.000
6	21.380	6.000	60.000	20.000	0.000	-4.844	8.022	7.476	0.013	10.000
7	21.380	6.000	60.000	20.000	0.000	-4.857	8.062	7.510	0.014	10.000
8	21.380	6.000	60.000	20.000	0.000	-4.857	8.034	7.513	0.013	10.000
9	21.380	6.000	60.000	20.000	0.000	-4.871	8.050	7.516	0.013	10.000
10	21.380	6.000	60.000	20.000	0.000	-4.866	8.054	7.506	0.013	10.000
11	21.380	6.000	60.000	20.000	0.000	-4.862	8.066	7.510	0.013	10.000
12	21.380	6.000	60.000	20.000	0.000	-4.871	8.062	7.506	0.013	10.000
13	21.380	6.000	60.000	20.000	0.000	-0.101	0.008	0.074	0.015	0.000
14	21.380	6.000	60.000	20.000	0.000	-0.092	-0.012	0.047	0.014	0.000
15	21.380	6.000	60.000	20.000	0.000	-0.088	-0.020	-0.017	0.006	0.000
16	21.380	6.000	60.000	20.000	0.000	-0.088	-0.008	-0.003	0.006	0.000
17	21.380	6.000	60.000	20.000	0.000	-0.092	-0.028	0.057	0.014	0.000
18	21.380	6.000	60.000	96.800	1.184	1.282	0.948	2.077	0.000	1.000
19	21.380	6.000	60.000	96.800	1.546	1.972	1.463	3.099	0.000	1.000
20	21.380	6.000	60.000	96.800	2.186	3.509	2.564	5.307	0.000	1.000
21	21.380	6.000	60.000	96.800	3.386	6.781	4.359	9.585	0.000	1.000
22	21.380	6.000	60.000	96.800	4.485	9.846	6.369	14.142	0.000	1.000
23	21.380	6.000	60.000	96.800	5.130	14.080	8.609	18.893	0.000	1.000
24	21.380	6.000	60.000	96.800	6.195	19.139	11.514	22.272	0.000	1.000
25	21.380	6.000	60.000	96.800	7.449	23.786	15.180	22.997	0.000	1.000
26	21.380	6.000	60.000	96.800	8.113	25.903	16.748	22.855	0.000	1.000
27	21.380	6.000	60.000	96.800	7.863	25.775	16.327	22.854	0.000	1.000
28	21.380	6.000	60.000	75.020	1.158	1.050	0.802	1.566	0.000	1.000
29	21.380	6.000	60.000	75.020	1.658	1.656	1.313	2.382	0.000	1.000
30	21.380	6.000	60.000	75.020	2.540	3.491	2.406	4.673	0.000	1.000
31	21.380	6.000	60.000	75.020	3.631	5.542	3.727	7.551	0.000	1.000
32	21.380	6.000	60.000	75.020	4.664	8.555	5.242	10.933	0.000	1.000
33	21.380	6.000	60.000	75.020	5.961	13.175	8.111	16.794	0.000	1.000
34	21.380	6.000	60.000	75.020	7.801	16.346	10.051	20.279	0.000	1.000
35	21.380	6.000	60.000	75.020	8.506	21.959	12.673	22.172	0.000	1.000
36	21.380	6.000	60.000	75.020	10.120	24.757	14.172	21.940	0.000	1.000

FIGURE 7.3: FULLY PROCESSED DATA FROM Fig.7.2 AS PRINTED OUT BY THE EDITED 'VIZCHECK' PROGRAMME. (DEPTH VALUES ARE GREATER THAN THE FIVE STANDARD VALUES AS LARGE IMMERSION WAS UNDER EXAMINATION IN THIS TEST)

7.2 PAPERTAPE PROCESSING

Programme 'TRANSLATE' was written in ALGOL by R. Harrington of the Computer Centre, and it simply converted the papertape voltage recordings from ASCII to EBCDIC, stored them on disc, and printed them out, numbered, in the form they appeared on the papertape (see Fig.7.2); ten channels per line and four digits per channel, in integer form, with a sign, and a space between each channel's data.

7.3 VISUAL CHECKING OF DATA

Programme 'VIZCHECK' read the integer voltage values stored by programme 'TRANSLATE', and multiplied them by preset conversion factors derived from the original alignment calibrations to give a data print-out in the appropriate units as shown in Fig.7.3. The printouts from 'TRANSLATE' and 'VIZCHECK' were then checked for obvious errors such as an incorrect setting of the immersion depth or indications of equipment malfunctions, and were then used as the basis for the required data processing.

7.4 PROCESSING THE DATA

Earlier sections have pointed out the need for various forms of data processing before the final data storage or plotting. The data processing was required in the following areas:

1. Elimination of significant zero errors in the force data.
2. Adjustment of the force calibration factors according to the in-practice calibrations.
3. Insertion of the accurate speed values from the Rating Car.
4. Standardisation of constant data values, such as blade angles.
5. Elimination of data acquisition system generated errors.

All the data processing was done by editing and altering the 'VIZCHECK' programme.

7.4.1 Zero Errors

Section 5.6 discussed the reasons why the force sensor zero values tended to drift, and noted that frequent checks and recordings were made of these values. Any recorded zero force errors greater

than 0.1 N and any torque zero errors greater than 0.01 Nm were eliminated in this processing stage. Two types of zero errors existed :

- (i) Errors constant with time;
- (ii) Errors which varied with time.

It was assumed that varying errors varied linearly between the two relevant zero recordings, and both types of zero errors were simply subtracted from the recorded force values.

7.4.2 Force Calibration Factors

The calibration factors used to convert the force sensor voltage recordings to actual force values were derived from the test in-practice calibration procedure, as noted in section 5.5.2. Some care was taken in obtaining these calibration factors. The calibration procedure conducted at the beginning and end of each day's testing (Fig.6.15) gave a data printout like the one shown near the beginning in Fig.7.2, from programme 'TRANSLATE'. About twelve recordings of the zero values and about six of the calibration values were made, and the force balance was shaken and vibrated between recordings so that hysteresis effects in the force sensors would show up in this output and could be averaged out. From these calibration and zero error recordings an average calibration factor for each force sensor was derived from the known magnitude of the applied in-practice calibration force. These calibration factors were then edited into the 'VIZCHECK' programme, correcting the original alignment calibration factors.

If the calibration procedure at the tank produced different calibration factors for the beginning and end of the day's tests, the difference was accommodated by a linear interpolation of the calibration factors. Normally the calibration factors were within 0.5% of each other, and no interpolation was necessary.

7.4.3 Speed of Advance

The Rating Car speed for each run down the tank was recorded in the test notebook. With the assistance of the results recorded by the speed of advance indicator these accurate speed values were entered into the appropriate data records, replacing the less accurate values given by the speed of advance indicator.

7.4.4 Constant Data Standardisation

The data that remained fixed for each data record, such as the date code, the wheel number, the blade angle, and the data status code, was read by the data acquisition system as voltage levels set by the potentiometers in the Buffer and Control Unit (section 6.3.1). Since the voltage levels varied a little in the millivolt ranges, these "constant" data values were not constant throughout a test. The plotting program 'LPWPLOT', required single-valued data for these constant data in its sorting procedure, so it was necessary to standardise the values in the data record to the proper single-valued numbers.

A similar procedure was required for the immersion depth transducer, though, as mentioned before (section 6.2.2) the actual immersion depth of the LPW may have varied quite markedly from the standardised recorded value. Consequently the immersion depth values recorded in the final data records were of the five preselected immersion depth values, rather than of the actual immersion depth values taken at the moment of data measurement.

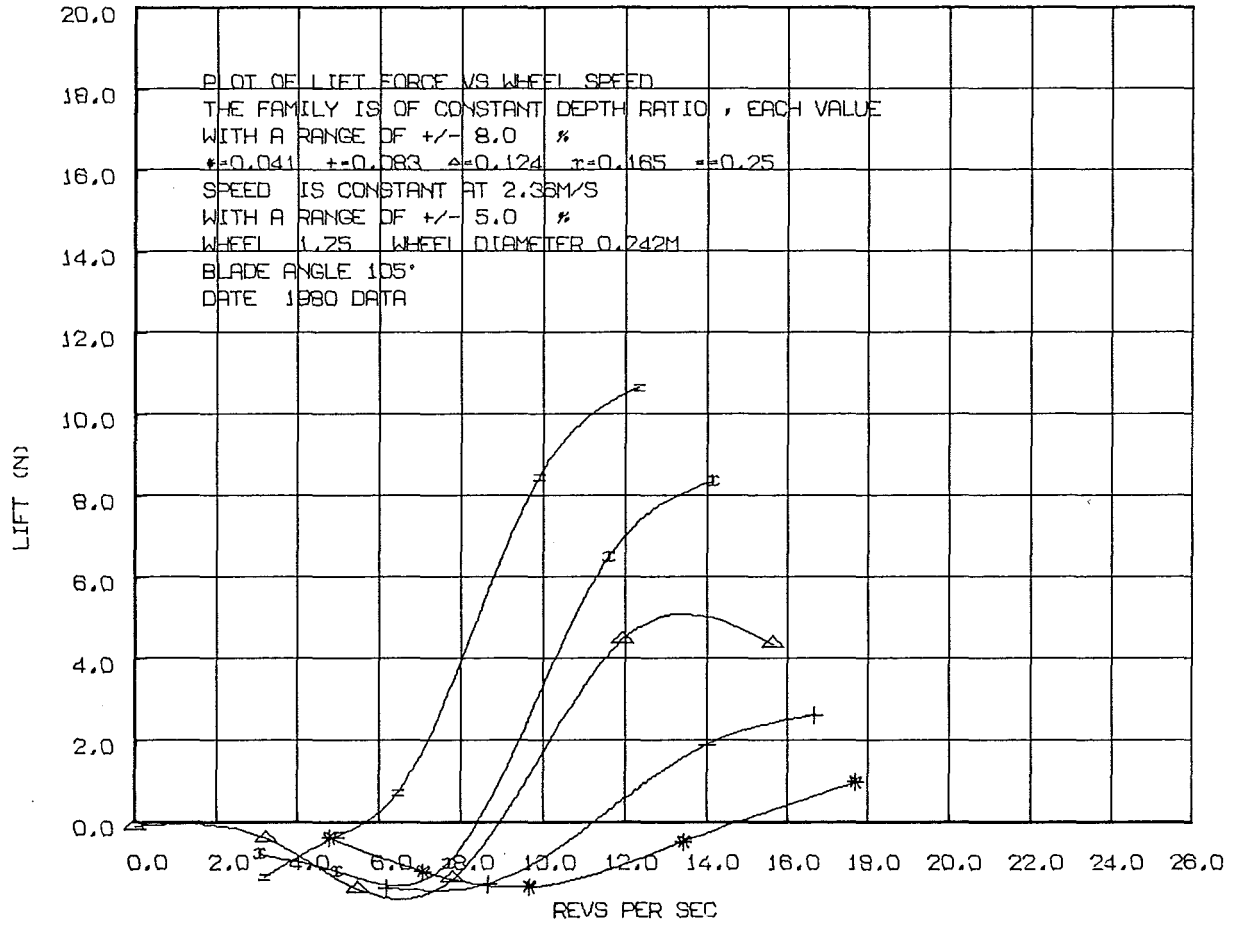
While five selected speeds of advance were set during the tests these were not always exactly achieved, as noted in section 5.9.4. However the actual speeds were measured reliably, so, rather than record the standard, preselected values as was done for the immersion depth data, the actual, accurately measured speeds were recorded.

7.4.5 Data Acquisition System Errors

Occasional transients in the mains voltage tended to trigger the Solartron to print a line of unrequired data. Data records such as these, and those recorded by mistake or including obvious errors were simply eliminated at this processing stage.

7.4.6 Conclusion For Data Processing

The processing procedure involved developing an edited form of the 'VIZCHECK' programme which included the required alterations so that its printed output was of fully processed error-free data such as that of Fig.7.3. Once this edited programme was running correctly the data was ready for permanent storage.



PLOT OF LIFT VS RPS AT 2.36M/S. WHEEL NO. IS 1.75 BLADE ANGLE IS 105.0

15 POINTS ARE OFF THE PLOT

THE DATA POINTS FOR EACH OF THE FAMILY OF CURVES IS LISTED BELOW

NO.	Y AXIS	X AXIS	SYMBOL
1	-0.41	4.79	*
2	-1.22	7.07	*
3	-1.61	9.66	*
4	-0.30	13.43	*
5	0.95	17.71	*
1	-1.62	6.21	+
2	-1.52	8.68	+
3	1.88	13.99	+
4	2.59	16.66	+
1	-0.13	0.00	A
2	-0.42	3.23	A
3	-1.66	5.50	A
4	-1.41	7.81	A
5	4.45	11.93	A
6	4.35	15.62	A
1	-0.81	3.05	X
2	-1.22	4.98	X
3	-1.02	7.64	X
4	6.47	11.60	X
5	9.34	14.12	X
1	-1.36	3.21	=
2	-0.33	5.04	=
3	0.70	6.46	=
4	8.45	9.90	=
5	10.64	12.32	=

FIGURE 7-4: THE COMPUTER-GENERATED PLOT AND DATA PRINTOUT PRODUCED BY PROGRAM "LPWPLOT".

7.5 DATA STORAGE

Data was stored at the Computer Centre on two magnetic tapes which were alternately updated with each day's test data, so that one always provided a backup if the contents of the other were lost in the copying process. The papertapes with their associated 'VIZCHECK' programme cards provided the final backup should both magnetic tapes be lost. In practice no backups were required.

Data was copied to the magnetic tapes by programme 'TRANSFERE' which was essentially the edited 'VIZCHECK' programme with the required Job Control cards for the copying procedure.

The stored data did not include the data status code, the calibration or the zero recordings. Only records of actual test data were retained. Data was stored in the form that it was read in: nine channels or items of data in the usual order (as shown in Fig.6.7 or in section 6.3).

During the copying process of new data to the magnetic tape records, corrections could be made to previously stored data which contained errors that had gone unnoticed during earlier processing procedures. Such errors were usually the incorrect assignment of speeds of advance to some records, and these errors became obvious in the plotting procedures. A catalogue of such corrections was kept to ensure that the data store contents was always known, or could be readily reconstructed if the backup storage was needed.

Once stored, the data could be accessed as required by suitable sorting programmes. Two forms of data analysis were undertaken. One simply listed the data with calculated values of the coefficients associated with it. This form was not often used, and programmes to do this type of work were written as necessary. (For example section 9.9.3 describes how practical force coefficients were developed from the data records.)

The other form of data analysis produced the plots for visual interpretation.

7.6 PLOTTING PROCEDURES

To be comprehended the data needed to be presented in a graphical form sufficiently representative of the physical situation as to

TABLE 7.5: PROGRAMME SEQUENCE FOR "LPWPLOT"

1. READ CARDS SPECIFYING THE REQUIRED PLOT.
2. READ THE DATA STORED ON MAGNETIC TAPE, SELECTING THE REQUIRED DATA WITHIN THE SPECIFIED TOLERANCES.
3. SORT SELECTED DATA INTO FAMILY MEMBER SETS AND ORDER IT.
4. AVERAGE ANY CLOSELY-GROUPED DATA VALUES IN ONE FAMILY MEMBER SET.
5. APPLY INTERPOLATING SMOOTHING ROUTINE TO CREATE A 50-POINT CURVE CONNECTING THE DATA POINTS.
6. REPEAT 4 AND 5 FOR OTHER FAMILY MEMBERS.
7. WRITE OUT ORDERED DATA ON PRINTOUT.
8. DRAW UP PLOT AXES, LABELS AND DOCUMENTATION.
9. PLOT DATA POINTS AS SYMBOLS.
10. PLOT SMOOTHED CURVES BETWEEN DATA POINTS.

allow the effects of the variables to be readily compared. Since the University Computer Centre had on-line plotting facilities a data plotting programme with the following requirements was planned. It needed:

- (1) To be able to select the required data from the data storage tapes and put it in the required order for plotting.
- (2) To provide a large selection of axes against which the data could be plotted.
- (3) To have the facility to plot data in a "family" of curves. For example: a plot might contain five curves each representing the effects at a different immersion depth.
- (4) The members of the family group needed to be readily distinguishable.
- (5) To be able to select data within a given tolerance band, from the data store.
- (6) To be able to link the plotted data points with appropriately smoothed curves.
- (7) Each plot had to be self explanatory so that a large number of plots could be readily sorted out.
- (8) Plots were required to fit on an A4 page.

The programme developed to fill these requirements was called 'LPWPLOT' and was fairly lengthy (700 lines). An example of a plot produced by it is shown in Fig.7.4 along with its associated data printout. A list of the programme's functions is shown in Table 7.5.

Of some note is the smoothing procedure used. This was a cubic spline interpolation subroutine largely based on one developed by Greville in "Mathematical Methods for Digital Computers". (1) From the set of data points this subroutine was made to produce a fifty-point curve passing through all the data points. Each actual data point was indicated by the symbol used for the curve (see Fig.7.4). The subroutine also employed an additional routine which calculated an average value for a group of closely-spaced points, to prevent the spline routine from going wild under such conditions.

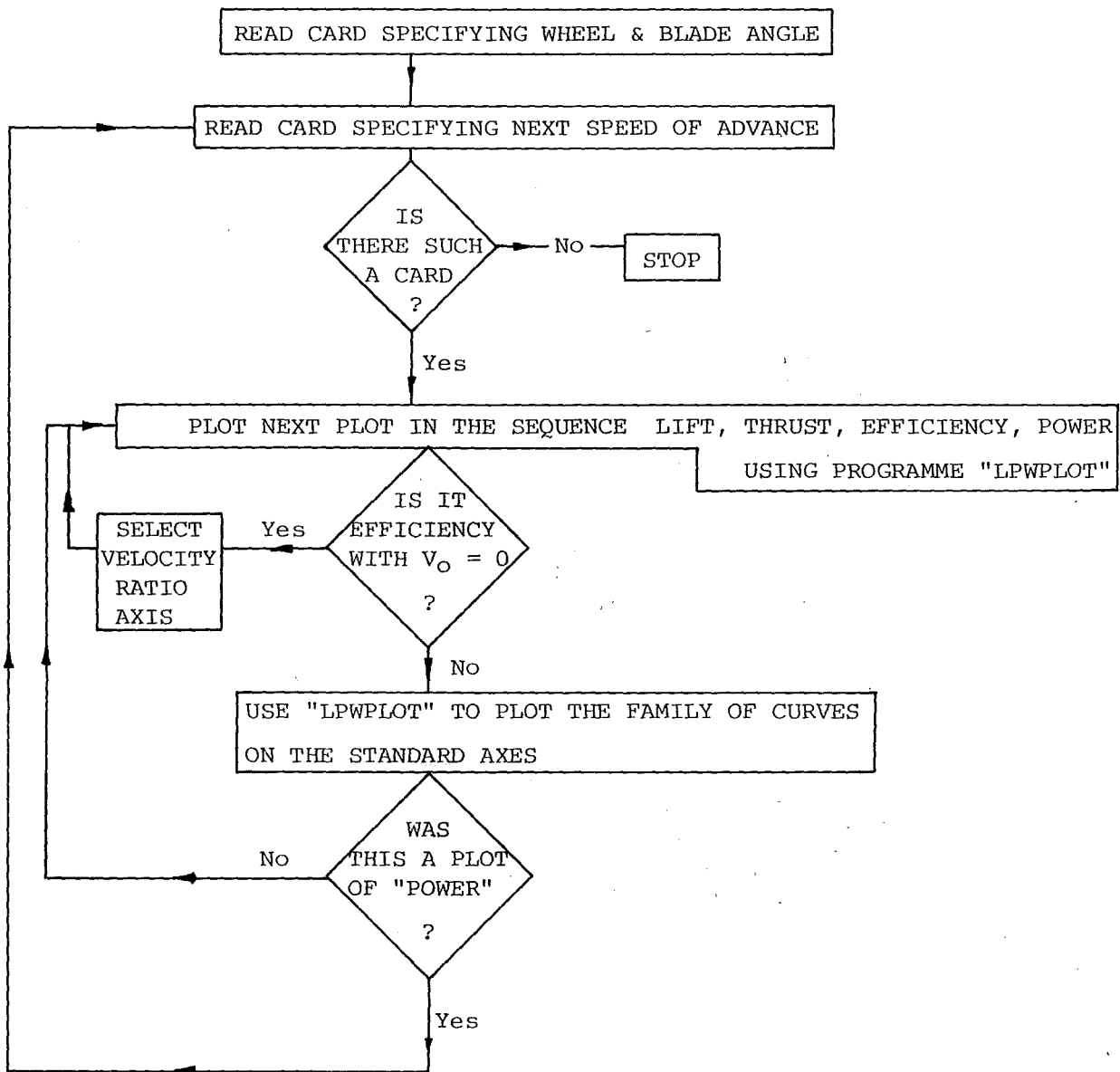


FIGURE 7.6: THE OPERATION OF THE MULTIPLE PLOTTING ROUTINE "ALTOGETHER"

While the curves produced would probably have been more representative of the real case had a least squares polynomial smoothing routine been used such a routine would not have produced a line to pass through all the data points. Both methods therefore have their disadvantages, and since the cubic spline routine was chosen the waviness of some of the curves in some plots has to be tolerated as a characteristic of this smoothing method, rather than of the data itself.

7.6.1 Multiple Plotting

Experience with the LPW tests made it clear that in order to gain a good intuitive understanding of LPW behaviour a number of plots would be required. These needed to contain all the variables and needed to relate them in a way that clarified their effects. While some authors, such as Helm and Volpich and Bridges, have attempted to condense all the information from one paddlewheel on to a few, or a single complex dimensionless plot (see for example Fig.4.30) it was felt that the effects of some of the variables were obscured by such simplifications so, with the aid of the computer plotting facilities the relatively long-winded but probably clearer approach was chosen, and larger numbers of plots were used to describe each wheel's performance.

It was a relatively simple task to adapt the programme 'LPWPLOT' to produce such an assemblage of plots automatically. The plotting routine which did this was called 'ALTOGETHER' and a block diagram of its function is shown in Fig.7.6.

While this programme was used to plot all the test data the Computer Centre plotting facilities took some time to cope with the volume of output required, with the result that it was often a week before the results of a day's testing at the testing tank were all available.

7.7 PRESENTATION OF MULTIPLE PLOTS

An assemblage, normally of 19 plots was chosen as the standard representation for each LPW, and such an assemblage for the standard LPW with flat blades at a blade angle of 60° is shown in Fig.7.7. (This figure is enlarged later in Figs.9.1, 2 and 3.) Each column of plots represents a different speed of advance, beginning with the static case on the left and finishing with the fully planing case on the right.

LIFT
EFFICIENCY THRUST
POWER

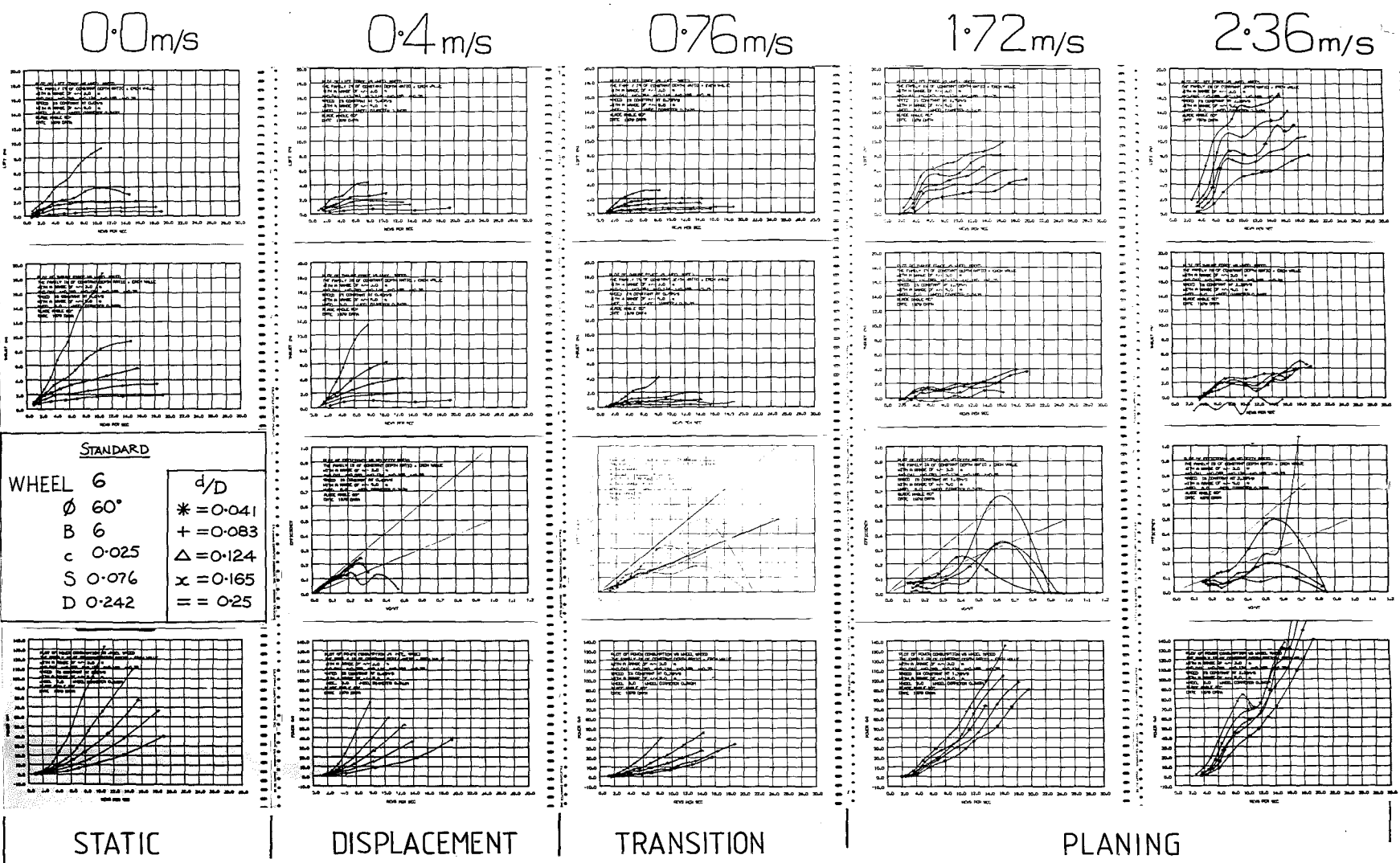


FIGURE 7-7: ASSEMBLAGE OF PLOTS DESCRIBING THE PERFORMANCE OF A SINGLE LPW
(This figure is enlarged in figs 9:1,2 & 3)

Each column contains a plot of Lift, Thrust, Efficiency and Power. For these plots the lift and thrust force values were plotted directly as measured from the results. Power was calculated from the torque and wheel revolutions measurements, so that:

$$P_{\text{expt}} = 2\pi n T_o \quad (7.1)$$

Efficiency was calculated from the power results as:

$$\eta = \frac{T V_o}{P_{\text{expt}}} \quad (4.45), (7.2)$$

where: P_{expt} = power from measured results
 n = wheel revolutions per second
 T_o = wheel torque as measured
 η = propulsive efficiency
 T = thrust force as measured
 V_o = speed of advance

Lift Thrust and Power were plotted against wheel revolutions per second, while Efficiency was plotted against velocity ratio since such a plot readily compared the actual efficiency with a straight line ideal maximum efficiency (marked on the plot) as noted in sections 1.4.1, 1.4.2 and 4.14.1.

This assemblage of 19 plots, each plot of A4 paper size, presented an access problem in itself, since there were 40 such assemblages once the testing was complete. Eventually each wheel's plots were set out on a 2 m x 1 m sheet of corrugated cardboard which allowed each wheel's data to be readily filed, or produced for comparison with the data of different wheels. The 19-plot assemblages of the LPW test data are shown in Appendix 4.

7.8 ACCURACY OF THE DATA PLOTS

The data in these plots includes measurement uncertainties and, being plotted by machine, has not had the guiding human hand to smooth the curves between errant points. Appendix 2 outlines the compilation of error estimates and identifies sources of measurement error with the conclusion that a given single data point will, 66% of the time,

TABLE 7.8: ERRORS IN THE DATA RECORDS ARE EXPECTED TO BE LESS THAN OR EQUAL TO THE ABOVE UNCERTAINTIES FOR 67% OF THE DATA. (THE 6.1% ERROR IN THRUST FORCE MEASUREMENTS IS NOT INCLUDED IN THESE ESTIMATES. THIS IS DISCUSSED IN SECTION 5.7.1, APPENDIX 2 AND APPENDIX 4).

MEASUREMENT ERRORS AT SOURCE

BLADE ANGLE:	$\pm 0.25^\circ$
IMMERSION DEPTH:	$\pm 4 \text{ mm}$
WHEEL ROTATIONAL SPEED:	$\pm 1.8\%$
THRUST FORCE:	$\pm(0.2 \text{ N} + 1\%)$
LIFT FORCE:	$\pm(0.2 \text{ N} + 1\%)$
TORQUE:	$\pm(0.02 \text{ Nm} + 1\%)$
SPEED OF ADVANCE:	$\pm 2\%$ (MAX: $\pm 5\%$)
WHEEL DIAMETER:	$\pm 1.2\%$ between wheels of differing blade angles. $\pm 0.4\%$ from diameter tabulated in Fig.5.18.

EFFECTS OF ALL UNCERTAINTIES ON PLOTTED DATA

LIFT FORCE:	\pm (THE LARGER OF: 0.5 N OR 10%)
THRUST FORCE:	\pm (THE LARGER OF: 0.5 N OR 10%)
EFFICIENCY:	$\pm 12\%$
POWER:	$\pm 6\%$

be subject to the magnitudes of error less than or equal to those shown in Table 7.8. This means, however, that discrepancies larger than those tabulated will be observable in the data records.

It should be mentioned that the thrust force data and efficiency data as recorded in Appendix 4 still contain the 6.1% error noted in section 5.7.1. This means that the thrust and efficiency values as plotted are 6.1% too large. It is clear from Table 7.8 that such an error is within the experimental uncertainty of any given data point, and because of this replotting of the data did not seem to be warranted.

7.9 CONCLUSION

Tank tests of LPW's constituted the major tasks of the project, largely fulfilling the data acquisition section of the secondary aims (see Fig 3.10, part A3). As well as the tank tests themselves, these tasks involved the design, construction and assembly of the force balance and the data logging equipment, together with the evolution of reliable experimental procedures and the development of data processing and plotting routines and a useable data filing and storage system. The last three chapters (Chapters 5, 6 and 7) have described the equipment procedures and programmes used in these tank tests.

CHAPTER 8

PHOTOGRAPHIC STUDIES8.1 INTRODUCTION

The photographic studies of the LPW in operation were undertaken in partial fulfilment of the tertiary aims, part A2 (Fig.3.10, section 3.6) which required sufficient data about LPW performance upon which to base theories of LPW operation. These studies then, filled a role similar to the force balance tank tests in providing such data. While the data itself was of a different nature than the force balance measurements, its value in explaining LPW operation was of almost equal importance.

This chapter describes the equipment and arrangements used for these studies while the actual results and conclusions drawn from them are included in with the general findings in the next chapters, Chapters 9, 10 and 11 as well as earlier in Chapter 4.

Three main areas of LPW operation were examined using photography and a video taperecorder. These were:

- 1) Studies of the spray and wake formation of a single LPW operating in open water, in the testing tank at Kainga.
- 2) Close-up studies of the LPW operating in flowing water in a glass-sided tank; this involved stroboscopic studies.
- 3) Records of the model LPW craft in operation.

Although some findings from this third area were pertinent to LPW operation, most were more relevant to the performance of the model LPW craft itself, so these findings will be left to the chapter relating to the model craft, (Chapter 12).

The other two studies helped clarify the following issues:

- (i) Wake formation and the generation of waves by the LPW: an area which was largely overlooked by paddlewheel researchers (as noted in Chapter 2).
- (ii) Flow around LPW blades: a study advocated by Beardsley as the next step in paddlewheel research. (1)

Both studies were of considerable value in explaining LPW and paddlewheel operation.

8.2 THE KAINGA TANK OPEN WATER STUDIES

The tank tests with the force balance involved the use of the spray guard shown in Fig.5.29 to prevent the spray from the LPW wetting the tank rails. This guard made observation of the spray and wake formations difficult during the force balance tests so a separate arrangement was built specially for the photographic study. It involved three main structures:

- 1) A new rig to hold and power the LPW.
- 2) A large cover to keep spray from the rails and the Rating Car, without interfering with spray and wake formation.
- 3) Cameras and lighting with suitable mounts.

8.2.1 The Photography Rig

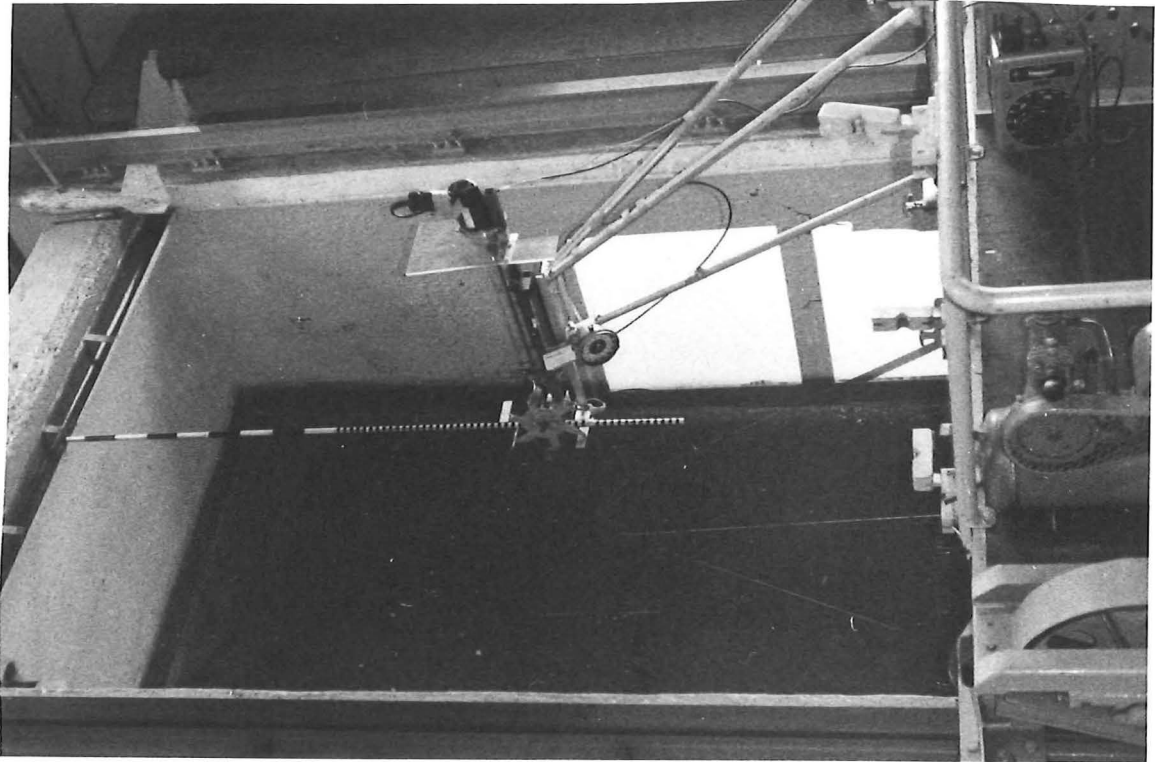
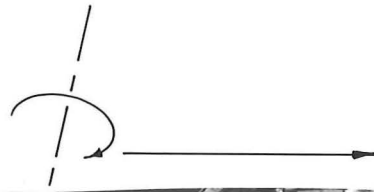
The rig is shown in Fig.8.1. It powered the LPWs by an electric drill supplied from a variac which could be used to vary the wheel rotational speed. The rig also had a screw adjustment to set the LPW immersion depth. A horizontal, graduated rod was attached to the rig just above the water surface to give a scale for the photographs, and a car speedometer, calibrated in revolutions per second, was mounted near the LPW and connected to the shaft so that, appropriately calibrated, it indicated its rotational speed. A code plate was mounted beside the r.p.s. indicator and codes on this identified the operating conditions for each photograph. Figures such as 4.19 (C) and (D) show these features.

The rig was mounted on a specially built frame which placed it well clear of the rear of the Rating Car so that wake and spray conditions were not obscured by it.

8.2.2 The Spray Cover

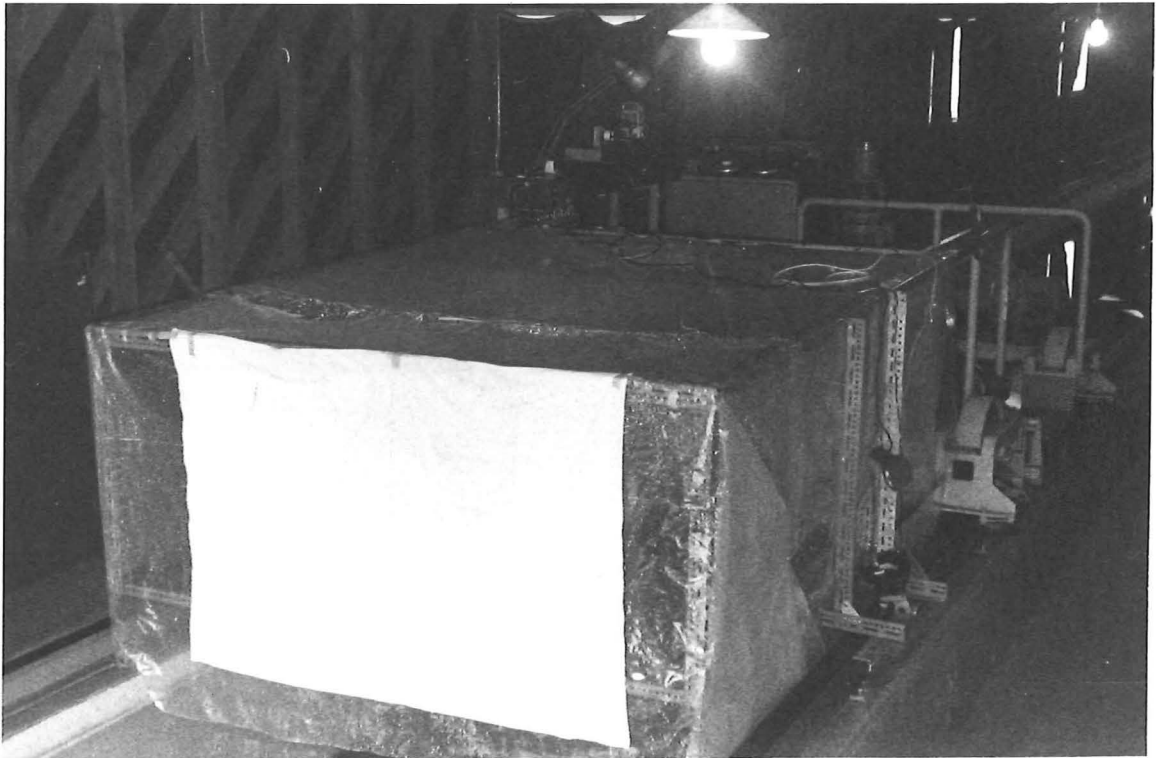
The spray cover was a structure measuring about 3 m x 2.3 m x 1.5 m and was sufficiently large to house the whole area under observation. It is shown in Fig.8.2. Its framework was made to be readily attached to the Rating Car handrails so that it could be quickly set up for the photography days. It moved with the car. Because the structure was

MOTION IN OPERATION



/2

FIGURE 8.1: THE PHOTOGRAPHY RIG MOUNTED ON THE REAR OF THE RATING CAR



/5

FIGURE 8.2: THE SPRAY COVER FROM THE REAR: IT HOUSES ALL OF THE WATER AREA SHOWN IN FIG.8.1

covered with clear polythene it allowed lighting and flash units to be shone through it. A white sheet was hung over the rear to help with light reflection, and to give some background contrast which would make the waves more readily visible.

8.2.3 Cameras and Lighting

The ideal photographic record was envisaged as one where two simultaneous high speed photographs from two different vantage points could be taken just after the LPW blade had entered the water. A series of five or so pairs of photographs would be taken with the wheel rotating at different speeds, for each run down the tank. Such a group of ten photographs would approximately illustrate the conditions in a normal test run down the tank with the force balance. If such photographs, with a view from the front and another from the side could always catch the LPW with a blade just immersed (the most important point in the blade passage) useful comparisons could be made between different wheels and blades.

In order to have enough data with which to make useful comparisons, a photography series was planned which would cover both the standard six-bladed wheel with blade angles of 60° under all standard conditions, as well as a representative sampling of other wheels and conditions. Such a series involved close to 250 pairs of photographs.

A camera and lighting system to achieve these ideals was designed as shown in Fig.8.3 and set up on the bench. It employed a pair of Nikon motordrive cameras operated from a single switch and battery pack; each camera contained enough film for 250 pictures which was sufficient for a day's photography. Lighting consisted of a pair of flash units, one for each camera, operated from a common power source and trigger, and supposedly, therefore, simultaneous in operation.

A magnetic pickup activated by the passing LPW blades triggered a stroboscope for visual observations, and since the stroboscope incorporated a phase deviation control, the LPW image observed under strobe lighting could be positioned as required with a blade just entering the water. A photoelectric SCR switch for the flash guns was to be triggered from the strobe light to ignite the flash units once the camera shutters were both open.

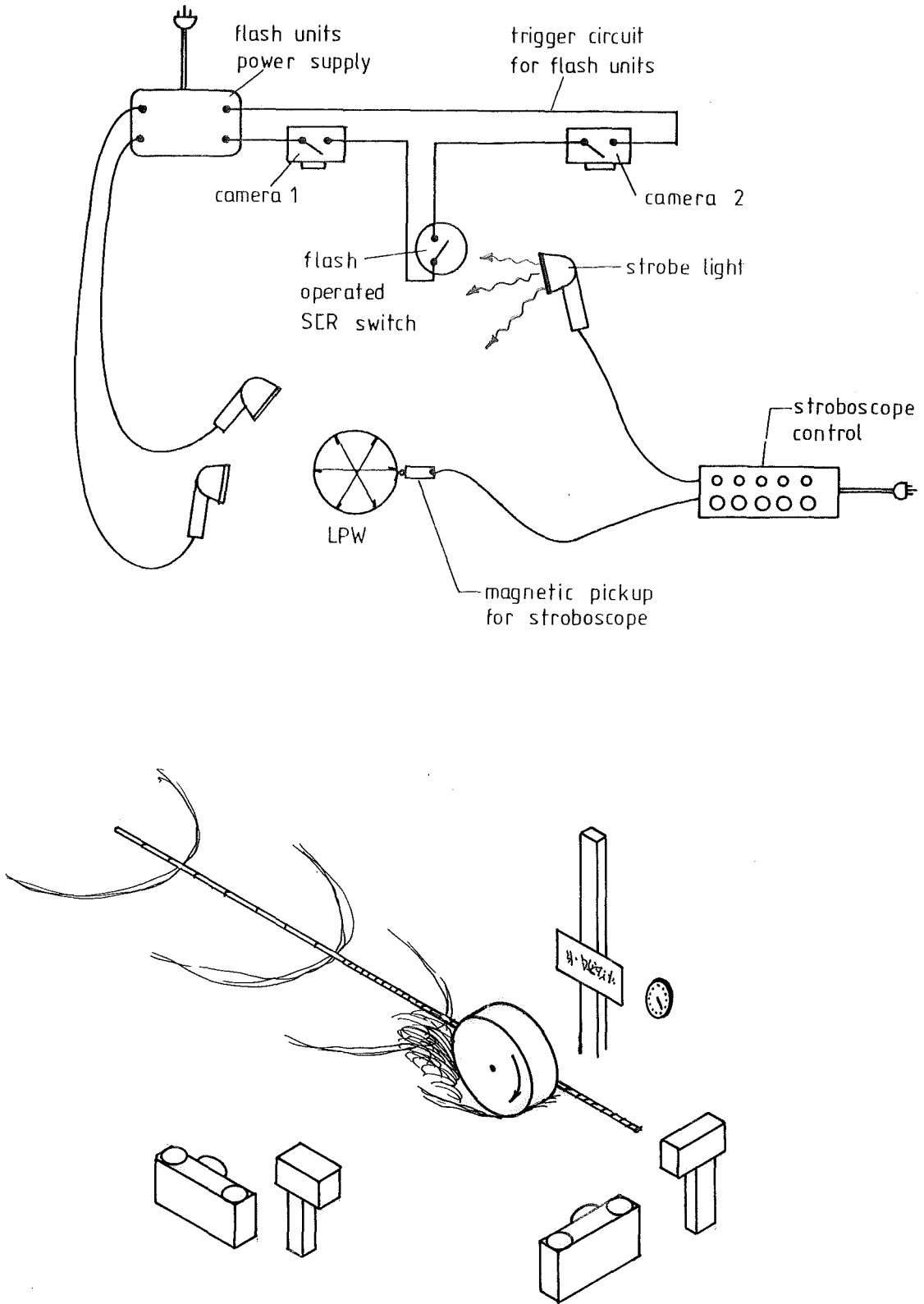


FIGURE 8.3 THE LIGHTING CIRCUIT AND THE CAMERA AND LIGHTING ARRANGEMENT FOR THE OPEN WATER STUDIES

A brief test run was conducted at the Kainga tank to check equipment assembly procedures and to find the correct camera settings for the light conditions, and a day was arranged when the photography series could be carried out.

8.2.4 Outcome of the Open Water Studies

Unfortunately a number of things rendered two photographic series somewhat less successful than they could have been. These were:

- 1) The paired Metz flashguns did not fire simultaneously and had long duration flashes resulting in partially blurred double images in many shots.
- 2) The photoelectric trigger for the flash guns, which worked on the bench, and in the stroboscopic photography studies (section 8.3) failed to work reliably at the Kainga tank, with the result that the LPW blades were positioned randomly in the photographs.
- 3) Although the flash gun triggering circuit included both camera shutters, the flash units seemed to be triggered by one camera only so that many shots from the other camera were only half exposed.
- 4) One film of 250 shots was largely destroyed during development.
- 5) Although the triggering circuitry was reassembled on the bench, flashguns replaced, and circuitry altered to accommodate capacitance effects so that it again worked well, another day's photography to repeat the first day's 500 shots at the tank similarly produced double images which were not synchronous with the stroboscope, and one film with pictures only partially exposed.
- 6) A third attempt was not possible partly due to difficulties in obtaining the use of the tank again, and partly because of the humiliation factor generated with the production of 1000 unsuccessful photographs.

However, the rather less than successful outcome was still a large number of useful photographs of LPW wakes under varying conditions of speed and immersion as well as a few shots showing blades just

entering the water as required. A rare and successful pair of photographs of the long-bladed wheel from the first series of photographs is shown in Fig.8.4, and these illustrate the intended results.

Table 8.13 lists the photographed conditions from both series. Of note is the wheel coded O which was the solid cylinder of the same dimensions as the LPWs. It was incorporated to illustrate the similarities of the LPW wakes to those of a stationary or rotating cylinder, and Fig.8.6 shows it operating in conditions similar to those shown in Fig.8.4.

8.3 CLOSE-UP STROBOSCOPIC STUDIES

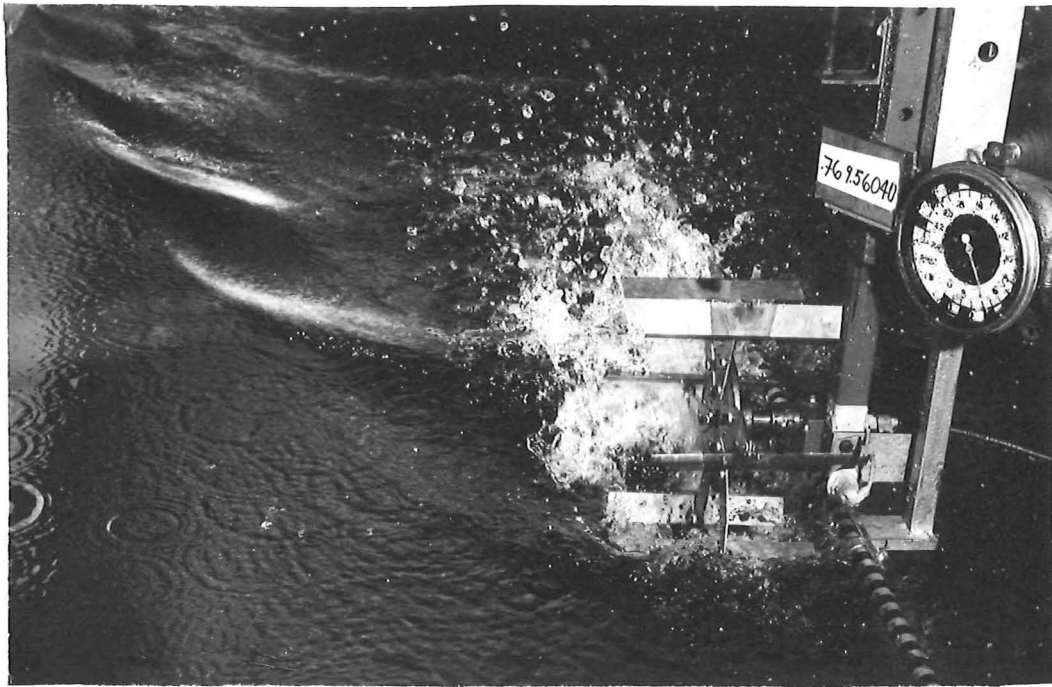
Close-up, underwater, high speed photographs of the flow around LPW blades at the Kainga testing tank would have been ideal for blade flow studies but it would have been a very difficult task to carry out. Therefore an easier, but slightly less satisfactory arrangement was decided upon for a first study of such flow conditions.

The Civil Engineering Department's Fluids laboratory has a glass-sided channel 0.16 m wide by 0.7 m deep and 6.1 m long. Its maximum flow velocity is about 3.2 m/s of supercritical flow at a depth of close to 0.18 m. It can also pass deeper slower moving subcritical flow. Since it was known that the two major modes of LPW operation were the displacement and planing modes, and that these could be approximately modelled with the LPW in conditions of subcritical and supercritical flow respectively, it was decided to observe and photograph both modes of operation in the flowing water channel, keeping in mind the limitations of the arrangement. (These limitations are discussed in section 4.16).

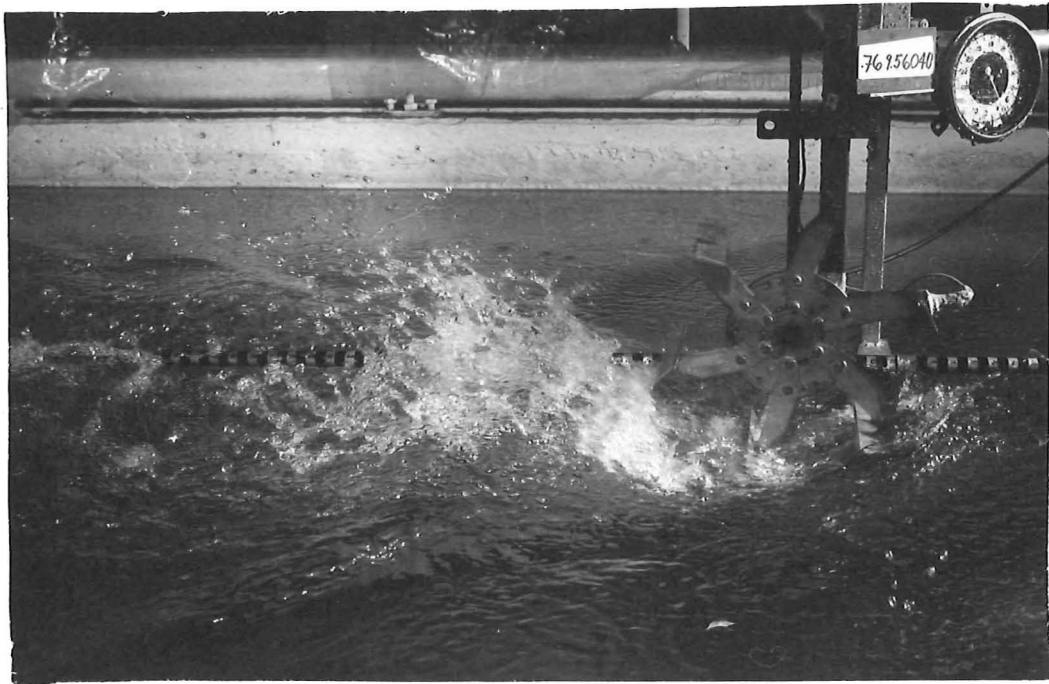
Since the equipment and tank were within the University, time could be spent in getting photographic and lighting equipment working properly before photographs were taken.

8.3.1 Equipment Arrangement

The rig to hold and power the LPW was essentially the same as the one used in the Kainga tank photography series. It was mounted on the channel top, could be raised or lowered by its screw adjustment, and was powered from a variac which controlled the LPW speed. It is shown set up in Fig.8.7.



1205A/24



1206A/42A

FIGURE 8.4: WHEEL CODED 9.5, WITH LONG BLADES PHOTOGRAPHED IN THE TESTING TANK SERIES IN THE HUMP CONDITION. NOTE THE WAKE. CONDITIONS: $D=242$ mm, $V_o=0.76$ m/s, $F_r=0.49$, $n=4.3$ rps, $\phi=60^\circ$, $d/D=0.17$, $d=40$ mm, $c=25$ mm, $s=152$ mm.



1300E/13A

$V_O=0.76$ m/s, $F_r=0.49$, $d/D=0.165$, $n=1$ rps

MOTION



1300E/14A

FIGURE 8.6 : THE CYLINDER OPERATING UNDER CONDITIONS CLOSE TO THOSE SHOWN IN FIG.8.4. NOTE THE SIMILARITY OF THE WAVE FORMATIONS.

$V_O=0.76$ m/s, $d/D=0.165$, $n=6$ rps

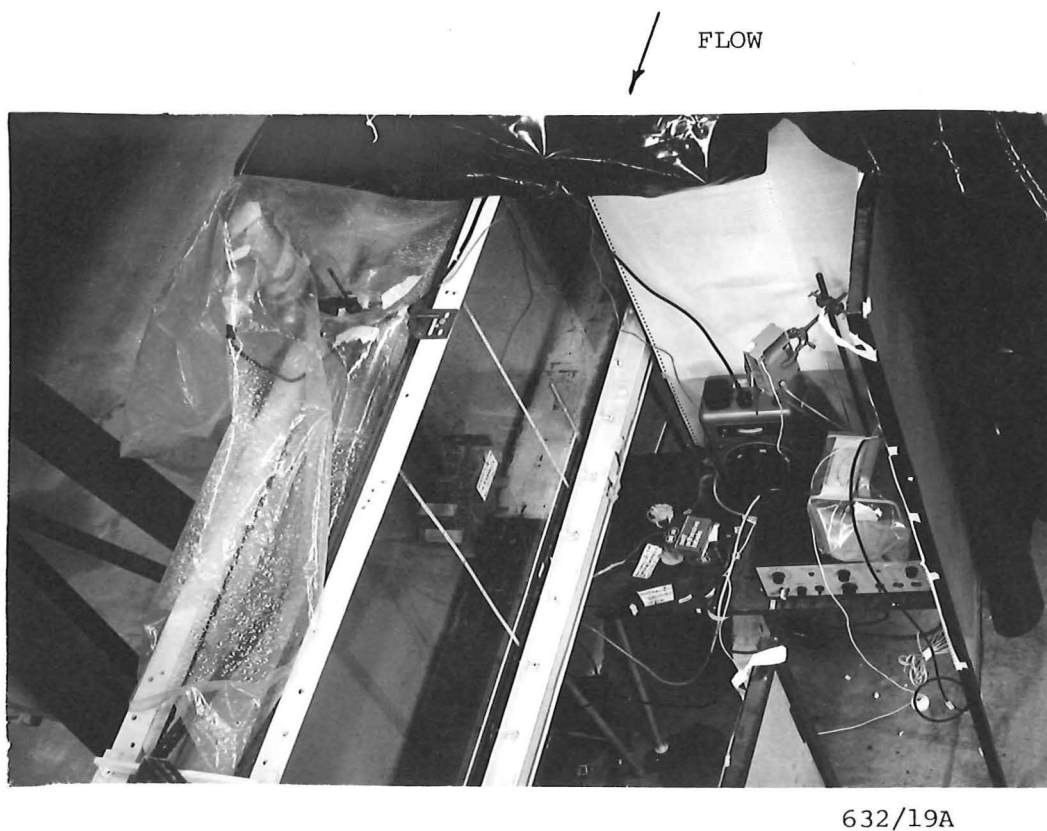
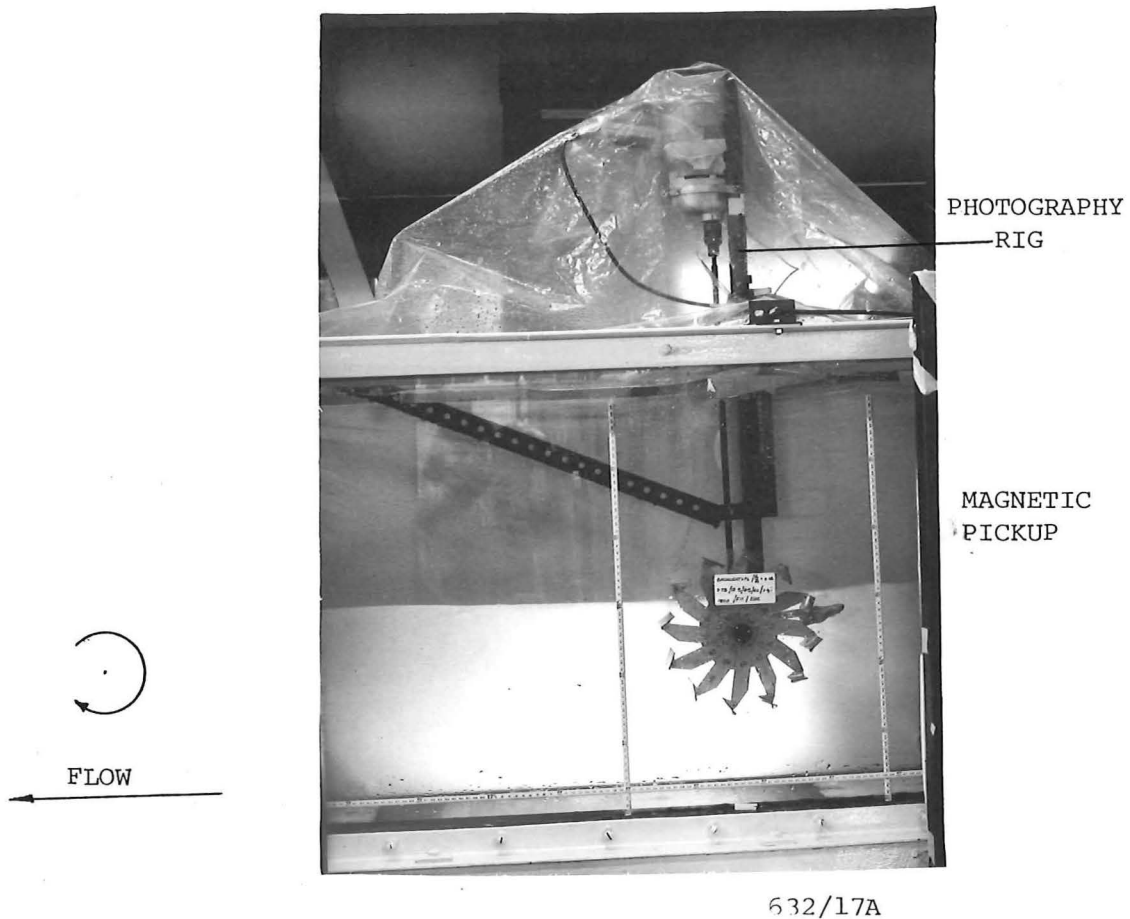
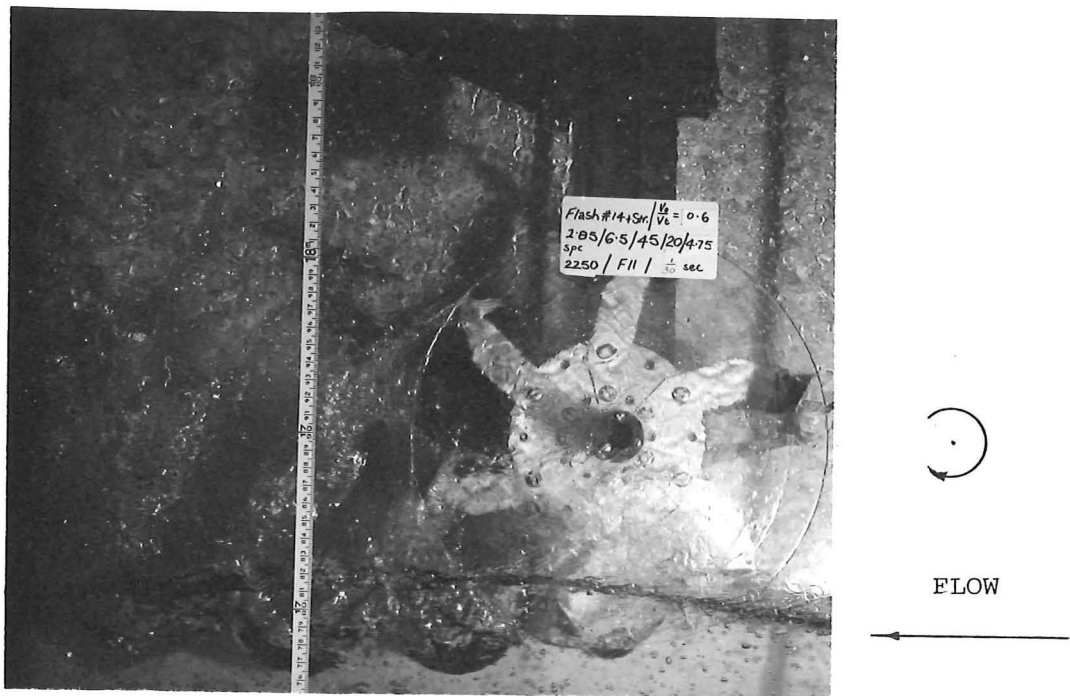


FIGURE 8.7: THE PHOTOGRAPHY RIG TOP, AND STROBOSCOPIC EQUIPMENT IN THE BLACKOUT CUBICLE BOTTOM. NO WATER IS FLOWING IN THESE VIEWS (STROBOSCOPE: BRÜEL & KJAER MOTION ANALYSER TYPE 4911)



630/41

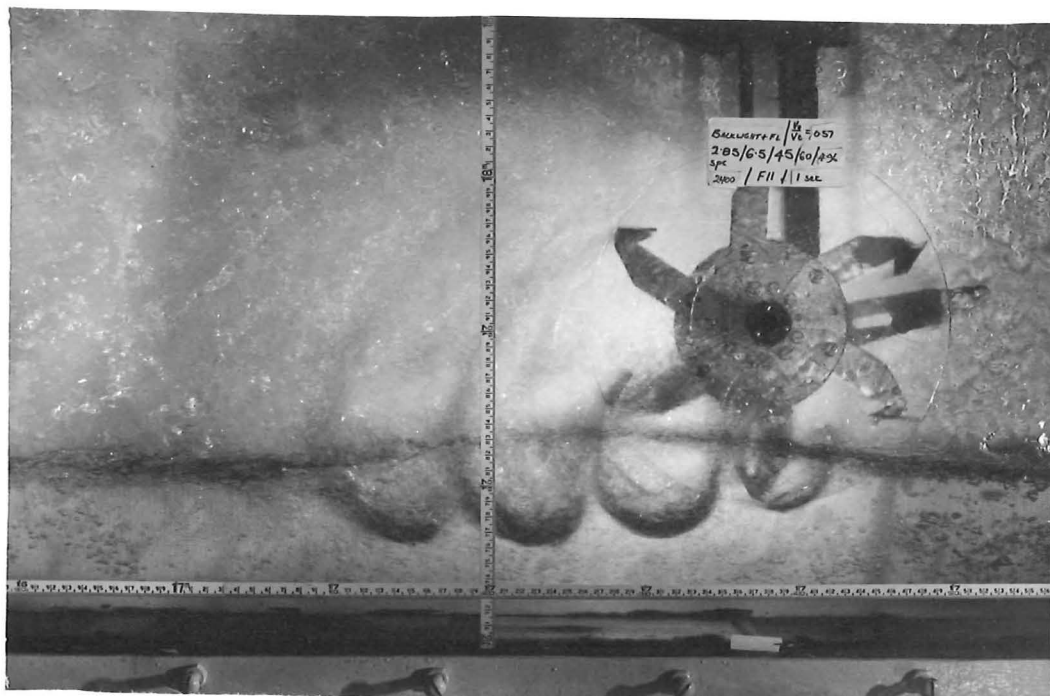
FIGURE 8.8: PHOTO OF THE PLANING CONDITION WITH A SINGLE FLASH FROM THE FRONT.

CONDITIONS: STANDARD BLADES, SIDEPLATES,
 $\phi = 45^\circ$, $d = 20$ mm, $V_0 = 2.85$ m/s, $n = 6.3$ rps



630/7

FIGURE 8.9: PHOTO AS FOR FIGURE 8.8 WITH STROBE LIGHTING, 20 DIFFUSED FLASHES FROM BEHIND



632/15

FIGURE 8.10: PHOTOGRAPH WITH A SINGLE FRONT-LIGHTING FLASH AND 20 BACKLIGHTING FLASHES FROM THE STROBOSCOPE

CONDITIONS: SIDEPLATES, $\phi=60^\circ$, $d/D=0.19$, $n=67$ rps, $V_O=2.85$ m/s, STD.DIMENSIONS, SUPER-CRITICAL FLOW MODELLING THE PLANING CONDITION



632/32A

FIGURE 8.11: TRANSITION MODE PHOTOGRAPH: THE WHEEL IS IN THE TROUGH CONDITION.

CONDITIONS: 12 BLADES, SIDEPLATES, $V_O=0.79$ m/s, $\phi=45^\circ$, $d/D=0.25$, $n=5$ rps, STD. DIMENSIONS, 12 BLADES, SUBCRITICAL FLOW

The 15 Watt stroboscope was triggered from the magnetic pickup near the LPW blades, and its phase deviation control and slow motion option were both useful for observations. (Lighting and circuitry arrangements are shown in Fig.8.12.)

A blackout cubicle was constructed around the tank close to the LPW, to assist observation and photography. Scales, and labels describing the operating conditions were simply stuck to the glass for the photographs.

The standard 242 mm diameter wheel used for observation in this study was fitted with 2 mm thick perspex sideplate discs out to the blade tips, which were used in an effort to keep the flow two-dimensional.

8.3.2 Lighting For Photography

Some attempts were made to take high speed photographs of the LPW in this tank using the camera flash alone, as shown in Fig.8.8, but such pictures illustrated only the instantaneous cavity and splash formations which did not represent very well, what could be observed using the stroboscope. While the stroboscope could be hand-held for observations the most satisfactory results when using it for photography seemed to be where it was arranged to give carefully diffused backlighting. Photographs taken with this lighting and a 1 second camera time exposure looked like the one in Fig.8.9. During such exposures the stroboscope light flashed about 20 times and this had the effect of averaging the splash formations and the cavity surfaces giving a more realistic image of conditions than a single picture would have given. While such pictures were satisfactory the final arrangement was one in which the camera flash gun was triggered once by the stroboscope light to light up the front of the wheel, the scales and the coded label, before leaving the stroboscope light to fill in the flow picture with the subsequent multiple flashes. The result of such an arrangement is shown in Fig.8.10, demonstrating the planing condition and in Fig.8.11 showing the transition zone. The circuitry and lighting layout is shown in Fig.8.12.

8.3.3 Limitations and Scope of this Study

The confines of the tank, as well as affecting wave velocity in the subcritical flow, (modelling the displacement mode) also affected the water surface level in the supercritical flow where the

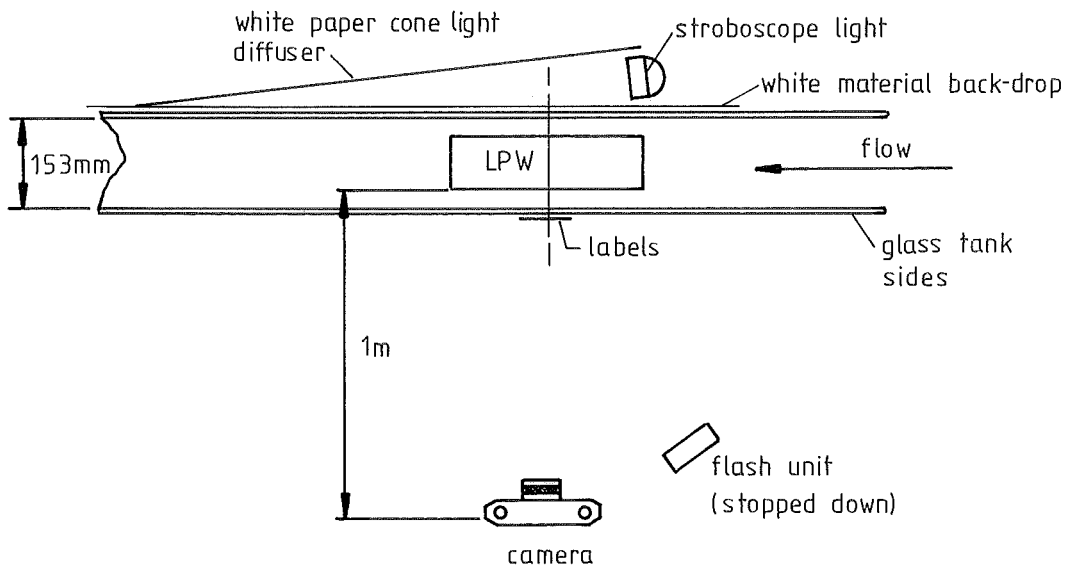
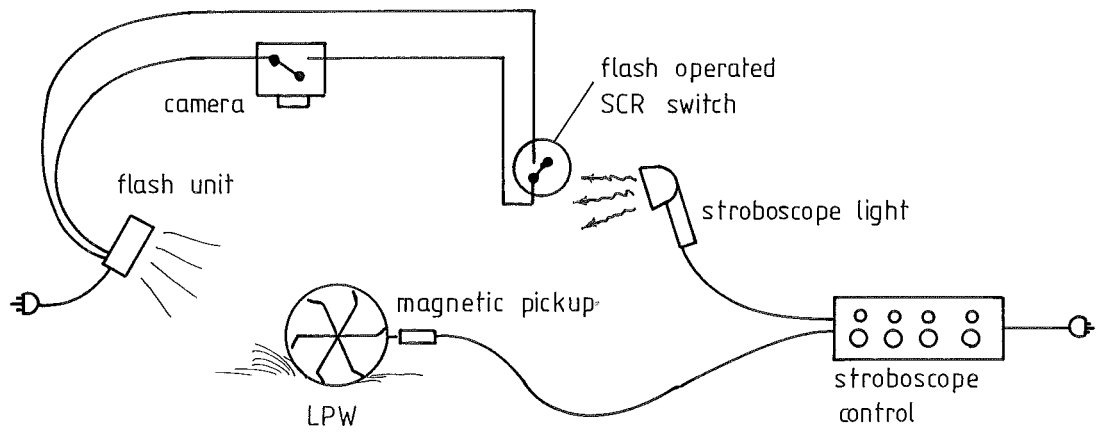


FIGURE 8.12 THE LIGHTING CIRCUIT (ABOVE) AND THE CAMERA AND LIGHTING ARRANGEMENT (BELOW), FOR THE STROBOSCOPIC STUDIES IN THE GLASS-SIDED TANK.

planing mode was modelled. The water surface in Fig.8.10 can be seen to bulge upwards where blade-generated cavities are present. This is simply a continuity effect caused when the blade cavity is thrust into water which is bounded on three sides by the tank sides and bottom. It would not be present if the LPW was in open water.

The closeness of the tank sides also amplified the effects of bowsplash (where, in the planing mode, water is splashed ahead of the wheel. See section 4.9.1). This splash tended to build up, partially blocking the flow. While this did not model the open water case either, it did provide a good opportunity to observe the onset of the bowsplash phenomenon.

The observations and photographs in this study were therefore largely qualitative in nature, so that while some approximate measurements could be taken from the photographs the main value of the study was to demonstrate the flow phenomena, and as such it became a useful reference during the development of the analytical models of the LPW performance, described in Chapter 4.

The series of photographs taken covered the flat-bladed LPW conditions, and Table 8.13 summarises the variables photographed.

8.4 VIDEO TAPE RECORDER STUDIES

The Department's JVC video camera and video tape recorder provided a further means of recording observational data, and videotaped records were made of a few runs of the Kainga testing tank, both of the force-balance operation and of the LPW on the photography rig.

A more extended series of videotaped records was made of the tests in the glass-sided channel, and Table 8.13 also notes which conditions were recorded in this way. Since these used the stroboscope in its slow-motion operation the pictures were particularly useful for subsequent observation, as more refined theories of flow around the blades were developed.

A problem encountered was that the scanning rate of the video camera, and the stroboscope flash rate were rarely synchronised so that the picture appeared to flicker erratically. However this hardly detracted from the value of the recordings for observational purposes.

TABLE 8.13: SUMMARY OF PHOTOGRAPHS AND VIDEO OF LPW TESTS

(MODEL CRAFT TESTS NOT INCLUDED)

WHEEL CODE	DESCRIP-TION	BLADE ANGLE ϕ	VELOCITY m/s (Froude No. F_r)						TANK *	VIDEO	FIGURE NUMBERS
			0 (0)	0.4 (0.29)	0.76 (0.49)	1.72 (1.12)	2.36 (1.53)	2.85 (1.85)			
0	Cylinder	-	✓	✓	✓	✓	✓		K		4.34, 8.6, 11.4 to 11.7
3	3 blades	45						✓	GS	✓	
4	4 blades	45						✓	GS	✓	
4		45			0.84				FW		8.14
4.75	Tyre +	90	✓	0.44	0.85	1.89			K		11.31
5	Roller-craft	-	✓						K		11.17
6	Std.Blades	15						✓	GS	✓	9.15
6		30						✓	GS	✓	
6		45						✓	GS	✓	8.8 to 8.10, 9.10, 9.27
6	Standard	60	✓	✓	✓	✓	✓		K	✓	4.19, 4.32, 4.33, 9.5 to 9.9
6		60						✓	GS	✓	4.19, 4.36
6		60					✓		FW		5.16
6		70						✓	GS	✓	
6		90						✓	GS		
6		90					✓		K		
7	Tyre -	90	✓	0.44	0.85	1.89			K		11.30, 11.32
9.5	Long blades	60			✓		✓		K		8.4
11	Cupped	135	✓						K		10.15
12		45			0.79			✓	GS	✓	8.11

* K = Kainga tank,

GS = glass sided flowing water tank,

FW = flowing water tank.

CONDITIONS

STANDARD DIMENSIONS

$$\phi = 45^\circ$$

4 blades

$$V_o = 0.9 \text{ m/s}$$

$$V_o/V_t = 0.5 \text{ top}$$
$$0.7 \text{ bottom}$$

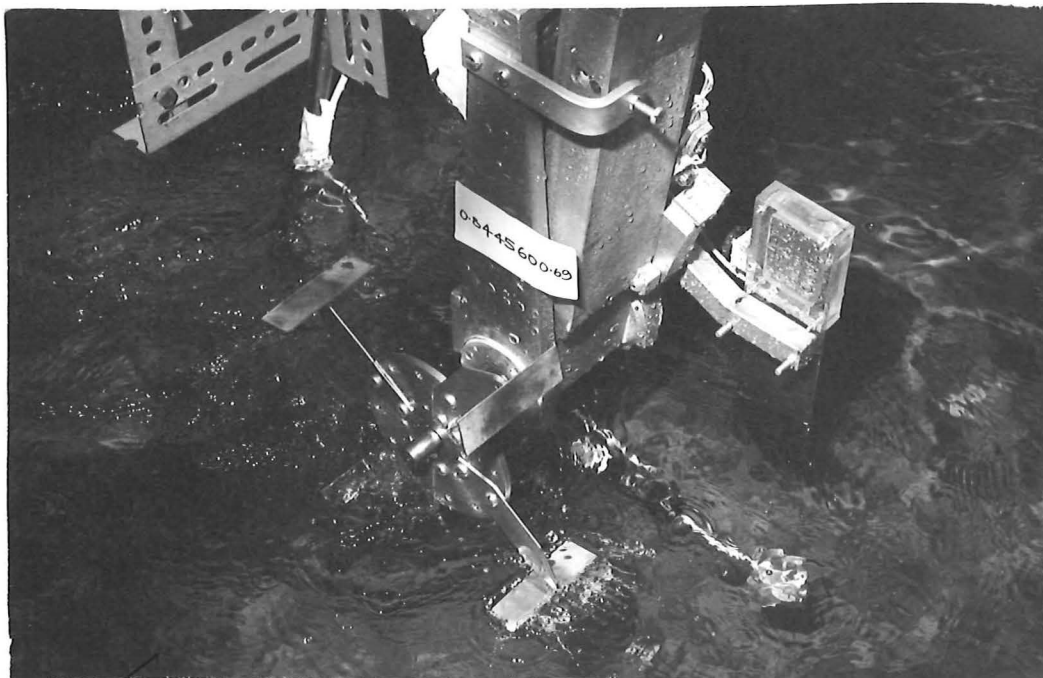
$$n = 2.4 \text{ rps top}$$
$$1.7 \text{ rps bottom}$$

$$d/D = 0.083 \text{ top}$$
$$0.25 \text{ bottom}$$



578/11

↑
FLOW



578/6

↙
FLOW

FIGURE 8.14: TWO PHOTOGRAPHS FROM THE 1978 SERIES SHOWING SPLASH EFFECTS AS BLADES ENTER THE WATER

8.5 OTHER PHOTOGRAPHS

Minor series of photographs were taken of the LPW in operation during the 1977 and 1978 tests in flowing water, and these series provided the starting points for the extended testing tank photography series described above in section 8.2. While in these earlier records no attempts were made to synchronise the photographs with blade entry, some of the pictures have proved more useful than those of the Kainga testing tank series because of the equipment malfunctions of the latter, and because they were taken from a greater variety of viewpoints. They have therefore been useful in subsequent analyses.

Two examples from the 1978 series are shown in Fig.8.14, and these show two effects of blade splash just as the blade enters the water where the blade and water surfaces are almost parallel.

8.6 CONCLUSIONS

These series of photographs and videotaped studies provided vital information clarifying the areas of LPW wake formation, and flow around LPW blades at entry and underwater. The findings from these studies have been useful throughout the project as the theories have been developed, and more systematic examination of the LPW photographs is undertaken in the next chapters.

CHAPTER 9

ANALYSIS OF THE RESULTS FOR THE LPW
WITH FLAT BLADES9.1 INTRODUCTION

Paddlewheel and LPW operation has been divided into four areas governed by the speed of advance of the wheel: the static, displacement, transition and planing modes. The theory section, Chapter 4, has defined limits to these areas, and has related them to the wake formations generated by the wheel. Since an operational LPW craft would be expected to run in the last of these areas, the planing mode, this area was concentrated on for the development of the impulse theory. This chapter, then, examines how well the theoretical limits between transition and planing apply in practice, and how closely the impulse theory and its accompanying predictions compare with the experimental results. Where relevant it draws upon the paddlewheel literature for comparisons. To conclude, it describes the development of coefficients which may be used to modify the theoretical model for use in the design and performance prediction of LPW craft discussed in subsequent chapters.

This chapter then fulfils parts 2 and 3 of the secondary aims loop in Chapter 3 (Fig.3.10) and allows the focus of the project to return from data gathering, to concentrate on assessing the value of the LPW concept.

9.2 RESULTS FROM THE TANK TESTS

This section examines the results from the LPW tank tests. These are in two forms, firstly the plotted data measured by the force balance described in Chapters 5, 6 and 7 and secondly the photographic records described in Chapter 8.

9.2.1 Measured Results for the Standard Wheel

The measured results from the tank tests with the force balance were stored on easily handled 19-plot assemblages as described in section 7.7 and shown in Fig.7.7. This figure is repeated and enlarged as Figs.9.1, 2 and 3. This data was not presented in the more conventional dimensionless form as it was seen as important to have the plots representing the real situation as closely as possible, to aid in an understanding of the many variables involved.

WHEEL NO: 6 (FB)

Blade Angle $\theta = 60^\circ$

Flat Blades, Standard Wheel

STATIC, $V_0 = 0$

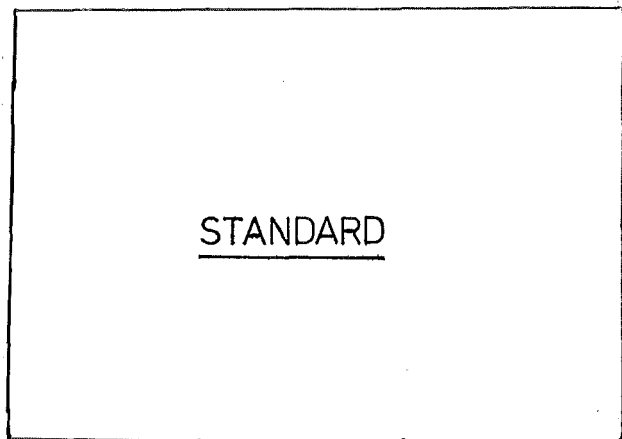
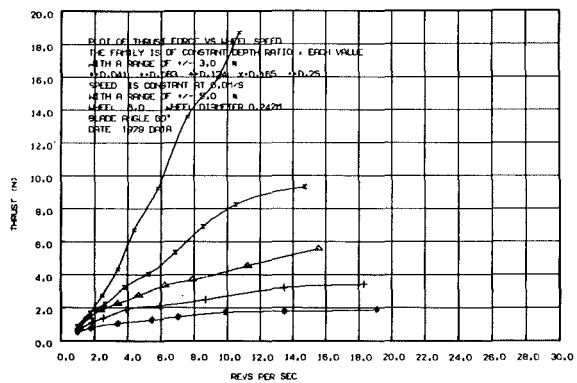
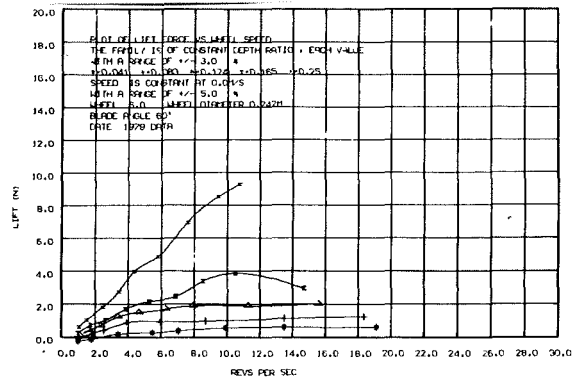
Diameter, $D = 242$ mm

Span, $s = 76$ mm $s/D = .31$

Chord, $c = 25$ mm $c/D = .1$

No. of Blades = 6

Symbols	Immersion ratio	Immersion angle	Immersion depth
	D/a	θ°	a (mm)
*	.041	24	10
+	.083	33	20
Δ	.124	41	30
x	.165	48	40
=	.25	60	60



See also:

Figs Sections
 1.2 Chapters 4
 9.5 to and 9
 9.10 etc.

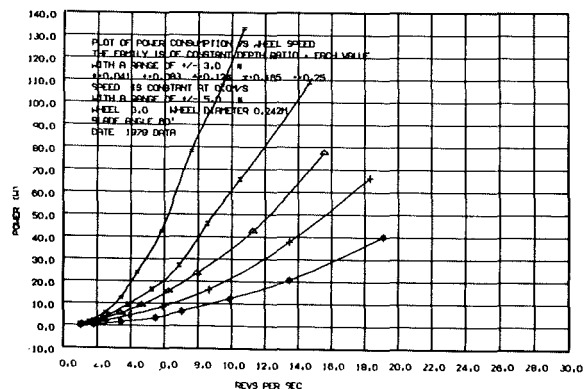


FIGURE 9.1: PLOTTED RESULTS FOR THE STANDARD WHEEL ENLARGED FROM FIGURE 7.7

Displacement, $V_0 = 0.4 \text{ m/s}$, $F_r = 0.26$

Transition, $V_0 = 0.76 \text{ m/s}$, $F_r = 0.49$

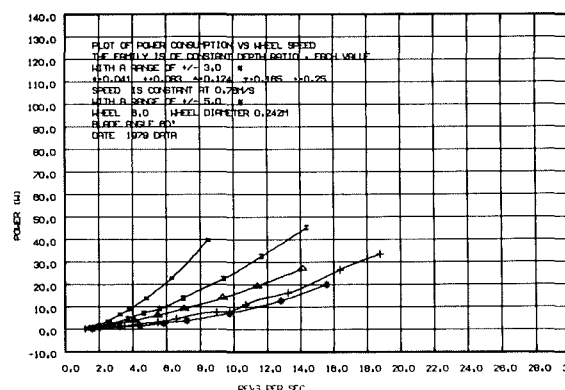
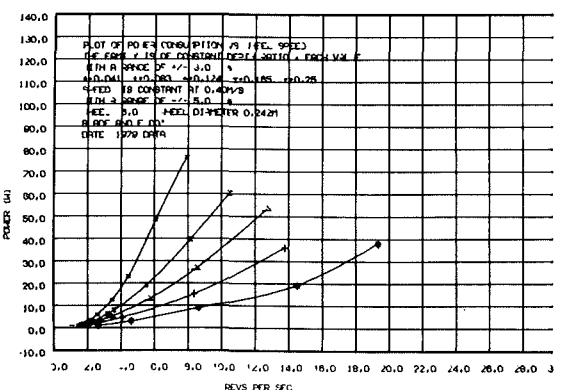
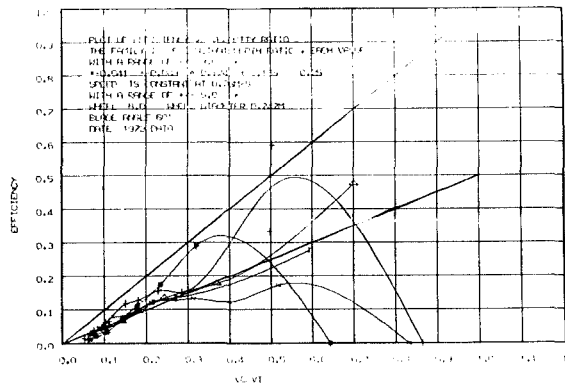
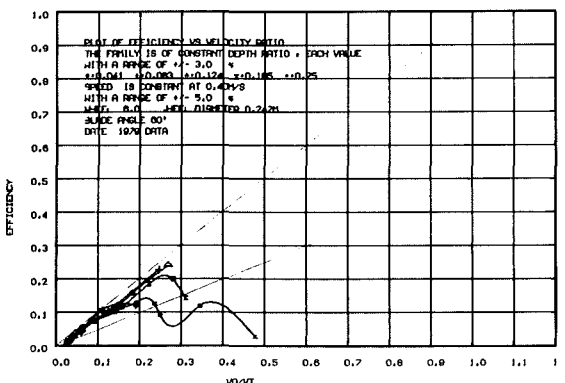
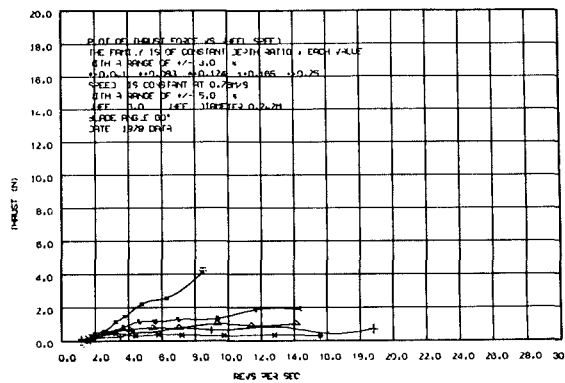
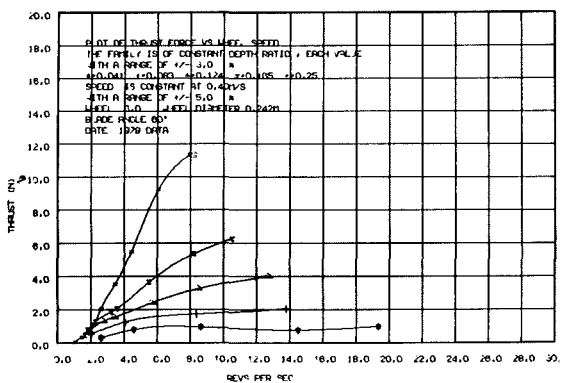
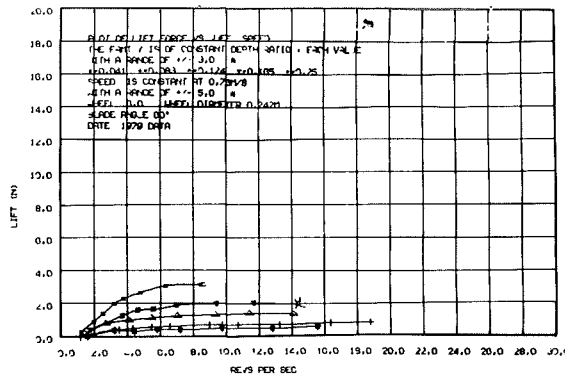
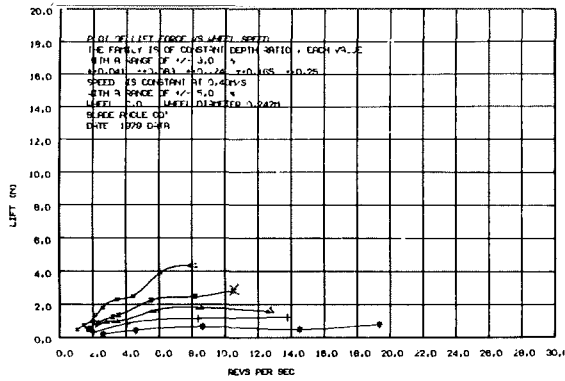


FIGURE 9.2: STANDARD WHEEL DISPLACEMENT AND TRANSITION RESULTS

Planing, $V_0 = 1.72 \text{ m/s}$, $F_r = 1.12$

Planing, $V_0 = 2.36 \text{ m/s}$, $F_r = 1.53$

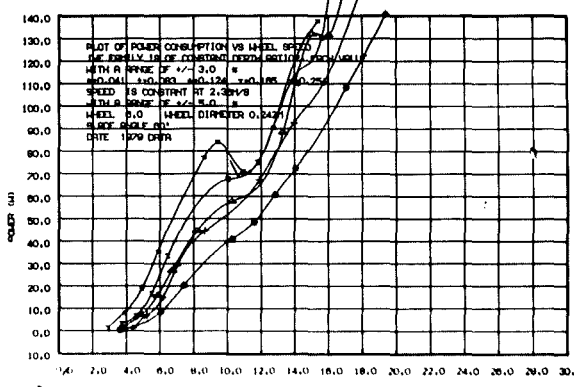
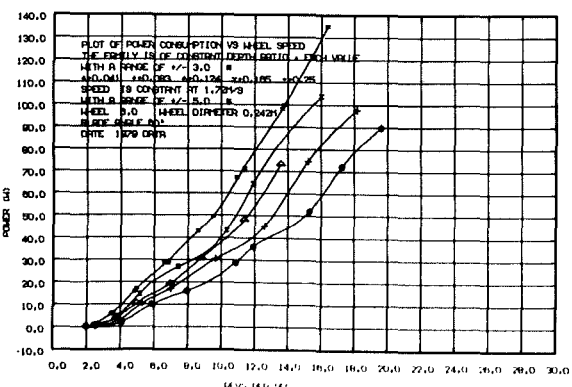
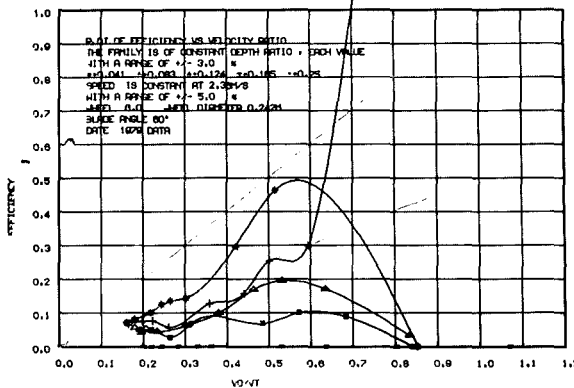
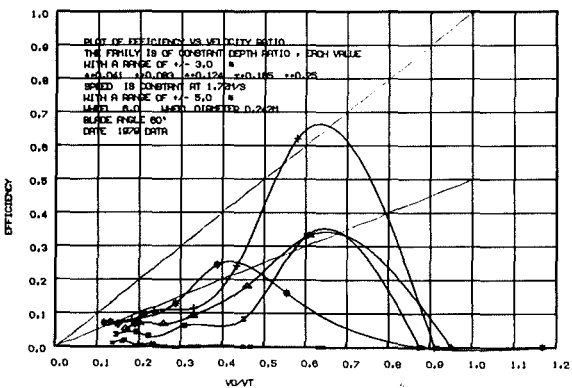
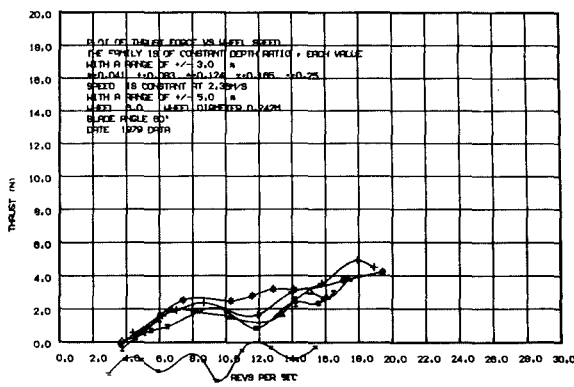
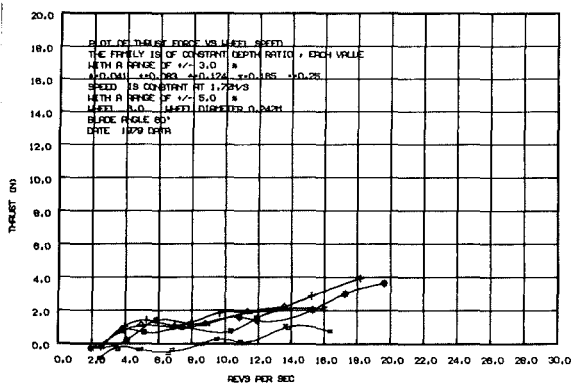
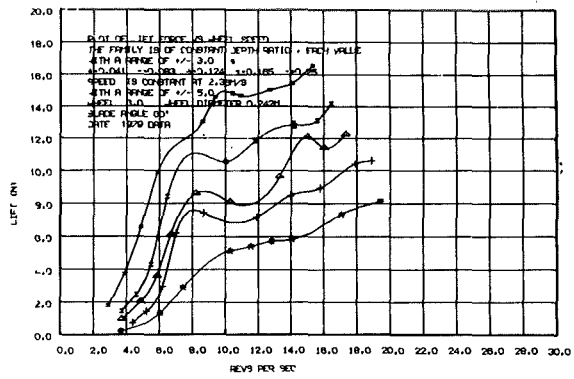
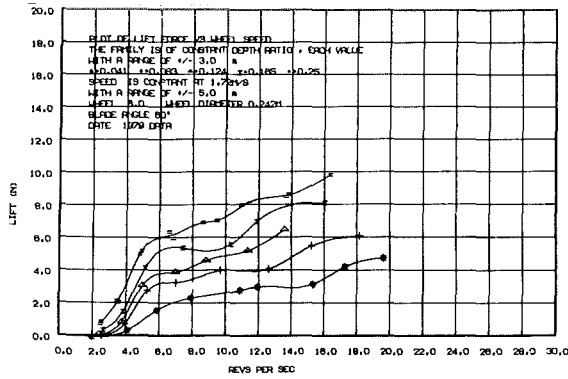


FIGURE 9.3: STANDARD WHEEL RESULTS FOR TWO PLANING SPEEDS (SEE APPENDIX 4 FOR RESULTS AT HIGHER SPEEDS)

A large number of the points covered in the theory section may be readily identified in the plots shown in Figs.9.1,2 and 3, which is the set of data for the standard wheel used in the development of the theory sections. Each individual plot contains five curves, one for each of the five immersion depths used. The curves may be distinguished by the symbols used to represent the actual data points as given in Fig.9.1 (Chapter 7 contains a description of the individual plots, and Fig.7.4 shows a plot in an enlarged form).

Each column of plots represents the results for a different velocity. Figure 7.7 shows the static mode on the left and the planing mode on the right. In this chapter this figure has been enlarged and broken up so that Fig.9.1 shows the static mode and Fig.9.3 shows the planing mode. The top row of plots is the lift force measurements, the second the thrust, the third the propulsive efficiency (no propulsive efficiency can be given for the static mode) and the bottom row the power consumed at each speed. The variation of the measured forces with the speed of advance, V_o , will be examined first.

9.2.1.1 LPW Forces in the Plotted Data. The lift and thrust forces in the static condition (Fig.9.1) can be seen to increase with wheel revolutions to an apparent limit. This limit, as described by Beardsley (1), is governed by the rate at which the water can be supplied to the wheel by the gravity-induced flow into the cavity that the moving blades scrape out. The more deeply immersed the wheel is, the greater the water spouting velocity into the cavity (1) and so the greater is the mass supplied to the rotor and consequently the greater are the forces before they reach this limit. Thus the forces, both lift and thrust, increase with immersion depth and with wheel revolutions up to this expected limit. These results agree with those of Beardsley. (1)

The next column in this case, in Fig.9.2 represents a velocity in the displacement mode. For this, the standard wheel, it is 0.4 m/s or a diametral Froude Number of $F_r = 0.26$. Both lift and thrust forces again increase with wheel revolutions and with immersion depth to the mass supply limit noted above. It can be imagined that once the blade tip speed is much greater than the speed of advance of the wheel (0.4 m/s) the mechanism of flow into the wheel cavity is much

the same as it was for the static condition, with a small additional flow into the front part of the cavity being largely balanced by a decreased flow into the rear part. So for displacement operation the forces are not unlike those for the static case.

The third column or in this case the second column in Fig.9.2, is of measurements taken at 0.76 m/s ($F_r = 0.49$), and this represents the transition zone for the smaller two immersions (10 mm and 20 mm with symbols * and +). For all immersion depths, in both the lift and thrust plots, the forces can be seen to reach upper limits at much lower wheel revolutions than they did in the displacement or static modes. This is because the wheel is now beginning to operate in the trough condition of the transition mode (see Figs.1.5, 4.32(B), 4.32(C), 8.4). The immersion depth of the wheel has, in effect been decreased by the formation of the wave trough which almost coincides with the wheel curvature. This limits the mass flow into the wheel cavity so that the force limits are reached sooner. Both lift and thrust forces, however, still increase with immersion depth.

The next column, column 1 in Fig.9.3, with the speed of advance $V_o = 1.72$ m/s ($F_r = 1.12$), represents the early planing condition for all immersion depths. (See Figs.4.33 and 4.36.) What has happened now is that, in Beardsley's terms: "the speed has become so great that the rotor is running away from the cavity before gravity-induced flow can supply it". (1) Now all the mass supplied to the rotor is horizontally entrained through the front. The mechanism of force generation has changed from one of flat plate drag, to one of impulsive momentum changes, with large accelerations occurring at blade entry. Blade entry conditions now become important in determining the direction of the resultant blade forces. A change may be observed in the thrust force curves. At this velocity they no longer increase with immersion depth and in fact the opposite is the case, so that the thrust curve for the deepest immersion (60 mm, with symbol = and $\frac{d}{D} = 0.25$) shows zero or negative thrust for most wheel revolutions.

This change in thrust forces with immersion depth as well as the fact that the lift force still retains its former relation with immersion depth is a result of the change of mass supply mechanism and the change to impulsive forces occurring at blade entry.

1. Beardsley, P.20

The character of the lift forces has also changed from that of the transition zone. The curves, at first concave downwards as wheel revolutions increase kink and become linear showing no tendency to become independent of wheel revolutions as before. This is now in the form of the force-rps plot of Fig.1.6. The initial parabolic section (1 to 5 rps) represents the lift force before surface cavity intrusion has begun to occur. (This pre-cavity intrusion section of the lift curves also has its equivalent in the thrust force curves though it is not easily recognisable at this blade angle.) Once surface cavity intrusion has begun, the parabolic sections give way (5 to 7 rps) to the linear section of the curves (7 rps onwards). The fact that the linear sections of the curves do not become independent of the wheel revolutions at planing speeds is another indication that different flow mechanisms control the mass supply to the rotor than in the displacement mode.

The next column (column 2 of Fig.9.3) is of results at a speed of 2.36 m/s ($F_T = 1.53$) which is well into the planing mode. This column has been the central reference for the development of the impulse theory in Chapter 4. It can be seen that the general character of both the lift and thrust curves is unchanged from the last column. The differences are that the force magnitudes are greater at this higher speed, and the zero crossing point (where $\frac{V_O}{V_t} = 1$) is now at higher wheel revolutions: these are differences that would be expected with an increased velocity. All the characteristics of the planing mode apply equally well to this speed as to the last: the parabolic sections, intersection regions and linear sections are still evident. Tests to higher speeds than this ($V_O = 3.71$ m/s and 5 m/s or $F_T = 2.41$ and 3.25, see Appendix 4; wheel 6 (FB), $\phi = 60^\circ$) show no evidence of a change from the character and form of curves shown in these last two columns for the planing mode. This suggests that once the LPW is in the planing mode, Froude, or gravity, effects are of minor importance as compared with dynamic effects (1) so that Froude scaling then becomes irrelevant. (Further effects of velocity are examined later in section 9.4.2.)

9.2.1.2 LPW Efficiency in the Data. The propulsive efficiency plots in Figs.9.2 and 3 will now be examined. Efficiency here is plotted against the velocity ratio, $\frac{V_O}{V_t}$, for reasons explained in sections 4.14 and 4.14.1. A diagonal on each plot representing

1. See also Beardsley, P.22

efficiency equal to velocity ratio gives the maximum theoretical value of efficiency. Unfortunately the recorded results are a little misleading in these plots, and this is for two reasons: first high efficiencies occur at high velocity ratios (low wheel revolutions) and this is where the forces are lowest and are most prone to measurement errors. Consequently there is a wide scatter of points and misleading efficiency peaks are present at these high velocity ratios. Further experiment would be required with more sensitive apparatus, to gather more accurate data in these regions. Second the plotting routine that produced these curves was programmed to set any negative efficiency values to zero, to prevent the curves from going off the page. Thus not only are the efficiency peaks open to question but the zero crossings are as well.

In spite of these limitations the plots show the following:

1) In all cases the propulsive efficiency curves increase with an increase in velocity ratio (decrease in wheel revolutions) to a peak value, before falling away to zero. Peak values occur at velocity ratios up to $\frac{V_o}{V_t} = 0.65$ in these particular results, suggesting that propulsive efficiencies of this same value may be reached under ideal conditions. All curves fall again to zero before the velocity ratio reaches unity. This indicates that this wheel needs some slip for propulsion: it concurs with comments on efficiency at high velocity ratios made in section 4.14.3 and thrust forces at high velocity ratios noted in section 4.8.

2) In all cases the propulsive efficiency decreases with immersion depth. This general conclusion holds for all blade angles and confirms the findings of Beardsley whose plot demonstrating the effect is shown in Fig.9.4. (See also section 9.4.8.1.)

3) In the displacement mode, with $V_o = 0.4$ m/s, the efficiency curves follow the maximum possible value closely before beginning to fall away from it at velocity ratios of 0.2 and 0.3.

4) In the transition zone, $V_o = 0.65$ m/s, the efficiency curves do not follow the theoretical maximum as closely, and after velocity ratios of 0.3 the curves diverge as the results become erratic at higher velocity ratios.

Conditions

18" diameter, 12 blades

typical blade shape

radial blade height = $0.088D$

$$\frac{nD}{\sqrt{gD}} = 0.67 = 3.1 \text{ rps}$$

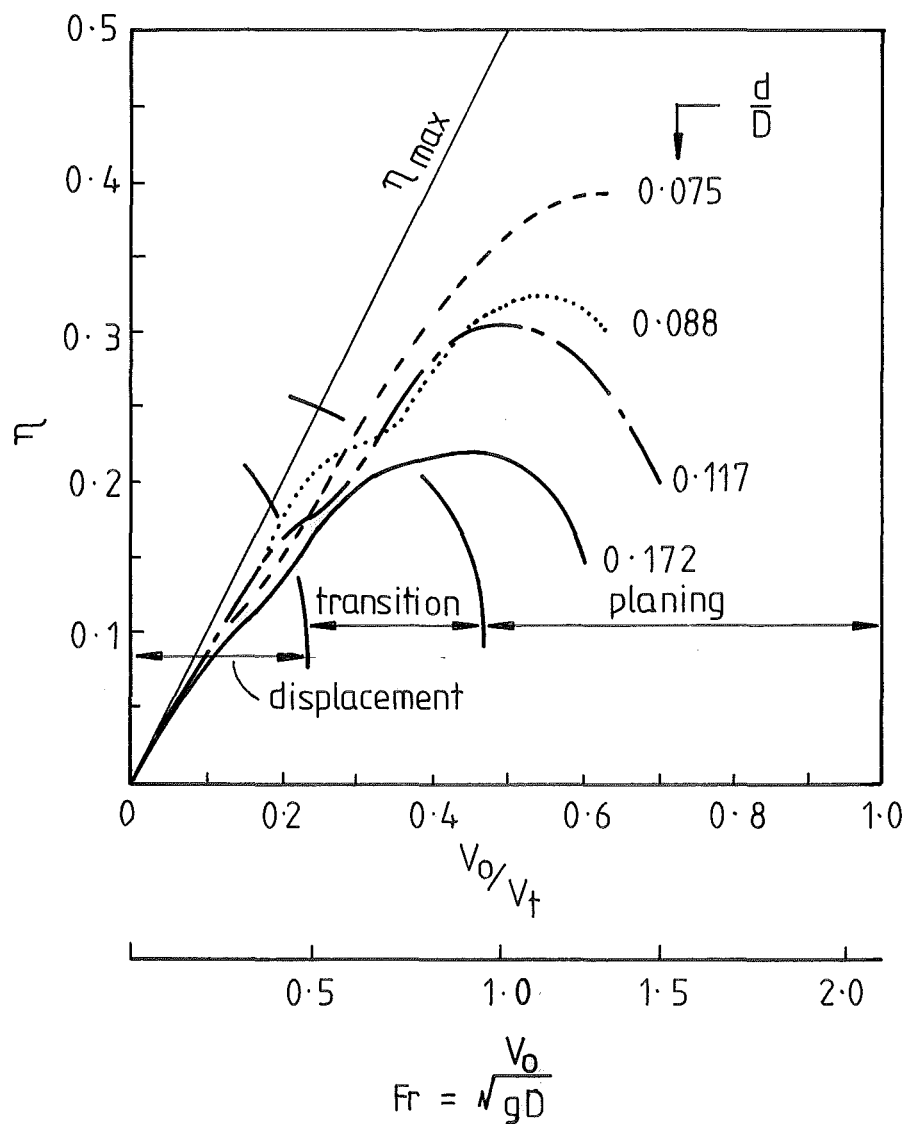


FIGURE 9.4 BEARDSLEY'S RESULTS SHOWING THE EFFECTS OF IMMERSION DEPTH ON PROPULSIVE EFFICIENCY.

5) In the planing mode, $V_o = 1.72$ and $V_o = 2.36$, the LPW was not turning fast enough to produce data at low velocity ratios (less than 0.1) but since the forces at high velocity ratios (0.4 to 0.8) have become more consistent the curves can be relied on a little more than those at lower velocities. In the planing mode at low velocity ratios (0.1 to 0.2) the curves are well below the theoretical maximum values and have become widely spread in proportion to the immersion depth. This represents the situation where the wheel is spinning fast, and cavity intrusion is well established. The planing mode is apparently, therefore, not such an efficient condition for the standard wheel to operate in as is a high rotational speed in the displacement mode, where efficiency is close to the maximum (point 3 above).

6) The peaks in the efficiency curves for both planing speeds, while not very reliable, suggest that propulsive efficiencies up to 0.5 may be achieved with shallow immersions ($\frac{d}{D} = 0.041$, or 10 mm in this case) and with this particular wheel ($\phi = 60^\circ$). Although this wheel is later shown not to be the most efficient propulsor, these results compare well with Beardsley's results shown in Fig.9.4.

9.2.1.3 Other Results for the Standard Wheel. The plots of power do not yield much new information though the observations that power consumption is lowest in the transition zone ($V_o = 0.76$ m/s) and thereafter increases rapidly with speed of advance, V_o , are useful.

As well as the measurements given in Figs.9.1, 2 and 3 for the standard wheel, and measurements at 3.71 and 5 m/s mentioned above, tests were run to cover the transition zone more fully, at $V_o = 0.96$ m/s and $V_o = 1.22$ m/s ($F_r = 0.62$ and 0.79) and tests at more extreme depths were carried out: 75 mm and 96 mm, ($\frac{d}{D} = 0.31$, $\theta = 67.7^\circ$; $\frac{d}{D} = 0.4$, $\theta = 78.1^\circ$). The results of these are recorded in Appendix 4, Wheel 6.

9.2.2 Photographic Records of the Standard Wheel

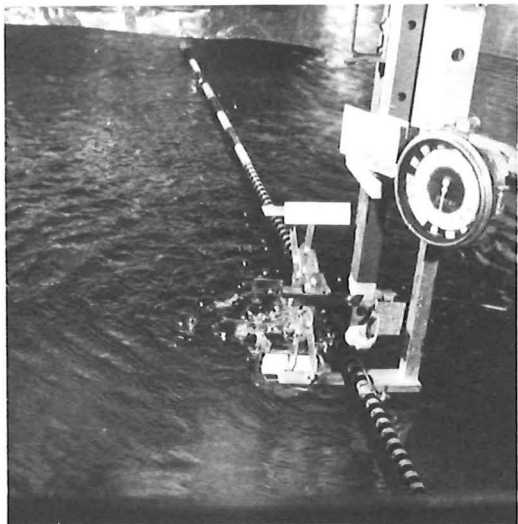
The arrangements used for the open water photographic series in the Kainga tank were described in section 8.2, while the results for the standard wheel are included here for comparison with the measured data in Figs. 9.1,2 and 3. While the photographic series made a thorough coverage of the standard wheel (Table 8.13) only representative

groups from the series are shown here. The wheel revolutions may be read from the meter in the photographs. Unfortunately it did not read reliably below 2 rps so that wheel rotational speeds less than this, as noted in the figures, have been estimated from the wakes in the photographs.

Beginning with the static condition ($V_o = 0$ m/s), Fig.9.5(A)-(E) shows a series of views of the LPW immersed 30 mm ($\frac{d}{D} = 0.124$) as the wheel revolutions are increased. Fig.9.5(D), with the wheel rotating at 6 rps, represents the limiting condition for the lift force, as indicated by a comparison with Fig.9.1 of the static condition at 30 mm immersion ($\frac{d}{D} = 0.124$, symbol Δ). Cavity pounding is beginning at this stage. This is a distinctly audible hissing, drumming sound of about 4 Hz which is believed to be caused by the cavity, scraped out by the blades, oscillating in and out against the spinning wheel. Fig.9.5(E) shows the wheel spinning at twice the last speed, and it shows more spray; cavity pounding is clearly evident at this stage when the wheel is observed in operation.

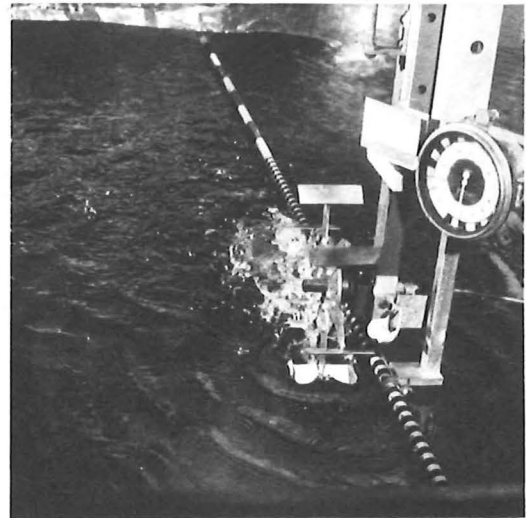
The low displacement speed of 0.4 m/s ($F_{\text{r}} = 0.26$) at the same representative immersion of 30 mm is shown in Fig.9.6(A)-(E). Fig.9.6(A) shows the wheel at a high velocity ratio ($\frac{V_o}{V_t} = 0.75$) and this makes it clear why the forces are small under such conditions at this low speed of advance. Fig.9.6(C) and (D) show the short wavelength waves generated by the wheel in the displacement mode. (These waves are also shown in Fig.4.32(A).) In Fig.9.6(E) cavity pounding is occurring as in the static case (Fig.9.5(E)) and little difference can be seen between these two views.

The next figure, Fig.9.7(A)-(E) shows the LPW at 0.76 m/s ($F_{\text{r}} = 0.49$) which is the centre of the transition zone for the standard wheel at 20 mm immersion ($\frac{d}{D} = 0.083$). The figure therefore shows the wheel at 20 mm immersion. In Fig.9.7(A) the wheel rotation is too slow for the typical transition zone waves to be formed; these are more evident in Fig.9.7(B) and (C). The side view of the standard wheel at 40 mm immersion with double span blades shown at 0.76 m/s in Fig.8.4, emphasises the transition wake and it can be seen that the blades almost follow the curve of the wave trough during their passage. Fig.9.7(D) and (E) show the wheel at higher rotational speeds where it can just be noted that the wave formation is somewhat



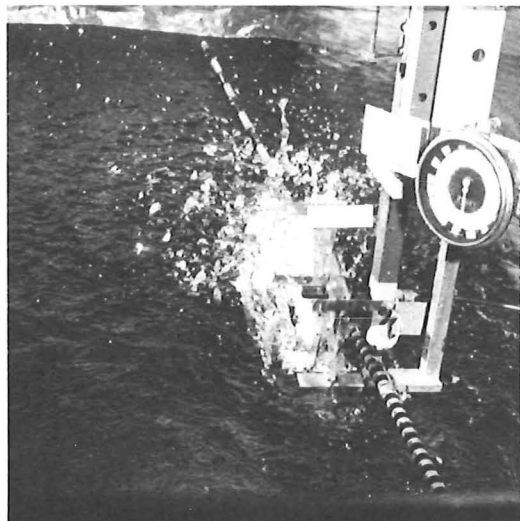
1300A/18A

(A) 1 RPS



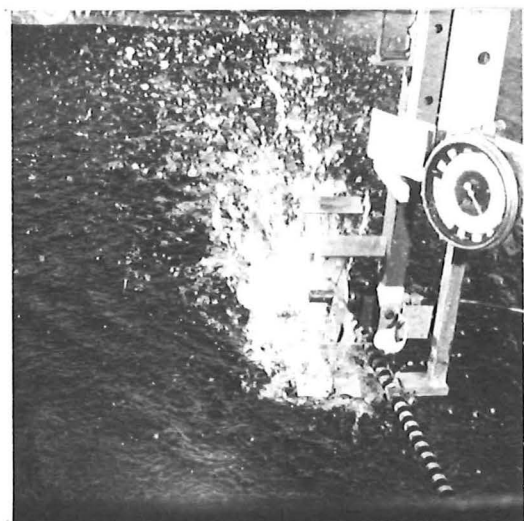
1300A/19A

(B) 2 RPS



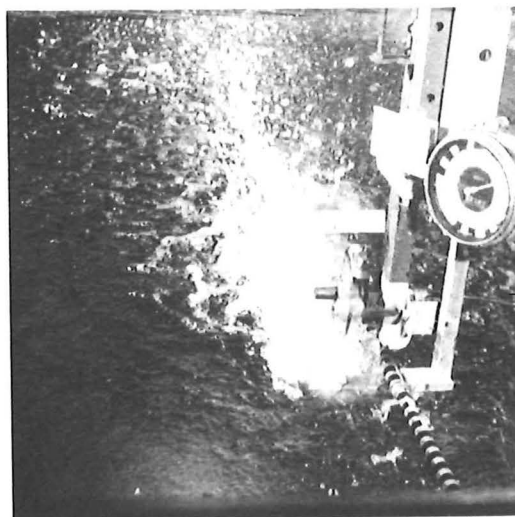
1300A/20A

(C) 3 RPS



1300A/21A

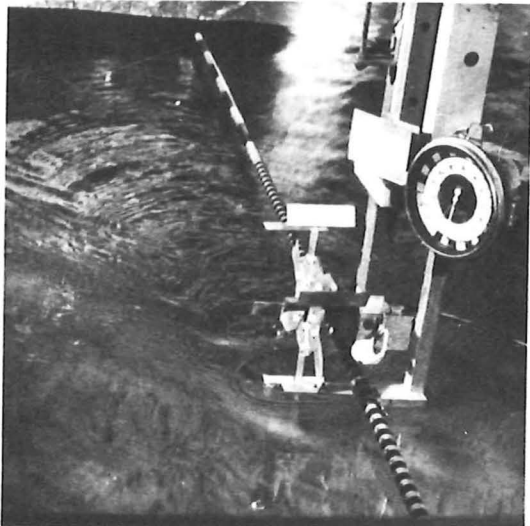
(D) 6 RPS



1300A/22A

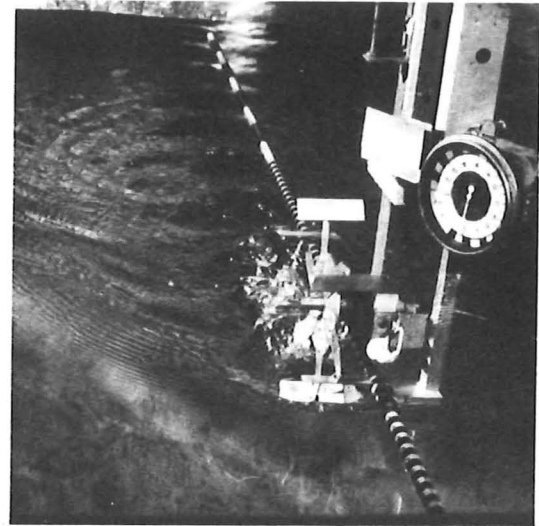
(E) 12 RPS

FIGURE 9.5: STATIC MODE, STANDARD WHEEL AT 30 mm IMMERSION
(WHEEL DIMENSIONS CONTAINED IN FIG.9.1)



1300B/36A

(A) 0.4 RPS $V_o/V_t = 0.75$



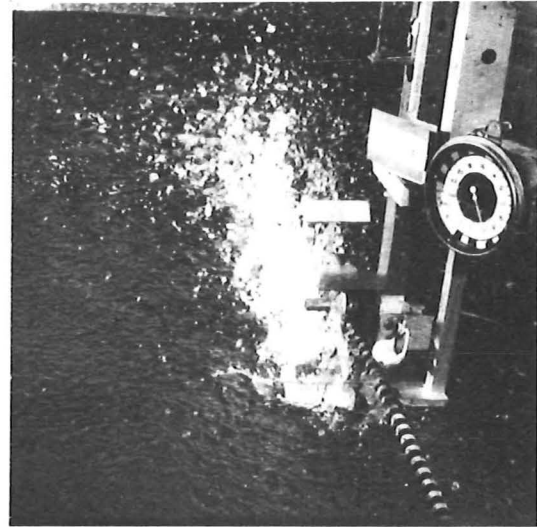
1300B/37A

(B) 2 RPS $V_o/V_t = 0.26$



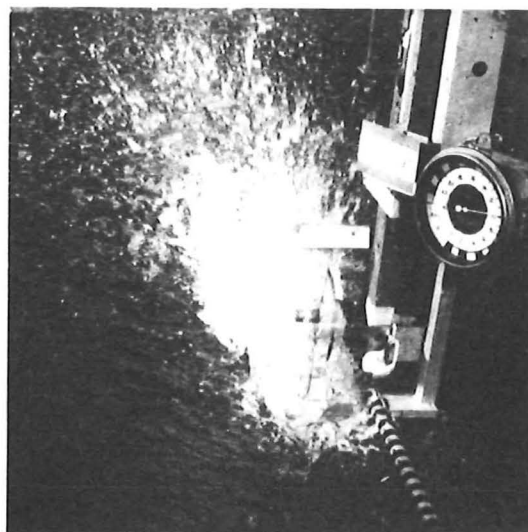
1300B/38A

(C) 3 RPS $V_o/V_t = 0.18$



1300B/39A

(D) 5 RPS $V_o/V_t = 0.11$



1300B/40A

(E) 10 RPS $V_o/V_t = 0.05$

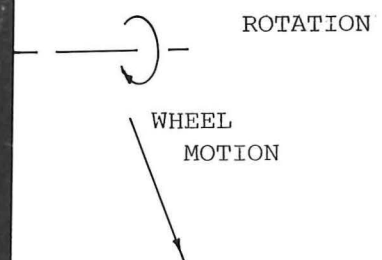
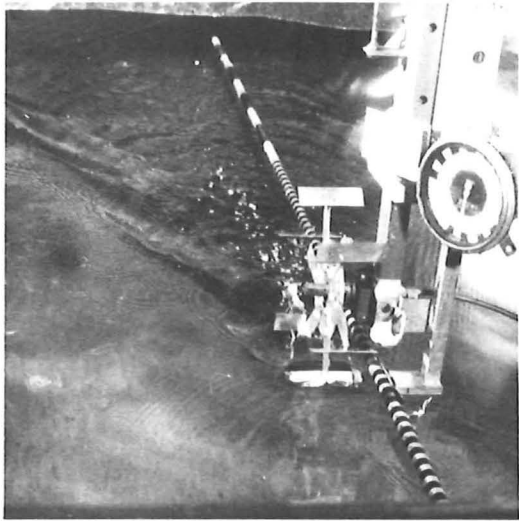
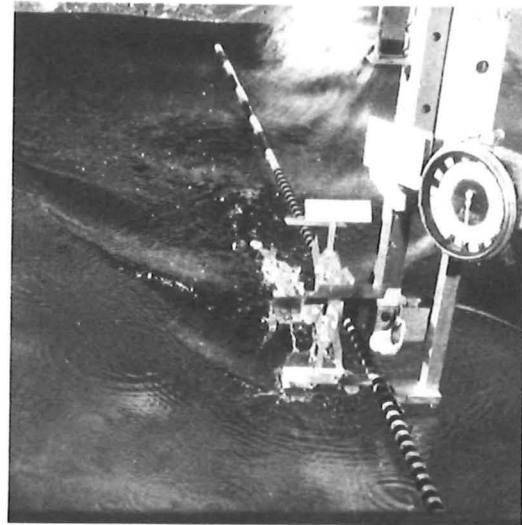


FIGURE 9.6: DISPLACEMENT MODE, STANDARD WHEEL AT 0.4 m/s AND 30 mm IMMERSION



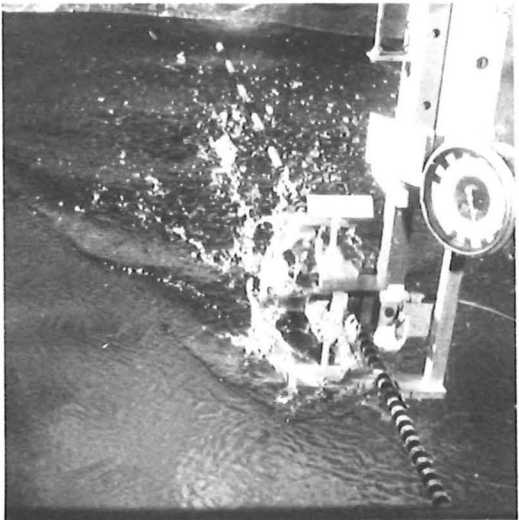
1300C/18A

(A) 1.2 RPS $V_0/V_t = 0.83$



1300C/19A

(B) 3 RPS $V_0/V_t = 0.33$



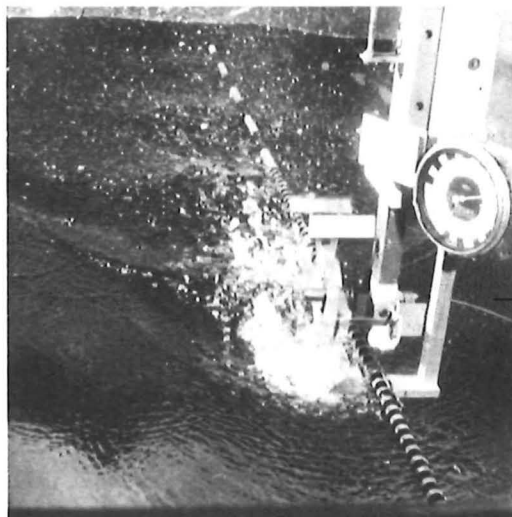
1300C/20A

(C) 4 RPS $V_0/V_t = 0.25$



1300C/21A

(D) 6 RPS $V_0/V_t = 0.17$



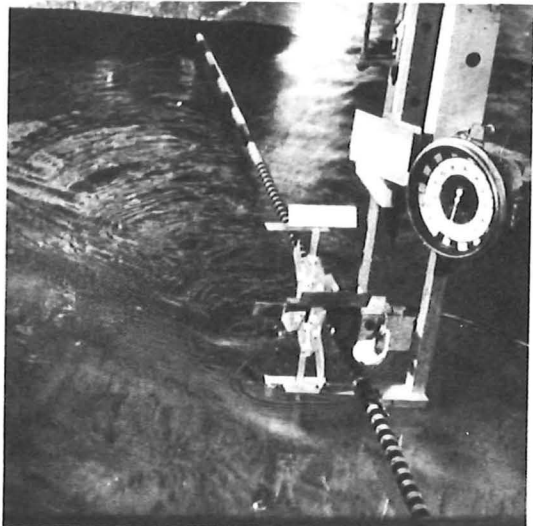
1300C/22A

(E) 11 RPS $V_0/V_t = 0.09$

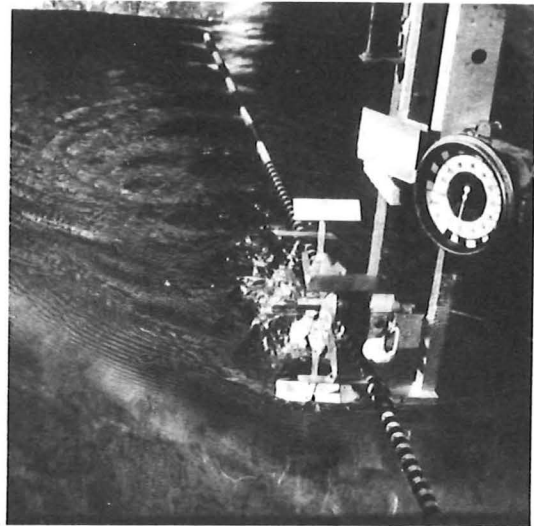
ROTATION

WHEEL
MOTION

FIGURE 9.7: TRANSITION ZONE AT 0.76 m/s AND 20 mm IMMERSION



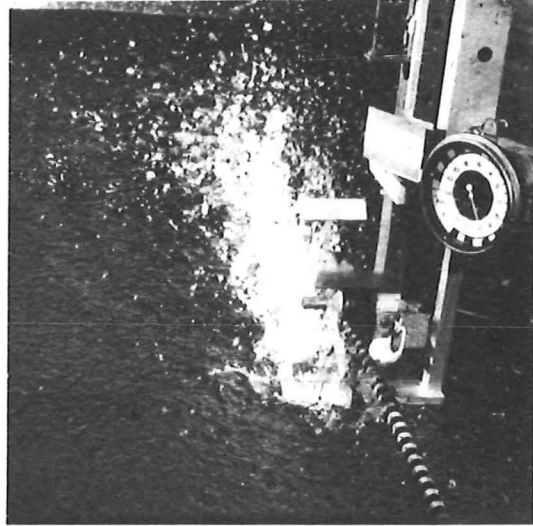
1300C/23A
 (A) 2.25 RPS $V_0/V_t = 2$



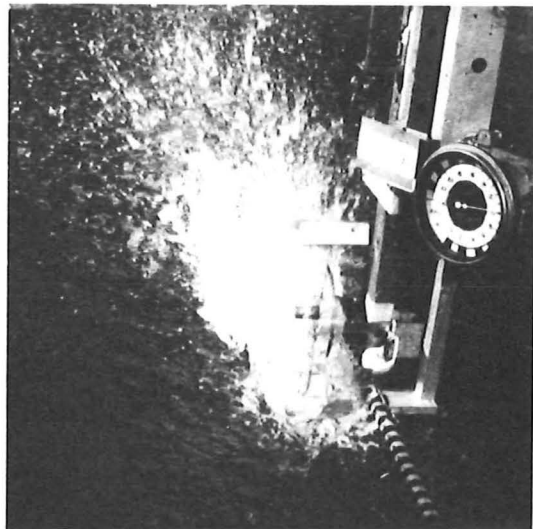
1300C/24A
 (B) 3.5 RPS $V_0/V_t = 0.65$
 (CLOSE TO LPW CRAFT OPERATING
 CONDITIONS)



1300C/26A
 (C) 5 RPS $V_0/V_t = 0.5$
 JUST BEFORE BOWSPASH



1300C/25A
 (D) 5 RPS, BOWSPASH CAVITY
 INTRUSION NOT YET OCCURRING



1300C/27A
 (E) 11.8 RPS $V_0/V_t = 0.19$
 MASSIVE BOWSPASH

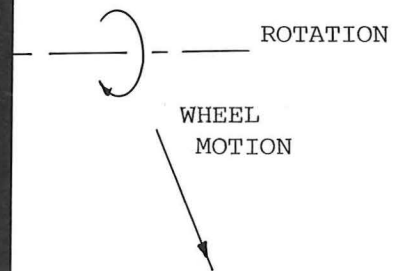
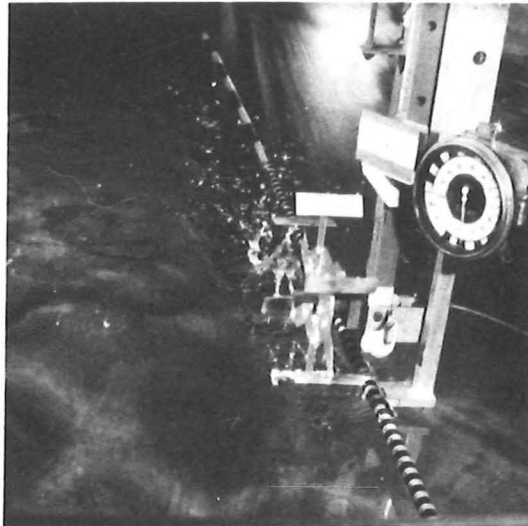
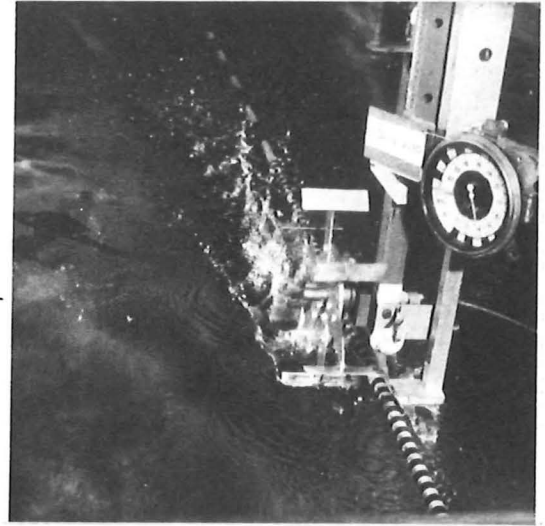


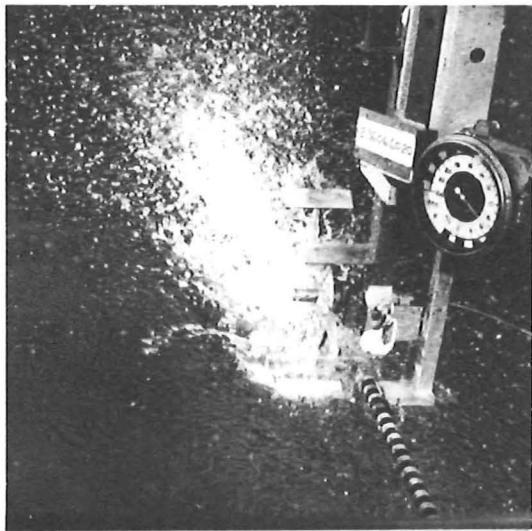
FIGURE 9.8: LOW PLANING SPEED. 1.72 m/s, 20 mm IMMERSION



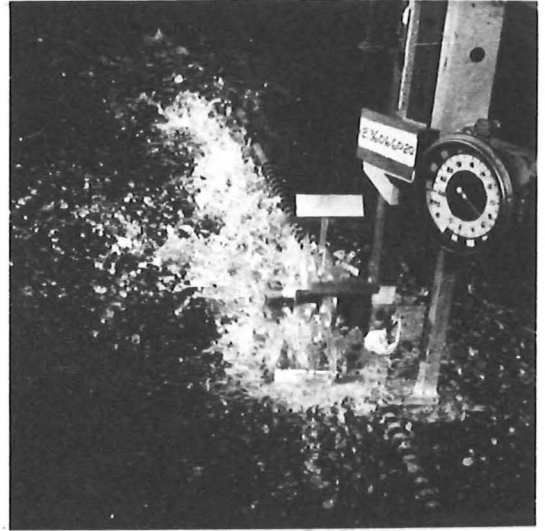
1300C/29A
 (A) 2.5 RPS $V_0/V_t = 1.25$



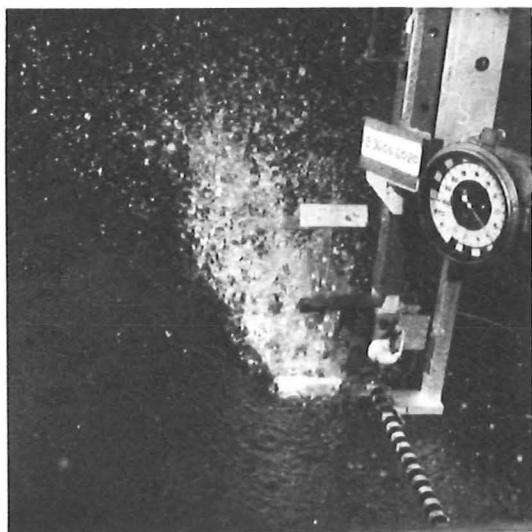
1300C/30A
 (B) 4 RPS $V_0/V_t = 0.78$



1300C/34A
 (D) 6.8 RPS $V_0/V_t = 0.46$
 BOWSPASH BEGINNING



1300C/33A
 (E) 7 RPS $V_0/V_t = 0.44$
 BOWSPASH; CAVITY INTRUSION
 BEGINNING.



1300C/32A
 (C) 6.5 RPS $V_0/V_t = 0.48$
 NO BOWSPASH



1300C/35A
 (F) 13.3 RPS $V_0/V_t = 0.23$
 EXTENSIVE BOWSPASH

FIGURE 9.9: PLANING SPEED, 2.36 m/s. 20 mm IMMERSION $d/D = 0.083$.
 (NOTE: PHOTOS ARE OUT OF SEQUENCE.)

less pronounced than it was at lower wheel revolutions. The reduction in the wheel stern wave height at high wheel revolutions seems to be because the spray leaving the wheel tends to flatten it. This phenomenon is more readily visible in the real situation. Of special note is the relatively small amount of spray thrown by the wheel at high wheel revolutions in Fig.9.7(E). This is a notable reduction when comparisons are made with the same wheel revolutions at higher and lower speeds of advance (Figs.9.6 and 9.8). This reduction is essentially because the wheel is operating in the wave trough so that the mass supply to the wheel is severely limited. Reference to the lift and thrust forces in Fig.9.2 at 0.76 m/s shows them to be minimal under these transition conditions. It is also clear from Fig.8.4 that the blades encounter water mainly at their point of entry rather than throughout their passage. This is in accordance with the definitions of the transition given later in section 9.4.2.1.

Under transition conditions no cavity pounding occurs; cavity pounding is a static and displacement phenomenon only. (See also Fig.8.11.)

Low speed planing conditions are shown in Fig.9.8(A)-(E), which has the wheel moving at 1.72 m/s ($F_T = 1.12$) and immersed 20 mm as before. The typical small oblique waves of the planing mode can just be seen in Fig.9.8(B). (See also Fig.4.33 for these waves.) This view shows the wheel operating at a velocity ratio of 0.65 which is close to the expected operating condition of the LPW craft. A structured splash can be observed behind the wheel and this is similar to that observed on the model LPW craft wheels (see Fig.12.12). Fig.9.8(C) shows a more jumbled splash behind the wheel and a little spray thrown ahead of the entering blade. In Fig.9.8(D), which is essentially for the same wheel revolutions, this small spray ahead of the blade has developed into bowsplash (described in sections 4.9.1 and 9.4.3.2). The wake behind the wheel is even more confused than before. These two views, (C) and (D), represent the intersection region of the force plots as shown for 1.72 m/s and 5 rps in Fig.9.3. Surface cavity intrusion will therefore be occurring in these views. Fig.9.8(E) shows the extensive bowsplash and wheel "crater" typical of the wheel at high revolutions in the planing mode. Under such conditions cavity intrusion has advanced so far that the whole blade passage seems devoid of water. Comparison with the same conditions in Fig.9.3 indicates that the lift and thrust forces are still

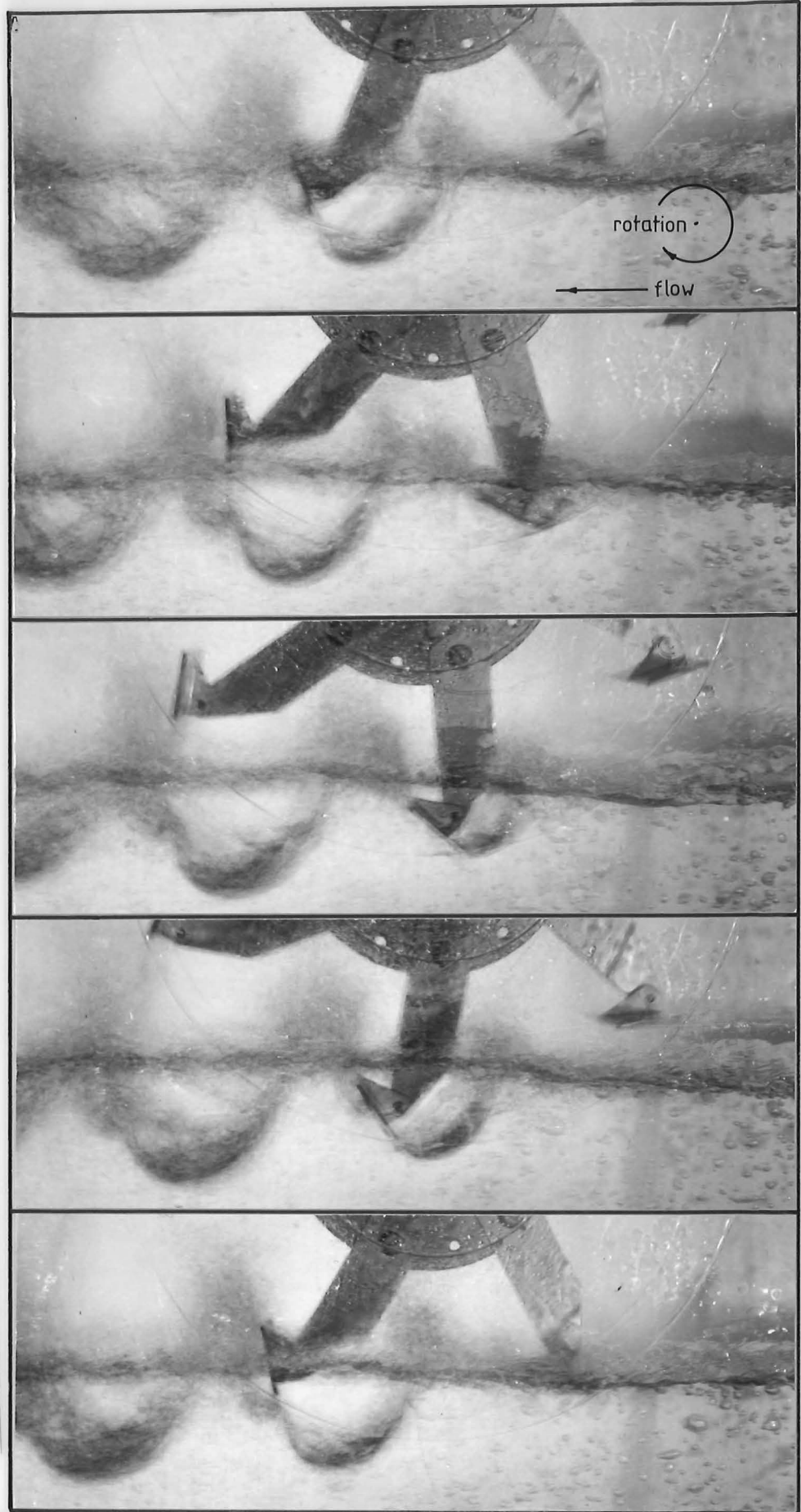


Figure 4: The passage of a blade through the water, in Condition 3.
 $V_o/V_t = 0.7$, $\phi = 45^\circ$, $d/D = 0.1$

increasing with wheel revolutions under these unlikely conditions. (See also Figs.4.19(A)-(E), 9.26.)

Figure 9.9(A)-(F) shows the LPW operating at 20 mm immersion and a higher planing speed: 2.36 m/s ($F_r = 1.53$). This speed was used to furnish the reference set of data used for the development of the impulse theory (and the coefficient equations in section 9.9). The figures are generally similar to those of the last speed in Fig. 9.8 (A)-(E). Fig.9.9(A) shows the wheel operating at a velocity ratio greater than one. Reference to Fig.9.3 at 2.36 m/s shows that under these conditions (wheel revolutions = 2.5) the thrust force will be negative, so that the water will be driving the wheel rather than vice versa, while the lift force will be small and positive. Fig. 8.8 (C), (D) and (E) show the onset of bowsplash. Careful comparison of the curves in Fig.9.3 with these three views indicates that bowsplash occurs at much the same time as surface cavity intrusion. (This is shown later in section 9.4.3.2.) Other views of the high speed planing condition are shown elsewhere in Figs.4.19 (A)-(D), 4.36, 8.8, 8.9, 8.10, 9.26.

9.2.2.1 Stroboscopic Records. Section 8.3 described the arrangement for stroboscopic photographs taken in the glass-sided tank. While a large number of such records were made, some of which appear elsewhere in this report, the most relevant to the LPW theory are those which apply at the expected operating condition of the LPW. It was noted above in relation to Fig.9.8(B) of the LPW in the planing mode, that the velocity ratio of 0.65 was close to the expected LPW operating condition of the LPW craft. A series of photographs taken under stroboscopic lighting in the glass sided tank at a velocity ratio of 0.7 is shown in Fig.9.10. This series shows the wheel turned about 10° clockwise in each successive exposure, and demonstrates the formation of the blade cavities and splash structure. A number of points may be made:

- 1) At this velocity ratio the 6 bladed wheel is operating before any form of cavity intrusion has begun and before bowsplash has started.

- 2) A small splash structure can be seen growing through the series at the forward end of the blade cavity: it may be imagined that this would increase with wheel revolutions to become the

bowsplash shown in earlier figures (Figs.9.8(E) and 9.9(F)).

3) A much more significant splash or spray formation can be seen at the rear of the blade cavity, and this can be seen to follow the blade as it leaves the water. (This can also be seen in Figs.9.8(B), 9.9(A) and (B), 8.9, 8.10.)

4) The cavity formed by the blade appears to be generated by the blade which moves tangent to its edge during the passage. The impulse theory, however, indicates that the movement of the water away from the point of entry is caused only at the point of entry where the blade strikes the water. This fact is illustrated later in Fig.9.15, and therefore in this figure (Fig.9.10) the fact that the cavity seems to be formed from the free streamlines behind the blade, is coincidental.

5) It may be noted in Fig.9.10(D) that the water is in the process of moving away from the inside edge of the blade to form another lobe on the cavity already present. This can be seen growing progressively in subsequent blade positions. It is proposed that this is formed by a secondary rearward impulsive force applied by the inner edge of the blade, to the water in view (B) or (C). This kind of complication is not taken into account by the impulsive theory which assumes action to take place at the blade tip. This lobe of the cavity can be seen to move away from the blade surface, allowing air entry. It clearly indicates that this part of the cavity is formed by an impulsive action rather than as the free streamline behind a passing flat plate.

6) The cavities left in the flow can be seen to broaden and deepen as they move away downstream from the wheel (also apparent in Figs.4.19(A) and (B)). This is a clear indication of the momentum exchange which took place at blade entry and the kinetic energy left in the flow by the LPW.

This figure has been most useful in clarifying high speed LPW performance.

9.3 THE IMPULSE THEORY, FORMER THEORIES AND EXPERIMENT

This section examines the theories of other experimenters developed to model the forces on paddlewheels, and it compares their results with those of the impulse theory and the experimental data. It shows why the impulse theory is the most suitable model for the LPW forces in the planing mode.

In the past paddlewheel forces were treated as flat plate drag forces, which, for the low speeds of operation in the displacement mode, was generally appropriate. The impulse theory as a model for high speed paddlewheel and LPW force generation is a departure from the traditional line of thinking in two respects. First, it assumes all the forces to be generated at the instant of blade entry, instead of throughout the blade passage as assumed by Volpich and Bridge, (1) and instead of at the bottom of the blade passage as implied in Beardsley's Surface Impulse Propulsion model. (2)

Second, it assumes the mass acted upon to be the induced mass of the semi-immersed blade; this mass being accelerated by an impulsive action at blade entry. Beardsley assumed all of the entrained mass flow to be accelerated impulsively in his momentum model, while Volpich and Bridge did not consider acceleration forces.

In the following sections these two assumptions of the impulse theory will be compared with the measured results and the predictions of the other theories.

9.3.1 Entry Forces Compared with Forces Throughout the Passage

This section examines the validity of the assumption that all the force is generated at blade entry, as opposed to the two alternative hypotheses (i) that the force is generated throughout the blade passage and (ii) that the force is generated at the bottom of the blade passage.

At this stage it is not the magnitude of the resultant force that is important but its direction. In the plotted data (Figs. 9.1, 2 and 3) the resultant force on the LPW has been resolved into lift and thrust components. A valid model of the resultant force

1. Volpich and Bridge, Part II, P.498
2. Beardsley, P.13

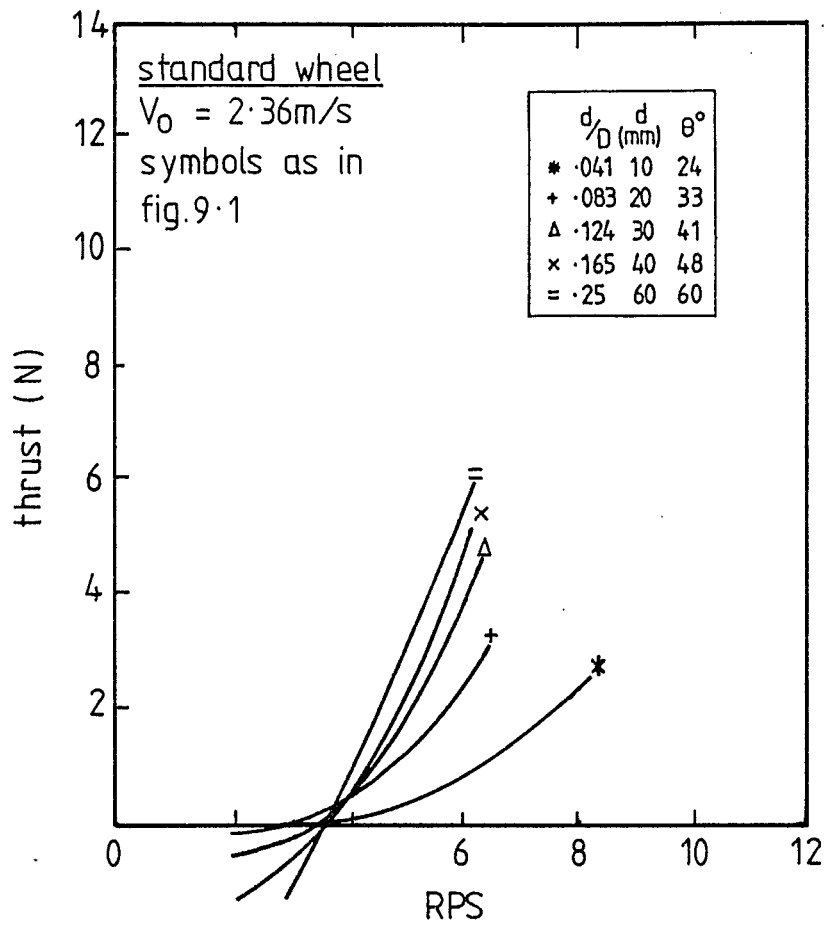
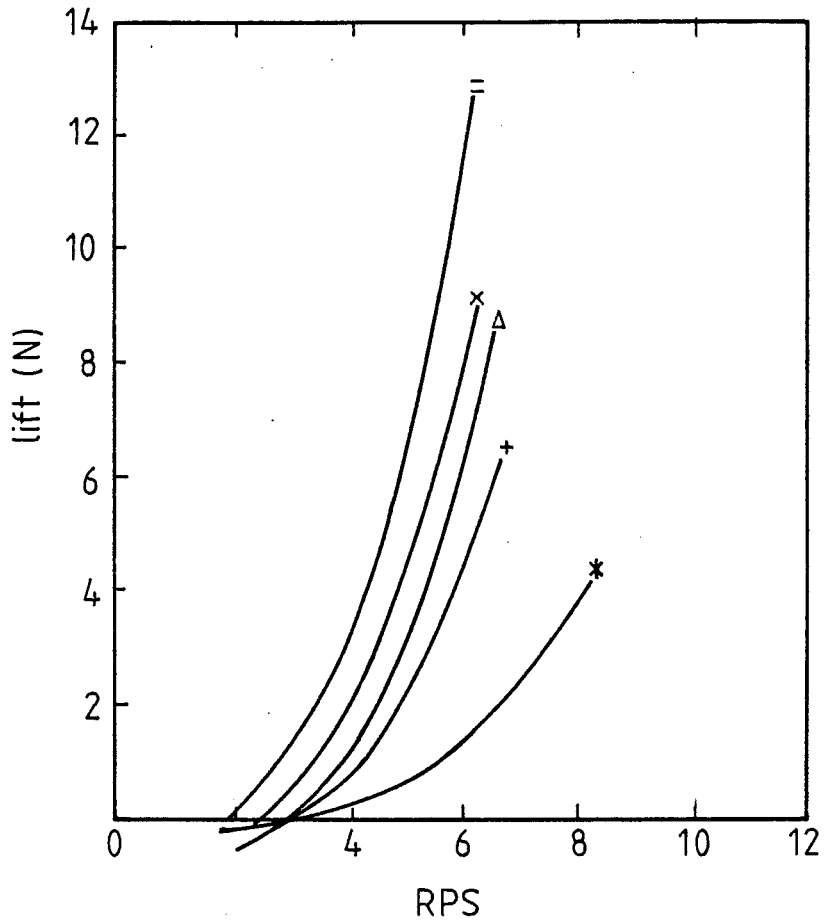


FIGURE 9.11 LIFT AND THRUST FORCES BEFORE CAVITY INTRUSION CALCULATED ON THE FLAT PLATE DRAG ASSUMPTION.

would be expected to show the lift and thrust components in the same relative proportions and with the same relationship with immersion depth.

If the lift and thrust forces are calculated on the basis of each of the three hypotheses for the standard wheel they may be compared directly with the plotted results in Figs.9.1, 2 and 3.

In Fig.9.11 the forces have been calculated on the basis of flat plate drag (after Volpich and Bridge (1)). In this method the force normal to the blade at a given point in the blade passage is calculated from the instantaneous velocity of the blade tip relative to the water (which is assumed to be still). The calculation uses the flat plate drag equation and employs well established coefficients (2) for the force normal to the blade. This normal force is resolved into lift and thrust components, and these components are averaged for all points through the blade passage to give the final lift and thrust forces. (To test this flat plate drag model a small FORTRAN programme 'BLADED DRAG' was developed early in the project. It was employed to perform these calculations and is given in Appendix 8).

As shown in Fig.9.11 the calculations represent the planing mode of the standard wheel with a forward speed of 2.36 m/s before cavity intrusion has begun to occur. Thus results up to 6 rps are present, and they may be compared with similar results in Fig.9.3. Fig.9.12, however, is a reproduction on the same scale of the experimental results for the same conditions, enlarged from Fig.9.3. It is apparent that the lift force curves compare well with those of Fig.9.11 both in magnitude, and in their relation to immersion depth. The thrust force curves, on the other hand, are different in magnitude, and opposite in relation to the immersion depth than those of experiment shown in Fig.9.12.

The results in Fig.9.13 have been calculated on the basis of Beardsley's approach. The governing assumptions in this case are:

- (1) All the horizontally entrained mass is acted upon.

1. Volpich and Bridge, Part II, P.498
2. E.S.D.U. Item 70015

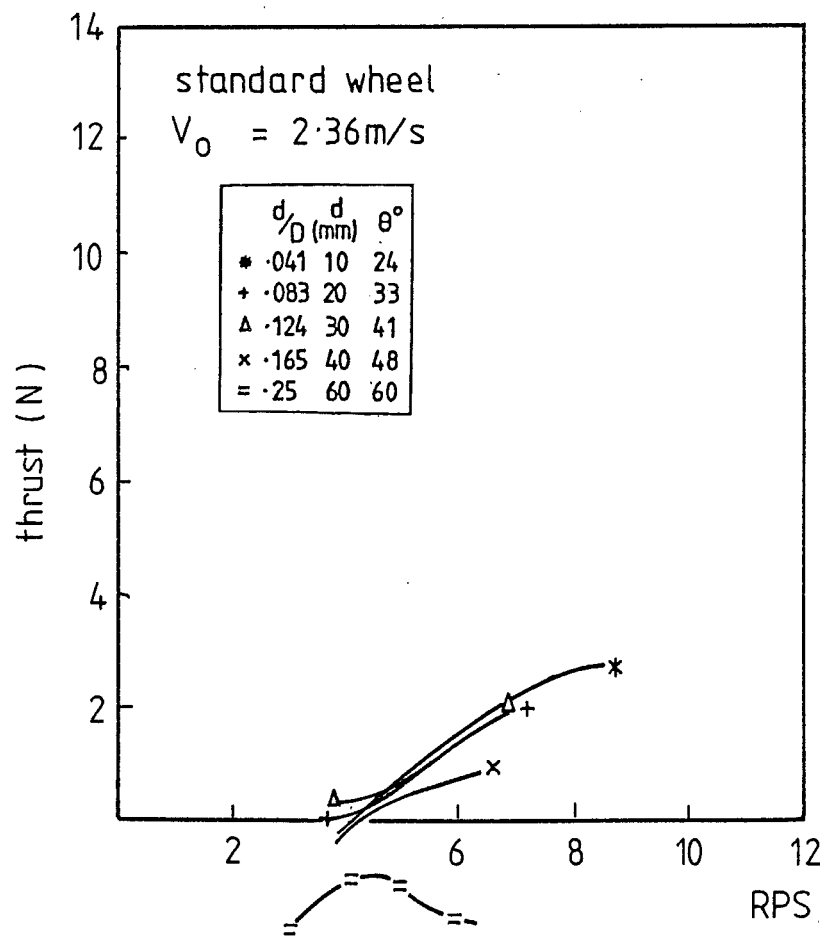
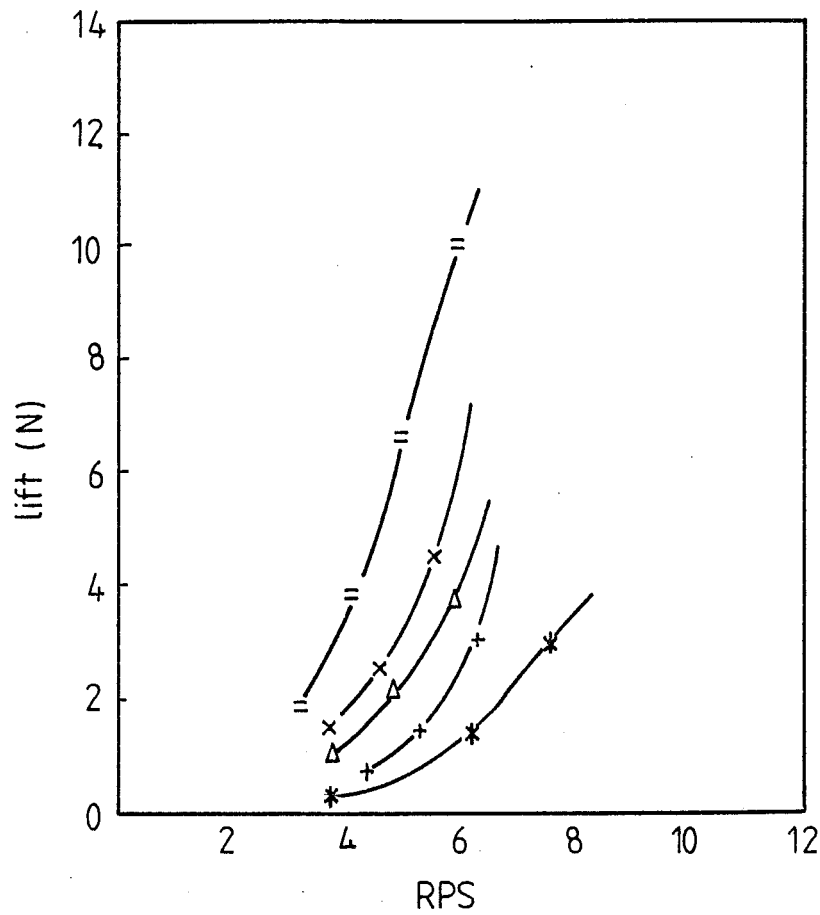


FIGURE 9.12 MEASURED RESULTS FOR THE STANDARD WHEEL BEFORE CAVITY INTRUSION (TAKEN FROM FIG 9.3)

(2) The forces occur as the blade passes the bottom of its passage (where it has maximum horizontal velocity rearwards).

(3) The forces are calculated using the perpendicular velocity expressions (4.20 and 4.21).

This final point was not part of Beardsley's approach but then he took no account of blade angle, ϕ . To use the expressions, α is set to zero, for the blade at the bottom of the passage. They now give the maximum velocity change occurring at this blade position. Multiplying by the entrained mass then gives the momentum change and hence the blade forces. In comparison with the experimental results of Fig.9.12 the following may be noted in Fig.9.13:

(1) Forces are linear with wheel revolutions. This is because the mass acted upon is independent of wheel revolutions. (It is the same as the entrained mass used in the impulse theory for the case after cavity intrusion, and is given by expression (4.7).)

(2) In spite of this difference, the lift force magnitudes, and their relationship to immersion depth compare well with the experimental results.

(3) Thrust forces, however, are much greater than those of experiment, and their order with immersion depth is again opposite to that of experiment. This model is further from the experimental results than the flat plate drag model of Fig.9.11.

Finally, Fig.9.14 shows the lift and thrust forces as calculated by the impulse theory for the same conditions. This assumes that the force occurs impulsively at blade entry and the mass acted upon is the induced mass of the immersing blades. The following may be noted:

(1) The vertical scale for both lift and thrust forces has been increased by a factor of three so that the figures may be readily compared. The fact that this theoretical approach produced such small forces, at first directed attention away from the impulse theory.

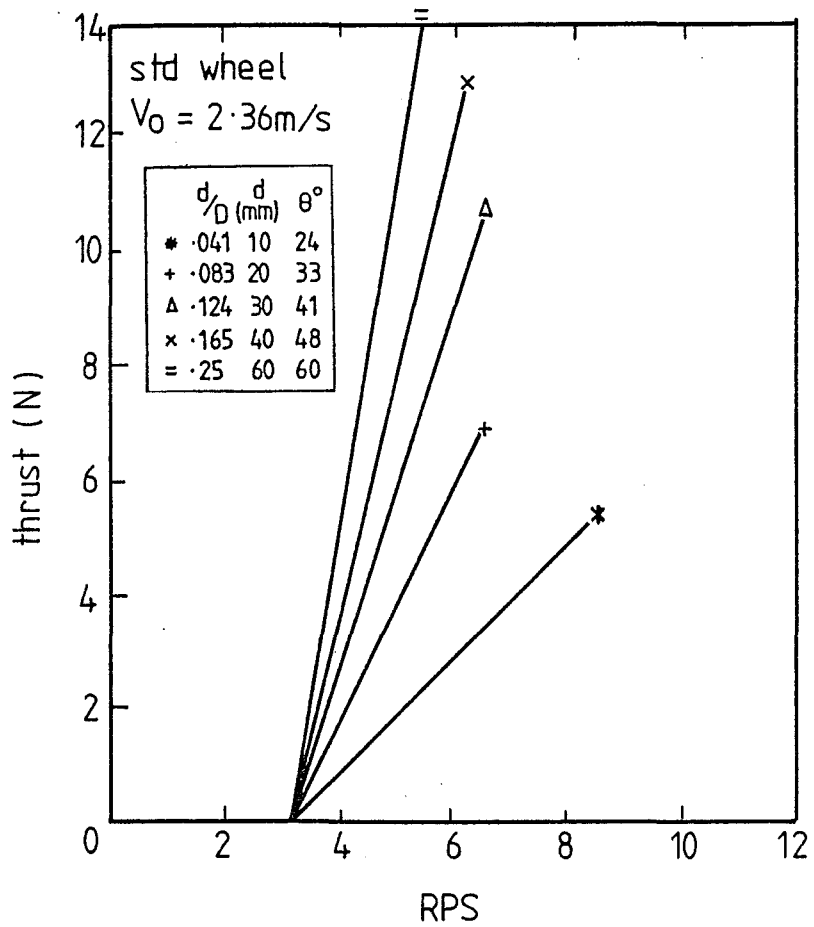
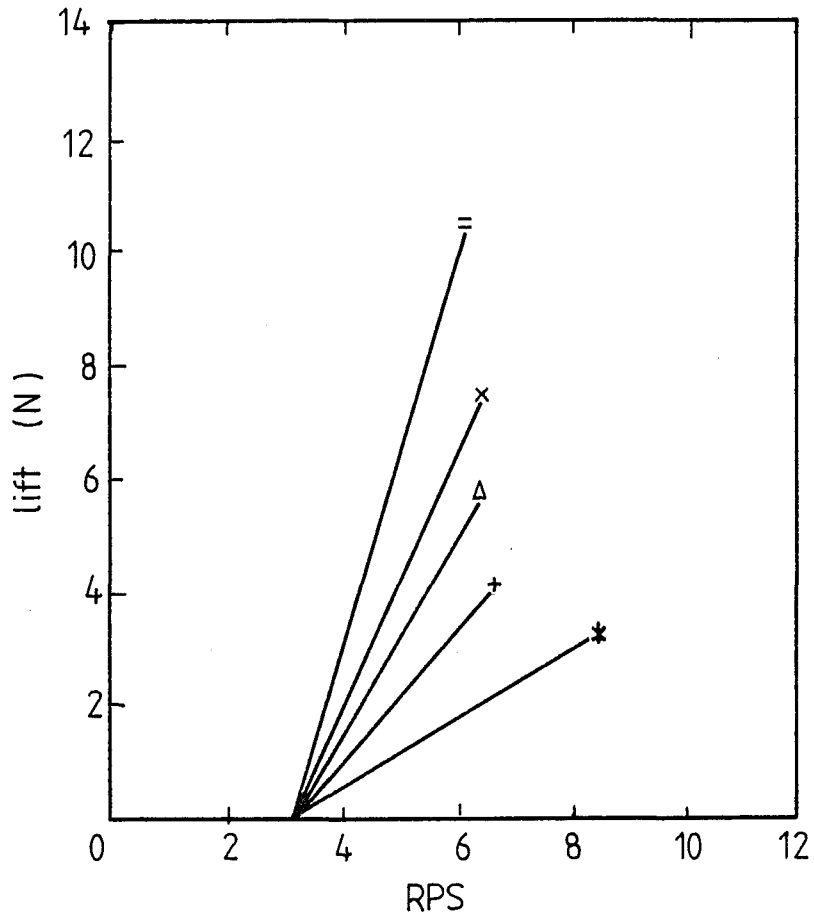


FIGURE 9.13 STANDARD WHEEL FORCES CALCULATED ASSUMING (a) FORCE OCCURS AT PASSAGE BOTTOM (b) ALL ENTRAINED MASS ACTUATED.

(2) In spite of the discrepancy in the force magnitudes it is clear that the curves in Fig.9.14 and those of experiment (Fig.9.12) have much the same relationship between lift and thrust, and with immersion depth: the thrust forces decrease with immersion depth and the magnitudes are small as compared to the lift forces as in Fig. 9.12.

It is apparent from the results calculated on the bases of these three hypotheses that the impulse theory hypothesis, assuming that all the force is generated at the moment of blade entry, gives the most accurate estimate of the direction of the resultant LPW force. This, however, is not the complete picture as the impulse theory fails to account for the magnitude of the resultant force.

9.3.2. Induced Mass and Flat Plate Drag in Experiment

A number of hypotheses may be proposed to account for the discrepancy in the force magnitudes as given by the impulse theory. The first three of these refer to the force equation, in this case the lift force equation, $L = \dot{m}\Delta V_v$, expression (4.11).

1) The calculated value of the change in vertical velocity, ΔV_v , is lower than in practice.

2) The calculated value of the induced mass per second, \dot{m} , is lower than in practice.

3) A combination of both of these.

4) Surface impact phenomena such as Wagner's wedge entry theory (see section 4.8) have not been taken into account.

5) There is a significant component of flat plate drag force still present in the high speed situation although the impulse theory assumed it to be insignificant (see section 4.5).

These hypotheses will each be examined briefly.

It is difficult to imagine for (1), that components of vector velocity could be a factor of three small, since vector estimates of flow generally afford a much more precise model of momentum changes than this.

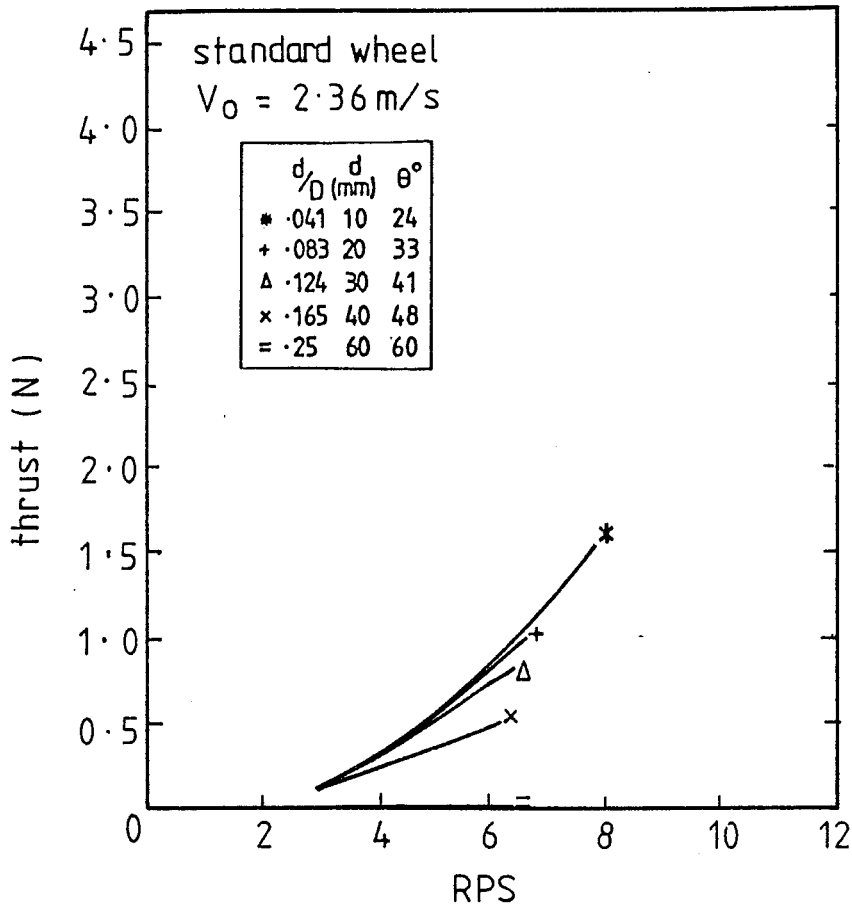
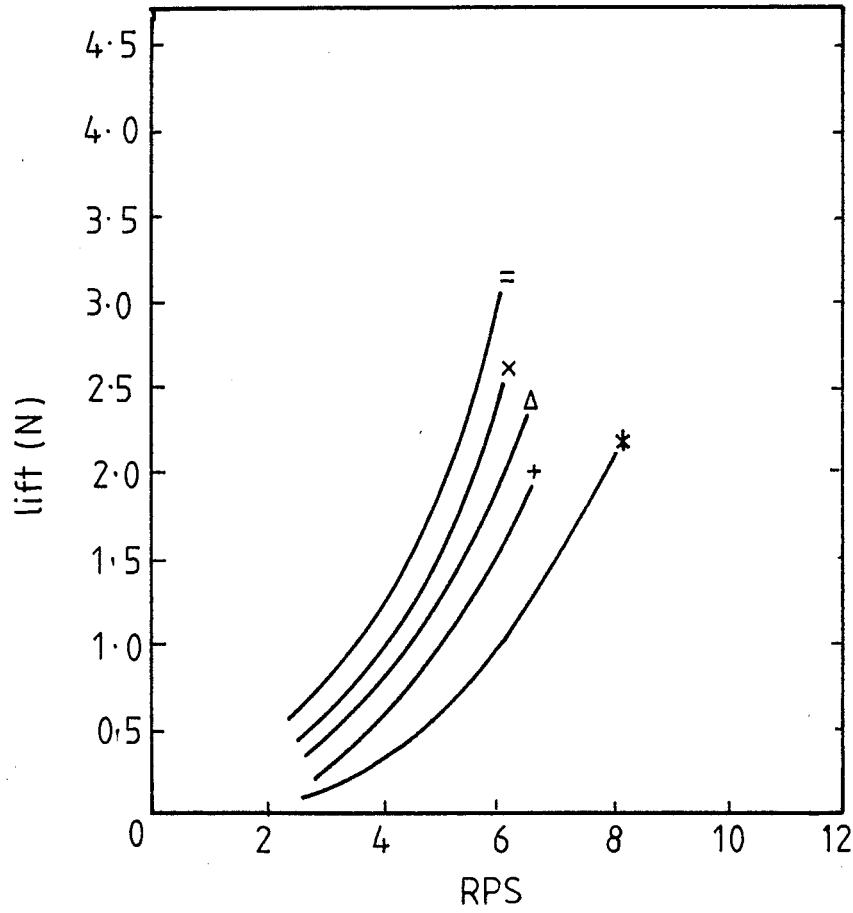


FIGURE 9.14 CALCULATED RESULTS BY IMPULSE THEORY FOR STANDARD WHEEL

In (2) it can be imagined that in the splash and other transient conditions of blade entry the normal analytical models of induced mass may not be entirely reliable, but a factor of three is too large a discrepancy to be reasonably considered.

For (3), then, it is barely conceivable that these two factors in combination could account for the discrepancy. Nevertheless at this stage the impulse theory coefficients have been based on this hypothesis as being the most easily dealt with of all the possibilities.

If the transient forces of hypothesis (4) were to be the reason for the force discrepancy the error would be expected to increase with the angle β between the blade and the water (see Fig.4.14 defining β) since this was one of the results of Wagner's theory (see section 4.8). This is clearly not the case, since the forces in Fig.9.14 are proportionally in error throughout the whole range of immersion depths shown. ($\beta = (\phi - \theta)$, and for the range of immersion depths shown, $\theta = 23.5^\circ$ to 59.7° , so that β covers the range of $\beta = 0^\circ$ to 36° , with no apparent increase or reduction of the forces because of this variation.)

In practice the most reasonable of these hypotheses is the last, (5). Unfortunately it complicates the picture of LPW forces.

First, it should be noted that cavity intrusion (as opposed to surface cavity intrusion, as shown in Fig.1.7) is occurring almost throughout the calculated range shown in Figs.9.11 to 9.14. This means that, should flat plate drag forces be calculated rigorously for Fig. 9.11 account should be taken of the fact that each blade would emerge into the previous blade cavity well before it had completed its passage back to the water surface. Thus the flat plate drag model of LPW forces shown in Fig.9.11 should really only involve calculations for the first part of the blade passage. This would necessarily reduce the magnitude of the resultant forces as well as giving a resultant force direction closer to that of the blade entry model. Calculations of flat plate drag for such a model involve the difficulty of estimating the position of the cavity left by the last blade.

Second, confusing this picture of steady flow flat plate drag forces is the fact, as outlined in section 4.6.5, that the impulsive action of the entering blade accelerates the water beneath the blade

to its entry velocity, then the blade decelerates relative to the water. This deceleration is sometimes so marked that air enters around the edges of the blade to the pressure side as shown in Fig.9.15. Any flat plate drag component of force must occur during the time when there is a velocity difference between the water and the blade, and the length of this time is clearly difficult to estimate. It is apparent that any flat plate drag addition to the impulsive entry forces will also occur only during the first moments of entry so that the direction of such forces will coincide with that of the impulsive entry forces.

Because of the difficulties associated with estimating the magnitude of this drag component analytically, it can, at present, only be assumed to be the major reason for the discrepancy between the theoretical and experimental force magnitudes. This discrepancy is incorporated into the impulse theory using the experimentally derived 'C' coefficients (see section 9.9). These coefficients, therefore, have magnitudes of about 3.

By way of conclusion it may be said that the conditions at blade entry have been confirmed by experiment to be the controlling factors in determining the direction of the resultant force on the planing LPW. Theoretical estimation of the magnitude of this force, however, is made difficult by the transient conditions under which the force is generated. Only its unsteady component may be readily estimated, the remainder being most easily dealt with by using an experimentally derived coefficient.

9.4 THE EFFECTS OF THE VARIABLES ON PERFORMANCE

This section examines each of the LPW variables in turn, comparing the theoretical predictions with measured results. Both LPW forces and propulsive efficiencies are used in these comparisons as the measures of performance.

9.4.1. The Use of Dimensionless Coefficients for Comparison Purposes.

It has been found useful to employ two sets of coefficients for the purposes of analysis in this chapter. These are the impulse theory coefficients, denoted 'C' and Beardsley's coefficients denoted

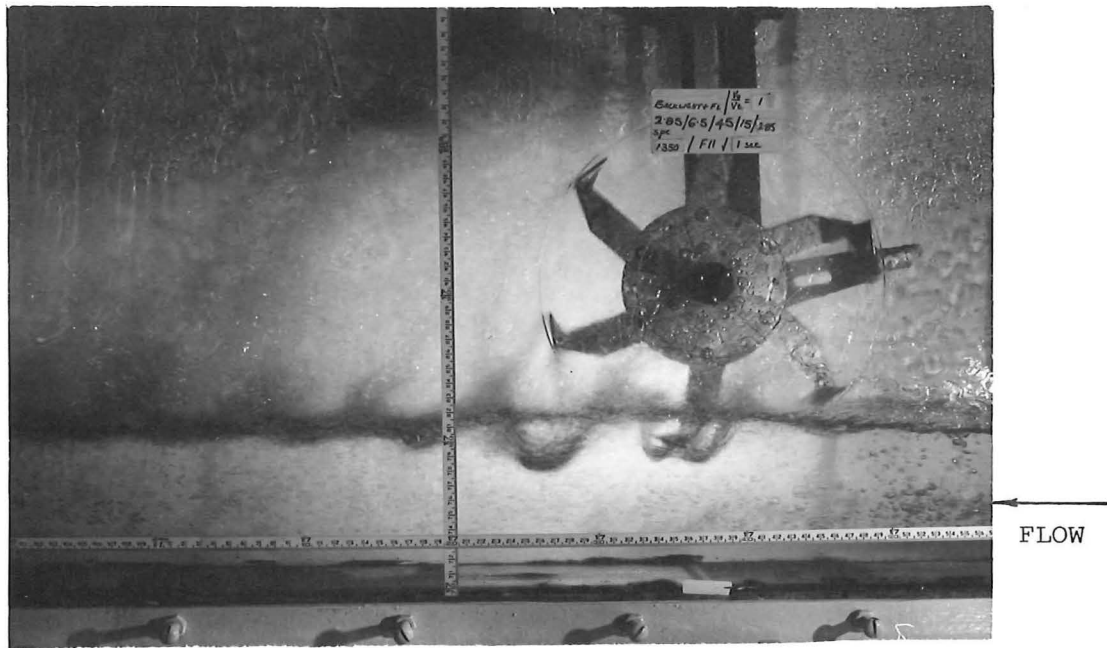


FIGURE 9.15: WATER CAN BE SEEN TO BE MOVING AWAY FROM THE PRESSURE FACE OF THE BLADE AFTER ENTRY. STANDARD BLADE DIMENSIONS, $\phi = 15^\circ$, $d/D = 0.1$, $V_o = 2.85$ m/s, $V_o/V_t = 1$, SIDEPLATES, SUPER-CRITICAL FLOW, PLANING

TABLE 9.16: THE FORCE COEFFICIENTS

"K" coefficients from Beardsley: (section 4.2.1)

$$\text{Lift: } K_L = \frac{L}{\rho n^2 D^3 s}$$

$$\text{Thrust: } K_T = \frac{T}{\rho n^2 D^3 s}$$

"C" coefficients from impulse theory: (section 4.7 and 4.8)

Before surface cavity intrusion:

$$\text{Lift: } C_L = C_{1L} = \frac{L}{V_v \dot{m}} = \frac{L}{\cos(\phi-\theta) (V_t \sin\phi - V_o \sin(\phi-\theta)) \frac{\pi}{8} \rho c^2 s n B}$$

$$\text{Thrust: } C_T = C_{1T} = \frac{T}{V_h \dot{m}} = \frac{T}{\sin(\phi-\theta) (V_t \sin\phi - V_o \sin(\phi-\theta)) \frac{\pi}{8} \rho c^2 s n B}$$

After surface cavity intrusion:

$$\text{Lift: } C_L = C_{2L} = \frac{L}{V_v \dot{M}} = \frac{L}{\cos(\phi-\theta) (V_t \sin\phi - V_o \sin(\phi-\theta)) \rho V_o s d}$$

$$\text{Thrust: } C_T = C_{2T} = \frac{T}{V_h \dot{M}} = \frac{T}{\sin(\phi-\theta) (V_t \sin\phi - V_o \sin(\phi-\theta)) \rho V_o s d}$$

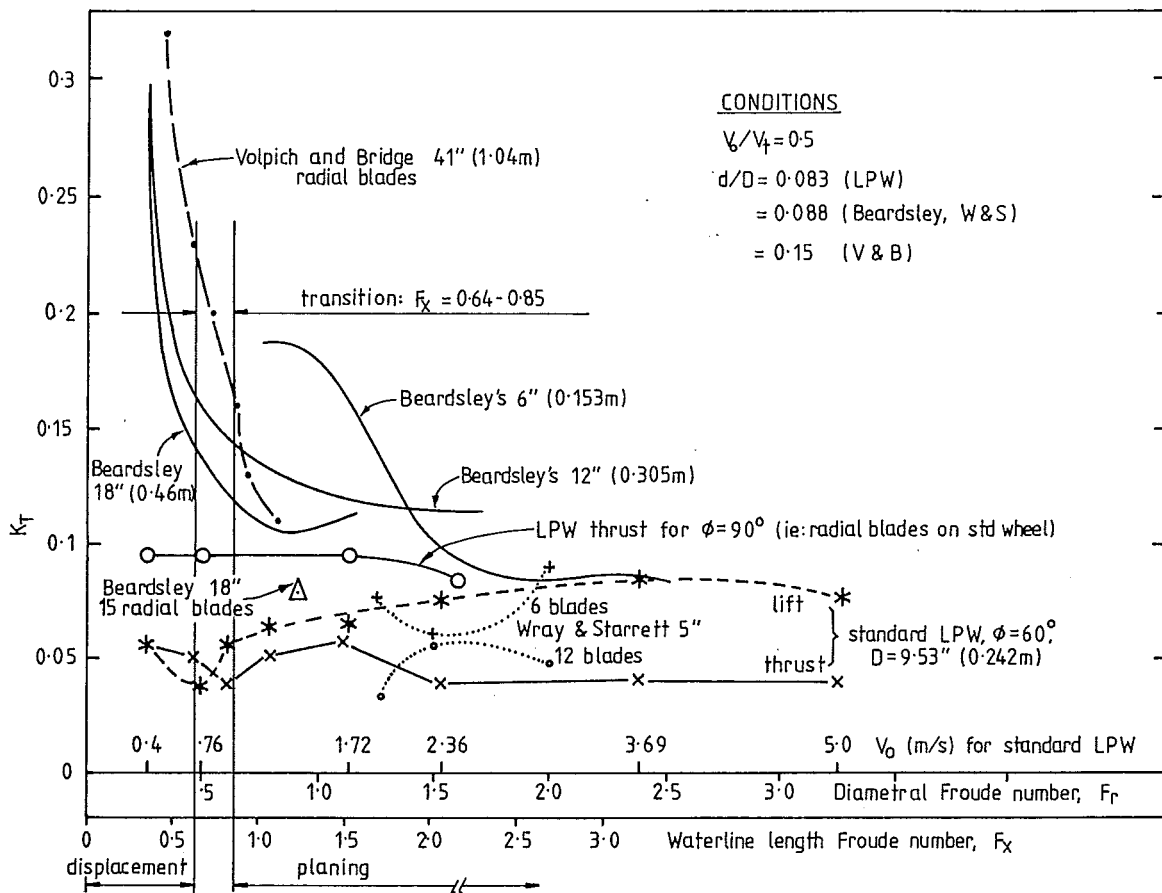


FIGURE 9.17: COMPARISONS OF THRUST COEFFICIENT VS VELOCITY

K FOR A VARIETY OF PADDLEWHEELS.

'K', and described in section 4.2.1. The impulse theory coefficients only apply in the planing mode for which the impulse theory was developed and are different in derivation both before and after cavity intrusion.

Beardsley's 'K' coefficients however are not so limited and are therefore used more often in the comparison of data both before and after cavity intrusion and throughout all the velocity conditions of operation. In such comparisons the differences in derivation of the two types of coefficients must be kept in mind. They are tabulated in Table 9.16.

9.4.2 Effects of Speed of Advance, V_0

Although paddlewheel researchers were not fully aware of the differences between displacement and planing modes of operation, those who tested wheels at high diametral Froude Numbers or high velocities have planing, propulsion data available for comparison. In Fig.9.17 such data has been reduced to Beardsley's K_T coefficient and a selection of LPW data can therefore be compared directly with the results of other paddlewheel researchers. The following points may be noted.

1) At low velocities in the displacement and transition zones the LPW results for lift and thrust for the standard wheel are low compared with those of Beardsley, and Volpich and Bridge. These LPW coefficients appear relatively constant throughout the range of velocity.

2) The results for the 90° LPW (that is, with radial flat blades) approaches the coefficient values of Beardsley's wheels at higher velocities. Beardsley's wheels were specially designed for propulsion, and had cupped blades as shown in Fig.2.9. This would suggest that purpose built propulsion blades such as Beardsley's may only have an advantage over flat blades in the displacement mode.

3) The 90° LPW results are marginally greater than those of Wray and Starrett who used a five inch diameter wheel with radial blades (see Fig.2.6).

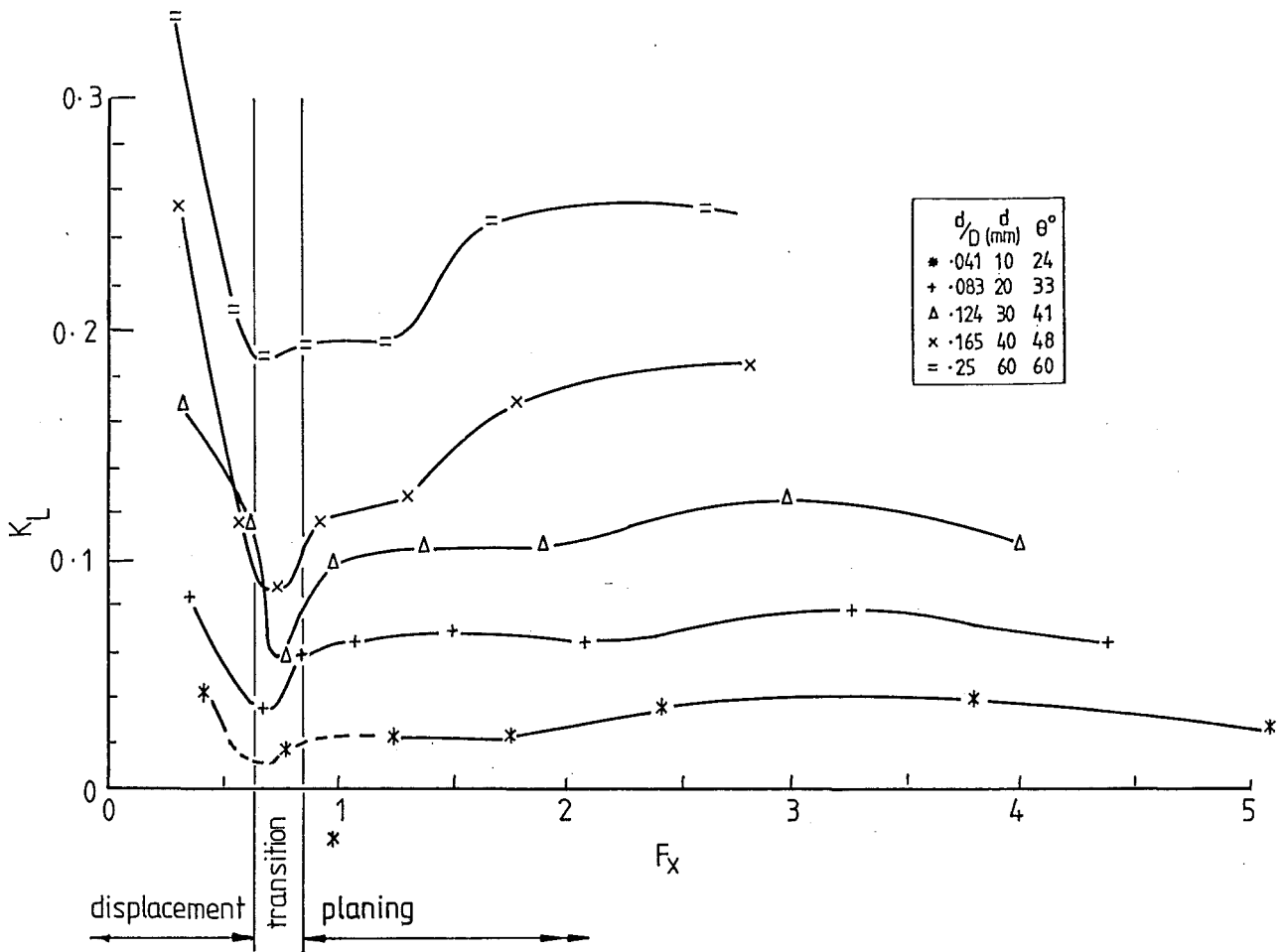


FIGURE 9-18: LIFT COEFFICIENT SHOWING TRANSITION DIP WITH WATERLINE LENGTH FROUDE NUMBER, F_x

4) One result is included for Beardsley's fifteen-bladed wheel with radial blades. This is lower in value than the 90° LPW results for the six-bladed LPW.

5) For the standard LPW with a blade angle of $\phi = 60^\circ$ the thrust coefficient is lower than those of the other wheels it is compared with, while the lift coefficient, included for comparison, seems to follow the trends of other results, especially at high velocities. It is apparent from this that the LPW has traded off some of its thrust for lift force.

In general these comparisons suggest that while the tested LPW appears to be giving low results in the displacement mode, when compared with other purpose built wheels its forces are closely comparable with those of other experimenters especially at higher Froude Numbers, in the planing mode. In such a comparison the fact that the standard LPW blades are angled must be kept in mind. As yet no good reason can be advanced as to why the LPW force coefficients are low in the displacement mode though this might be a diameter effect as implied by Wray and Starrett's results.

Beardsley suggested that at high Froude Numbers, as speed is increased the thrust coefficient should remain constant for a fixed velocity ratio. (1) His results up to $Fr = 2.5$, as shown in Fig.9.17, generally confirmed this. LPW results have been obtained at still greater Froude Numbers with the continuation of the trend expected by Beardsley as also shown in Fig.9.17. This finding supports Beardsley's momentum model of paddlewheel forces (2) upon which was based the LPW impulse theory (see sections 4.2.1 and 4.3) thus tending to confirm both approaches.

The fact, then, that the force coefficients become independent of velocity at planing speeds supports Beardsley's assertion and implies that once the wheel is planing Froude effects may be neglected and constant velocity ratio (V_o/V_t) is a sufficient velocity condition for velocity scaling. This is a useful conclusion for a high speed craft.

9.4.2.1 The Displacement to Planing Transition. It was shown in section 4.15.2 how the wakes for the displacement to planing

1. Beardsley, P.20

2. Beardsley, P.13 equation 8 and P.20

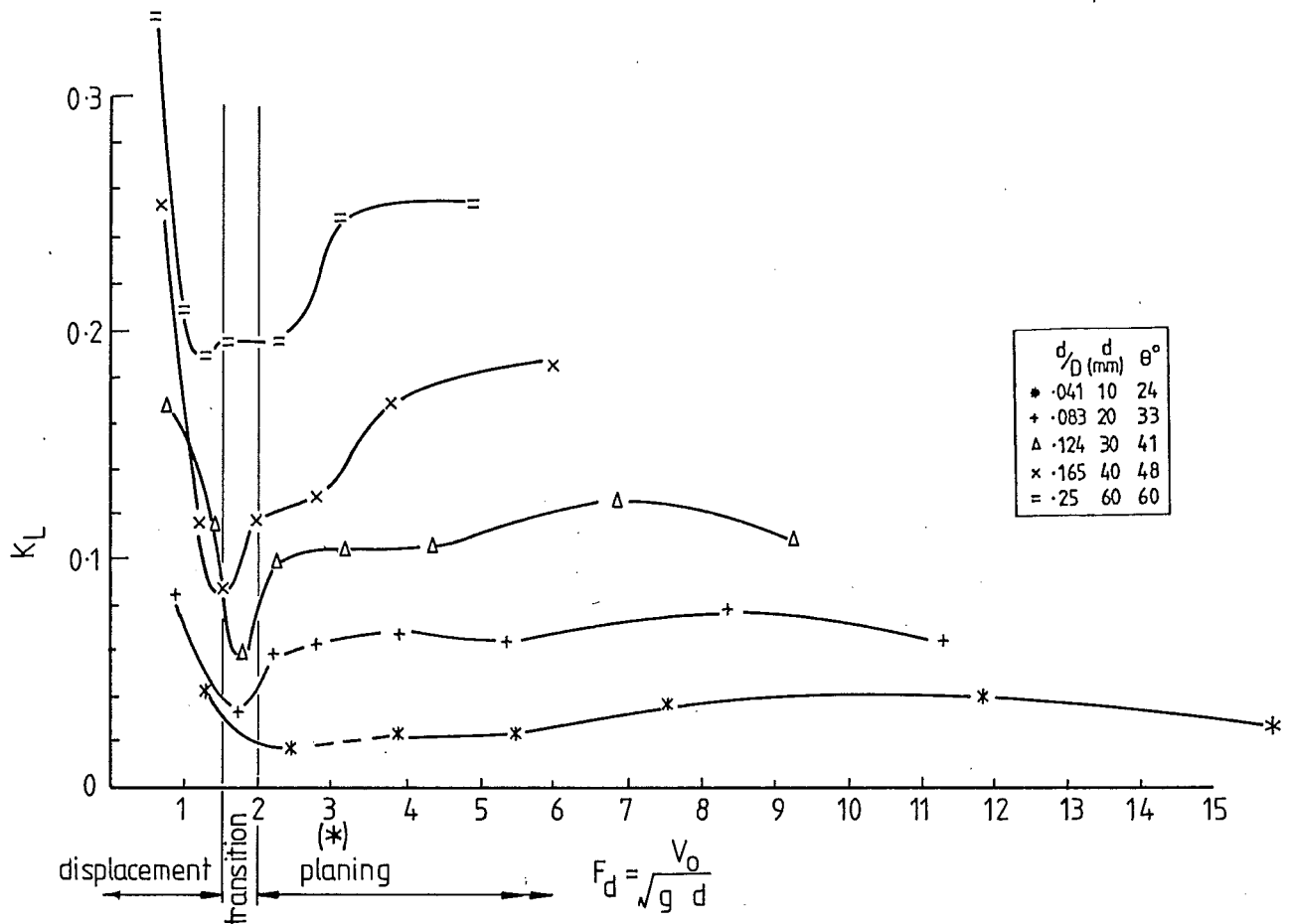


FIGURE 9-19: LIFT COEFFICIENT WITH BEARDSLEY'S DEPTH FROUDE NUMBER, F_d

transition for the LPW or paddlewheel are similar to those for the same transition for planing boat hulls. The same value of the Froude Number based on waterline length can be used in both cases to define the change. This change can be observed as changes in the wave formations of the LPW wake as already shown in Figs.9.5 to 9.9 and 4.32 and 4.33. Based on Beardsley's transition parameter (1) a range for the waterline length Froude Number was seen to be $F_x = 0.64$ to 0.85 for the transition (section 4.15.2).

Beardsley defined the depth Froude Number (1) :

$$F_d = \frac{V_o}{\sqrt{g d}} \quad (4.51), (9.1)$$

where V_o = speed of advance

g = gravitational acceleration

d = immersion depth.

He considered that a transition relating gravity flow and immersion depth occurred where the flow into the cavity changed from chiefly gravity induced to chiefly horizontally entrained.

This project has considered the change in the forces over the transition to occur for different but closely related reasons to those of Beardsley namely the transition occurs when the forces begin to be generated chiefly at blade entry rather than throughout the cavity. Both descriptions are helpful in showing what is occurring during the transition.

It is of value to examine the 'K' coefficients, with immersion for the standard wheel through this transition, to see how well the changes in them correspond with the transition zones described by Beardsley and by this project. These are shown in Fig.9.18, which gives the lift coefficient, K_L against the waterline length Froude Number, F_x , while Fig.9.19 shows the lift coefficient against Beardsley's depth Froude Number F_d , for the standard LPW.

The following points may be made:

1. Beardsley, P.20

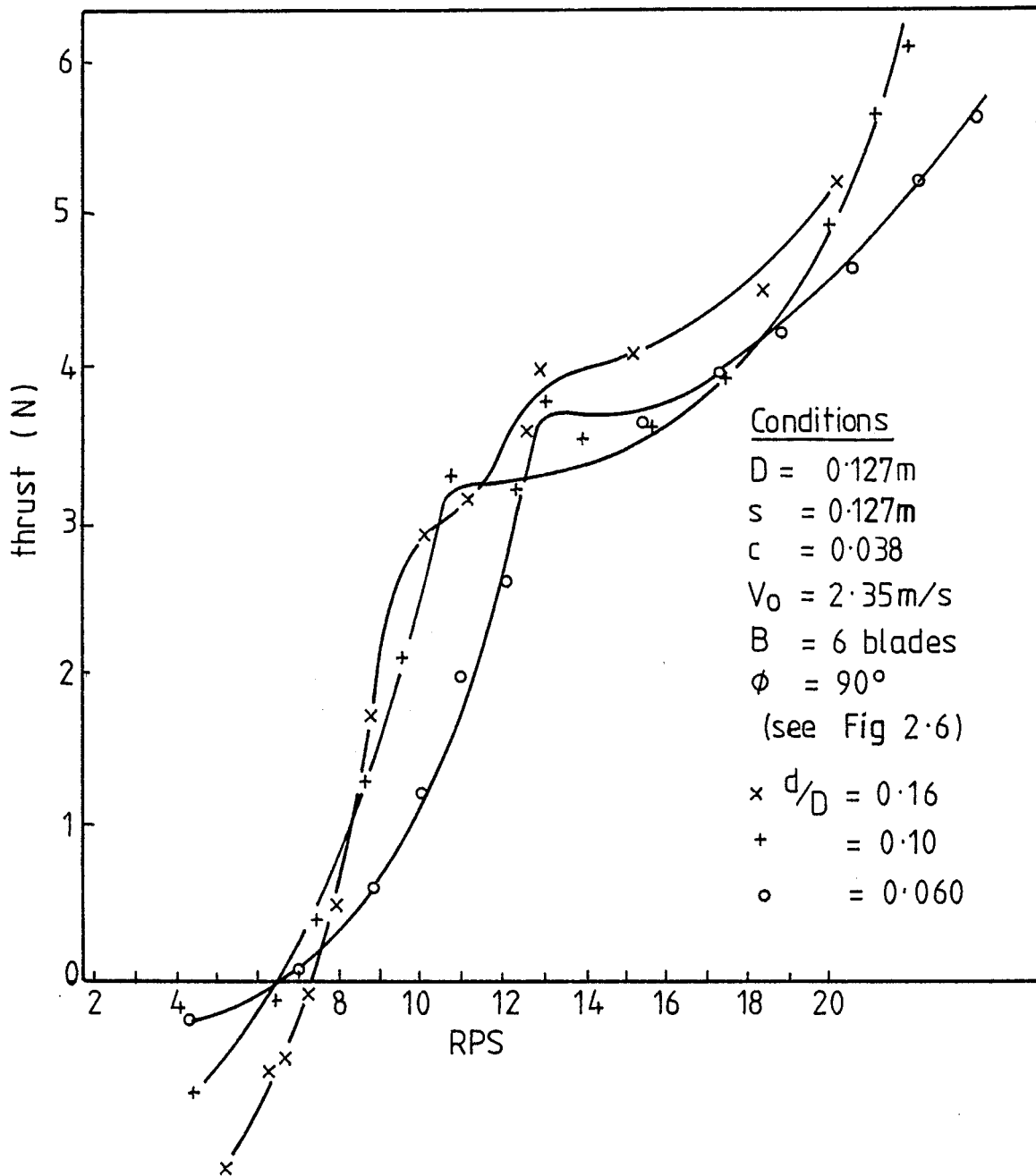


FIGURE 9.20 WRAY AND STARRET'S RESULTS FOR THEIR 0.127 m (5 INCH) WHEEL IN THE PLANING MODE.

(W & S, pg 73, Fig 11.)

1) The dip in the K_L curves corresponds well with the chosen transition zone for the waterline length Froude Number in Fig.9.18, as does the change in character of the K_L plots. The exception is the smallest immersion depth ($d/D = 0.04$, symbol *) which appears anomolous and is shown dotted. This may be because of the larger errors present in small force measurements for small immersions.

2) The K_L curves replotted using Beardsley's depth Froude Number in Fig.9.19 do not show quite such a good correspondence between the dip in the curves and his chosen transition zone. It is apparent, however, that either transition parameter used ($F_d = 1.5$ to 2 or $F_x = 0.64$ to 0.85) will give a fair indication of where the 'K' coefficients change their character.

3) In all cases the curves show a different character each side of the transition zone. Before it they seem to be dependent upon Froude (or gravity) effects while after it they tend to become independent of Froude Number (gravity) effects. This point is significant for the scaling of forces with changes in velocity, or Froude Number as noted above in section 9.4.2. It is also indicative of the different mechanisms being brought into play each side of the transition zone, as also noted above.

The transition zone, then, occurs as predicted by the waterline length Froude Number based on experience with normal planing craft, as well as by Beardsley's method. The former method is preferred here simply to be consistent with the established planing craft transition zone.

9.4.3 Effects of Wheel Rotational Speed, n , V_t

The effects of the rotational speed of the LPW have been noted in part in the preceding sections of this chapter and occur through most of the remainder as incidentals to the figures and topics under discussion. The effects are described here as a way of bringing together these scattered references and outlining some puzzling results. Planing speeds only will be used for comparison with the theory.

As the wheel revolutions per second increase from rest at a speed of advance in the planing mode, the rotor is at first driven by the water as long as the velocity ratio is greater than one. (In Fig.9.3 at $V_o = 2.36$ m/s this is the case when wheel speed is less

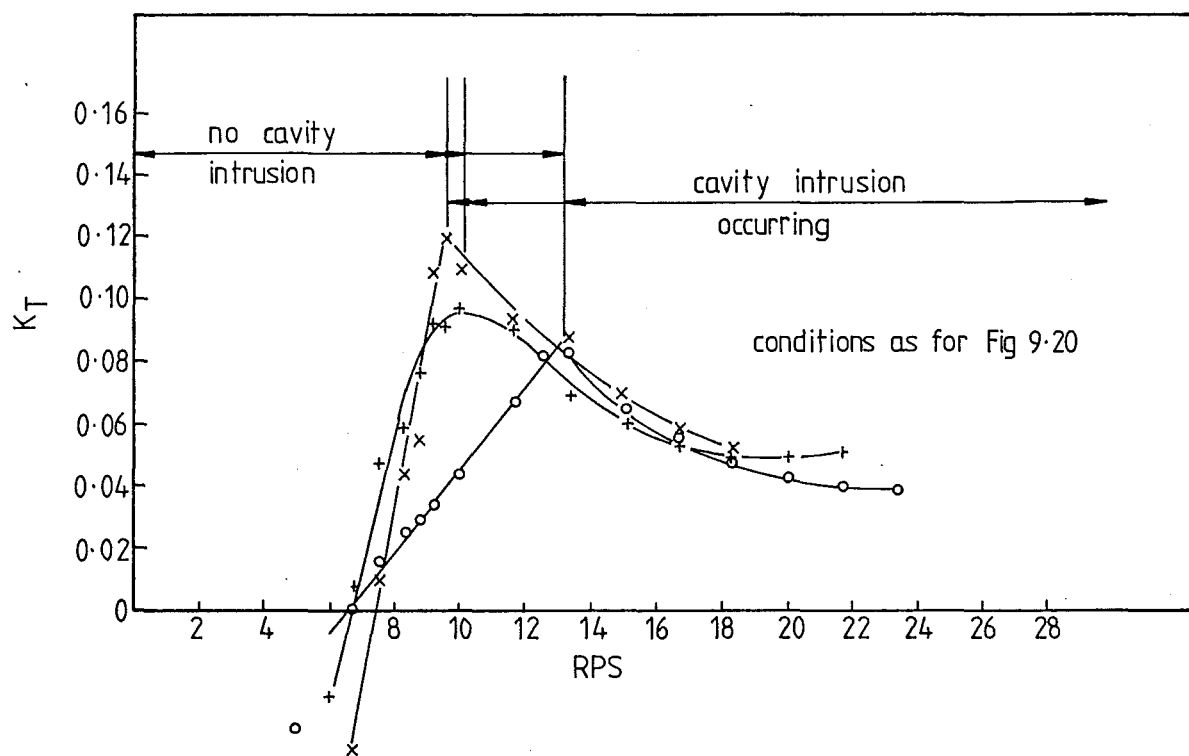


FIGURE 9-21: WRAY & STARRETT'S RESULTS REPLOTED AGAINST K_T .

than 3.1 rps). Under such conditions the lift force may be positive while the thrust is still negative. (This was noted in Fig.9.9(A) and discussed in sections 9.22, 4.8 and 4.14.3.)

As the wheel speed increases and the velocity ratio becomes less than one, both lift and thrust become positive and increase almost parabolically with wheel speed. The blades leave cavities in the water (see Figs.4.25, 4.36, 8.11, 9.8(B), 9.9(B), 9.10) until the wheel speed is great enough for these cavities to begin to interfere with the entry of the incoming blades, whereupon surface cavity intrusion occurs, (Fig.4.19(A) and (B)).

In the plots of force against rps in Fig.9.3 the forces appear to increase with the square of wheel revolutions before surface cavity intrusion. Wray and Starrett also plotted their data on similar axes as shown in Fig.9.20 and the initial portions of their thrust curves are similar to those of the LPW data. Both the impulse theory and dimensional analysis (in expressions (4.2), (4.23), (4.25)) predict that these forces should be largely dependent upon the square of wheel revolutions. Thus a plot of Beard'sley's 'K' coefficient (expression 4.3) against wheel revolutions for the lift force should show no dependence of K_L upon wheel revolutions before cavity intrusion occurs. Such a figure is shown later in Fig.9.26, where it is apparent that this is not the case. Before cavity intrusion K_L has a linear relationship with wheel revolutions. This result was also found to exist in Wray and Starrett's data, a sample of which is re-plotted in 'K' coefficient form in Fig.9.21..

It would at first appear that this relationship exists because as the wheel speed increases (velocity ratio decreases) the angle of attack of the blades increases, as shown in Fig.4.13. This angle change would thus cause the forces to increase by more than the square of the wheel revolutions.

In the impulse theory, however, this variation is taken into account by the maximum velocity expressions (expressions 4.20 and 4.21 in section 4.6.7) so that the impulse theory 'C' coefficients should show no dependence upon wheel revolutions before cavity intrusion. These 'C' coefficients for the lift force have been plotted against wheel revolutions in Fig.9.22 where it appears that this linear relationship with wheel revolutions still exists.

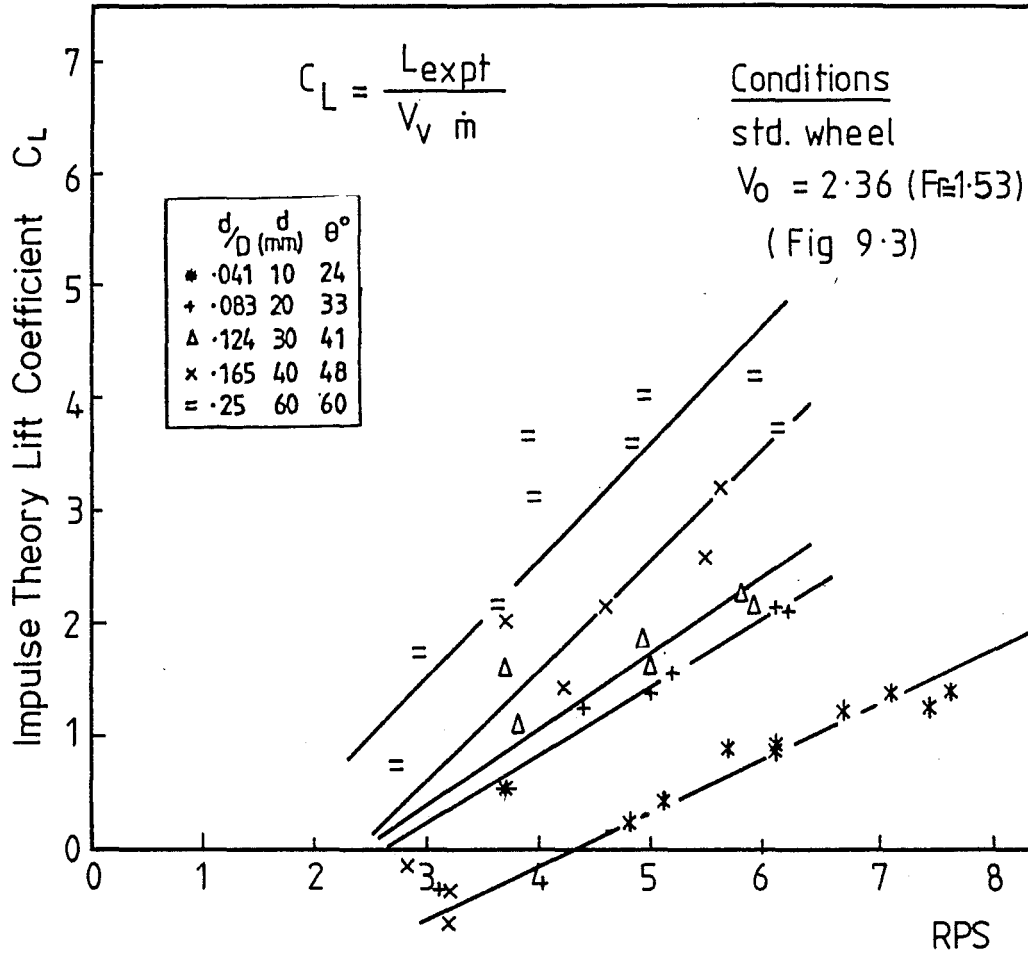


FIGURE 9.22: THE IMPULSE THEORY LIFT COEFFICIENTS SHOW A LINEAR DEPENDENCE UPON WHEEL REVOLUTIONS BEFORE CAVITY INTRUSION

At present the reason for this extra dependence of LPW forces upon wheel revolutions is not clear. While it may be related to the blade exit forces, which have been ignored by the theory so far, no confirming evidence is yet available. It thus appears that the parabolic section of the force-rps plots may really be part of a cubic relation.

As wheel revolutions increase towards cavity intrusion, bow-splash begins to occur. This is possibly simultaneous with the onset of cavity intrusion though it may be unrelated (see sections 9.43.2 and 4.9.1, and Figs.9.8(D), 9.9(D), 4.19(A)-(E)). This is the intersection region of the force-rps plot where the force-rps relationship changes from the apparently parabolic (or cubic) to an almost linear one.

After cavity intrusion, the impulse theory has not defined the induced mass per blade and has assumed, along with Beardsley, that all the entrained mass is acted upon. While dimensional analysis, and Beardsley's 'K' coefficients indicate that the forces should, as before, relate to the square of the wheel revolutions (expressions 4.2 and 4.3) the impulse theory predicts, in expressions 4.26 and 4.27 of section 4.7.1 that the forces should have nearly a linear dependence upon wheel revolutions; the extra variation with wheel revolutions beyond a linear relation being accounted for by the effect of the increase in angle of attack noted above, and still present in the expressions.

Reference to Fig.9.24 (later) (or Figure 9.3 or 1.6) shows that after cavity intrusion has occurred the forces apparently have a linear dependence upon wheel revolutions. This is in contradiction to dimensional analysis or Beardsley's 'K' coefficient predictions, but is in line with the impulse theory. As a check on the impulse theory prediction, the forces after cavity intrusion have been plotted another way.

Fig.9.23 shows the experimentally derived 'C' coefficient for lift after cavity intrusion, plotted, in this case, against velocity ratio. A linear relationship between the coefficient and the velocity ratio indicates an inverse relationship between the coefficient and wheel revolutions. This means that the forces predicted by the

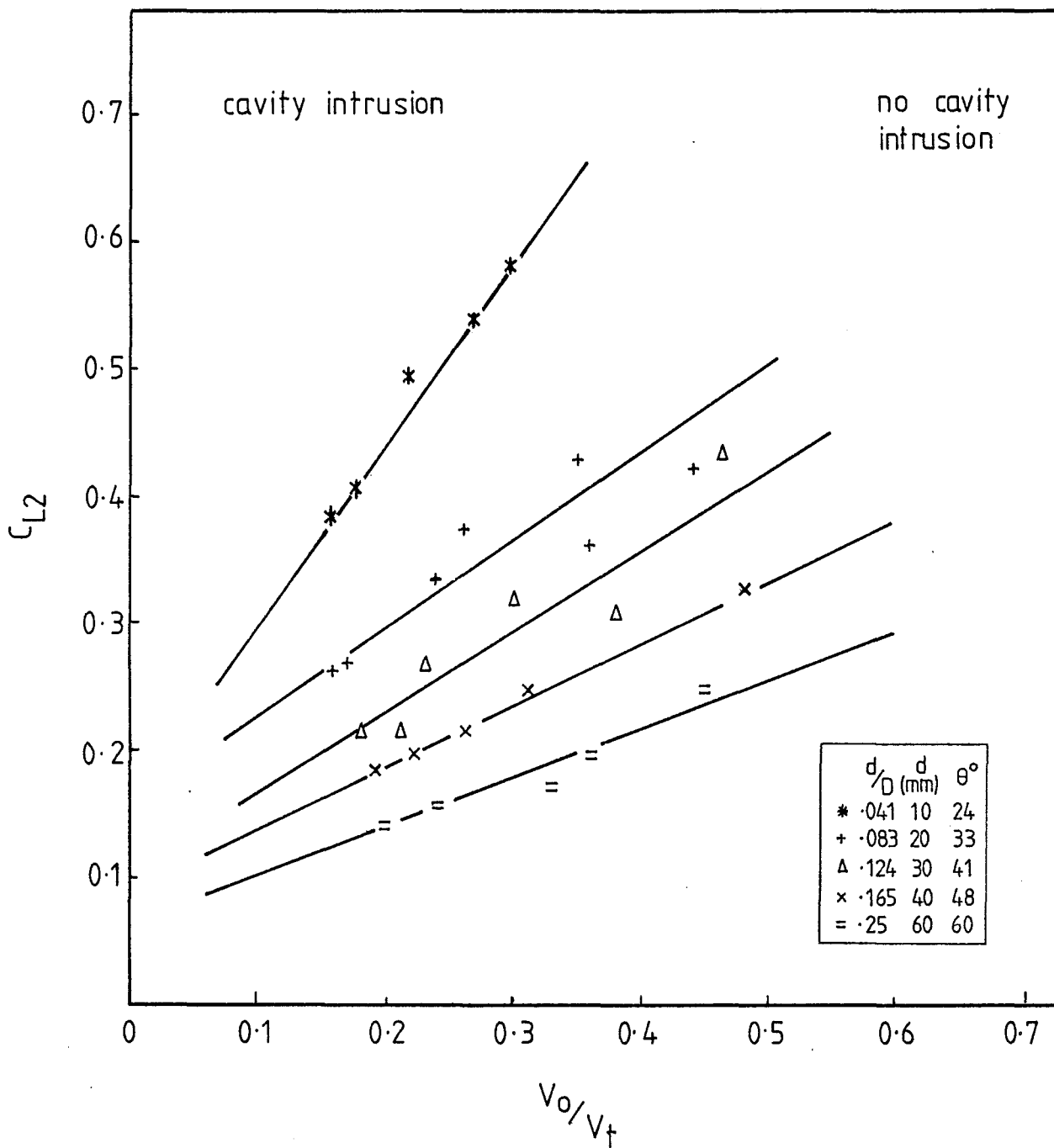


FIGURE 9.23 THE IMPULSE THEORY LIFT COEFFICIENT AFTER CAVITY INTRUSION, FOR THE STANDARD WHEEL.

impulse theory would be too strongly dependent upon wheel revolutions: something less than this relationship is found in experiment. It will also be seen that the values for the 'C' coefficients are less than unity, reflecting the fact that not all the entrained mass is acted upon as induced mass, as assumed for this case after cavity intrusion.

Thus the effects of the wheel revolutions upon the LPW forces are quite complex and some aspects of this variable have yet to be clarified.

9.4.3.1 Surface Cavity Intrusion. Surface cavity intrusion was described in section 1.4.1 and Fig.1.7 and an analytical method of estimating it was given in section 4.9.3 and Appendix 5. This present section shows how it was estimated from the experimental results in their usual form, and compares the theoretical estimates with the experimental ones.

Shown in Fig.9.24 are the lift and thrust curves for the standard wheel in the planing mode ($V_0 = 2.36$ m/s) at an immersion depth of 30 mm. (These curves are taken from Fig.9.3.) Superimposed on the curves are parabolic and linear sections (shown dotted) which have been sketched in by eye. The intersections of the dotted parabolas and the dotted linear sections have been taken as the point where surface cavity intrusion begins. As can be seen, it is different for the lift and thrust curves, a variation not unexpected in experimental results.

The value calculated analytically is 6.4 rps and this is shown on the figure as well.

It is assumed that cavity intrusion is one and the same phenomenon for both lift and thrust components of the resulting force, so that in this case the analytical estimate seems a reasonable figure.

The general reliability of the analytical method was assessed by estimating the beginning of surface cavity intrusion (S.C.I.) by eye as described above, throughout the measured results for flat-bladed LPWs. The values of wheel revolutions thus obtained were

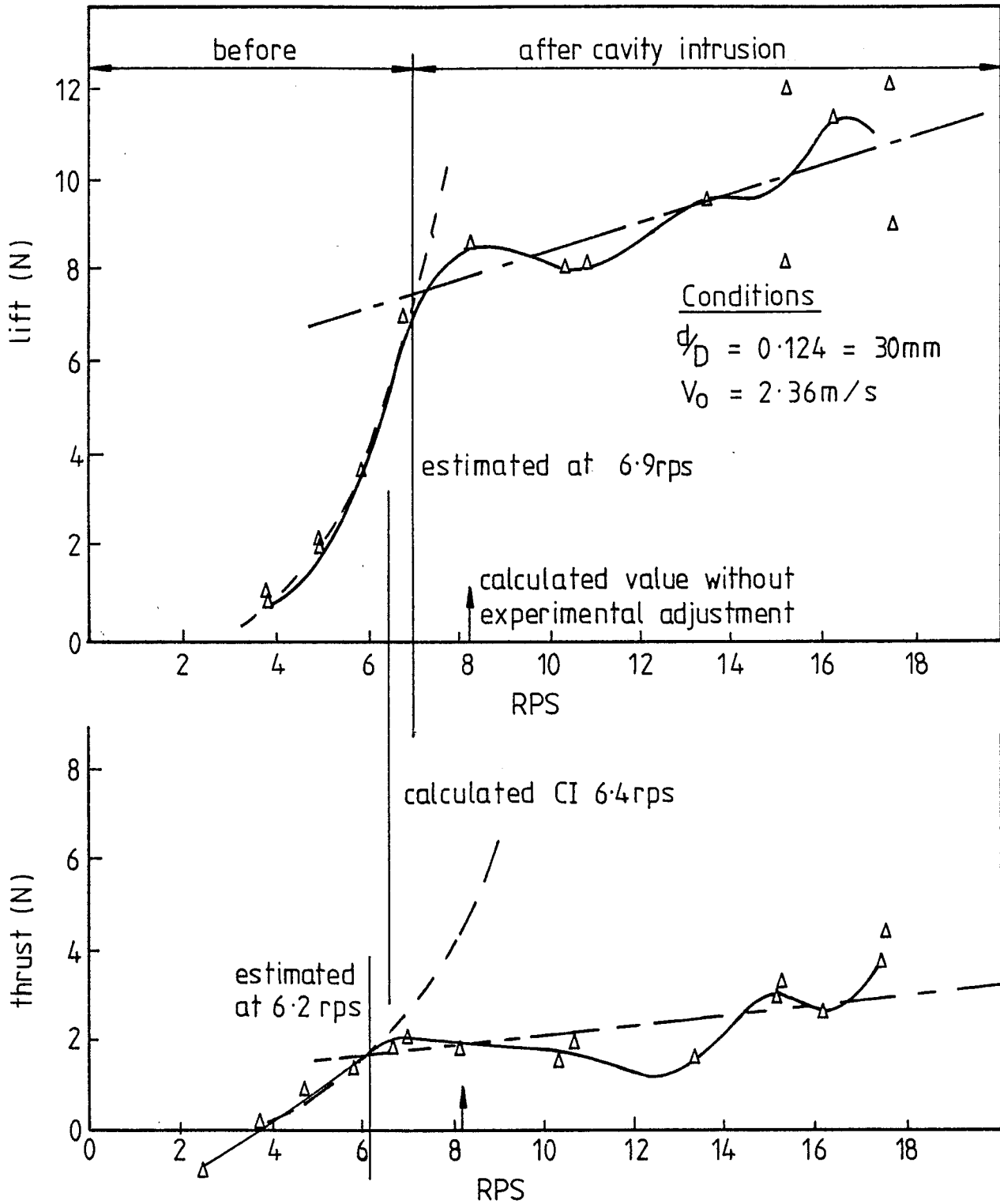


FIGURE 9-24 METHOD USED TO ESTIMATE SURFACE CAVITY INTRUSION FROM THE FORCE DATA (DERIVED FROM FIG 9-3)

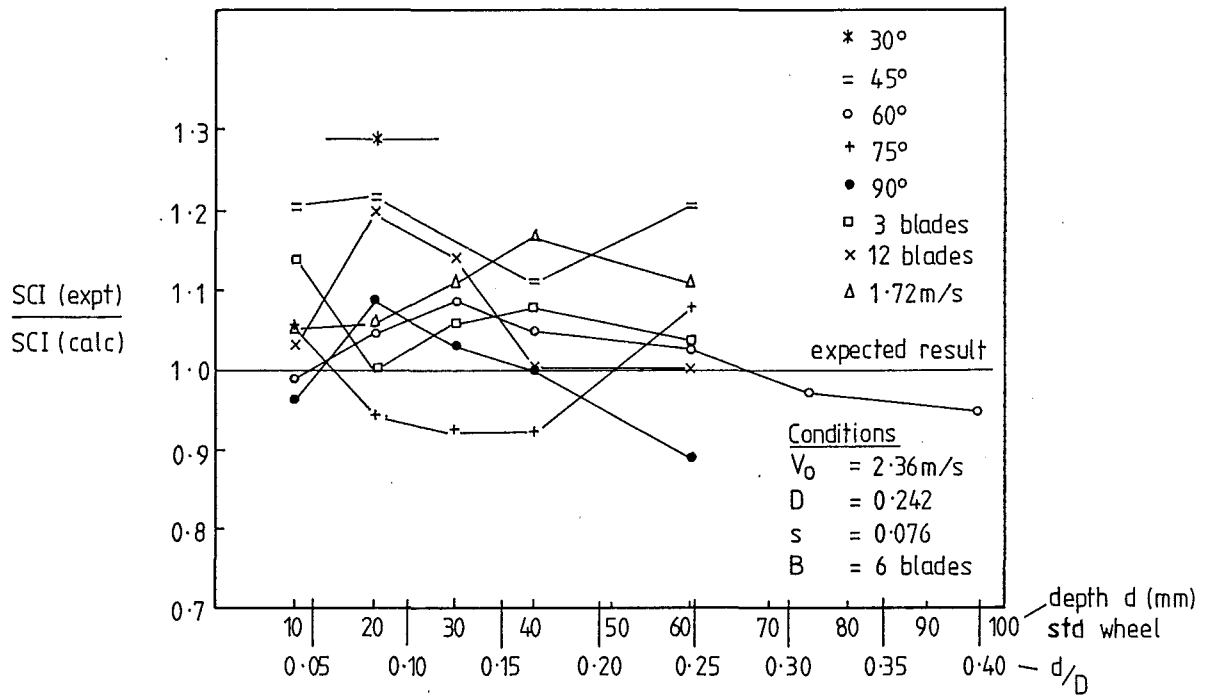


FIGURE 9.25: COMPARISON BETWEEN ESTIMATED AND CALCULATED SURFACE CAVITY INTRUSION RPS.

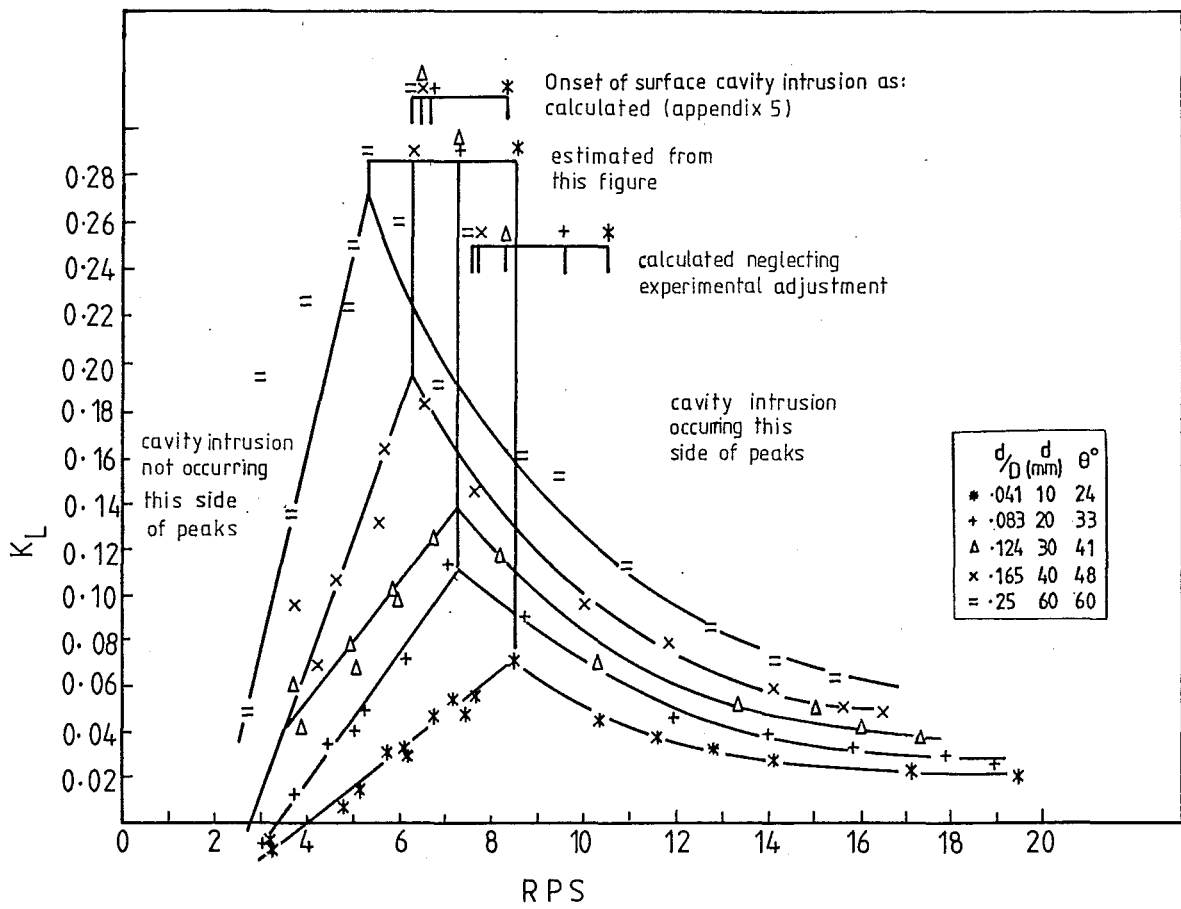


FIGURE 9.26: THE 'K' COEFFICIENTS EMPHASISE THE EFFECT OF SURFACE CAVITY INTRUSION

compared with the analytical estimates in a ratio: (experimental S.C.I.)/(analytical S.C.I.). The values of this ratio were plotted against immersion depth as shown in Fig.9.25. The expected value for the ratio was, of course, unity.

The following points may be noted :-

(1) There seems to be no consistent variation of the ratio with immersion depth: the analytical method seems quite valid in this respect.

(2) On the whole the analytical method slightly underestimates the wheel revolutions at the onset of surface cavity intrusion; since most points lie above the expected value of one.

(3) The results seem to vary a little with blade angle so that the analytical method underestimates the onset of cavity intrusion at blade angles of 45° and less.

In general the figure indicates that the analytical model predicts the phenomenon reliably enough for most purposes.

While the above method of estimating surface cavity intrusion by eye has used the data in the standard form, a more emphatic illustration of its presence is seen in plots of Beardsley's 'K' coefficients. Fig.9.26 is a plot of K_L against wheel revolutions for the standard wheel in the planing mode (2.36 m/s) and the peaks of the curves can be seen to occur close to the analytical estimates of the onset of cavity intrusion.

It was pointed out in Appendix 5 that an experimental adjustment is contained in the analytical estimate for surface cavity intrusion. If this was not included, the calculated value back in Fig.9.24 would be 8.2 r.p.s. as shown. The calculated values for surface cavity intrusion without this adjustment are also shown in Fig.9.26. It is clear from this figure that the adjustment chosen gives a more reasonable estimate than the calculations without it.

9.4.3.2 Bowsplash in Observational Data. Bowsplash as seen in this project is the mound of aerated water pushed ahead of the LPW under certain conditions in the planing mode. Its probable

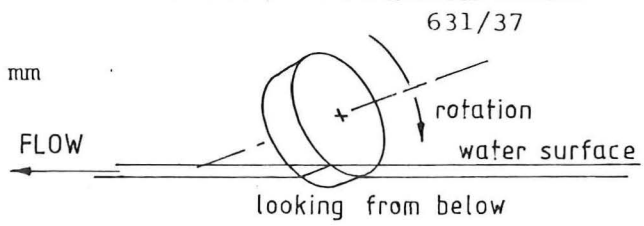
mechanism was described in section 4.9.1 and shown in Fig.4.19 (A)-(E). It can also be seen in Figs.9.8 and 9.9.

The concepts of the impulse theory and cavity intrusion have satisfactorily described LPW forces without reference to this phenomenon so that its presence may in fact be of little consequence for a real craft. Nevertheless it will be described here because of its possible relation to surface cavity intrusion and thence to force generation, as well as its presence in model craft tests.

Fig.9.27 shows two photos taken from beneath the 6-bladed, $\phi = 45^\circ$ LPW in operation in supercritical flow in the glass-sided tank (as described in section 8.3). These photos were taken at the wheel rotational speed where bowsplash was just beginning. There is barely any detectable difference in wheel rotational speed between the two, yet in the second, bowsplash has begun to build up as evidenced by the froth on the upstream side of the wheel against the glass. The photos were taken to highlight the position of the cavity left by the last blade in relation to the incoming blade. It may be seen that the distance between the forward edge of the cavity and the rear edge of the incoming blade is close to half the chord of the blade. Much the same distance may be observed in Fig.4.19 (A) and (B). This distance is reminiscent of the experimentally derived distance, of the same magnitude, required between the cavity edge and the blade heel for the calculation of the surface cavity intrusion conditions in Appendix 5, and it suggests that the two phenomena may be related. To test this idea an examination was made of the photographic records, for the standard wheel under open water conditions at the Kainga tank. A range of wheel revolutions within which bowsplash began to occur was obtained for each immersion depth, and the results were plotted in Fig.9.28 with the experimental and analytical estimates of cavity intrusion. It is clear from this figure that at immersion depths greater than 10 mm for the standard wheel (immersion ratios greater than $\frac{d}{D} = 0.04$) bowsplash occurs at a lower wheel speed than cavity intrusion. It also seems from Fig. 4.19 (b) for a wheel with four blades, and from observations of the wheel with twelve blades that bowsplash generally occurs just before the onset of surface cavity intrusion, though this conclusion has yet to be checked for wheels other than the standard wheel.



CONDITIONS. STANDARD WHEEL,
 $\phi = 45^\circ$, SIDEPLATES, $d = 30$ mm
 $V_0 = 2.85$ m/s, $V_0/V_t = 0.54$



631/36

FIGURE 9.27: STROBOSCOPIC VIEWS OF PRE-BOWSPASH (ABOVE) AND BOWSPASH CONDITIONS. NOTE THE GAP BETWEEN THE CAVITY FORWARD EDGE AND THE BLADE REAR EDGE

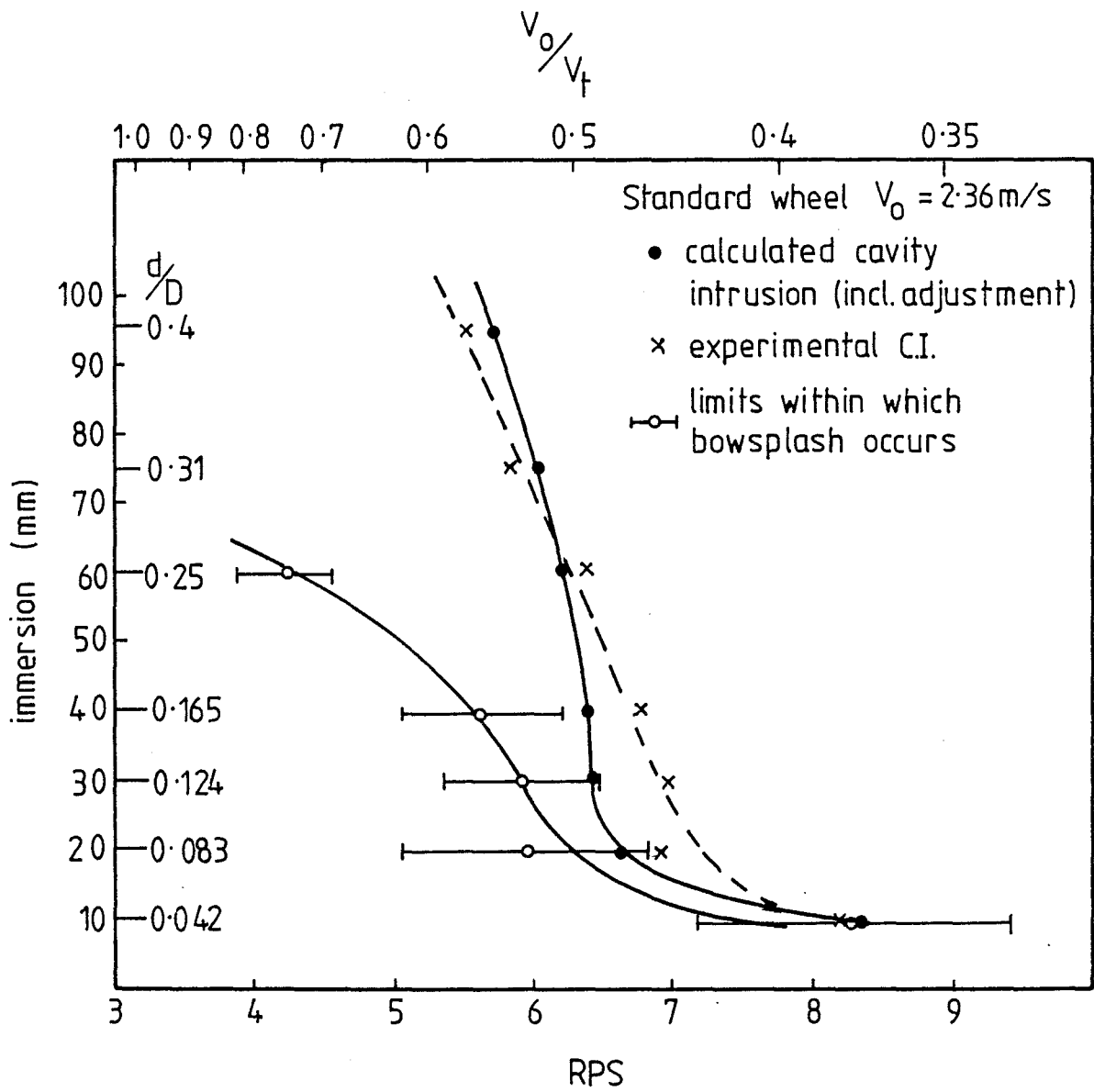


FIGURE 9.28 BOWSPASH OCCURS AT LOWER WHEEL REVOLUTIONS THAN SURFACE CAVITY INTRUSION.

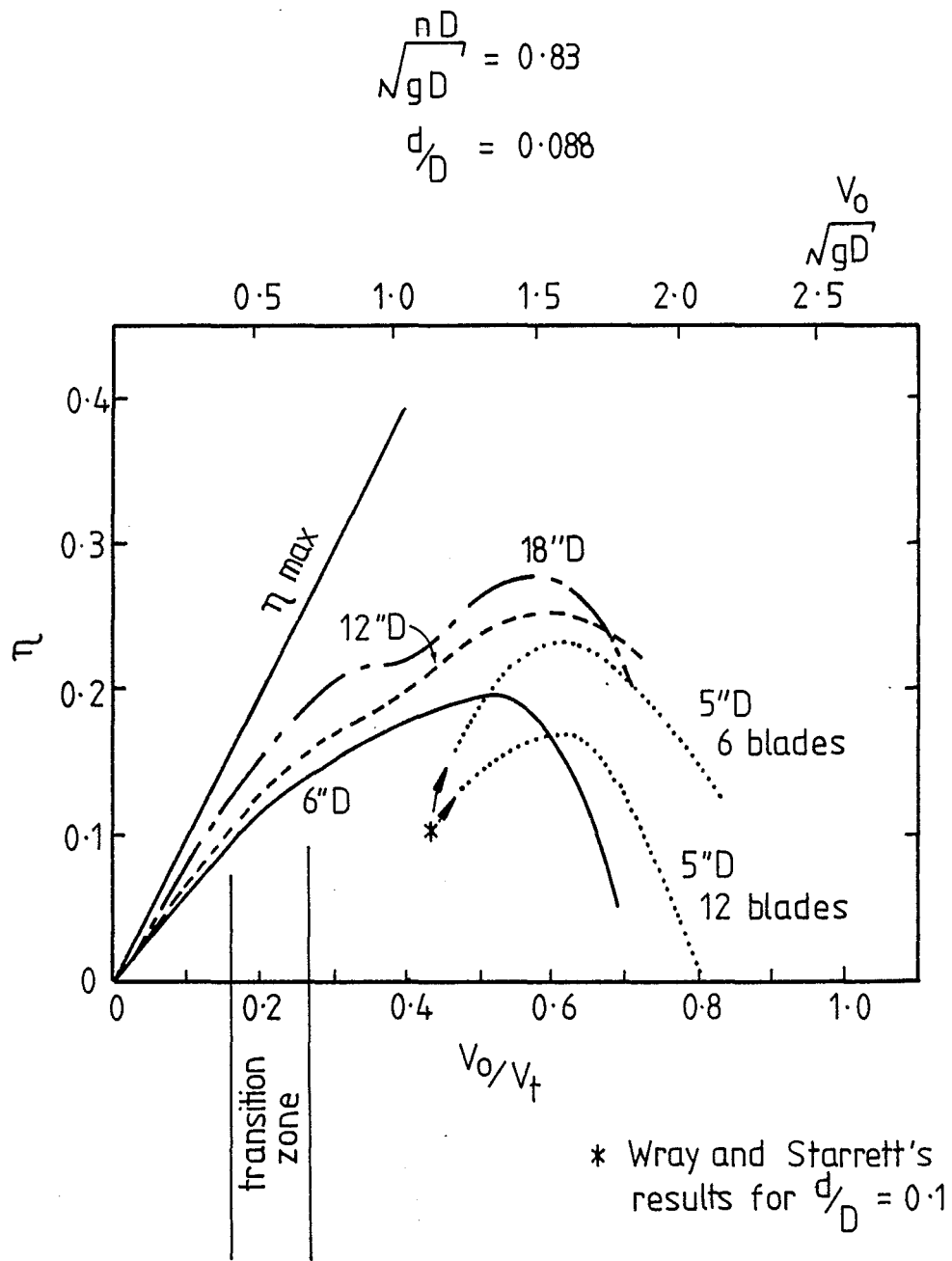


FIGURE 9-29: BEARDSLEY'S RESULTS SHOWING EFFICIENCY WITH WHEEL DIAMETER PLOTTED AGAINST VELOCITY RATIO AT CONSTANT WHEEL REVOLUTIONS.

As yet, it is not clear how this phenomenon affects the performance of the LPW, and while it is at present believed to increase the wave drag markedly, observed loss of propulsion, when bowsplash occurs, may in fact be a result of the concurrent onset of cavity intrusion, limiting the propulsive thrust forces instead.

9.4.4 Effects of Wheel Size, D

The literature of paddlewheels contains a number of attempts to analyse the effect of wheel size since this is important if results are to be scaled to full-sized wheels. Volpich and Bridge tested geometrically similar wheels of 0.518 m (1.7 ft) and 1.036 m (3.4 ft) in diameter and found essentially no difference between the force or propulsive efficiency results between the two (1) (section 2.2.3). Wray and Starrett tested a 0.127 m (5 in) diameter wheel and apparently produced results which indicated degradation of performance because of wheel size (see Fig.9.17 in section 9.4.2) though as pointed out in section 2.2.5 there were a number of other possible explanations for their results. (2)

Beardsley tested wheels of 0.152 m, 0.305 m, and 0.457 m (6 in, 12 in and 18 in) in diameter at an immersion of $\frac{d}{D} = 0.088$ (section 2.2.6). (2) Some of his data are shown in Fig.9.17. Although he found unexpected values for the smallest wheel (0.152 m) he considered this to be a result of inaccuracy of measurement at the low speeds of advance. He concluded that his force coefficient results for varying diameter were reasonably consistent for the conditions tested. His efficiency curves for the same tests showed a small but steady increase in propulsive efficiency with diameter. His results are reproduced in Fig.9.29. Based on this propulsive efficiency variation he suggested test wheels should be at least 0.3 m in diameter. This was discussed in section 5.8.1.

This LPW project tested three wheel sizes close to Beardsley's tested diameters. In this case the wheels were 0.152 m, 0.242 m (the standard wheel) and 0.383 m in diameter. All were geometrically similar to the standard wheel with blade angle, $\phi = 60^\circ$. It was not possible to gather a large amount of data for the largest wheel as it readily overloaded the force balance motor.

1. Volpich and Bridge, Part 1, P.348
2. Beardsley, P.15

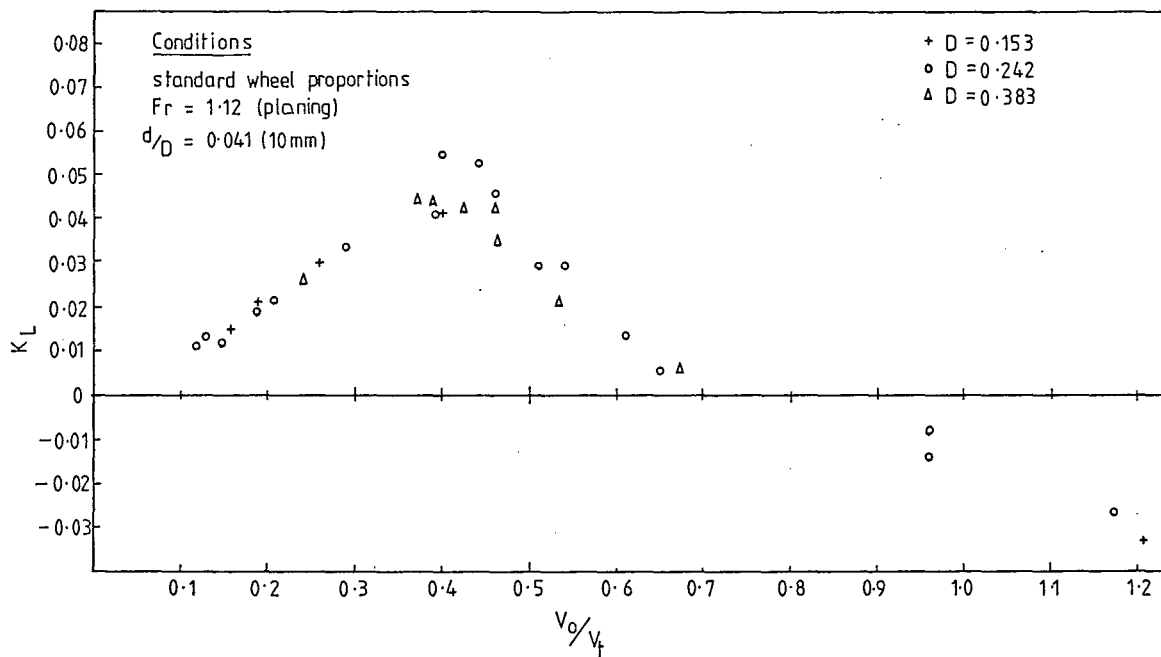


FIGURE 9-30 LIFT COEFFICIENT SHOWING NO VARIATION WITH WHEEL DIAMETER

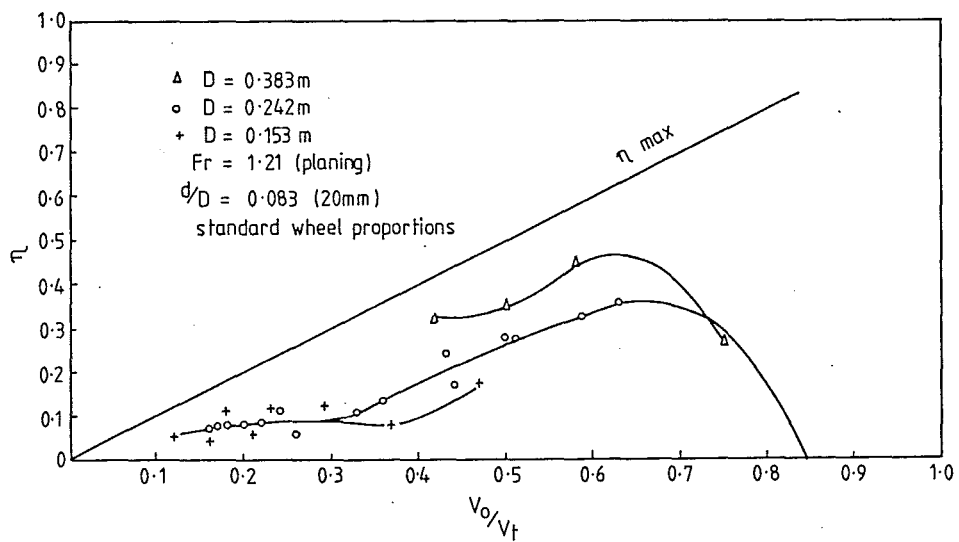


FIGURE 9-31 LPW EFFICIENCY INCREASES WITH DIAMETER AT WORKING VELOCITY RATIOS

With these three wheels the trends found by Beardsley were confirmed. Fig.9.30 shows the LPW lift coefficients, K_L , for the three wheel diameters at the immersion ratio $\frac{d}{D} = 0.041$. The lift coefficient was chosen as thrust forces are small for the wheel with a blade angle of $\phi = 60^\circ$ in the planing mode, and lift forces would be expected to vary with diameter in the same way as the thrust forces. It is clear from this figure that the coefficient values show no distinguishable trend with diameter. This was found to hold for all immersion depths and velocities in the planing mode where the three diameters could be compared.

This confirms Beardsley's conclusion that force coefficients are consistent with diameter, though in this case only the high speed planing results have been examined.

An examination of the propulsive efficiency, η , for the three sizes of wheel while a little more confusing generally supports Beardsley's findings. As shown in Fig.9.31 the efficiency values above a velocity ratio of 0.3 are seen to increase with diameter. This figure is again representative of the range of planing velocities and immersion depths compared.

It would be appropriate to conclude, in the light of Beardsley's similar findings, that force coefficients in the planing mode do not alter with increase in wheel diameter from wheels as small as 0.152 m, while propulsive efficiency increases in the operational range with increase in wheel diameter at least up to 0.383 m and possibly up to 0.518 m though not beyond this size, since this was the diameter of the small wheel in Volpich and Bridge's results. Reliable scaling of propulsive efficiency would seem to require wheels at least as large as the size suggested by Beardsley (0.3) and possibly as great as 0.518 m, though scaling of forces and force coefficients seems to be satisfactory down to wheels of 0.152 m diameter.

9.4.5 Effects of Blade Span and End Plates, s

The effect of blade span was investigated by Volpich and Bridge and by Beardsley with the common conclusion that thrust force increases directly with span with no change in propulsive efficiency. (1) Because of this Beardsley included a term for span in his thrust

1. Beardsley, P.16

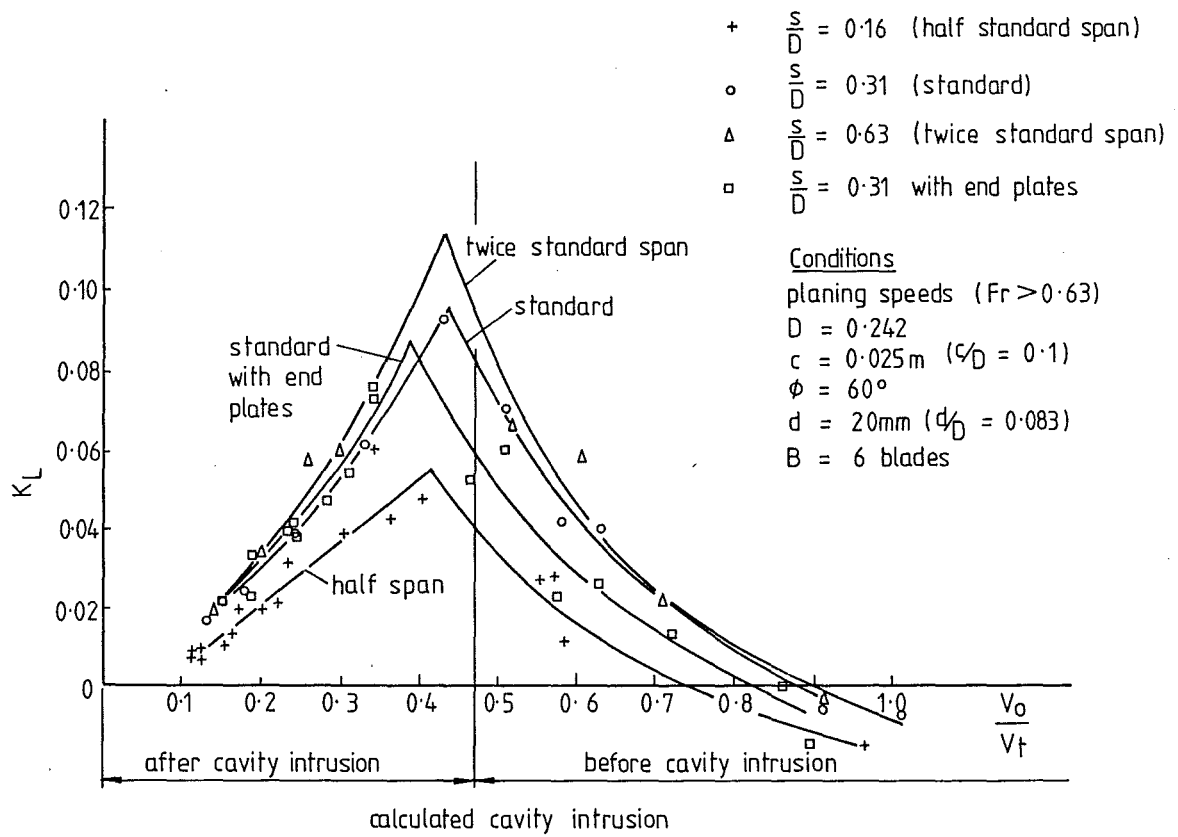


FIGURE 9.32: THE EFFECT OF SPAN ON THE LIFT COEFFICIENT

coefficient, K_T , thereby normalising it for span equal to diameter, (expression (4.2)). Beardsley suggested that for open-ended rotors, with no endplates, with spans less than half the rotor diameter a degradation may be found.

The LPW tests on the standard wheel all had spans of 0.31 D. Thus by Beardsley's reckoning a force degradation effect might be expected.

To test this a series of results were taken with span to diameter ratios of $\frac{S}{D} = 0.16$, $\frac{S}{D} = 0.31$ (the standard wheel) and $\frac{S}{D} = 0.63$. Additionally the standard wheel was tested with endplates extending to the blade tips. These plates were of 2 mm thick perspex and may be seen in all photographs of the wheel in the glass-sided tank; for example Fig.9.27.

The results of these tests generally showed that a fall off in force coefficient values may be expected with $\frac{S}{D} < 0.3$. Thus wheels with spans less than the standard wheel span were the only ones to show the loss. Fig.9.32 was prepared to show these results and the following points may be noted:

(1) The wheel with blades of half the standard span ($\frac{S}{D} = 0.16$) show a markedly lower force coefficient than the other wheels throughout the range of velocity ratios tested. This was typical at other immersion depths as well.

(2) The results for the standard span ($\frac{S}{D} = 0.31$) and twice the standard span ($\frac{S}{D} = 0.63$) give results which barely differ especially before cavity intrusion, suggesting that $\frac{S}{D}$ may be as low as 0.3 without appreciable effect. This is lower than the $\frac{S}{D} = 0.5$ suggested by Beardsley as the beginning of this effect.

(3) Endplates on the standard wheel actually reduced its force coefficient before cavity intrusion (in this case the lift coefficient) while making no difference after cavity intrusion. This is apparently because the endplate discs themselves throw up a thin sheet of spray (observed during the tests) which is sufficient to reduce the lift coefficient at high velocity ratios (low wheel revolutions).

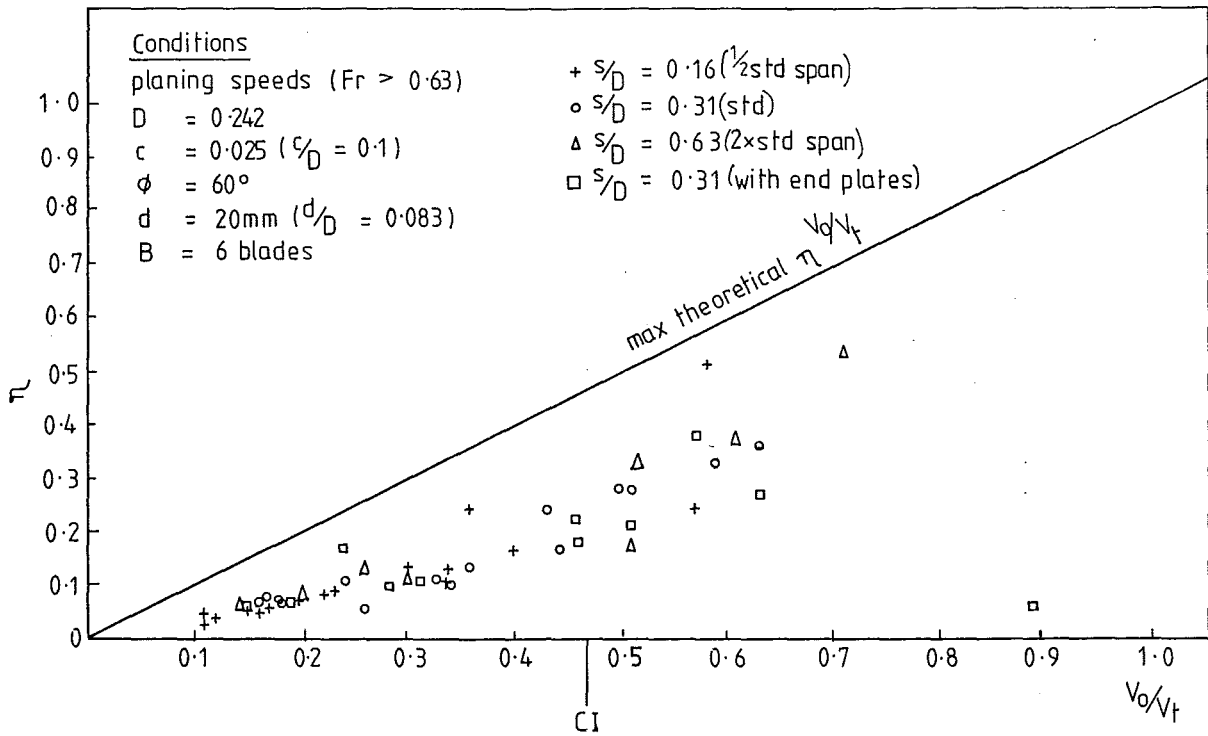


FIGURE 9.33 THERE IS NO EFFECT OF SPAN OR END PLATES ON EFFICIENCY

The effect of span variation on propulsive efficiency is shown in Fig.9.33. It can be concluded with Beardsley that variation in blade span, even to small values (minimum of $\frac{S}{D} = 0.16$) has no effect on propulsive efficiencies at least up to velocity ratios of 0.6. (Section 4.11 and in particular section 4.11.4 showed how, theoretically, power per unit thrust may be reduced, and therefore propulsive efficiency increased, by an increase in blade span or chord. It must be pointed out that these sections do not contradict the above findings of no change in propulsive efficiency with increase in blade span. This is because the expressions in section 4.11 do not assume constant velocity ratio for such improvements in power consumption. Thus, for a given fixed thrust force these expressions allow an increase in velocity ratio if the span is increased, so that in Fig.9.33 an increase in propulsive efficiency would be achieved by an increase in span by a movement to the right. The expressions of section 4.11 do not suggest therefore that the efficiency curves themselves move closer to the optimum value of efficiency for an increase in blade span.)

The following observation may be made: The standard wheel endplates (wheel labelled 6.5, see Appendix 4 for results) on the static and displacement modes shows a lower limit to the lift and thrust forces than the standard wheel does (see Fig.9.1 and 2). This is believed to indicate that in the static and displacement modes the mass supplied to the standard open ended wheel by gravity induced flow comes not only through the bottom of the wheel cavity but also through the sides. When the sideplates are present (as in wheel 6.5) the upper limit of the force is necessarily reduced.

In the planing mode, however, no mass supply comes through the sides of the wheel since it is all horizontally entrained, so the endplates no longer have any effect, and the forces are therefore the same as those of the standard wheel without endplates.

9.4.6 Effects of Blade Chord, c

There is little in the literature to assist in consideration of blade chord effects. This is probably because paddlewheels were not often operated with the inside or top edge of the blade immersed below the water level so that blade chord effects were hardly different than immersion depth effects. (1) Blade chord does become a more important consideration with the LPW. In the displacement mode the

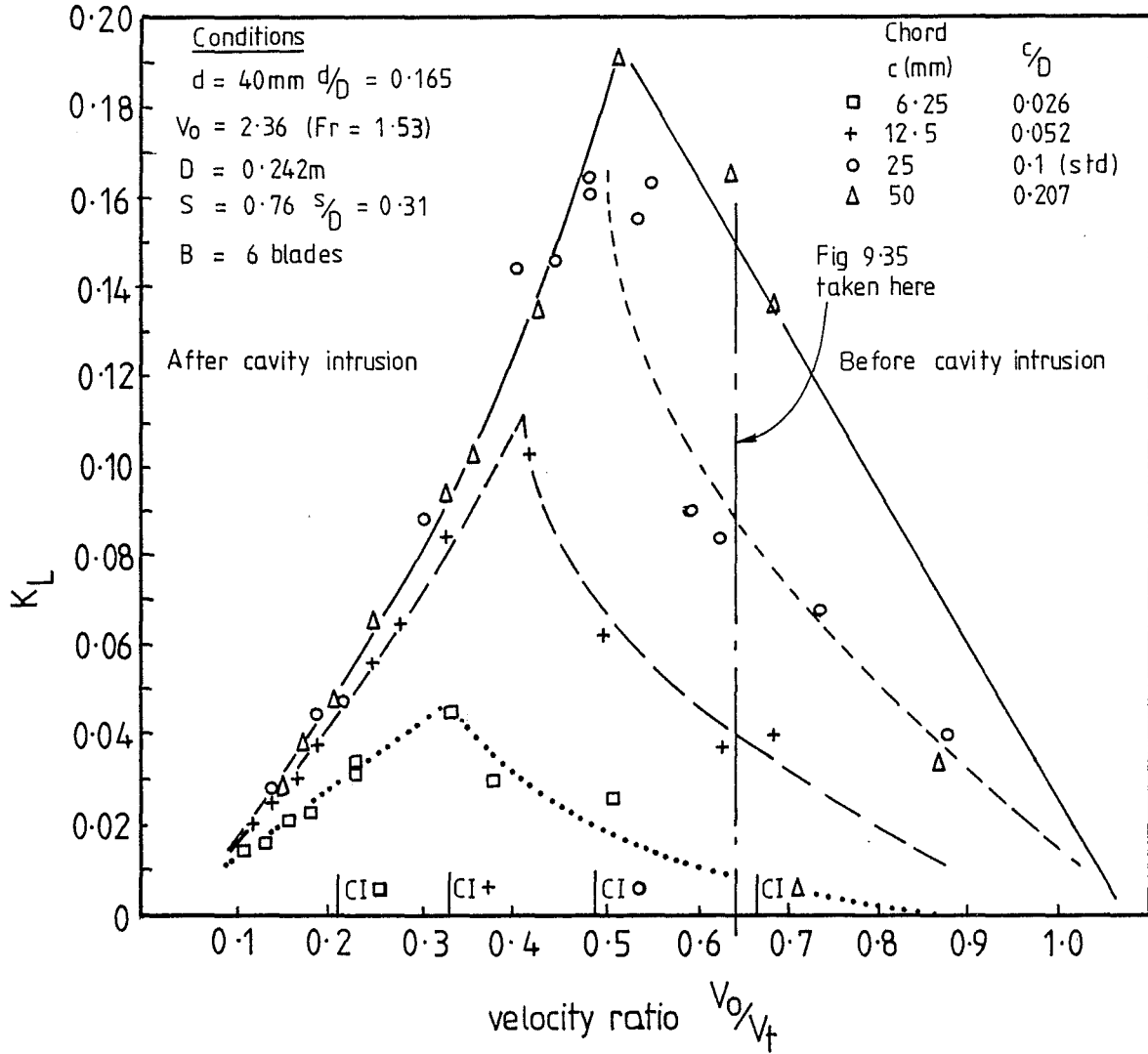


FIGURE 9.34: EFFECT OF BLADE CHORD ON LIFT COEFFICIENT

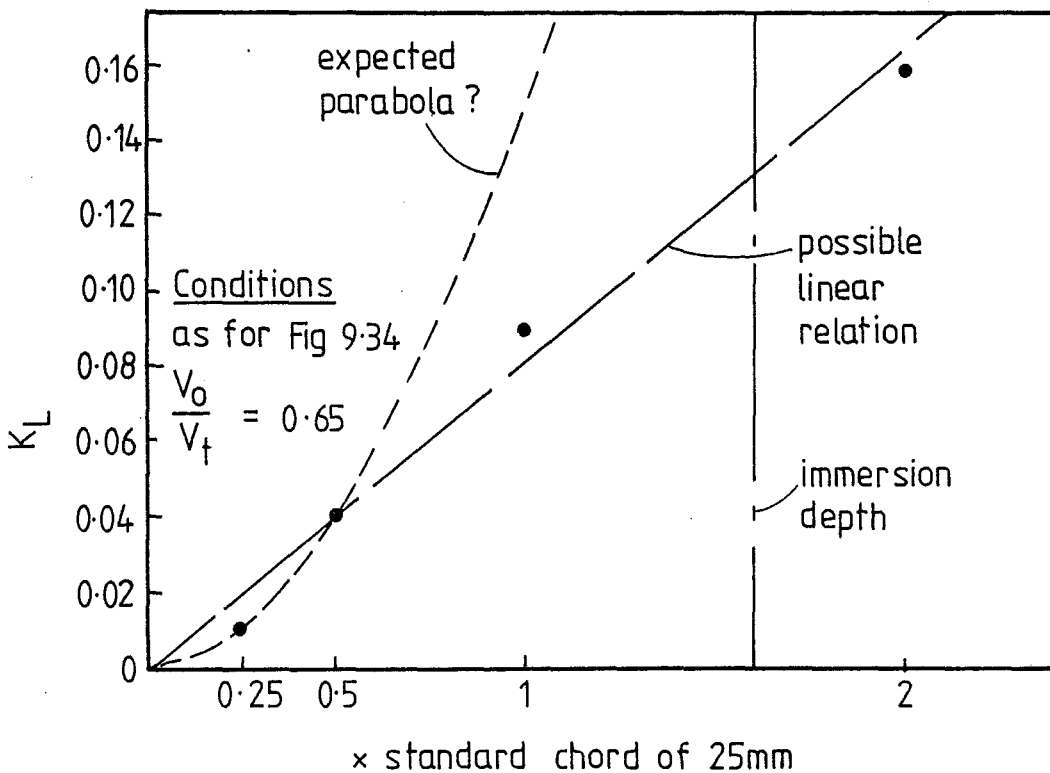


FIGURE 9.35: RELATIONSHIP BETWEEN K_L AND BLADE CHORD BEFORE CAVITY INTRUSION.

blades, set at an angle, may readily become fully immersed during their passage. In this case the immersed area of blade is important in determining the blade forces and this is proportional to blade chord. In the planing mode the blade chord has a different effect again. Before surface cavity intrusion the blade chord determines the volume of the induced mass per blade which is acted upon by the blade. By the impulse theory this induced mass, and hence the blade force is proportional to the square of the blade chord. This is given by relation 4.15 (section 4.5) for the induced mass per blade:

$$m' = \frac{\pi}{8} \rho c^2 s \quad (4.15), (9.2)$$

where m' = induced mass per blade at entry
 ρ = water density
 c = blade chord
 s = blade span.

Thus any increase in blade chord should dramatically increase the mass acted upon by the wheel, and so by section 4.11.3 reduce the power requirements for a given craft.

Offsetting this promising advantage, however, is the fact that the impulse theory assumed all the induced mass to be actuated at the blade tip, though, in fact, as the chord is increased the centre of mass of the induced mass per blade will move towards the wheel axis and therefore be on a smaller radius than before: (discussed in section 4.11.3 and Fig.4.27).

After surface cavity intrusion the impulse theory predicts that blade chord will have no effect on the induced mass since only the outer part of the blade meets the water surface at all. (See Fig.1.7(C) showing surface cavity intrusion.)

These factors have produced a complex picture of the supposed effects of blade chord, for comparison with the experimental results.

The LPW tests included a comparison of four blade chords: one quarter, half, one and two times the standard blade chord ($\frac{c}{D} = 0.026, 0.052, 0.013$ and 0.026). The results of these tests are plotted in the form of the 'K' lift coefficients against velocity ratio in Fig.9.34. This coefficient form contains no allowance for

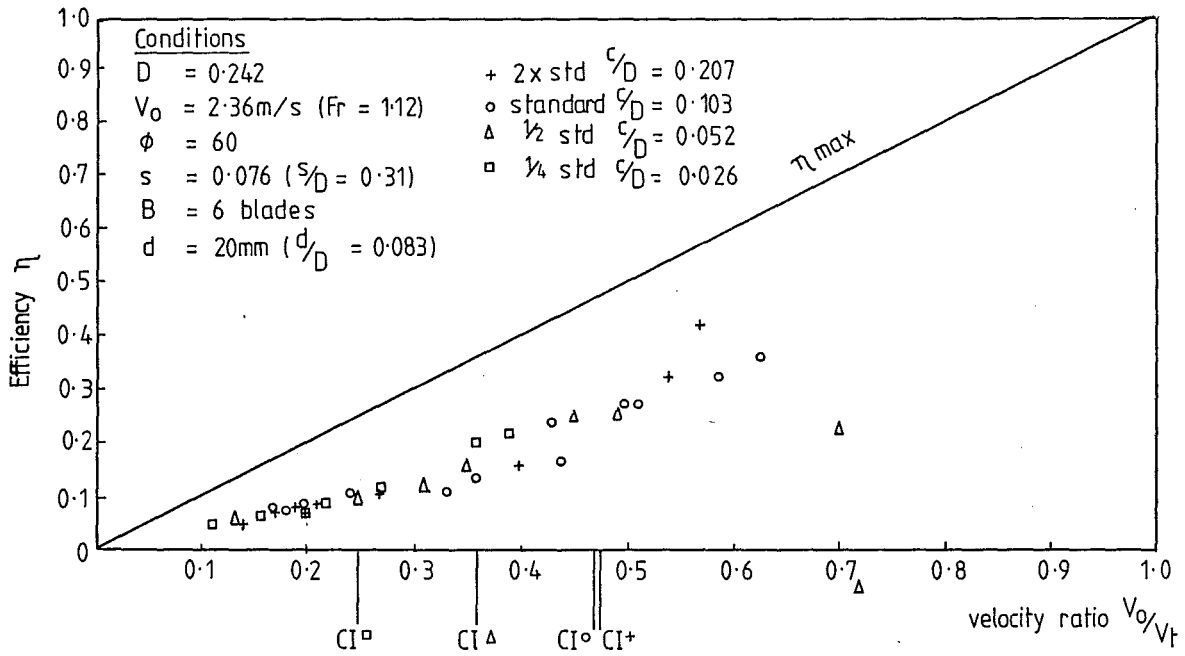


FIGURE 9.36 EFFICIENCY WITH BLADE CHORD: THERE ARE NO TRENDS WITH BLADE CHORD

variations in chord (as it does for blade span; see Table 9.16) so any variation with chord should show. The following points may be noted:

1) Before surface cavity intrusion (the right hand side) the coefficient values are strongly dependent upon blade chord. Fig.9.35 is a plot of this relationship, K_L vs c , from Fig.9.34 before cavity intrusion for $\frac{V_o}{V_t} = 0.64$. This point is marked on Fig.9.34. The relationship shown in Fig.9.35 is close to linear and cannot readily be fitted to a parabola as predicted by the impulse theory induced mass relation which is shown dotted in Fig.9.35. There are two possible explanations for this observed linear relationship between the 'K' coefficient and the chord c :

- (a) The proximity of the water surface, the assumption that all induced mass is located at the blade tip, the effects of splash, the fact that the blades do not enter the water parallel to the surface and other factors assumed for the induced mass in the impulse theory (section 4.5) may all combine to reduce the effect of and increase in blade chord.
- (b) The flat plate drag description of force generation may be more appropriate since in the flat plate drag equation, force (and hence the force coefficient) is linearly dependent upon blade chord, as shown in Fig.9.35, whereas in the impulse theory (expressions (4.23) and (4.25)) the force depends upon the square of the blade chord.

2) The impulse theory prediction (expression (4.27)) that after surface cavity intrusion the forces are independent of blade chord so that all the curves of Fig.9.34 should coincide, does not seem to hold. The fact that the curves for the two larger chord values ($\frac{c}{D} = 0.1$ and $\frac{c}{D} = 0.207$) seem to coincide is probably because the larger chord blades do not become fully immersed (immersion is $\frac{d}{D} = 0.165$ for a chord ratio of $\frac{c}{D} = 0.207$). At smaller blade chords there seems to be some relation between blade chord and force coefficient which appears less than linear. This suggests a rather more confusing situation than predicted by the impulse theory, and is as yet not understood.

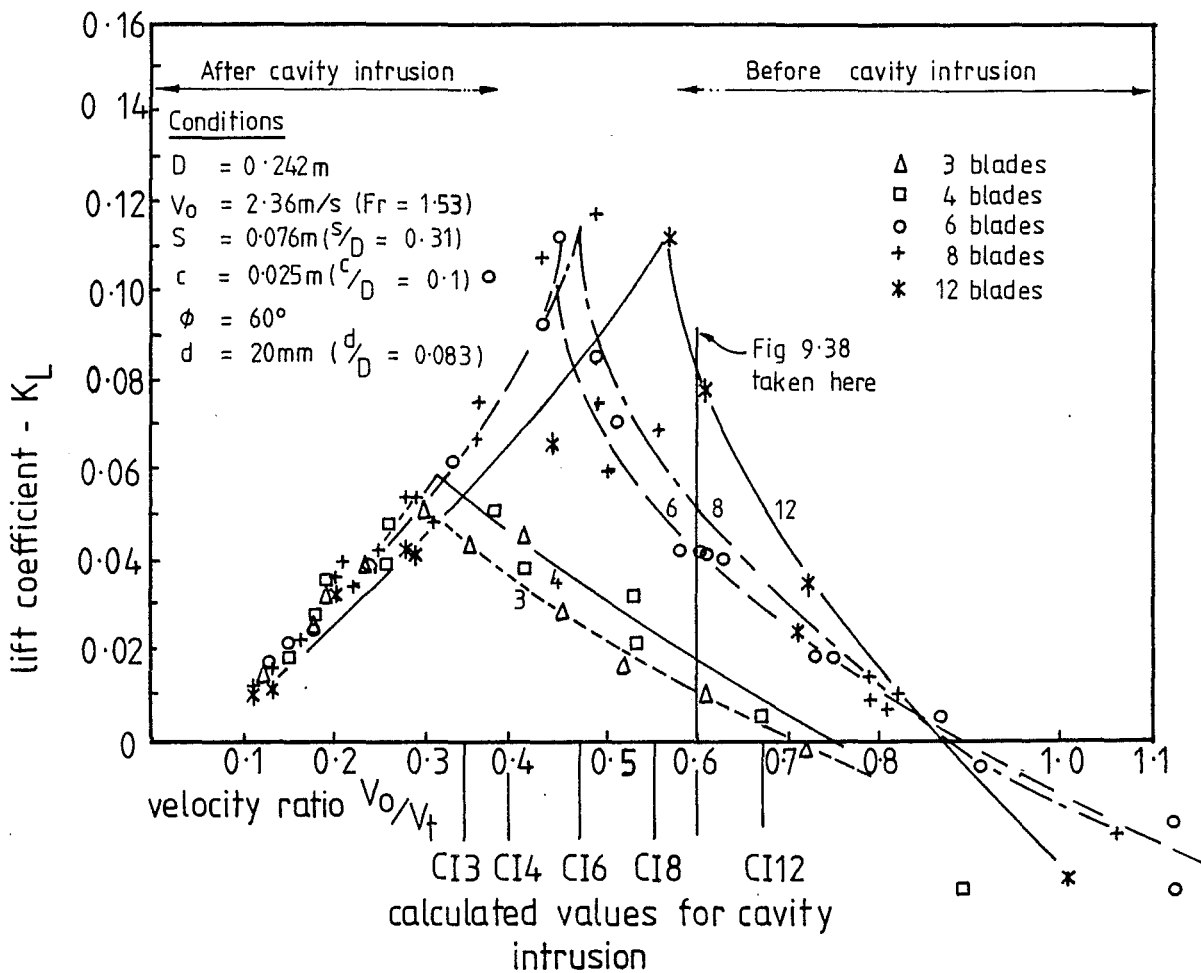


FIGURE 9-37: EFFECT OF THE NUMBER OF BLADES ON K_L .

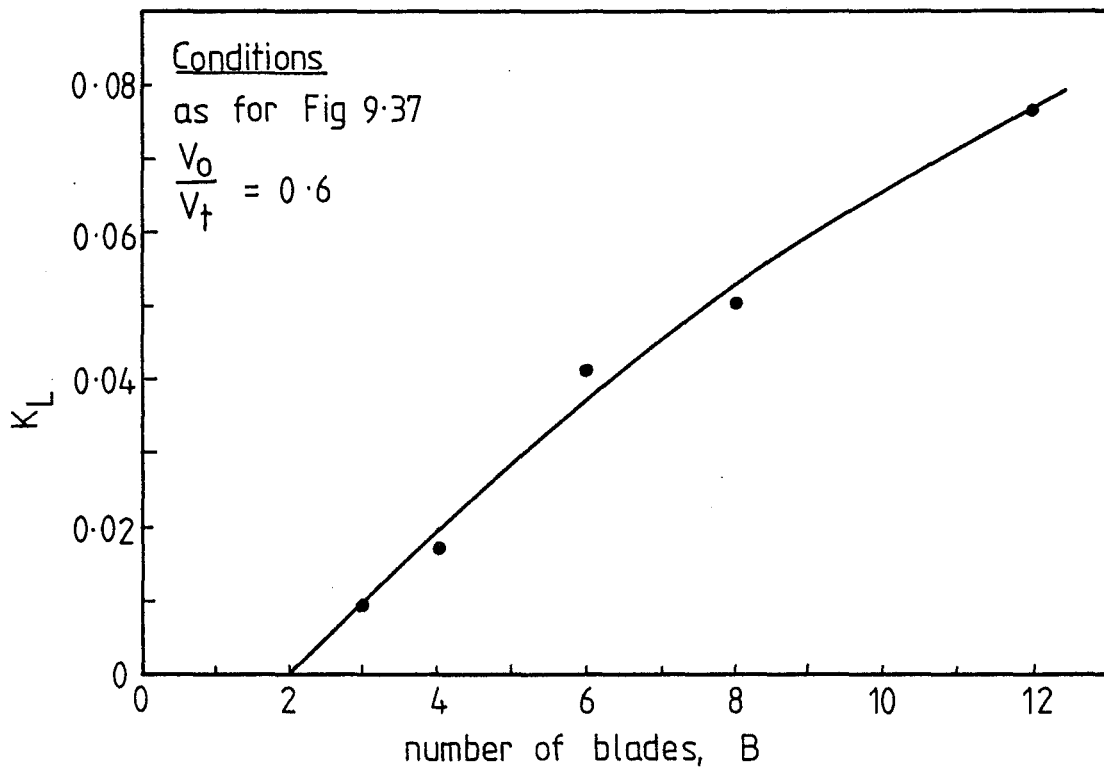


FIGURE 9-38: RELATIONSHIP BETWEEN K_L AND THE NUMBER OF BLADES BEFORE CAVITY INTRUSION.

3) Calculated values of surface cavity intrusion marked on the horizontal axis in Fig.9.34 coincide with the curve peaks only for medium blade chords, suggesting that the theoretical estimates of surface cavity intrusion begin to break down for very large and very small blade chords.

Efficiency would be expected to vary in much the same way with blade chord as with blade span, since an increase in both blade chord and blade span increase the mass acted upon per blade. The caution included regarding power reduction for increase in blade span in the last section (9.4.5) applies equally well to the case for the blade chord. It may be expected then, that an increase in blade chord would have no effect on propulsive efficiency as was the case with an increase of span.

A plot of propulsive efficiency with blade chord is given in Fig.9.36. Any variation of efficiency with blade chord is within the scatter of data points. This trend was the same for all immersion depths examined.

It can be concluded that while for small blade chords the forces may increase parabolically with chord increase as predicted by the impulse theory the general result is that before surface cavity intrusion an increase in chord causes a linear increase in force coefficient. After surface cavity intrusion an increase in chord causes a less-than-linear increase in force coefficients. The reasons for these effects are not yet clear.

Propulsive efficiency seems unaffected by changes in chord both before and after cavity intrusion, though careful analysis of the data indicates a possible advantage for smaller chords.

9.4.7 Effects of the Number of Blades, B

This variable has produced confusing results each time it has been examined, so that Beardsley concluded that the number of blades should be between six and twenty though the reasons for this were not clearly understood. (1) It is felt that much of the confusion was caused by the presence of the transition in some data, as well as the effects of cavity intrusion which takes place at different velocity ratios for different numbers of blades, thus making comparisons difficult.

Conditions

18" diameter
shaped blades

$$d/D = 0.088$$

$$\sqrt{\frac{nD}{gD}} = 0.58 = 2.7 \text{ rps}$$

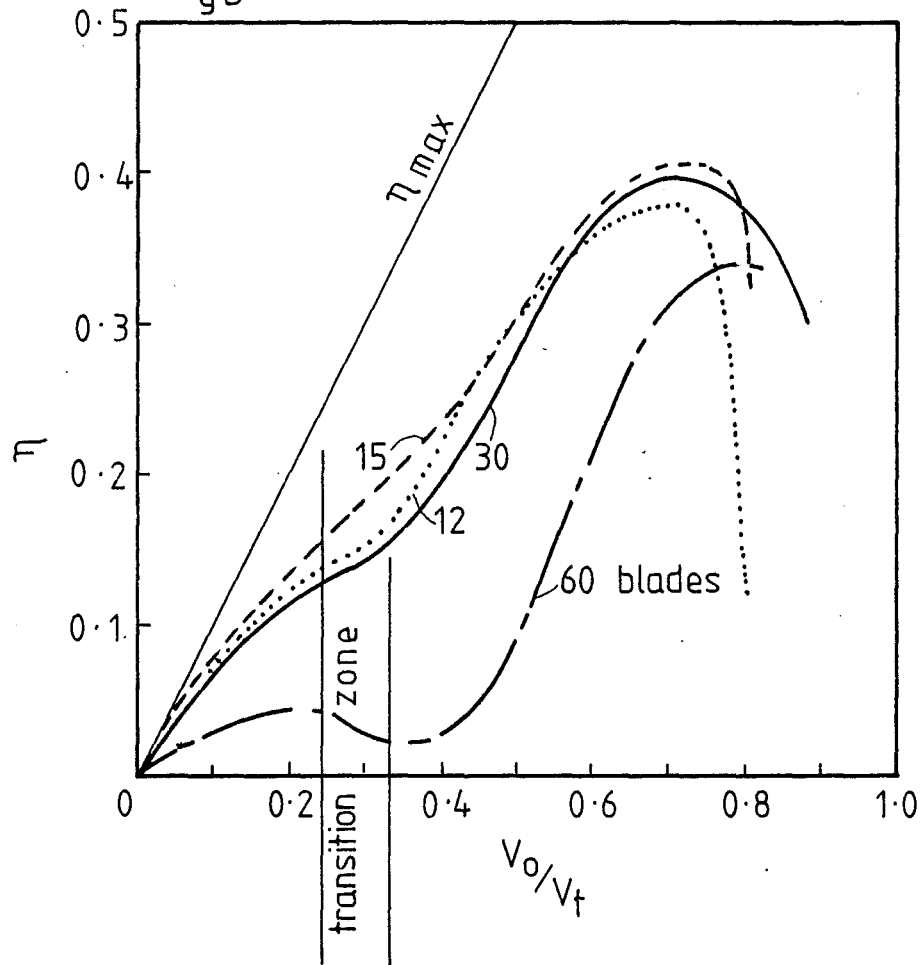


FIGURE 9.39 BEARDSLEY'S RESULTS FOR EFFICIENCY WITH VARYING NUMBERS OF BLADES.

(Beardsley P. 15)

The impulse theory predicts simply that before cavity intrusion the forces (and 'K' coefficients) should vary linearly with the number of blades: This is a result of the induced mass flow rate equation 4.16:

$$\dot{m} = \frac{\pi}{8} c^2 s \rho n B \quad (4.16), (9.3)$$

where B is the number of blades

which is part of the lift and thrust force equations, (4.23) and (4.25). After cavity intrusion the impulse theory suggests there should be no variation in force with the number of blades since all the entrained mass is acted upon by the blades, whatever the number.

The impulse theory itself makes no prediction for propulsive efficiency with the number of blades. Section 4.11.3 notes, however, that efficiency would be expected to be a maximum just before surface cavity intrusion, so that in as much as a change in the number of blades moves the point of operation towards this condition improvements in efficiency may occur. Section 4.14 notes that the larger the number of blades the more water is carried above the surface by them, the more rotational kinetic energy is left in the wake by them, and the greater their air drag. For these reasons a larger number of blades would be expected to give a lower efficiency.

The effect of the number of blades on the 'K' lift coefficient is shown in Fig.9.37. These points may be noted:

1) Before surface cavity intrusion the coefficients are almost linearly dependent upon the number of blades. This is essentially as predicted by the impulse theory: Fig.9.38 taken from Fig.9.37 at the point shown clarifies this relationship.

2) After surface cavity intrusion (to the left) the curves almost converge to a single line as predicted by the impulse theory. There seems to be some degradation in the lift force coefficients for the larger number of blades as would be expected of the lift coefficient if more water was thrown up by more blades.

3) The six and eight blade values before cavity intrusion seem to be somewhat higher than would be expected of a linear relationship. This is evident both in Fig.9.37 and in Fig.9.38 and

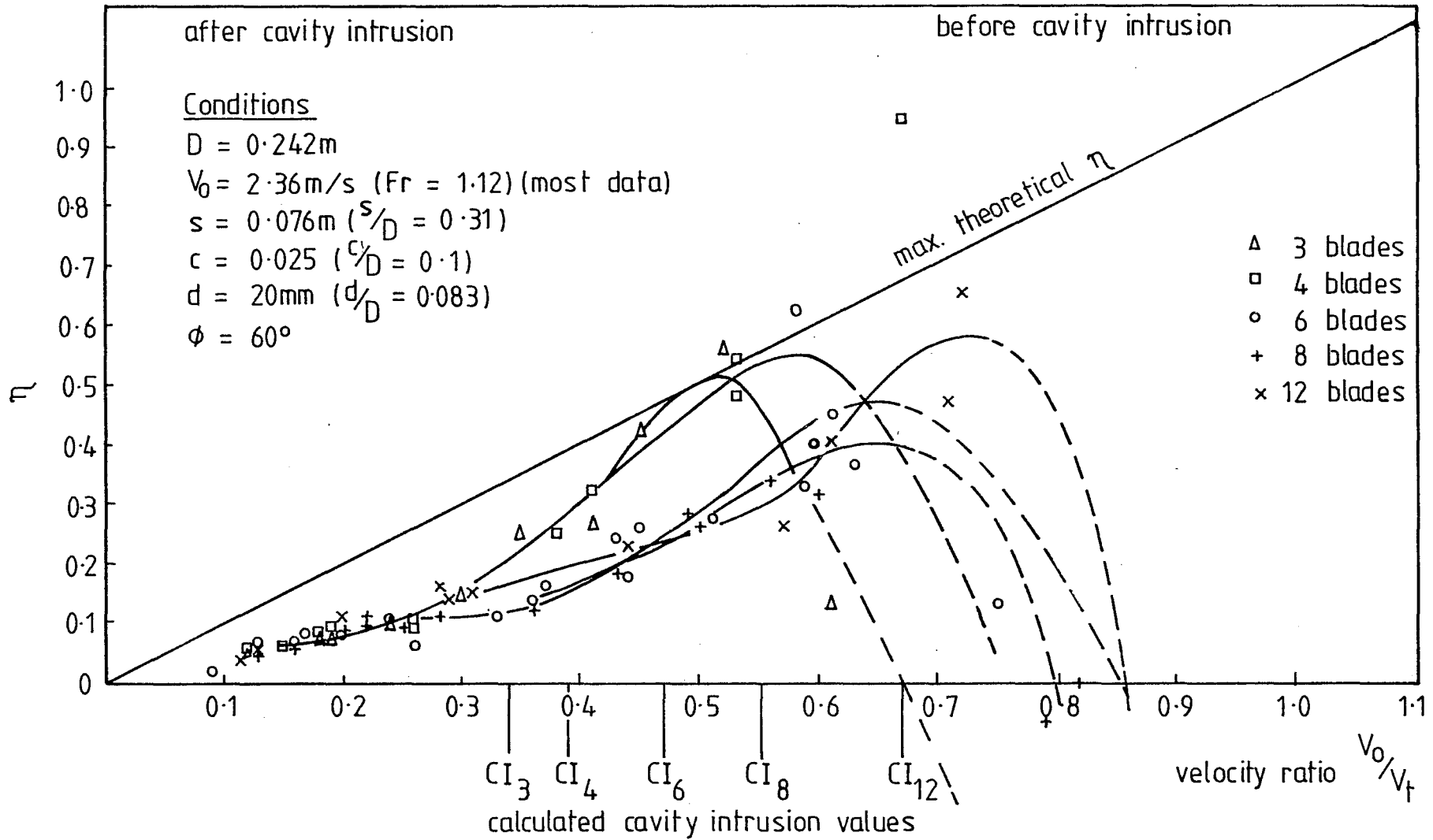


FIGURE 9.40 VARIATION OF EFFICIENCY WITH THE NUMBER OF BLADES

seems to suggest an optimum for lift force at these blade numbers. This is however only a marginal advantage and may in fact be only present in the test wheels.

4) The cavity intrusion values as calculated are close to, but do not exactly coincide with the peak lift coefficient values. This helps to support the analytical method for estimating surface cavity intrusion in regard to blade numbers.

The effects of the number of blades on propulsive efficiency were examined by Beardsley who used wheels with curved blades. His results are shown in Fig.9.39 where the lowest number of blades he tested was twelve. Unfortunately his results cover the transition zone as shown but the peaks of his curves are in the planing mode and therefore comparable with LPW results. It is difficult to estimate the equivalent of surface cavity intrusion for Beardsley's wheels because his blades were curved, but it is probable that the dip in the curve for the sixty-bladed wheel is largely such an effect.

The efficiency results for the LPW with varying blade numbers are given in Fig.9.40 where the immersion ratio is close to that of Beardsley's results in Fig.9.39. The following points may be made:

1) Unfortunately there are not enough data points at the high velocity ratio end of the plot to adequately define the efficiency peaks which exist there. As well as this the points in this region are scattered and unreliable: both of these factors are because the measurement forces and wheel rotational speeds were low under these conditions.

2) The calculated positions of surface cavity intrusion are marked on the plot and in all cases the efficiency curve peaks occur at a higher velocity ratio (lower wheel revolutions) than where cavity intrusion occurs (to the right of the cavity intrusion points in the plot). While this supports the assertion of section 4.14.3, that maximum efficiency should occur just before surface cavity intrusion some doubt is thrown on the relationship between these variables by the 3 blade efficiency peak, which seems to occur well before the calculated cavity intrusion point.

3) The larger the number of blades the further to the right (the higher the velocity ratio) the efficiency curves are taken. The peaks, however, do not approach the ideal efficiency as closely. These trends are both present in Beardsley's results in Fig.9.39.

4) After surface cavity intrusion the efficiency curves for all cases join into a single line with a value about half the ideal propulsive efficiency. (This value depends upon blade angle.)

5) Peak efficiency values compare well with Beardsley's peak values in Fig.9.39 even though the 60° blades of the LPW's were not intended solely for propulsion as were Beardsley's wheels, and the LPW's were half the diameter of Beardsley's wheels.

6) For the range of blade numbers tested both by Beardsley and in this project in Figs.9.39 and 9.40, the peak efficiencies occur between velocity ratios of 0.5 and 0.8; 12 or 15 blades would seem to give the greatest efficiency peaks at a velocity ratio of about 0.72, supporting Beardsley's assertion that paddlewheels should have between 12 and 20 blades. (1)

7) The six and eight blade LPW efficiency peaks seem to be low compared to the other results. It is not clear whether this is a real trend or simply a lack of reliable data points for these wheels.

8) While $\eta = 0.55$ is the maximum propulsive efficiency shown here, higher values were observed in the data for smaller immersion depths.

To conclude: the force coefficients were found to vary with the number of blades largely as predicted by the impulse theory while propulsive efficiency values showed the expected variation with surface cavity intrusion and gave maximum efficiency peaks for twelve (to fifteen) blades for the immersion depth examined.

9.4.8 Effects of Blade Angle, ϕ and Immersion Depth, d, θ

The blade angle variable is a pivotal component in the operation of the LPW, since it is this which divides the resultant wheel force into appropriate lift and thrust components. It is found to be intimately related to the immersion depth and the close relationship

between these factors has been discussed in terms of the thrust to lift ratio in section 4.10.1 and is examined later in this chapter in section 9.5. Here the relationship is examined from the broader perspective.

Very little is contained in the literature on blade angles, as such, though there is some discussion in terms of the angles of feathering blades. Volpich and Bridge hold that blades should be kept vertical during their passage for optimum performance, (1) and this assumption appears to be general in paddlewheel literature, on the grounds that the blades should enter and leave the water without excessive shock or splash. Results indicate that the feathering wheels give up to 10% better propulsive efficiency than radial wheels. (2) Barnaby notes that by contrast radial blades are "...wasting power by thrusting downwards at entry and upwards at exit." (3)

Immersion depth, on the other hand, has been examined more extensively and the general findings are summarised by Beardsley: "...greater blade immersion depth produces increased thrust and torque and lower maximum propulsive efficiencies." (4)

The LPW project has indicated both by theory and experiment that blade forces depend upon both blade angle and immersion depth. Fig. 4.24 showed this relationship for the theoretical wheel force, (section 4.10.3) and a similar figure produced from the experimental results is shown in Fig.9.41. As can be seen the vertical scales are in terms of the force divided by an induced mass flow rate, \dot{m} . In both the theoretical results in Fig.4.24 and the experimental results in Fig. 9.41 the same induced mass flow rate has been assumed, as that given by expression (4.16). In comparing the experimental and theoretical figures the following may be noted:

1) The experimental values are around one quarter of the theoretical values since the experimental mass flow rate is about four times as large as the theoretical one. This discrepancy has already been discussed (section 9.3.2) and is later dealt with using coefficients (section 9.9).

2) In spite of this the peaks of the experimental curves occur at the same angles as the peaks of the theoretical curves so

1. Volpich and Bridge, Pt.II, P.493 3. Barnaby, Art.176
 2. Volpich and Bridge, Pt.I, P.352 4. Beardsley, P.19

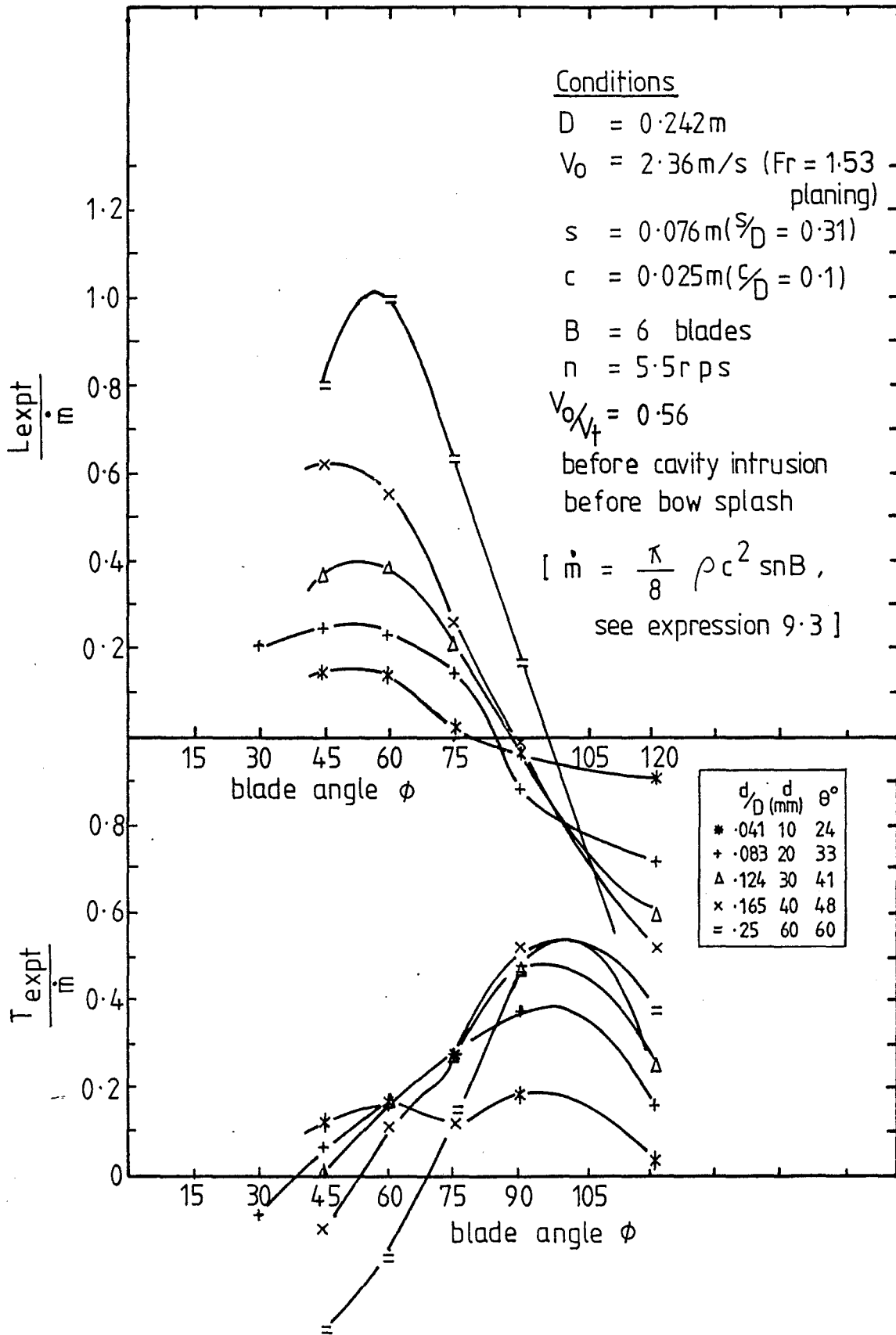


FIGURE 9.41: EXPERIMENTAL LIFT AND THRUST ENTRY FORCES WITH BLADE ANGLE ϕ

that theoretically and experimentally, maximum lift may be obtained for blade angles $\phi = 40^\circ$ to 60° and maximum thrust may be found between $\phi = 90^\circ$ and $\phi = 105^\circ$ for the velocity ratio of these results. (These peaks shift a little with changes in velocity ratio.)

3) For blade angles less than 60° the relation between the different immersion depths is the same for both theory and experiment, while for blade angles greater than 60° the experimental curves for both lift and thrust begin to fold over each other, and in the theoretical case they remain in their previous order. The two following points help to clarify why this might occur:

4) The impulse theory takes no account of blade exit forces. Certain conditions of blade exit would be expected to throw more water up than others; these would be large blade angles and deep immersions. From these considerations it would be expected that lift forces would be lower than those predicted by the impulse theory when blade angles and immersions are large. This is apparently what is occurring in the plot of the lift force in Fig.9.41 where at large blade angles the curves pass through zero earlier than they do in the theoretical curves of Fig.4.24. These exit forces would not be expected to influence the thrust forces.

5) The range of force variation with immersion depth is much greater in the experimental plot than in the theoretical. In the experimental results it appears that the magnitude of both the lift and thrust forces is more dependent upon immersion depth than in the theoretical results. A partial explanation for this is the fact that for the smaller immersion depths the blades will at no time during the passage become fully immersed. Thus it would be unreasonable to assume the same induced mass for small immersion depths than for the large. This assumption, however, has been made for Fig.9.41 because of the difficulty of accurately determining the induced mass of a partly immersed blade. The result of this is that the forces for the small immersion depths in the experimental results of Fig.9.41 appear smaller than they would, had this been taken into account. (See section 9.9.1 for a method of estimating this limited chord.)

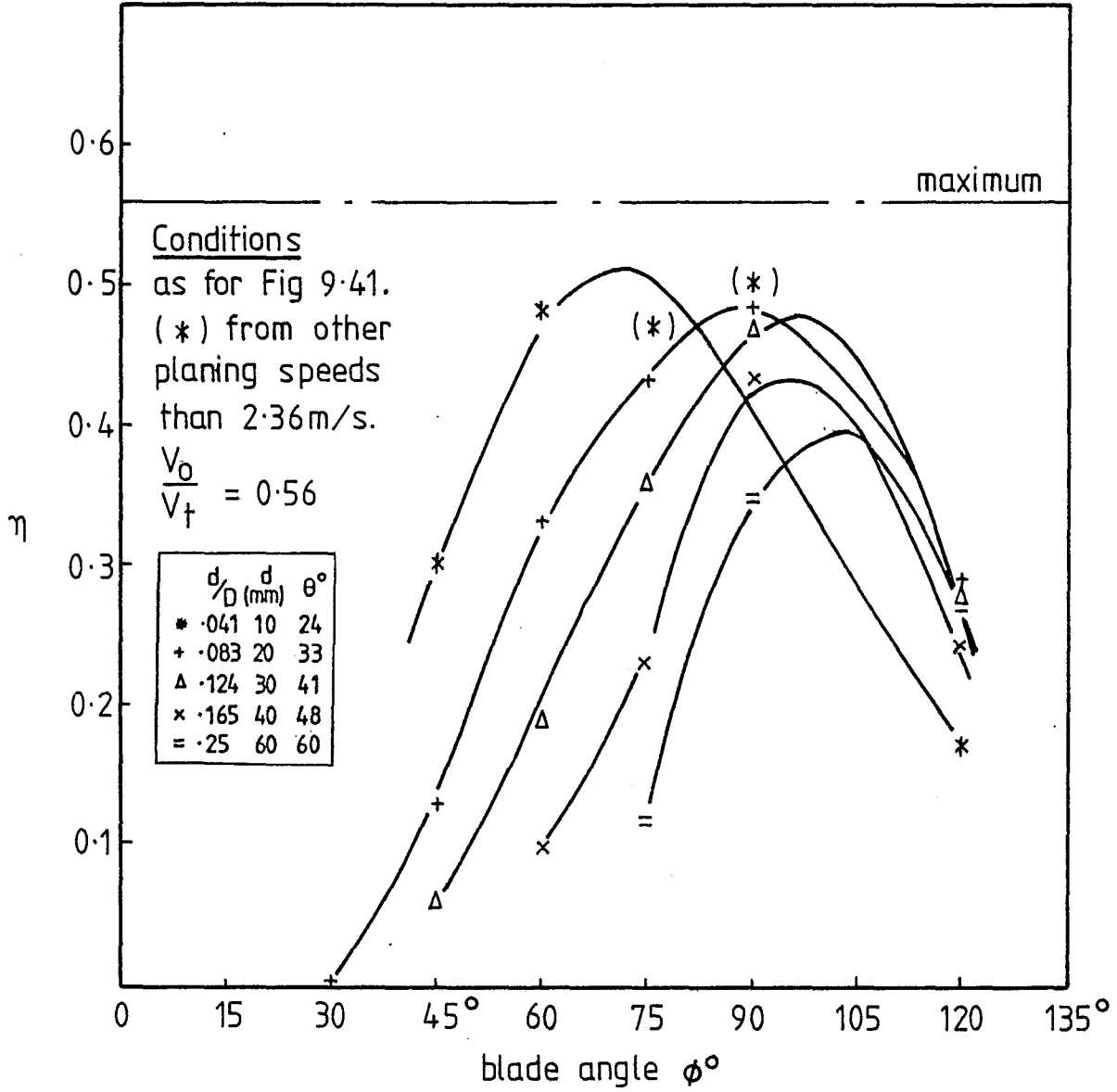


FIGURE 9.42 PROPULSIVE EFFICIENCY WITH BLADE ANGLE

6) For blade angles of $\phi = 90^\circ$, and over, the experimental thrust results indicate that thrust is dependent upon immersion depth. This confirms the general conclusion given by Beardsley when it is remembered that Beardsley's results, and those of most researchers will be for blade angles between $\phi = 90^\circ$ and 130° . (Beardsley's (1) were 120° , see Fig.2.9).

7) The theoretical results for thrust over $\phi = 90^\circ$ do not follow this trend with immersion depth. This seems to be related to the fact that the theoretical results are not as strongly related to immersion depth as the experimental results and in this case has the theoretical model contradicting the experimental results. Put another way a greater vertical spread of the thrust curves of Fig.4.24 would show such dependence of thrust upon immersion depth.

Appendix 4 contains data plots like those of Figs.9.1. 2 and 3, for blade angles of 45° , 75° , 90° and 120° , where the effects of blade angle may be compared to the results of the standard wheel ($\phi = 60^\circ$) in Figs.9.1, 2 and 3. The most notable feature of these results is that the lift force before cavity intrusion is almost non-existent when the blade angle is close to 90° . This is different than the theoretical prediction and is reflected later in the coefficient equations Fig.9.47(H).

In conclusion, then, the lift and thrust forces vary with immersion depth and blade angle to a large extent as predicted by the impulse theory, through both lift and thrust forces, in practice, show a stronger dependence upon immersion depth than that indicated by the theory; the lift forces are smaller at large immersion depths and large blade angles in experiment apparently because water is lifted out on blade exit under these conditions.

9.4.8.1 Propulsive Efficiency with Immersion Depth. Beardsley's finding of an inverse relationship between propulsive efficiency and immersion depth (see Fig.9.4) is supported by the LPW results for the planing mode almost without exception. The efficiency plots of Figs. 9.1, 2 and 3 are typical of LPW results, and Fig.9.42 shows the relationship with blade angle ϕ .

The reason for this inverse relationship with immersion is believed to be that at smaller immersion depths the blades move more nearly horizontally during their passage and are therefore not .."wasting power thrusting downwards at entry and upwards at exit."(1)

This finding suggests that for a given craft larger wheels immersed proportionally less would give an improved performance in terms of propulsive efficiency, while this would seem to be at the expense of lift force.

9.4.8.2 Propulsive Efficiency and Blade Angle. Propulsive efficiency for a velocity ratio of 0.56 is plotted against blade angle as shown in Fig.9.42 and the following noted:

1) Efficiency can be seen to have the inverse relationship with immersion discussed in the above section (section 9.4.8.1), though this relationship seems to become less distinct when the blade angle, ϕ , is greater than 90° .

2) Efficiency peaks for the immersion depths shown, occur when the blade angle is between 70° and 105° , suggesting 90° is an optimum value.

3) The fact that the efficiency value at the blade angle $\phi = 120^\circ$ and $\frac{d}{D} = 0.083(+)$ is less than the value for the same immersion depth for $\phi = 60^\circ$, seems to explain why the LPW results for $\phi = 60^\circ$ compare well with the efficiencies of Beardley's wheels designed specifically for propulsion, but which had blade angles of $\phi = 120^\circ$ at the tips. (See section 9.4.7 point 5, and Fig.2.9 showing Beardley's wheel. See also section 10.9.)

4) Since the velocity ratio has been fixed at 0.56 for this figure this is also the maximum theoretical efficiency as marked in the figure.

By way of conclusion it may be said that the LPW results show the expected decrease in efficiency with immersion as found by other researchers, while the LPW experiments have given a broader perspective to this finding by showing that the blade angle, also, has a strong influence on propulsive efficiency.

9.5 THE THRUST TO LIFT RATIO IN EXPERIMENT

One result deriving directly from the impulse theory was the simple but useful expression for the thrust to lift ratio as given by expression (4.31):

$$\frac{T}{L} = \tan (\phi - \theta)$$

where T = thrust force
 L = lift force
 ϕ = blade angle
 θ = depth angle.

This relationship is found to be present in the experimental results, which helps to confirm the emphasis on blade entry in the impulse theory and justifies the use of the expression (4.31) as a means for dealing with the relationship between the LPW forces. As predicted by the impulse theory, this relationship is found to exist for the planing LPW both before and after surface cavity intrusion.

The plot shown in Fig.9.43 was prepared from the standard wheel results, using also some results for the standard wheel at greater immersion depths. (These results are tabulated in Fig.7.3.)

The expected result is shown dotted and the two cases, before and after cavity intrusion have been drawn in as linear relationships. Several points may be made:

(1) Straight lines may justifiably be drawn through the clusters of data points in both cases though the data points are scattered, especially for the case before cavity intrusion where the forces are small. This generally confirms the expected linear relationship between the $\frac{T}{L}$ ratio and $\tan (\phi - \theta)$.

(2) The slope of both lines is somewhat at variance with the slope of the expected result, though the deviations are barely beyond the scatter of experimental points. These deviations become understandable if the relation is rewritten as follows :

$$\frac{T}{L} \cdot \frac{C_L}{C_T} = \tan (\phi - \theta)$$

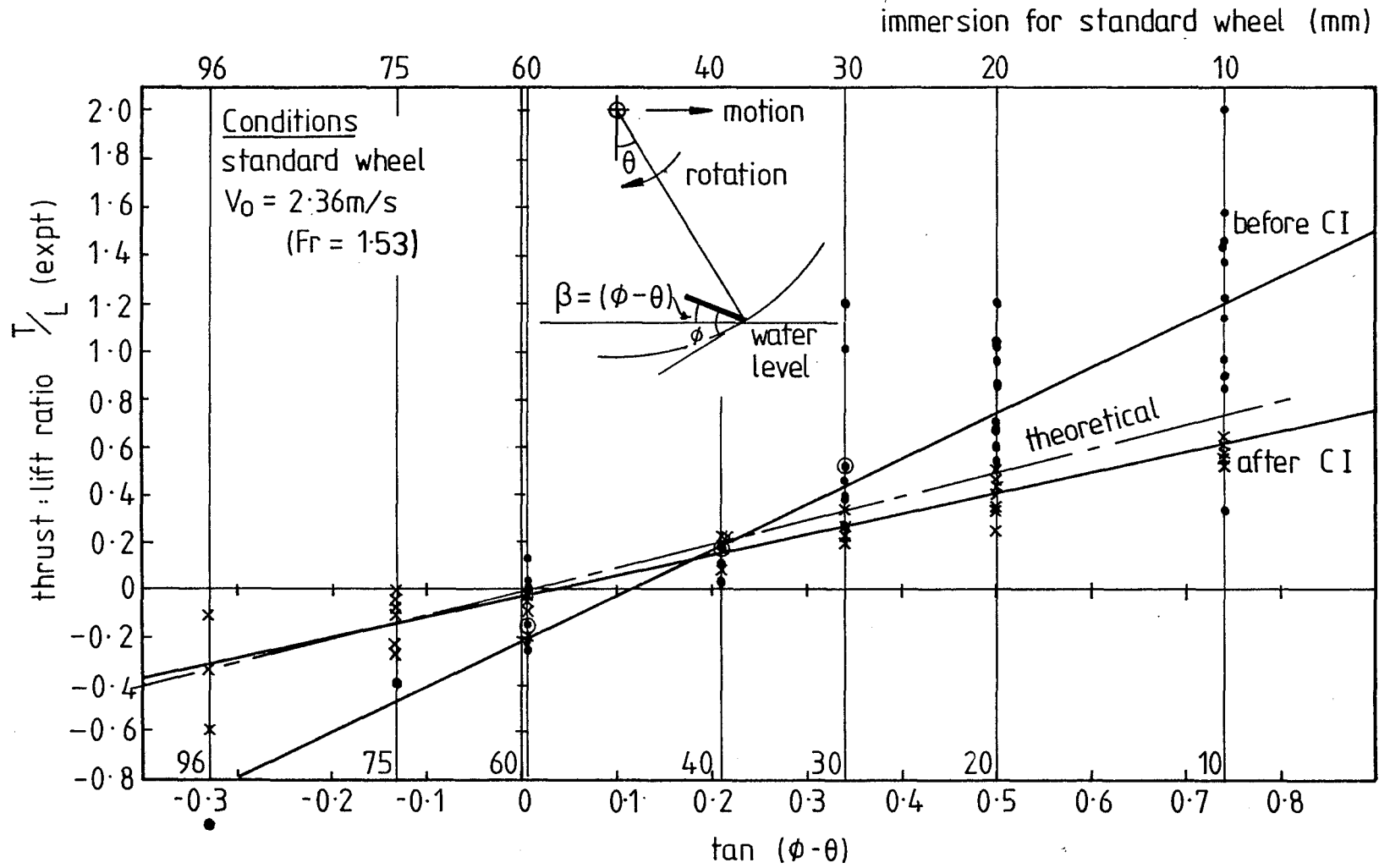


FIGURE 9.43 : EXPERIMENTAL THRUST TO LIFT RATIO AGAINST TAN β
TO TEST RELATION 4.31

where C_T = impulse theory thrust coefficient (section 9.9)

C_L = impulse theory lift coefficient.

It is apparent that the deviation of slope from the expected, for the two cases, is because $C_T \neq C_L$.

(3) Both lines, as drawn, fail to pass through the origin. The scatter of points, however, just allows both lines to be drawn through the origin within the uncertainty of the figure. It remains unclear as to whether this trend is really a deviation from the theoretical relationship.

Thus with some reserve regarding this final point, the thrust to lift relationship as proposed by the theory is found to hold in the experimental results.

9.6 WINDAGE LOSSES WITH LPW'S

The windage losses associated with the LPW have been treated in two separate ways:

- 1) Rotational air drag of the LPW's in still air which absorbs some of the wheel torque;
- 2) Frontal drag of the rotating LPW's, which increases the drag of the LPW craft.

To determine the first of these, a brief set of experiments was conducted during the final debriefing of the force balance. The coefficient used for this, KP_w was discussed, in theory, in section 4.13.2. The ideal test to determine such a coefficient would involve moving the rotating wheel at the required speed of advance through air while appropriately shielding the "immersed" lower portion. Torque measurements would then be made. Proper measurements of this sort could not be readily made at the Kainga testing tank because the LPW was in the air wake of the Rating Car and it was not seen as important enough to set the equipment up specially for such tests. Instead the force balance was mounted on the bench and the wheel rotated in the open, clear of obstacles, and torque measurements made over a range of wheel revolutions. The results obtained were expected only to give an estimate of these losses.

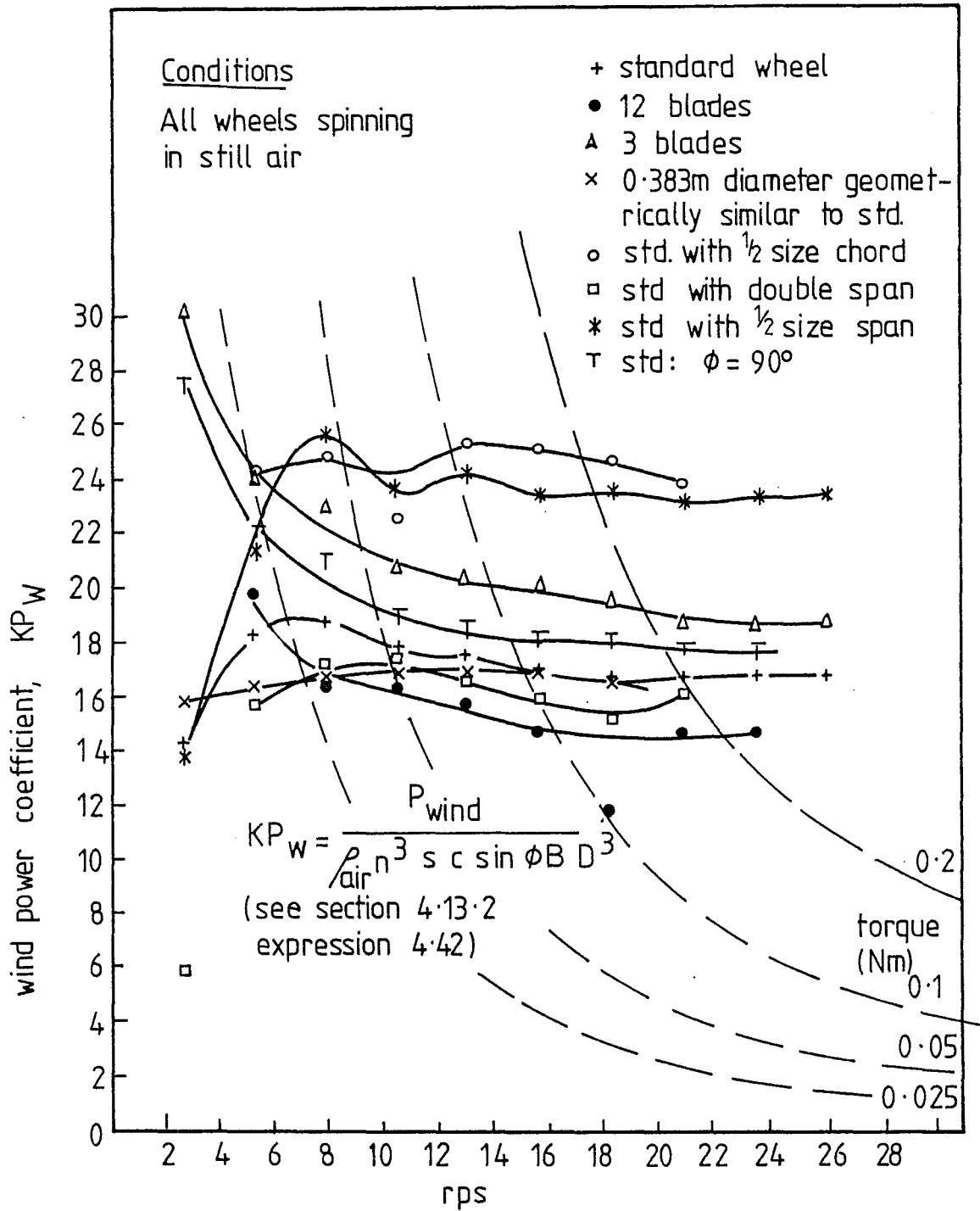


FIGURE 9.44 WIND POWER COEFFICIENT WITH A CROSS SECTION OF LPW VARIABLES: n, ϕ, B, D, s, c

From the measurements of torque, the windage power coefficient, KP_w , was calculated and the results were plotted in Fig.9.44 against wheel revolutions. The following may be noted:

1) The actual torque magnitudes were 0-0.5 Nm often being at the bottom limits of the resolution of the torque sensor, so that where the torque was especially small (as at low wheel revolutions) the results contained considerable scatter.

2) For blade chords less than $0.1D$ and blade spans less than $0.3D$ KP_w increases from the general grouping of other results. (These same reduced span and chord dimensions cause degradation in the LPW forces, as discussed in sections 9.4.5 and 0.4.6).

3) There is a small dependence of KP_w upon the number of blades, B .

Although these small deviations exist it seems that for wheels likely to be used a reasonable estimate for $KP_w = 16.0 \pm 1.5$.

The second windage loss to LPW's is that of frontal drag associated with a rotating wheel in a moving air stream. A single exploratory test was undertaken to determine the worth of undertaking more extensive tests, with the result that the rotating LPW frontal drag may be treated simply with known drag coefficients.

For this test a model craft LPW was held in the chuck of an electric drill which was mounted on the wind tunnel balance in such a way that the wheel axis was perpendicular to the air flow, and the wheel rim just cleared the tunnel floor. The drag of the drill and rotating LPW was determined, and the drag of the running drill without the LPW was subtracted from it. Interference between the drill and the wheel was neglected. The small wheel used ($D = 0.152$ m) had a Reynolds Number of 9.2×10^4 for the conditions of the test, and the resulting drag coefficient value was $C_D = 0.14$. This drag coefficient value is found to be very close to drag coefficient values for equivalently short cylinders, with surface roughness, in flow of the same Reynolds Number. (1)

It was found that beyond a certain minimum value the speed of rotation had only a marginal effect on the drag force.

It seems, then, that the frontal drag of the rotating LPW may be treated as that of the equivalent, rough cylinder and the drag coefficient for all expected speeds and sizes of LPW's will probably be close to $C_D = 0.14$.

9.7 SPRAY FORCES AND LOSSES

Under some conditions the LPW throws up a large plume of spray. This generally occurs at low velocity ratios when the wheel is spinning fast. No measurements of the amount of water lifted as spray by the LPW was attempted during the tank tests. Subsequent model LPW craft tests, however, have indicated that such spray can give significant additional lift forces if it is redirected by spray guards. These extra lift forces generally occur before the model has lifted off and the wheels are turning fast relative to the water. There seems also to be a significant drag force introduced to the model craft as the spray strikes its spray guards.

One observation made during the tank tests indicates the magnitude of spray forces. The splash guard shown in Fig.5.29 was occasionally lifted by spray under high speed operating conditions. This box could be pivoted about its forward attachment to the Rating Car, by a force of 11.5 N applied at its rear edge. The spray thrown up inside the box by the enclosed LPW must have exerted forces exceeding this value. Since LPW lift forces were rarely over 20 N this suggests that under some conditions LPW spray may be employed to give an additional lift force against suitable spray deflectors of about 50% of the normal lift given by the LPW.

It should be pointed out, however, that in normal high speed operation the model LPW craft made very little spray.

9.8 POWER ESTIMATES AND MEASUREMENTS

An attempt was made in the theory section 4.14 to make out a power budget for the LPW, by estimating where its power was consumed. This total power estimate, given in expression (4.43), is repeated below. In this expression all the factors, bar one, could be assessed, the remaining term for power lost to spray has yet to be estimated.

$$P_i = P_T + P_{\text{lost}} + P_L + P_w + P_{\text{spray}} + P_{\text{rot}} \quad (4.43) \cdot (9.4)$$

where P_i = total input power
 P_T = thrust power, for propulsion
 P_{lost} = horizontal kinetic energy left in wake
 P_L = power required for lift
 P_w = rotational windage loss
 P_{spray} = power lost in energy of spray
 P_{rot} = power left as rotational KE in water

Evaluation of each term in this relation is found to depend strongly upon the magnitude of the LPW forces involved. For example the lift power as given by expression (4.41) was:

$$P_L = \frac{L^2}{2 \dot{m}} \quad (4.41), (9.5)$$

It has already been noted that the lift force found by experiment is about three times as great as the theoretical lift force (section 9.3.2, and section 4.8) and this is allowed for by a coefficient primarily attached to the induced mass flow rate, \dot{m} . Thus the lift force equation (expression (4.11)) is modified to:

$$L_{\text{expt}} = V_v (\dot{m} C_L)$$

where V_v = vertical velocity change in the water
 L_{expt} = lift force by experiment
 C_L = induced mass coefficient for lift or impulse theory lift coefficient.

(This is described more fully in section 9.9).

Any realistic estimate of the lift power, P_L , should include the experimental values for lift and induced mass flow rate, so that expression (9.5) becomes

$$P_L = \frac{(L_{\text{expt}})^2}{2 \dot{m} C_L} \quad (9.6)$$

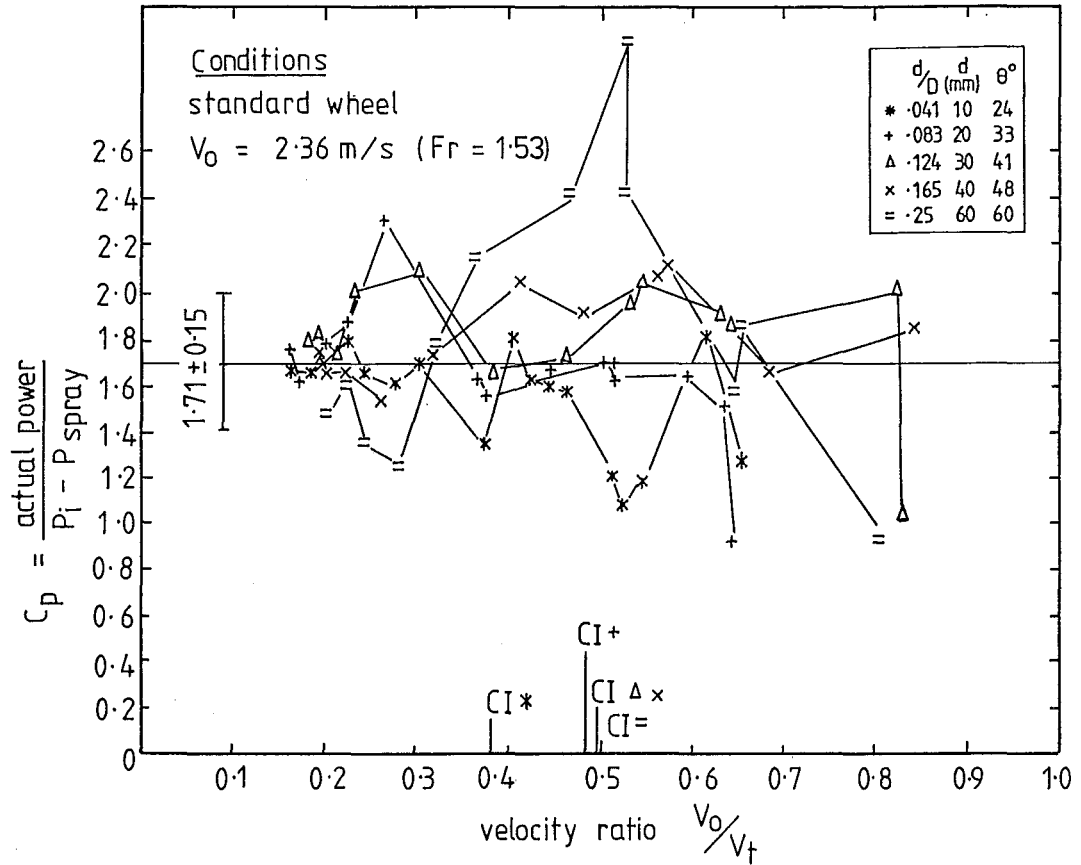


FIGURE 9:45: ACTUAL POWER/CALIBRATED POWER, OVER THE VELOCITY RATIO RANGE FOR THE STANDARD WHEEL IN THE PLANING MODE

and since $L_{\text{expt}} = C_L \cdot L_{\text{theory}}$ this may be rewritten:

$$P_L = \frac{(L_{\text{theory}})^2 C_L}{2 \dot{m}}$$

where L_{expt} = experimental lift force
 L_{theory} = $V_v \cdot \dot{m}$ by expression (4.11)
 \dot{m} = induced mass flow rate
 C_L = impulse theory lift coefficient attached to \dot{m}
 P_L = power used in lift.

The same sort of procedure may be used to find the values of the forces and induced mass flow rates in each of the terms in the expression for input power, P_i , above (expression (9.4)); except for the P_{spray} term. The other terms in expression (9.4) may be listed:

$$P_T = T_{\text{expt}} V_o \quad (\text{from (4.32)})$$

$$P_{\text{lost}} = \frac{(T_{\text{expt}})^2}{2 \dot{m} C_T} \quad (\text{from (4.33)})$$

$$P_w = 16.0 (nD)^3 S c \sin\phi B \quad (\text{from (4.42), and section 9.6})$$

$$P_{\text{rot}} = 0.345 C_L \dot{m} n^2 c^2 \quad (\text{from section 4.13.3), (9.7)}$$

In order to test the power estimate given by expression (9.4) the coefficient computer programme (see section 9.9.3) was run for the standard wheel in the planing mode and the total input power P_i less the value lost to spray, P_{spray} , was calculated using the above expressions. The resulting value was then compared with the actual experimental power, in a ratio denoted C_p . Thus:

$$C_p = \frac{\text{Actual Power}}{P_i - P_{\text{spray}}} \quad (9.8)$$

The results of this comparison are shown in Fig.9.45 which contains the data for the standard wheel only. These points may be made:

- 1) A mean value for C_p is about 1.7 and this value seems to hold up to high velocity ratios (0.8) where the scatter of data points makes it difficult to estimate.
- 2) There is some inverse dependence of C_p with immersion depth, this being more pronounced at higher velocity ratios.
- 3) Brief examination of other blade variables suggests that this value for C_p is general, though for low planing speeds ($F_x = 0.85$ to 1) it is a little higher, at 1.9, and at larger diameters it is probably lower perhaps even approaching 1.0 when D exceeds 0.5 m.
- 4) The figure indicates that the proportion of the total LPW power lost to spray as well as other undetermined losses, amounts to between 60 and 100% more than the power consumed by the known mechanisms. While this is a large proportion to be unaccounted for, it is felt that at this stage of LPW development this is not unreasonable.
- 5) It is doubtful that there is any merit in finding values of C_p for other LPW variables since the value found above is already dependent upon the coefficient equations and the theoretical model, both of which contain uncertainties. It is felt, therefore, that this value for C_p is best left as a general adjustment to the power estimates, keeping in mind that discrepancies with scaling are likely to be on the conservative side (see section 9.4.4).

The main value of the result shown in Fig.9.45 is that, given the impulse theory and the impulse theory "C" coefficients the power consumed by the LPW may be calculated with sufficient reliability to be used in design calculations, without further recourse to the experimental results.

9.9 THE COEFFICIENT EQUATIONS

The impulse theory of LPW forces developed in section 4.7 does not give the actual forces found by experiment. For this reason the impulse theory "C" coefficients have been developed to modify the impulse theory forces to represent those found in the real situation.

In the basic force equations, for example the equation (4.11) for the lift force:

$$L = \dot{m} V_v \quad (4.11)$$

the coefficient has been imagined as applying to the induced mass flow rate, \dot{m} , (as discussed in section 4.8) so that the equation for the lift force found by experiment becomes:

$$L_{\text{expt}} = C_{1L} \dot{m} V_v \quad (9.9)$$

where C_{1L} = impulse theory lift coefficient, before C.I.

\dot{m} = induced mass flow rate

V_v = vertical component of maximum perpendicular velocity.

Two distinct approaches are contained in the impulse theory of section 4.7, one for the conditions before, and the other, after surface cavity intrusion. Since these two approaches have widely different ways of estimating the induced mass flow rate they also have different coefficients. Coefficients before cavity intrusion are denoted " C_1 " and after cavity intrusion they are denoted " C_2 ". The appropriate coefficients can only be used once it is known whether the LPW is operating before or after surface cavity intrusion (cavity intrusion estimation is outlined in section 4.9.3).

Close comparison of the experimental forces and the impulse theory forces showed that these induced mass " C " coefficients are slightly different for lift and thrust forces, and vary to some extent with each of the many LPW variables. While this makes it clear that the impulse theory, as it stands, does not give a complete picture of LPW forces, it can be employed for design calculations if these coefficients are known.

Some time was spent, then, in determining coefficient values for each of the LPW variables using the computer programme described later in this section (section 9.9.3). Consequently the force coefficients, such as C_{1L} above, have been found to be the product of a number of functions, each one representing the amount the LPW force varies from theory with the variable concerned. Thus, employing the notation used in the computer programmes the lift coefficient before cavity intrusion C_{1L} , may be expressed:

$$C_{lL} = SF1.CF1.BF1L.dF2.RPS1L.VOF1.DIAF1.\phi F1L \quad (9.10)$$

This expression has been termed the lift coefficient equation. Each of the terms in this equation represents a simple function which indicates how the lift force differs from the theory with that variable. For example SF1 is given by the function:

$$SF1 = (3.18 s/D)^{0.8} \quad (9.11)$$

where SF1 = span function before cavity intrusion
 s = span of blades
 D = wheel diameter.

The terms in expression 9.10 (such as expression 9.11) have been called the variable functions. They are given in full in Table 9.46(B) with their notation, as well as the variable functions for all the other coefficient equations used. For further clarification, the variable functions have been plotted in Fig.9.47 (A)-(Q) and are described more fully in section 9.9.2.

There is a similar expression to the lift coefficient equation (9.10), for thrust before cavity intrusion, one for both the lift and thrust after cavity intrusion, and two further coefficient equations apply to the case when immersion depth is less than 0.1D before cavity intrusion. This makes six coefficient equations in all, as shown in Table 9.46 (A).

In this project most design calculations for the LPW craft have been performed by computer (Programme 'LPWCRAFT' described in section 13.6 and listed in Appendix 7) and it has been a relatively simple matter to incorporate the coefficient equations and their various terms into the programmes as they stand in Table 9.46. For hand computation of LPW forces, however, the values of these coefficient equations may best be established by reference to the plotted values of each of the terms in Fig.9.47. (Appendix 6 contains a worked example of LPW force calculations.)

9.9.1 Limited Chord at Small Immersion Depths

Before the coefficient equations can be used, special considerations need to be given to the blade chord.

TABLE 9.46 (A)THE COEFFICIENT EQUATIONS

Before surface cavity intrusion; depth ratios greater than 0.042:

$$\text{Lift:} \quad C_{1L} = SF_1 \cdot CF_1 \cdot BF_{1L} \cdot dF_1 \cdot RPS_{1L} \cdot VOF_1 \cdot DIAF_1 \cdot \phi_{F1L}$$

$$\text{Thrust:} \quad C_{1T} = SF_1 \cdot CF_1 \cdot BF_{1T} \cdot dF_1 \cdot RPS_{1T} \cdot VOF_1 \cdot DIAF_1 \cdot \phi_{F1T}$$

Before surface cavity intrusion with depth ratios less than 0.042:

$$\text{Lift:} \quad C_{10L} = SF_1 \cdot CF_1 \cdot BF_{1L} \cdot dF_1 \cdot \underline{RPS_{10L}} \cdot VOF_1 \cdot DIAF_1 \cdot \phi_{F1L}$$

$$\text{Thrust:} \quad C_{10T} = SF_1 \cdot CF_1 \cdot BF_{1T} \cdot dF_1 \cdot \underline{RPS_{10T}} \cdot VOF_1 \cdot DIAF_1 \cdot \phi_{F1T}$$

After surface cavity intrusion:

$$\text{Lift:} \quad C_{2L} = SF_2 \cdot CF_2 \cdot BF_2 \cdot dF_2 \cdot RPS_{2L} \cdot VOF_2 \cdot DIAF_2 \cdot \phi_{F2L}$$

$$\text{Thrust:} \quad C_{2T} = SF_2 \cdot CF_2 \cdot BF_2 \cdot dF_2 \cdot RPS_{2T} \cdot VOF_2 \cdot DIAF_2 \cdot \phi_{F2T}$$

TABLE 9.46 (B)

THE VARIABLE FUNCTIONS

(These are depicted in graphical form in Fig.9.47 A-Q)

(A) SPAN FUNCTIONS

$$SF1 = (3.18s/D)^{0.8}$$

$$SF2 = \sqrt{3.18s/D}$$

$$\text{If } s/c > 3 \quad SF2 = 1.0$$

(B) CHORD FUNCTIONS

$$CF1 = (D/(0.1c_{lim}))^{0.3}$$

$$\text{If } c_{lim}/D \geq 0.1 \quad CF1 = 1.0$$

$$CF2 = (10c/D)^{0.33}$$

$$\text{If } c/D \geq 0.103 \quad CF2 = (D/10c)^{0.13}$$

(C) BLADE NUMBER FUNCTIONS

$$BF1L = X \cdot B^{0.28}$$

$$BF1T = X/B^{0.62}$$

$$BF2 = X/B^{0.25}$$

$$\text{where } X = (27.0/(B^2 + 25)) \sin^2(\pi(B-3)/14) + 0.8$$

(D) IMMERSION DEPTH FUNCTIONS

$$dF1 = (d/D)^{0.6}$$

$$(E) \quad dF2 = (D/d)^{0.667}$$

(F) VELOCITY FUNCTIONS

$$VOF1 = (\sqrt{gD}/V_0)^{0.07}$$

$$VOF2 = (V_0/\sqrt{gD})^{0.21}$$

(G) DIAMETER FUNCTIONS

$$DIAF1 = 1.0$$

$$DIAF2 = D^{0.12}$$

TABLE 9.46(B) cont'd.

(H) BLADE ANGLE FUNCTIONS *

$$\phi_{F1L} = \phi^{0.15} \sin 2\phi$$

$$\phi_{F1T} = \phi^{-0.25} (1.0 + \cos^2 2\phi)$$

$$(J) \quad \phi_{F2L} = \phi^{-0.25}$$

$$\phi_{F2T} = \phi^{-0.25} (0.9 + 0.6 \cos^2 2\phi)$$

WHEEL REVOLUTION FUNCTIONS

$$(K) \quad RPS1L = 6.524 (V_t/V_o - 0.843)$$

$$(M) \quad RPS1T = 26.31 (V_t/V_o - 0.843)$$

$$(N) \quad RPS10L = 27.93 (V_t/V_o - 1.299)$$

$$(P) \quad RPS10T = 136.74 (V_t/V_o - 1.299)$$

$$(Q) \quad RPS2L = 0.04934 (1.0 + 5.401 V_o/V_t)$$

$$RPS2T = 0.03854 (1.0 + 5.511 V_o/V_t)$$

- Notation: ...1... Before surface cavity intrusion
 ...2... After surface cavity intrusion
 ...10... Before surface cavity intrusion, $\frac{d}{D} < 0.041$
 ...L A lift function
 ...T A thrust function
 s Blade span (m)
 D Wheel diameter (m)
 c Blade chord (m)
 c_{lim} Limited blade chord (section 9.9.1) (m)
 B Number of blades
 d Immersion depth (m)
 g gravitational acceleration (m/s/s)
 V_o Speed of advance (m/s)
 * ϕ Blade angle (radians)
 V_t Blade tip velocity relative to wheel axis (m/s)

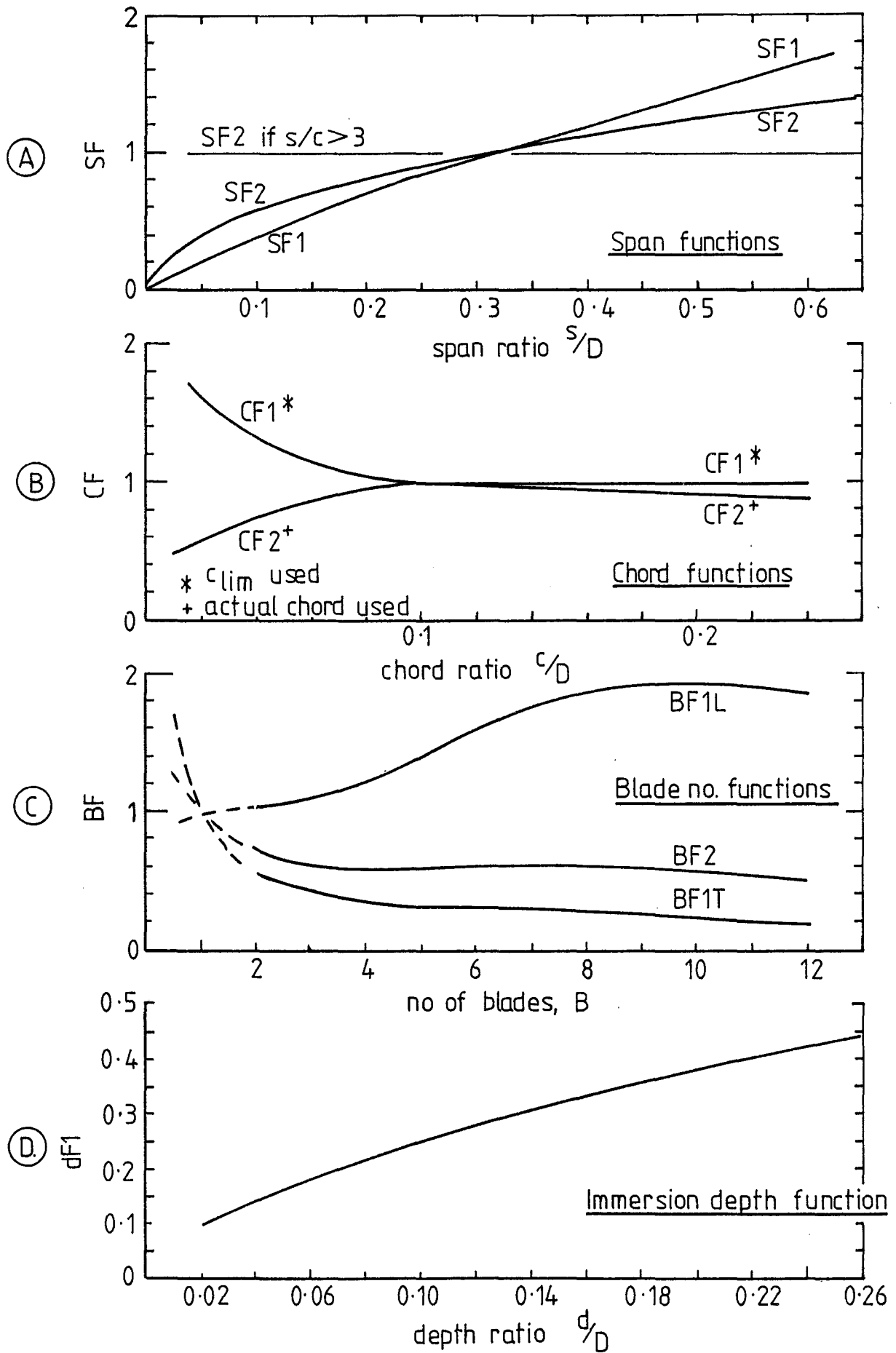


FIGURE 9.47: THE VARIABLE FUNCTIONS IN GRAPHICAL FORM.

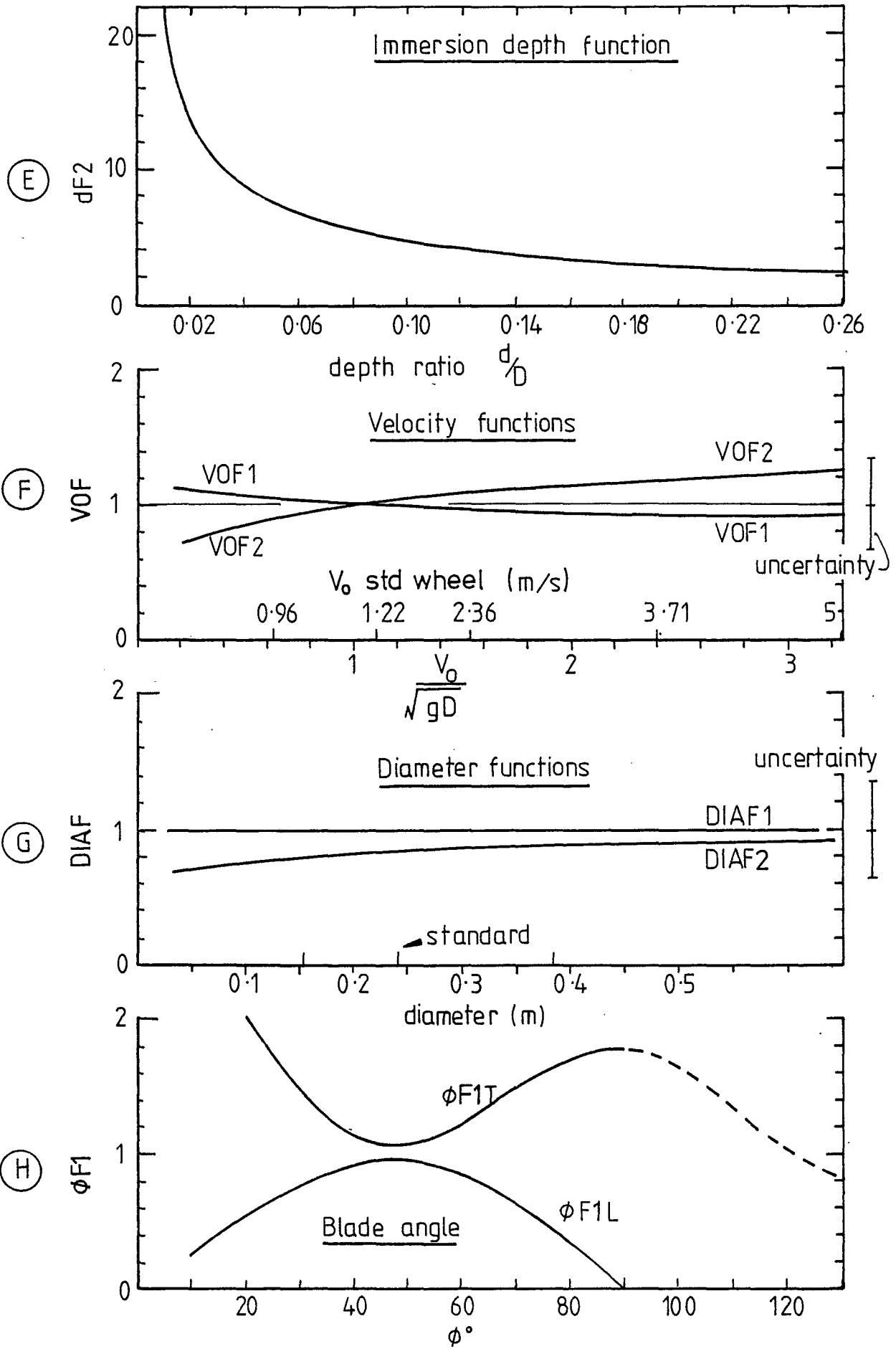
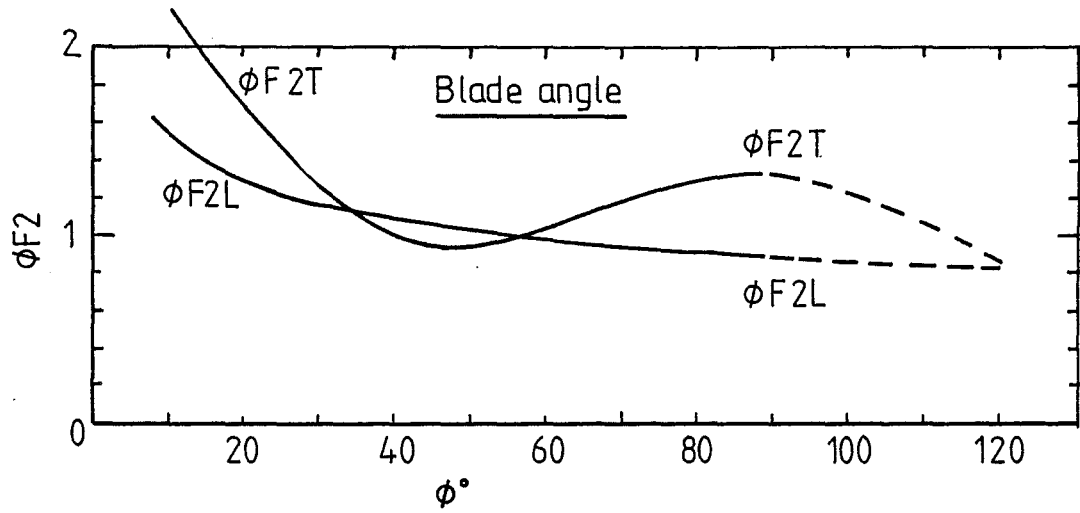
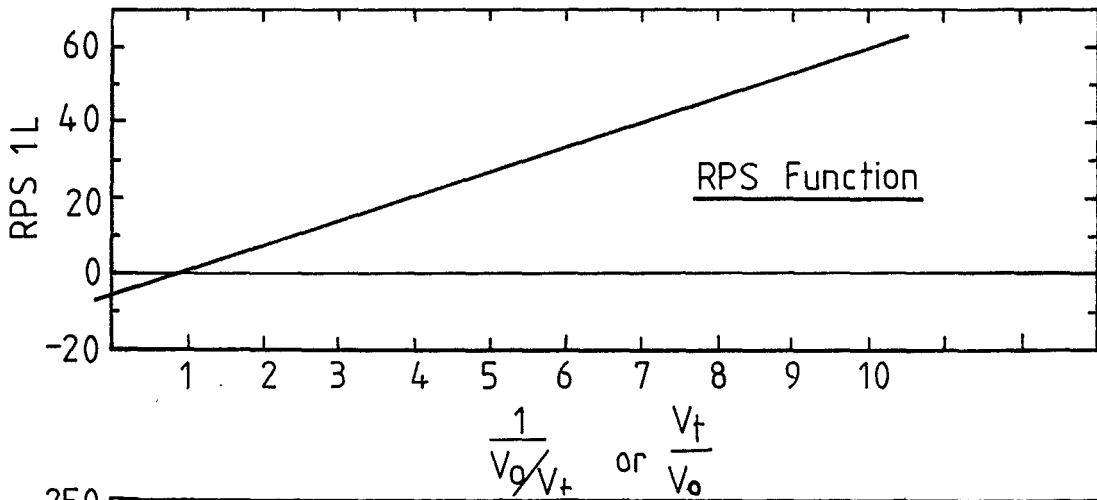


FIGURE 9.47 (cont)

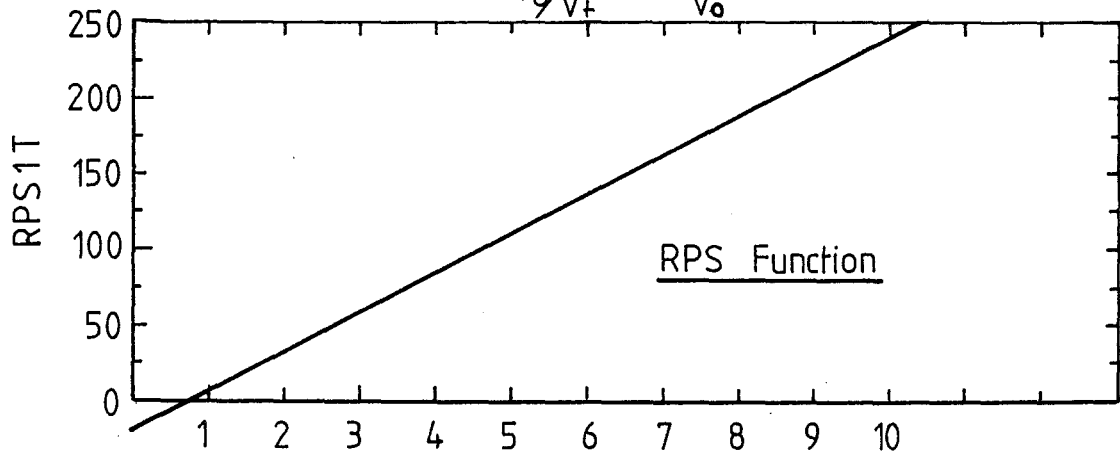
(J)



(K)



(M)



(N)

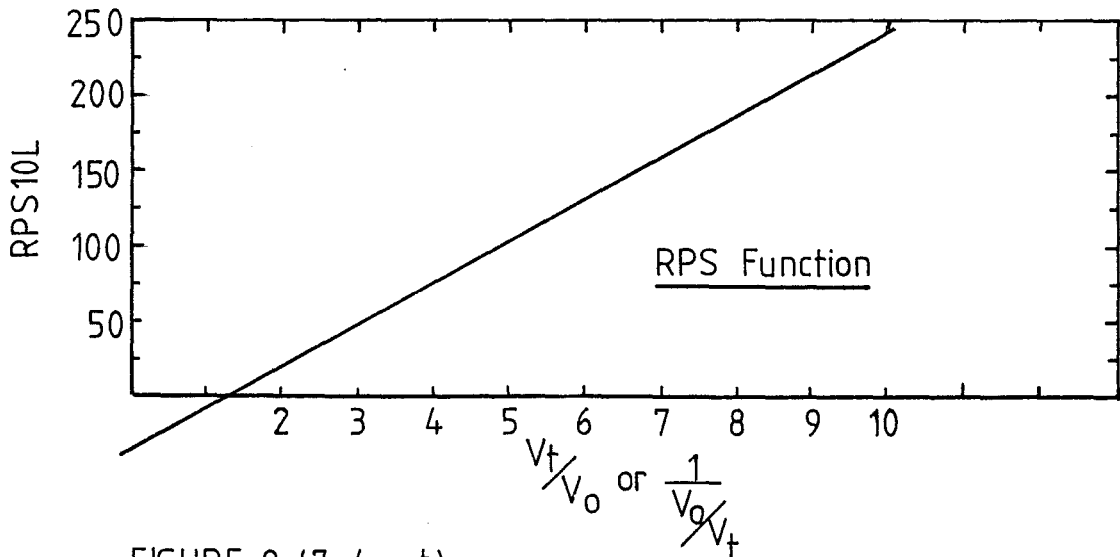


FIGURE 9-47 (cont)

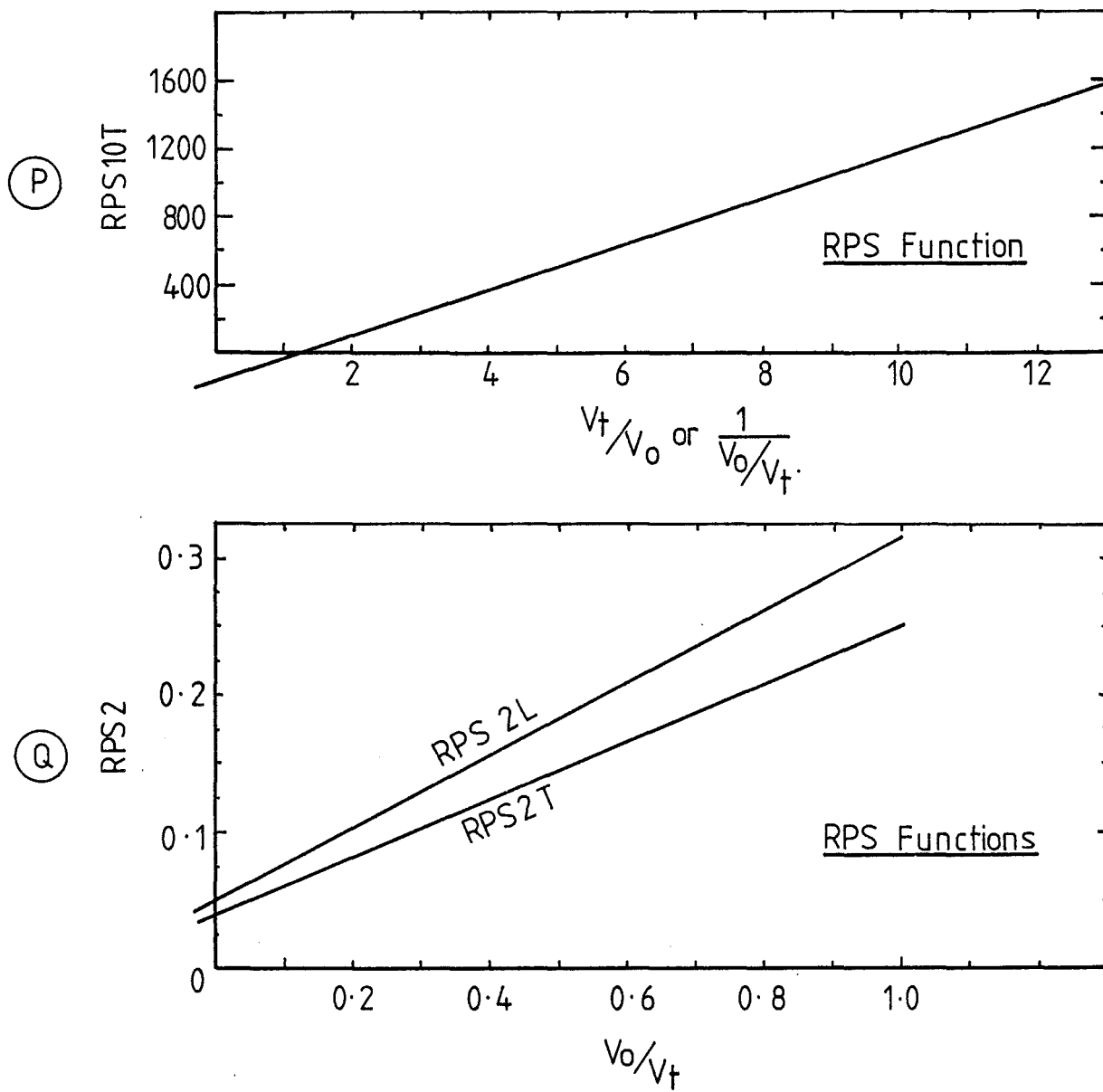


FIGURE 9.47 (cont)

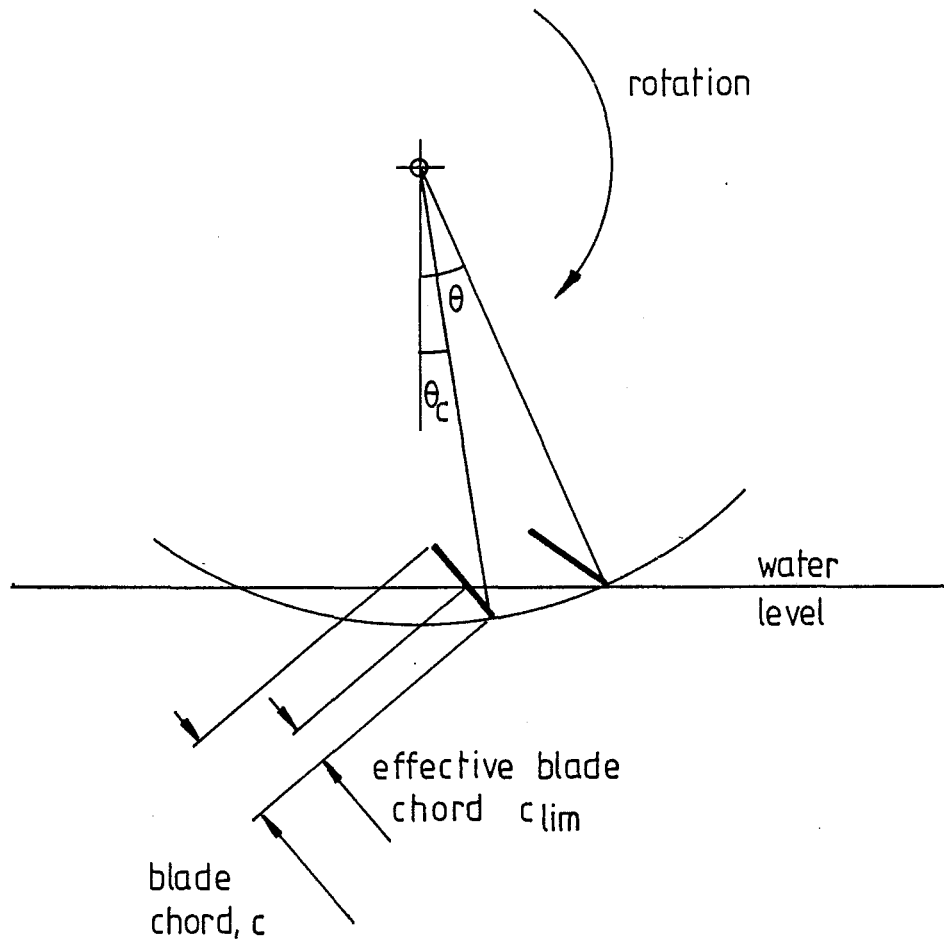


FIGURE 9-48 ESTIMATION OF EFFECTIVE BLADE CHORD AT
 θ_c FOR SMALL IMMERSIONS

If the immersion depth is small - somewhat smaller than the blade chord it is apparent that the blade will not become fully immersed during its passage. In this case it is difficult to know what the effective blade chord will be and, therefore, what the induced mass per blade, based on this chord, by relation (9.2) should be. In order to calculate LPW forces at small immersions a suitable method is required to estimate the effective chord. A number of methods have been tried and the method now used, while empirical, appears satisfactory though it has not been rigorously tested. This assumes that the effective part of the immersed blade chord can be determined when the wheel, turning slowly, has moved 7° past the point of entry, plus an extra amount inversely proportional to the depth angle, θ . As an expression this motion is given by:

$$\theta_c = \theta - 7^\circ - 4.5 \left(\frac{30^\circ}{8}\right)^2 \quad (9.12)$$

At the angle θ_c the effective blade chord can be measured as the immersed blade chord, as shown in Fig.9.48.

The effective blade chord may be calculated from the geometry of Fig.9.48 or measured from sketches. Alternatively these values may be read from Fig.9.49 which indicates how this theoretically limited chord varies with blade angle and immersion depth.

In the calculation of LPW forces this limited chord c_{lim} is the value used in the relation (9.3) for the induced mass flow rate and it is the value used in the variable function for chord in the coefficient equations. (Table 9.46(B) part (B) or Fig.9.47(B).)

To clarify the use of the coefficient equations in the calculation of LPW forces a worked example is included in Appendix 6.

9.9.2 The Variable Functions of the Coefficient Equations

The term "variable function" is used to describe an expression which modifies the theoretical effect of the LPW variable, to match its actual effect in practice. A set of variable functions is used to make up the coefficient equation. The variable functions and coefficient equations have been shown in Table 9.46 and Fig.9.47 (A) - (Q).

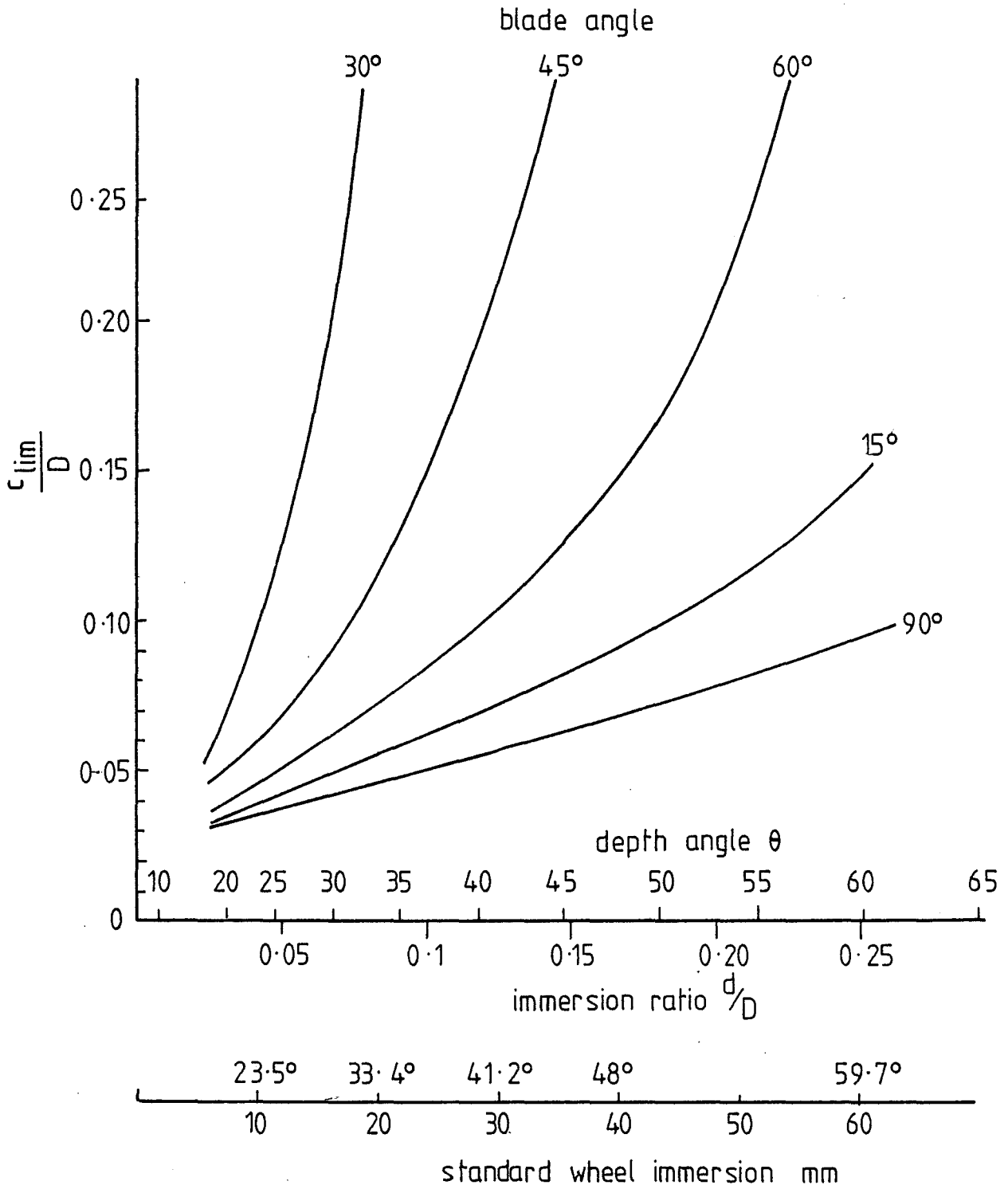


FIGURE 9.49 LIMITED EFFECTIVE CHORD, c_{lim} , WITH ϕ AND d .

In developing these functions it has often been necessary to introduce constants. For example BFlT in Fig.9.47(C) for a six-bladed wheel would be expected to have a value near one. As shown, this function for blade numbers has a value of 0.27, so that it should be increased 3.7 times to suit the actual results. This constant, 3.7, and others introduced by other variable functions have in each case been incorporated into the wheel revolution constants, Fig.9.47 K,M, N,P and Q. For this reason these wheel revolution functions vary widely in magnitude. When all the terms in each coefficient equations have been multiplied together the coefficient equation maximum values are close to 4, as they accommodate the major discrepancy between theory and practice discussed in sections 9.3.1 and 9.3.2.

Several further points may be made about the variable functions:

- 1) The variable functions for both velocity and wheel diameter (Fig.9.47 (F) and (C)) show little variation from the expected values of unity. While some variation from unity is shown, this is within the experimental uncertainty marked on these two plots. It would, therefore, appear safe to scale LPW forces in terms of diameter and velocity as indicated by dimensional analysis and expect the results to be reliable. (Note, however, that propulsive efficiency varies with diameter as shown in Fig.9.31 and discussed in section 9.4.4.)
- 2) The second pair of coefficient equations for the small immersion depth case ($\frac{d}{D} < 0.042$) before cavity intrusion seem to be closely related to the use of the chord limit, for small immersions (section 9.9.1). These separate equations, and indeed the chord limit itself, may yet both prove to be unnecessary. Since this relationship has not yet been closely examined these coefficient equations remain at present as a functional part of the scheme.
- 3) The variable functions for wheel revolutions before cavity intrusion (Fig.9.47 K,M,N and P) are plotted against the inverse of velocity ratio (that is, against wheel revolutions in a dimensionless form). These show linear plots which do not pass through the origin. This latter point indicates that LPW forces in fact fall to zero at wheel revolutions different from those indicated by the impulse theory. This has already been noted (sections 4.8, 4.14.3, 9.2.2) as being a probable result of blade exit forces and is in accordance with the propulsive efficiency falling to zero before the velocity ratio reaches unity (section 4.14.3).

TABLE 9.50: CALCULATION STEPS USED BY PROGRAMME "ADDEDMASS"
IN THE DEVELOPMENT OF THE COEFFICIENT EQUATIONS

1. Read data from magnetic tape: $\phi, d, n, T, L, T_o, V_o$, wheel code..
2. Assign appropriate diameter span chord and number of blades for the wheel code.
3. Calculate preliminaries: $\frac{V_o}{V_t}$, V_t , θ .
4. Call subroutine "XYVG" to calculate angle of attack, γ (see expression (4.18)).
5. Calculate limited chord for small immersions (see expression (9.12)).
6. Call subroutine "CIRPS" to calculate wheel revolutions at which surface cavity intrusion occurs (see Appendix 5).
7. Calculate mass flow rate appropriate to cavity intrusion conditions (expressions (4.16) and (4.7)).
8. Calculate coefficient equations from variable functions (Table 9.46, Fig.9.47).
9. Calculate vertical and horizontal components of \max^m velocity expressions, V_v and V_h (expressions (4.20), (4.21)).
10. Calculate theoretical lift and thrust at blade tip using coefficient equations, \max^m velocity expressions, and induced mass flow rates (expressions (4.23), (4.25)).
11. Calculate experimental:theoretical ratio e.g.: $CCL = \frac{L_{\text{expt}}}{L_{\text{calc}}}$.
12. Repeat steps 3-11 for blade centre of pressure conditions.
13. Write out all data and resulting ratios.
14. Stop.

4) The fact that the variable functions for wheel revolutions before cavity intrusion have a linear dependence upon wheel revolutions has already been noted in regard to the effects of wheel rotational speed, section 9.4.3. In Fig.9.47 K,M,N and P the consistent tendency towards this linear relation is emphasised, indicating that LPW forces (and paddlewheel forces) are dependent upon the cube of wheel revolutions rather than their square, as proposed by the theory. At present this difference between theory and practice remains unexplained.

9.9.3 Computer-Aided Development of the Coefficient Equations

To aid in determining the coefficient equations and the related variable functions shown in Table 9.46 and Fig.9.47 a FORTRAN programme called 'ADDEDMASS' was developed. Its function was to perform the calculations involved so that curve fitting could be performed by graphical methods. A chart outlining its functions is given in Table 9.50, but in brief its task was: to read each data record from the magnetic tape (described in section 7.5), then take the LPW operating conditions and perform theoretical force calculations. These, it then adjusted by the chosen coefficient equations and compared the results with the experimental values in a ratio.

The final ratios could be plotted against any one of the LPW variables so that the dependence of the coefficient equations on that variable could be determined. The coefficient equations in the programme could then be adjusted and the programme re-run. By this iterative process the coefficient equations and variable functions were ultimately determined.

The coefficient equations therefore represent the variation of the experimental results from the theory, put into an analytical form. They are the same variations from theory discussed in earlier sections of this chapter, that have now been more broadly and soundly based on all the available data, rather than just on the selections shown in Figs. 9.37 or 9.40.

The obvious test of such equations is to check whether they can be used in conjunction with the impulse theory to reproduce any selected measured results. It would require considerable testing to cover the field, but as an example Fig.9.51 shows the impulse theory-coefficient equation version of the lift and thrust forces

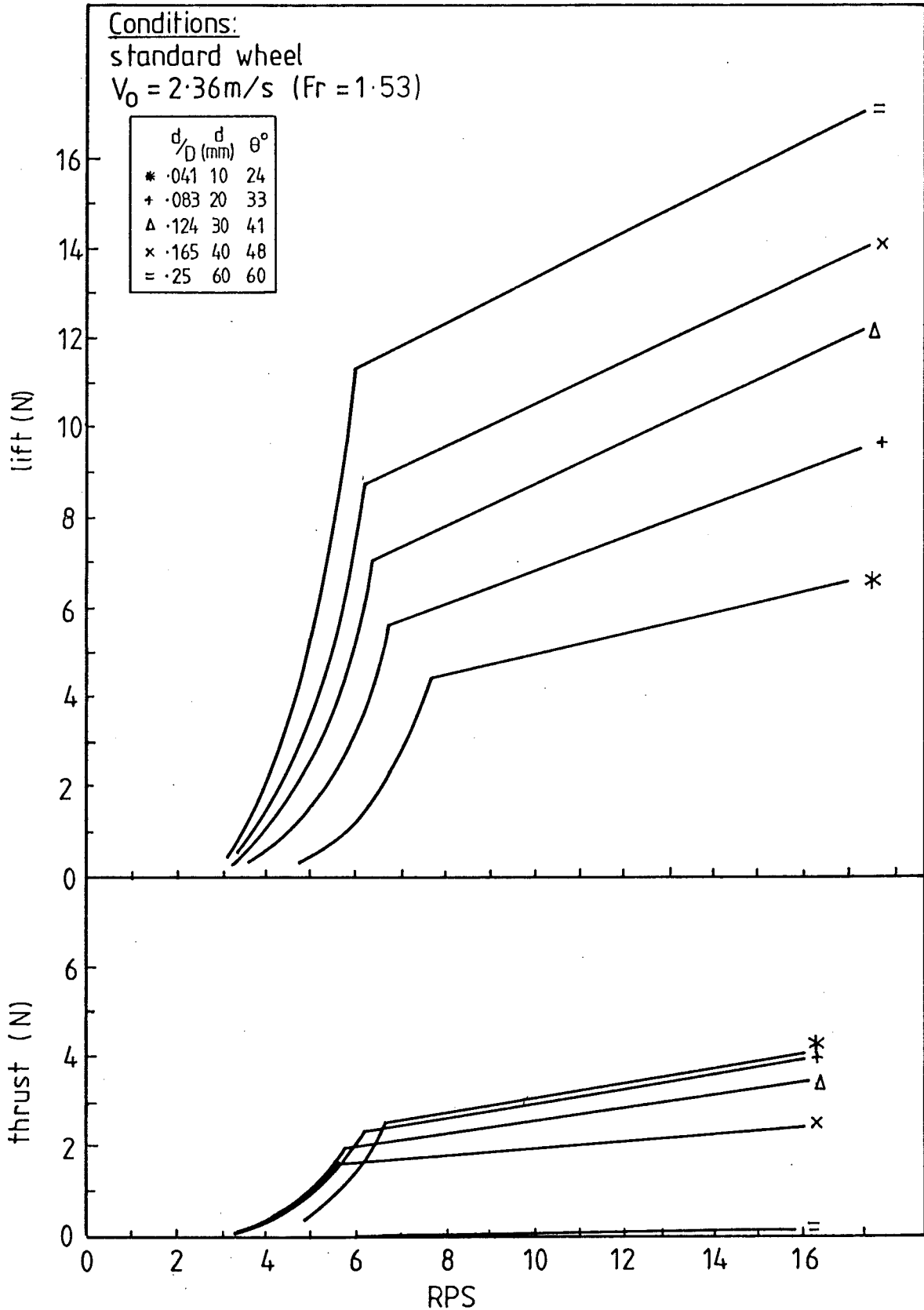


FIGURE 9.51: RESULTS FOR THE STANDARD WHEEL AT 2.36 m/s GENERATED BY THE IMPULSE THEORY USING THE COEFFICIENT EQUATIONS. THIS COMPARES WITH FIG. 9.3. (PRODUCED USING PROGRAMME "LPWCRAFT", APPENDIX 7)

for one set of conditions, the standard wheel at 2.36 m/s. Comparison may be made with the equivalent experimental results in Fig.9.3. As would be expected there are small differences to be found between these theoretical and experimental results, though there are none of major significance.

Several points may be added, concerning the programme 'ADDEDMASS'.

1) It includes the estimation of cavity intrusion contained in Appendix 5 and uses this to determine which coefficient equations are used.

2) It employs the relation (9.12) to limit the blade chord for small immersion depths (as shown in Fig.9.49).

3) It was felt that realistically the force calculations should be performed at the blade centre of pressure rather than at the blade tip. A position 40% back from the blade tip was chosen as an average value and the programme was designed to repeat all the coefficient calculations at this point as well as at the blade tip.

4) The coefficient equations were actually developed for this 40% chord position rather than for the blade tip. While this means that the coefficient equations do not strictly apply to conditions at the blade tip, little variation was found between the two sets of calculations so that the coefficient equations, as they stand, are considered to apply to calculations at the blade tips.

5) This same programme was altered and used to calculate the values of " C_p " the ratio of experimental to calculated power as discussed in section 9.8.

9.10 CONCLUSIONS

This chapter has compared the LPW theory and experimental results and noted the differences between the two. It has developed coefficients which, while they do not explain these differences, enable the theoretical model to reproduce the experimental results. Strictly speaking these coefficients only apply to the measured data

but the whole purpose of developing them was to allow the theoretical models to be used to predict full size craft performance.

As will be seen in section 12.8 these theoretical models were tested against the performance of the model LPW craft, before their predictions were extrapolated to the design calculations for a full-sized craft in Chapter 13.

The most distinct difference between theory and the experimental results was in the dependence of the forces on wheel revolutions. The fact that the forces appear to depend upon the cube of the wheel revolutions rather than the square as proposed by the theory suggests that, should any improvement be made to the impulse theory, this discrepancy would be the most appropriate starting point.

CHAPTER 10

RESULTS FOR ROTORS WITH CURVED BLADES10.1 INTRODUCTION

The impulse theory as a description of LPW forces, outlined in Chapter 4 and compared with experimental results in Chapter 9, was concerned only with flat-bladed LPW's. It is apparent that flat blades may not give the best performance characteristics for a chosen application and that blades, curved in their chordwise direction, could be devised to better control the entrained flow. This chapter then, examines how some of the concepts upon which the impulse theory was based may be used to suggest worthwhile variations in blade shape. It then examines the tank test results for LPW's with curved blades as well as one associated test of the LPW with alternating blades of different angles. From the findings a generalised set of results is formed.

This chapter assists in the secondary aims loop parts 2 and 3 of Fig.3.10 by providing data, and some further information on how the LPW works.

10.2 ANALYTICAL APPROACHES TO FLOW PAST SHAPED BLADES

Force equations were developed in the impulse theory on the basis of a two dimensional vector diagram model of the fluid flow encountering the flat blade at its entry (see sections 4.6 and 4.7). This flow was assumed to occur in such a way that momentum changes took place only normal to the plane of the blade. It involved the flow dividing at a stagnation point and leaving the blade in two directions, the proportions flowing each way being modelled by the vector velocities.

Curved blades, however, can be arranged to cause the flow to move almost completely in one direction across the blade face as shown in Fig.10.1. Here the flow is started by the tip entering the water and is then steadily redirected by the remaining portion of the blade, which follows. This can be advantageous as all the flow can be directed in the required direction to give the momentum change necessary for the chosen resultant force. This seems more

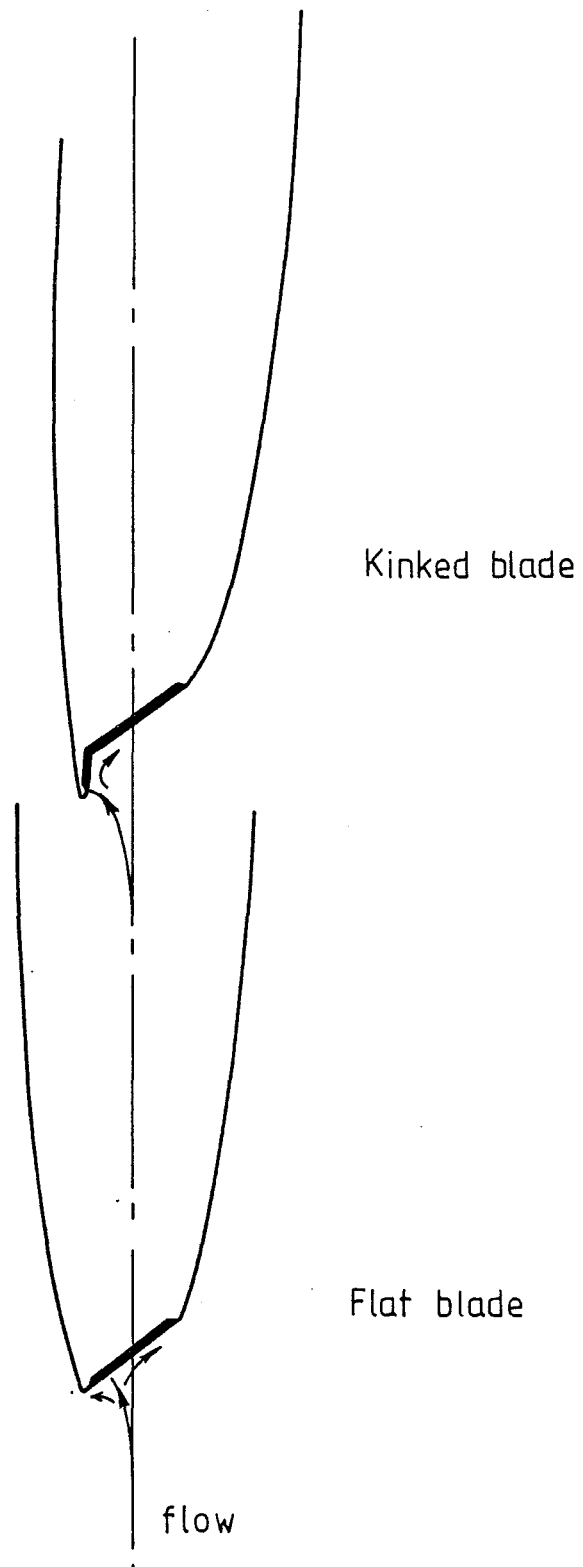


FIGURE 10.1 SKETCHES SHOWING THE EFFECT ON THE CAVITY AND FLOW AROUND A KINKED AND FLAT BLADE (BOTH FULLY IMMERSED)

purposeful and efficient than the flat blade flow which spreads from the blade in both directions. From this consideration the analysis of curved blade operation would seem to lend itself to the entry and exit vector diagram treatment used for centrifugal pump design.

There are a number of complicating factors, however, to such a straightforward approach to curved blade analysis. These are generally that, because of changes in immersion depth and velocity ratio the wheel does not always operate under the chosen conditions, and when this happens, analysis becomes very difficult, no longer giving the sort of workable results that the impulse theory can give for flat blades over a wide variety of conditions. There are methods available for determining the magnitude and direction of the resultant force on an arbitrarily shaped plate with an attached cavity, fully immersed in a steady flow. (1) Such methods could probably be used to determine the forces on curved LPW blades.

This project, having developed and tested a satisfactory theoretical model for flat LPW blades has, therefore, stopped short of extending or restructuring the analysis to cover the performance of curved blades even though it is probable that shaped blades will ultimately provide optimum LPW performance.

A less rigorous analysis of curved-bladed LPW's not extending to mathematical models, may be undertaken by systematically comparing the results of tests with those of the better understood flat-bladed LPW's. In this way some typical characteristics can be identified and, therefore, to some extent, understood.

10.3 SHAPED BLADES IN THE PADDLEWHEEL LITERATURE

(Curvature in this chapter always refers to curvature in a chordwise direction. No spanwise curvature is considered.)

While radial paddlewheel blades have generally been flat, feathering paddlewheel blades have usually been slightly concave on the pressure face. Volpich and Bridge's tests with shaped blades showed a significant improvement in propulsive efficiency of up to 12% with curved blades over flat blades. (2) While they do not state

1. T.Y. Wu p.38
2. Volpich and Bridge, Part II, P.486

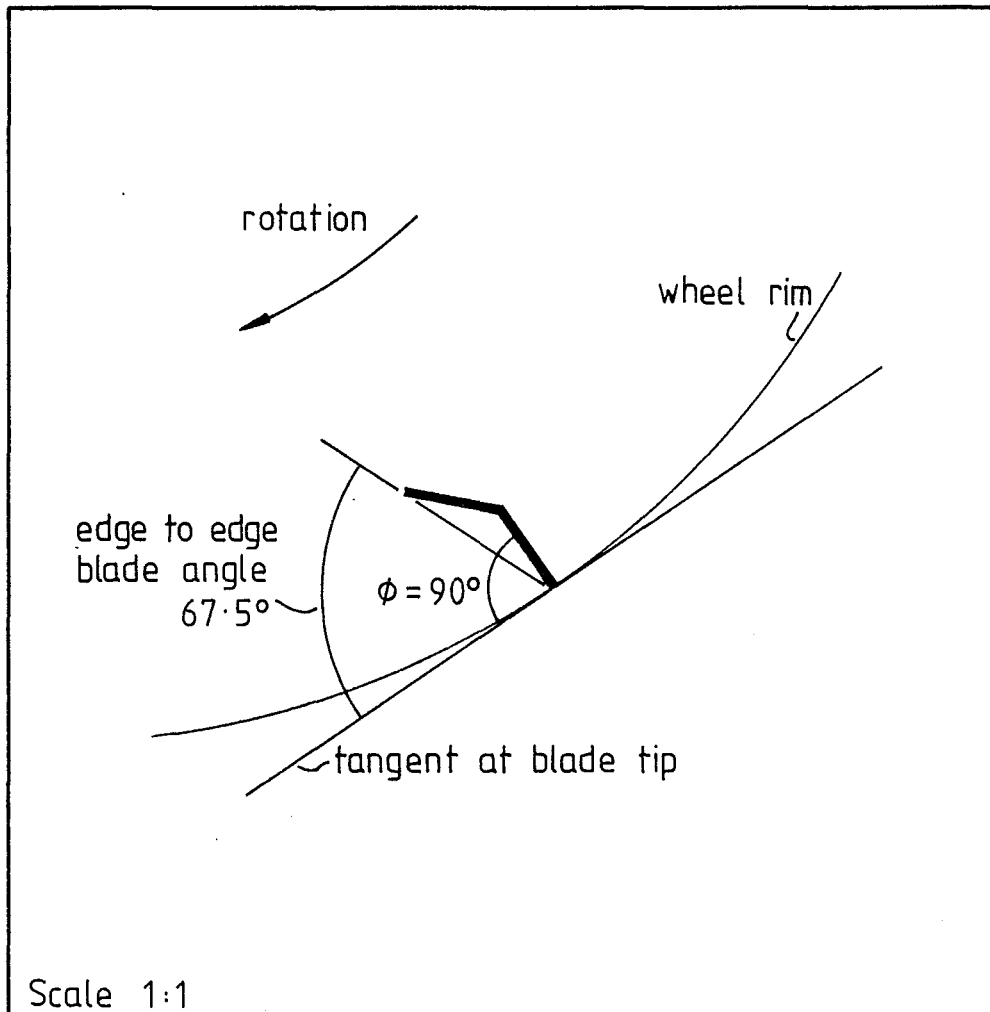


FIGURE 10.2 CONVENTIONAL BLADE ANGLE ϕ , AND
THE EDGE TO EDGE BLADE ANGLE

what the curvature was it would appear to have had a radius half the wheel radius. (1) They found still greater improvement with sharp edged blades, but made no attempt to explain why either of these improvements might have occurred.

Helm's results from his deeply immersed feathering wheels showed that none of the shapes he tried showed overall superiority. (2) His tests covered a range from flat to a curvature of radius a little less than the radius of the wheel.

Beardsley tested two types of shaped blades as well as flat blades. He attempted to design his curved blades to enter and leave the water smoothly and his other shaped blades were angular versions of these curved ones. (See section 2.2.6, Fig.2.9.) Beardsley concluded that blade shape was of considerable importance in that it controlled local flow during the momentum exchange process. (3) Perhaps because his smoothly curved blades did not perform as well as their angular counterparts, he felt that more information on blade flow conditions is needed to provide a basis for blade design.

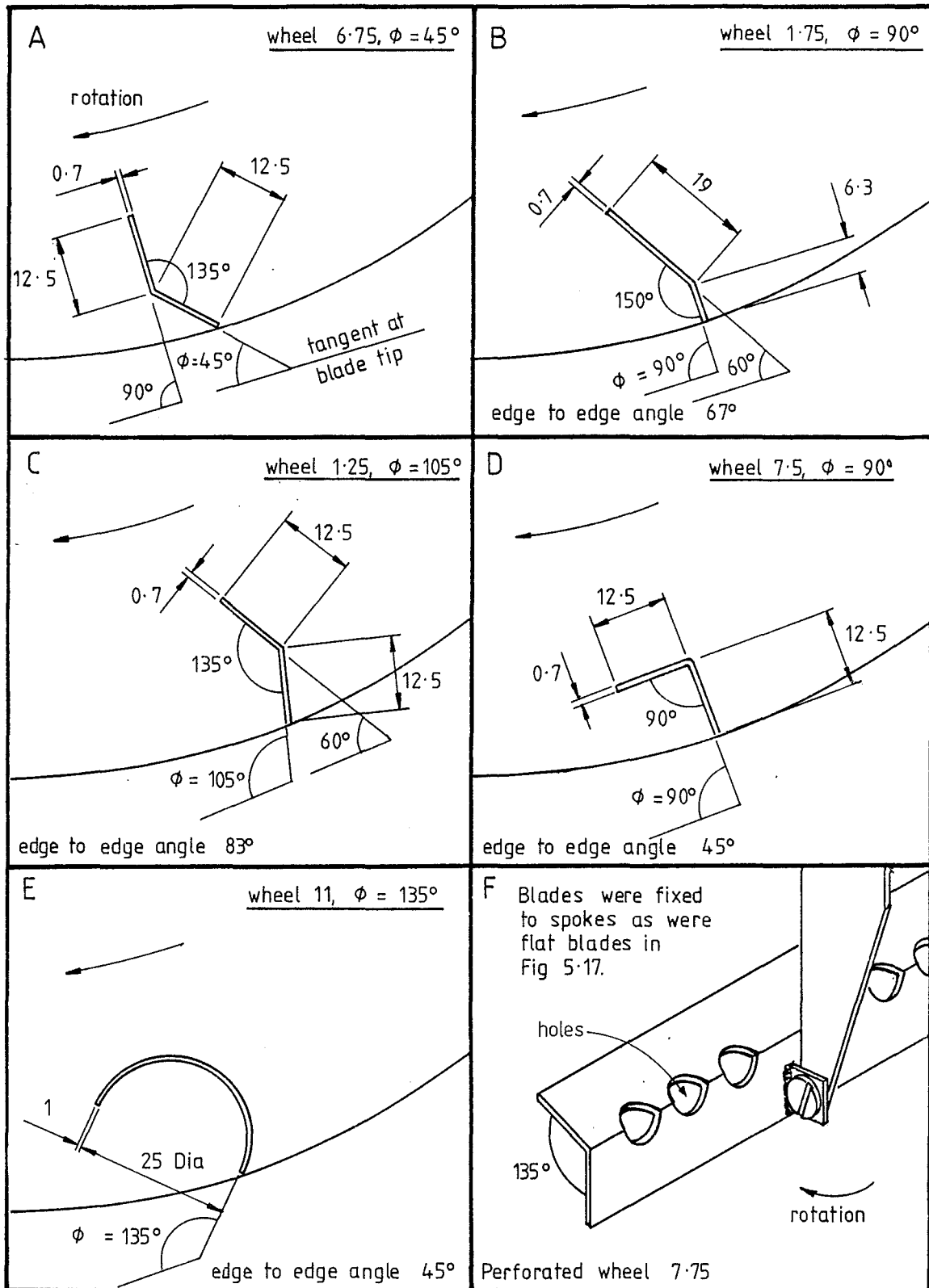
The literature, then, does not provide an altogether clear picture of what to expect in terms of blade performance with curved blades. The LPW results described in this chapter however, begin to clarify this area.

10.4 GENERALISED FINDINGS FOR CURVED BLADED WHEELS

While the tests of LPW's with curved blades were not planned as a systematic series they may be arranged in order of curvature from convex (on the pressure face), through the flat blade to concave, and the results examined with respect to this classification. A further convention adhered to is that the blade angle, ϕ is taken as the angle of the blade tip to the tangent of the wheel. This is the same definition of blade angle as was used for flat blades, as shown in Fig.1.2.

The blades examined in this section are shown in Fig.10.3, which also shows the normal method of attachment to the basic LPW test wheel.

1. Volpich and Bridge, Part I. P.340, Fig.4 3. Beardsley, pp.19 & 24
 2. Beardsley, P.17.



Dimensions - mm
 Scale 1:1

FIGURE 10.3 CURVED BLADES EXAMINED IN THIS CHAPTER.

It is of some help to outline the main findings of this section before examining each blade type in turn, so that meaningful threads may be followed through the otherwise confusing results. The following generalisations, then, help to bring order to the results:

- 1) The blade tip seems to have a strong influence upon the performance of a curved blade so that comparison of the performance of a curved blade with that of a flat blade of the same blade angle as its tip will show strong resemblances.
- 2) An edge-to-edge blade angle may be generated on a curved blade as shown in Fig.10.2. A refinement of point (1) above is that the thrust force of a curved-bladed LPW most closely resembles the thrust force of the flat-bladed LPW with the same blade angle as the tip of the curved blade; the lift force, by contrast, most closely resembles the lift force of the flat-bladed LPW with the same blade angle as the edge-to-edge blade angle of the curved blade.
- 3) It may be partly deduced from the above two findings that slightly concave blades are found to have the advantages of good lift and thrust forces inherent in the flat blades from which they derive. (See for example wheel 1.75, $\phi = 90^\circ$, in Figs.10.3(B) and 10.7, 8 and 9 which has the lift advantage of the edge-to-edge angle of 67° and the thrust advantage of the $\phi = 90^\circ$ toe.)
- 4) As expected, small immersions generally show performance characteristics of flat blades that have the same angle as the tips of the blades, while deeper immersions show more of the effects of the whole blade.
- 5) The above four findings apply most consistently to slightly concave blades (which are the most useful) and begin to break down with other sorts of blades.

A convention used in this chapter to help identify which wheels are being referred to is as follows: For curved bladed wheels as shown in Fig.10.3 above, the wheel code number followed by its blade angle (at the tip) is used as the reference. For flat bladed wheels the letters FB followed by the blade angle define them. For example the standard LPW would be referred to as FB, $\phi = 60^\circ$ since it has flat blades and its blade angle is 60° .

All wheels examined in this chapter have 6 blades.

10.5 CONVEX BLADES: WHEEL 6.75, $\phi = 45^\circ$

(See Appendix 4 and Fig.10.3(A))

This wheel had 6 blades of the standard chord of 25 mm ($\frac{C}{D} \doteq 0.1$) which were bent so that the vertex of the bend ran spanwise along the centre to make an outer portion, or tip set at $\phi = 45^\circ$ to the wheel tangent, and an inner portion or heel close to an angle of 90° to the tangent (See Fig.10.3(A).) The purpose of testing this blade configuration was to discover whether it would give the good lift performance of a FB, $\phi = 45^\circ$ wheel and the good thrust performance of a FB, $\phi = 90^\circ$ wheel; to see whether the tendency of FB, $\phi = 45^\circ$ blades to produce negative thrust at deep immersions (see Figs. 4.24, 9.41, Appendix 4 wheel 6, $\phi = 45^\circ$) could be offset by providing a heel, or inner portion of the blade set at 90° , this coming into play to generate more thrust at these deep immersions. (This greater thrust for FB, $\phi = 90^\circ$ is seen in Appendix 4 wheel 6, $\phi = 90^\circ$ or in Fig.9.41.)

The results for this wheel are given in Figs. 10.4, 5 and 6 where the following may be noted:

Lift: In the static and displacement modes lift is slightly less than for the FB, $\phi = 45^\circ$ wheel (Appendix 4, wheel 6, $\phi = 45^\circ$) at small immersions. At larger immersions lift is significantly lower than for FB, $\phi = 45^\circ$. In the planing mode lift seems to be no different than for the FB, $\phi = 45^\circ$ wheel.

Thrust: At all speeds the thrust seems to be no different from that of the FB, $\phi = 45^\circ$ wheel, being low at small immersions and small or negative at larger immersions.

Efficiency: With the low and negative thrust values, efficiencies are also low, reflecting again the results of the FB, $\phi = 45^\circ$ wheel.

These results confirmed the finding (Point (1) in the generalised findings) that tip conditions most strongly influence the wheel performance. This convex blade configuration failed to encompass the good points of both FB, $\phi = 45^\circ$ and FB, $\phi = 90^\circ$ blades and directed attention away from blades with convex surfaces. The conclusion con-

WHEEL NO: 6.75

Blade Angle $\phi = 45^\circ$

Shaped Blades

Diameter, $D = 242$ mm

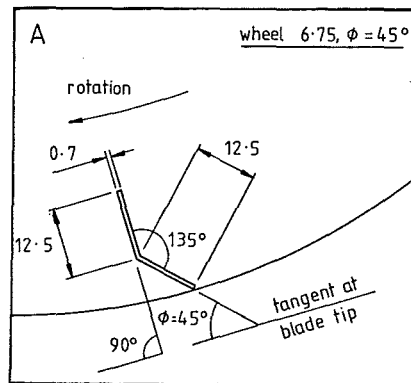
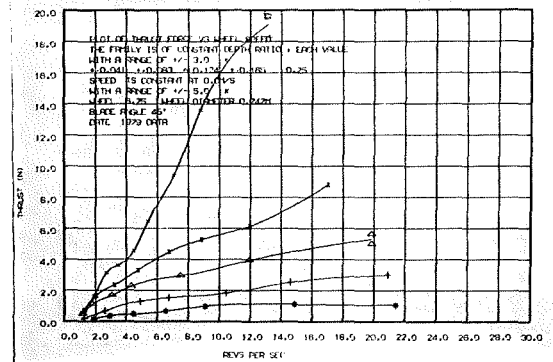
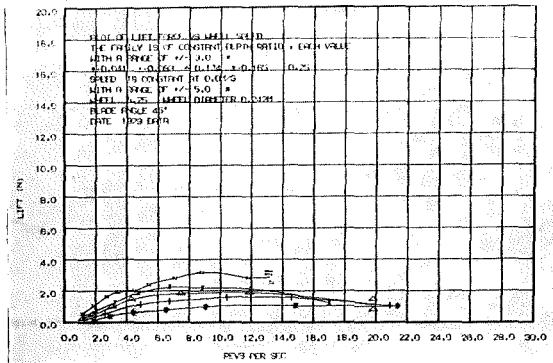
Span, $s = 76$ mm $s/D = .31$

Chord, $c = 25$ mm $c/D = .1$

No. of Blades = 6

STATIC, $V_o = 0$

Symbols	Immersion ratio	Immersion angle	Immersion depth
	D/ρ	ϕ_o	d (mm)
*	.041	24	10
+	.083	33	20
Δ	.124	41	30
x	.165	48	40
=	.25	60	60



See also:

Figs	Sections
10.3	10.5
10.4 to	
10.6	

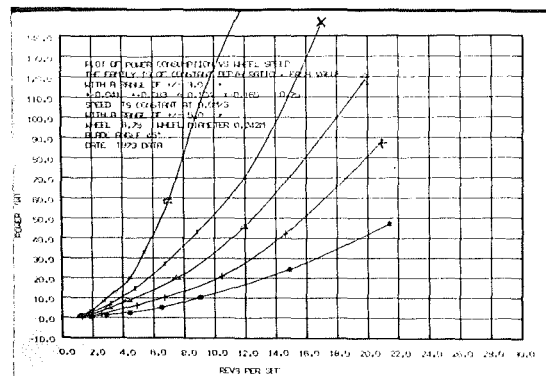


FIGURE 10.4: WHEEL 6.75, $\phi = 45^\circ$ IN THE STATIC CONDITION

Displacement, $V_0 = 0.4 \text{ m/s}$, $F_r = 0.26$

Transition, $V_0 = 0.76 \text{ m/s}$, $F_r = 0.49$

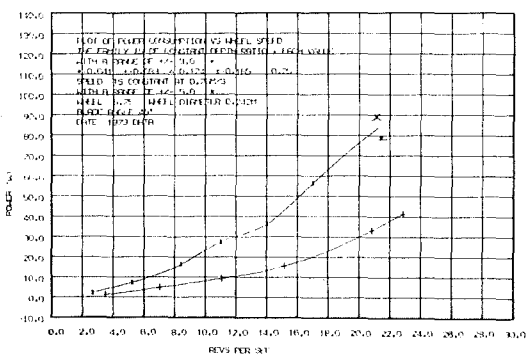
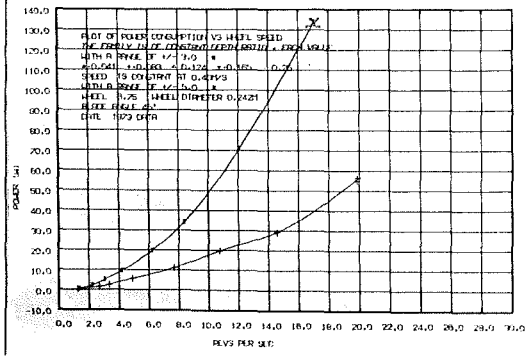
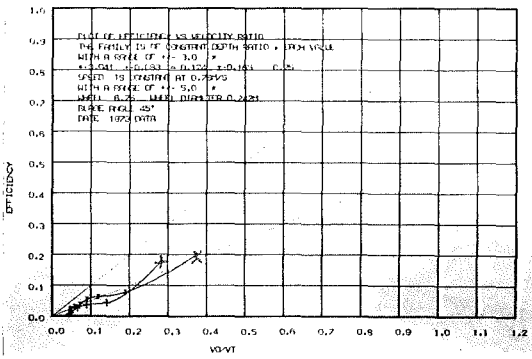
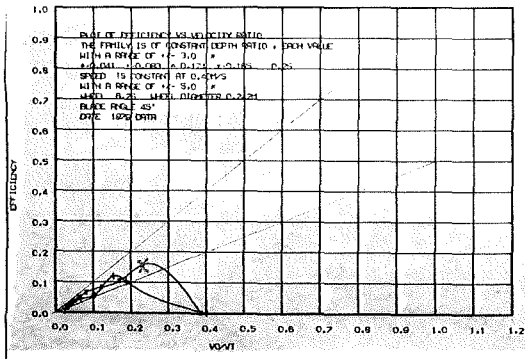
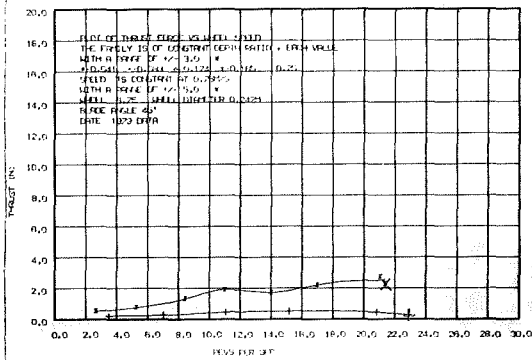
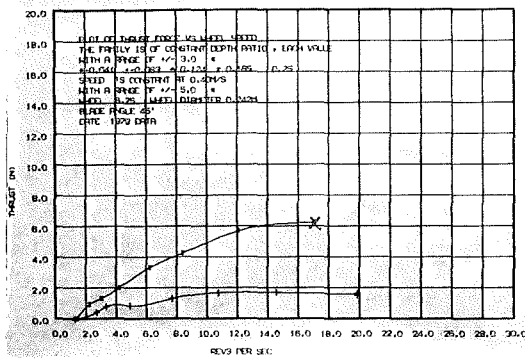
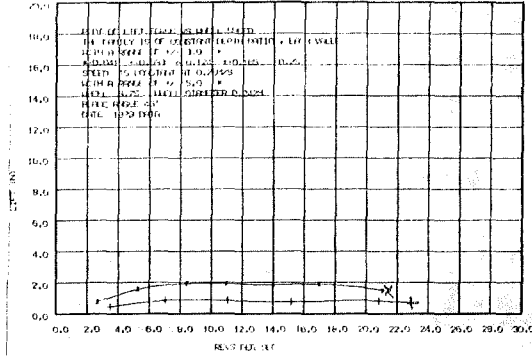
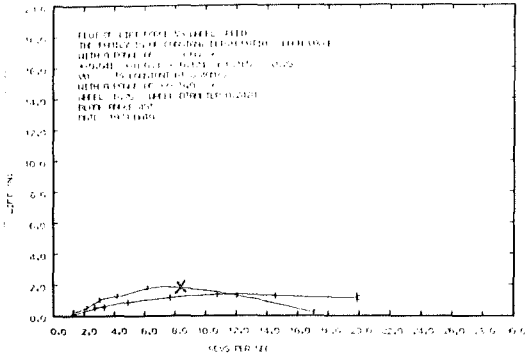


FIGURE 10.5: WHEEL 6.75, $\phi = 45^\circ$

Planing, $V_0 = 1.72 \text{ m/s}$, $F_r = 1.12$

Planing, $V_0 = 2.36 \text{ m/s}$, $F_r = 1.53$

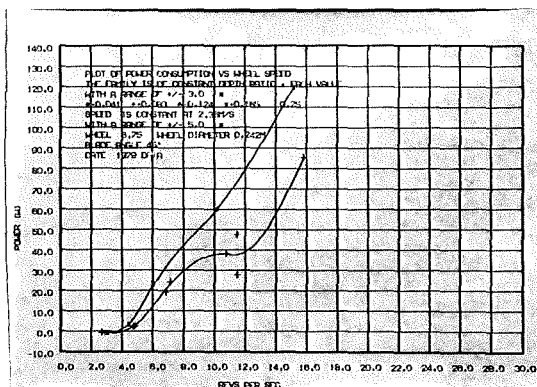
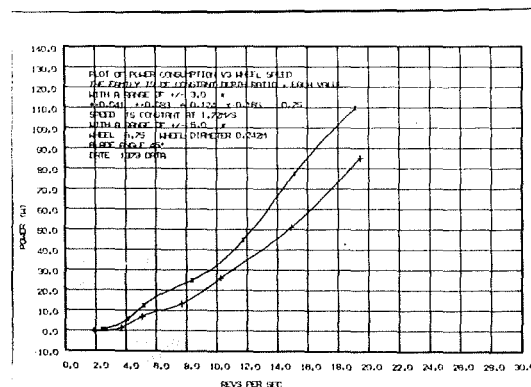
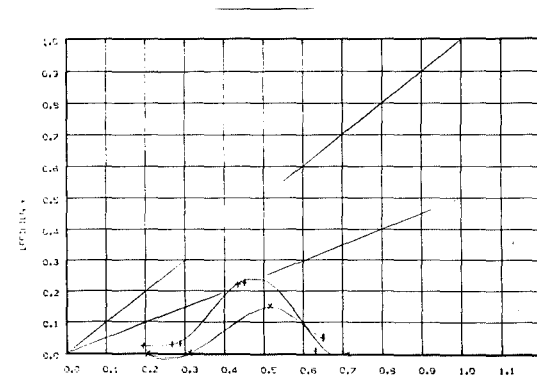
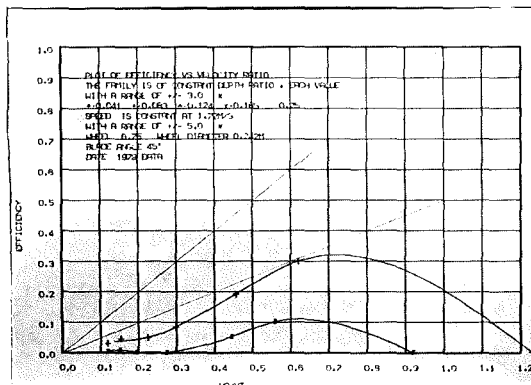
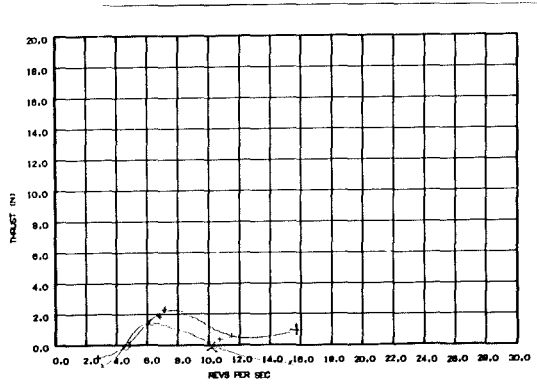
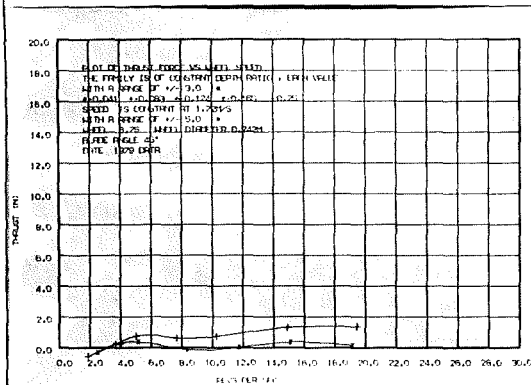
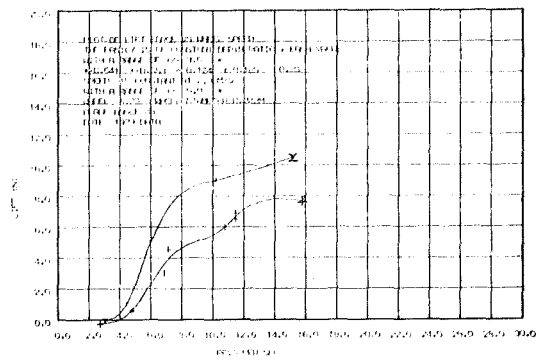
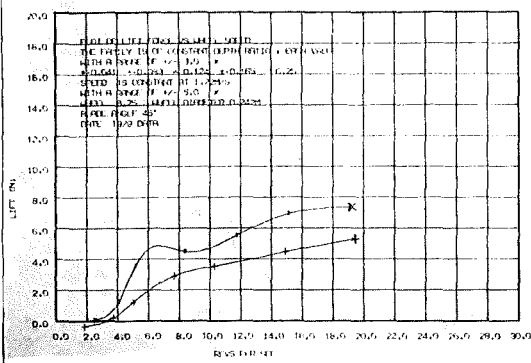


FIGURE 10.6: WHEEL 6.75, $\phi = 45^\circ$, PLANING OPERATION

cerning edge-to-edge blade angle did not apply in this case of convex blades.

10.6 SLIGHTLY CONCAVE WITH SMALL TOES: WHEEL 1.75, $\phi = 90^\circ$

(See Appendix 4 and Fig.10.3(B))

The next in the series from convex blades are flat blades which were dealt with in Chapter 9. The series continues with blades with a small amount of concavity only. These were again of the standard chord of 25 mm. They were bent so that the vertex of the bend ran spanwise at a distance of 6.25 mm, or one quarter of the chord away from the blade tip. This gave a blade which had the outer quarter set at 150° from the inner heel as shown in Fig.10.3(B). For this test the outer quarter was set at $\phi = 90^\circ$ so that the slightly concave blade had the inner heel set at 60° to the tangent. The blades thus had an edge-to-edge blade angle of 67° , not much larger than the heel angle of 60° . The purpose of testing these blades was similar to that of the last one, to discover whether it would give the good lift of the FB, $\phi = 60^\circ$ wheel (the standard wheel, results shown in Figs. 9.1, 9.2 and 9.3) with the good thrust performance of the FB, $\phi = 90^\circ$ wheel (Appendix 4, wheel 6, $\phi = 90^\circ$). Since the tip was known to be more effective than the rest of the blade, it was reduced to only one third of the area of the rest of the blade to discover how well this might redress the balance between the effects of the two blade portions.

The results in Figs.10.7, 8 and 9, although not containing data for all immersions show a good performance:

Lift: For all speeds the lift forces generated are marginally lower than for the standard wheel FB, $\phi = 60^\circ$, while being usefully greater than the low lift generated by FB, $\phi = 90^\circ$, especially in the planing mode at low wheel revolutions. This is the result that would be expected from point (2) above suggesting that lift would be related to the flat bladed wheel with the same blade angle as the edge-to-edge blade angle here.

Thrust: Again for all speeds thrust forces are good, being only slightly lower than those of the FB, $\phi = 90^\circ$ wheels and considerably greater than those of the FB, $\phi = 60^\circ$ wheels, especially through the transition zone and in the planing mode. This is the result that would be expected from

WHEEL NO: 1.75

Blade Angle $\phi = 90^\circ$

Shaped Blades

Diameter, $D = 242$ mm

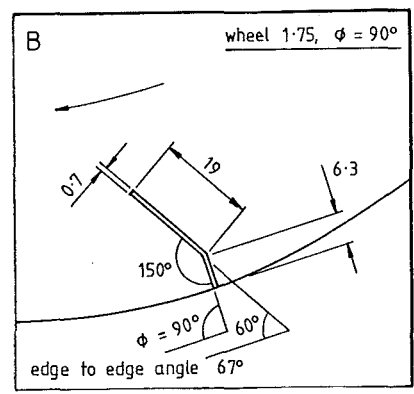
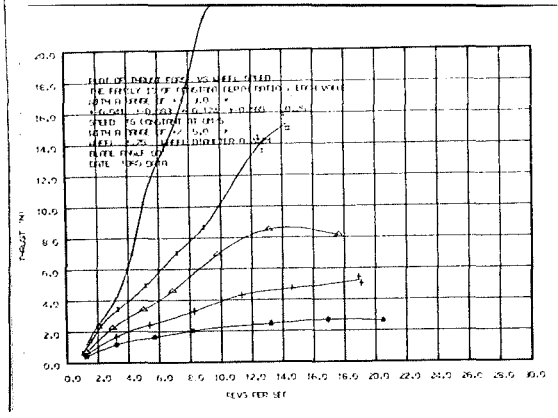
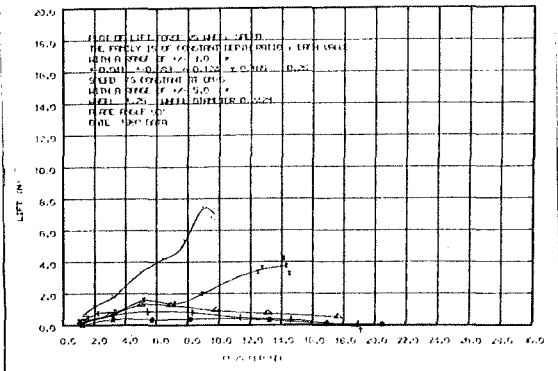
Span, $s = 76$ mm $s/D = .31$

Chord, $c = 25$ mm $c/D = .1$

No. of Blades = 6

STATIC, $V_o = 0$

Symbols	Immersion ratio	Immersion angle	Immersion depth
	D/d	θ°	d (mm)
*	.041	24	10
+	.083	33	20
Δ	.124	41	30
x	.165	48	40
=	.25	60	60



See also:

Figs	Sections
10.3	10.6
10.7 to	
10.9	

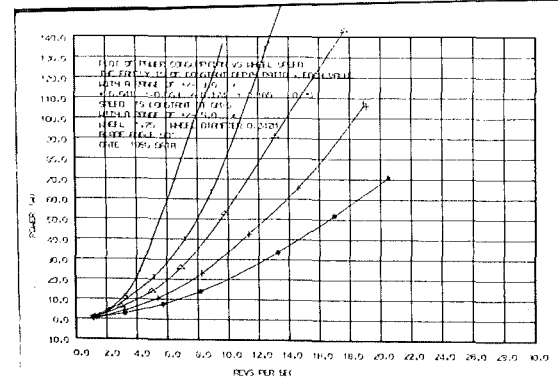


FIGURE 10.7: WHEEL 1.75, $\phi = 90^\circ$, SLIGHTLY CONCAVE BLADES, IN THE STATIC CONDITION

Displacement, $V_0 = 0.4 \text{ m/s}$, $F_r = 0.26$

Transition, $V_0 = 0.76 \text{ m/s}$, $F_r = 0.49$

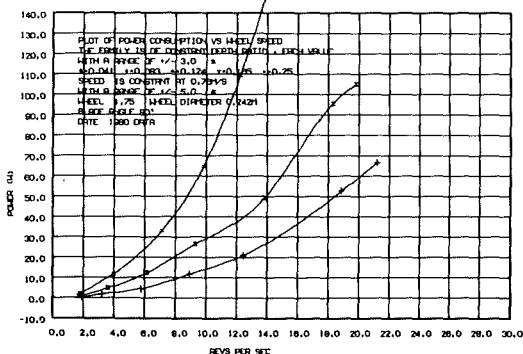
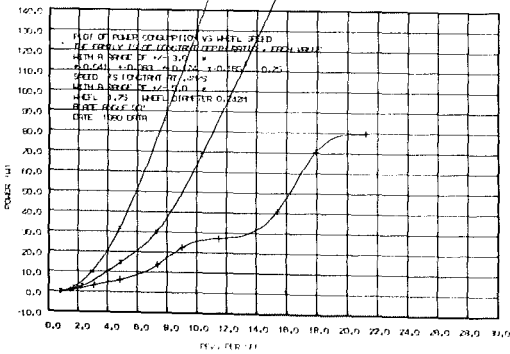
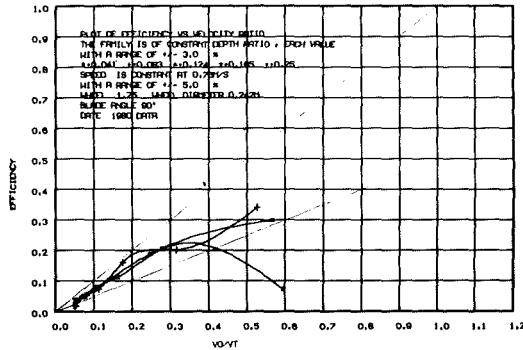
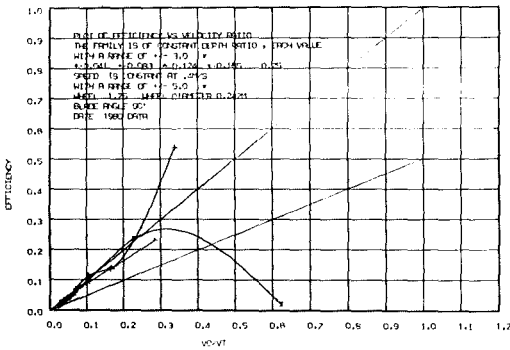
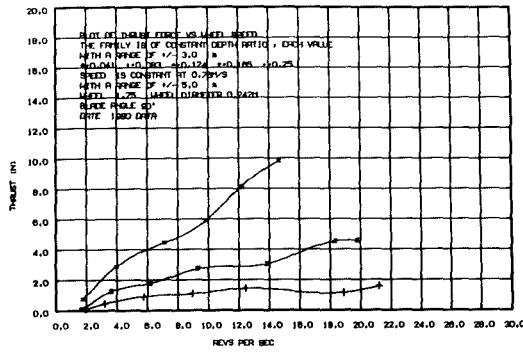
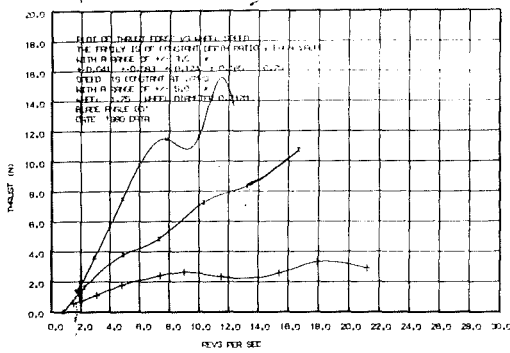
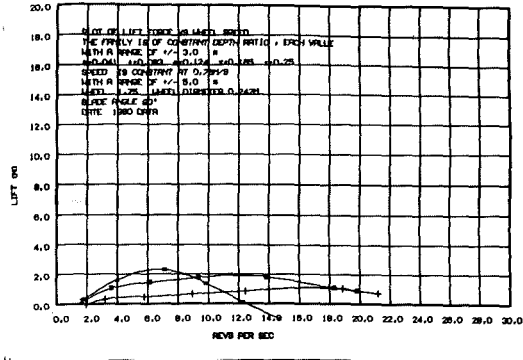
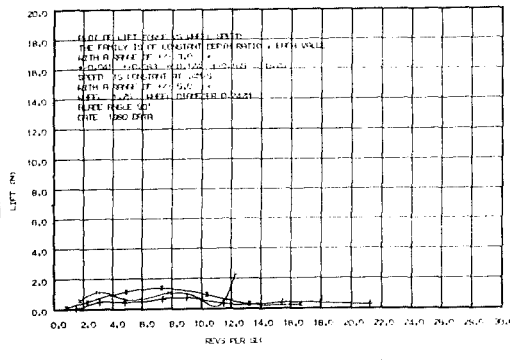


FIGURE 10.8: WHEEL 1.75, $\phi = 90^\circ$, DISPLACEMENT AND TRANSITION

Planing, $V_0 = 1.72 \text{ m/s}$, $F_r = 1.12$

Planing, $V_0 = 2.36 \text{ m/s}$, $F_r = 1.53$

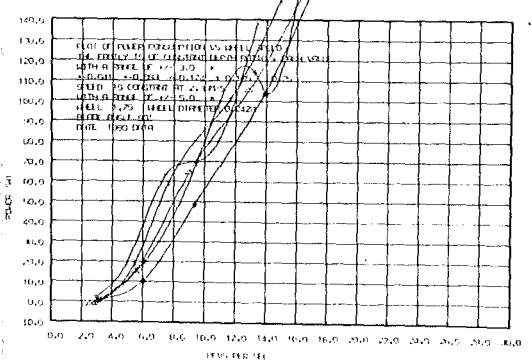
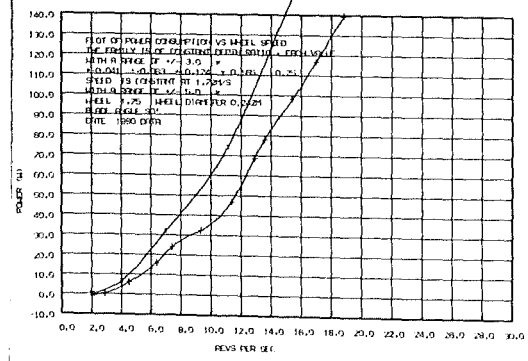
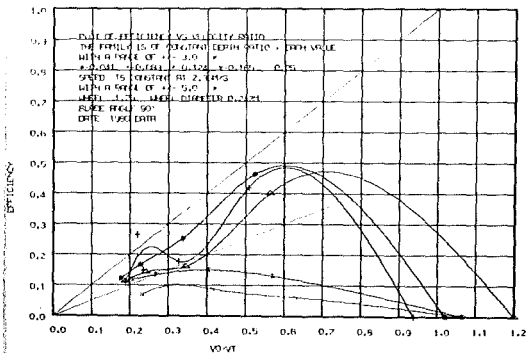
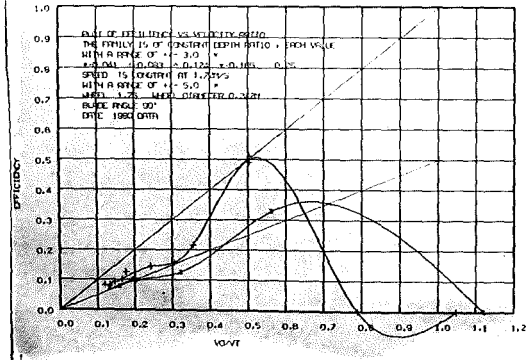
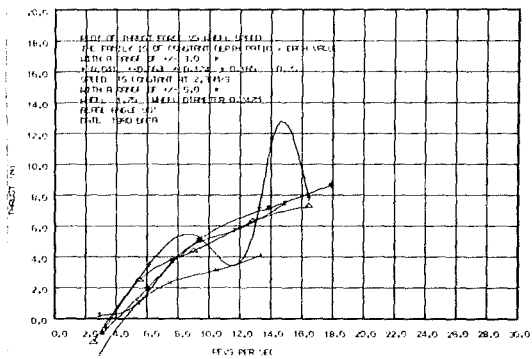
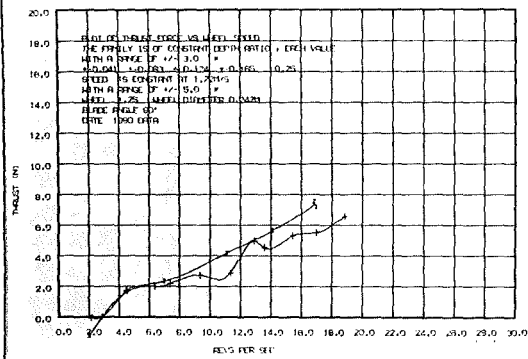
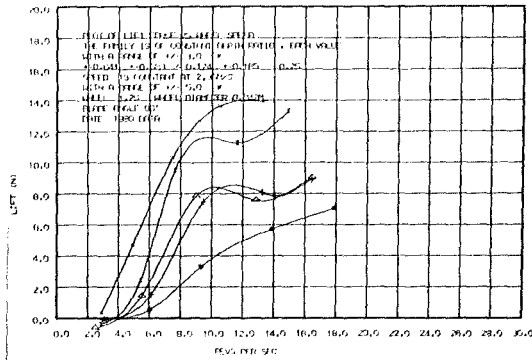
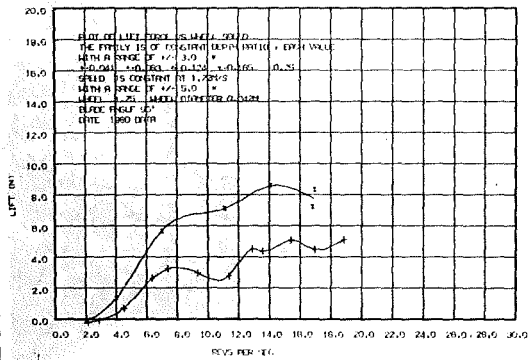


FIGURE 10.9: WHEEL 1.75, $\phi = 90^\circ$, PLANING OPERATION

points (1) and (2) above in the generalised findings (section 10.4).

Efficiency: This is a little lower than for FB, $\phi = 90^\circ$, especially for deep immersions where the 60° heel would have most effect. Efficiency is, however, throughout, markedly greater than efficiency for the FB, $\phi = 60^\circ$ wheel shown in Fig.9.1, 2 and 3.

This blade configuration in large part confirmed all the findings outlined in the generalised findings, section 10.4 above, and gave the best overall performance of any LPW. It was also tested on the model LPW craft which to date has shown it to be the most practical blade shape for traction through the displacement and transition zones, and for lift and traction at high speeds in the planing mode. (See the end of section 12.8.)

This blade shape was also tested at some immersion depths for a blade angle $\phi = 105^\circ$ where it performed well as a propulsor, as would be expected of its tip blade angle, and poorly as a lift device as would be expected from its edge-to-edge blade angle. Its results are shown in Appendix 4.

10.7 EQUAL SIZE TOE AND HEEL: WHEEL 1.25, $\phi = 105^\circ$

(See Appendix 4, and Fig. 10.3(C))

This blade type was more concave than the last, having an angle of 135° between the toe and heel. It was chronologically the first in the series of tests with concave blades and was tested at three tip angles, $\phi = 75^\circ$, $\phi = 90^\circ$ and $\phi = 105^\circ$, as well as in a perforated version at $\phi = 90^\circ$. The blades were again formed from flat blades of the standard chord of 25 mm. They were bent so that the vertex of the bend ran spanwise along the blades at mid chord. The tip in this case was set at $\phi = 105^\circ$ and the heel was than at 60° . These blades were shaped the same as the convex blades of wheel 6.75, $\phi = 45^\circ$ above, but they were turned around the other way. They are shown in Fig.10.3(C).

The purposes in examining this series were:

- 1) To attempt to get a better combination of lift and thrust than given by the constituent flat blades, FB, $\phi = 45^\circ$ and FB, $\phi = 90^\circ$.

WHEEL NO: 1.25

Blade Angle $\phi = 105^\circ$

Shaped Blades

Diameter, $D = 242$ mm

Span, $s = 76$ mm $s/D = .31$

Chord, $c = 25$ mm $c/D = .1$

No. of Blades = 6

Symbols	Immersion ratio	Immersion angle	Immersion depth
	d/D	θ°	d (mm)
*	.041	24	10
+	.083	33	20
Δ	.124	41	30
x	.165	48	40
=	.25	60	60

See also:

Figs	Sections
10.3	10.7
10.10 to	
10.12	

STATIC, $V_o = 0$

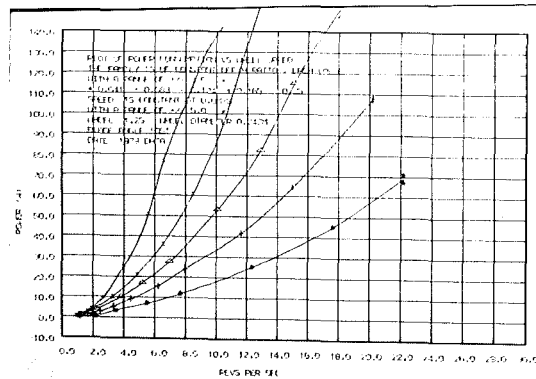
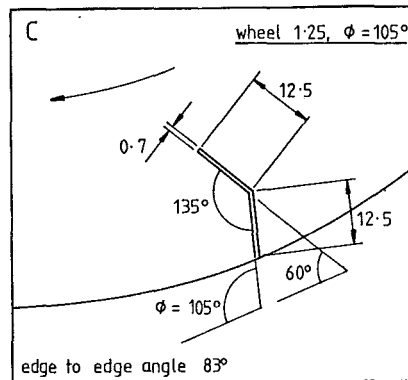
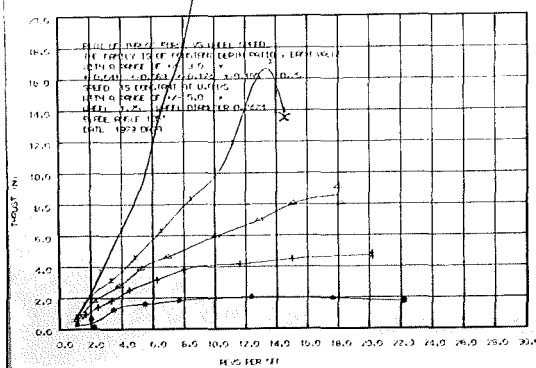
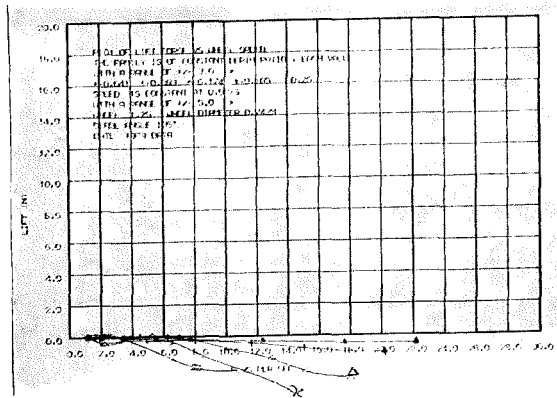


FIGURE 10.10: WHEEL 1.25, $\phi = 105^\circ$ STATIC OPERATION. NOTE NEGATIVE LIFT AND HIGH THRUST

Displacement, $V_0 = 0.4 \text{ m/s}$, $F_r = 0.26$

Transition, $V_0 = 0.76 \text{ m/s}$, $F_r = 0.49$

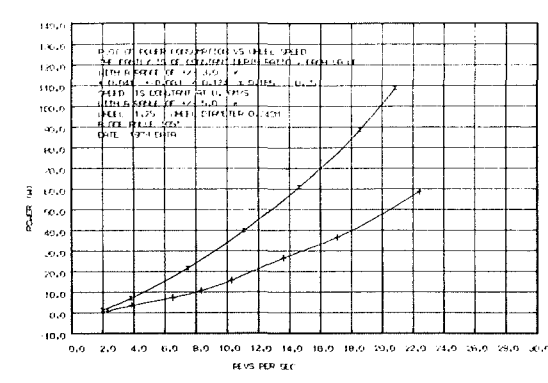
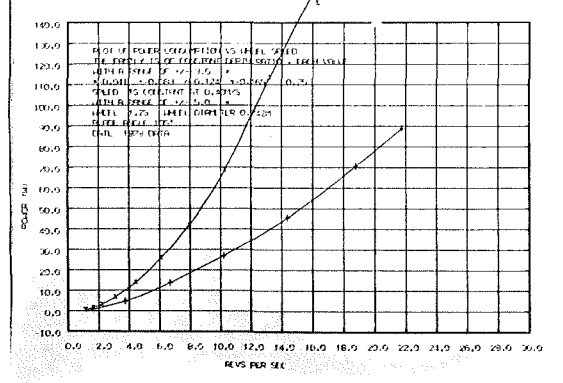
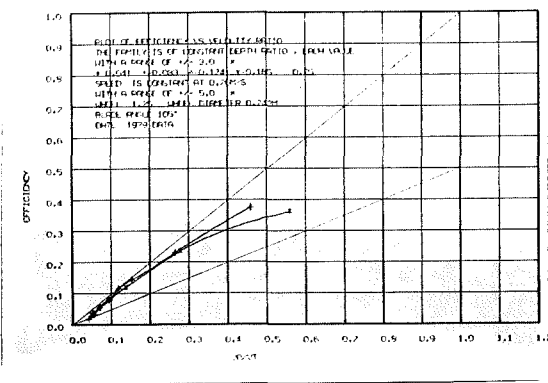
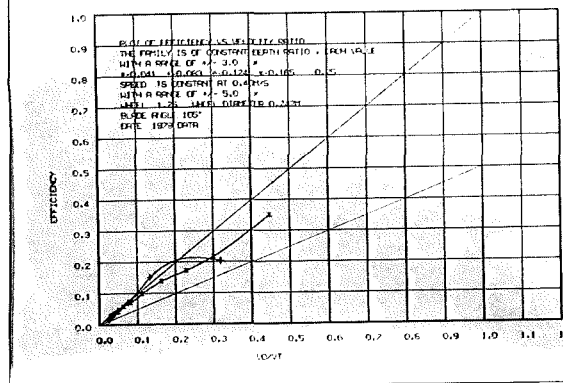
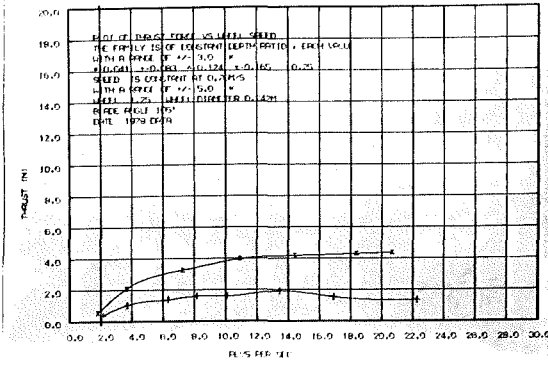
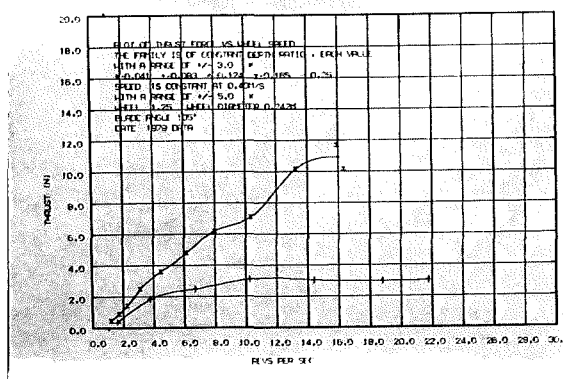
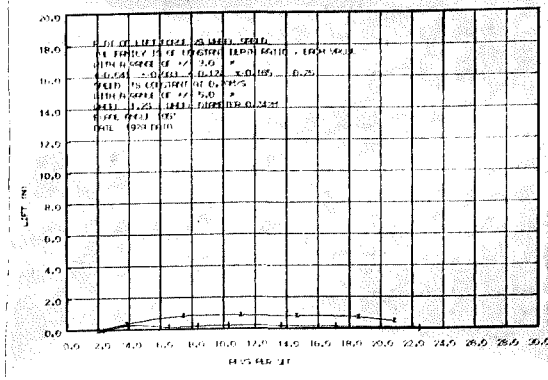
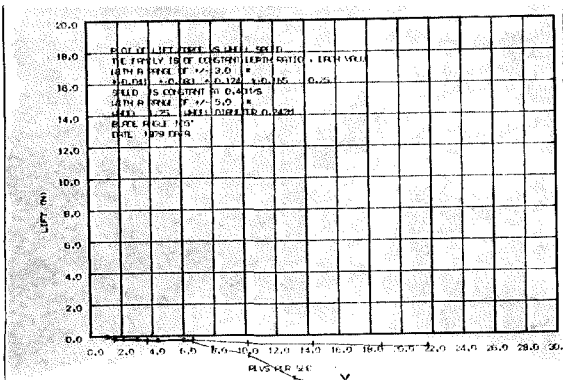


FIGURE 10.11: WHEEL 1.25, $\phi = 105^\circ$ DISPLACEMENT AND TRANSITION. NOTE THE CHANGE FROM NEGATIVE TO POSITIVE LIFT AT TRANSITION

Planing, $V_0 = 1.72 \text{ m/s}$, $F_r = 1.12$

Planing, $V_0 = 2.36 \text{ m/s}$, $F_r = 1.53$

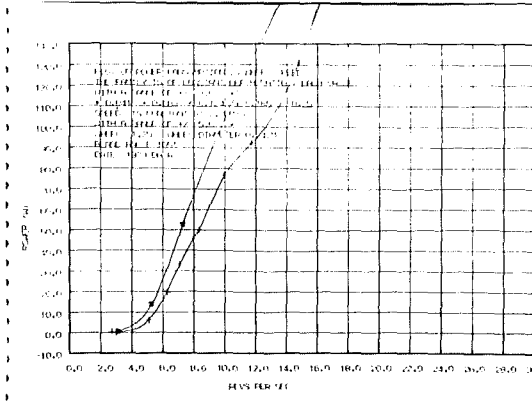
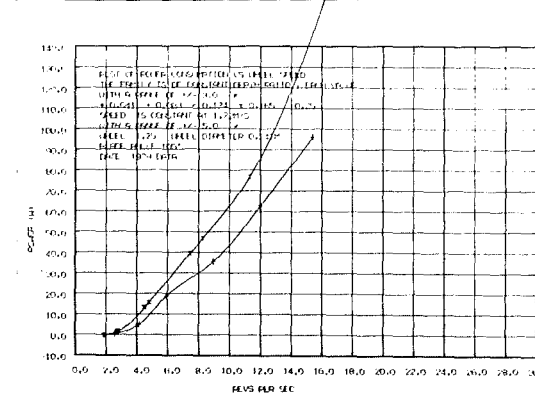
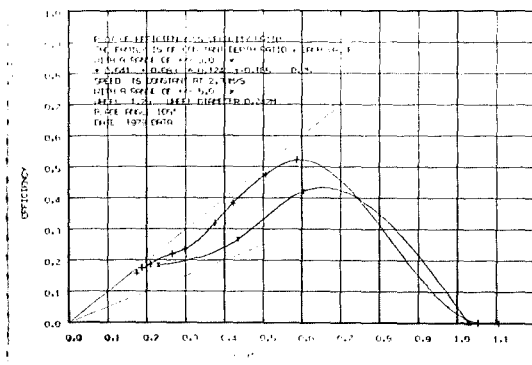
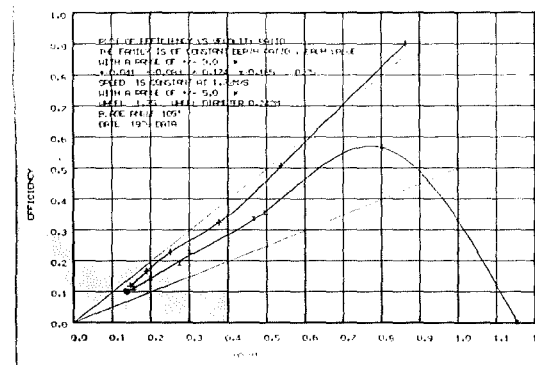
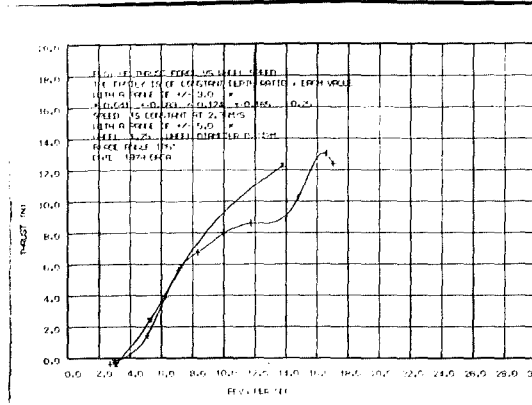
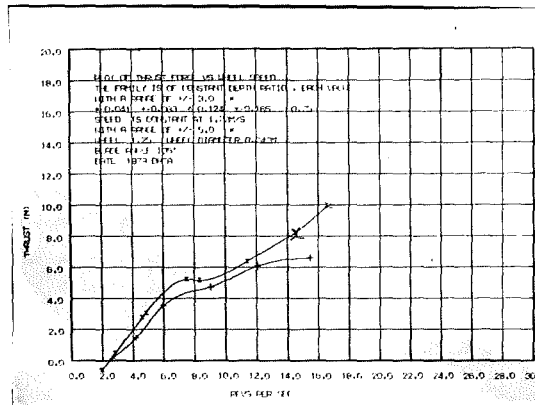
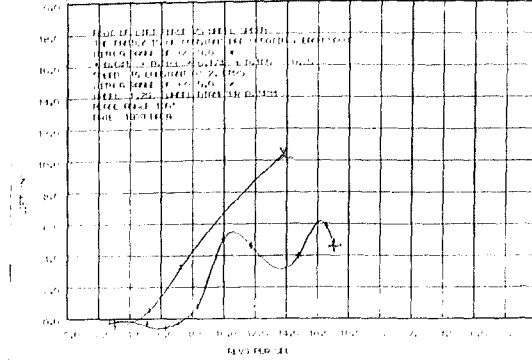
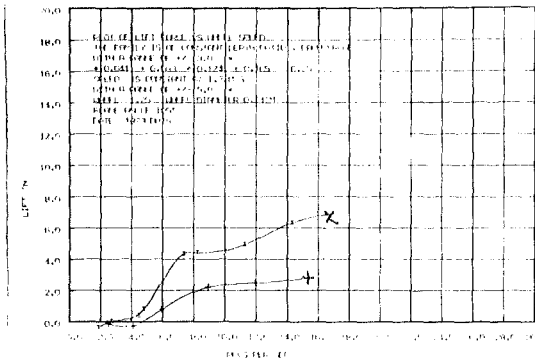


FIGURE 10.12: WHEEL 1.25, $\phi = 105^\circ$ PLANING OPERATION

- 2) To examine the effects of angle changes on concave blades.
- 3) To confirm that forces would be reduced with perforated blades as would be expected.

The results are shown in Figs.10.10, 11 and 12. While not all immersions were examined the results are as follows:

Lift: In the static and displacement modes lift is negative, and once planing, lift becomes positive only after cavity intrusion (6 rps at 2.36 m/s). With the edge-to-edge blade angle of 83° these results would be expected to closely follow those of the FB, $\phi = 90^\circ$ wheel (point (2) in the findings above, (section 10.4), and comparison with FB, $\phi = 90^\circ$ results in Appendix 4 shows that results are in fact very close, lift magnitudes throughout being possibly a little less than for FB, $\phi = 90^\circ$.

Thrust: From point (2) in the generalised findings and reference to Fig.4.24 and Fig.9.41, it would be expected that thrust would be a little less than for FB, $\phi = 90^\circ$ and greater than for FB, $\phi = 120^\circ$. (Results for FB, $\phi = 120^\circ$ are in Appendix 4.) This is not quite the case, however, and thrust is seen to be greater than FB, $\phi = 90^\circ$ throughout the range. In fact the thrust of this blade at this angle was the greatest of any of the bladed LPW's tested.

Efficiency: Although there was not a broad selection of results, especially at high velocity ratios, the results available suggest efficiencies at least as good as the FB, $\phi = 90^\circ$ results, better than for FB, $\phi = 120^\circ$, and on much the same level as those for the last blade shape examined, namely wheel 1.75, $\phi = 105^\circ$. These high efficiencies, especially at high velocity ratios ($\frac{V_o}{V_t} > 0.6$) lend support to the idea that for high efficiency blades should be designed so that the tips enter at small angles of attack, reducing shock entry losses. This idea was noted earlier in section 4.6.6 and Fig.4.15 and was the idea behind Beardsley's curved blades, Fig.2.9. (1)

This blade at this angle was the best in terms of thrust and propulsive efficiency of any bladed LPW. Its efficiency exceeded that of Beardsley's "typical" blades which are not dissimilar in

shape in their outer portion (Fig.2.9). With its poor lift, however, this blade shape would not be suitable as a lifting device; good lift blades seem to require shock or impulsive blade entry to generate a useful lift force, and they consequently have lower propulsive efficiencies.

10.7.1 Variation in Blade Angle with These Concave Blades

(See Appendix 4, wheel 1.25)

This same blade shape was tested at a tip angle of $\phi = 90^\circ$ and $\phi = 75^\circ$. The results were unremarkable in that they, without exception, supported the findings outlined in section 10.4 above. It may be said therefore that the effects of blade angle upon slightly concave blades like this one are little different than the blade angle effects on flat blades as shown in Figs. 4.24 and 9.41, as long as the edge-to-edge blade angle is used for determining lift variation, and tip angle is used for determining thrust variation.

10.8 PERFORATED CONCAVE BLADES: WHEEL 7.75, $\phi = 90^\circ$

(See Appendix 4 and Fig.10.3(F))

It is sometimes of value to test well established assumptions in new situations, especially if differences of opinion may be settled by such action. For this reason wheel 1.25, $\phi = 90^\circ$ (section 10.7 and Fig.10.3(C) above) had the blades altered by drilling six 6 mm holes along the vertex of the bend as shown in Fig.10.3(F). The expected results were a reduction in both lift and thrust as compared with those of the parent wheel, wheel 1.25, $\phi = 90^\circ$. Comparison between the results for the two wheels in Appendix 4 (wheel 1.25, $\phi = 90^\circ$, and wheel 7.75, $\phi = 90^\circ$) confirms that this is the case, showing that forces have been reduced approximately in proportion to the area reduction (9%) while efficiency seems to remain unaltered.

10.9 RIGHT-ANGLED CONCAVE BLADES: WHEEL 7.5, $\phi = 90^\circ$

(See Appendix 4 and Fig.10.3(D))

This is the next stage in blade concavity from wheel 1.25, and although only results from the planing mode are available they provide some valuable insights. Once again the blades were formed from flat blades of 25 mm chord, which in this case were bent at right angles so that the vertex of the bend ran spanwise along the centre of the blade. With the tip set at $\phi = 90^\circ$ the inner portion

or heel was set parallel to the tangent, or at 0° as shown in Fig. 10.3(D). With this arrangement the edge-to-edge blade angle was 45° . The results are given in Fig.10.13.

Lift: Lift would be expected to be close to that of FB, $\phi = 45^\circ$ (Appendix 4, wheel 6, $\phi = 45^\circ$) and this is found to be the case but only after cavity intrusion has occurred. Before cavity intrusion lift seems to be low, more like the zero lift of the FB, $\phi = 90^\circ$ wheel before cavity intrusion. (See Appendix 4, wheel 6, $\phi = 90^\circ$). This is not altogether in line with the prediction of point (2) in the generalised findings suggesting that lift varies with edge-to-edge blade angle. After cavity intrusion, however, the lift forces are high, being higher than for any LPW tested; they are closest to those of FB, $\phi = 45^\circ$ as expected.

Thrust: From the generalised findings thrust would be expected to be almost as high as for FB, $\phi = 90^\circ$ results. This is not the case, however, and thrust is lower, being nearest to that of FB, $\phi = 75^\circ$ (Appendix 4, wheel 6, $\phi = 75^\circ$). This seems too great a reduction to be simply a result of the reduced effective blade chord at $\phi = 90^\circ$, and seems to be affected by the nearby heel of the blade.

Efficiency: Propulsive efficiency seems poor as this wheel has traded its thrust and propulsive efficiency for lift and unknown losses.

This blade type seems unsuitable for use on the LPW craft because of its low lift before cavity intrusion in the planing mode, where the LPW would normally operate. It should be kept in mind however, because its high lift forces may be of some special use.

For this wheel the generalised findings of section 10.4 are beginning to break down, as noted in section 10.4 point (5).

Of some special note is the possible effect of the 0° heel portion of the blade on the thrust and propulsive efficiency. It is probable that if this part of the blade was simply removed thrust and efficiency would be higher, like that of FB, $\phi = 90^\circ$ wheels while lift would be lower, also like that of the FB, $\phi = 90^\circ$ wheels. This part of the blade, then, seems to generate a large part of the lift force at the expense of thrust and efficiency. This sort of action is worth investigating further.

PLANING SPEEDS

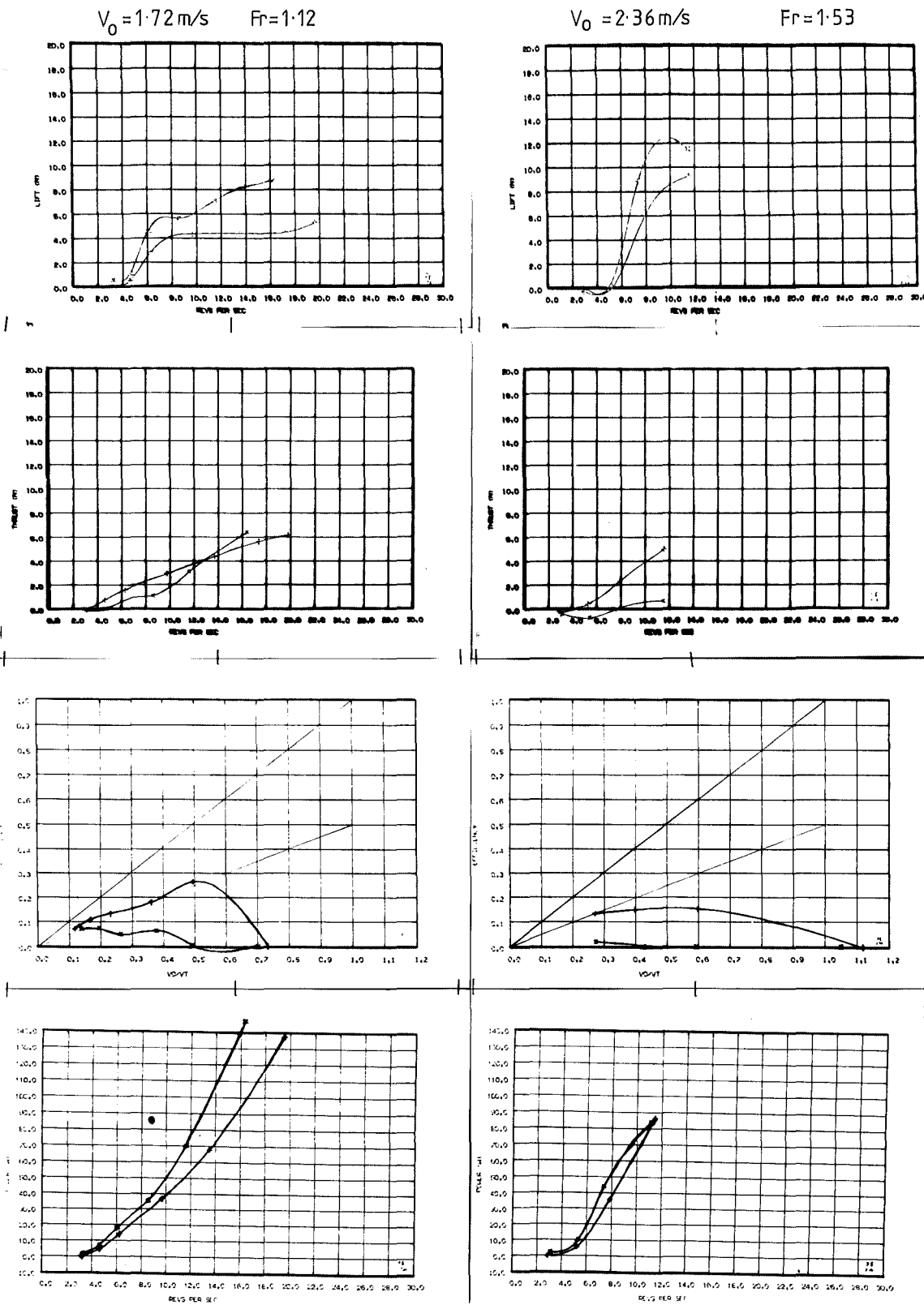


FIGURE 10.13: WHEEL 7.5, $\phi = 90^\circ$, PLANING OPERATION (ONLY)

It would appear that Beardsley's "typical" blades and smoothly curved blades (see Fig.2.9) may have demonstrated lower efficiencies than flat bladed LPW's because they had similar heels to this blade. (1) It is also likely that Beardsley's wheels would have demonstrated appreciable lift like this wheel, if it had been measured. (2) (It was also suggested earlier that the lower efficiencies recorded by Beardsley may have been a result of his blade tip angles of $\phi = 120^\circ$ as noted in section 9.4.8.2.)

10.10 SEMICIRCULAR CONCAVE BLADES: WHEEL 11, $\phi = 135^\circ$

(See Appendix 4 and Fig.10.3(E))

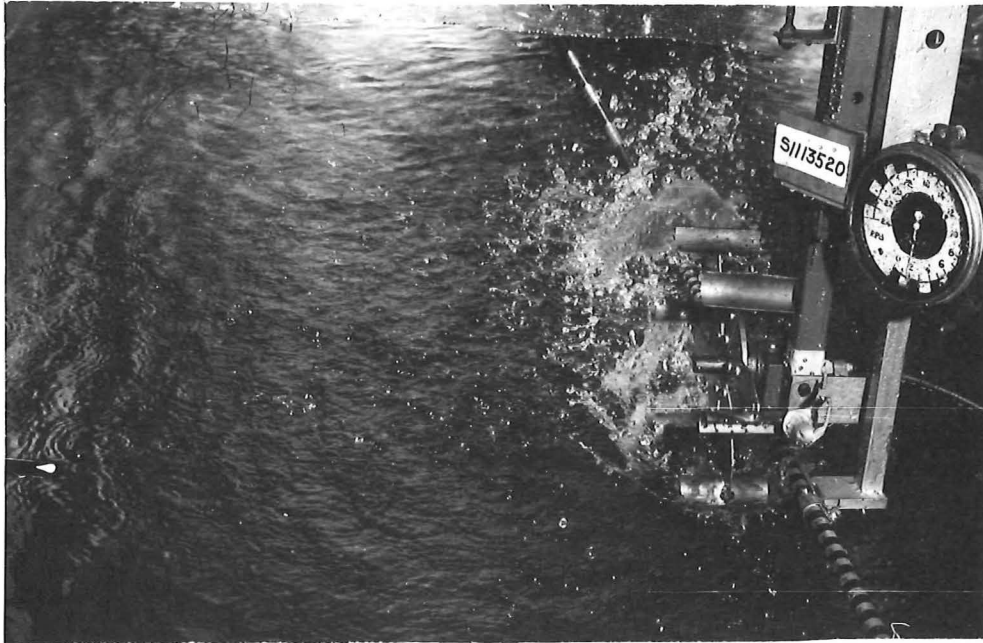
Next in increasing concavity are blades of a semicircular concave form as shown in Fig.10.3(E), and photographed in static mode operation in Fig.10.14. They were made by cutting 25 mm internal diameter copper tube down the centre. The actual surface area of the blades was therefore greater than the others tested by a factor of $\frac{\pi}{2}$. These blades were tested at only one blade tip angle of $\phi = 135^\circ$ and this setting gave them an edge-to-edge blade angle of 45° . The purposes in testing these blades were to see whether smooth blade entry would give high efficiency, to find out if they threw up more water because of their cupped shape and to provide a (rough) comparison with Beardsley's curved blades (3) (see section 2.26 and Fig.2.9). The results are shown in Figs.10.15, 16 and 17.

Lift: Static, displacement and transition lift forces are low, and at deep immersions they become negative at high wheel revolutions. This trend with wheel revolutions appears to indicate the blades are picking up spray. The edge-to-edge blade angle of 45° would suggest much higher lift forces should be reached than are found, so it seems that in this case (as for the last) the edge-to-edge blade angle comparison with flat blade results is beginning to break down. In the planing mode lift forces are small or negative before cavity intrusion (~ 6 rps at 2.36 m/s) as they were for the last wheel, 7.5, $\phi = 90^\circ$, and at small immersions after cavity intrusion they remain small as suggested by point (4) regarding small immersions in the generalised findings (section 10.4). For larger immersions, however, lift forces after cavity intrusion are exceptionally large and would appear to exceed those for FB, $\phi = 45^\circ$ which should compare with the edge-to-edge blade angle of this wheel. At planing speeds spray thrown up by the

1. Beardsley, P.19, Fig.15.

3. Beardsley, P.18

2. Beardsley, P.15



1205B/6A

FIGURE 10.14: WHEEL 11 WITH THE CUPPED BLADES AT 3 RPS
IN THE STATIC CONDITION. $d/D = 0.08$,
 $D = 0.242$ m

WHEEL NO: 11

Blade Angle $\phi = 135^\circ$

Shaped Blades

STATIC, $V_o = 0$

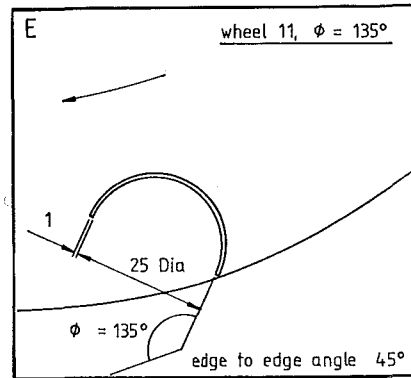
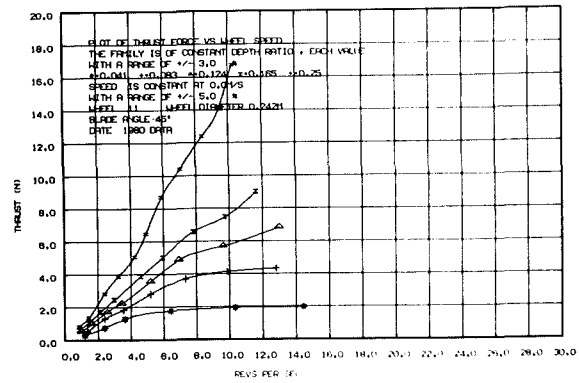
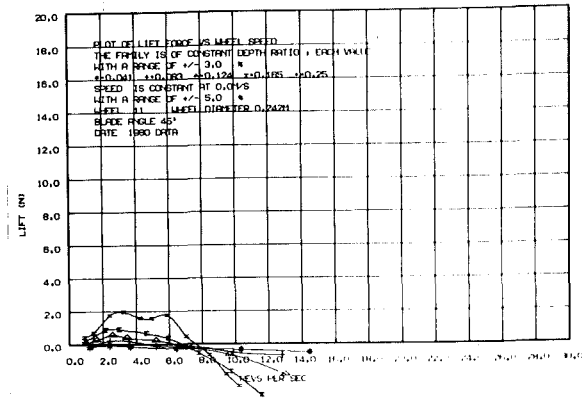
Diameter, $D = 242$ mm

Span, $s = 76$ mm $s/D = .31$

Chord, $c = 25$ mm $c/D = .1$

No. of Blades = 6

Symbols	Immersion ratio	Immersion angle	Immersion depth
	D/d	θ°	d (mm)
*	.041	24	10
+	.083	33	20
Δ	.124	41	30
x	.165	48	40
=	.25	60	60



See also:

Figs 10.3, 10.14 to 10.17
 Sections 10.10

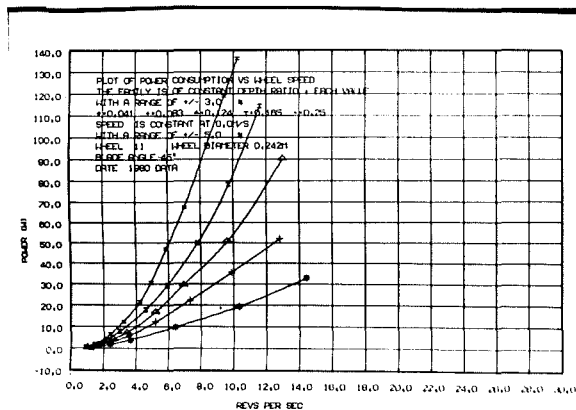


FIGURE 10.15: WHEEL 11, $\phi = 135^\circ$, STATIC OPERATION

Planing, $V_0 = 1.72 \text{ m/s}$, $F_r = 1.12$

Planing, $V_0 = 2.36 \text{ m/s}$, $F_r = 1.53$

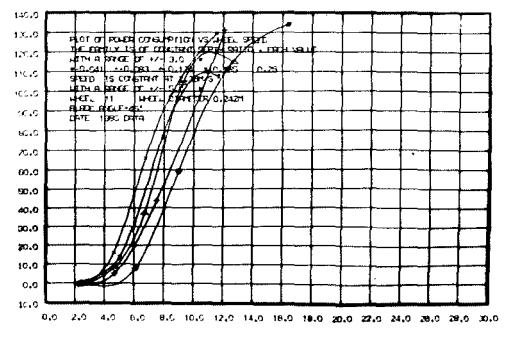
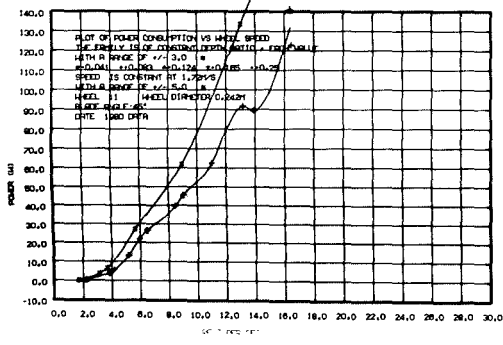
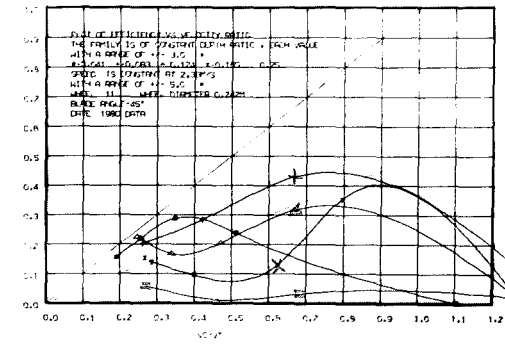
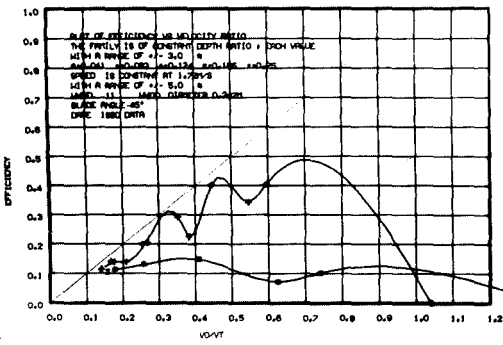
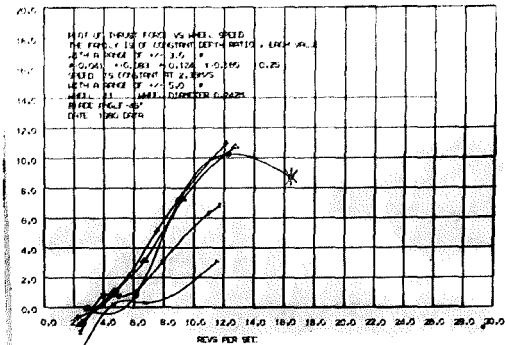
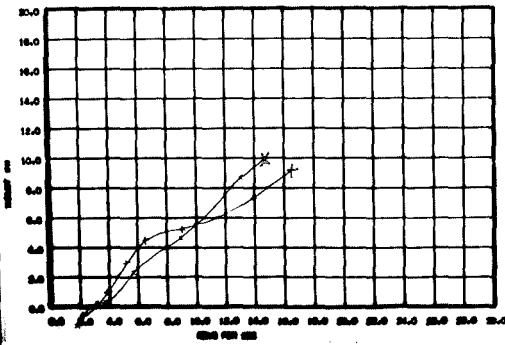
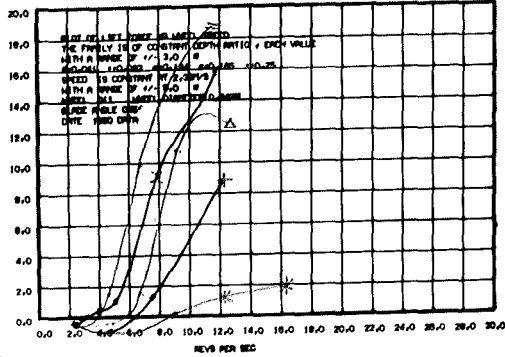
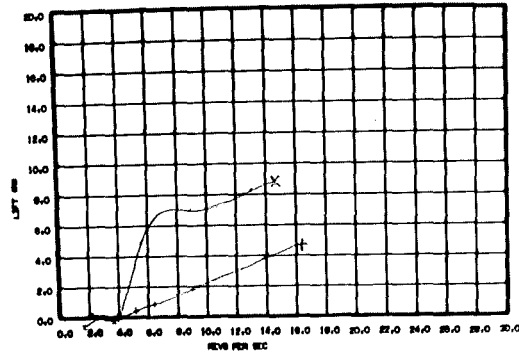


FIGURE 10.17: WHEEL 11, PLANING OPERATION

blades is not seen to reduce the lift at all at high wheel revolutions. Thus for deeply concave blades the lift force can no longer be predicted at all speeds from flat blade results based on the edge-to-edge angle. This prediction does, however, seem to hold after cavity intrusion in the planing mode.

Thrust: Below planing speeds thrust is greater than for $FB, \phi = 90^\circ$ and rivals that of the best propulsor to date, wheel 1.25, $\phi = 105^\circ$, Figs.10.10, 11 and 12 (see section 10.7 above). It in fact exceeds the results of wheel 1.25 through the transition zone where its very high blade angle can be imagined as scooping up water from the edge of the wave trough. Once in the planing mode, thrust forces can be seen to be small before cavity intrusion but then to continue to exceed those of $FB, \phi = 105^\circ$ after cavity intrusion. It is clear that points (1) and (2) in the generalised findings (section 10.4) have also broken down in predicting the expected thrust forces in this case - thrust force is much in excess of what would be expected of a $FB, \phi = 135^\circ$ wheel, as shown by Fig.4.24 or Fig.9.41.

Efficiency: The fact that thrust in the planing mode does not develop fully until after cavity intrusion, prevents the efficiency from being high at high velocity ratios (low wheel revolutions) where the peaks of efficiency curves normally occur. Efficiency cannot be high at low velocity ratios (high wheel revolutions) after cavity intrusion because of the theoretical limitation that efficiency must be less than velocity ratio. The efficiency results are therefore flattish curves which are not as good as those of other reasonable propulsors, for example $FB, \phi = 90^\circ$, and instead show mediocre values like those for $FB, \phi = 60^\circ$. These flattish curves show a general similarity to Beardsley's efficiency results. (1)

Inferences from Fig.4.13 indicate that ideal entry conditions with zero angle of attack, γ , should occur at velocity ratios of about $\frac{V_o}{V_t} = 0.75$ for this blade angle of $\phi = 135^\circ$. Reference to the efficiency curves for the planing mode in Fig.10.17 shows no evidence at all of specially high propulsive efficiencies occurring at this velocity ratio. The hypothesis proposing high efficiencies for good entry conditions is therefore not supported in this case.

1. Beardsley P.17, Fig.12 and 13.

This wheel clearly did not fit in with the general trends of the findings for curved blades, possibly because of its much greater curvature. It is therefore the least well understood, but since it demonstrated large forces, both lift and thrust, in the planing mode it may be worth investigating further. In the meantime this blade shape is best avoided on LPW craft.

10.11 DIFFERING ANGLES ON ALTERNATE FLAT BLADES: WHEEL 1

(See also results in Appendix 4)

While this wheel does not have curved blades its intended purpose was most closely related to those of curved blades.

It was relatively easy to test a wheel with three flat blades at $\phi = 45^\circ$ alternating with three at $\phi = 90^\circ$, to again investigate the possibility of obtaining the lift advantage of the $\phi = 45^\circ$ blades with the thrust advantage of the $\phi = 90^\circ$ blades. Wheel 1, $\phi = 45^\circ$, $\phi = 90^\circ$ was used to assess the value of this configuration at only two immersion depths. The results are shown in Figs.10.18, 19 and 20.

Lift: In the static and displacement modes lift is a little lower than for FB, $\phi = 45^\circ$ blades alone (Appendix 4, wheel 6, $\phi = 45^\circ$) and much greater than for FB, $\phi = 90^\circ$ (Appendix 4, wheel 6, $\phi = 90^\circ$). Deeper immersions show a small decline in lift with increased wheel revolutions which suggests that the wheel is throwing up spray. (This was also evident at displacement speeds for the model craft where this wheel type caused it to submerge by throwing up a large amount of water.) In the transition zone lift is little different from the FB, $\phi = 45^\circ$ wheel. Once planing, lift forces before cavity intrusion are low, but after cavity intrusion, they are again similar to those of the FB, $\phi = 45^\circ$ wheel. Thus in terms of lift this wheel generates forces which model those of one of the most advantageous blade angles for lift, that of $\phi = 45^\circ$, except, unfortunately, before cavity intrusion, in the planing mode where it would be expected to operate.

Thrust: Up to the transition speed thrust is a little greater than for the FB, $\phi = 45^\circ$ wheel and less than for the FB, $\phi = 90^\circ$ wheel. Once planing, however, the thrust curves take a peculiar form: before cavity intrusion (before 6.1 rps at 2.36 m/s) they begin to increase with wheel revolutions as would be expected of a three-bladed, FB, $\phi = 90^\circ$ wheel and then after cavity intrusion they follow the FB, $\phi = 45^\circ$ results which have low or negative thrust with an

inverse relation between thrust force and immersion depth.

Efficiency: In the planing mode the efficiency values are not high at high velocity ratios, comparing with FB, $\phi = 60^\circ$ or FB, $\phi = 75^\circ$ wheels before cavity intrusion has begun. After cavity intrusion these efficiencies become low and negative as does the thrust force at low velocity ratios, or higher wheel revolutions.

This blade configuration shows no special advantages for the LPW craft. Instead it poses a number of confusing questions concerning the behaviour of the flow through the wheel and the forces generated. Until the flow is better understood this configuration should be avoided on LPW craft. No further tests have been conducted on this wheel type as a result of these findings.

10.12 CONCLUSIONS

A good working understanding of all curved LPW blades has not yet been achieved, but attention has been directed to the most promising areas. Convex blades have not been found useful since they seem to act little differently than flat blades of the same blade angle as their tip angle. Highly concave blades (angle between toe and heel being less than 90° , as for wheel 11, section 10.10 above) may yet prove valuable since large forces can be generated by them, but this project has not been able to adequately clarify flow around them and has found them to have low efficiencies. Attention has again been directed elsewhere. Wheels with alternating blades at different angles have produced poor and confusing results.

Blades of small concavity have been found, however, to be able to combine a number of the advantages found in widely different flat-bladed wheels. A method of satisfactorily predicting their performance by comparison with the performance of flat blades has evolved. These generalised results were noted earlier in the chapter (section 10.4 above) and while they do not offer the sort of analytical precision of the impulse theory for flat blades, they do at least enable usable predictions to be made of the capabilities of these, the best LPW's tested to date.

WHEEL NO: 1 (FB)

Blade Angle $\phi = 45^\circ, 90^\circ$

Flat Blades, Alternate angles

STATIC, $V_o = 0$

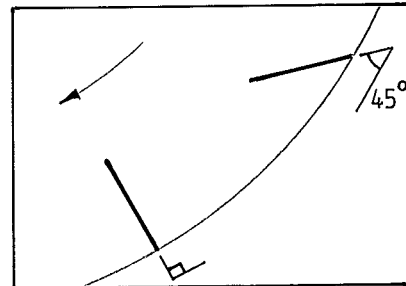
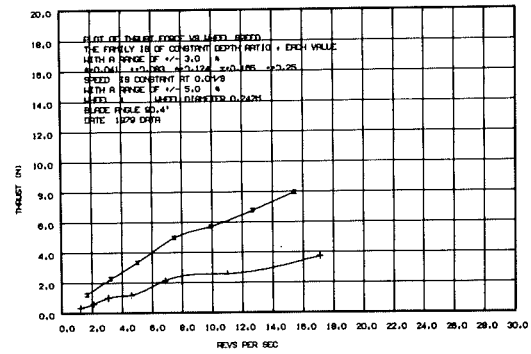
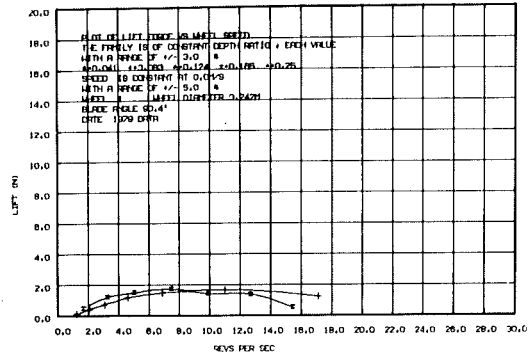
Diameter, $D = 242$ mm

Span, $s = 76$ mm $s/D = .31$

Chord, $c = 25$ mm $c/D = .1$

No. of Blades = 6

Symbols	Immersion ratio	Immersion angle	Immersion depth
	D/a	θ_o	a (mm)
*	.041	24	10
+	.083	33	20
Δ	.124	41	30
x	.165	48	40
=	.25	60	60



See also:

Figs 10.18 - 10.20 Sections 10.11

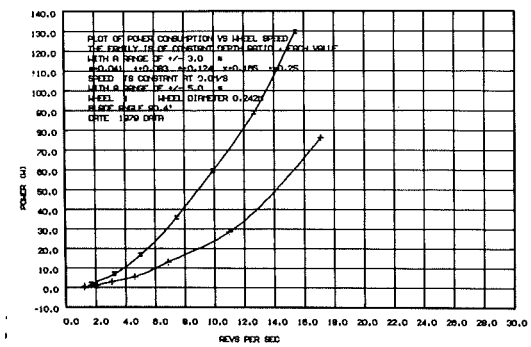


FIGURE 10.18: WHEEL 1, $\phi = 90^\circ, 45^\circ$ ALTERNATING. STATIC

Displacement, $V_0 = 0.4 \text{ m/s}$, $F_r = 0.26$

Transition, $V_0 = 0.76 \text{ m/s}$, $F_r = 0.49$

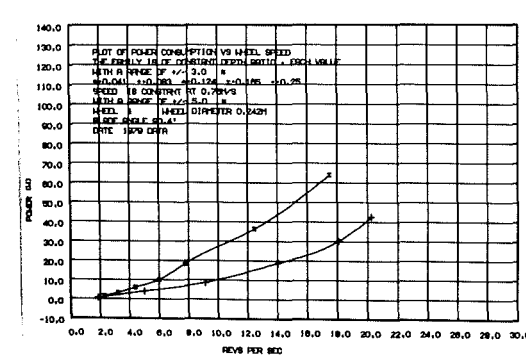
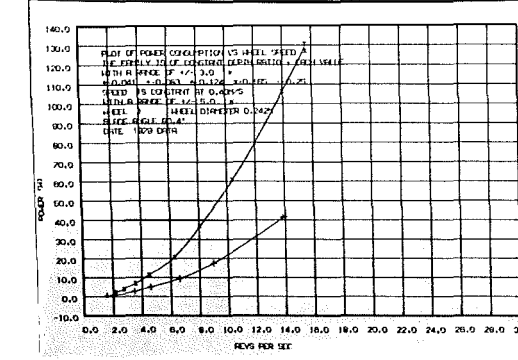
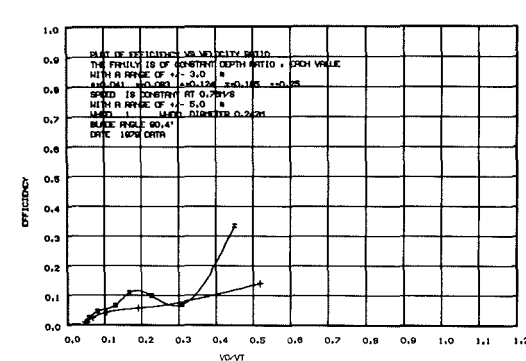
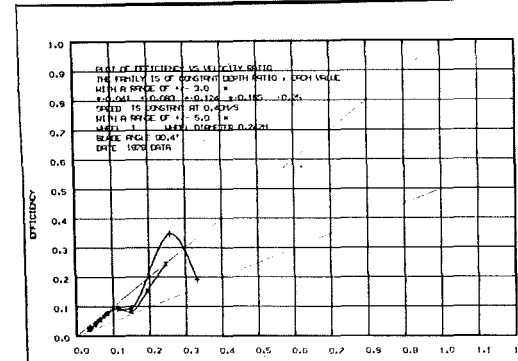
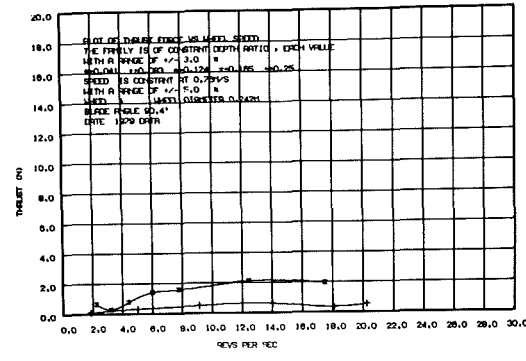
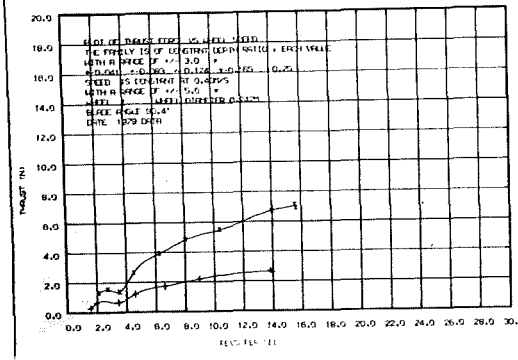
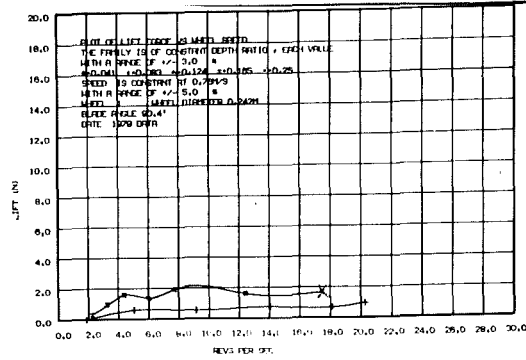
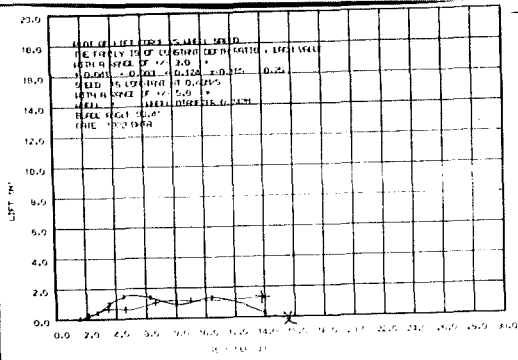


FIGURE 10.19: WHEEL 1, $\phi = 90^\circ, 45^\circ$. DISPLACEMENT AND TRANSITION

Planing, $V_0 = 1.72 \text{ m/s}$, $F_r = 1.12$

Planing, $V_0 = 2.36 \text{ m/s}$, $F_r = 1.53$

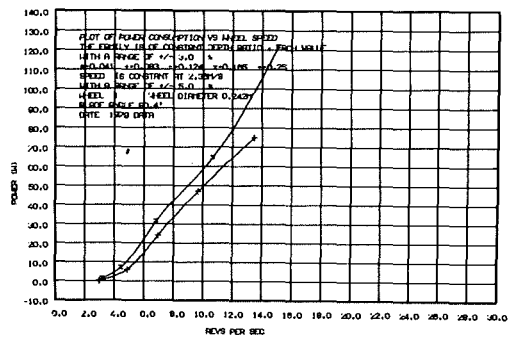
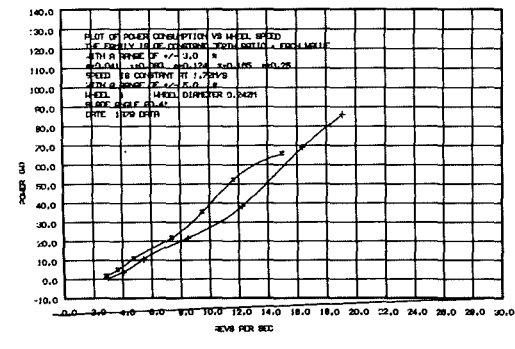
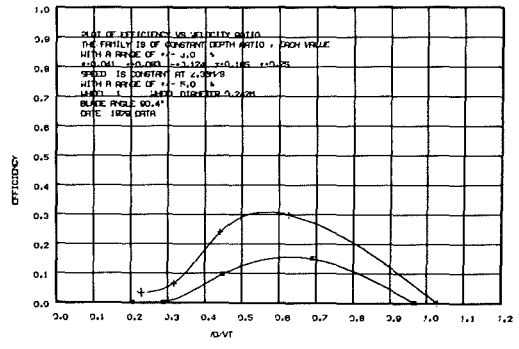
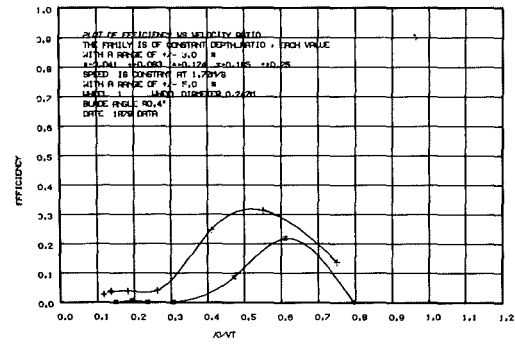
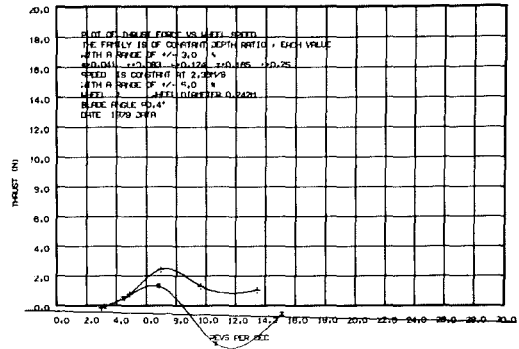
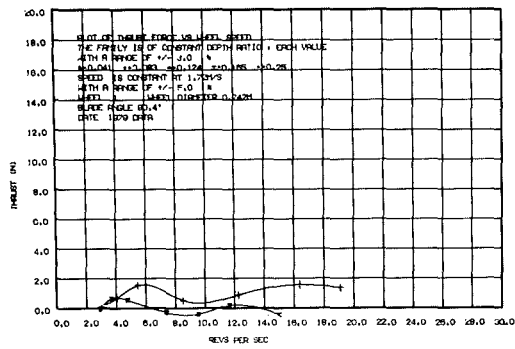
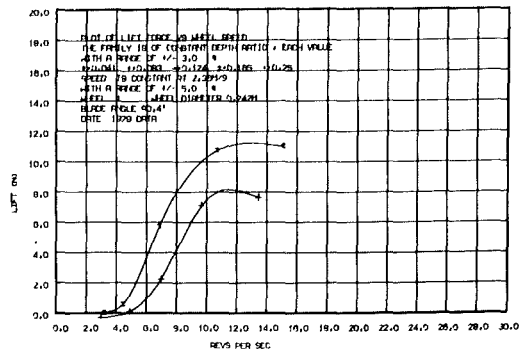
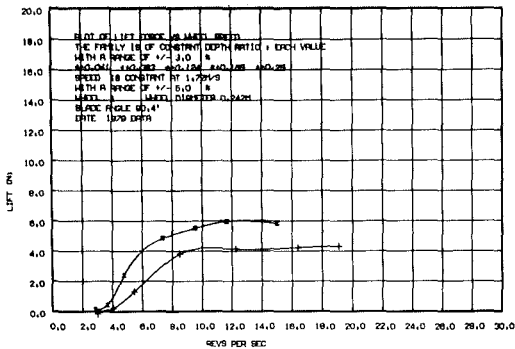


FIGURE 10.20: WHEEL 1, $\phi = 90^\circ, 45^\circ$, PLANING OPERATION

CHAPTER 11

RESULTS FOR CONTINUOUS SURFACE ROTORS USED AS LPW'S11.1 INTRODUCTION

Apart from the usual LPW configuration of blades mounted on a relatively empty space structure there are a number of variants of overall wheel form which can be imagined as having some advantage in LPW-type applications. One such variant is a wheel type with a continuous surface beneath the blades such as a cylinder, with blades mounted around it. Rotors of this sort were examined by Kearsey, Wray and Starrett, and Beardsley, with Kearsey being the only one to examine lift forces. This chapter examines the results of this project's tests of wheels of this sort, in the following order:-

- 1) A smooth cylinder with the same dimensions as the standard LPW.
- 2) A model of Kearsey's inflatable, flexible-skinned Rollercraft wheel, and a metal wheel with cupped blade forms like those of the Rollercraft wheel.
- 3) A small ribbed tractor tyre, tested with the tread pointing in each of the two possible directions.

This variety of wheels was tested in order to broaden the base of the experimental work and thereby discover any notable qualities or disadvantages in such wheels when they are seen as lifting, as well as propulsion devices. Like the last chapter, this one was able to identify common results, which in this case appear to apply to all wheels with continuous surfaces beneath the blades.

This chapter assists in the secondary aims loop parts 2 and 3 of Fig.3.10, by providing a data source from which hypotheses may be formed and against which new ideas may be compared.

11.2 GENERALISED FINDINGS FOR CONTINUOUS SURFACE WHEELS

The following results were found more or less throughout the data of the wheels examined in this chapter. Since it is easier to make sense of the results of each wheel if the generalised findings are known, they are presented first.

(1) These wheels create wake patterns like those of the LPW in the static, displacement and transition modes. In the planing mode, unlike the LPW, they generally exhibit bowsplash for all wheel revolutions. (The normal LPW exhibits bowsplash only after a certain wheel revolutions is reached in the planing mode; see section 9.4.3.2).

Lift Force Findings:

(2) In the static, displacement and transition zones, high speed rotation of these wheels causes them to pick up water making a fountain of spray. This results in negative lift forces which become increasingly negative with increases in immersion depth and wheel revolutions. This effect is less noticeable in the planing mode.

(3) As speed of advance is increased from static, any buoyancy forces present decrease because of changes in flow around the wheel (at fixed immersion).

(4) As speed of advance is increased from static, some dynamic lift is generated by the flow meeting the front surfaces of the wheel, and this increases with speed, opposing the loss of buoyancy. This effect is enhanced by the presence of blades on the wheel surface.

(5) Rotation of a bladed wheel of this sort, in the planing mode, generates impulsive blade entry forces like the LPW forces. This seems to enhance both lift and thrust forces.

Thrust Force Findings

(6) The wavedrag of these wheels exceeds skin friction and increases with speed of advance as would the wavedrag of a boat hull. In the planing mode this drag seems to be further increased by the development of bowsplash.

(7) Rotation of these wheels produces positive thrust which in some conditions is sufficient to overcome the wavedrag.

It is worth noting particularly, that the lift forces generated by these sorts of wheels are relatively complex, comprising buoyancy, planing forces and impulsive blade entry forces, opposed by loss of buoyancy and the throwing up of spray.

11.3 THE SMOOTH CYLINDER: WHEEL 0

(Results also in Appendix 4)

While it was hardly imagined that a solid smooth cylinder would perform in any way as well as the LPW there are a number of reasons why running a series of tests on such a wheel of the same dimensions as the LPW would be of value:

- 1) The wake patterns from a moving cylinder, either rotating or stationary would be a useful reference for comparison with LPW wakes.
- 2) The cylinder is an extreme form of the LPW or paddlewheel as it can be imagined as having an infinite number of blades. It therefore serves as a limiting case of the LPW form where, unlike operational LPW's water is completely prevented from passing through the wheel circumference.
- 3) Claims have been made that a smooth cylinder is capable of providing dynamic support while rolling over a water surface at speed. Since this is essentially the LPW concept it deserves some investigation. (Such ideas were noted in sections 2.3.4, 2.4.1, 2.4.2, 2.4.3.)

For these reasons, then, a solid cylinder was fabricated of wood, waterproofed, and tested on the LPW force balance over the standard series of immersions and speeds, as well as being examined photographically.

11.3.1 Force Balance Tests

These tests were generally no different than the force balance tests of the LPW's as described in section 6.4.2. They involved lift, thrust and torque measurements at a series of wheel revolutions (including zero rps) for the five immersion depths and five speeds of advance examined for the LPW's.

The measurement and interpretation of the lift forces in this case, however, requires some explanation. It is clear that the stationary cylinder, partly immersed will experience a buoyancy force. Once moving while held at a constant immersion the flow around the cylinder changes the immersed volume, so that the buoyancy force alters; dynamic forces also appear, and rotation of the moving cylinder changes the flow and the forces further. Since the LPW in its usual

WHEEL NO: 0

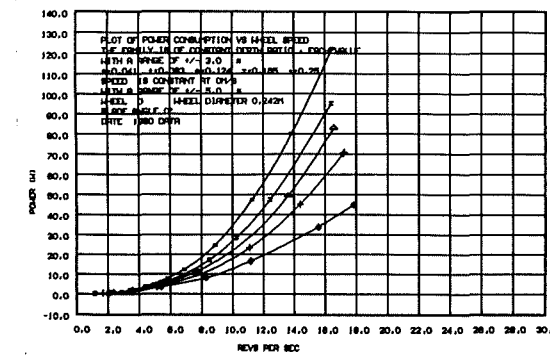
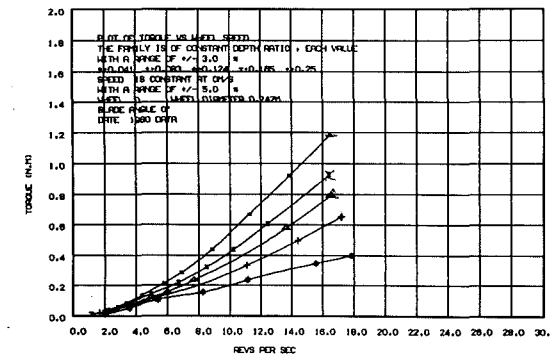
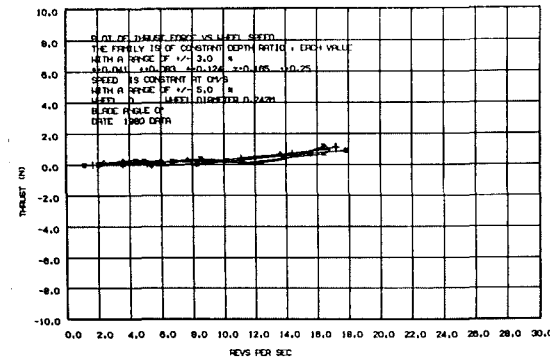
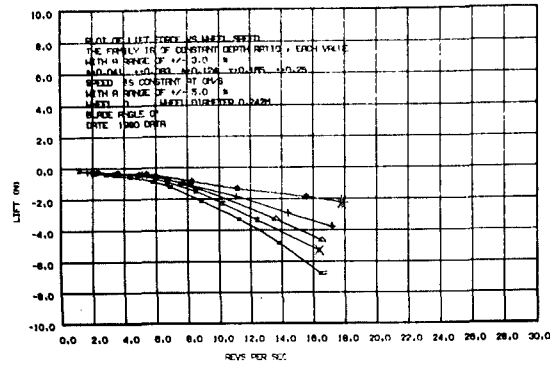
Solid Cylinder

Diameter, $D = 242$ mm

Span, $s = 76$ mm $s/D = .31$

STATIC, $V_o = 0$

Symbols	Immersion ratio	Immersion angle	Immersion depth	Buoyancy force (N)
	D/d	θ°	d (mm)	
*	.041	24	10	.48
+	.083	33	20	1.4
Δ	.124	41	30	2.4
x	.165	48	40	3.7
=	.25	60	60	6.6



See also:

Figs	Sections
11.1 - 11.9	11.3
8.6	

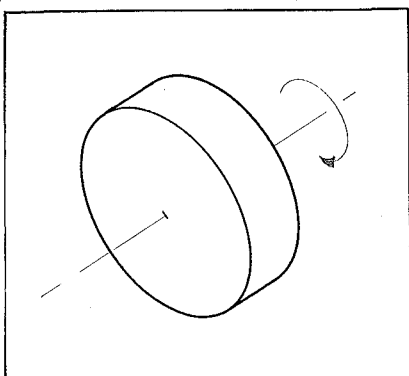


FIGURE 11.1: WHEEL 0, THE SOLID CYLINDER WITH LPW DIMENSIONS

WHEEL 0, CYLINDER

Displacement, $V_0 = 0.4 \text{ m/s}$, $F_r = 0.26$

Transition, $V_0 = 0.76 \text{ m/s}$, $F_r = 0.49$

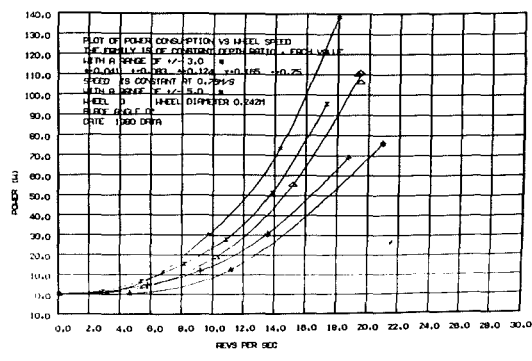
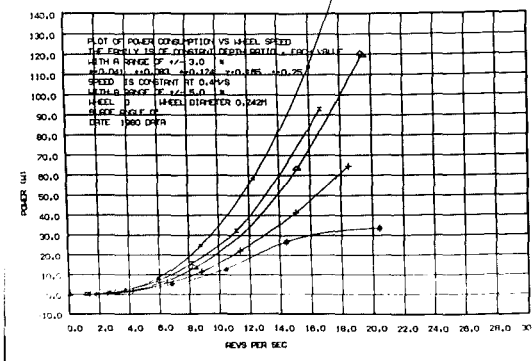
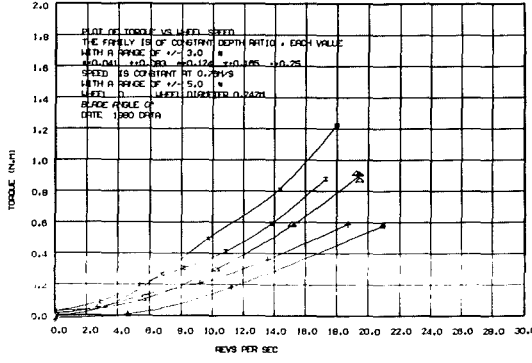
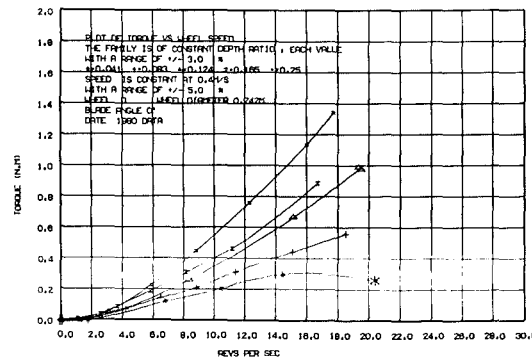
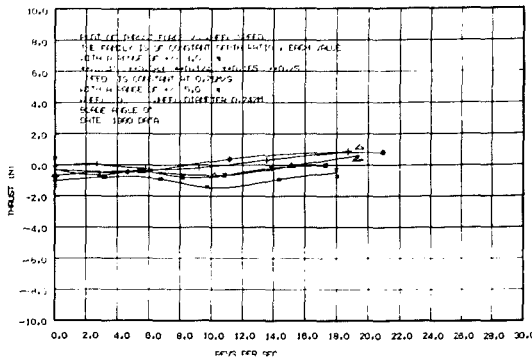
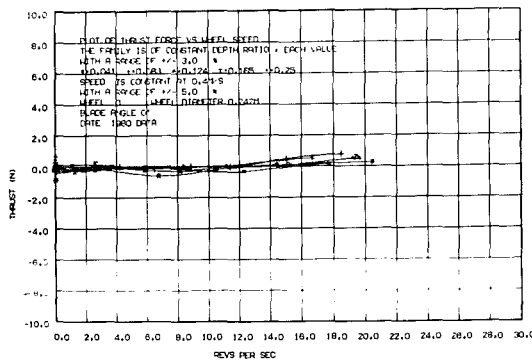
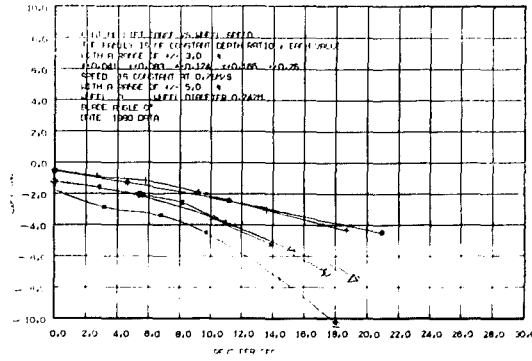
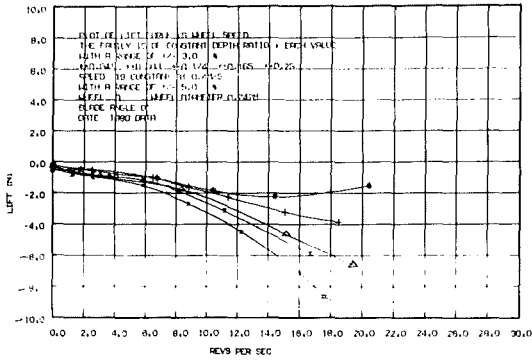


FIGURE 11.2: WHEEL 0, DISPLACEMENT AND TRANSITION RESULTS

WHEEL 0, CYLINDER

Planing, $V_0 = 1.72 \text{ m/s}$, $F_r = 1.12$

Planing, $V_0 = 2.36 \text{ m/s}$, $F_r = 1.53$

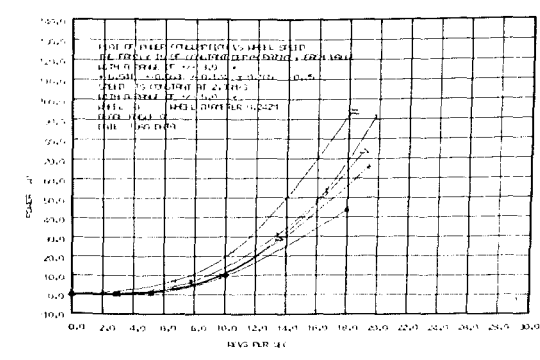
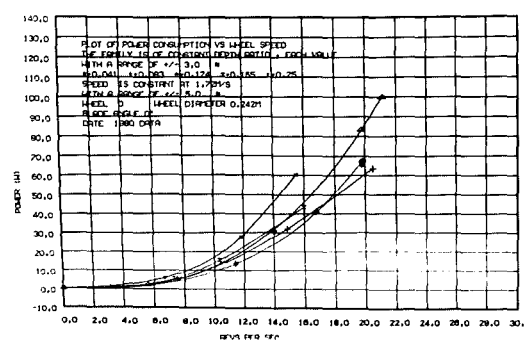
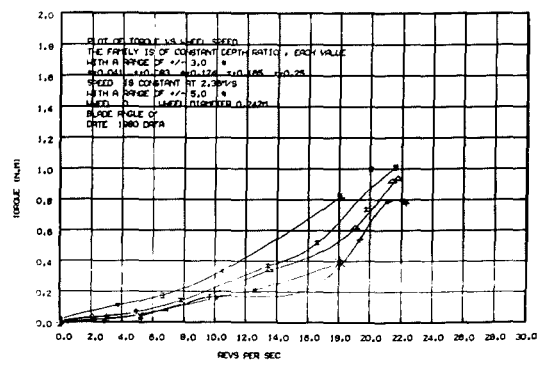
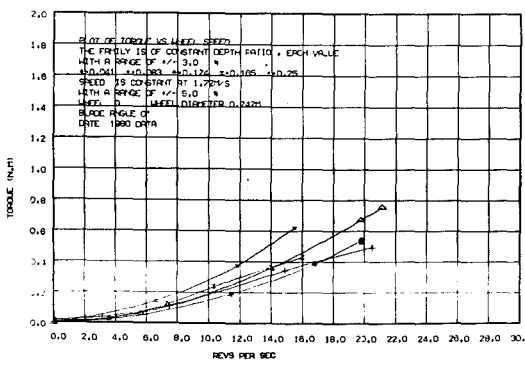
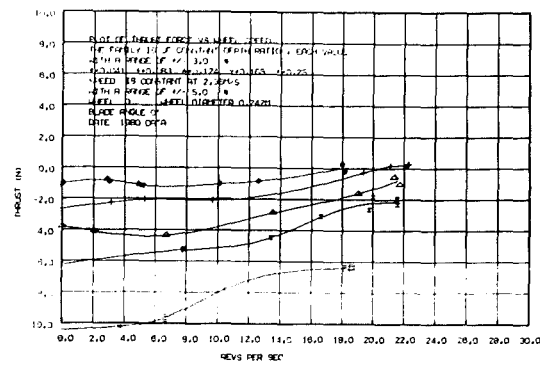
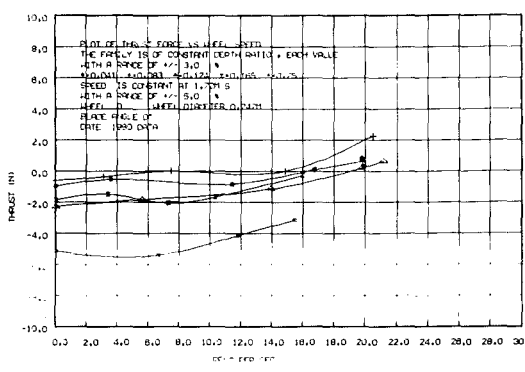
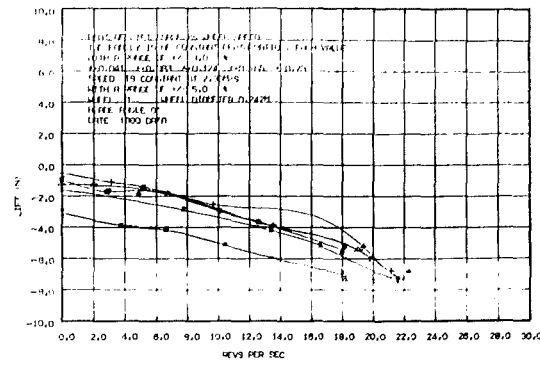
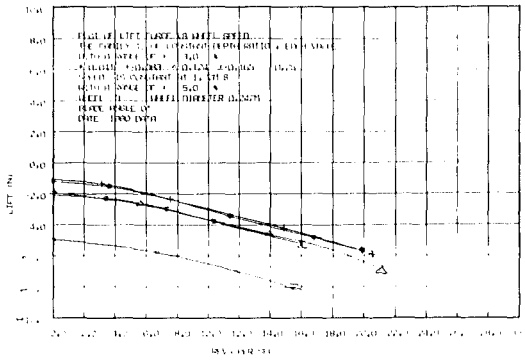


FIGURE 11.3: WHEEL 0, IN THE PLANING CONDITION

form has negligible buoyancy forces this extra, varying buoyancy contribution to the vertical forces experienced by the cylinder, confuses direct comparisons between the two. As a way of providing a common starting point between LPW lift and the dynamic lift generated by the cylinder, the static buoyancy forces of the cylinder were zeroed out before the start of the test runs, so that before the cylinder was in motion the lift force was seen by the force balance to be zero. For their comparison with the dynamic forces, the static buoyancy forces have been tabulated with the results in Fig.11.1.

Once in motion, then, the lift forces were generated by these mechanisms:

- a) Changes in buoyancy;
- b) Dynamic forces such as the lifting or planing forces generated as the flow meets the convex cylinder surface;
- c) Additional effects caused by rotation, such as the throwing of spray.

As can be seen these, only in a small part, relate to the LPW forces as described by the impulse theory, the common ground being that in both cases they are generated by the wheels in motion.

The results of the force balance tests are shown in Figs.11.1, 11.2 and 11.3 and these are set out in much the same way as the LPW test results as shown for example in Figs.9.1, 2 and 3. Two differences may be noted: first, propulsive efficiency has been replaced by wheel torque since negative thrust values produced meaningless efficiency results, and second, the lift and thrust force plots have zero force occurring half way up the scale to accommodate negative force values. Discussion of these results is as follows:

Lift: (1) At no condition of velocity, immersion or wheel revolutions tested do the lift forces of the smooth cylinder become positive. This at first seems to be a direct contradiction to the claims of the proponents of the Hydroler concept (section 2.4.1) and the cylinder vehicle concept (section 2.4.3). Closer scrutiny of the results is required. It may be argued that the planing speeds at which this smooth cylinder was tested were too low for positive

lift forces to become evident. If this was the case, it would be expected that the lift results for the two planing speeds, clear of confusing displacement and transition wakes, would show evidence of increasing lift with speed of advance. This can in fact be found in Fig.11.3 where for virtually all values of immersion and wheel revolutions there is a trend towards positive lift with increase in speed, which seems too pervasive to be experimental error. This positive-going trend is likely to have the following explanation: the reduction in lift at zero wheel revolutions with increase in speed from $V_0 = 0$ (static, Fig.11.1) is caused by a reduction in buoyancy forces because of changes in the flow around the cylinder. Opposing this reduction in lift force would be the planing forces generated by the sloped convex surface meeting the flow. (This is more in evidence at low wheel revolutions in wheel 5.5, $\phi = 105^\circ$, which has no buoyancy to lose and is discussed later in section 11.5. It is also outlined in points (3) and (4) in the generalised findings, section 11.2, above). Since the buoyancy forces may only be reduced by a fixed amount as tabulated in Fig.11.1, and dynamic forces increase with the square of the speed of advance, there must be a speed where the dynamic lift forces exceed the loss of buoyancy and the lift forces would then become positive. Extrapolation from the two sets of results in Fig.11.3 suggests that this would occur between $V_0 = 4$ to 8 m/s, a finding which is not inconsistent with the Hydroler measurements. (1) These lift results, then, while showing no positive lift do not contradict the claims of the proponents of cylinder vehicles and in fact show evidence for positive dynamic lift at speeds beyond those for which the tests were conducted.

(2) As required by the above explanation, the magnitude of the lift force at zero wheel revolutions can be seen to become increasingly negative as speed is increased, until planing speeds are reached whereupon this trend is reversed. As noted above this is probably a result of flow changes causing alterations in the wheel buoyancy forces, and this seems to be supported by the fact that at no point (at zero wheel revolutions) do these negative lift force magnitudes exceed the buoyancy force magnitudes tabulated in Fig.11.1. (Point (3) in the generalised findings, section 11.2 above.)

(3) The effect of speed of rotation is, throughout, to decrease the lift force. This effect seems to be a result of water sticking to
1. Lombardini and Fidderman, Fig.11.

the wheel surface and being thrown up (the fountain effect) as shown for a range of wheel revolutions in Fig.11.4 (A-E) for the static case. This is also shown at constant, high wheel revolutions through the other stages of advance velocity; displacement, transition and planing, in Fig.11.5 (A),(B) and (C). It can be seen that this effect is less pronounced when the planing mode is reached in Fig.11.5(C). (These figures demonstrate point (2) in the generalised findings, section 11.2 above.)

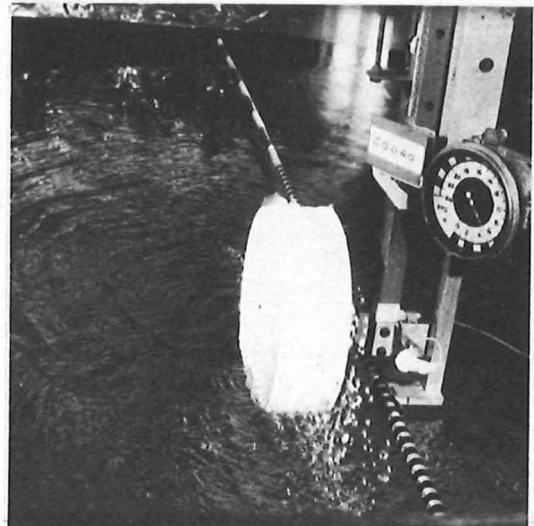
Thrust: (1) At low or zero wheel revolutions in Figs.11.1, 2 and 3, thrust is negative - drag is positive, and this drag becomes increasingly large with speed of advance, and increase in immersion depth. This is most apparent after planing speeds have been reached and seems related, there, to wave formation, especially bowsplash. These wave formations are shown for the case of approximately zero rim to water speed ($\frac{V_o}{V_t} \doteq 1$) in Fig.11.6, (A) to (D). This clearly demonstrates the problem generally overlooked by those proponents of cylinder vehicles who hold that since skin friction may be reduced by rotating the cylinders at $\frac{V_o}{V_t} = 1$ drag will not exist. (Point (6) in generalised findings, section 11.2 above.)

(2) Throughout the range of test results in Figs.11.1, 2 and 3, thrust forces showed a small but consistent increase with wheel revolutions. At low wheel revolutions, around $\frac{V_o}{V_t} = 1$, when there is practically no relative velocity between the wheel rim and the water this thrust increase was negligible, suggesting that drag forces are composed mostly of wave drag, with the skin friction component being very small. At high wheel revolutions ($\frac{V_o}{V_t} < 0.12$) this skin friction component increased significantly so that the thrust forces even became slightly positive at small immersions, thus overcoming the wavedrag. The mechanism for this increase in thrust with wheel revolutions may have two components. First, it seems that the rotation of the wheel reduces the height of the bowsplash as can be seen by comparing the two cases in Fig.11.7 (A)-(D). This would appear therefore to reduce the amount of water pushed ahead of the wheel and thereby reduce the drag. Second, it can be seen from Fig.11.7(D) that the water picked up by the wheel is also thrown rearwards so that skin friction of the cylinder in this case is being employed to get a grip on the water for propulsion. (Point (7) in the generalised findings, section 11.2 above.)



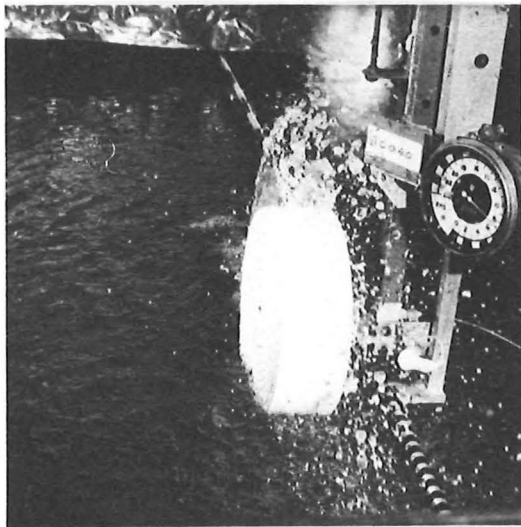
(A) 1 RPS

1300E/2A



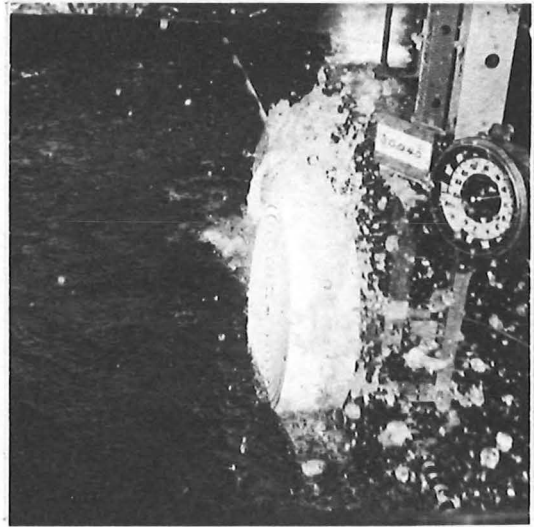
(B) 5 RPS

1300E/3A



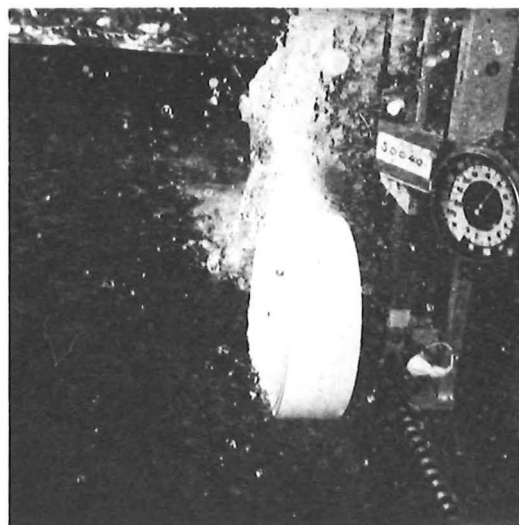
(C) 7 RPS

1300E/4A



(D) 11 RPS

1300E/5A



(E) 14 RPS

1300E/6A

FIGURE 11.4: THE CYLINDER IN THE STATIC MODE ($V_0 = 0$ m/s) AS WHEEL REVOLUTIONS INCREASE. NOTE WATER STICKING TO THE WHEEL, CREATING THE FOUNTAIN EFFECT

FIGURE 11.5: MORE WATER APPEARS TO STICK TO THE WHEEL IN THE DISPLACEMENT AND TRANSITION CONDITIONS, (A) & (B), THAN IN THE PLANING CONDITION, (C). 1.4 RPS THROUGHOUT



(A)

1300E/11A



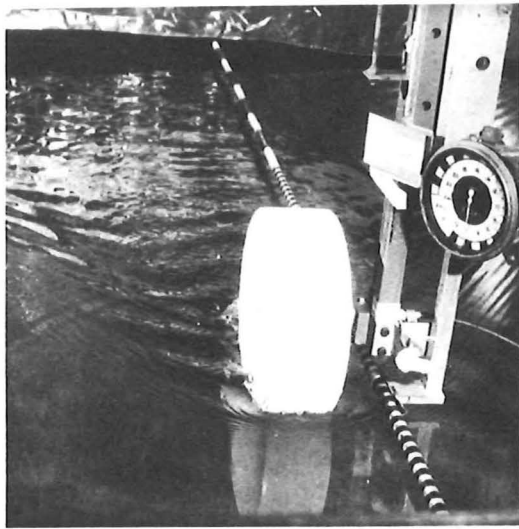
(B)

1300E/16A



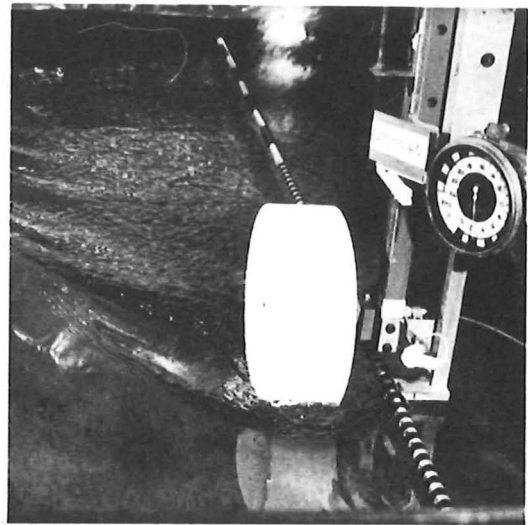
(C)

1300E/21A



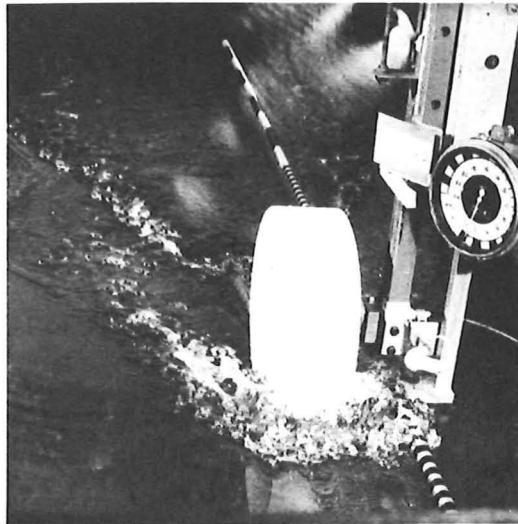
1300E/7A

(A) DISPLACEMENT 0.4 m/s



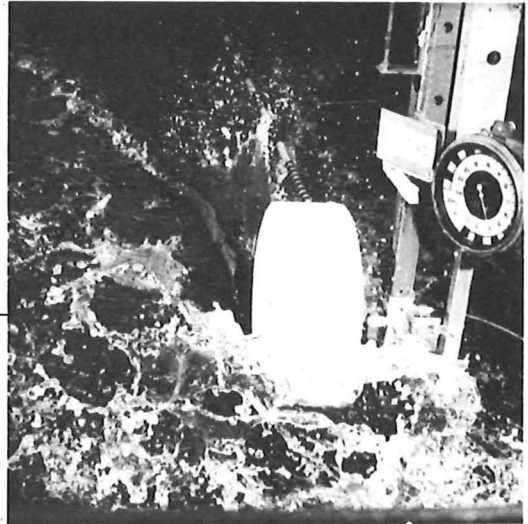
1300E/12A

(B) TRANSITION 0.76 m/s



1300E/17A

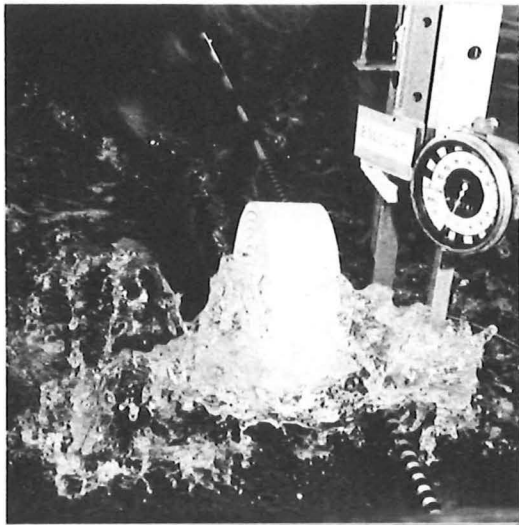
(C) PLANING 1.72 m/s



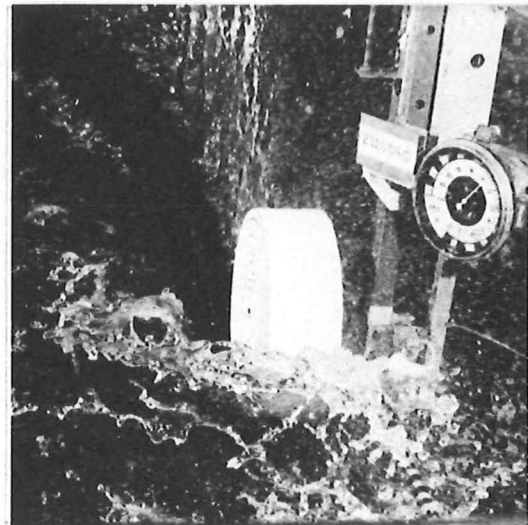
1300E/23A

(D) PLANING 2.36 m/s

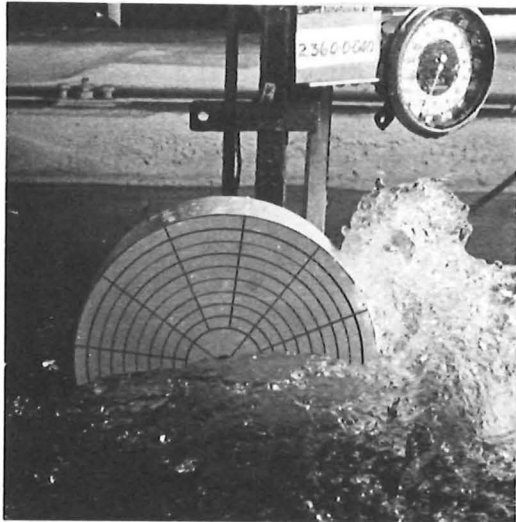
FIGURE 11.6: THE CYLINDER OPERATING AT DIFFERENT SPEEDS OF ADVANCE AT A VELOCITY RATIO CLOSE TO UNITY IN EACH CASE. IMMERSION IS CONSTANT THROUGHOUT AT 40 mm. ($d/D = 0.17$)



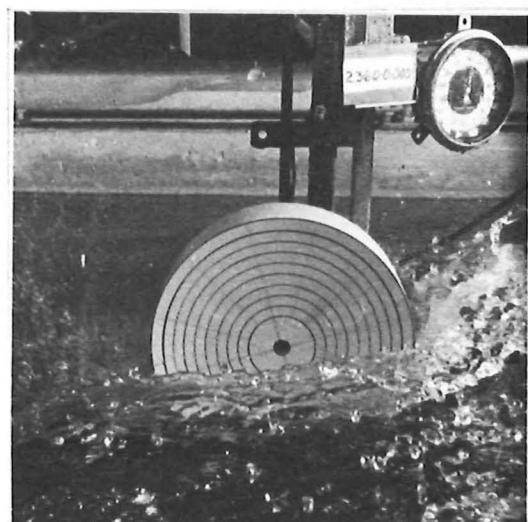
(A) 1300E/22A



(B) 14 RPS 1300E/25A



(C) 0 RPS 1206F/34



(D) 16 RPS 1206F/37

WHEEL MOTION


WHEEL MOTION


FIGURE 11.7: SHOWING THE DIFFERENCE IN BOWSPASH FOR THE CYLINDER IN THE PLANING CONDITION BETWEEN ZERO ROTATION (A) & (C) AND A HIGH ROTATION OF 15 RPS (B) & (C) ($V_0 = 2.36$ m/s)

(3) These thrust results indicate that, if thrust alone was considered, then a light smooth cylinder of LPW dimensions, fixed at a constant immersion of $\frac{d}{D} = 0.083$ (or 20 mm in this case, symbol '+'), would be able to maintain positive thrust at very high wheel revolutions right through the transition and planing modes. Whether or not this traction could be retained to higher speeds than those tested is not clear.

In contradiction to this final point, if both lift and thrust results are considered it appears that a weightless powered smooth cylinder of LPW dimensions would, in fact, not be able to reach planing speeds unassisted because the negative lift created at the high wheel revolutions necessary for positive thrust, would overcome the buoyancy forces and cause it to submerge and slow down before it could traverse the transition zone. A larger cylinder would be expected to have the same relationship between lift and thrust while exhibiting a larger buoyancy force compared to lift and thrust forces so that it may be possible for such a cylinder to successfully traverse the transition zone and reach planing speeds as claimed by proponents of cylinder vehicles. Scaling of these results, however, requires both Froude and Reynolds Number equivalence so that sound predictions become difficult to make.

It is interesting, therefore, that neither the lift nor thrust results can be said to clearly contradict the claims made for the Hydroler or the Russian cylinder vehicle.

11.3.2 Photographic Records

While some of the photographs of the cylinder in operation have already been discussed several comparisons of these results with those of the standard wheel in Figs. 9.5 to 9.9 and 9.27 may be usefully made.

1) As with the LPW, bowsplash for the cylinder did not occur until the planing mode was reached. This was noted in relation to the LPW in section 9.4.3.2 and shown in Fig. 9.27. For the cylinder it can be seen in Fig.11.6 (C) and (D) and 11.7 above. (Points (1) and (6) in the generalised findings, section 11.2.)

2) Bowsplash with the LPW in the planing mode, only occurs near cavity intrusion and at wheel revolutions over this limit (Figs. 9.8, 9.9 and 9.27) whereas for the cylinder bowsplash occurs

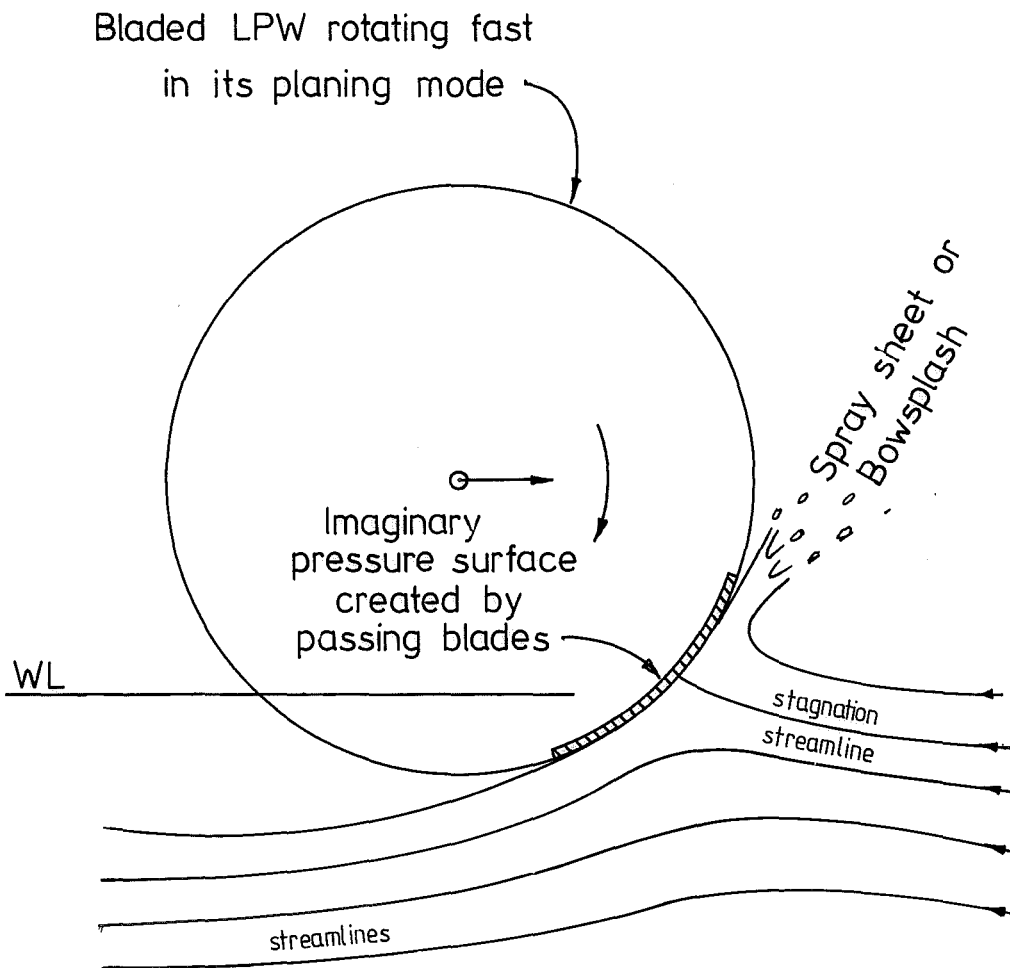


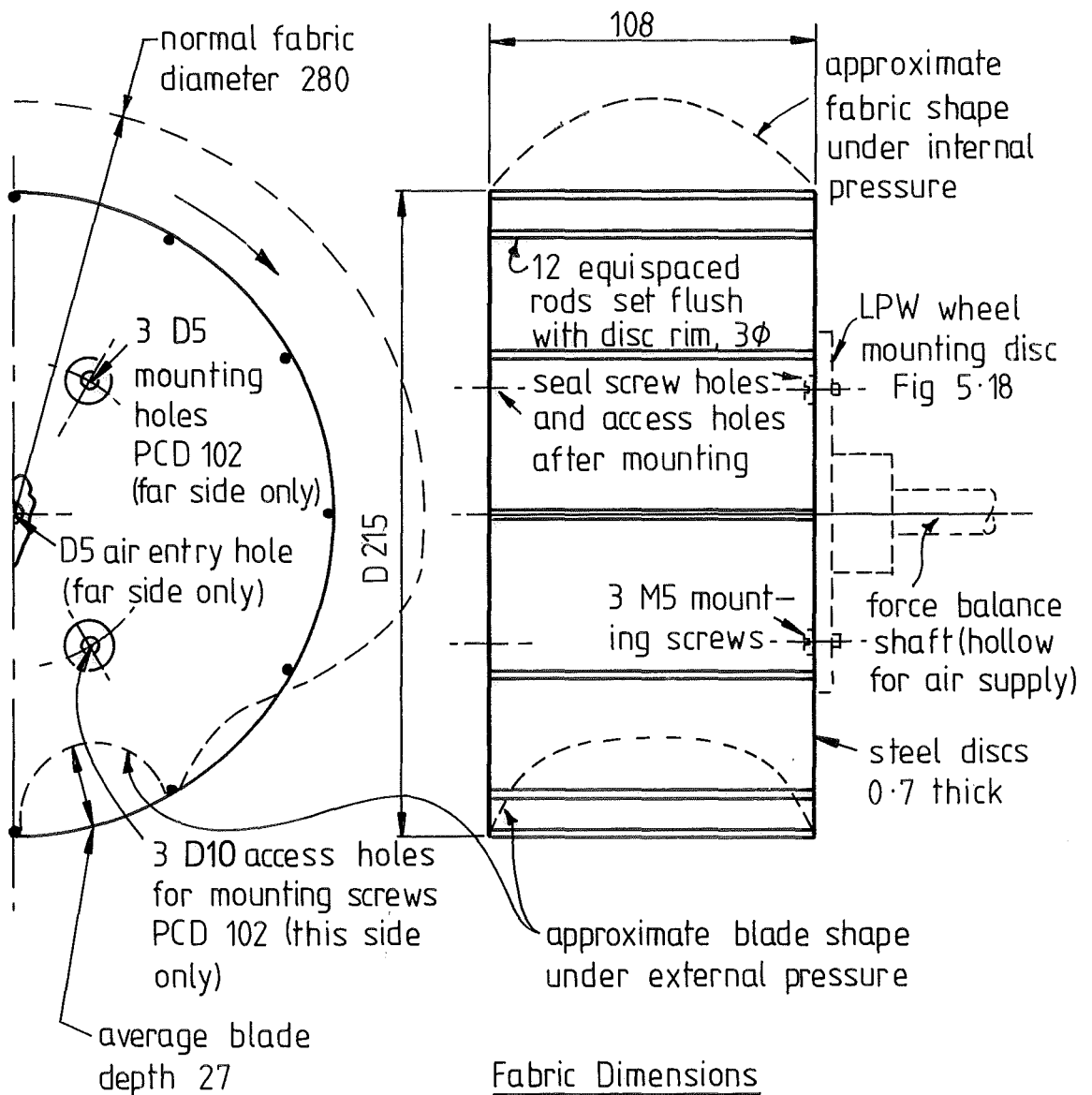
FIGURE 11-8: BOWSPASH LIKENED TO THE SPRAY SHEET OF A PLANING SURFACE. (Compare Fig 4-17).

K

throughout the planing speeds independently of wheel revolutions. This is shown by Fig.11.7. It appears that for the cylinder the bowsplash is derived from the "sheet" of spray thrown forward, as is the case with a flat planing surface (shown in Fig.4.17) and this suggests that the bowsplash of LPW's may be visualised as a related phenomenon where an imaginary planing surface or "pressure surface" is created by the nearby passage of the LPW blades. This is shown in Fig.11.8. (Bowsplash was also discussed earlier in section 4.9.1.)

3) The cylinder wakes may be compared with LPW wakes with many features common to both. The range of speeds of advance for the cylinder for one rotational speed were shown in Fig.11.6, (A)-(D) and these may be compared with Figs. 9.5 to 9.9 for all the conditions of advance of the LPW. The displacement mode wavetrain of short wavelength waves is especially clear in the cylinder case of Fig.11.6 (A) which shows a wave peak half way along the wheel. This is not nearly so clear in the LPW case (Fig.9.6) where the blade impacts have set up interference patterns of their own. (Point (1) in the generalised findings.)

4) Unlike most LPW's the cylinder carries water sticking to its surface right over the top and back down. This is visible in Fig.11.4 (A) and (B). At higher wheel revolutions this feature changes as shown in Figs. 11.4 (C)-(E) and 11.5, where the cylinder is rotating at 14 rps and shows graphically how water may be thrown up in a large fountain even by a smooth cylinder. As noted above this creates the negative lift shown in Figs.11.1 and 11.2 which seems to be most pronounced in the transition zone. (Point (2) in generalised results section 11.2.) This sort of phenomenon was observed on the model LPW craft operating in the displacement and transition zones, with any wheel which tended to trap water by preventing it from traversing through the rim. Since such a fountain usually generated sufficient negative lift to cause the model to submerge, wheels that created it were best avoided. This fountain effect does not seem nearly so pronounced in the planing mode as shown in Figs. 11.4 (E) and 11.7 (B) and (D), probably because the water is able to separate from the wheel low down rather than be held against it as in trough or displacement conditions.



3rd angle
dimensions in mm

Fabric Dimensions

0.10 thick woven sealed nylon
125 between discs,
10 additional each side for
attachment to discs: 145 total
980 circumference
folds must be introduced at
the disc edges on attachment.

FIGURE 11-10 THE INFLATABLE 12-BLADED ROLLERCRAFT WHEEL TESTED IN THIS PROJECT

11.3.3 Conclusion for Wheel O

These cylinder tests have helped to confirm the ideas on LPW wake formation, have demonstrated bowsplash and the throwing of spray; or fountain effect also found in some LPW's and have put the claims of cylinder vehicle proponents in perspective. While the tests do not show the cylinder to be a viable competitor with the LPW, neither do they fully discount the possibility that cylinder vehicles may develop workable lift and thrust forces at high planing speeds or with different dimensions. In that they have demonstrated many of the characteristics common to these sorts of wheels, these results have provided a reference for discussion of the following wheel types which have "blades" on a continuous surface.

11.4 ROLLERCRAFT INFLATABLE WHEEL TESTS: WHEEL 5

(Results in Appendix 4)

The buoyant inflated roller of Kearsy's work was described in section 2.3.2. If it could live up to the claims made for it, it would be a serious competitor for the LPW concept. For this reason, and since it was felt that the force measurements performed by Kearsy were in some doubt (see section 2.3.2 and 4.16, 4.16.1 and 2) it was decided to perform an investigative test series on a model inflatable Rollercraft wheel similar to the one tested by Kearsy.

11.4.1 The Tested Wheel

The inflatable Rollercraft wheel, being largely fabric is difficult to dimension in ways sufficiently accurate to be reliably compared with dimensions of "hard" wheels, such as the LPW's. The inflatable wheel made by the author for these tests was intended to be geometrically similar to Kearsy's test wheel but owing to some confusion as to dimensions, it is different in a number of ways. This is unlikely to detract from the general trends of the results, however. The dimensions are given in Fig.11.10.

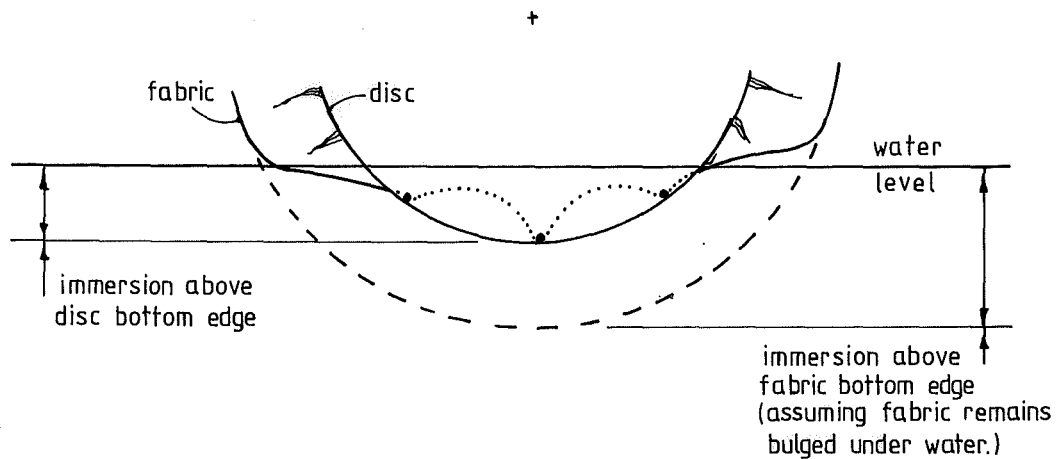
The disc size was seen as the dimension equivalent to the LPW diameter since this was the dimension to the immersed blade tips in both cases. While the inflatable wheel disc size at 215 mm was smaller than the usual LPW diameters, the span was larger, so that forces calculated on a "K" coefficient basis (see sections 4.2.1, 9.4.1 on the use of "K" coefficients) should be of the same magnitude

TABLE 11.11: COMPARISON BETWEEN THE DIMENSIONS OF KEARSEY'S ROLLERCRAFT WHEEL AND THIS PROJECT'S ROLLERCRAFT WHEEL

	KEARSEY'S WHEEL		THIS PROJECT'S WHEEL	
DISC DIAMETER	242 mm	D	215 mm	D
FABRIC OUTSIDE DIAMETER	304 mm	1.26D	280 mm	1.3D
WHEEL SPAN	152 mm?	0.63D	108 mm	0.5D
NUMBER OF BLADES	12		12	
BLADE DEPTH	38 mm	0.16D	27 mm	0.13D
SKIN: WOVEN SEALED NYLON	0.13 mm		0.1 mm	

TABLE 11.12: THE TWO INTERPRETATIONS OF IMMERSION DEPTH

		IMMERSION ABOVE DISC BOTTOM EDGE	FRACTION OF DISC DIAMETER	IMMERSION ABOVE FABRIC BOTTOM EDGE	FRACTION OF FABRIC DIAMETER	θ TO DISC EDGE
		KEARSEY'S WHEEL		32.3 mm	0.13 D	2½" = 64 mm
		64 mm	0.26 D	3¾" = 95 mm	0.31	61.9°
		96 mm	0.40 D	5" = 127mm	0.42	78.1°
THIS PROJECT'S WHEEL	*	8.8	0.041 D	41.1	0.15	23.5°
	+	17.9	0.083 D	50.16	0.18	33.4°
	Δ	26.7	0.124 D	59	0.21	41.2°
	x	35.5	0.165 D	68.7	0.24	48.0°
	=	53.8	0.25 D	86.1	0.31	59.7



as LPW forces and force results would therefore be comparable. Since the wheel diameters differ, wheel revolutions in the resulting force plots, however, will not compare directly with those of the LPW force results.

Kearsey's actual test wheel dimensions are compared to the dimensions of this test wheel in Table 11.11. (In respect of Kearsey's wheel span, there is some confusion. Kearsey's test wheel as shown in his published article (1) appeared to have a smaller span than stated in his thesis and shown in Table 11.11.) Immersion depth figures have two possible interpretations: they may be measured from the supposed fabric diameter as done by Kearsey, or from the edge of the disc as carried out in these tests. These two conventions give the two sets of immersion results shown in Table 11.12. As will be seen, Kearsey tested to much greater immersions than normally undertaken for LPW tests, and his immersion depths and ratios were referred to fabric diameter. The tests by this project covered the range of immersion ratios examined in the LPW tests, but these ratios were referred instead to the disc diameter.

Once the wheel was made, it required some adaptations to the force balance since, unlike the LPW's, it needed a continuous supply of low pressure air to keep it inflated. This was accomplished by delivering the air through the driveshaft as shown in Fig.11.13. The air supply itself was arranged as also shown in Fig.11.13 and was intended to give a steady air pressure of 25 mm water. This value was comparable with low pressures used by Kearsey, whose tests covered a range of air pressures from atmospheric to 5 inches of water (127 mm). It is likely that in operation the air pressure supply fluctuated as much as $\pm 30\%$, with the simple arrangement shown in Fig.11.13.

11.4.2 Test Procedure

Before each test the immersion depth was set then the air turned on. The lift force was set to zero, annulling the buoyancy effects just as was done for the solid cylinder described in section 11.3.1. In this case it involved getting an average zero with the wheel turning slowly (about $\frac{1}{2}$ rps) since buoyancy varied as the

1. Hovercraft and Hydrofoil, September 1971, p.23, Fig.17

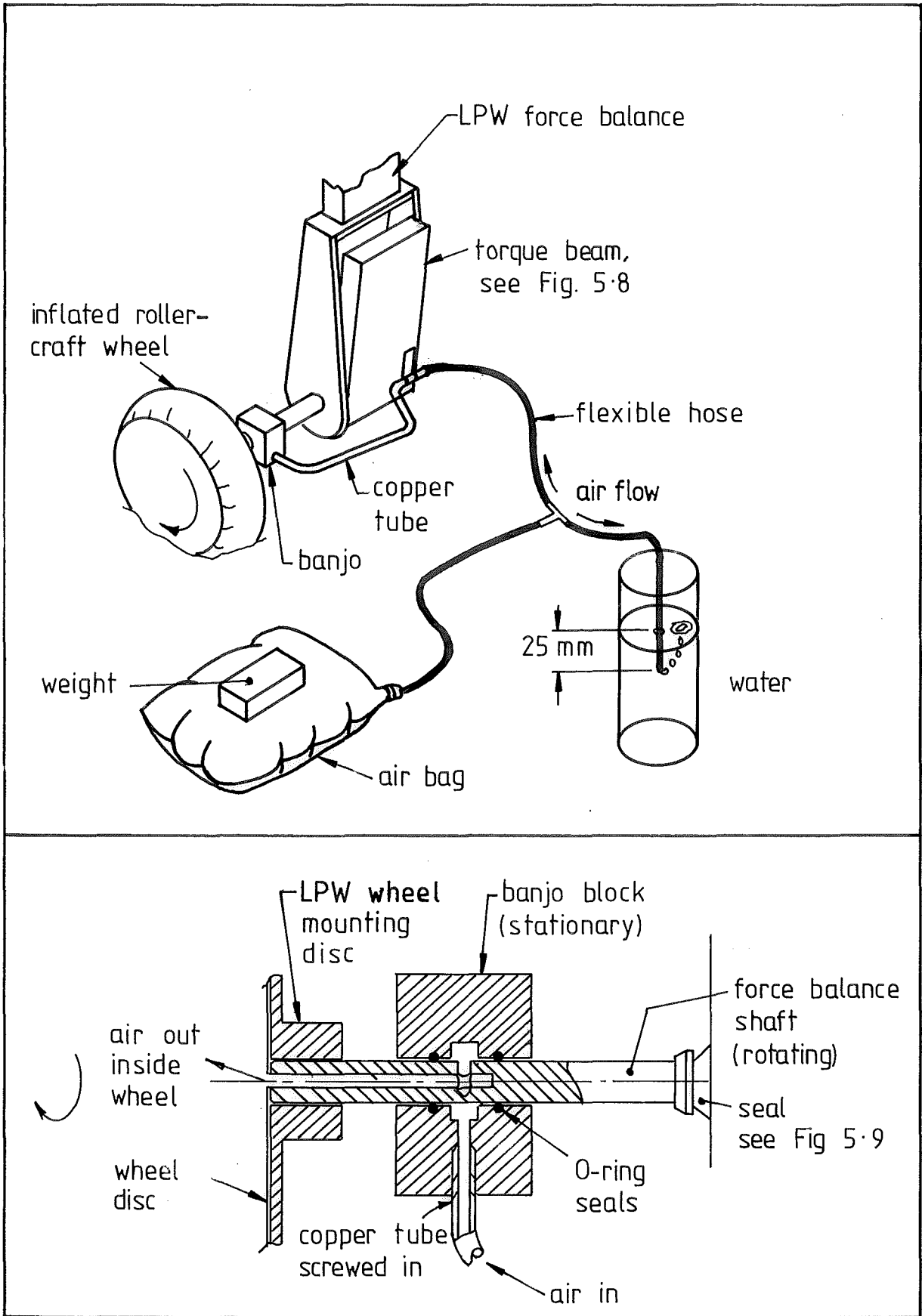


FIGURE 11.13 SCHEMATIC OF AIR SUPPLY TO ROLLERCRAFT WHEEL (TOP) AND DETAILS OF THE SUPPLY THROUGH THE SHAFT (BOTTOM)

water deflected the fabric. Static buoyancy was recorded separately and is given in Fig.11.14. Results of lift force recorded in the tests therefore gave only dynamically generated forces as was the case for the cylinder.

Once the lift sensor had been zeroed, torque and thrust sensors were zeroed. The Rating Car was then run down the tank at the chosen speed and a set of readings taken at different wheel revolutions (including zero rps). At the end of the run the air was checked to ensure it was still running. In other respects, the tests proceeded as described in section 6.4.2 for the LPW tests, the main differences being zeroing and buoyancy forces, and taking drag readings with zero wheel revolutions.

11.4.3 Results For Wheel 5, The Rollercraft Wheel

The results of the inflated Rollercraft wheel as tested on the LPW force balance are shown in Figs.11.14, 15 and 16. As was done with the cylinder results, the plots are presented with the zero force value half way up the axis so that negative values may be accommodated. For midrange speeds results for only two immersion depths have been recorded. The speeds of advance are the same as used for the LPW tests, but in this case they represent different Froude Numbers (F_r) because of the different diameter(s) of the flexible rotor. The speed of 0.76 m/s which normally represents the transition zone for the smallest two immersions of the LPW, still represents a transition speed for this Rollercraft wheel independent of which diameter (fabric or disc) is taken, and which value of the immersion angle θ is taken (to the disc edge or to the fabric edge). (See section 4.15.2 regarding transition conditions.) Thus the velocities at which the Rollercraft wheel was tested still represented displacement transition and planing velocities though strictly the results may not be directly compared with those of the LPW's at the same velocities, because Froude Numbers (F_r) are a little different.

The following points may be noted in the force results in Figs.11.14, 15 and 16:

Lift: In the static, displacement and transition zones the lift force is close to and just less than zero for no wheel revolutions; this is, of course, after buoyancy forces have been removed.

(See Test Procedure above.) As wheel revolutions are increased lift decreases in each case. A decrease in lift also occurs with an increase in immersion depth. These results are the same as the cylinder results, where it was suggested that the wheel picking up water was the cause of negative lift (point (2) in the general findings, section 11.2 and Figs.11.4 and 11.5 above). Certainly this would seem to be supported by Fig.11.17 where the wheel is in the static mode, and picking up water much as the cylinder did in Fig.11.4(C) at much the same rps.

Beyond the transition zone with the wheel not rotating lift differs from that of the cylinder (see Fig.11.16) in that it now becomes increasingly positive with increase in speed of advance. Apparently, at zero wheel revolutions, the fabric can arrange itself between the rods of the Rollercraft wheel in such a way as to present a planing surface to the oncoming flow, thereby generating considerable lift without any rotation, albeit at the cost of considerable drag. This is different from the cylinder results in Fig.11.3 and it seems that the "blades" of the Rollercraft wheel are therefore essential in generating this larger lift force at zero wheel revolutions. (Point (4) in the generalised findings, section 11.2.) Once the wheel begins to rotate in the planing mode, however, this lift force is lost, decreasing with increase in wheel revolutions to values near zero lift, before increasing again as wheel revolutions are increased beyond the point where the rim speed equals the speed of advance (that is once $\frac{V_o}{V_t} < 1$, or $n > 3.5$ rps at $V_o = 2.36$ m/s). This is also different from the results of the cylinder where lift decreases steadily with increase in wheel revolutions (Fig.11.3).

These lift results suggest that the Rollercraft wheel in the planing mode acts, at zero wheel revolutions like a high lift planing surface, providing lift which is lost as the wheel begins to rotate, only to be replaced at higher wheel revolutions by lift forces similar to the LPW impulse forces which are now generated at least partly by the "blades". (See point (5) in the generalised findings above.) This of course could not occur with the cylinder because it has no blades.

Although the Rollercraft wheel forces should not be directly compared with LPW forces in the planing mode because of the small

WHEEL NO: 5

Internal Pressure = 25 mm water

Inflatable Rollercraft wheel

Diameter, D = 215 mm (disk)

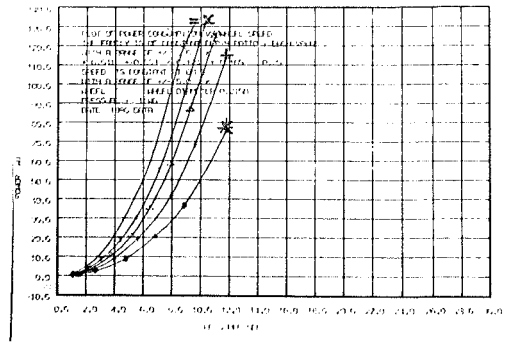
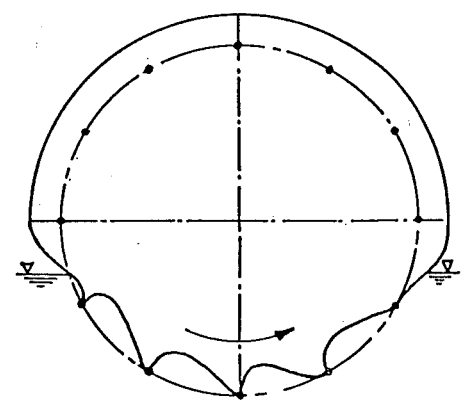
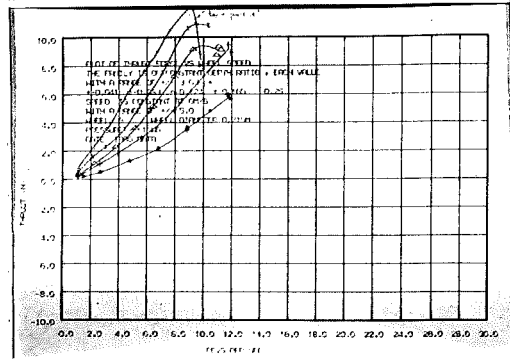
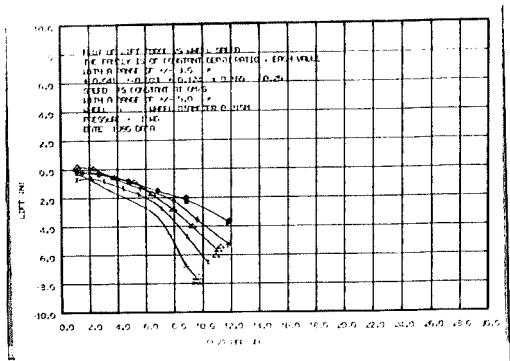
Span, s = 108 mm s/D = 0.5

Chord: blade depth = 27 mm

No. of Blades = 12

STATIC, $V_o = 0$

Symbols	Immersion ratio	Immersion angle	Immersion depth	Buoyancy force (N) ± 0.2
	D/d	θ_o	d (mm)	
*	.041	24	9	0.5
+	.083	33	18	1.1
Δ	.124	41	27	2.4
x	.165	48	36	3.5
=	.25	60	54	5.8



See also:

Figs 11.10 - 11.14 Sections 11.4

FIGURE 11.14: ROLLERCRRAFT INFLATABLE WHEEL RESULTS FROM THIS PROJECT. BUOYANCY FORCES HAVE BEEN SUBTRACTED FROM LIFT FORCES SO THAT LIFT RESULTS REPRESENT DYNAMIC EFFECTS ONLY

ROLLERCRAFT WHEEL

Displacement, $V_0 = 0.4 \text{ m/s}$, $F_r = 0.28$

Transition, $V_0 = 0.76 \text{ m/s}$, $F_r = 0.52$

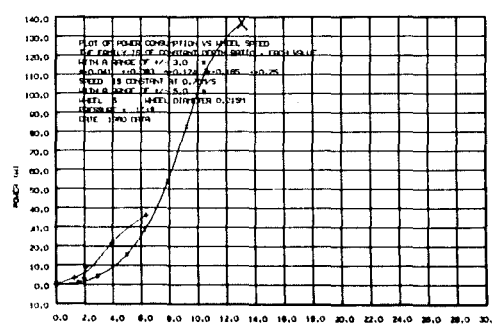
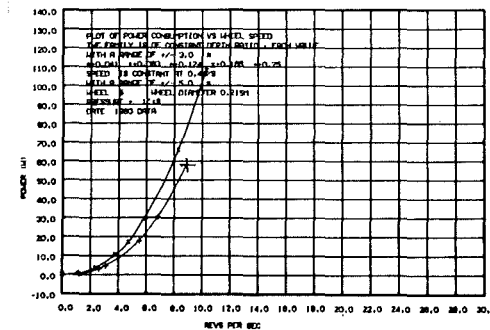
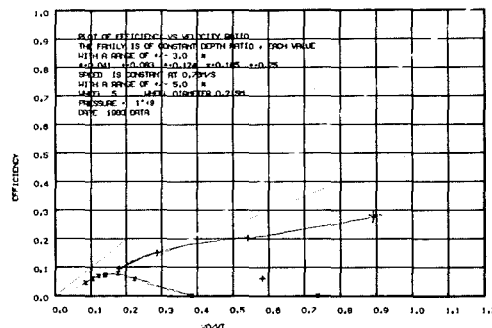
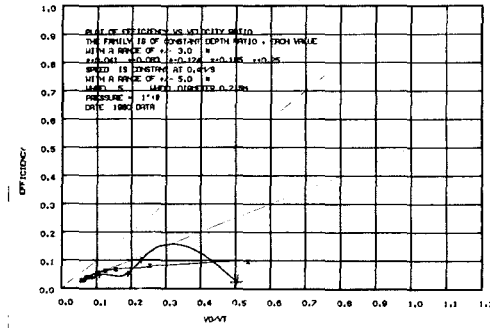
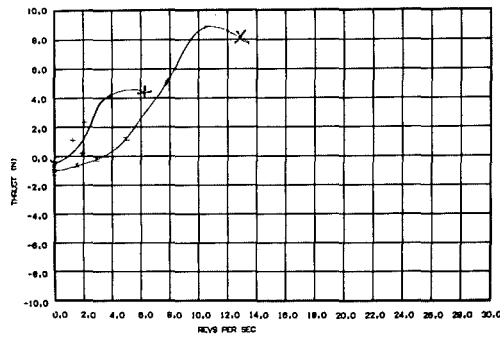
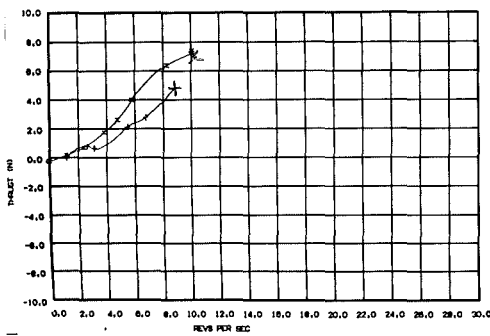
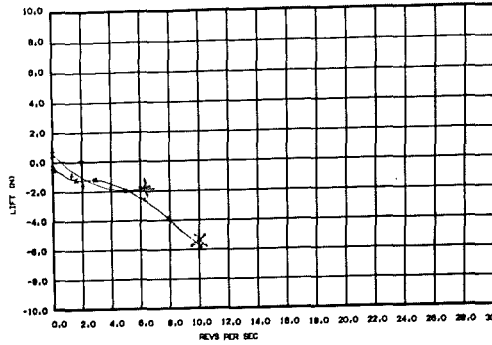
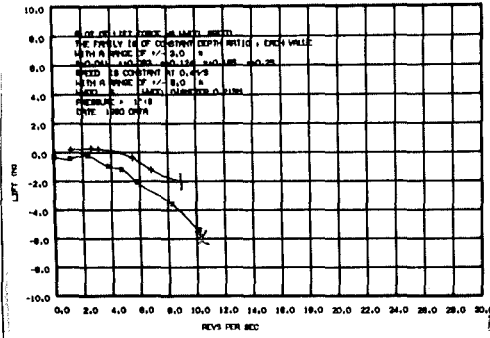


FIGURE 11.15: THE ROLLERCRAFT WHEEL IN DISPLACEMENT AND TRANSITION. NOTE THAT FROUDE NUMBERS (F_r) ARE BASED ON DISC DIAMETER IN THIS CASE

ROLLERCRRAFT WHEEL

Planing, $V_0 = 1.71 \text{ m/s}$, $F_r = 1.18$

Planing, $V_0 = 2.36 \text{ m/s}$, $F_r = 1.63$

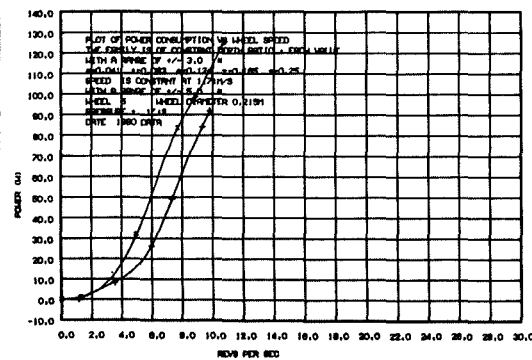
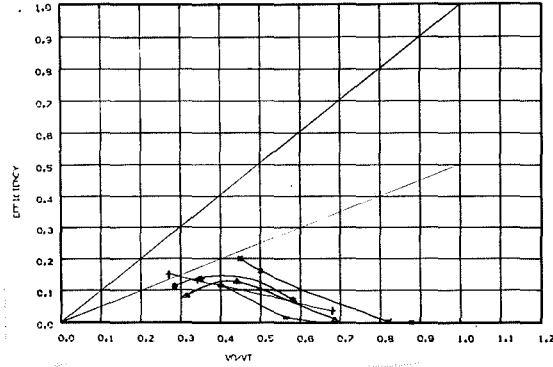
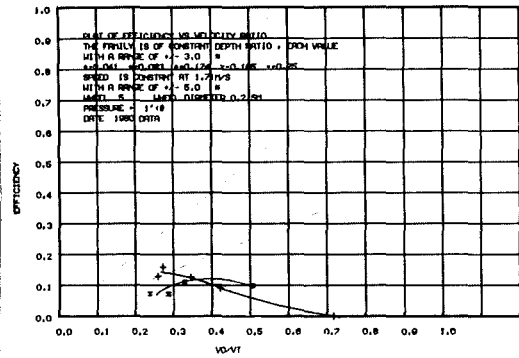
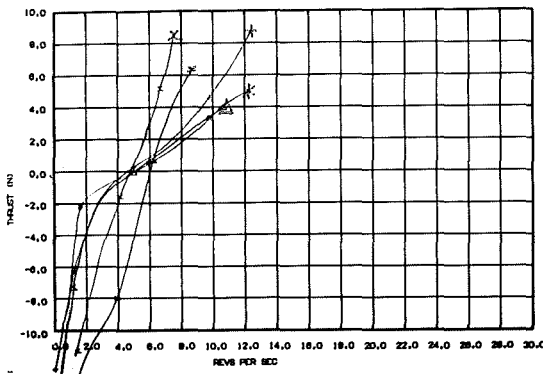
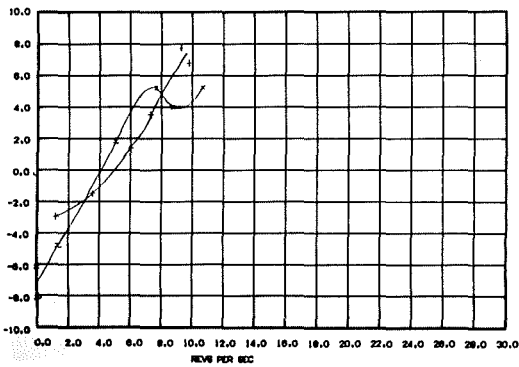
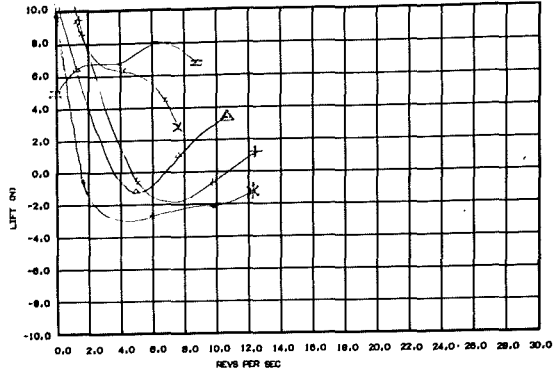
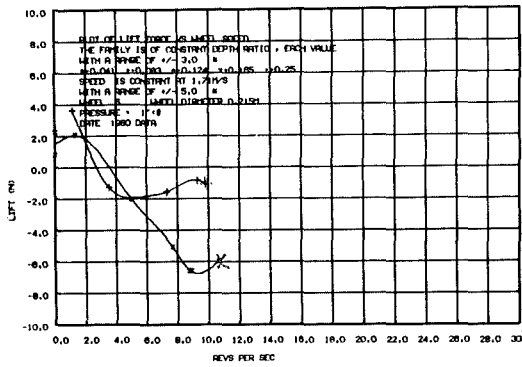


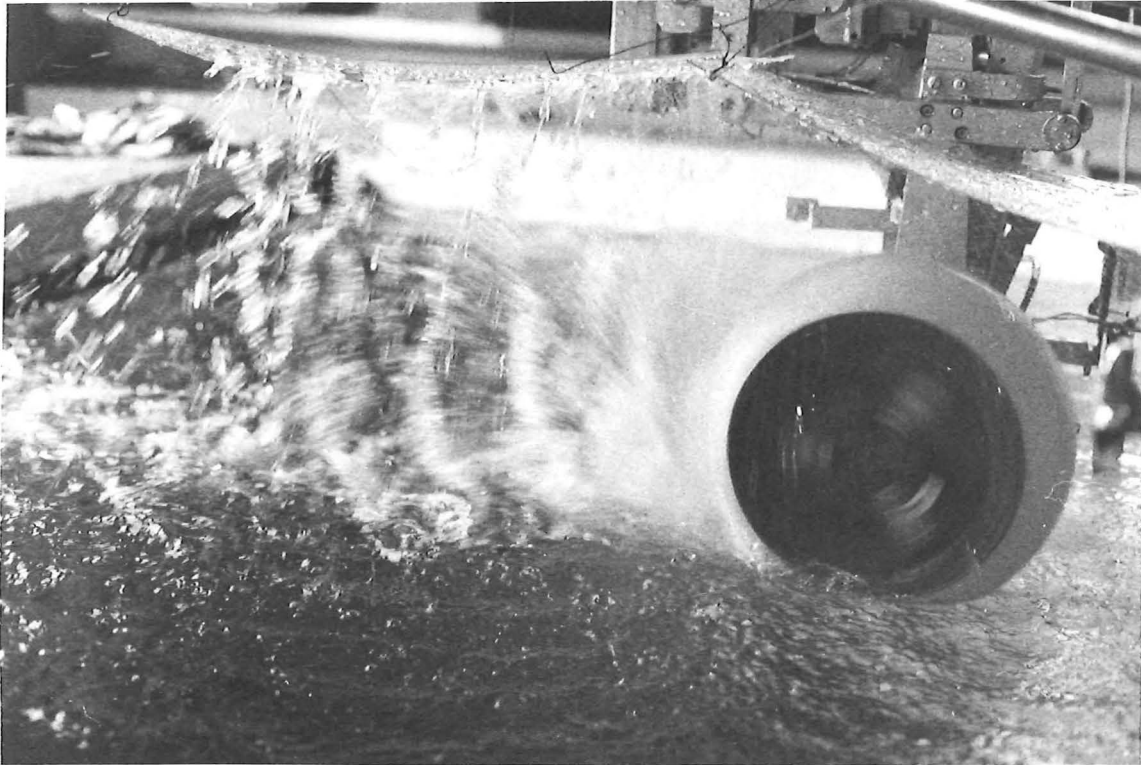
FIGURE 11.16: THE ROLLERCRRAFT WHEEL RESULTS FROM THIS PROJECT FOR PLANING OPERATION

differences in Froude Numbers of the velocity it is quite clear that the lift forces, once the wheel is rotating at speed, are small compared with those generated by the six-bladed LPW, such as FB, $\phi=60^\circ$ in Figs. 9.1, 2 and 3. (It should be remembered that for the Rollercraft wheel the actual "lift" forces would include some extra buoyancy forces less than or equal to those tabulated in Fig.11.14.)

Thrust: Thrust forces for the Rollercraft wheel contrast strongly with those of the cylinder. In the static condition, Fig.11.14, thrust forces increase with wheel revolutions and immersion depth, and apparently do not reach any mass supply limit with revolutions like the limit found in LPW results, (see section 9.2.1.1). (Point (7) in section 11.2.) This seems to occur because the immersions of the fabric can be much greater than the disc immersions; the fabric can "balloon" to greater depths and grab more water during its passage even though it would normally form "blades" between the rods (see Fig.2.12). Certainly large oscillations of the force balance support this explanation. (See later discussion, section 11.4.4.)

This trend of thrust increasing steadily with wheel revolutions is present in the displacement results as well as in the transition zone results (Fig.11.15). While LPW results except good propulsors at large immersions reach limits in the transition zone, and become independent of increases in wheel revolutions, the Rollercraft wheel forces still seem to increase with revolutions in this zone. This is a valuable result and may explain why Kearsey apparently experienced no problem in traversing the transition zone in his Rollercraft (see section 2.3.2).

Once planing speeds are reached (Fig.11.16) drag forces become evident at low wheel revolutions (velocity ratios $\frac{V_o}{V_t} > 1$ or $n < 3.5$ rps at $V_o = 2.36$ m/s). These forces may be large, as in the 2.36 m/s results, but would be of little significance unless a Rollercraft was under tow with its wheels locked. By comparison LPW's have very small drag forces at zero wheel revolutions at planing speeds. Once wheel revolutions increase ($\frac{V_o}{V_t} < 1$ or $n > 3.5$ rps at $V_o = 2.36$ m/s) thrust forces increase (drag forces decrease) until thrust forces become positive at velocity ratios of about $\frac{V_o}{V_t} = 0.6$, or $n = 6$ rps at $V_o = 2.36$ m/s. It is significant that this does not occur at $\frac{V_o}{V_t} = 1$ ($n = 3.5$ rps at $V_o = 2.36$) and this seems to be caused by the presence



/20

FIGURE 11.17: THE ROLLERCRAFT WHEEL OF THIS PROJECT AT 6 RPS IN THE STATIC MODE

of bowsplash which, unlike the LPW case, persists more or less throughout the range of wheel revolutions from zero upwards. (Points (1), (6) and (7) in the generalised findings.) Because the results are somewhat erratic it is not clear whether thrust forces are proportional to immersion depth or not.

The magnitudes of these drag and thrust forces in contrast to the lift forces seem to be relatively large, and tentative comparisons with LPW forces suggest that planing mode thrust may be as good as that of good LPW propulsors such as wheel 1.25, $\phi = 105^\circ$ (section 10.7).

Efficiency: Efficiency results have been plotted against a velocity ratio determined from the disc diameter. It is worth pointing out that the derivation of propulsive efficiency from measurements (see section 7.4.5) contains no diameter or span dimensions so that the efficiency results are not affected by whether fabric or disc diameter is to be used.

Although the results are scattered it is clear that they are low compared to LPW efficiencies, peak values generally being around $\eta = 20\%$. There are two possible reasons for this. First, the thrust forces do not become positive until velocity ratios are relatively small ($\frac{V_o}{V_t} < 0.6$) as noted above. Thus the efficiency curves tend to be confined to the left of the efficiency plot where even the ideal efficiencies are small. Second, the immersions of the tested Rollercraft wheel are large if they are measured against fabric diameter, and for most paddlewheels and LPW's efficiency decreases with immersion depth. Examination of the efficiency curves here shows that this trend of decreasing efficiency with immersion depth also exists for the Rollercraft wheel. Comparisons between the Rollercraft efficiency results and those of the FB, $\phi = 90^\circ$ wheel at roughly the same immersion ratio ($\frac{d}{D} = 0.17$ based on fabric diameter) shows that the FB, $\phi = 90^\circ$ wheel, generally a good propulsor, demonstrates an equally low efficiency at this immersion. This suggests that should the Rollercraft wheel be immersed much less its propulsive efficiencies might be higher. This speculation tends to be supported by the results shown in the next section (section 11.5) where the metal model of the Rollercraft wheel demonstrated high efficiencies at small immersions.

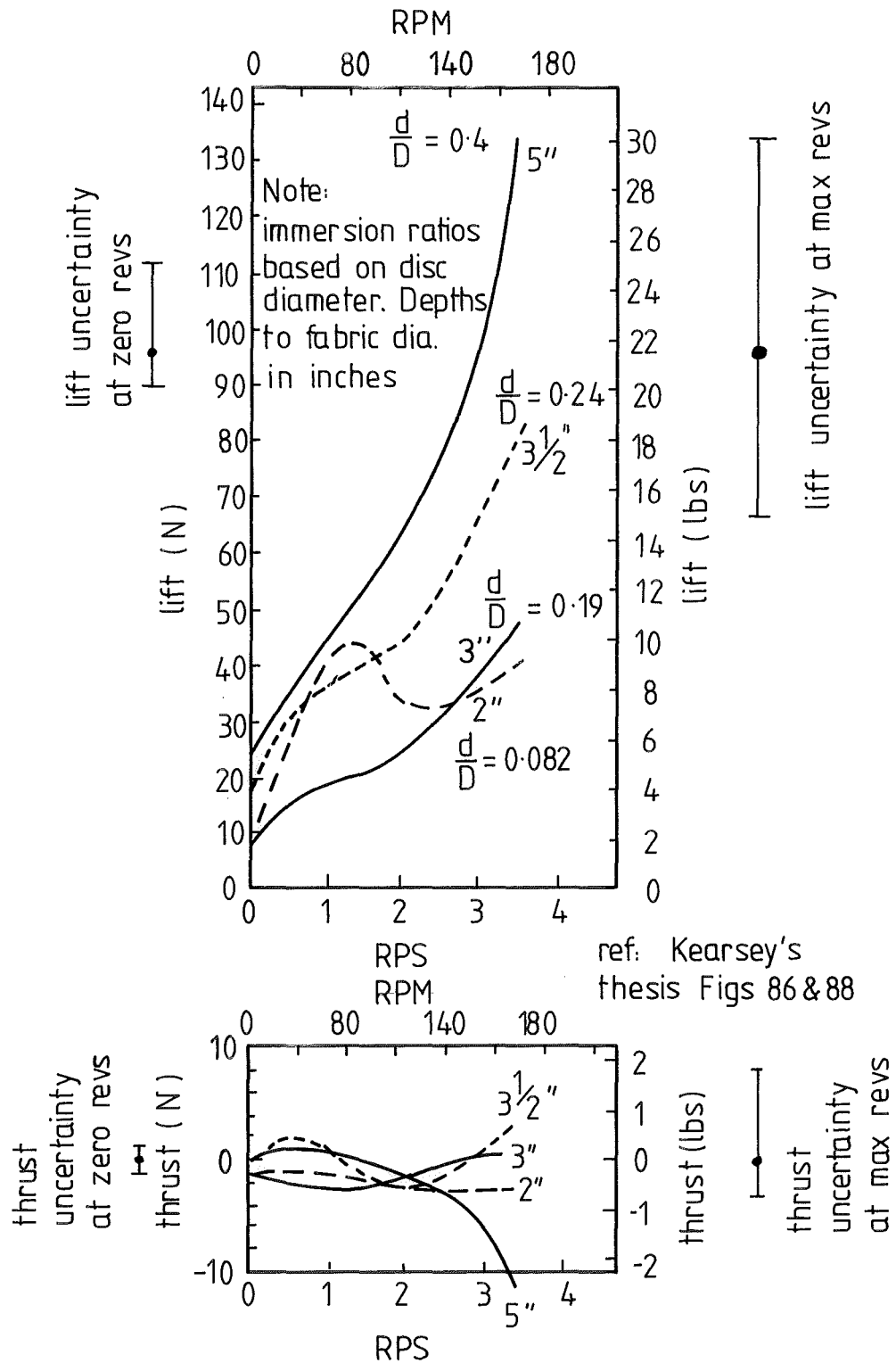


FIGURE 11-18: KEARSEY'S RESULTS FOR HIS INFLATABLE WHEEL AT 1.52m/s ($Fr = 0.99$, DISC) IN THE EARLY PLANING MODE. INTERNAL PRESSURE: 25mm WATER.

Although Rollercraft wheels were intended to operate at large immersions (1) ($\frac{d}{D} \doteq 0.25$) they generate some lift at speed, so that smaller immersions for high speed running might be expected, in which case improved operational efficiency might also be possible with speed.

11.4.4 Observations

In the static and displacement modes a type of cavity pounding was observed (see section 9.2.2). In this case it seemed more as though, at high wheel revolutions, the wheel "grabbed" at about 3 Hz, and it is likely that a cavity pounding type of phenomenon was coupled with the fact that once a "blade" caught, it could billow and scoop up a relatively large quantity of water. It also seemed to entrain quantities of air which may or may not have been related to this phenomenon, but was also observed by Kearsley. (2)

It is felt that the somewhat erratic force results are a result of these low frequency oscillations caused by the billowing fabric. Since the force balance damping system had a half second response time (see section 5.4.6 and 6.3.1) large oscillations of about 3 Hz could affect the recorded results.

With the wheel stationary, checks were made by feeling beneath it, that the "blades" did actually form. Under water the fabric seemed to bend very easily and while the "blades" did not seem to take shape with the wheel stationary, it was not difficult to imagine them readily forming as sketched by Kearsley (see Fig.2.12) once the wheel was rotating, and it was equally easy to imagine the fabric billowing to trap water or air during its passage. It has been speculated that at higher wheel revolutions (8 - 10 rps) the blades may not have been forming at all, in which case traction was achieved by the folds and creases in the fabric rather than the forming of "blades" between the rods. Some evidence for this was available in, unfortunately, poor quality underwater photographs which are not shown here. It is difficult to know what effect this might have on ultimate performance.

Poking at the fabric of the wheel under water showed that transmission of pressure along the air line was virtually instantaneous

1. Kearsley's Thesis, Fig.110
2. Kearsley, Fig.31 and Hovercraft & Hydrofoil, Sept. 1971, P.22, Fig.13

at the low flows used. This helped to confirm that air pressure was uniform throughout the air supply system.

11.4.5 Comparison With a Sample of Kearsley's Results

For the purposes of comparison with the force measurements from the Rollercraft wheel tests in this project some of the measurements made by Kearsley are shown in Fig.11.18. It must be remembered that Kearsley's wheel dimensions were a little different than those used in this project, as outlined in Table 11.11, and Kearsley's measurements were made in a water channel with a flow velocity of 1.52 m/s (5 fps). This placed the tests barely beyond the transition zone in the early planing mode though it is unlikely that this has much relevance in the channel flow situation. The results should therefore be comparable with the early planing results in Fig.11.16, in trends. Magnitudes would be expected to be a little larger than those of Fig.11.16 since Kearsley's wheel (may have) had a greater span.

Comparison between the two sets of results in Figs.11.16 and 11.18 shows the following:

- 1) The trends of both lift and thrust forces differ markedly, seeming to have the opposite relationship to wheel revolutions.
- 2) While Kearsley's lift force magnitudes are far in excess of the measurements taken in this project, the thrust force magnitudes are much smaller.
- 3) Although Kearsley's results cover a wider range of immersion depths, the trend of increasing lift with immersion depth is reflected in both sets of results. In this respect alone the results seem to agree.

11.4.6 Conclusions For Wheel 5

While this project's test results of a Rollercraft wheel attempted to reproduce only one set of the many sets of measurements made by Kearsley, the large differences between the two tend to support the claim made in section 2.3.2 that Kearsley's measurements were not a valid indication of Rollercraft wheel forces. Ironically the results of the tests in this project seem to suggest that the Rollercraft wheel forces are in some cases, better than those of the LPW, and indicate that the Rollercraft wheel would be able to propel a

light craft through the transition zone to planing speeds where increasing lift forces and better efficiencies, than at lower speeds, may be achieved. The results also suggest, however, that in the form it was tested in this project, the Rollercraft wheel did not provide sufficient lift or propulsive efficiency to compete with the better LPW configurations.

This comparison, then, while not confirming Kearsley's results, nevertheless seems to have shown the Rollercraft concept to be a possible competitor for the LPW concept.

11.5 THE HARD ROLLERCRAFT WHEEL: WHEEL 5.5, $\phi = 105^\circ$

(Results also in Appendix 4)

A twelve-bladed metal wheel was designed with the usual LPW dimensions, having large cupped blades which were intended to model Kearsley's self-forming fabric blades. It is shown in Fig.11.19. Its purposes were:

1) To clarify some of the confusing results of the flexible Rollercraft wheel. It was felt that such a wheel made hard, instead of flexible would help to show what was, and was not caused by floppy fabric.

2) To discover whether some of the advantages of the flexible Rollercraft wheel, such as its good traction through the transition zone, could be reproduced with a hard wheel.

3) To examine, in the LPW context, what happens when blades are mounted on a solid rim rather than being in the open like other LPW blades.

Unlike the flexible Rollercraft wheel the hard version had no form of sideplates, and its span was 0.31 D as for the LPW's rather than 0.63 D for Kearsley's wheel (disc diameter) or 0.5 D for this project's flexible Rollercraft wheel (disc diameter).

11.5.1 Results for Wheel 5.5

The forces the hard wheel generated would be expected to compare directly with twelve-bladed LPW forces because of the similarity in dimensions, and while force magnitudes would be

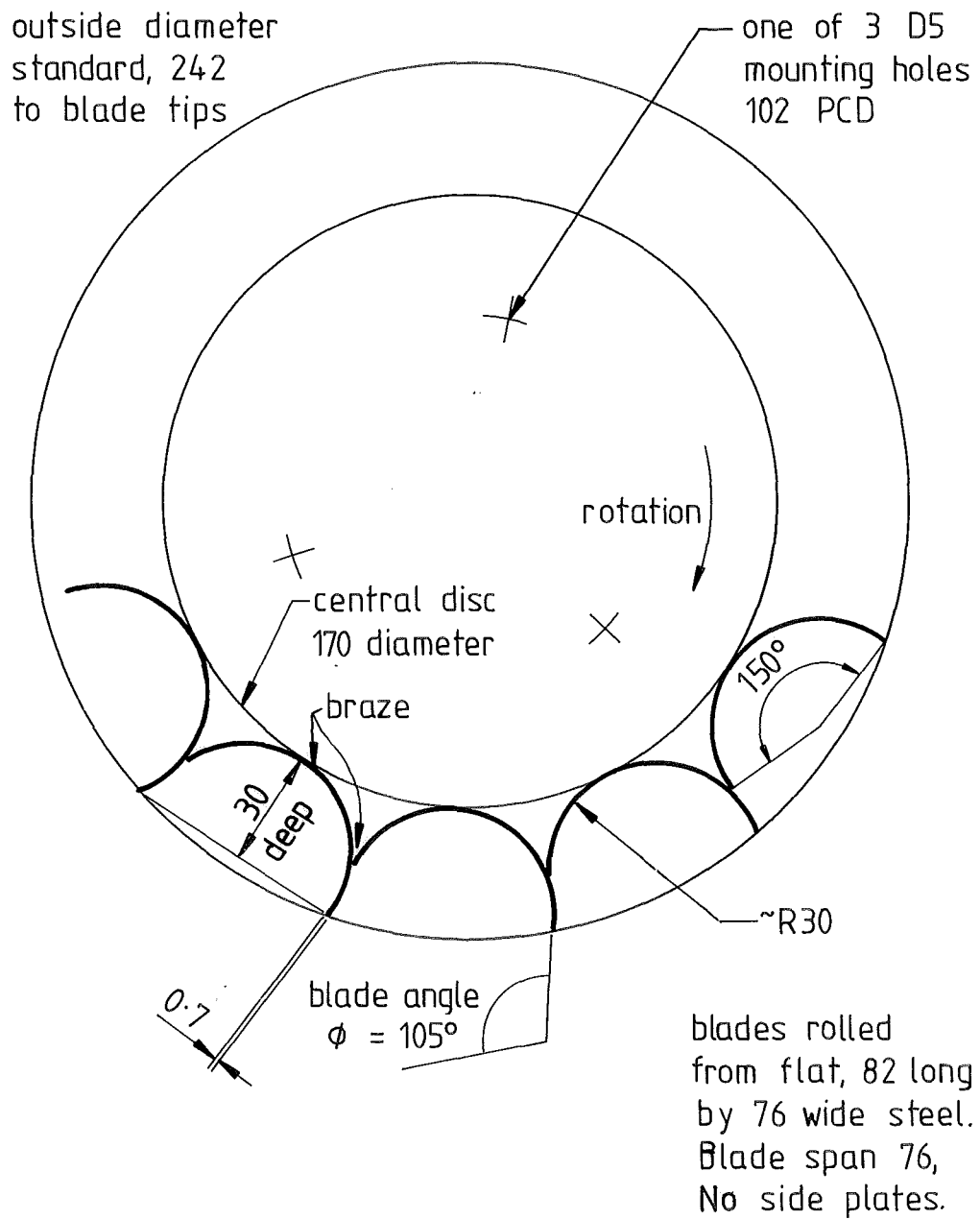


FIGURE 11.19 DIMENSIONS OF WHEEL 5.5, THE METAL IMITATION OF THE INFLATABLE ROLLERCRAFT WHEEL SHOWN IN FIGURES 11.10 & 11.17.

comparable with those of the flexible Rollercraft wheel of this project the wheel revolutions or velocities would not correlate exactly. The results for the hard Rollercraft wheel (wheel 5.5, $\phi = 105^\circ$) are shown in Figs. 11.20, 21 and 22 and comparisons will be made with those of the flexible Rollercraft wheel, wheel 5 in Figs. 11.14, 15 and 16.

Lift: In the static and displacement modes the hard Rollercraft wheel demonstrates lift forces which became increasingly negative with wheel revolutions. The effect is increased strongly with increase in immersion demonstrating lift forces more negative than those observed in any other wheel. While this same trend may be seen in Figs. 11.14 and 15 for the flexible Rollercraft wheel the effect there is not as pronounced. It is felt that at deep immersions water is trapped in the cups of the hard wheel, and not being able to escape towards the wheel axis as it can with other LPW's it is thrown upwards creating the fountain effect and causing this large negative lift. This is believed to be the reason why LPW's, with blades mounted on a cylindrical surface, tended to immerse the model LPW craft at low speeds as will be described in section 12.6.3. The fact that this negative lift was not nearly as pronounced with the flexible Rollercraft wheel in Figs. 11.14 and 15 seems to be because the fabric reforms into a cylinder on exit from the water, ejecting trapped flow before it can be lifted far. This is shown occurring in Fig. 11.17 and is the process described by Kearsley for the suppression of spray with flexible Rollercraft wheels. (1) For this reason the flexible Rollercraft wheel does not display negative lift forces any greater than those of the smooth cylinder, while the metal imitation does.

In the transition zone, lift for the hard Rollercraft wheel is very small for all immersions. It is not altogether clear why this should be. This result is in contrast to that of the flexible Rollercraft wheel which has a surface to which the water sticks so that it shows negative lift in this zone, like the smooth cylinder, Figs. 11.2 and 11.15.

In the planing mode (Fig. 11.22) the lift forces for both the hard and the flexible Rollercraft wheels have similar trends. Two

1. Hovercraft and Hydrofoil, September 1971, P.22

aspects of these trends are of note:

1) At low wheel revolutions before the wheel rotation reaches water speed ($\frac{V_o}{V_t} > 1$, $n < 3.1$ rps at $V_o = 2.36$ m/s) higher lift is exhibited. Such results compare well with those of the flexible Rollercraft wheel (Fig.11.16) where it was surmised that lift at zero or low wheel revolutions was a result of the wheel presenting concave planing faces to the incoming flow. (Point (4) in the generalised results, section 11.2.)

Once wheel revolutions are increased lift at first falls, as with the flexible Rollercraft wheel then increases again. As wheel revolutions are further increased the effects of cavity intrusion can be observed indicating that the blades are acting like LPW blades; see Fig.11.22 (Point (5) in the generalised findings). These effects could not be discerned in the flexible Rollercraft wheel results though the related bowsplash was noted as present. Lift magnitudes for the hard Rollercraft wheel, while generally a little better than those of the flexible Rollercraft wheel are very modest by LPW standards. (Compare, for example, with the six-bladed LPW in Fig.9.3.)

As noted for the flexible Rollercraft wheel, lift in the planing mode at low wheel revolutions (Fig.11.22) appears to be generated by planing forces at first, and at higher wheel revolutions this is replaced by the impulsive forces of the entering blades. The hard Rollercraft wheel results, being much less scattered than those of the flexible wheel show this trend more clearly and reinforce the result that for deep immersions this change of mechanism involves positive lift for all values of wheel revolutions, while for small immersions the lift force falls below zero during this change. See especially Fig.11.22 compared to Fig.11.16.

Thrust: For static, displacement and transition regions the hard Rollercraft wheel thrust forces are as high as those of the good LPW propulsors such as $FB, \phi = 90^\circ$, and even exceed that of wheel 1.25, $\phi = 105^\circ$ (section 10.7) through the transition zone. While this is an exceptionally good propulsive performance by LPW standards, the mass limit reached with increase in wheel revolutions

WHEEL NO: 5.5

Blade Angle $\phi = 105^\circ$

Hard Rollercraft wheel

Diameter, $D = 242$ mm

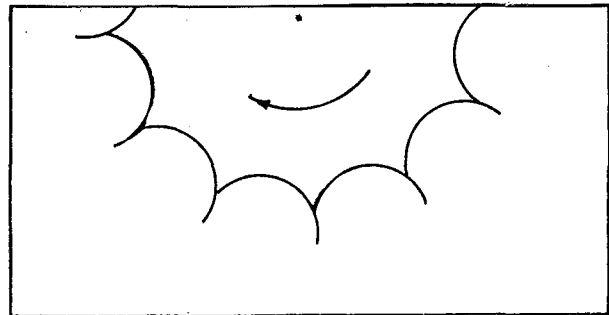
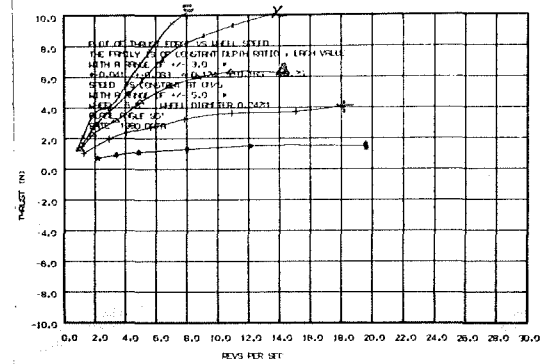
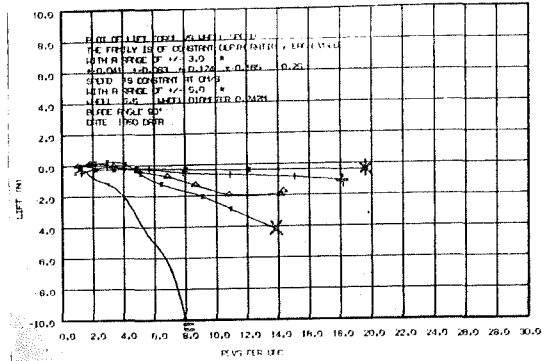
Span, $s = 76$ mm $s/D = .31$

Chord; blade depth = 30 mm

No. of Blades = 12

STATIC, $V_o = 0$

Symbols	Immersion ratio	Immersion angle	Immersion depth
	D/d	ϕ^o	d (mm)
*	.041	24	10
+	.083	33	20
Δ	.124	41	30
x	.165	48	40
=	.25	60	60



12 BLADES

See also:

Figs	Sections
11.19	11.5

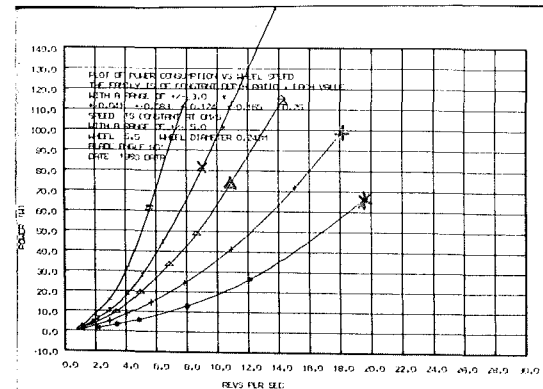


FIGURE 11.20: WHEEL 5.5, $\phi = 105^\circ$. THE METAL IMMITATION OF THE ROLLERCRAFT WHEEL

WHEEL 5.5, $\phi = 105^\circ$

Displacement, $V_0 = 0.4 \text{ m/s}$, $F_r = 0.26$

Transition, $V_0 = 0.76 \text{ m/s}$, $F_r = 0.49$

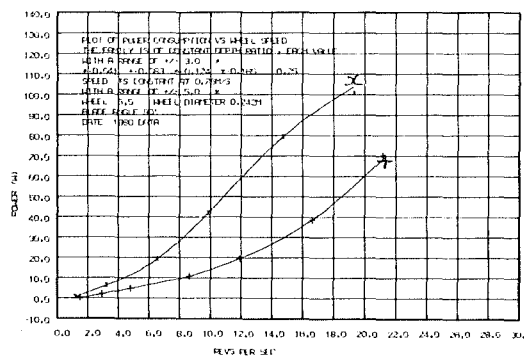
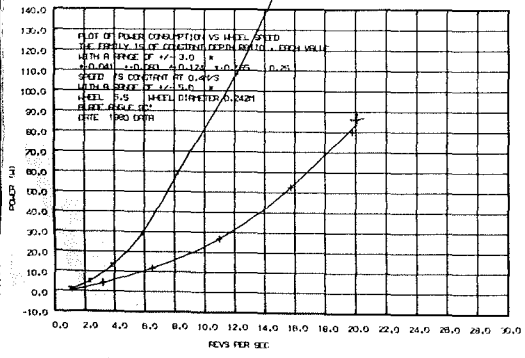
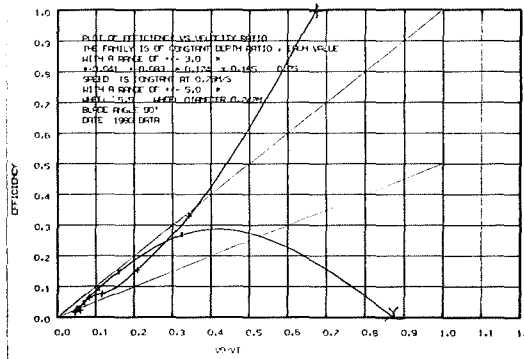
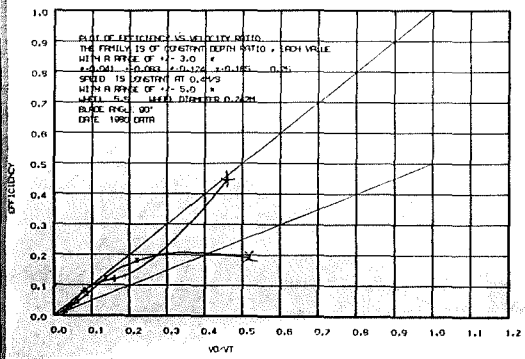
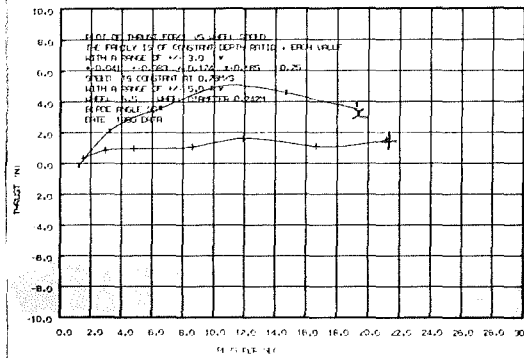
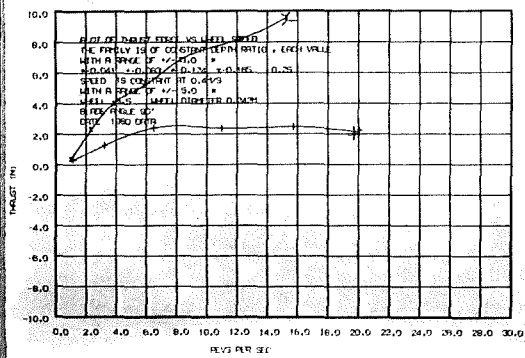
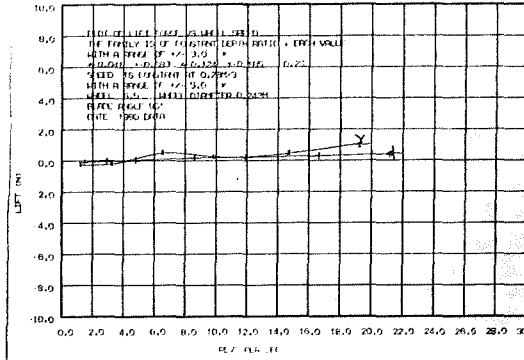
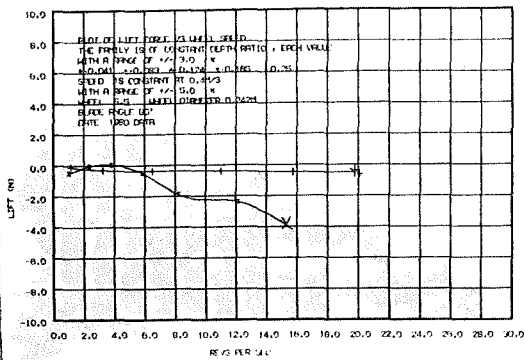


FIGURE 11.21: WHEEL 5.5 IN THE DISPLACEMENT AND TRANSITION CONDITIONS

WHEEL 5.5, $\phi = 105^\circ$

Planing, $V_0 = 1.72 \text{ m/s}$, $F_r = 1.12$

Planing, $V_0 = 2.36 \text{ m/s}$, $F_r = 1.53$

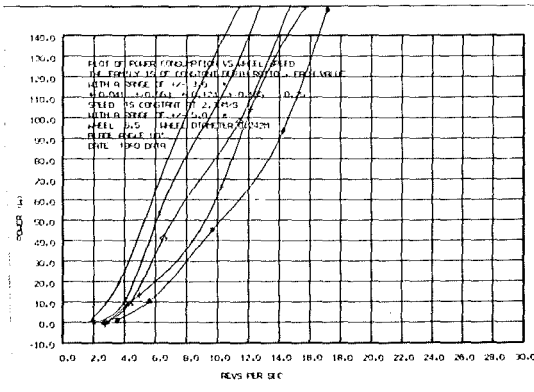
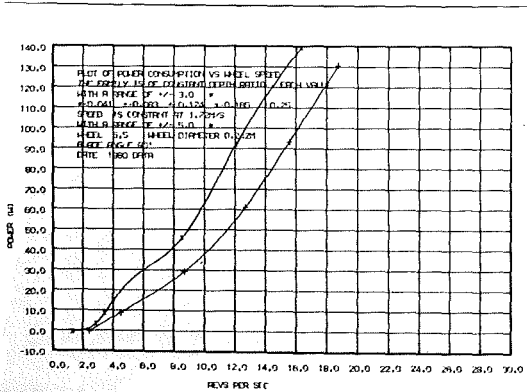
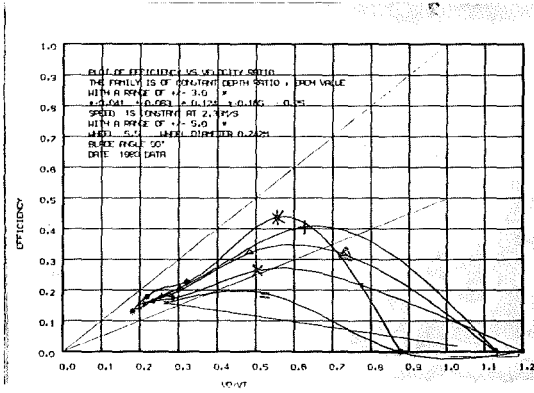
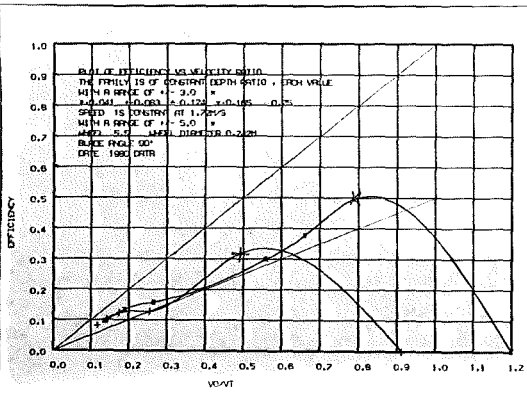
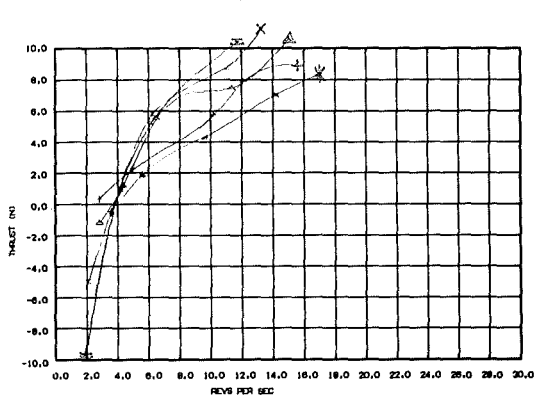
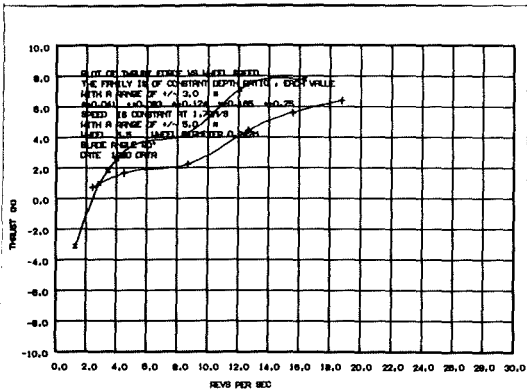
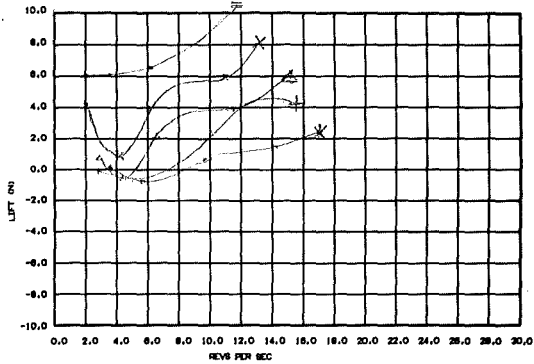
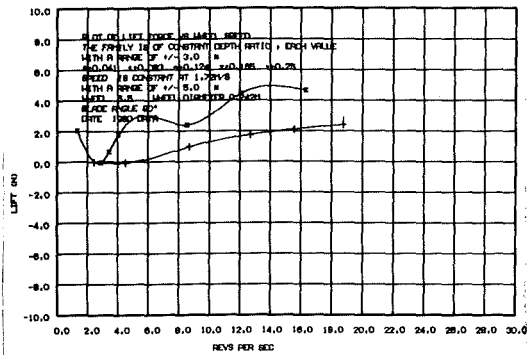


FIGURE 11.22: WHEEL 5.5 IN THE PLANING MODE

is still evident throughout static, displacement and transition zones. (This was discussed in section 9.2.1.1.) These transition zone thrust force values are still exceeded by those of the flexible Rollercraft wheel, which shows only a hint of the mass supply limit. This seems to confirm the idea that the billowing fabric is responsible for its special transition zone performance.

Once planing, the thrust results show a good propulsion performance though in this case not quite as good as the best LPW propulsors. These thrust results are in excess of those produced by the flexible Rollercraft wheel and, more important, increase from drag to positive thrust at a velocity ratio of $\frac{V_o}{V_t} \doteq 0.8$ ($n \doteq 4$ rps for $V_o = 2.36$ m/s) rather than at $\frac{V_o}{V_t} = 0.6$ as in the case of the flexible Rollercraft wheel. At low revolutions the hard wheel demonstrates large drag forces similar in magnitude to those given by the flexible Rollercraft wheel.

Efficiency: As for most LPW results, efficiency is close to the optimum for displacement and transition modes, after which it tends to fall away from the optimum values. Efficiency is inversely proportional to immersion depth and peaks rising to $\eta = 0.4$ to $\eta = 0.5$ for small immersions compare rather poorly with those of good LPW propulsors such as FB, $\phi = 90^\circ$.

In general, while not a useful wheel in itself in LPW terms, the hard Rollercraft wheel has helped clarify some of the functions of the flexible fabric of the flexible Rollercraft wheel, and has also helped confirm the somewhat erratic measurements of the flexible wheel. It has also begun to clarify the fountain type effect shown in Figs. 11.4 and 11.5 of the cylinder, this being a disadvantage of LPW's with blades mounted on a cylinder, and has again demonstrated the contribution to lift at low revolutions in the planing mode afforded by the surface beneath the blades.

11.6 TRACTOR TYRE TESTS: WHEEL 7, $\phi = 90^\circ$ AND WHEEL 4.75, $\phi = 90^\circ$

(Results also in Appendix 4)

Tests on a miniature ribbed tyre resembling the rear tyre of a farm tractor were conducted for three reasons:

1) It is conceivable that once the LPW project was complete and became publicised a New Zealand farmer would report that this had been done before, and describe how in his tractor at speed and out of control he had approached the farm pond and skittered crazily across its surface to arrive safely and astonished at the other side. Apart from such a report being an affront to academic pride, it was felt that the performance of the most LPW-like road wheels under LPW operating conditions was of some value to assess the possibility of their adaption to the LPW form.

2) Many small amphibious vehicles use their wheels as propulsors in the displacement mode as noted in section 2.3.3. It seemed of some value, therefore, to examine and quantify the performance of a sample tyre.

3) This wheel had thick "blades" or tines, and these were not parallel to the wheel axis. These two variables were not examined as part of the LPW tests, so it was hoped that the results might give some indication of the effects of these variables.

The relevant dimensions of the tested tyre are given in Fig.11.23. As can be seen its outside diameter was 298 mm (one foot, slightly worn) and while it had 30 tines, these only reached half way across the wheel and were staggered so that it was effectively a fifteen-bladed wheel. To examine the effect of the tines not being parallel with the wheel axis, the tyre was tested twice, once for each direction of the tread. The normal direction for the tread of a driving wheel is one where the marks left on the ground point towards the rear of the vehicle. This was denoted the normal direction; the tyre the other way round was called the retrograde direction. Results with the wheel in the normal direction were denoted: wheel 7, $\phi = 90^\circ$ and the retrograde wheel tests were classified: wheel 4.75, $\phi = 90^\circ$. Thus the tyre in the normal direction would be expected to throw water out sideways from the wheel, while in the retrograde direction it would pull water in towards its centreline.

Several points should be noted with respect to the plotted results in Figs.11.24, 25 and 26 for the normal direction and Figs. 11.27, 28 and 29 for the retrograde direction:

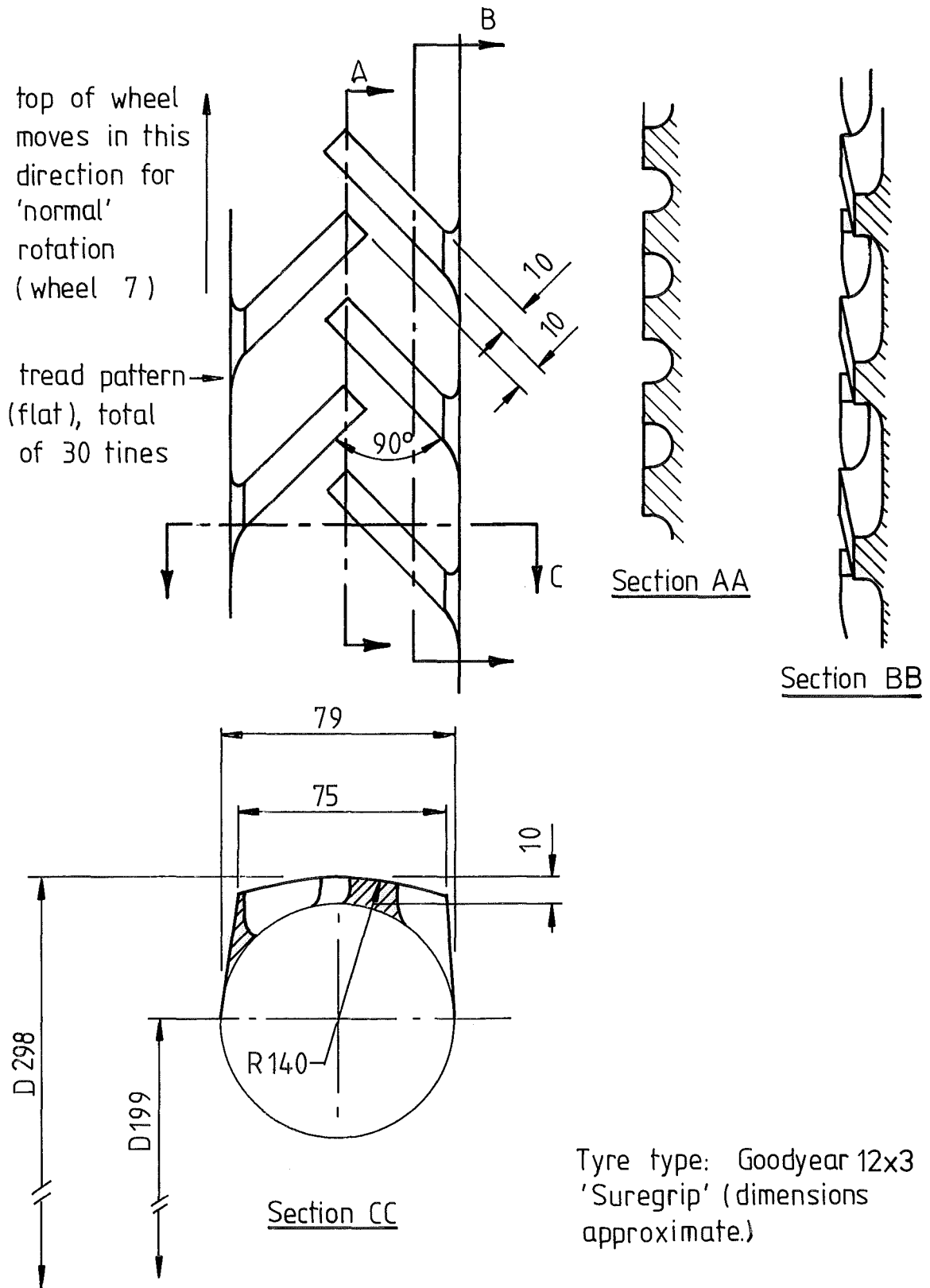


FIGURE 11-23: DIMENSIONS OF TYRE TREAD FOR WHEELS 7 (NORMAL DIRECTION), & 4.75 (RETROGRADE DIRECTION).

1) As for previous wheels buoyancy forces have been zeroed out, and in this case have not been recorded separately.

2) The lift and thrust scales on the plots are different from each other, and different from the scales for LPW plots. As for the cylinder and Rollercraft wheels, the scale zero values do not occur at the bottom of the plots but in the centre to accommodate negative forces.

3) Immersions are in the standard ratios used on the LPW's, and in this case are referred to the outside diameter at the centre of the wheel. They are tabulated in Fig.11.23.

4) Speeds of advance have been scaled to give Froude Numbers corresponding to those of the LPW tests.

The results in Figs.11.24, 25 and 26 and 11.27, 28 and 29 may now be discussed in terms of the findings from the cylinder (section 11.3) and the Rollercraft wheels (sections 11.4 and 11.5).

Lift: The following results can be compared with the cylinder (Figs.11.1, 2 and 3) and Rollercraft results (Figs.11.14, 15 and 16):

1) Through displacement and transition zones lift would be expected to be negative, this effect increasing with immersion and wheel revolutions as the wheel throws up spray sticking to its surface. This was observed in the flexible Rollercraft wheel, the hard Rollercraft wheel and the cylinder.

Reference to the relevant sections of the force results for the tyre in both directions (Figs.11.24 and 25 and Figs.11.27 and 28) shows these to be the trends in both cases. With the wheel in the retrograde direction (Figs.11.27 and 28) the effect is not so pronounced. The suggestion that these negative forces arise because the wheel is lifting water into the air is confirmed by Fig.11.30 (A-E) for the wheel in the transition zone with the tyre in the normal direction. The wheel in the retrograde direction can be seen to throw up less spray than this in Fig.11.31 and while this explains the smaller lift loss for this wheel it is not clear why the blades in the retrograde direction cause this to occur, since the opposite effect might be expected.

2) In the planing mode lift results would be expected to be not unlike those of the Rollercraft wheel, while differing from those of the cylinder. In this case the lift force would be expected to be positive at zero wheel revolutions, caused by convex planing faces meeting the flow, then fall as wheel revolutions increased, to rise again as the blades began to act like LPW blades.

Reference to Figs.11.26 and 11.29 for the tyre in the planing mode shows that these effects are present in the results for both tyre directions though they are not as pronounced as for the Rollercraft wheel, being perhaps half way between those of the Rollercraft wheel and the cylinder. The initial lift at zero wheel revolutions still seems present, though small. Results at zero revolutions look more like those of the smooth cylinder. This is not unexpected as the tyre tines are small compared with the Rollercraft wheel blades. Increase in lift at higher revolutions is evident for both tyre directions, but is more pronounced for the tyre in the retrograde direction, probably because it does not throw up as much water as in the other direction as was noted to be the case in the displacement and transition zones discussed in (1) above.

3) Lift forces would be expected to show an increase with increase in velocity over the two planing speeds. This was observed in the cylinder results but not evident in either Rollercraft wheel results. It was explained as being caused by the increase in planing forces generated by the flow meeting the convex cylinder surface.

Reference to Figs.11.26 and 11.29 shows that in both cases this increase in lift force with velocity is evident. It would seem therefore that at higher planing speeds lift forces might become positive for all immersions and speeds of rotation, as was thought to be the case for the cylinder in section 11.3.1.

4) In the planing mode lift forces, either positive or negative would be expected to have magnitudes proportional to their immersion depths. This is found to be the case in Figs.11.26 and 11.29 and this is consistent with the cylinder and Rollercraft wheel results, and those of point (2) in the general findings.

WHEEL NO: 7

Blade Angle $\phi = 90^\circ$

Tyre, forward direction

STATIC, $V_o = 0$

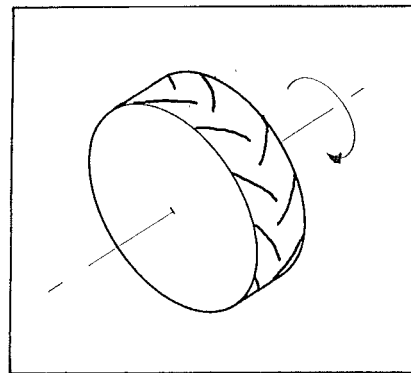
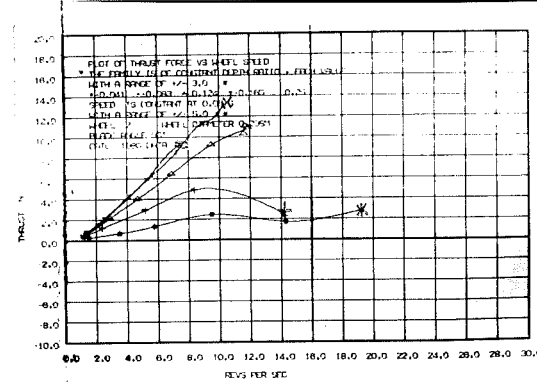
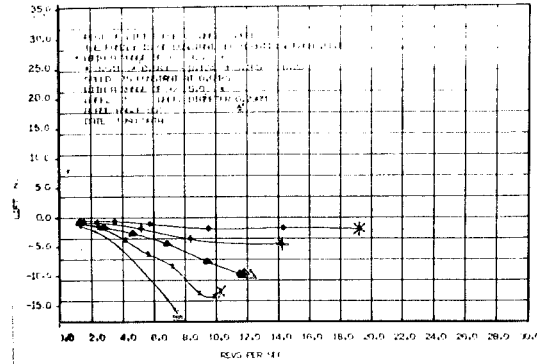
Diameter, $D = 298$ mm

Span, $s = 75$ mm $s/D = .25$

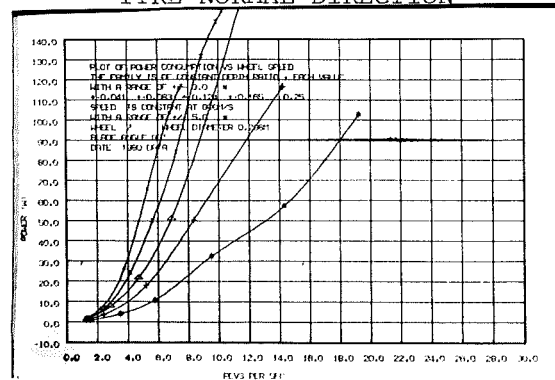
Chord, $c = 10$ mm $c/D = .03$

No. of Blades = 15 each side.

Symbols	Immersion ratio	Immersion angle	Immersion depth
	D/d	θ^0	d (mm)
*	.041	24	12
+	.083	33	25
Δ	.124	41	37
x	.165	48	49
=	.25	60	74



TYRE NORMAL DIRECTION



See also:

Figs	Sections
11.23 - 11.26	11.6
11.30 - 11.32	

FIGURE 11.24: WHEEL 7, $\phi = 90^\circ$. THE TRACTOR TYRE ROTATING IN THE NORMAL DIRECTION

WHEEL 7, $\phi = 90^\circ$
TYRE NORMAL DIRECTION

Displacement, $V_0 = 0.44 \text{ m/s}$, $F_r = 0.26$

Transition, $V_0 = 0.85 \text{ m/s}$, $F_r = 0.49$

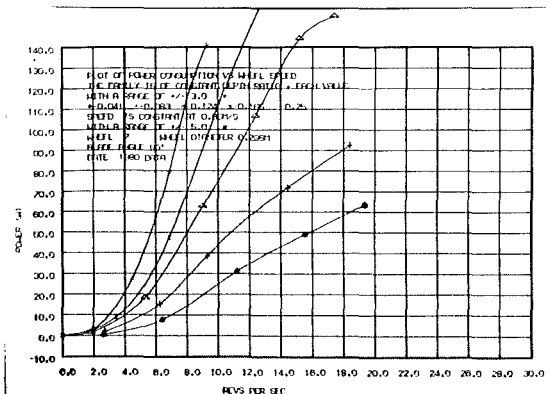
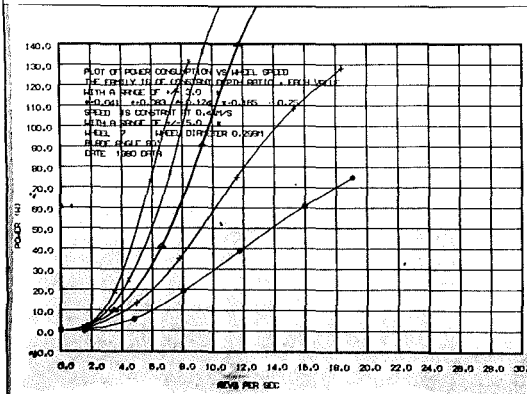
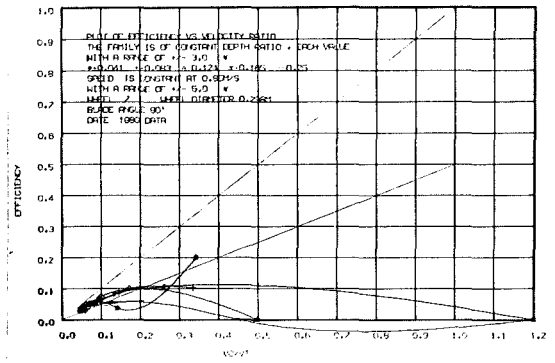
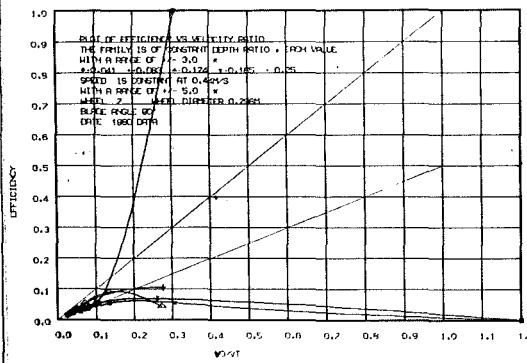
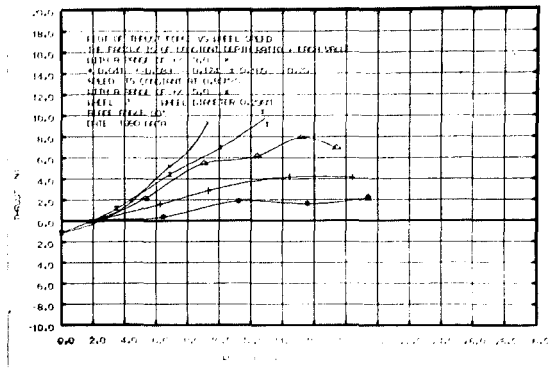
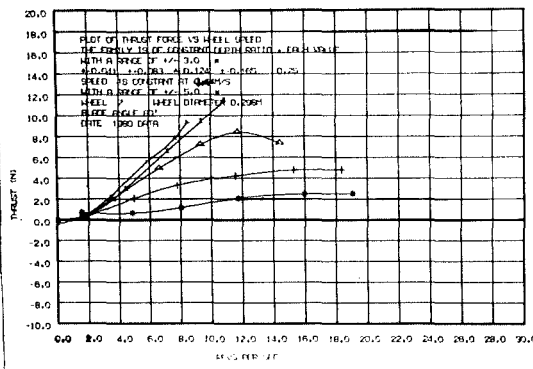
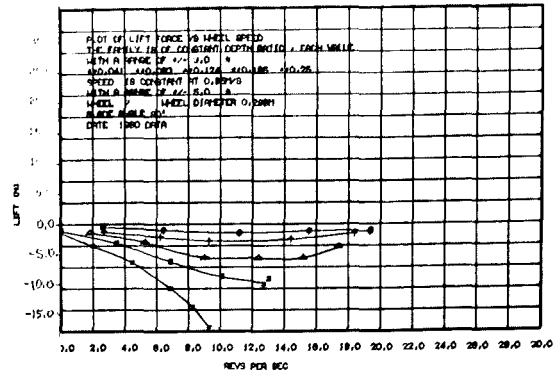
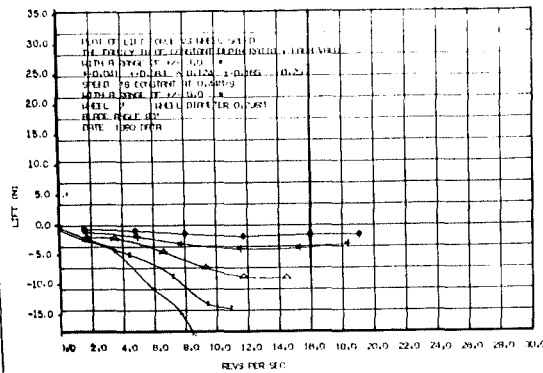


FIGURE 11.25: TRACTOR TYRE NORMAL DIRECTION DISPLACEMENT AND TRANSITION CONDITIONS

WHEEL 7, $\phi = 90^\circ$

TYRE NORMAL DIRECTION

Planing, $V_0 = 1.89 \text{ m/s}$, $F_r = 1.12$

Planing, $V_0 = 2.6 \text{ m/s}$, $F_r = 1.53$

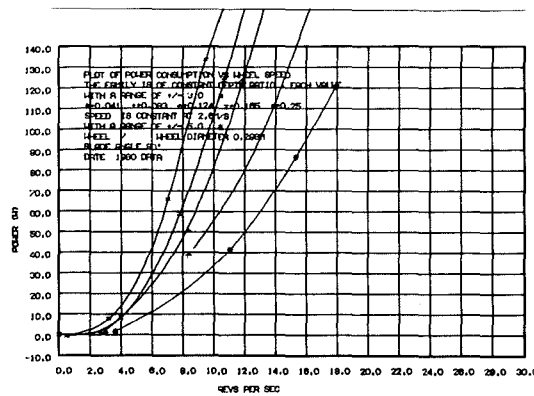
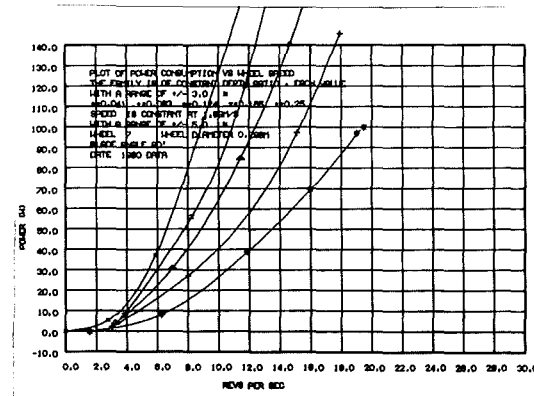
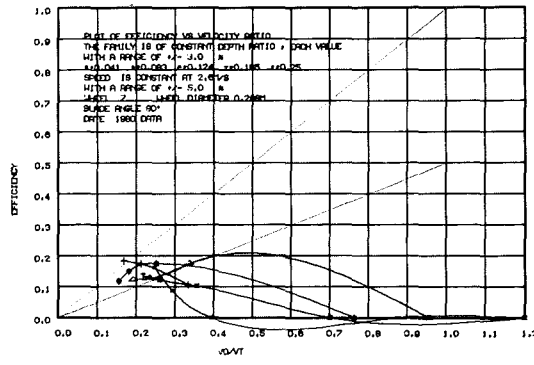
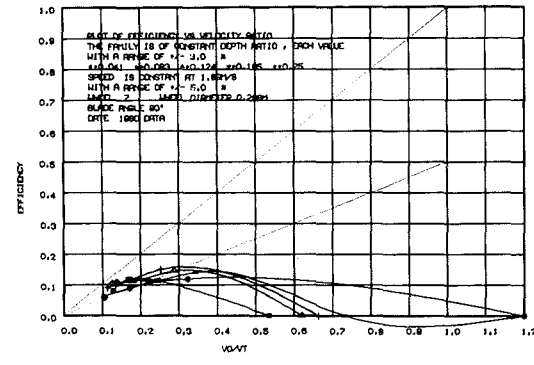
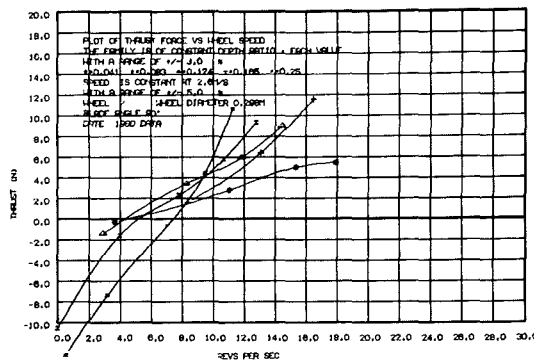
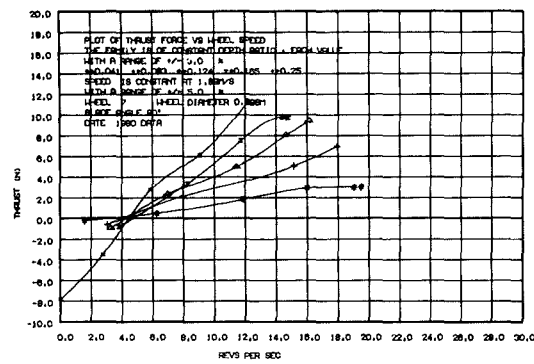
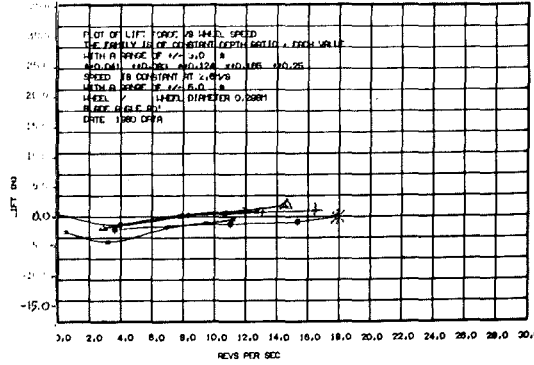
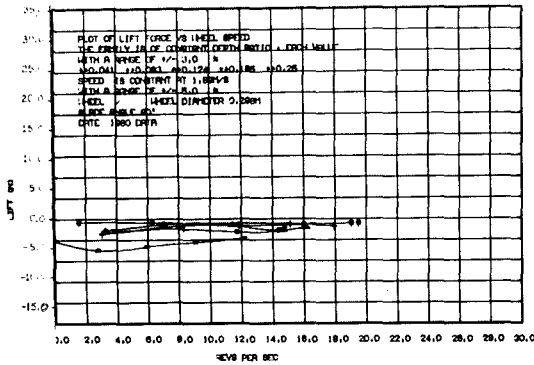


FIGURE 11.26: TRACTOR TYRE, NORMAL DIRECTION, PLANING

WHEEL NO: 4.75

Blade Angle $\phi = 90^\circ$

Tyre, retrograde direction

STATIC, $V_o = 0$

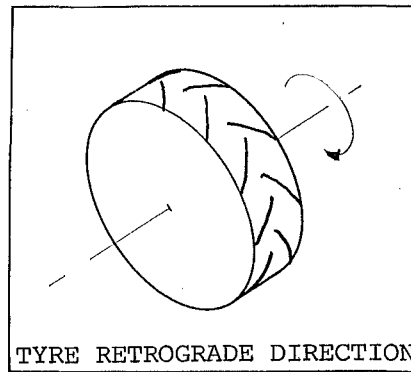
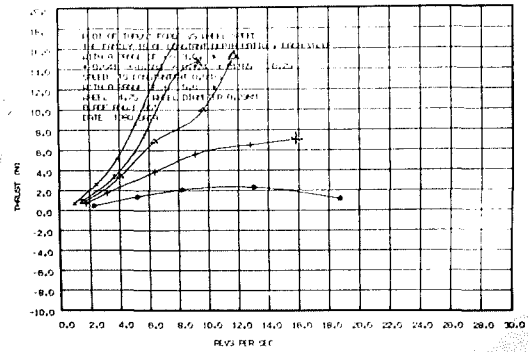
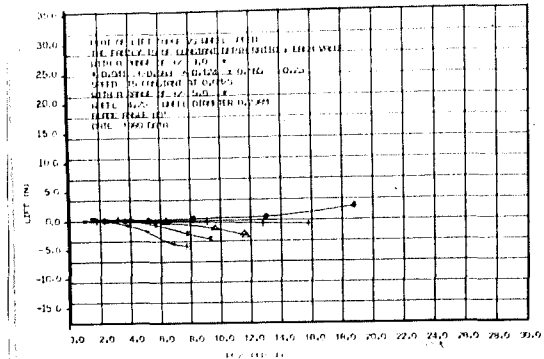
Diameter, $D = 298$ mm

Span, $s = 75$ mm $s/D = .25$

Chord, $c = 10$ mm $c/D = .03$

No. of Blades = 15 each side.

Symbols	Immersion ratio	Immersion angle	Immersion depth
	D/a	θ°	d (mm)
*	.041	24	12
+	.083	33	25
Δ	.124	41	37
x	.165	48	49
=	.25	60	74



See also:

Figs 11.27 - 11.32 Sections 11.6

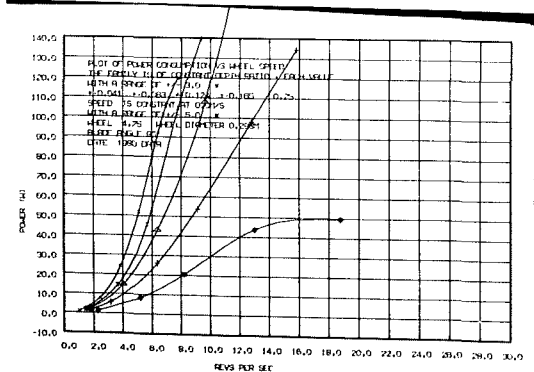


FIGURE 11.27: WHEEL 4.75, $\phi = 90^\circ$. THE TYRE TURNED AROUND SO THAT ITS TREAD FACES THE OTHER WAY

WHEEL 4.75, $\phi = 90^\circ$
TYRE RETROGRADE DIRECTION.

Planing, $V_0 = 1.89 \text{ m/s}$, $F_r = 1.12$

Planing, $V_0 = 2.6 \text{ m/s}$, $F_r = 1.53$

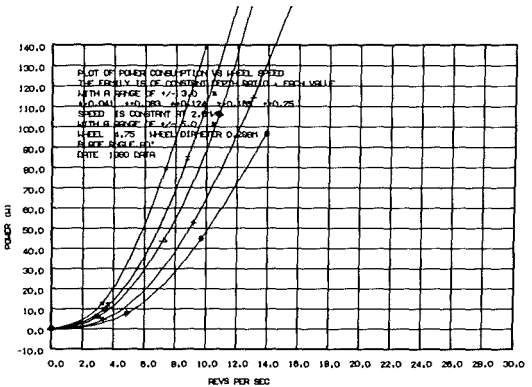
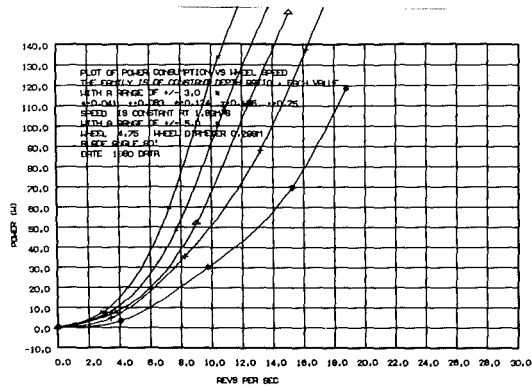
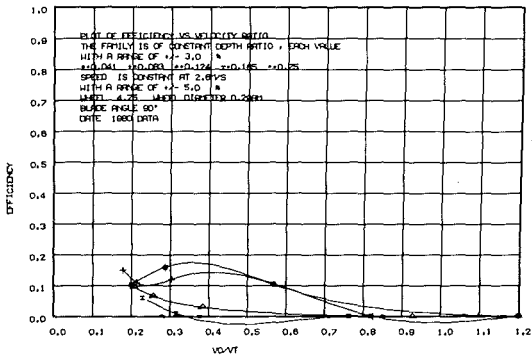
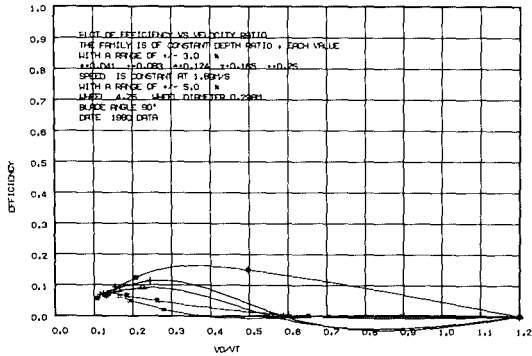
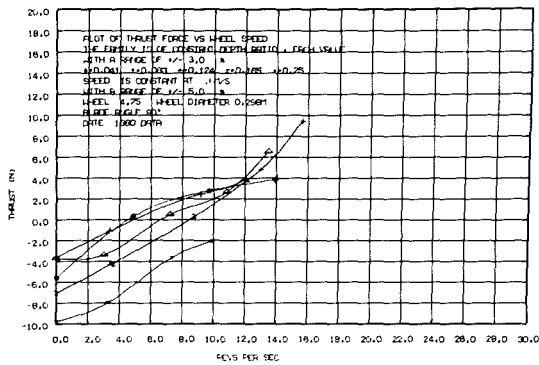
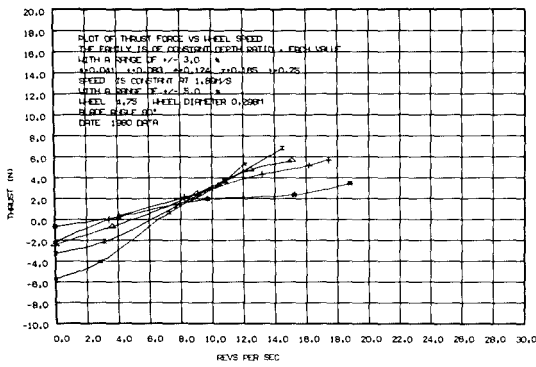
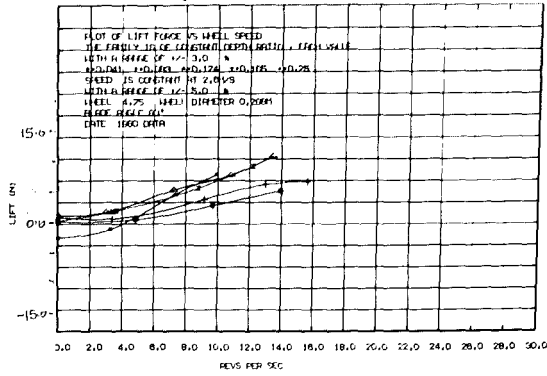
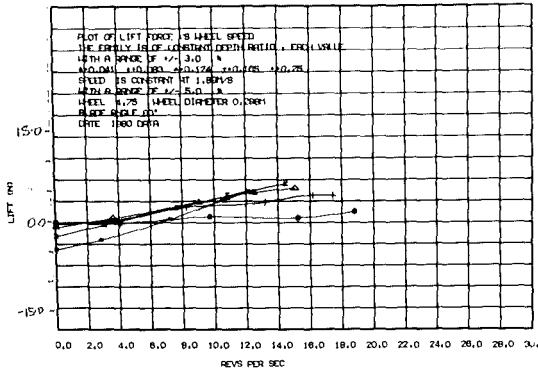
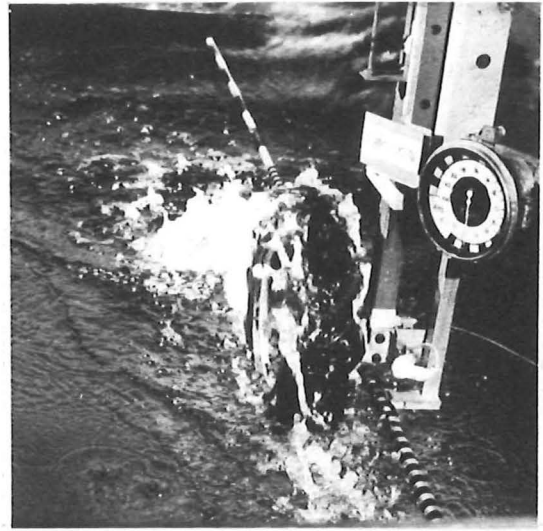


FIGURE 11.29: TRACTOR TYRE, RETROGRADE DIRECTION, PLANING



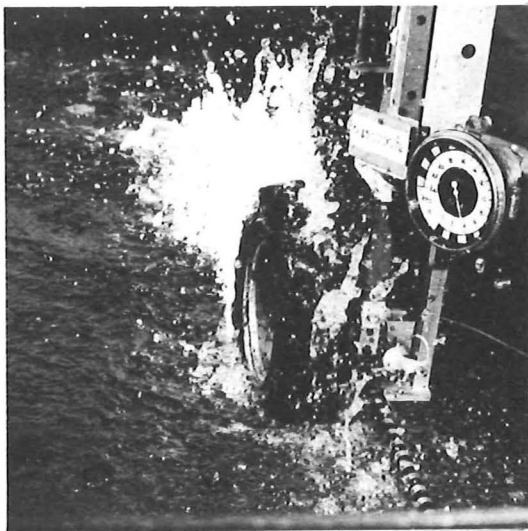
1300D/35A

(A) 0 RPS



1300D/36A

(B) 2 RPS



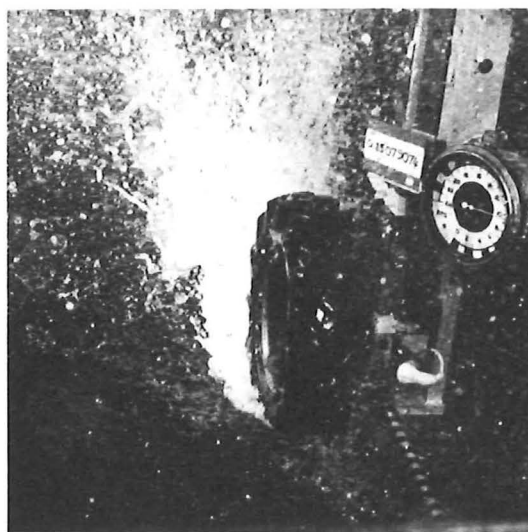
1300D/37A

(C) 4 RPS



1300D/38A

(D) 6 RPS



1300D/39A

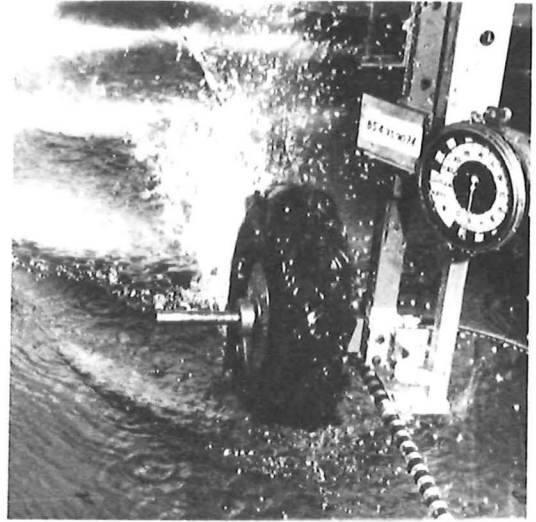
(E) 10 RPS

FIGURE 11.30: WHEEL 7, $\phi = 90^\circ$: THE TYRE IN THE NORMAL DIRECTION IN THE TRANSITION MODE SHOWING THE PICK UP OF WATER (0.85 m/s)



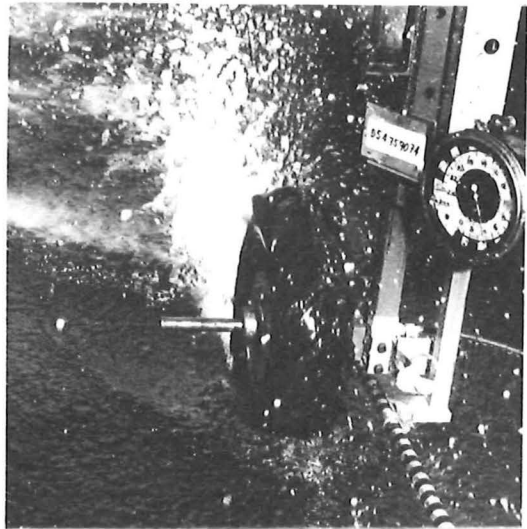
(A) 1 RPS

1205C/31



(B) 2 RPS

1205C/32



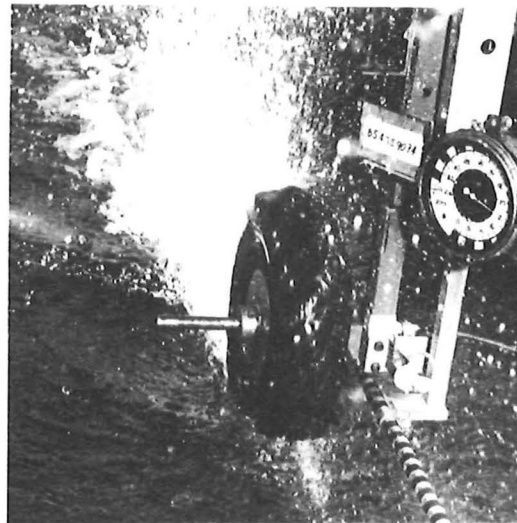
(C) 4 RPS

1205C/33



(D) 6 RPS

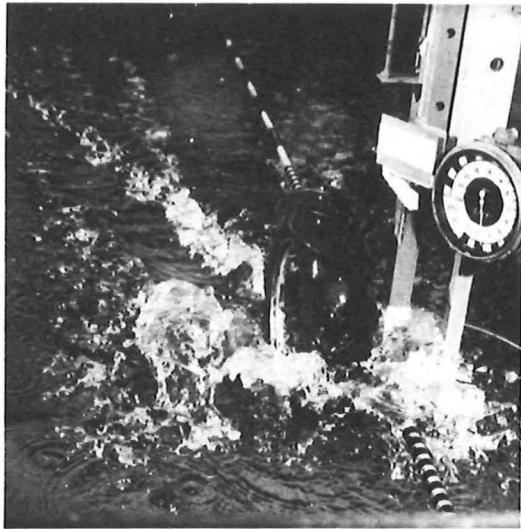
1205C/34



(E) 8 RPS

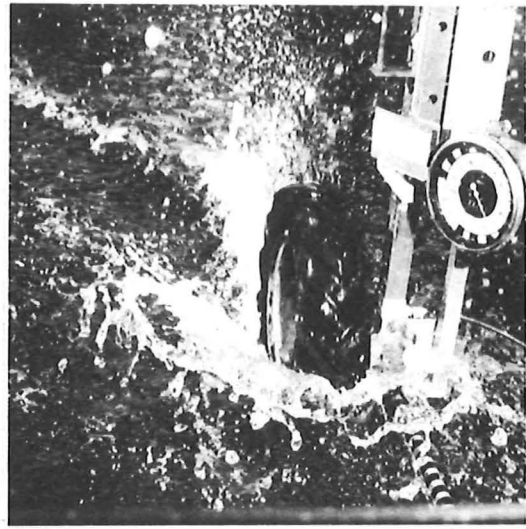
1205C/35

FIGURE 11.31: THE TYRE IN THE RETROGRADE DIRECTION OF ROTATION (WHEEL 4.75) IN ITS TRANSITION CONDITION SEEMS TO THROW UP LESS SPRAY THAN IN THE FORWARD DIRECTION (IN FIG.11.30)



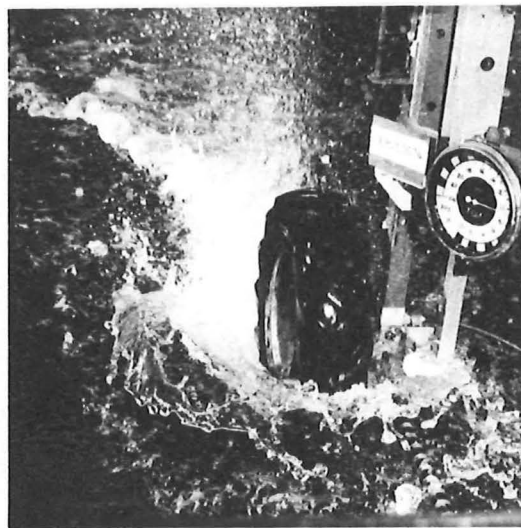
(A) 1 RPS

1300E/1A



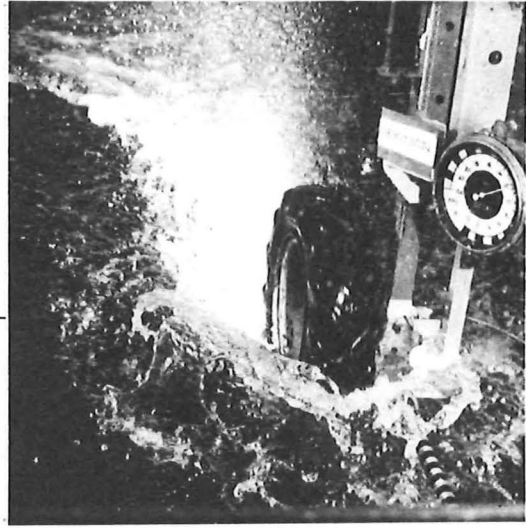
(B) 5 RPS

1300E/41A



(C) 9 RPS

1300E/42A



(D) 12 RPS

1300E/0

WHEEL MOTION

FIGURE 11.32: WHEEL 7, $\phi = 90^\circ$: THE TYRE IN THE NORMAL DIRECTION IN THE PLANING MODE AS REVOLUTIONS INCREASE (1.89 m/s)

Thrust: Again results are compared with expected trends from Rollercraft wheels (Figs.11.14, 15 and 16) and cylinder results (Figs.11.1, 2 and 3):

1) In the static displacement and transition zones drag at zero wheel revolutions would be expected to increase with speed of advance, and immersion depth. Rotation of the wheel would be expected to overcome this drag giving positive thrust, as was shown by the Rollercraft wheels, and to a much smaller extent by the smooth cylinder.

Reference to these thrust results in Figs.11.25 and 11.28 shows this to be the case for the tyre in both directions. The tyre in the retrograde direction demonstrates more grip on the water, giving more thrust over these speeds. While the mass limit, as found by the LPW results (section 9.2.1.1) is apparent at small immersion depths, results at larger immersions show remarkable traction in the transition zone when compared to LPW trends.

2) In the planing mode at zero revolutions drag would be expected to be large, as for the Rollercraft wheels and the cylinder, this turning into positive thrust at high wheel revolutions as the impulsive forces generated by the blades overcome the wavedrag of the planing wheel.

Reference to the tyre results in Figs.11.26 and 11.29 shows just such trends - these conforming well to results half way between those of the cylinder with no blades where thrust is regained only at excessive wheel revolutions, and the hard Rollercraft wheel with pronounced blades where thrust is regained at much lower wheel revolutions with velocity ratios near 0.6. The tyre with small blades, shows thrust overcoming wavedrag at velocity ratios around 0.5 ($n = 6$ rps at $V_0 = 2.6$ m/s). These thrust values do not become particularly large, and it is clear from Fig.11.32 (A) - (D) that the large bowsplash present in the planing mode at all wheel revolutions prevents this.

Efficiency: Efficiency results for the tyres are low, generally not rising above $\eta = 0.2$. This is largely because the wavedrag needs to be overcome by the wheel, and this is not achieved

until it is rotating fast ($\frac{V_o}{V_t}$ is small). As was the case for the flexible Rollercraft wheel, this restricts efficiency results to the left of the efficiency plots where ideal values themselves are low. As might be expected paddlewheel, and LPW efficiencies all exceed values achieved by these tyres.

11.6.1 Conclusions for Tyre Tests

These tyre test results have essentially consolidated the general findings from other wheels having surfaces beneath their blades. Rather remarkably the lift force trends indicate that a high speed tractor may just be able to skitter across a farm pond, though the speed would have to be unusually high and other conditions would need to be carefully chosen. Thrust results in the displacement and transition zones are exceptional and while propulsive efficiency is poor the traction afforded by these tyres, especially at deep immersions, rather justifies their use for the propulsion of small amphibious vehicles, if only low speeds are expected.

Several questions remain unanswered by these tests. While blades not parallel to the wheel axle have been shown to produce differing results in the two sets of tyre results, it is not clear why this should be the case. It is also unclear why the tyres do not rapidly reach the mass supply limit to their forces, especially in the transition zone where LPW forces were generally low because of this limit. And finally, while it is clear that tyres, as they stand, can provide lift and propulsion like the LPW it is not clear what effect the thick tines have or whether they could be readily adapted to become LPW type blades.

11.7 CONCLUSIONS

The wheel studies in this chapter have broadened the base of the LPW work by discussing the effects of different wheel configurations and organising the results into generalised findings which make workable predictions possible. While this has not added significantly to the theoretical understanding of the LPW it has, in a practical sense, shown the areas where problems may be found with this type of wheel; these problems are likely to be encountered if the LPW configuration is altered in the direction of a combination road and water wheel.

Unlike the results of Chapter 9, from which the impulse theory was developed, this chapter's contribution to the project remains as a resource of data against which ideas and future theoretical developments may be measured.

CHAPTER 12

THE MODEL PROTOTYPE LPW CRAFT12.1 INTRODUCTION

This chapter examines the results of a long series of tests on the small, 4 kg, four-wheel-drive, radio controlled, model LPW craft, powered by a model aeroplane engine. While these tests were the most frustrating and rewarding part of the project they are only given a relatively minor emphasis here, since the more controlled, experimental work at the testing tank, and the development of a workable theory offered more of fundamental value in determining the capabilities and limits of the LPW concept. Nevertheless the model tests provided much that was essential, in practical terms, to demonstrate the viability of the concept. This chapter describes these practical findings.

The purposes of building and testing a working model LPW craft may be divided into four areas:

- 1) To establish more firmly the validity of the results of the earlier, marginally successful model LPW craft tests, which set out to show that such a craft could be built and operated. (These earlier tests were described in section 3.5.)
- 2) To further demonstrate and discover the unique problems associated with the LPW craft-problems that could not show up in tank tests of an isolated wheel.
- 3) To provide a realistic testbed for the LPW's themselves and thereby help to verify promising experimental and theoretical results.
- 4) To attempt an answer to the fundamental question posed by this project: "How well can the LPW craft be made to work", by a direct demonstration of model prototype performance.

It will be seen from Fig.3.10 that the implementation of these purposes fits in the context of the tertiary aims of the project, while point (4) above returns the focus to the question that the project attempts to answer - the primary aim. Points (2), (3) and (4) above

will be examined in turn in the following sections.

12.2 BACKGROUND

To date two model LPW craft have been built, both undergoing a series of alterations and revisions. The first never ran more than 15 to 20 meters before stopping for one of a variety of reasons. It was built using materials and a model motor to hand in early 1977, before data was available from the first force balance tests. It was originally designed for tethered running round a pole but later, during 1978 simply launched in a straight line - its short runs never requiring it to be tethered. Its final specifications are given in Table 12.1 and it was shown in an early form in Fig.3.8 and final form in Fig.3.9. After many alterations it was retired having barely demonstrated its feasibility but having added significantly to the understanding of such a craft. The main lessons learnt from this craft were:-

1) The idea of a craft running on the water supported by dynamic forces produced by the wheels was shown to be possible: the craft ran without any flotation on two runs, indicating it was totally supported on its wheels.

2) More power than was originally installed was found to be necessary for this size of craft. This was later confirmed by the results of the 1979 tank tests.

3) Longitudinal instability was shown to be a significant problem and the torque reaction from the wheels tended to aggravate this. The craft often reared and dived especially in tests before the centre of gravity was placed well forward.

4) Appropriate torque matching between the motor and the wheels was necessary; at this early stage this was a trial and error process.

12.3 THE RADIO CONTROLLED MODEL

During 1979 a more powerful, radio controlled model was designed, based on the experience gained from the earlier craft. Its original specifications are given in Table 12.2, the assembly drawing of the chassis and transmission is shown in Fig.12.3 and the assembled craft

TABLE 12.1: FINAL SPECIFICATIONS FOR THE ORIGINAL
MODEL LPW CRAFT

Four-wheel drive, non-steerable model intended for free running.

Track:	350 mm
Wheelbase:	311 mm
Float:	Length: 653 mm
	Width: 216 mm
	Draught: 20 mm
Construction:	Polystyrene foam and wood
Craft weight:	2.14 kg
Motive power:	2.5cc model aircraft engine rated at 207 W at 260 rps (0.27 hp at 15,700 rpm)
Transmission:	Toothed belt drive to $\frac{1}{4}$ inch shafting and bevel gears
	Reduction Ratio: 8.67:1 overall
Bearings:	Fibre
L.P.W.'s:	FB, $\phi = 60^\circ$; D = 153 mm, s = 48 mm, c = 16 mm, 6 blades. (No.2 in Table 12.22)

TABLE 12.2: ORIGINAL SPECIFICATIONS FOR THE SECOND
MODEL LPW CRAFT

Four-wheel drive radio controlled model.

Track:	324 mm, front and rear
Wheelbase:	418 mm
All up weight:	3.5 kg
Float:	Length: 820 mm
(See Fig.13.2)	Width: 220 mm max
	Draught below axles: 32 mm min (variable)
Construction:	Polystyrene foam and wooden stringers
Steering:	Ackermann on front wheels
Chassis:	Aluminium tube, and 7 mm ply. No suspension or brakes
Motive Power:	O.S. 40 FSR radio control type 6.5cc motor Rating: 821 W at 267 rps (1.1 hp at 16,000 rpm)
Transmission:	Toothed belt drive from motor to driveshaft
	Reduction: 3.8:1
	Bevel Gear reduction drive to front and rear axles, 2:1
	Overall reduction: 7.6:1
	Shafting: $\frac{1}{4}$ inch throughout
	Bearings: Stainless steel shielded, type SKF WY $\frac{1}{4}$ inch No clutch or differentials
Radio Control:	Futaba 2 channel type FP-2G with combined receiver and servos Control functions: steering and throttle.
Centre of Gravity:	141 mm behind and 12 mm above front axle
Movement of Inertia:	0.139 kgm ² @ CG, about axis parallel to axles
LPW's:	Diameter: 153 mm
	Types: See Table 12.22

ready for its first runs shown in Fig.12.4. Some of the design features were as follows:

1) Since it was meant to demonstrate the principle of a fast amphibious craft its general arrangement was that of a four-wheel-drive road vehicle with Ackermann steering in the front wheels and rear wheels in line behind the front wheels. Although it was possible that such steering and general arrangement might not be the ideal for a water craft of this sort, this arrangement is known to perform well on land, so that to demonstrate it on water would immediately confirm it as a successful amphibian. Other arrangements may have been used such as skis in place of the front wheels, or differential type steering, but these would not have been suitable for a road vehicle.

2) The wheelbase was chosen so that at the transition zone trough speed, the wave train from the front wheels would tend to cancel the wave train of the rear wheels, enabling the rear wheels to negotiate what was believed to be the most difficult stage before lift-off. The wheelbase could be altered by simply using longer chassis members, and providing a driveshaft extension (see Figs.4.19(E), and 12.10 showing the long wheelbase version).

3) The float was of polystyrene foam, sealed, and could be easily cut, changed or added to, until a workable configuration was found.

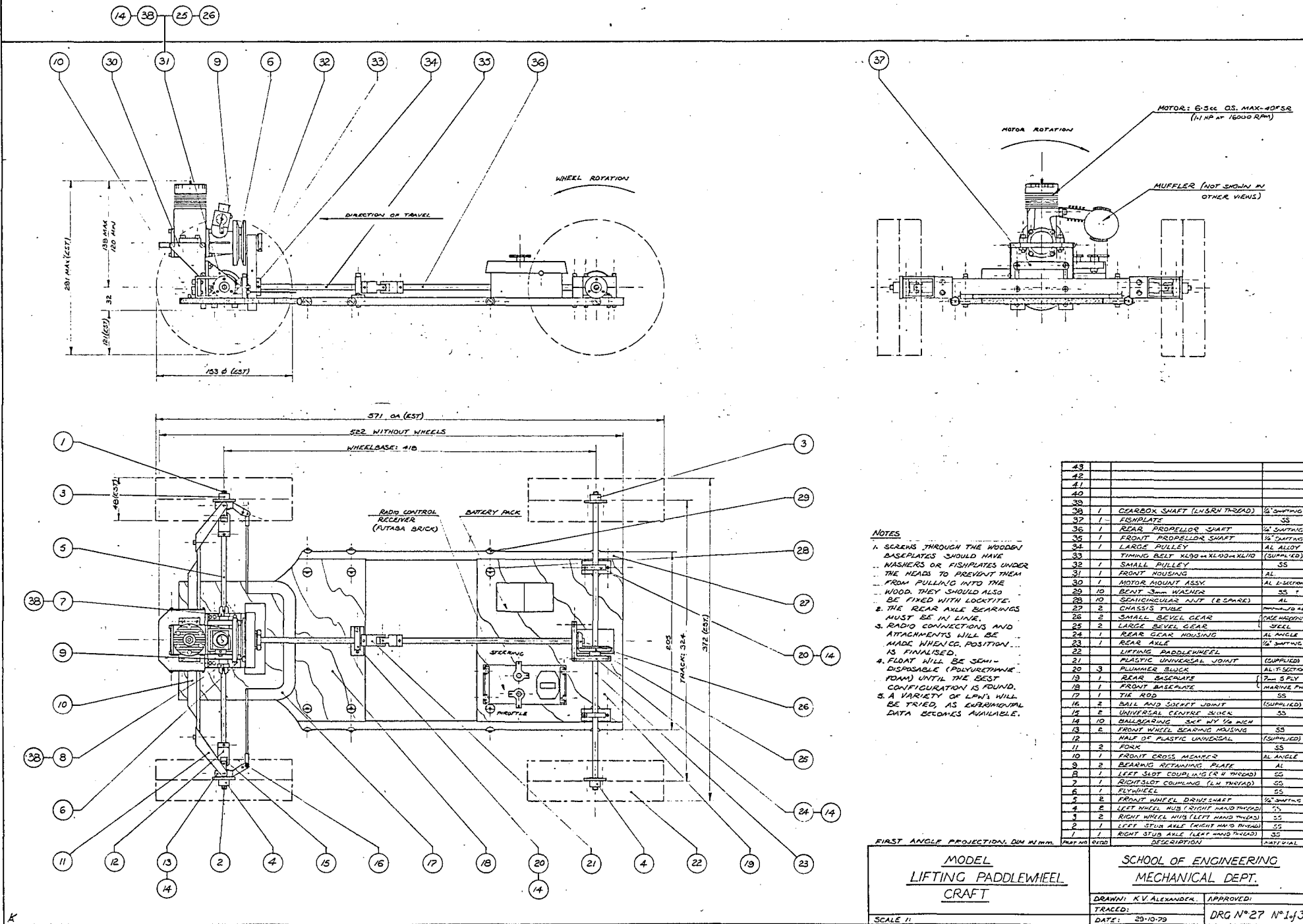
4) The centre of gravity was well forward to balance the torque reaction of the wheels, and provide good longitudinal trim under power, after lift-off.

5) Spray guards over the wheels were deliberately left off so that spray formation could be observed. Such guards could easily be added if required.

6) The craft was designed to come apart easily under heavy loadings or for regular alterations, repairs and maintenance (Fig.12.5).

The main chassis components and transmission were made by the Departmental Workshop while the hull, radio control installation and linkages, wheels, motor, tank, air cleaner and other additions were

FIGURE 12.3: CHASSIS ASSEMBLY DRAWING FOR THE MODEL LPW CRAFT.



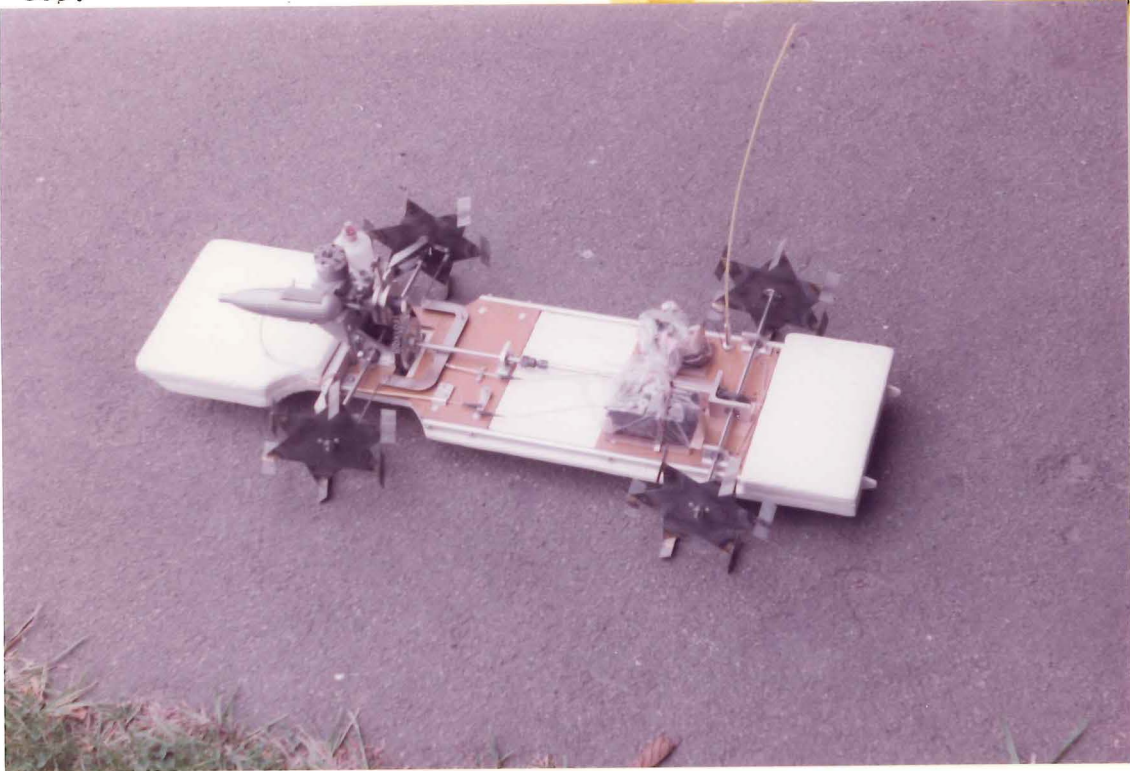


FIGURE 12.4: THE MODEL READY FOR ITS FIRST RUNS (WHEELS 2)



FINAL AIR CLEANER DESIGN

FIGURE 12.5: THE MODEL AT A LATER STAGE, DEMONSTRATING ONE RETRIEVAL METHOD, THE FACILITY WITH WHICH THE CRAFT COMES APART AND THE AIR CLEANER IN ITS FINAL FORM. (WHEELS: REAR 23, FRONT 7.)

installed later, and adapted to the changing conditions of operation.

Once construction was complete the expected teething problems had to be dealt with, and it wasn't until the twelfth trip to the model boat lake that the craft ran successfully and under a measure of control. Once successful runs had been achieved the work of clarifying performance parameters and the testing of a variety of LPW's began.

12.4 RECORDING CRAFT PERFORMANCE

Getting the model to operate consistently under a chosen set of conditions was one thing, while the reliable recording of distinguishable results was quite another. In order to distinguish between results of craft performance, a number of techniques were employed.

1) Each test in a particular series was coded with a binary number, and a pattern of flags (sticky labels) was stuck to the craft aerial so that it represented this code (numbering from bottom to top). This was generally visible in photographs. Each series of tests started these numbers at the beginning again.

2) The LPW's themselves were painted in different colours, and in colour photographs they could readily be identified.

3) Before each test a chart was drawn up. It contained the binary code, and it recorded the particular parameters under test. It was photographed prior to the test runs. (See Fig.12.6.)

4) Variations in the craft superstructure also helped to identify tests, for example long or short wheelbase versions, different aircleaner designs, hull additions and so on.

These methods were generally successful in identifying photographic records.

There were three main forms of lakeside data records. These were:

(1) Still Photography: Colour photographs were taken by the assistant, Mr K. Fairweather, with a hand held motordrive camera.

This enabled a series of views to be taken at a maximum rate of just over two photographs per second when necessary. Over 300 pictures were taken in this way; these included photographs of the test identification chart. There were a number of other photographs taken in a less systematic fashion by other photographers and these, taken for reasons other than simply keeping a record often provided additional useful information when they could be matched to the tests in question.

(2) Black and White Video Recordings: These provided invaluable information on the craft dynamics, while the sound track recorded the engine note from which engine speed could later be determined. Two or three minutes of video record was generally more than enough to demonstrate the craft performance under each test situation. Close to 1½ hours of video recordings were made; these included views of the test identification chart at the beginning of each test. These video recordings had considerably less resolution than the still camera views, so these two records complemented each other.

3) Written Records: These were made after each test and enlarged upon at the end of each day's testing. They contained such things as the binary code, the features under test, performance characteristics of note, motor mixture settings, fuel types, breakdowns, modifications, whether or not photos and video were taken, and so on.

(4) Measurements: Actual quantitative measures of craft performance were not easily, nor often undertaken. One set of tests recorded static thrust of the model, and the final series took speed measurements by timing the craft over a measured distance.

12.5 MODEL PREPARATION AND EXPERIMENTAL PROCEDURE

Prior to each test series considerable organisation was required. Thorough preparation normally took more than a day and it was unusual not to have some repairs to be made. Before the tests the procedures in Table 12.7 were undertaken.

Christchurch is fortunate to have a model boat lake not far from the University. This was ideally suited to the model tests which were always conducted there. Because of the vagaries of the weather, the

Front
of
Craft

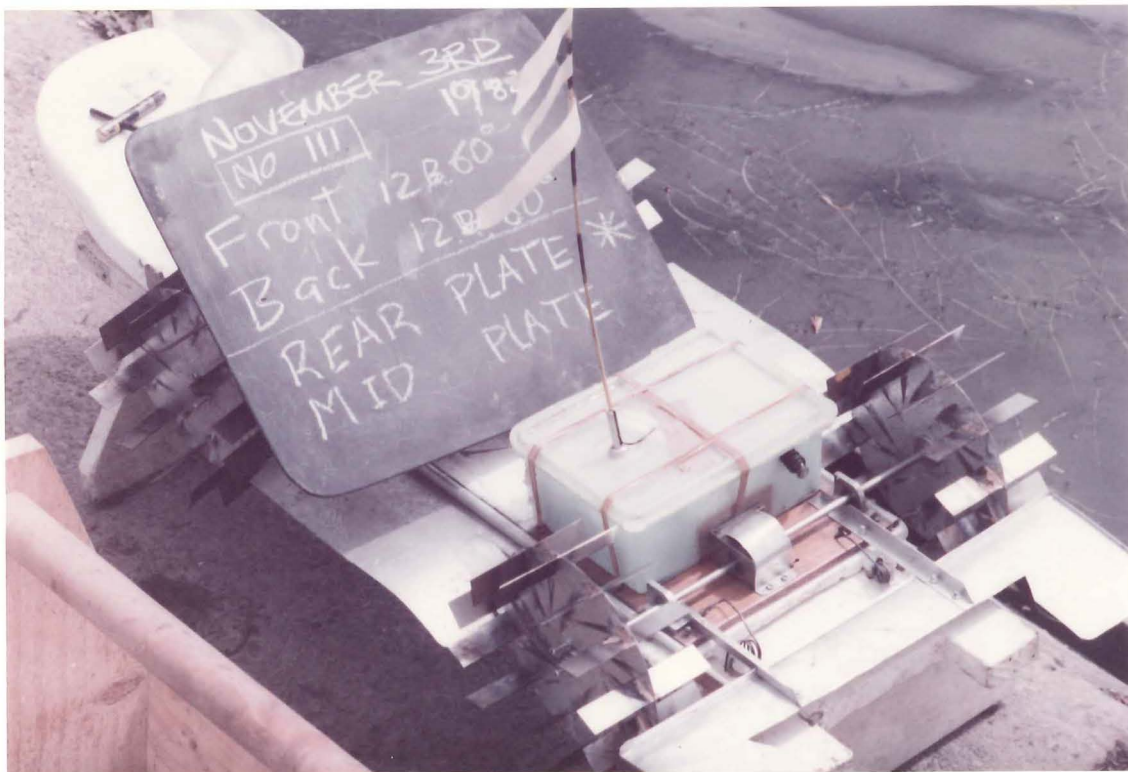


FIGURE 12.6: THE MODEL ON ITS STAND WITH THE DESIGNED WHEELS (NO.3) (SECTION 12.8), THE MID-SECTION AND REAR PLATES, THE TEST IDENTITY CHART AND THE CORRESPONDING AERIAL FLAGS IN BINARY CODE.

TABLE 12.7: PROCEDURES BEFORE A TEST SERIES

Read the results of the previous test series.

Make new wheels to be tested.

Dismantle model, flush out bearings, make repairs and alterations.

Reassemble model and check all screws and transmission grubscrews.

Buy fuel, spare belts and glowplugs.

Arrange to borrow video camera and recorder, and put video batteries on charge.

Charge starter motor batteries, radio batteries and check glowplug.

Install radio receiver and batteries in waterproof radio box on model.

Plan test programme.

Organise assistance for the tests - video camera operator, still camera operator, transport.

Assemble all equipment, tools, cameras and check through equipment checklist.

TABLE 12.8: PROCEDURES AT THE LAKESIDE

1. Unload and assemble equipment and model on the jetty. Connect up and test video equipment, load still camera, put tools and radio transmitter handy.
2. Mount LPW's on the model.
3. Make out chart describing the test to be undertaken (Fig.12.6) and attach binary code flags to radio receiver aerial.
4. Record intended test and binary code in writing, and take still and video shots of the test chart.
5. Fuel up the model, check water trap in fuel pressure line, connect up glowplug, get engine running using the starter motor.
6. Turn on radio receiver, then transmitter, check both steering and throttle operation; leave transmitter handy.
7. Hand launch model fast or slow as required. Take over transmitter.
8. When possible steer the model past the jetty for acceleration and high speed runs, for the camera records.
9. After a suitable variety of performance trials, return the model to the jetty, stop the motor, return craft to the stand and turn off radio equipment.
10. If the model has stopped in the lake it is to be retrieved, and radio equipment turned off. (Fig.12.5.)
11. Clean off weed and empty any water from motor, aircleaner and radio box.
12. Discuss performance, make written records, repairs and alterations. Continue the same test at 5 above, or a new test at 2 above.

model motors, equipment breakdowns and the inevitably wet conditions, the lakeside tests were rather less than ideally controlled. Nevertheless, at the lakeside the tests followed a fairly regular procedure as contained in Table 12.8. About half the runs ended with the model out in the lake from where it had to be retrieved (Fig.12.5) and if the craft had rolled over or submerged, the motor had to be blown out thoroughly before it would run again. Four hours was usually the extent of a day's testing by which time the various batteries were running low.

In all there were 25 trips to the lake, covering tests with 29 different sets of wheels.

12.6 PROBLEMS AND CHARACTERISTICS OF THIS CRAFT

This section covers point (2) in the introduction to this chapter in looking at problems unique to this type of craft as found in the model tests. In this analysis they fall into the following five areas which will be examined in turn:

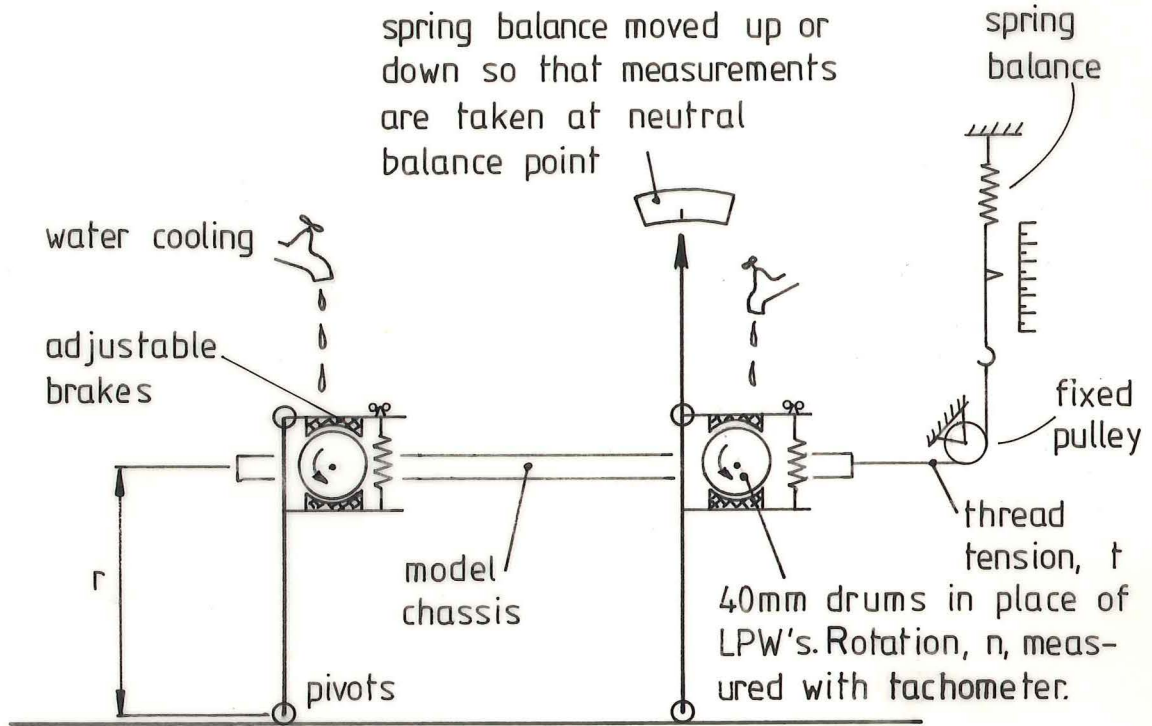
- (1) Motor output and power requirements.
- (2) Obtaining craft lift-off from a static start.
- (3) Craft stability in all modes of operation.
- (4) Steerage.
- (5) Land performance.

12.6.1 Motive Power and Power Requirements

In the first model tests and in the early stages of the second model tests, considerable time and effort was spent in simply trying to keep the model engines running under the wet conditions of low speed model operation. The difficulties had three aspects.

(1) The torque matching between the motor and wheels was inappropriate: gear ratios were too high so the motor either stalled at launch or ran much too slowly to develop the required power.

(2) Inexperience with these motors meant that fuel mixtures were not properly adjusted. Canterbury Model Power Boat Club members were consulted and their experience readily rectified this difficulty.



torque from all 4 wheels $T_0 = tr$
 power from all 4 wheels $P = 2\pi ntr$

FIGURE 12.9 SCHEMATIC OF THE MODEL'S CHASSIS DYNAMOMETER

34/57/9



FIGURE 12.10: THE DYNAMOMETER IN PREPARATION FOR TESTS WITH THE LONG WHEELBASE VERSION OF THE MODEL

(3) The motor often stopped because it ingested too much water and spray. A series of air cleaners (eg:Fig.12.10) and water traps was designed, used and lost to the bottom of the pond before the final satisfactory form evolved(it can be seen in Fig.12.5) which generally allowed the motor to keep running in the most unlikely conditions. Ironically high speed runs with the designed LPW's were successfully conducted without the air cleaner (Fig.12.20) (which had been lost earlier that particular day) and it only really seemed necessary when the model operated in the displacement mode and threw up more spray.

As noted above, the original estimates of craft power requirements were too low and the model craft motors were upgraded in capacity from 2.5cc for the first model to 6.5cc and 10cc in the second. The difficulty with estimating craft power requirements had two aspects:

(1) There were no reliable LPW experimental power measurements available for the first model tests nor for most of the second model tests.

(2) Although the manufacturers rated power for the motors was known, the actual power output under these operating conditions, the shape of the power curves and the model craft transmission losses were all unknown. These factors were of considerable importance since these small two-stroke model motors often have steep power curves and their performances tend to be very sensitive to fuel variations, air temperature and humidity. So not only were power requirements unknown, but power available was unknown as well.

By the time the testing tank results had been processed and the theory developed to an extent where power requirements could be estimated with some reliability (see sections 4.14 and 9.8) the model had been running successfully for some time. At this stage dynamometer tests to determine the model power output were planned to ascertain how well the model was performing in comparison with its predicted performance based on tank test data and theoretical work.

A model chassis dynamometer was required to measure the power output at the wheels under the loadings and wheel revolutions expected in practice. Apparatus for this purpose was designed and

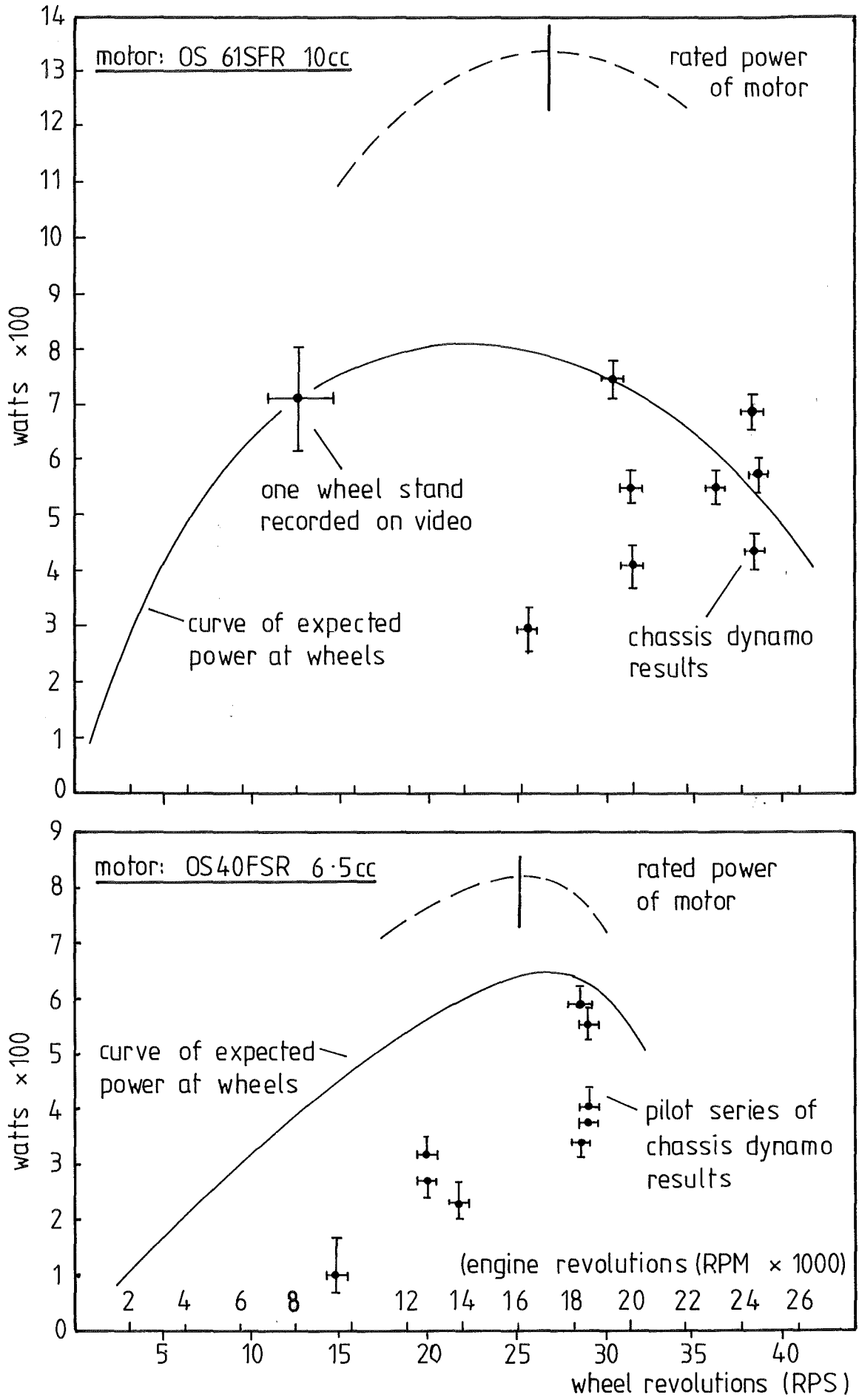


FIGURE 12.11 RESULTS OF CHASSIS DYNAMOMETER TESTS GIVING POWER AT LPW's FOR BOTH MOTORS USED.

built by the author. It is shown schematically in Fig.12.9 and a photograph of it being prepared for operation is shown in Fig.12.10. The most pertinent features were that the craft weight was supported by the "wheels", small cast iron drums in this case, so that the bearings were loaded as they would be in practice, and the torque produced by the wheels was averaged by the apparatus, and could be determined from the spring balance measurements and the torque arm length.

In operation water cooled the drums and the motor, and once the brakes had been applied, wheel rotational speed was measured with a hand-held tachometer while the spring balance was read.

The apparatus, while providing results, was not easy to operate in its first form: for example the brakes could not be quickly and evenly applied, and the spring balance had to be moved vertically to obtain measurements with the apparatus in a balanced condition. Unfortunately the 10cc model motor broke a connecting rod when it was run too fast during the dynamometer tests, so that at the time of writing only a few scattered results had been obtained from the 10cc motor and those from a pilot series for the 6.5cc motor. These are shown in Fig.12.11 and while they are not considered, by any means, to be a satisfactory test of the motor capabilities they are of some value for this project for the following reasons:

(1) In both sets of results there are cases of widely differing power outputs from the motor at the same wheel revolutions and with the same fuel settings. Aside from the possibility of undetected dynamometer faults, these results seemed consistent with the varying performance found in practice.

(2) As expected, no measurements exceeded the rated power output of the motors. This helps to validate the dynamometer results.

(3) The tests of the 6.5cc motor gave one result of 588 watts, this being 233 watts below the rated output of the motor. This figure of 233 watts can therefore be taken as an upper limit to transmission losses.

(4) Curves may be drawn through both sets of results as shown in Fig.12.11. These are the best estimates at present of the model

craft power output. It must be remembered, however, that under the right conditions when the model ran well, it may have been using more power than these curves show, possibly as much as the motor rated outputs.

It is apparent from this discussion and attempted measurements that reliable estimates of LPW craft power consumption are not easy to obtain from model motors, which tend to give unpredictable performances. Such measurements may have to be left until a full-sized prototype can be developed.

12.6.2 Achieving Lift-Off

"Lift-off" is the term used to describe how the craft goes from floating during low speed running through an intermediate stage of hull planing to the condition where, at high speed, it is supported only on its wheels with the hull clear of the water. Getting the model LPW craft to achieve lift-off was one of the most confusing areas of the model tests. Now that the process is better understood it is apparent that a classification of the various stages of the craft's progress during lift-off clarifies matters. These stages may be classified in terms of displacement, transition and planing type modes for both the LPW and the craft hull. In this classification the wheel mode is followed by the hull mode as follows:

(1) Displacement-displacement: Apart from static conditions this is the slowest mode of craft operation. The wheels themselves are in the displacement mode (see Fig.9.6), and the craft, in the displacement mode, is supported almost completely by the buoyancy of the hull.

(2) Transition-displacement: The LPW's are in their transition zone (see Fig.9.7) while the hull, having a longer waterline length is still in the displacement mode. The model craft just beyond this condition is shown later in Fig.12.15 and this was originally believed to be a difficult stage for the wheels to go through. In practice this has not been the case at all, though if hull drag was excessive such difficulties might arise.

(3) Planing-displacement: The wheels have just entered the planing mode (Figs.9.8 and 9.9) while the craft is still moving in its displacement condition. If the wheels are rotated fast, as they

often need to be to traverse this stage, a large bowsplash will develop in front of the LPW's as shown with the model earlier in Fig.4.19(E). This bowsplash may be excessive if the wheels are still relatively deeply immersed, which they are likely to be if the hull has not been lifted far. This was often the case during model tests. On the other hand if the craft has sufficiently low hull drag or the wheels generate enough thrust they will not be able to reach a high enough velocity ratio for bowsplash to begin to occur (see discussion of bowsplash in sections 4.9.1, 4.9.3, 9.4.3.1 and 9.4.3.2). Thus the craft may traverse this stage without the appearance of bowsplash at all.

It is also possible that if the craft is light enough it will be lifted clear of the water before this stage is reached. Although it is unlikely, this stage could therefore be avoided altogether and the craft would go directly to planing-flying, point (6) below.

Once the LPW's are planing another problem arises: if deeply immersed, or if the blades have a small blade angle ϕ , then the angle $\beta = (\phi - \theta)$ may be negative. This being the case then by expression 4.22 the thrust force in the planing mode will also be negative (see section 4.10.2). This sort of condition can be seen for FB, $\phi = 45^\circ$ in Appendix 4 (wheel 6, $\phi = 45^\circ$) where, for the immersion ratio $\frac{d}{D} = 0.165$ (symbol ' χ ') thrust is positive for the wheel in the displacement and transition zones but becomes negative once planing is reached. If this is the case the LPW's cannot provide traction beyond the wheel transition zone and craft speed is limited to the wheel transition speed. To cope with this, wheels can be given blade angles ϕ , which are large and such wheels can therefore provide positive thrust through the wheel transition zone at large immersions. This was one of the early problems with the model and was overcome by having high blade angles, greater than 90° , or cupped blades (see Fig.12.21 and Table 12.22) and while these solved this transition zone problem they provided insufficient lift for lift-off.

(4) Planing-transition: The wheels are still in their planing mode with or without bowsplash, while the hull is making the transition to planing. This is the "hump" speed for the hull and therefore its drag will be increasing rapidly with speed. Once again the craft may not be able to traverse this stage if the wheels do not have enough thrust to overcome this increasing hull drag. This also was observed

to be the limit to the model craft speed in many instances during the model craft tests at the lake.

On the other hand hull drag may be levelling off with increase in speed, especially if the LPW's now with the assistance of the planing forces generated by the hull are able to lift the hull high in the water, and therefore decrease the drag.

Alternatively this stage may be by-passed altogether if LPW lift forces are sufficient to lift the hull clear of the surface before its hump speed is reached. (Hull hump speed or transition speed may be found approximately from the hull waterline length since it occurs when $Fr \doteq 0.75$. See section 4.15.2.)

Interestingly the short wheelbase version of the model apparently managed to avoid the high drag of the hull in its transition zone by lifting the bow out first, thus shortening the hull waterline length so that it was automatically planing. In this case the wheel torque fortuitously provided a suitable mechanism to make this change. Model hull transition speeds were about 2.1 m/s for the short wheelbase version and 2.3 m/s for the long wheelbase version.

(5) Planing-planing: Both the wheels and the hull are in their planing modes in this stage. At least some of the craft support is gained from the hull's dynamic forces. Many of the LPW's tested achieved this state, giving quite high speeds (about 5 m/s max.) but not operating as truly lifting devices. In fact purely thrusting paddlewheels could also achieve this same state, and indeed, this is what Wray and Starrett hoped to do (see Fig.2.5) and was also the intended use of Beardsley's Surface Impulse Propulsion concept. (1) This can be seen to be the model craft condition in Fig.12.12 where the model craft's stern is in the water and the rear wheels are deeply immersed (to about $\frac{d}{D} = 0.2$). In this state the LPW's may, or may not be generating bowsplash depending upon the conditions of velocity ratio, immersion, blade angle and number of blades. In Fig.12.12 bowsplash is not evident from front or rear wheels and velocity ratio, as determined from the splashes left by the front wheel blades is quite high (about 0.64), just consistent with conditions of no bowsplash (see Fig.9.28). As before, this condition



FIGURE 12·12: THE MODEL IN THE PLANING-PLANING CONDITION. THE REAR OF THE HULL IS IN THE WATER, AND THE REAR WHEELS DEEPLY IMMERSSED ($d/D \doteq 0.3$, $V_0 \doteq 4\text{m/s}$, WHEELS: F 8, R 20)

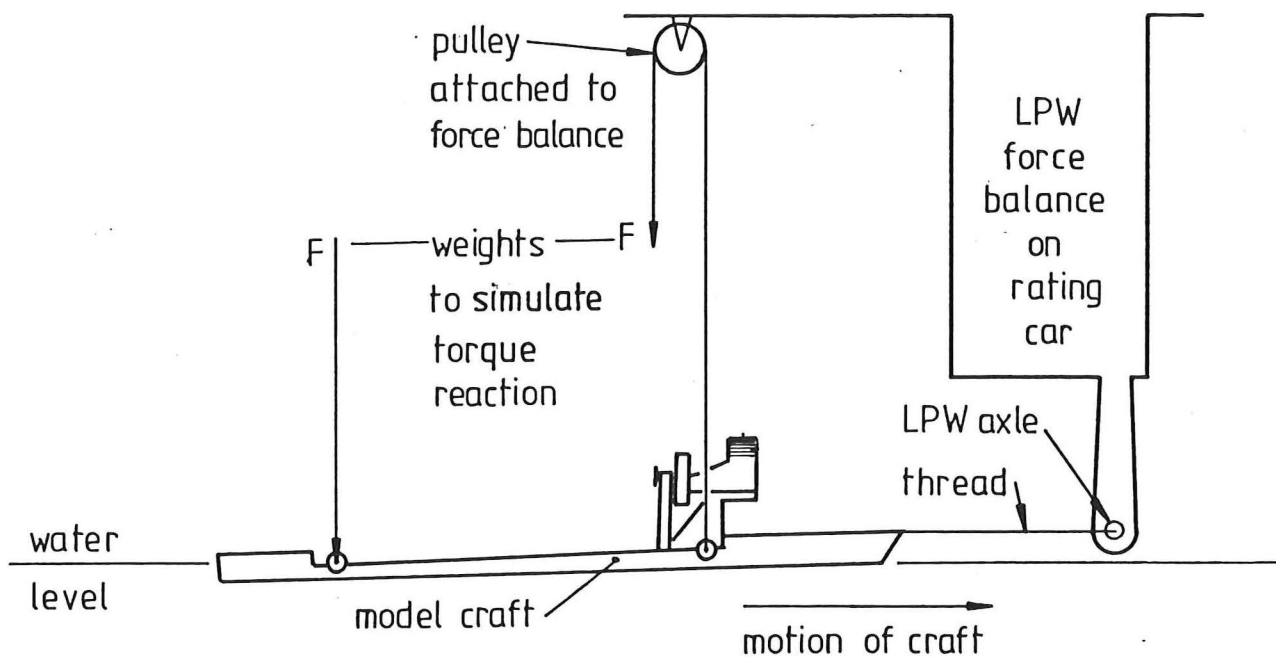


FIGURE 12·13: THE ARRANGEMENT FOR THE TOWING TESTS OF THE MODEL WITHOUT LPW'S IN PLACE, AT THE KAINGA TESTING TANK. (PLANING ANGLE, α , WAS NOT MEASURED.)

may be avoided altogether if sufficiently large lift is generated by the LPW's to lift the hull clear at speeds below the craft planing speed.

(6) Planing-flying: This is the condition which can be uniquely achieved by the lifting paddlewheel. The wheels are in a high speed planing condition while the craft hull is raised clear of the water (see Fig.12.20). Under this condition the hull drag is reduced to air drag and spray drag which is presumed to be small compared to the former hull drag. Thus once this condition is achieved, speed rapidly increases and the LPW's begin to operate at high velocity ratios (low slip). Under optimum conditions the speed could be arranged to increase until the craft was operating at its maximum propulsive efficiency (see section 13.2.10).

While these states are clear now they were not apparent in the early stages of the model tests, where emphasis upon wheels for propulsion to overcome hull drag diverted attention away from the importance of wheels with adequate lift. As an example in Figure 12.12 the model is fitted with cupped-bladed wheels to overcome hull drag. Cupped blades while providing good thrust only give lift after cavity intrusion (see section 10.10 on cupped blades). In Figure 12.12 the wheels are not demonstrating bowsplash, so they will be operating before cavity intrusion and therefore providing insufficient lift for lift-off. Such cupped blades never achieved the planing-flying condition on the model.

Once attention returned to lifting wheels of suitable dimensions lift-off was readily achieved from a static start.

12.6.2.1 Hull Drag Measurement. To assist in analysis of the lift-off stages, drag tests on the model hull, in its early form, without the LPW's in place, were undertaken at the Kainga tank. These tests simply involved towing the craft at a series of known speeds, with the towing thread attached to the force balance shaft so that the drag could be recorded as negative thrust on the LPW data recording system. Weights were added to the rear of the hull and the bow was lifted by similar weights over a pulley, to represent the effects of wheel torque. This is shown schematically in Fig.12.13. These were only intended as order of magnitude tests as it was fully expected that the hull drag in still water was likely to be different from the hull drag under operating conditions with the LPW's generating

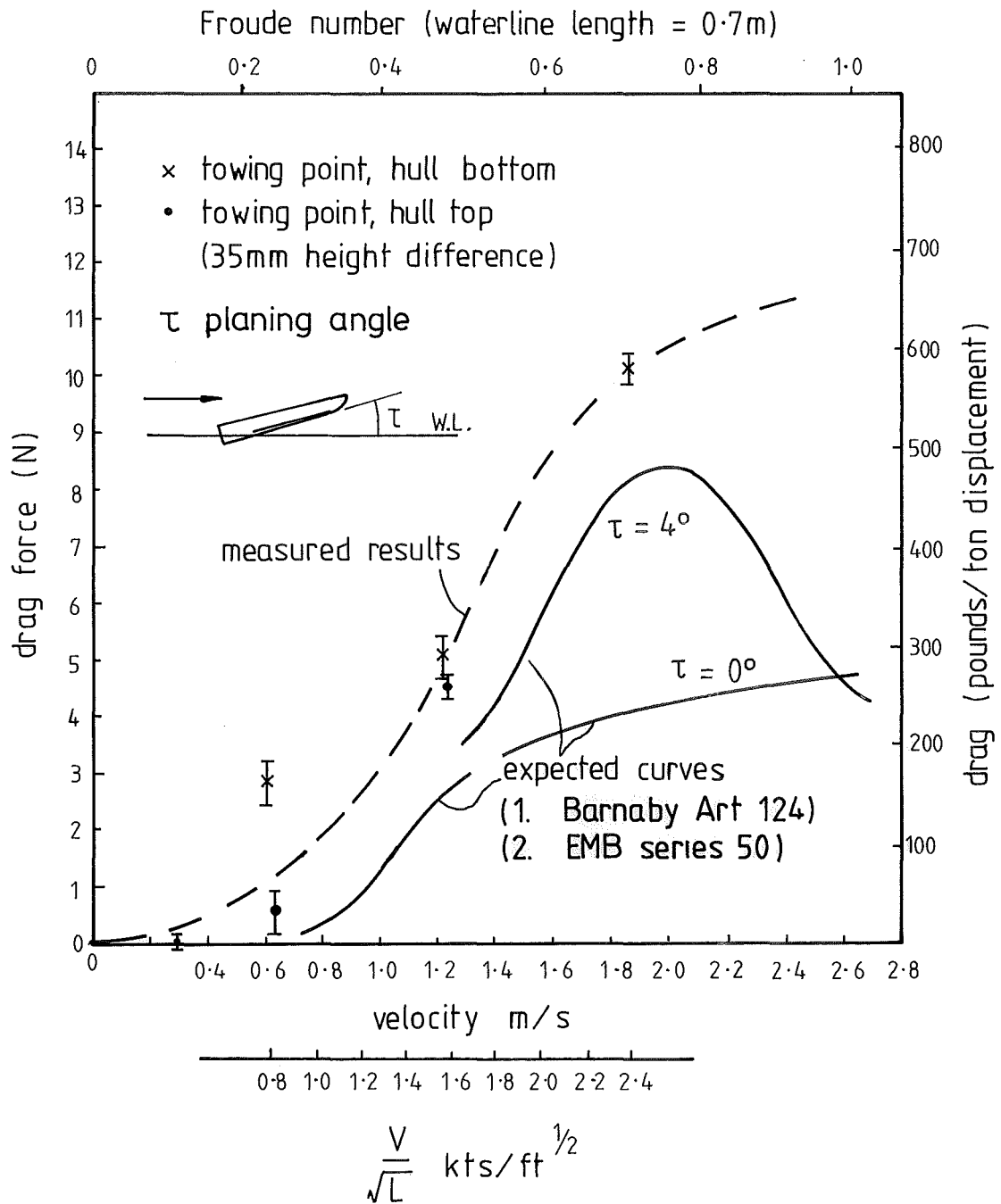


FIGURE 12.14 RESULTS OF TOWING TESTS ON THE MODEL CRAFT.

(see point (3) above and section 4.10.2). Such plates with height adjustment screws can be seen in Fig.12.17 in front of the front wheels and between the front and rear wheels. Earlier versions can be seen in Fig.12.15. These plates have only made slight differences to lift-off difficulties though their effects have yet to be thoroughly assessed. Once the optimised LPW designs were found to be successful, tests on these plates lapsed.

The effects of spray on craft lift-off are possibly of some significance. Although no measurements have yet been attempted it can be imagined that the large amounts of spray thrown up at lift-off speeds would add to craft drag. Equally, however, it can be seen that this spray may aid in lifting the craft as much of it is intercepted by the mid-section and rear plates. These effects, still not assessed are discussed further in section 12.8 and Table 12.23.

12.6.3 Stability

Although water craft operate in a medium which makes them inherently less stable than vehicles on land, this fact was easy to overlook in adapting a road vehicle configuration to water use. Stability needs to be considered separately for each of the conditions of hull speed:

- (1) Static buoyant stability.
- (2) Stability at low speeds with the hull in the displacement or transition conditions.
- (3) Stability with the hull planing.
- (4) Dynamic stability of the craft after lift-off.

In examining these conditions the following aspects need to be kept in mind:

- (1) The effects of wheel torque.
- (2) Longitudinal stability.
- (3) lateral stability.
- (4) Dynamic effects.

Of these four aspects the effects of wheel torque were the most significant and easily overlooked. As already noted the second model was designed with its centre of gravity well forward, 25% of the wheelbase length behind the front axle, to balance the effects of motor torque.

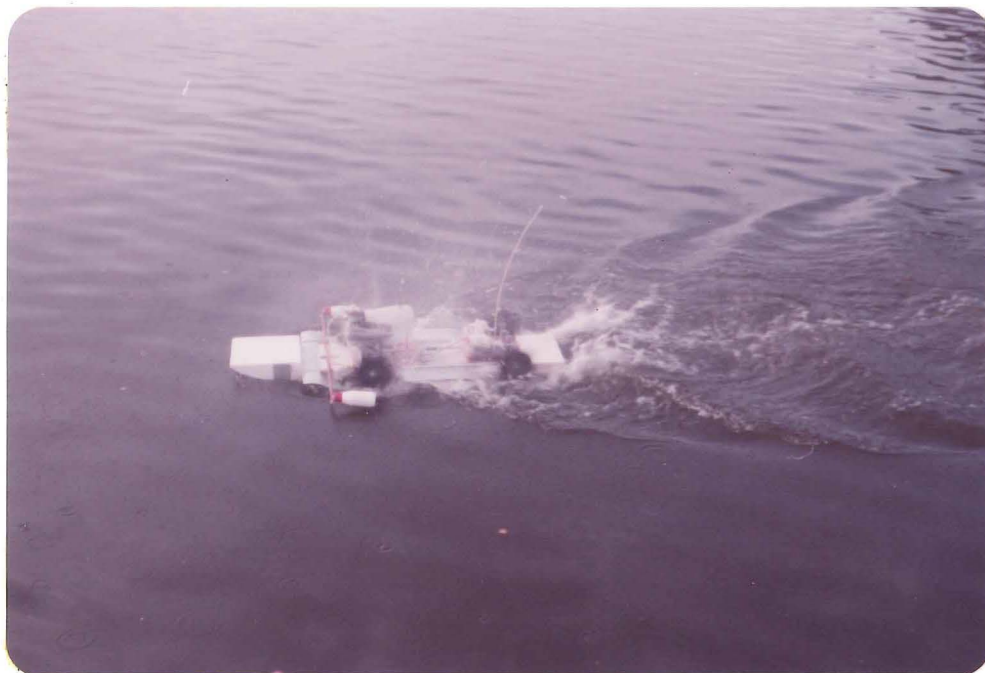


FIGURE 12.15: THE MODEL JUST BEYOND THE TRANSITION-DISPLACEMENT CONDITION, WHICH WAS THE SPEED LIMIT FOR THESE WHEELS FROM A STANDING START (WHEEL 2). NOTE OUT-RIGGERS AND ENLARGED BOW. ($V_0 \doteq 0.9$ m/s)

FIGURE 12.16: THE MODEL IN AN EARLIER FORM, IN THE PLANING-FLYING CONDITION AFTER A HAND LAUNCH. THE SAME WHEELS ARE IN USE (WHEEL 2), $V_0 \doteq 4$ m/s. NO MID-SECTION OR REAR PLATES ARE IN USE.



Each of the conditions of hull speed will be examined in turn and the most significant stability factors noted in each case.

12.6.3.1 Buoyant Stability. With the centre of gravity well forward the centre of buoyancy had also to be well forward so that the floating craft had a reasonable attitude which did not interfere with its displacement motion. The hull was necessarily flat bottomed to allow it to be lifted clear of the water at speed, and narrow enough to fit between the wheels. With the motor mounted as high as it was, the centre of gravity was about 12 mm (0.08D) above the water level so that this hull did not have particularly good roll stability: if the craft was tilted 55° to 60° from the horizontal it overturned. In the most recent form the radio box on top of the hull contributed to the buoyancy of the aft end, and being placed high it helped a little in preventing the craft from completely overturning on occasions.

12.6.3.2 Stability in the Hull Displacement and Transition Modes. This was the least stable condition of all for the model. In early tests it was found necessary to mount outriggers on the craft to prevent it rolling over at these speeds (see Fig.12.15 above). The reasons for this instability can now be generally attributed to the torque reaction and fountain effect created when any one of the craft wheels became too deeply immersed. Lateral stability could be lost if, for example, the craft was turned sharply, when, because of its high centre of gravity it would list and immerse the outside front wheel. This wheel then absorbed most of the motor torque, which had the primary effect of rotating the craft around the inclined front axle and caused a confusing set of conditions which either righted the craft or caused it to roll over, out of the turn.

This lateral instability in the displacement-displacement mode was largely corrected by two alterations. The first was to add more buoyancy to the craft bow by extending it forwards and upwards. This prevented the craft from immersing either front wheel deeply. The second was to place horizontal plates between the front and rear wheels (see Figs.12.5, 12.10, 12.15, 1.3). While these helped to convert wheel spray to lift at high speeds and kept front wheel spray from striking the rear wheels, their primary purpose was for lateral

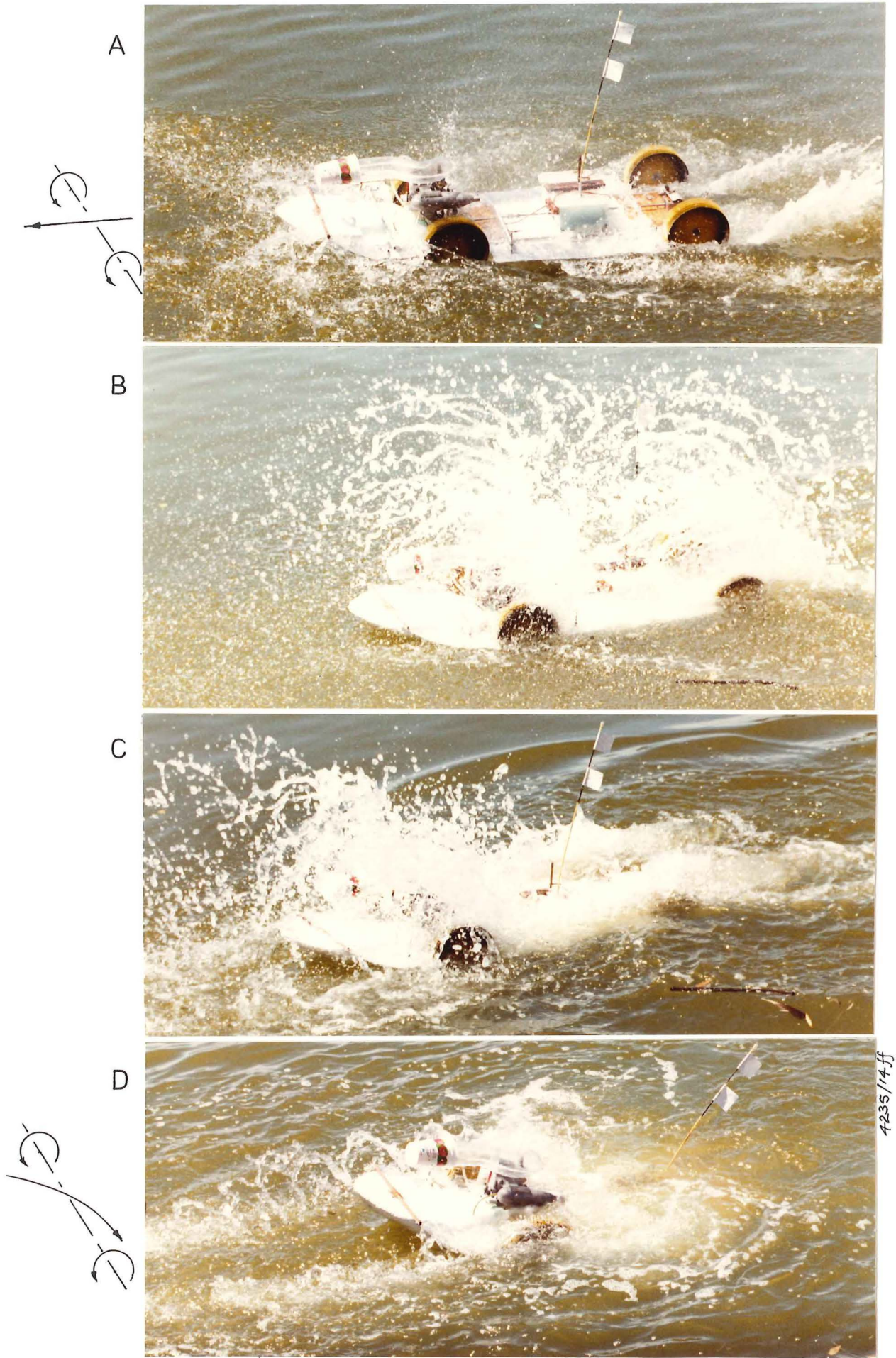


FIGURE 12.17: THE FOUNTAIN EFFECT CAUSING THE MODEL TO SUBMERGE. THE SEQUENCE COVERS ~5 SEC. (WHEELS: 24, MESH)

stability in this displacement-displacement condition. It was unclear at first why they helped, but it seems now that these plates redirected water thrown up by the front wheels in the fountain effect, which seems to occur with all wheels at deep immersions ($\frac{d}{D} > 0.5$). In intercepting this flow the plates created substantial righting moments which restored craft equilibrium. These two methods proved quite adequate for displacement-displacement stability and the outriggers were removed.

It is clear that a lower centre of gravity would greatly assist in reducing this sort of instability.

Longitudinal instability was also a problem with some wheels in the displacement-displacement mode. Wheels which combined the properties of poor thrust with the ability to create the fountain effect, caused these difficulties. Their operation seemed to be as follows: thrust was not sufficient to keep the craft moving faster than the wheel transition speed. At this speed, or slower the rear wheels produced substantial fountains and so created large negative lift forces. Since the centre of buoyancy of the craft was well forward and the plates behind the front wheels redirected spray from them, the front of the craft stayed up and the rear was pulled down. Once the rear wheels were fully immersed their torque reaction rotated the craft round the rear axle. The whole effect was that the craft would slow down and be caught up by its trailing wavetrain whereupon it would halt, and reverse downwards into the water under a fountain, sometimes rolling over in the process. This formidable behaviour is shown in the sequence in Fig.12.17 (A)-(D) for the mesh wheels (No.25 Table 12.22). The process in this figure began with a hand launch at about 1.5 m/s, into the planing-displacement condition (note bow splash in Fig.12.17(A)), and the motor stopped before the craft became completely submerged, just after (E).

It is interesting to note that most of the other wheels responsible for this reaction, (Nos. 27, 28 and 29 in Table 12.22), would maintain traction and keep the craft running if it was launched into the planing-planing mode to start with. This response only occurred when the wheels themselves were in the displacement or transition mode.

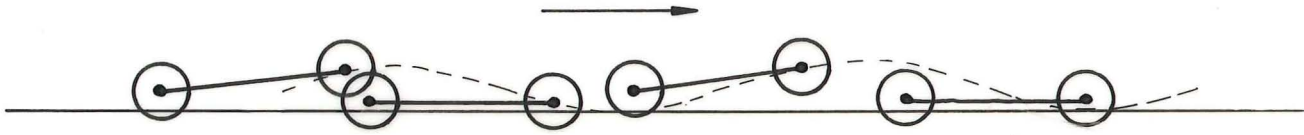


FIGURE 12.18: THE BOUNCING MOTION: FRONT WHEELS OFTEN LEFT THE WATER COMPLETELY, REAR WHEEL IMMERSION DECREASED AT HIGH POINTS.



FIGURE 12.19: WHEN THE BOUNCING WAS EXCESSIVE THE MODEL LEFT THE WATER COMPLETELY. STEERING WAS DIFFICULT UNDER THESE CONDITIONS. (WHEELS F7, R19)

12.6.3.3 Stability in the Hull Planing Mode. As the craft speed increased from the hull displacement mode so did the craft stability. Support came increasingly from the wheels which provided relatively widely spaced points of suspension compared with the support of the hull buoyancy forces. Steering now produced less roll and the wheels in their planing condition were unable to carry water around to create the fountain effect and negative lift.

Once the hull was planing, however, a new set of dynamic stability problems arose. Apart from the dynamic effects of the wheels themselves which acted like undamped elastic supports as discussed in (4) below, the hull seemed to act like many flat-bottomed planing hulls and executed a porpoising motion with a frequency of about 2.75 Hz. While in this case the action was probably assisted by the wheel lift, it looked very similar to the behaviour of high powered planing boats. This phenomenon has been studied at length by boat designers and others who have found that instabilities arise from an interaction between vertical and pitching motions which tend to increase as the planing angle becomes small, the immersed surface becomes large, or the speed is increased. Variation in these factors, then, can cause the porpoising craft to become increasingly unstable, or can cause the oscillations to die out. (1) The model craft with the hull in its planing mode demonstrated both these extremes. In general it "bounced" along as shown in Fig.12.18 and occasionally the oscillations stopped and it then had the chance to pick up speed and achieve proper lift-off, though usually such clean runs had to be interrupted by turns which started the oscillations again. Sometimes, however, oscillations built up so that the craft leapt clear of the water, Fig.12.19, and on one or two occasions these leaps ended in dives terminating the run. Normally this bouncing motion about the rear axle or craft stern was not of such an extent as to necessitate the craft being slowed down for its safety.

This porpoising motion in the hull planing mode was of concern from two points of view, first, with the front wheels clear of the water much of the time, steering the craft was difficult, and second, this motion repeatedly immersed the full length of the hull which increased hull drag considerably so that with many of the wheels tried, the craft could not attain speeds that would have allowed them

to lift it clear of the water. Some time was spent in trying to understand the causes of this motion so that it could be prevented. Apart from the fact that the hull itself seemed to be porpoising several other factors may have contributed to the motion:

(a) As noted already, the wheels acted like undamped springs on the four corners of the craft.

(b) The motor speed could be heard to vary in time with the motion: if the front wheels left the water, motor speed increased and therefore motor torque decreased. This reduced the torque reaction around the rear axle, and allowed the bow to fall back again. Immediately the front wheels entered the water the motor came under load so its speed reduced and torque increased which, with the assistance of the lift forces generated by the front wheels, lifted the bow out again. This mechanism doesn't require any contribution from the craft hull.

(c) Another possible mechanism seems a little less likely to cause the rotational motion about the rear axle that was normally observed, but it may be responsible for the less often observed vertical motion. By the expression 4.31:

$$\frac{T}{L} = \tan (\phi - \theta) \quad (4.31) \quad (12.1)$$

if lift is assumed to be roughly constant and a little less than the weight of the craft, then with the hull in the water, planing, drag and therefore thrust must be relatively large for steady motion. Any increase in thrust tends to decrease the immersion angle θ since the blade angle ϕ is fixed and equality in the expression must be maintained. Reduction in the immersion angle, θ lifts the craft clear of the water and this reduces the drag dramatically, so that the craft accelerates, velocity ratio increases, thrust decreases and to keep the equality, the immersion angle θ increases so that the craft falls back on to the water surface, starting the cycle again.

While (b) above seems the most likely explanation as it is consistent with the method used to stop it ((4) below), the explanation (c) should not be overlooked.

A number of methods have been tried to dampen out these oscillations:

(1) Weight shift methods: Loads of up to 0.5 kg (0.13 of the craft weight) were placed on the craft bow to both stop its lifting clear of the water and to change the craft's moment of inertia. Such efforts were uniformly unsuccessful in preventing this porpoising motion though they did lower its frequency to about 1.5 Hz (on the long wheelbase version).

(2) Changing the wheelbase: The craft wheelbase was increased from 418 to 600 mm. This simply lowered the bounce frequency also.

(3) Reducing lift from the front wheels: This was accomplished by reducing the front wheel blade size to a quarter of rear blade area (Fig.12.12) which showed no change in the bouncing. Blade area was then reduced to zero and simple discs were put on instead of the front wheels. The craft could not be run satisfactorily with these in place, since with no traction at the front, and most of the hull drag ahead of the rear wheels, steering became very sensitive and unstable, so that each run ended with the craft turning sharply from a gentle turn and rolling itself over before the planing-planing condition could be reached. Effectively negative lift with positive thrust was given to the front end by using the flat-bladed wheels, $FB, \phi = 75^\circ$ mounted backwards which made them $FB, \phi = 105^\circ$ wheels. In this case craft steering was good but the negative lift didn't stop the bounce.

(4) Plates behind the rear wheels: These can be seen in Figs. 12.6, 12.20 and 13.3. This method seemed entirely effective in preventing the buildup of the porpoising-type bounce. It apparently operates in the following manner: As the rear wheels immerse they throw up more spray which, in striking these rear plates generates a moment about the rear axle having the opposite sense to the torque reaction of the craft around the rear axle. Thus these plates tend to counteract any rearing of the craft especially when it coincides with an increased immersion of the rear wheels. In action this moment appears to operate in phase with the mechanism that causes the porpoising and successfully damps it out.

These plates also had a disadvantage in that in some circumstances they prevented the craft from making its transition to the hull planing mode. This seemed to occur because they tended to hold

the craft bow down rather than letting it rear through the transition mode as described above (section 12.4.2, point 4, Planing-transition mode).

Since this final method worked it would appear that the explanation of the bouncing motion is largely contained in (b) above. If this is the case the bouncing motion could probably also be prevented by governing the motor speed.

What appears to be the same or a related bouncing motion has been observed in some large earthmoving vehicles which have no suspension other than their large tyres. At speed they can get into a galloping, fore-and-aft bounce which varies the motor speed. That these vehicles have little inherent damping in their suspension, and that the motor speed varies with the bounce tends to indicate similarities in the mechanism.

Lateral stability in the planing-planing mode was considerably better than in the hull displacement mode, though with the high centre of gravity the craft still tended to roll on sharp turns. Often, therefore, it was preferable to slow the craft down to negotiate turns.

12.6.3.4 Stability After Lift-Off. This was potentially the most stable condition since, like hydrofoil craft, the suspension points were now spread widely, at the corners of the craft rather than within the hull boundaries. Dynamic problems in the model were still present though these had altered a little in character. With the craft moving faster the motor and wheels were running faster and nearer to their design speeds, so that the torque was lower, enabling the craft to sit evenly on the front and rear wheels as intended. (Compare Fig.12.12 where the hull is planing and has the stern immersed, with Fig.12.20 where the hull is flying and is parallel to the water surface.) The rotation bounce around the rear axle in this situation gave way to a fore-and-aft galloping motion similar to that of earthmoving machinery described above. This could build up to a condition where the craft ended a bounce with a dive. This occurred with the first model when its flotation was removed, and with the second model, with the optimised LPW's, it was again successfully dealt with by using the plates behind the rear wheels, seen on the planing-flying model in Fig.12.20 (also in Fig.13.3).



FIGURE 12.20: THE SHORT WHEELBASE MODEL WITH BEST WHEEL DESIGN (WHEEL NO.17) IN THE PLANING-FLYING CONDITION AT ABOUT 9 m/s. NOTE THE VERY SMALL IMMERSION AND ONLY A LITTLE SPRAY; NO AIR CLEANER WAS REQUIRED AT SPEED.

A new oscillation mode began only after lift-off. The craft sometimes went into relatively rapid lateral oscillations (about 6 Hz), as first one side then the other bounced out of the water. This was also observed on the original model craft. It was noted on the second model that sometimes only the rear wheels went into these oscillations, as the light, rear part of the chassis was able to twist sufficiently to allow this to happen. The evident solution is to stiffen the chassis torsionally and to increase the craft's moment of inertia about the fore and aft axis.

This oscillation did not cause as much concern as longitudinal porpoising motions, though it did slow the craft a little.

12.6.4 Steering

Most of the steering problems associated with normal road vehicles were encountered, one way or another on the model craft during water-borne operation. Steerability varied from almost none at all to excessively sensitive steering causing the craft to spin and flip over at speed. Most of the problems were comprehensible in terms of road vehicle steering analysis, and while tests have not been carried out to specifically identify steering problems the following observations may be given:

(1) Understeering: occurred when (a) the front wheels were bouncing out of the water much of the time, and (b) the craft had wide rear wheels of high traction compared to those at the front. Since the craft had no differentials on its axles wide wheels made it difficult to turn without necessitating large changes in slip.

(2) Oversteering occurred when both: (a) the bow was well down in the water as it might be when there were high lift wheels on the back and low lift wheels on the front, and (b) the rear wheels gave more traction than the front. The classic demonstration of this case was with discs on the front, since these provided neither lift nor thrust and the craft steering was excessively sensitive as noted above (section 12.6.3.3, point (3)).

(3) With the partly flexible steering linkages on the model, steering shimmy often developed. This involved the front wheels turning rapidly from left to right at around 6 Hz. This effect was

exaggerated with wide wheels. It was successfully dealt with by adding a small oil filled damper into the steering system, much in the way it is installed in four-wheel-drive off-the-road vehicles.

(4) With high lift wheels (the optimised FB, $\phi = 60^\circ$ LPW's or wheel No 3, Table 12.22, see section 12.8 later) at high speed the craft was very "light" on its wheels and tended to slither like a car on ice. The danger was that the wheels would grip irregularly as they struck wavelets, and this caused the steering to be rather erratic so that sometimes high speed slides developed, which resulted in the craft overturning. Blades with more traction and a little less lift (developed from wheel 1.75, $\phi = 90^\circ$) gave considerably better control with an improved performance. (Wheel No.17 in Table 12.22 and Fig.12.21.)

(5) As already noted, steering in the hull displacement condition had to be undertaken cautiously since the high centre of gravity tended to roll the craft.

(6) Virtually all the model LPW's were made with a central disc which extended beyond the edges of the blades. It was believed that these discs would provide the necessary lateral resistance for steering to be accomplished. It is not clear how important these discs were nor how necessary it was to extend their edges beyond the blade tips.

It was felt that a number of the steering difficulties may have occurred because of inappropriate steering geometry. For example, since the point of support for the flying LPW craft is the point of blade entry rather than the point directly below the wheel axle some consideration needs to be given to a suitable castor angle. There is no castor angle in the model steering and this may be the cause of the shimmy noted in (3) above.

At present the steering control of the model craft could at best be described as satisfactory, but efforts have so far been concentrated elsewhere. It is clear that steering can be rapid enough to roll the craft over which is a more severe manoeuvre than would normally be required. What is needed then is a method of

better controlling this steerage capability rather than the development of a different system altogether.

12.6.5 Land Performance

Land performance was never of much concern as the capabilities of four-wheel-drive vehicles are already well understood. The LPW's used on the model were normally not robust enough for land use but the craft was run on land on several occasions and successfully driven from land to water directly into the planing-planing mode. Model cars of the same power as the model LPW craft normally have centrifugal clutches and brakes and the few runs on land with the LPW craft showed how useful these are: the land seems to have many more trees and bystanders than the model boat lake. For such reasons as these, and because runs from land to water didn't show anything that could not be ascertained from hand launches, land runs were generally avoided.

12.7 THE MODEL CRAFT AS A TESTBED FOR LPW'S

Once the model was running reliably it could be used as a testbed for the variety of promising LPW's. There are three aspects of this testbed role to be considered:

(1) Consolidating the results for the LPW's from the testing tank with performance results from the craft: Conditions of operation for the LPW in the testing tank differ considerably from those on the craft. Volpich and Bridge found differences in their results to the extent that paddlewheels giving 80% propulsive efficiency in tank tests could only be expected to give 35 - 40% overall efficiency in practice. Part of the reason for this was that in operation the wheels could not be arranged to operate at the conditions of slip (or velocity ratio) where peak efficiencies occurred. (1) It was of some importance, therefore, to identify such problems with the LPW's.

(2) The effects of different LPW's on craft performance: It was not always apparent from tank tests which wheels would propel the craft through its transition to lift-off nor which would provide good steerability, and so on. Such properties could only be found with craft tests.

1. Volpich and Bridge, Part III, P.520-523

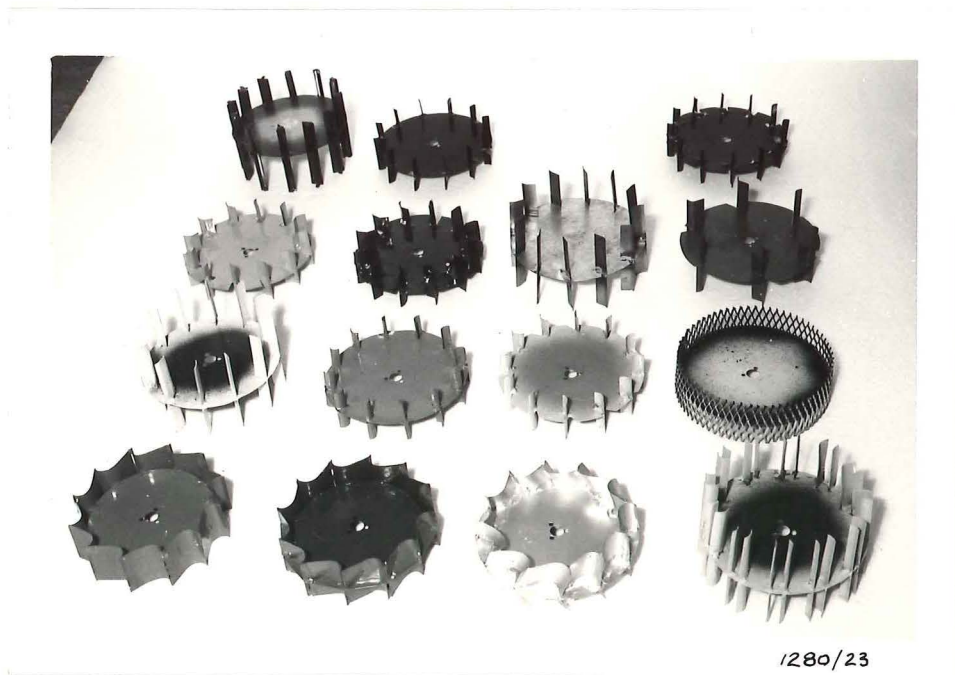
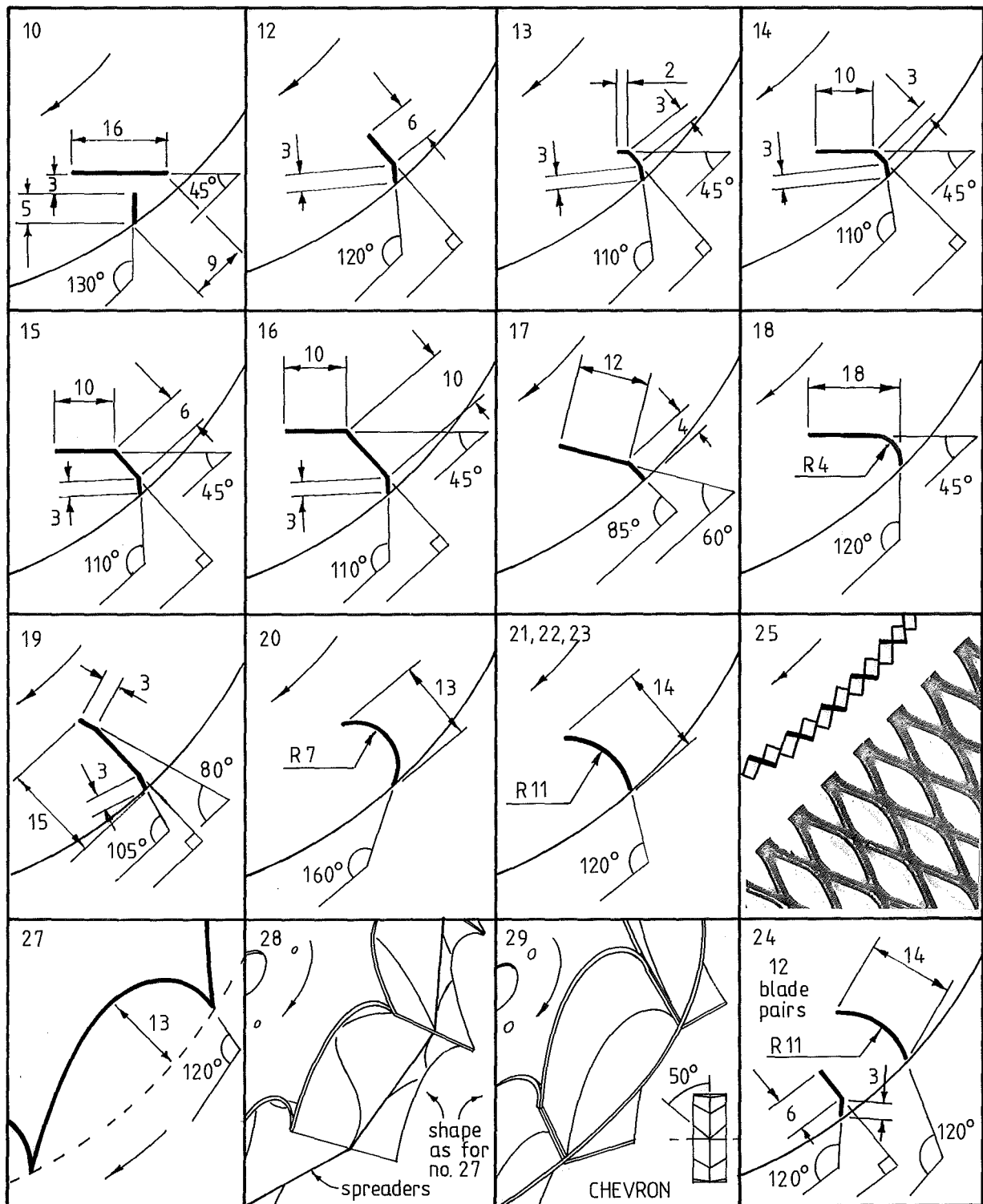


FIGURE 12.21(A): SOME OF THE WHEELS TESTED ON THE MODEL,
SET OUT IN THE ORDER SHOWN IN FIG.12.21(B)



Drawing scale 1:1 (except 28 & 29)

FIGURE 12.21 (B): DETAILS OF SHAPED BLADES FOR LPW's TESTED ON THE MODEL. NUMBERS ARE AS IN TABLE 12.22.

FIG.12.22: TEST CONDITIONS AND RESULTS FOR LPW'S TESTED ON THE MODEL

	A	B	C	D	E	F	G	H	I	J	K	PERFORMANCE					Q	
	COLOUR CODE (centre colour last)	SHAPE FB = flat blades	CHORD c (mm)	BLADE TIP ANGLE ϕ	BLADE SPAN S (mm)	NO. OF BLADES B	FULL SET OF 4, OR FRONT AND REAR	ENGINE USED (capacity cc)	CRAFT WHEELBASE, LONG OR SHORT	TANK TEST WHEEL NUMBER	TANK TEST RESULTS IN FIG. NUMBER	DISPLACEMENT OPERATION	MAINTAINED PLANNING-PLANNING WITH THROM START	ACHIEVED PLANNING- PLANNING UNASSIST- ED	ACHIEVED LIFT-OFF	STEERAGE G:Good,F:Fair P:Poor		COMMENT
1	-	FB	17	45	48	6	4	2.5		6		-	x	x	x	-	First model only see Fig.3.8	
2	-	FB	16	60	48	6	4	2.5 6.5	S	6	9.1,2&3	✓	✓	x	✓	P	First and second models. See Figs. 3.8,12.4,12.15,12.16	
3	-	FB	20	60	96	12	4	10	S	9.5		✓	✓	✓	✓	F	Designed wheels. See section 12.8, Fig.12.6	
4	Ochre	FB	16	75	48	6	4,R,F	6.5 10	S,L	6		✓	✓	x	✓	P		
5	-	FB	16	75	72	6	R	6.5	S	-		✓	-	-	-	-	No fair test. Spot welded blades came off	
6	White	FB	16	90	48	6	4,R,F	6.5	S	6		✓	✓	x	(x)	F	With these on rear & No.4 on front craft achieved lift-off, $V_o/V_c = 0.38$	
7	Yellow	FB	9	90	48	12	4,R,F	6.5	S,L	-		✓	✓	X	x	F	Used on front when testing wheel pairs, No.10,11,19,24. Figs.12.5,12.19	
8	-	FB	8	90	48	6	F	6.5	S	-						F	Front only, low lift attempt. Section 12.6.3, Fig.12.12	
9	Ochre	FB	16	105	48	6	F	6.5	S	-						G	FB, $\phi=75^\circ$ reversed. Front only.	
10	Purple Silver	2 part hybrid	15		45	96	12	R	10	S	-	-	✓Thrust & ✓Lift	-	-	-	Exces- sive Sensi- tivity	Rear only with 7 on front. Not fairly tested
11	Orange Purple	FB	16		Alternating 45, 90	96	12	R	10	S	(1)		SUBMERGE	x	x	x		Rear only with 7 on front. Fountain effect

	A	B	C	D	E	F	G	H	I	J	K	L	M	N	O	P	Q
12	Black	kinked	10	120	48	12	4	6.5 10	S,L	(1.75 $\phi=105^\circ$)		✓	✓	✓	x	F	Good propulsion - only wheels, Fig.1.3
13	D Green	kinked with heel	9	110	48	12	4	10	L	-		✓	-	✓	x	F	No.15 with much heel removed
14	D Green	"	16	110	48	12	4	10	L	-		✓	-	(✓)	x	F	Series with in- creasing centre to blade
15	Orange	"	20	110	48	12	4	10	L	-		✓	(✓)	(✓)	x	F	Little differ- ence in perform- ance between all 4
16	Purple	"	23	110	48	12	4	10	L	-		✓	✓	(✓)	x	F	
17	-	kinked	16	85	96	12	4	10	S	(1.75 $\phi=90^\circ$)		✓	✓	✓	✓	F	Best wheel design, based on 3 above. Fig.12.20
18	Green	cupped with heel	20	120	78	6	R	6.5	L	-		✓	-	x	x	-	Not fully tested
19	Yellow Purple	slightly cupped	15	105	96	12	4	10	S	-	-	✓	-	✓	x	F	High torque, good thrust. Fig. 12.19
20	Blue	cupped	13	160	48	12	4,R	6.5 10	S,L	(11)		✓	✓	✓	x	F-G	Good propulsors Fig.12.12
21	L Blue, Blue.	Shallow cupped	14	120	48	12	4,R	6.5 10	S,L	-	-	✓	✓	✓	x	F-G	
22	Silver Blue	"	14	120	48	24	4	10	L	-	-	✓	✓	✓	x	F-G	Very good propulsors
23	Gold Blue	"	14	120	96	12	4,R	10	L,S	-	-	✓	✓	✓	x	P-F	Very good propulsors. Fig. 12.5
24	Blue Purple	Shallow Cupped	14,9	105, 120	96	24	4,R	10	S	-	-	✓	-	✓	x	P	High torque wheelstands
25	Black Yellow	Mesh	3	45	48	65 or 130	4	10	L	-	-	SUB	x	x	x	-	One run with wheels in each direction.
26	"	"	"	135	48	65 or 130	4	10	L	-	-	SUB	x	x	x	-	Consistently submerged, see Fig.12.17
27	Red	Solid surface	(15)	120	48	12	4	10	L	-	-	✓ SUB	x	x	x	G	Generally poor. Tendency to submerge
28	Red Brown	" with spread- er	(15)	120	48	12	4	10	L	-	-	SUB	x	x	x	F	Barely maintained planing- displacement mode. Submerged on slowing down.
29	Silver	" chevron	(15)	120	48	12	4	10	L	-	-	SUB	x	x	x	-	

(3) Continuation of tests on new wheels: Once the tank testing programme had been completed it was not practical to set the equipment up again for further tests. Model tests, on the other hand, could be undertaken as required and such tests were useful as the impulse theory was being developed. (Table 12.22, Column J, notes which LPW's were tested only on the model.)

The criteria for assessing the performance of the LPW's on the model were simple since they depended on observers' impressions. They can be usefully classified as:

(a) Displacement stability: did the wheels tend to roll the craft over or submerge it in the displacement-displacement mode?

(b) Achieving the planing-planing mode: did the wheels enable the craft to go from a displacement-displacement condition through the hull transition to the planing-planing condition?

(c) Flying performance: did the wheels either allow the craft to fly from a high speed hand launch, or lift-off and fly from the planing-planing mode?

From these criteria it is apparent that the ideal LPW, as far as these tests were concerned, was one which allowed the craft to operate safely in the displacement mode, could transport it through the hull transition and, after planing, could lift it off completely for high speed flying operation. Clearly the form and weight of the craft hull, and the power available would have some bearing upon whether the wheels performed as required, and changes in these variables between tests had to be taken into account in assessing the various wheels.

In the earlier tests, (pre-1981) the model craft had never reached the planing-planing mode from a displacement start. These tests usually involved throw launches and neglected this second criterion, (b), altogether. Effort, therefore, was concentrated on improving the LPW's that first achieved this passage from hull displacement to hull planing, and these were "blacks" (No.12) and "blues" (No.20, see Table 12.22), which were primarily thrust wheels. Attention, therefore, focused on thrust performance with blade angles or tip angles of $\phi = 90^\circ$ to $\phi = 130^\circ$, and lift was neglected as a

factor assisting in achieving the planing-planing condition. These thrust wheels, however, never properly achieved lift-off though some impressive runs were made in the planing-planing mode (see for example Fig.1.3 which shows the "blacks" (No.12) in the planing-planing mode at the top of a bounce; this figure is therefore something of a misrepresentation as it shows the operation of a primarily thrust paddlewheel rather than a true lifting paddlewheel). Once the theory had been developed attention returned to larger span, high lift wheels and these were found to fulfil all three of the performance criteria without much trouble, providing there were enough blades of sufficient span.

In this testbed series some effort was made to test complete sets of four wheels of the same type, and while this meant a lot of time spent in construction, normally undertaken by K. Fairweather, the results of tests with all four wheels the same were clear-cut in their indications. The wheels tested in this way on the model are shown in Fig.12.21(A) and (B) and the results of the tests, based on the above criteria are given in Table 12.22.

While tests were also performed with differing pairs of wheels on the front and rear the results could not readily demonstrate the wheel capabilities, and such tests were usually undertaken to look at craft performance rather than wheel performance.

The testbed work constituted the major portion of the model tests and experience with the unique characteristics of the LPW craft grew as the work proceeded. It was not until the final test series that attention turned to the optimisation of craft water performance using the LPW's designed on the basis of the experimental and theoretical work in earlier chapters.

12.8 PERFORMANCE OF THE CRAFT WITH PURPOSE-DESIGNED LPW'S

Towards the end of the project when the theory had been developed, along with the coefficient equations, there was enough information available to attempt to design suitable flat-bladed LPW's for the model craft. This could have been done by hand using calculations like those shown in Appendix 6 but with the number of variables involved in a necessarily iterative task it was more appropriate to use a computer programme employing the theoretical

relations for lift and thrust (expressions 4.22 to 4.27) and the coefficient equations (see Table 9.46). Once written this programme was also suitable for craft of any size so that full-sized craft LPW design could also be performed. This computer programme, 'LPWCRAFT' is described more fully, along with its assumptions and limitations in the next chapter, and the listing is contained in Appendix 7.

This programme, then, was used to assist in the design of a suitable set of LPW's for the model craft. The objectives of this design process were twofold:

- (a) To produce LPW's that would enable the craft to fly well.
- (b) To assess the validity of the design procedure by comparing predicted performance with actual performance.

The wheels were chosen to match the available gear ratio and craft configuration and the resulting "optimised" LPW's and their performance is recorded as No.3 in Table 12.22. They were essentially high lift wheels with the blade angle $\phi = 60^\circ$. While only a brief set of tests have been undertaken with these wheels to date they have provided a useful reference point.

With these wheels, lift-off was readily achieved, and speed over a measured distance of 56 m averaged 5.6 m/s. Later tests using wheels with slightly concave blades (No.17 in Table 12.22) tended to confirm observers' reports that the craft was accelerating throughout the run so that a speed nearer 9 m/s is probably a more realistic indication of its final speed (see further discussion below). At these speeds the size of the lake restricted the acceleration distance so that full performance speeds were unlikely to be reached. It must also be pointed out that no effort was made to choose conditions or tune the engine for speed runs at this stage. and only five runs were made with these wheels, so better performances could well be achieved.

The predicted and actual performance figures are shown in Table 12.23 and the differences between these results provide a starting point from which the design process may be improved while at the same time giving an indication of its present accuracy.

Before discussing the implications of the results shown in the table some notes on how the data were derived are necessary.

(1) There are four sets of results. Column (a) lists the actual craft performance figures to date, as recorded and discussed in earlier sections of this chapter. Column (b) contains performance predictions using the computer programme which used theoretical models and the coefficients derived from the tank tests: no account was taken of the effects of spray. Columns (c), (d) and (e) contain a set of similarly calculated results assuming the spray has an increasing effect on craft drag (and hence thrust). Columns (f), (g) and (h) contain another set of results which assume, additionally, that the spray contributes 3N per wheel to the lift force; the wheels have therefore to lift 3N less each, though still overcoming the increased drag caused by spray.

(2) All the theoretical power results have been estimated on the basis of the Power Budget described in section 4.14, the power coefficient, C_p , described in section 9.8, expression (9.8), and an extra contribution based on the effect of diameter on propulsive efficiency as shown in section 9.4.4.

(3) The wheel speed of 25 revolutions per second was calculated from the maximum engine speed recorded during the test runs with these wheels, and all results in the table have been based on this value. (Changes in the wheel speed markedly change craft speed, power and immersion in the calculated predictions.)

(4) Actual immersion values for the model were difficult to determine since the craft was never very steady, and the wheels regularly left the water altogether (see Fig.12.20). Immersion was rarely as much as 20 mm when recorded by photographs and the video camera, so the value of 15 mm is the best that could be given.

(5) The lift from all four wheels must equal craft weight unless there is a contribution to the lift from spray as assumed in columns (f), (g) and (h) when wheel lift and spray contribution must equal craft weight.

TABLE 12.23: ACTUAL MODEL PERFORMANCE, AND PREDICTED MODEL PERFORMANCE UNDER A VARIETY OF SPRAY INFLUENCES. WHEELS USED, NO.3 AND NO.17, TABLE 12.22.

	Actual performance to date	Theoretical performance neglecting spray	Theoretical performance if spray progressively increases drag			Theoretical performance if spray reduces lift and progressively increases drag		
	a	b	c	d	e	f	g	h
POWER (W)	500 - 800W? (Fig.12.11)	518	542	566	596	432	466	470
VELOCITY (m/s)	~ 9	13.5	13.25	11.6	9.45	12.82	10.52	8.6
WHEEL REVOLUTIONS (rps)	25 max.	25	25	25	25	25	25	25
VELOCITY RATIO	0.42 - 0.75	1.12	1.11	0.97	0.79	1.07	0.88	0.72
IMMERSION (mm)	≤ 15	28.5	21	14	10	16.3	11.5	7.4
WHEEL LIFT (N per wheel)	6 - 9.81	9.81	9.81	9.81	9.81	6.81	6.81	6.81
SPRAY LIFT (N per wheel)	≤ 4	0	0	0	0	3	3	3
AIR DRAG (N)	.085 to 0.27	0.62	0.59	0.45	0.30	0.55	0.37	0.25
SPRAY DRAG (N)	?	0	0.59	1.36	2.04	0.55	1.12	1.7
TOTAL DRAG (N)	?	0.62	1.18	1.82	2.34	1.1	1.49	1.95
VELOCITY AT LIFTOFF AT 25 RPS (m/s)	2.1 ±0.15	2.44	2.44	2.45	2.45	1.93	1.93	1.94

CRAFT WEIGHT = 4 kg OR 9.81 N PER WHEEL

(6) A spray contribution to the lift of $\leq 4N$ per wheel was decided upon for column (a) after measuring the forces required to bend the side and rear plates to the extent observed in photographs. Spray lift forces may be greater than this if the spray strikes the underside of the craft rather than these plates, though this seems unlikely.

(7) Air drag throughout was based on the air drag results of brief wind tunnel tests which ascertained that craft air drag for the model may be given by:

$$\text{Drag} = 0.0034 (V_0)^2$$

where Drag = air drag in newtons

$$V_0 = \text{craft speed, m/s}$$

(Note that the drag equation in this form avoids having to assess the craft frontal area.)

(8) Spray contribution to drag has been increased progressively through each of the two sets of theoretical results examining its effects, since as yet no methods have been devised to estimate its contribution experimentally. It may, however, be imagined to be significant under some conditions when spray from the front wheels strikes the midsection plates and rear wheels.

Now the predicted performance and actual performance figures in Table 12.23 may be compared:

(1) The theoretical results in column (b), which ignore the effects of spray, differ markedly from the actual results, in terms of velocity, velocity ratio, immersion and power. It is not clear whether the model would be able to achieve speeds of 13.5 m/s. Given ideal conditions and appropriate handling of spray speeds of 11 m/s might be attainable.

(2) The theoretical results in column (e) for no spray contribution to lift and a high spray contribution to drag show a better overall agreement with the actual performance figures in column (a).

TABLE 12.24: MODEL BOAT SPECIFICATIONS AND PERFORMANCE FIGURES
COMPARED TO THE MODEL LPW CRAFT

BOAT CODE	WEIGHT (kg)	SPEED (m/s)	INSTALLED POWER (W)	ENGINE CAPACITY (cc)	HULL LENGTH (mm)	SPECIFIC POWER ($\frac{\text{HP}}{\text{ton.kts}}$)	SPEED COEFFICIENT $\frac{\text{kts}}{(\text{ton})^{1/2}}$
A	3.45	14.2	1120	7.5	900	16.03	71.2
B	3.0	12.5	560	3.5	840	11.9	64.1
C	5	15.6	1570	10	900	14.11	73.5
D	4.75	15.6	1570	10	900	14.86	74.1
E	3.75	13.3	750	6.5	760	10.54	65.7
F (Hydroplane)	9.07	18	1865	11.8	1100	8.01	76.8
G	3.5	15.1	820	6.5	780	10.89	75.5
LPW craft	4	9	700-900 (measured) 1343 (rated)	10	860	136-17.5 21.8	440

(3) Column (h), with spray affecting lift and drag, shows good overall agreement except for the calculated power, with a velocity a little lower than achieved by the model. Since it would be expected that the model would achieve higher speeds than this, the spray effects assumed in this column may be greater than those that occur in practice. This tends to be confirmed by comparisons of lift-off velocities.

(4) The design system, using the computer programme, when altered in the direction that would be expected if spray effects are significant, gives performance figures close to those observed in practice. While this tends to confirm the hypothesis regarding the effects of spray as well as helping to validate the design process these deductions have yet to be consolidated by further practical results.

(5) The results in Table 12.23 cover a range in which the actual performance is found, and indicate a possible maximum speed, should the effects of spray be removed.

Since the LPW, wheel 1.75, $\phi = 90^\circ$ was found to have superior all round performance in the testing tank tests (see section 10.6 above), a set of such wheels (No.17) was constructed for the model, with the same number of blades and span as the designed FB, $\phi = 60^\circ$ wheels above (No.3). With their small, $\phi = 90^\circ$ toes, these new wheels provided better thrust without significant loss of lift and gave the following results when tested on the model:

(1) The passage from a standing start through to lift-off was achieved effortlessly with no evidence of wheel bowsplash.

(2) Steerage was better than with wheels No.3.

(3) Acceleration was relatively rapid so that 8.63 m/s was achieved over the measured distance with the craft exhibiting lateral oscillations (discussed in section 12.6.3) and apparently still accelerating.

(4) Plates behind the rear wheels stopped longitudinal oscillations without any noticeable effect on the ability of the craft to traverse its hull transition zone.

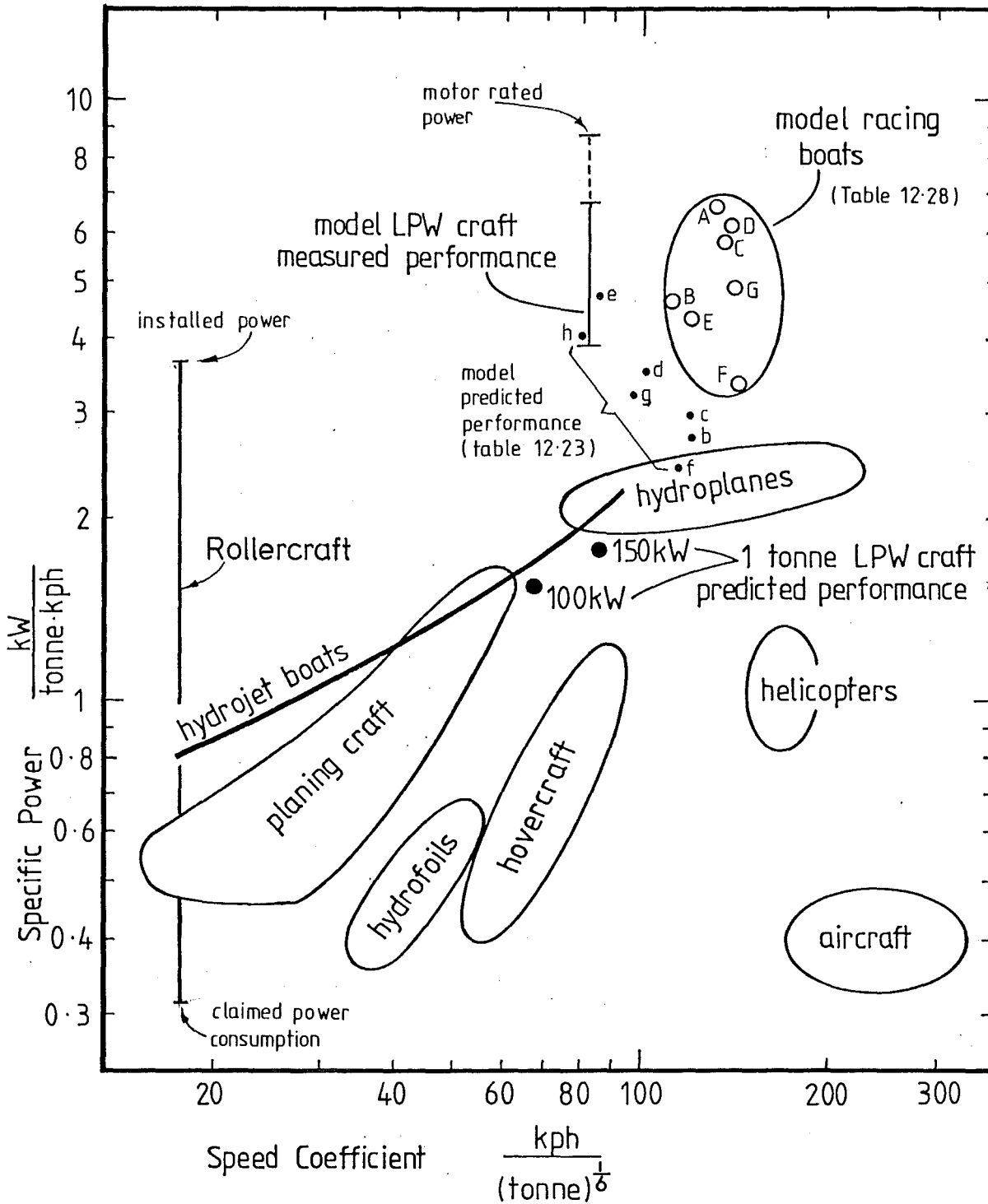


FIGURE 12-25 MODEL BOAT AND MODEL LPW CRAFT PERFORMANCES COMPARED WITH FULL SIZE CRAFT.
 (Sources: Silverleaf and Cook, Hamilton Marine)

At the time of writing these wheels were the best performers according to all the criteria for assessing them, in section 12.7 above.

The objectives of the computer aided design of the LPW's were therefore largely met. This process produced flat-bladed wheels which enabled the model to perform well, providing a reference set of results which showed up the differences between the predicted and actual performance figures. The fact that the performance was improved upon by using curved-bladed LPW's, shown to be superior in tank tests, tended to confirm the validity of the present picture of craft operation and wheel performance. As a result of these tests the design process has been given its first evaluation, and while it is clear that there are questions yet to be answered and improvements to be made, it seems to be on the path to becoming a valid predictor of the LPW craft performance.

12.9 PERFORMANCE COMPARED WITH CONVENTIONAL CRAFT

The fundamental question posed by this project (section 3.6): "How well can the LPW craft be made to run across the surface of the water on its wheels?" may be given a first tentative answer on the basis of the model performance to date. Since, at this stage, the model capabilities with appropriately designed wheels have not been thoroughly explored this will inevitably make it a conservative answer.

Comparison of the performance figures of small model craft with those of full-sized craft often prove misleading, so a survey of performance figures of model power boats with similar engine capacities to that of the LPW craft was made for the purposes of a more realistic comparison. It should be noted that these small craft are run by enthusiasts who have spent much of their spare time perfecting their boats so that the figures given would be close to optimum values for the boat types assessed.

The results of this survey are given in Table 12.24 and plotted on a commonly used plot in Fig.12.25. In this figure (12.25) the vertical scale represents an overall hydrodynamic "efficiency", relating the power required to propel a specified all-up weight at a stated speed; the lower end of the scale is more "efficient",

using less power. As can be seen the model boat results, while showing that the craft are fast for their weight, indicate that they are "inefficient" compared with their full-sized counterparts. The model LPW craft results to date are not as good as the performance figures of these models. The performance figures as calculated for Table 12.23 for the LPW craft under various conditions of spray drag have been plotted on this figure where it can be seen that some of these are close to the model's present performance while others compare well with the performance figures of the model boats. The latter, however, neglect spray effects, though they were made at the observed wheel revolutions of 25 rps. While alterations to the gear ratio, spray effects, LPW blade span and angle may improve performance, the capabilities of the present model would be expected to lie somewhere between the performance to date and the best predicted performance values, (f) and (b) in Fig.12.25 and Table 12.23.

From this it may be said that while the model LPW craft has shown itself capable of considerable speed over a water surface, it has yet to perform as well as model planing boats of similar weights and engine capacities. It could be anticipated that results near the predicted performance might be achieved with the sort of enthusiastic effort afforded by model makers.

On the other hand, the land performance of the LPW craft has always been better than that of model power boats, and it is worth noting that even with this present measured water speed of 8.63 m/s the model LPW craft exceeds the water speed capabilities of all full-sized amphibious vehicles in production other than the hovercraft.

12.10 CONCLUSION

This chapter has described work which not only puts experimental and theoretical results on a realistic footing but also covers experience that would be invaluable if the LPW was to be put to practical use in whatever context. While at the time of writing the model LPW craft water performance is only fair by comparison with other water craft its size, its present performance combined with its amphibious capability makes it unusually fast on the water for any amphibious vehicle.

CHAPTER 13

CONSIDERATIONS IN THE DESIGN OF A PROPOSED FULL-SIZED CRAFT13.1 INTRODUCTION

The project this far has produced a large data source, has derived an analytical model and has provided experience from the series of model prototype tests. The analytical description of LPW forces has been adjusted with coefficients derived from the tank test results and it has been checked against the prototype model tests. From this quantity of information it is possible to attempt the design of a full-sized prototype LPW craft. This chapter examines the design considerations for such a craft, drawing upon all aspects of the project's findings, then proceeds to work through the design calculations for a small man-carrying craft.

Since it has been found useful in practice to use the computer to perform the necessarily iterative calculations required to refine the governing dimensions of the craft the programme used is described and its limitations noted. While the predicted performance of this craft can only be given within broad limits at this stage it allows some comparison with the performances of other water craft and so permits an answer, if at this stage a tentative one, to the fundamental question of how well a man-carrying LPW craft may work on water.

13.2 GENERAL FEATURES OF LPW CRAFT OPERATION

The operation of the LPW craft is not straightforward. It involves trade-offs and balances: it requires weight for speed, it reduces drag at the expense of deeper immersion, it trades off low lift-off speed for maximum speed, and so on. This section examines these effects and why they occur in relation, specifically, to the design of the LPW craft.

13.2.1 The Craft Hull

It is necessary that the LPW craft have some form of buoyant hull to float it at low speeds. Considering first this hull it is apparent that like a boat hull it gains its support from two sources, firstly its buoyancy and secondly any lift generated from its motion through the water. For a planing hull form the buoyancy forces are

predominant at Froude Numbers, based on waterline length, below $F_R \doteq 0.75$ after which the dynamic forces provide an increasingly significant proportion of the craft support. (1) Drag forces arise from the wavemaking resistance, skin friction, and induced drag associated with the dynamic lift. Wave drag is a maximum at around $F_R = 0.68$, then falls away to be replaced by the induced drag, which depends upon the hull trim, and the skin friction which depends upon the wetted area and the square of the speed. (1) At high speeds the skin friction is the predominant drag force with air drag increasing in importance at very high speeds.

13.2.2 The Hull With LPW's

With the addition of LPW's to the hull further factors need to be considered. At low speeds the LPW's create their own wakes which complicate the wavetrain of the hull and hence the wavedrag of the craft. At higher speeds, before craft lift-off, they may make considerable spray which, as has been seen may contribute to the support of the hull and increase its drag (section 12.8 and Table 12.23). For the craft to accelerate to lift-off speeds the thrust force of the deeply immersed LPW's must overcome the hull drag, as well as overcoming any additional spray drag and wavedrag they create.

13.2.3 The Thrust to Lift Ratio

At any condition of craft speed the immersion of the LPW's is governed by the combined lift forces, namely hull buoyancy forces, hull dynamic lift forces, wheel lift forces and any spray or aerodynamic lift contributions present. With the immersion depth fixed the immersion angle of the LPW's, θ , is also fixed and this determines the relationship between the lift and thrust forces generated by the LPW's as given by the expression (4.31):

$$\frac{T}{L} = \tan (\phi - \theta) \quad (4.31), (13.1)$$

where T = thrust force (of four wheels)

L = lift force (of four wheels)

ϕ = blade angle (Fig.1.2)

θ = immersion angle (Fig.4.2)

It should be noted that while this expression was derived for the lift and thrust of a single LPW it applies just as well to the set of four LPW's on a craft, if L and T are taken as the combined lift and thrust forces for all four wheels, and θ (the immersion angle), is assumed to be the same for all four wheels.

Before lift-off the thrust, T , is equal to the craft drag plus the acceleration force, while the lift, L , is only the LPW's contribution to the craft support, not yet equalling the craft weight.

After lift-off the lift force, L , may be considered, in a first approximation, to be constant and equal to the weight of the craft. (In fact spray and aerodynamic lift may contribute to the craft support as well but these unknown contributions will be neglected at this stage.) This being the case the immersion angle, θ , is governed only by the blade angle ϕ and the thrust force T in the expression (13.1) above. If the blade angle is kept constant, as it has been on all LPW's so far, then the immersion by (13.1) is inversely proportional to the thrust force alone, which is equal to the craft drag and acceleration forces. So as the thrust increases the craft rises, and as the thrust decreases the craft is lowered.

The mechanism which controls this relationship between the thrust force, T , and the immersion is not immediately apparent in the expression (13.1) but is as follows: if the craft, moving at a steady speed, experiences an increase in the drag force it slows down and as long as the wheels continue to rotate at the same speed the velocity ratio of the wheels decreases. The LPW's therefore experience greater slip or more "skidding" than before and by the basic force equation (expressions (4.5 and (4.11)), $F = \dot{m} \Delta V$, increase the acceleration of the water they act upon. This increases both lift and thrust forces so that the thrust balances the increased drag and the lift causes the craft to rise further in the water. (This mechanism can be seen more clearly by working through the lift and thrust expressions (4.23) and (4.25)). A decrease in craft drag similarly causes the craft to sink further into the water.

This interaction between lift, thrust and immersion for the flying LPW craft is a fundamental feature of its operation.

13.2.4 Scaling With the Thrust to Lift Ratio

If, in expression (13.1) for the thrust to lift ratio, the thrust is replaced by the craft drag force at a steady speed, and the lift is replaced by the craft weight force the expression may be rewritten:

$$\frac{T}{L} = \frac{\text{Drag}}{\text{Weight force}} = \tan (\phi - \theta) \quad (13.2)$$

In scaling the LPW craft at a given fixed speed, the drag force varies approximately in proportion to the square of the scaling factor, while the weight force varies as the cube of the scaling factor. Thus for an increase in craft scale, with the expected increase in drag and weight, the thrust to lift ratio will decrease in inverse proportion to the scaling factor. This means that for no alteration of blade angle, or speed with scaling, the larger craft will have a larger immersion angle, θ , and will therefore not be lifted, proportionally, as high out of the water as its smaller counterpart.

Geometrical similarity of immersion conditions may however be obtained if the $\frac{T}{L}$ ratio can be kept constant with scaling. This is achieved if the thrust (or drag) is adjusted by changing the craft speed. Since craft drag is proportional to the square of its speed the appropriate change in craft speed will be by the square root of the scaling factor.

This is a not unexpected Froude type of relationship for scaling craft size and speed. Thus, for example, a scaled up LPW craft with a scaling factor of 5 will weigh 125 times as much as the original and will operate at immersion conditions geometrically similar to those of the original at a velocity $\sqrt{5}$ times as great as the original craft velocity.

13.2.5 The Theoretical Speed Limit

The change in immersion with the change in the LPW thrust as noted above in section 13.2.3 has obvious limits. The drag or thrust increase which causes the craft to rise in the water can go only so far before the craft lifts right out of the water. Immersion at this point is zero and so $\theta = 0$ also. This limit therefore occurs when:

$$\frac{T}{L} = \tan \phi \quad (13.3)$$

under which conditions the wheels must be turning infinitely fast to maintain the lift and thrust forces; the velocity ratio is therefore zero at this point as well. As long as the blade angle, ϕ , is less than 90° this expression allows the calculation of a theoretical maximum velocity from a drag equation such as:

$$\text{Craft Drag} = \frac{1}{2} \rho_a (V_{\max})^2 A C_D + \text{Spray Drag} \quad (13.4)$$

where ρ_a = density of air

V_{\max} = maximum velocity of craft

A = craft cross-sectional area

C_D = craft air drag coefficient.

The maximum velocity, V_{\max} , will be determined when the craft drag is equal to the thrust, T , in expression (13.3). (The lift, L , in expression (13.3), of course, will be the craft weight force, as the craft is assumed to be in the flying condition at this limiting velocity).

This maximum velocity limit may be increased by three methods:

(1) A decrease in craft spray drag or cross-sectional area allows the craft to reach a higher speed before the limiting thrust is reached.

(2) An increase in the weight of the craft increases L in expression (13.3) so that T may increase in proportion to maintain equality; thus a heavier craft could go faster.

(3) The blade angle, ϕ , may be increased in expression (13.3) so that for a given craft weight the thrust and hence the craft drag may be increased allowing a higher maximum velocity in expression (13.4).

The theoretical maximum speed for a given craft is subject to some adjustment when a practical craft is considered. A real

craft will not be able to reach the zero immersion required by relation (13.3) as it will only rise out of the water to a point where the wheels, spinning faster with decreasing immersion, absorb all the power from the motor. This will put a lower practical limit on the speed than the theoretical maximum. Another adjustment is required when it is noted that in the real case expression (13.1) contains a number of the variable functions of the coefficient equations. Rewriting (13.1) to incorporate the coefficient equations gives the following form:

$$\frac{T}{L} = C_{\beta} \tan (\phi - \theta) \quad (13.5)$$

$$\text{where } C_{\beta} = \frac{4.28 \text{ BF1T } \phi 1T}{\text{BF1L } \phi 1L} \quad \text{before cavity intrusion}$$

$$C_{\beta} = \frac{0.83 \phi 2T}{\phi 2L} \quad \text{after cavity intrusion}$$

$$C_{\beta} = \frac{5.19 \text{ BF1T } \phi 1T}{\text{BF1L } \phi 1L} \quad \begin{array}{l} \text{before cavity intrusion} \\ \text{at immersions } \leq 0.041D \end{array}$$

(Notation may be found in Table 9.46 for the variable functions shown here.)

Expression (13.3) then becomes:

$$\frac{T}{L} = C_{\beta} \tan \phi \quad (13.6)$$

which defines the conditions for maximum velocity when the force coefficients are taken into account.

One further point regarding this maximum craft speed is that if the blade angle, ϕ , is greater than 90° in (13.1) or (13.5) a velocity limit will not be reached in this way. As the thrust in (13.1) is increased the angle $\beta = (\phi - \theta)$ approaches 90° . If ϕ is greater than 90° , θ increases but approaches a limiting value greater than zero. In practical terms this would mean that the LPW craft hull would rise as speed increased, to a fixed height above the water surface where it would remain with the LPW's virtually locked into the water surface at this limiting immersion angle θ . While this seems to have an advantage over the blades which would lift the craft right out of the water it appears at present that LPW's

must have blade angles less than 90° to lift off and run at lower speeds. This property of blades with angles greater than 90° may however be incorporated into LPW's with curved blades to provide a practical solution to the speed limitation, and immersion changes with changes in drag.

13.2.6 The Craft Slowing Down

If the drag of a craft in steady motion after lift-off is suddenly decreased, the craft increases its speed, the velocity ratio $\frac{V_O}{V_t}$ of the wheels increases, and it sinks further into the water by expression (13.1). This would be the craft's response for example to a tailwind gust. A decrease in the rotational speed of the LPW's would cause a similar increase in velocity ratio $\frac{V_O}{V_t}$, and consequently a similar lowering of the craft, or increase in immersion. It is apparent then, that if the craft drag was markedly reduced, the velocity suddenly increased by running down a wave for example, or the wheels suddenly slowed, the immersion could increase so much that the hull would be let down on to the water surface. This might and might not be a useful response. On the one hand it could be likened to the "sea crash" of the hydrofoil craft (1) where the hull is suddenly and sometimes dangerously immersed at flying speeds above lift-off, and on the other hand it could be a useful way to bring a speeding craft to a relatively sudden stop.

It can be seen however from expression (13.1) that for small blade angles, ϕ , thrust may be allowed to become negative while the lift remains positive and the immersion angle, θ , stays usefully small, still holding the craft aloft. It would seem possible, therefore, that the blade angle might be arranged so that this "sea crash" behaviour could be avoided, and the craft allowed to slow down even with negative thrust from the wheels, but still with sufficient positive lift to hold it up until relatively low speeds were reached. Possibly curved blades or variable angle blades could be used to accomplish such a sedate, rather than sudden, halt if this "sea crash" behaviour proved to be a problem.

13.2.7 The Thrust to Lift Ratio at Lift-Off

It was seen in Chapter 12 that the model LPW craft achieved lift-off with the wheels in the planing mode. This being the case, there is no need to resort to descriptions of the wheel forces that

apply to its displacement and transition operation, as the impulse theory, and hence the expression (13.1), are all that is relevant at craft lift-off speeds.

At lift-off the forward speed may be such that the craft hull is in its displacement, transition or planing mode and this depends upon the conditions of drag and the blades employed on the LPW's. Whatever the hull operation condition, as the lift force generated by the LPW's increases they take more of the weight of the craft and therefore their immersion is governed increasingly by their own contribution to the craft support, over the hull buoyancy and planing forces. Lift-off may occur when the lift force from the LPW's is equal to the craft weight though this can only happen if the immersion of the wheels, at which the lift force is generated, is small enough for the hull to be clear of the water. As noted above, the immersion of the LPW's of the flying craft depends upon craft thrust and consequently its drag. The ironic implication of this is that, for LPW's with high blade angles at least, a craft requires drag (or acceleration) in order to decrease its immersion to a point where it can lift clear of the water. A craft with smaller blade angles is not so confined so that, for example, LPW's with a blade angle of $\phi = 60^\circ$ might achieve lift-off with an equal immersion angle of $\theta = 60^\circ$ with no thrust at all, as shown by expression (13.1): if this immersion (of $\frac{d}{D} = 0.25$) was sufficient to lift the craft clear of the water no thrust or drag would be necessary. Such low blade angles, however, run into the other side of the problem. In their providing small thrust forces when deeply immersed they may be unable to keep the craft moving forward at the required speeds for lift-off and they would be in danger of spinning too fast to avoid developing bowsplash, or of becoming immersed to an extent where their thrust becomes negative (see section 4.10.2). It is apparent from this, that a high drag, as might be found at a hull transition speed, may be an aid to lift-off as long as the craft can reach the required speeds without bowsplash and cavity intrusion absorbing too much of the craft power.

It is possible with light, high powered craft that lift-off may be achieved at relatively low forward speeds if the LPW's can be made to generate sufficiently large forces at small speeds of advance, in spite of the presence of cavity intrusion and bowsplash.

This, however, is unlikely to occur in practice as the high hull drag at hull transition provides a convenient boost for lift-off.

13.2.8 LPW's With Variable Blade Angles

It should be evident from the foregoing sections that the blade angle has a controlling influence on much of the LPW craft operation, so that a good case might be made for LPW's with blades whose blade angle could be varied while the craft is in motion. The blade angle might be changed in the following ways. At low speeds, before lift-off speeds were reached, the angle would be set at 90° , or greater, to provide high thrust and a high velocity ratio thus avoiding bowsplash and cavity intrusion. Once lift-off speed was reached an increase in wheel revolutions with a reduction in blade angle to $\phi = 60^\circ$ would maintain thrust while lifting the craft clear to accelerate away to higher speeds. Once high speeds were reached the spray and air drag would be such that the high thrust would lift the craft too high and out of the water with these low blade angles causing the wheels to lose traction. At this point the blade angle could be increased again, reducing the lift and allowing adequate immersion for traction, thus avoiding the speed limitation for smaller blade angles. Angles greater than 90° might be used to hold the craft down at a selected level above the water surface (see above in section 13.2.5) thus counteracting aerodynamic lift forces and preventing bouncing.

Once it was required to slow down, the blade angle could be reduced again to 60° or 45° to maintain the craft in a flying attitude while the wheels slowed allowing the craft to lose speed and sink back on to the surface when conditions were right. Alternatively if a sudden stop from the flying condition was required the wheels could be slowed with the blade angles still high, and the hull would lower on to the water at speed bringing the craft to a relatively rapid halt.

At this stage of LPW development it is difficult to envisage a fixed blade shape which could combine all these capabilities - but it is also difficult to envisage a simple sound, reliable mechanism that would alter the blade angles for 12 blades on 4 wheels as required. While a variable blade angle seems so advantageous it is probable that enough of the required properties may be combined in a fixed, shaped blade to enable a practical craft to perform well.

13.2.9 Blade Angle For a Fixed Flat-Bladed LPW

For a craft with fixed flat bladed LPW's the selection of the blade angle requires a choice between contradictory requirements. On the one hand the blade angle sets the maximum craft speed by expression (13.3) and this indicates that the larger the blade angle the greater the craft maximum speed. On the other hand large blade angles mean greater immersions at lower speeds and may not lift the craft clear of the water at the maximum speeds to which the wheels can propel the hull. (This was the case for the model craft with wheels numbered 12, 20 and 21 in Table 12.22.) While these contradictory requirements may be met to some extent by adjusting other variables such as blade span, and compromising the high speed limit the difficulties are better overcome by using shaped blades. (Wheels Number 3 in Table 12.22 were an example of this compromise in the case of the model LPW craft.) Nevertheless blade angles of $\phi = 60^\circ$ and $\phi = 75^\circ$ have been found to be the most satisfactory for flat-bladed wheels on the model craft.

13.2.10 Shaped Blades

Shaped blades can be arranged to avoid some of the difficulties encountered with flat blades. While the theory does not apply directly to such blades, deductions can be made on the basis of the experimental results in Chapter 10 which indicated ways they could be treated like flat blades. The possibilities for shaped and hybrid blades are great and while a number of innovative ideas have been suggested and tried the simplest and most promising one only will be discussed as an example. The probable functioning of the wheel 1.75, $\phi = 90^\circ$ in the data (section 10.6 or Appendix 4 and wheel No.17 in the model tests, Table 12.22 and Fig.12.21) is as follows:

It is clear that the speed limit of flat-bladed wheels with $\phi = 60^\circ$ would be increased if they had toes set at 90° as wheel 1.75, $\phi = 90^\circ$ has, since at high speeds the immersion would decrease until only the $\phi = 90^\circ$ toes were being immersed. In this condition they would generate relatively little lift so that immersion would decrease no further while traction could remain effective. These wheels would then have a higher speed limit than their parent wheels with flat blades at $\phi = 60^\circ$. A limit to this decrease in immersion could possibly be set if the toes were set at angles greater than 90° so that by (13.1) the immersion angle, θ , could not decrease

below $\theta = (\phi - 90^\circ)$. In this case they would tend to hold the craft down as speed increased, effectively preventing any theoretical speed limit.

The data for wheel 1.75, $\phi = 90^\circ$ (Figs.10.7, 8 and 9) indicate that this wheel has considerably more thrust than the flat bladed wheels, especially those with low blade angles. This suggests it would be specially suitable for propelling the craft to lift-off speed while maintaining a high velocity ratio and therefore preventing bowsplash, and cavity intrusion. The high angle at its tip stops it from producing negative thrust at deep immersions (see section 4.10.2) and its high lift, almost as great as for FB, $\phi = 60^\circ$ blades, allows it to lift the hull clear at relatively low speeds, just as high lift wheels would. Examination of Fig.10.9 indicates that as wheel revolutions are decreased with the wheel in the planing mode, lift becomes zero at the same time, or before the thrust. This suggests that a wheel with these blades would have difficulty in allowing a craft to slow gracefully from high speed without dropping the hull on to the water surface.

Shaped blades have yet to be well understood but it seems that for the above reasons, as well as the fact that the model craft performed well with them, these wheels would be a better choice for a full-sized craft design than flat-bladed wheels. There is no reason why fixed-bladed wheels with even better characteristics may be developed if required.

13.2.11 Choice of Velocity Ratio for Cruising Operation

It seems possible to arrange the velocity ratio to be at almost any value required between 0 and 1, depending upon what is considered to be the optimum value for a cruising LPW craft.

It can be seen in Fig.9.3 showing the results for the standard wheel that at low wheel revolutions the lift and thrust forces may continue to exist even at velocity ratios approaching $\frac{V_o}{V_t} = 1$. For example in Fig.9.3 at 3 rps the velocity ratio is 1.03, lift is positive for most immersions and while thrust has become negative at this velocity ratio evidence from tests at higher speeds (Appendix 4, wheel 6, $\phi = 60^\circ$, 5 m/s) suggests it may remain positive to velocity ratios as high as 0.92 for this blade angle.

At the other extreme the foregoing discussion of speed limits (section 13.2.5) has shown that as the speed increases towards the theoretical maximum the wheel revolutions increase until the velocity ratio approaches zero.

Thus by varying the LPW dimensions and craft speed a condition may be found between the extremes of velocity ratio where the LPW operates most efficiently. A number of factors may be considered in relation to choosing this velocity ratio:

(1) Section 4.14.3, while indicating that the velocity ratio should be as high as possible for theoretically high efficiencies, has noted why a practical limit below $\frac{V_o}{V_t} = 1$ would be expected.

(2) The experimental work, while generally showing propulsive efficiencies to peak around velocity ratios near $\frac{V_o}{V_t} = 0.6$ for 6-bladed wheels, was not really able to give reliable results at high velocity ratios so that it might be possible to reach such high velocity ratios as 0.92 in practical craft at high speeds.

(3) It has been noted (section 4.11.3) that the wheels should operate at a velocity ratio greater than that at which cavity intrusion or bowsplash occur, though as near to these as possible.

(4) While a certain velocity ratio may be chosen, the forces generated at the speeds involved must satisfy the thrust to lift ratio expression (13.1) and maintain the craft at a suitable height above the water surface.

These may be used, then, as the criteria for choosing a craft velocity ratio for optimum operating conditions, though this does not prevent the craft from operating at other velocity ratios at the extremes of its capabilities.

13.2.12 Span, Chord and the Number of Blades

At a velocity ratio before cavity intrusion and bowsplash occurred, where the cruising, full-sized craft would be expected to operate, the mass supply, governing the generation of the lift and thrust forces, and the power per unit force, is controlled by blade chord, number of blades and blade span (see sections 4.11.3 and 4.11.4). Since changes in span were seen to involve few other

complications and they behaved largely according to the impulse theory they will be discussed first. The effects of blade chord and the number of blades will be similar, though they involve other influences as well.

Although changes in wheel span cannot change any of the variables in the thrust to lift ratio relation (13.1), they can effect the wheel revolutions and hence the velocity ratio required to generate given lift and thrust forces. The thrust to overcome a known craft drag at a given velocity before cavity intrusion is given by a form of the thrust equation derived from expression (4.23) and (9.9):

$$T = \sin(\phi-\theta) \left(\sin\phi - \frac{V_o}{V_t} \sin(\phi-\theta) \right) \frac{\pi^2}{8} \rho c^2 s B D n^2 C_T \quad (13.7)$$

where T = thrust force
 ϕ = blade angle
 θ = immersion angle
 V_o = speed of advance
 V_t = blade tip speed = $\pi n D$
 ρ = water density
 c = blade chord
 s = blade span
 B = number of blades
 D = wheel diameter
 n = wheel revolutions per second
 C_T = a thrust force coefficient before cavity intrusion (Table 9.46)

(It should be noted that C_T is a function of n , the wheel revolutions.) For all other factors remaining constant, changes in V_t and n (which are related) may be affected by changes in c , B or s , all of which affect the mass supply to the rotor (section 4.5). A change in blade span, s , therefore, can have a small effect on the velocity ratio or wheel revolutions at a given steady speed of advance. This effect is only small because in expression (13.7) the span, s , is to the power one while the wheel revolutions, is cubed. (n is incorporated in V_t and C_T .) This small change in velocity ratio with span may result in similar small changes in the speed of advance where the optimum velocity ratio defines cruising speed.

Variation in blade span, in practice, has only a small effect on craft power; an increase in span reduces the craft power as outlined in section 4.11.4, but in the real situation the force coefficients (such as C_T in expression (13.7) above) tend to reduce this advantage to less than would be expected from the theory. (See Fig.13.8(F).)

Changes in span, however, have useful consequences at lift-off velocities. Bowsplash and cavity intrusion appear to inhibit lift-off and these effects may be avoided if the number of blades is small enough or the velocity ratio large enough. With an appropriately large blade span a high velocity ratio may be maintained thus avoiding bowsplash while the LPW's still supply sufficient lift and thrust for lift-off. This high velocity ratio might also be enhanced by blades of large chord which could have their greatest effect just before lift-off when the LPW's were deeply immersed. (See Fig. 13.8(C).)

The effects of the number of blades on propulsive efficiency were discussed in section 9.4.7 and while this suggested that 12 or 15 blades seemed to give the best peak efficiencies the model LPW craft operated with 6 and 12 blades with the 12 bladed wheels possibly performing better than those with 6 blades. Apart from these factors there is an upper limit to the number of blades which is dictated by the onset of cavity intrusion. For a craft moving at a steady speed, an increase in the number of blades causes an increase in the velocity ratio for the generation of the same forces. This would normally be an advantage as a higher velocity ratio allows a higher efficiency. As was the case for an increase in span, however, an increase in the number of blades produces only a relatively small increase in the velocity ratio because in expression (13.7) n is cubed while B is only to the first power. The limit to the number of blades arises, then, because the velocity ratio at which cavity intrusion occurs increases in direct proportion to the increase in the number of blades while the velocity ratio itself is only decreased by the cube root of the increase in the number of blades for the production of the same forces. Thus increases in the number of blades soon bring the operating conditions to a velocity ratio where cavity intrusion and bowsplash occur. This is to be avoided and a balance must be met between the number of blades and

the blade span so that cavity intrusion and bowsplash should not be encountered at the conditions of lowest velocity ratio, such as lift-off.

13.2.13 Large Spans and High Velocity Ratios

There remains some doubt as to the validity of the experimental efficiency results at high velocity ratios, because the small forces under these conditions introduced large experimental errors (see section 9.2.12). While this doubt remains it is worth examining the potential of operation at high velocity ratios.

The theory of sections 4.11.1 and 4.12 indicate that the power per unit force decreases with an increase in span and this suggests that span should be as large as possible. This requires the LPW's to become more like rollers than wheels. Such rollers would have to operate at large velocity ratios to achieve the promised power savings, and there is even the theoretical possibility of them operating with velocity ratios greater than one. The force equations for lift and thrust ((4.23) and (4.25)) both allow the forces to be positive with velocity ratios over unity, and by a simplistic deduction from the theory of efficiency in section 4.14 and Fig.1.9, efficiencies may also be greater than one. While it is clear that such effects as noted in section 4.14.3, which discussed the limits to efficiency, would prevent this, it is not yet known whether large rollers for LPW's perhaps with many blades would be able to achieve high propulsive efficiencies at high velocity ratios or whether their results would simply confirm those of the present uncertain LPW testing tank data, that peak efficiencies may be found at velocity ratios between 0.6 and 0.8.

13.2.14 Selection of Wheel Diameter

There are two ways a change in wheel diameter might be conceived:

- (1) Change in diameter with the blade span and chord remaining unchanged.
- (2) Change in diameter with proportional changes in blade dimensions: this gives a geometrically similar wheel to the original.

For a given craft travelling at a fixed speed neither type of diameter change can effect the thrust to lift ratio relationship (13.1). The only effect for such a craft in respect of this ratio is that different diameter wheels, while having the same immersion angle, θ , and immersion ratio, $\frac{d}{D}$, will dictate a different absolute immersion, d (Fig.4.5). This determines the height the flying craft would travel above the water surface and therefore may have some controlling effect on lift-off conditions, where larger wheels would be expected to hold the craft higher at lift-off and be less susceptible to immersions that would cause them to produce negative thrust with negative angle β (see section 4.10.2).

Both types of diameter change, however, cause changes in the wheel revolutions required to produce the forces, as governed by the force equations like (13.7). The first type of diameter change maintains the velocity ratio: blade tip speed, V_t remains constant but since the diameter has changed in the relation

$$V_t = \pi n D \quad (13.8)$$

the wheel revolutions, n , change in compensation. There are three sources of craft power variation for this sort of diameter change:

(1) If the diameter is small there are scale effects with diameter change as discussed in section 9.4.4, and below.

(2) If the velocity ratio is altered in the direction of cavity intrusion less power is required since more of the incoming mass is being acted upon. (See section 4.11.3 and Fig.13.8(E).)

(3) As well as (2) above there may be a practical optimum velocity ratio at which the LPW is most efficient. If a diameter change altered the velocity ratio in the direction of this optimum an improvement in power consumption would be expected.

The second type of diameter change changes the velocity ratio as well as the wheel revolutions, but only because of the changes in blade span and chord also. Variation in span and chord have already been discussed above (section 13.2.12) and the effects are little different in this case, being governed by the force equations such as (13.7). The alteration of velocity ratio caused

by this sort of diameter change would only be advantageous if it allowed the LPW to operate at a velocity ratio nearer its optimum for the chosen speed of advance, as noted in (2) and (3) above.

It was found in the tank test data that while there was the expected variation of LPW forces with different sizes of geometrically similar wheels, the efficiency and therefore power consumption improved with increase in wheel size. (See section 9.4.4, Table 9.46(B) and Fig.9.47(G).) It appeared from the data of Volpich and Bridge that this scale effect would not be found in wheels greater than 0.5 m in diameter while for wheels smaller than this, like those of the model, it had to be taken into account. Normally the wheels of a full-sized craft would be beyond this scale effect so that it need not be considered in such cases.

13.3 DESIGN UP TO LIFT-OFF

There are two major areas of craft operation to be considered in LPW craft design:

- (1) Operation before and up to lift-off when floatation, stability and thrust to overcome hull drag, are of most importance.
- (2) Operation after lift-off when all the elements of the flying condition interact.

The critical conditions for which the LPW's must be designed are those of lift-off and maximum speed, between which extremes the most economical or efficient cruise speed may be found.

The first area, operation before, and up to lift-off is considered in this section. Since this is of secondary interest compared with flying operation, many of the design points are derived directly from experience with the successful forms of the model LPW craft discussed in Chapter 12. These design considerations fall readily into three areas:

- (1) Design of the LPW's for thrust and lift up to lift-off.
- (2) Craft stability during hull borne operation.
- (3) Hull design to suit the special needs of the craft.

13.3.1 LPW Design Before Lift-Off

LPW design has to be undertaken keeping in mind the fact that unless a variable blade angle is used, the LPW must be able to operate under all craft conditions: not only must it be able to hold the craft aloft during flying operation but it must also be able to provide traction up to lift-off speeds, and hoist the hull clear of the water at lift-off speeds. The requirements of the LPW for each of these areas of operation need to be discussed; those before lift-off being noted here and the others in subsequent sections.

Before lift-off the main function of the LPW's is to provide sufficient thrust to reach speeds where lift-off can be achieved. The emphasis, then, is on traction to overcome hull drag and lift is of minor importance. The following points may be made.

(1) LPW's which caused the model to submerge in its displacement-displacement mode should be avoided (see section 12.6.3).

(2) At low speeds before lift has developed significantly LPW's will be deeply immersed.

(3) All LPW's tested provided high thrusts at deep immersions in their displacement mode of operation before transition speeds were reached. LPW's with blades at any angle will therefore propel the craft up to these speeds, and since hull drag is usually still small most wheels readily traverse this zone to begin planing operation.

(4) Once the wheels are operating in their planing mode their action can be described using the impulse theory:

(5) By the impulse theory for flat blades the requirements of deep immersion and high thrust are in opposition. The factor $\sin(\phi-\theta)$ in the thrust equation (expression (4.23)) tends towards zero as the immersion, and the immersion angle, θ , increase. (see section 4.10.2). Deep immersion, then, means low thrust, and small immersion high thrust.

(6) Because of this, it may be necessary to employ special methods to provide low speed traction. These were discussed in section 12.6.2 in regard to the model but may be listed:

- (a) Plates or foils to artificially lower the surface of the incoming flow, to decrease θ at blade entry.
- (b) Variable blade angle, ϕ .
- (c) High blade angle, ϕ (though this has disadvantages at lift-off).
- (d) Concave blades like those of wheel 1.75, $\phi = 90^\circ$.
- (e) Hybrid blades like No.10 in Table 12.22, or Fig.13.11.

(7) With wheels in the planing mode bowsplash and cavity intrusion can develop, with attendant difficulties.

(8) As craft speed increases and the hull begins to lift out as a result of its planing forces and the LPW lift, the thrust force will increase, tending to compensate for the higher drag at higher speeds.

(9) Thrust and lift both increase with increase in craft speed, as long as velocity ratio and immersion remain unchanged. In practice this factor in conjunction with (8) above means that there is a 'hump' speed where the craft drag is large in proportion to the available craft thrust; if thrust is insufficient the craft will not get past the hump speed. (See Fig.13.9(B) later.)

Assuming the craft has negotiated this difficult stage the requirements of the LPW's at lift-off may be examined.

13.3.2 LPW Design at Lift-Off

Several points may be made:

(1) Cavity intrusion should preferably not be occurring at lift-off, and calculations of wheel dimensions should be based on this.

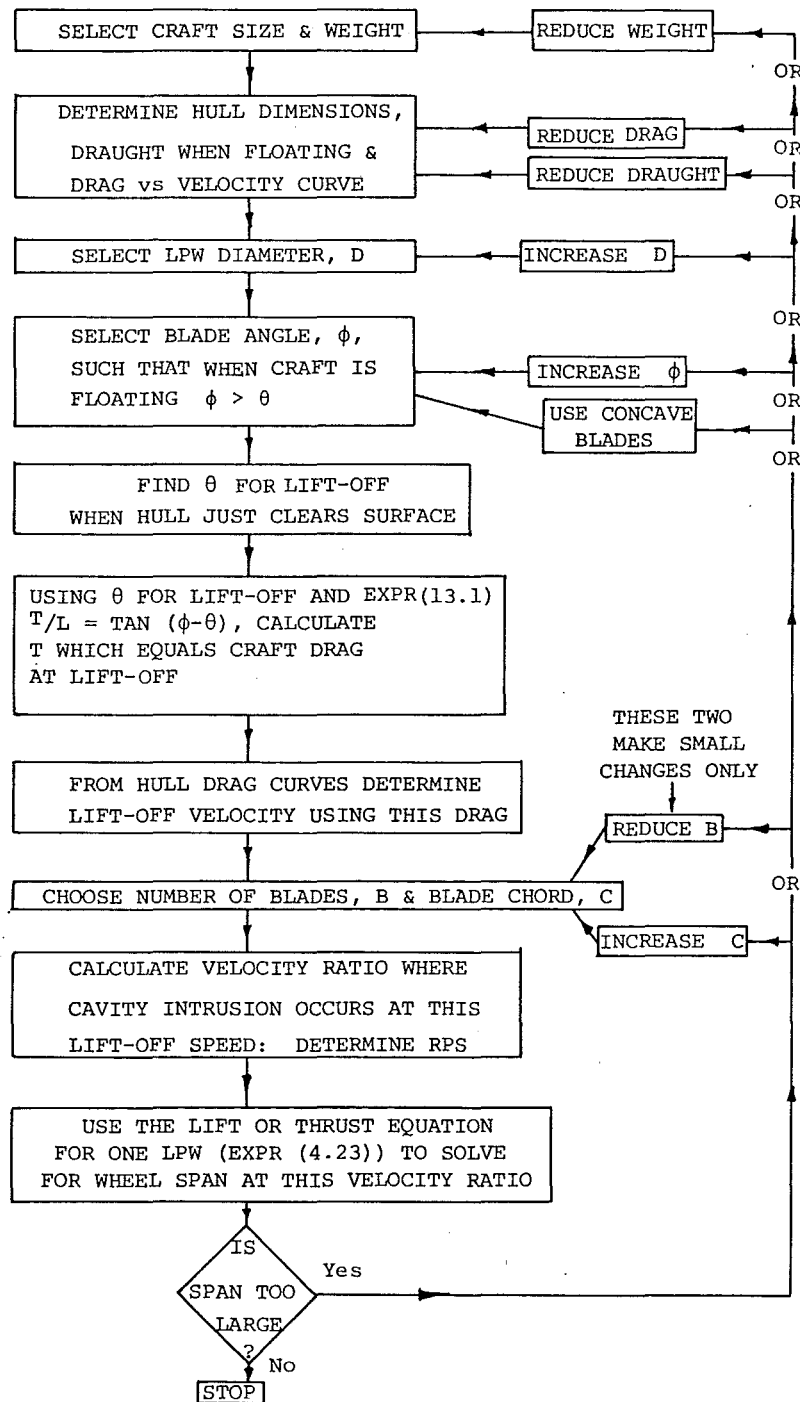


FIGURE 13.1: A SUITABLE SCHEME FOR THE DESIGN OF FLAT-BLADED LPW'S FOR LIFT-OFF.

(2) The immersion angle, θ , of the wheels where the hull just clears the water needs to be known.

(3) The conditions of hull drag, craft weight, and wheel diameter should be such that the thrust to lift ratio (expression (13.5)) can be satisfied at lift-off.

(4) While lift-off may be assumed to occur at a steady speed, the craft may also be assumed to be accelerating if the thrust force is large enough to overcome hull drag, so that the force required for accelerating the craft may be added to the craft drag in the thrust to lift expression (13.5).

(5) Immediately after lift-off the hull drag will decrease dramatically. It is probable that at first thrust will remain constant (thus holding the craft aloft by the thrust to lift ratio, expression (13.1)) accelerating the craft away to higher speeds.

A process suitable for the design of flat-bladed LPW's for lift-off conditions is shown in Fig.13.1 where it can be seen that the scheme centres around the thrust to lift ratio, and the assumption of cavity intrusion just not occurring at lift-off. It allows iterative loops to adjust the LPW dimensions if they exceed practical limits.

13.3.3 Craft Stability Up to Lift-Off

It was found necessary for the model craft to incorporate a number of features to prevent instabilities in its operation before lift-off (see section 12.6.3). Although these were important on the model largely for its stability with extreme types of wheels, they should at first be incorporated into the full-sized craft design for safety purposes until good reasons can be found for leaving them out:

(1) The position of the centre of gravity and the craft wheel base needs to be selected so that the craft sits evenly on the water at its cruising speed and cannot lift the front wheels from the water under maximum motor torque at any speed. There may, however, be some advantage in having the hull rear somewhat if it has difficulty in reaching lift-off once in its planing mode (see section 12.6.3.3 or the decrease in the hull drag at Froude Numbers greater than 1.2 for an increase in hull trim angle τ in Fig.13.4).

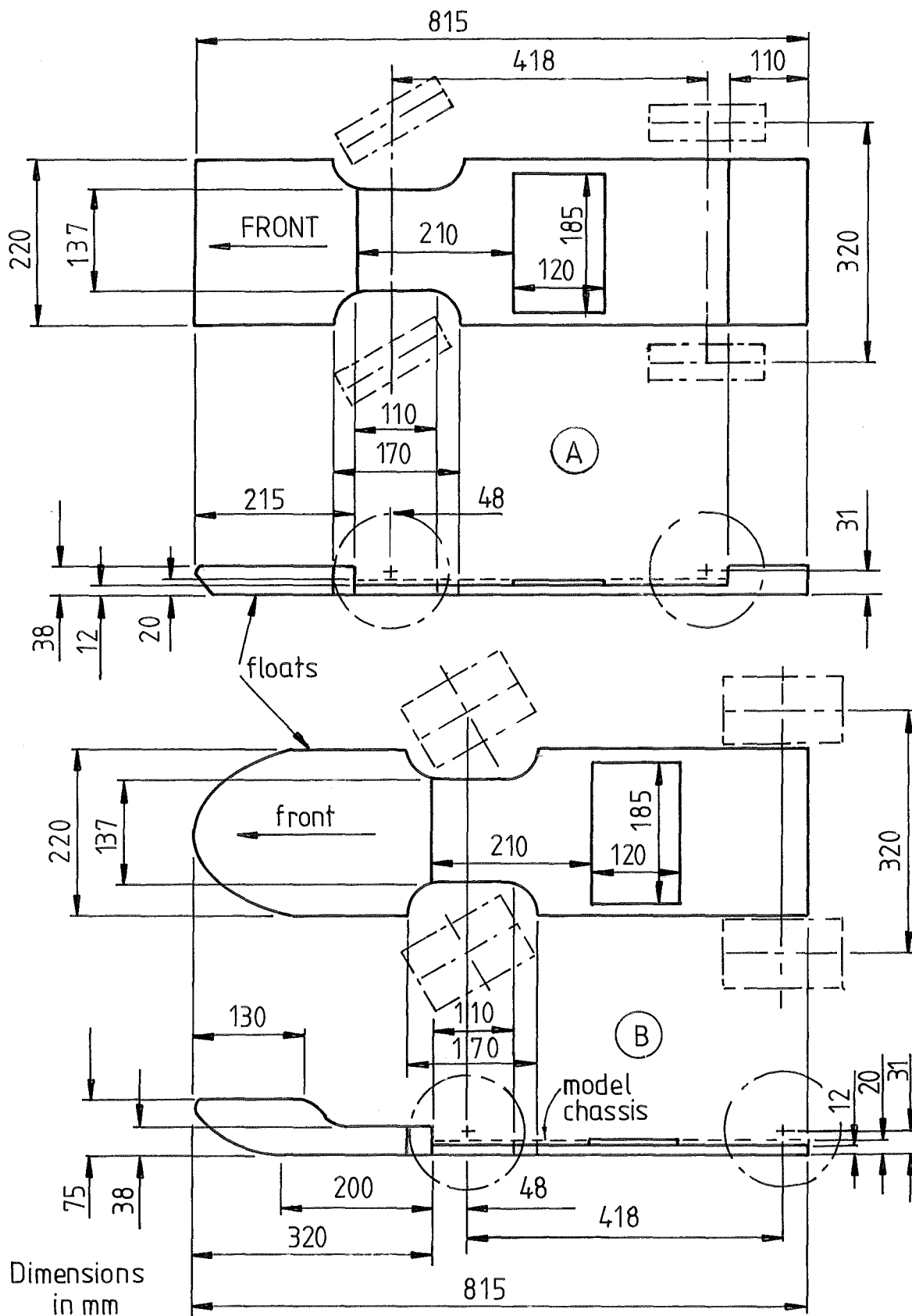


FIGURE 13-2: MODEL LPW CRAFT FLOATS; (a) WAS THE ORIGINAL AND (b) THE FINAL VERSION. THE LONG WHEELBASE MODEL USED VERSION (b) WITH AN EXTENDED STERN.

On the other hand, if the craft centre of gravity is too far forward the rear LPW's readily lift the craft stern before the front ones can lift the bow at low speeds and with the bow consequently deeply immersed it becomes difficult for high speeds to be reached. Finally, it should be noted that planing hulls alter their trim as they advance from displacement to planing type wakes and this may have some bearing on the placement of the craft longitudinal centre of gravity position.

(2) The centre of gravity should be kept as low as possible to prevent the rolling on corners experienced by the model craft in the displacement mode (section 12.63), though a judicious choice of hull may help to overcome this. A limit to the steering lock may also be necessary to avoid this.

(3) Buoyancy should be arranged so that craft floating trim is reasonable, although on the model LPW craft this seemed less important than having reserve buoyancy available above the waterline at the bow to prevent the craft nosing in, or immersing a front wheel on corners. The amount of excess buoyancy required is not clear though Fig.13.2 shows the dimensions of the model floats which were and were not adequate in this respect. It should be noted that (A) in Fig.13.2 while seeming inadequate was never tried with mid-section plates (Fig.13.3) so that its reserve buoyancy may in fact have been sufficient with these. Conservative design would choose a design based on (B) for a first full-sized craft.

(4) Mid-section plates: the dimensions of these are shown in Fig.13.3, as used on the model craft. At present little is known about the best dimensions or positions for these other than that they should be placed just behind the front LPW's as shown in Figs.13.3, 1.3 and 12.20 to redirect any spray fountain generated during low speed operation. These plates also help during high speed operation to supply lift from the front wheel spray, and to redirect water from the front wheels, which would otherwise complicate the operation of the rear wheels. While these advantages are evident they also seem to present a large surface area that would cause spray drag at speed.

(5) Plates behind the rear wheels never seemed necessary for displacement operation of the model and they even seemed to

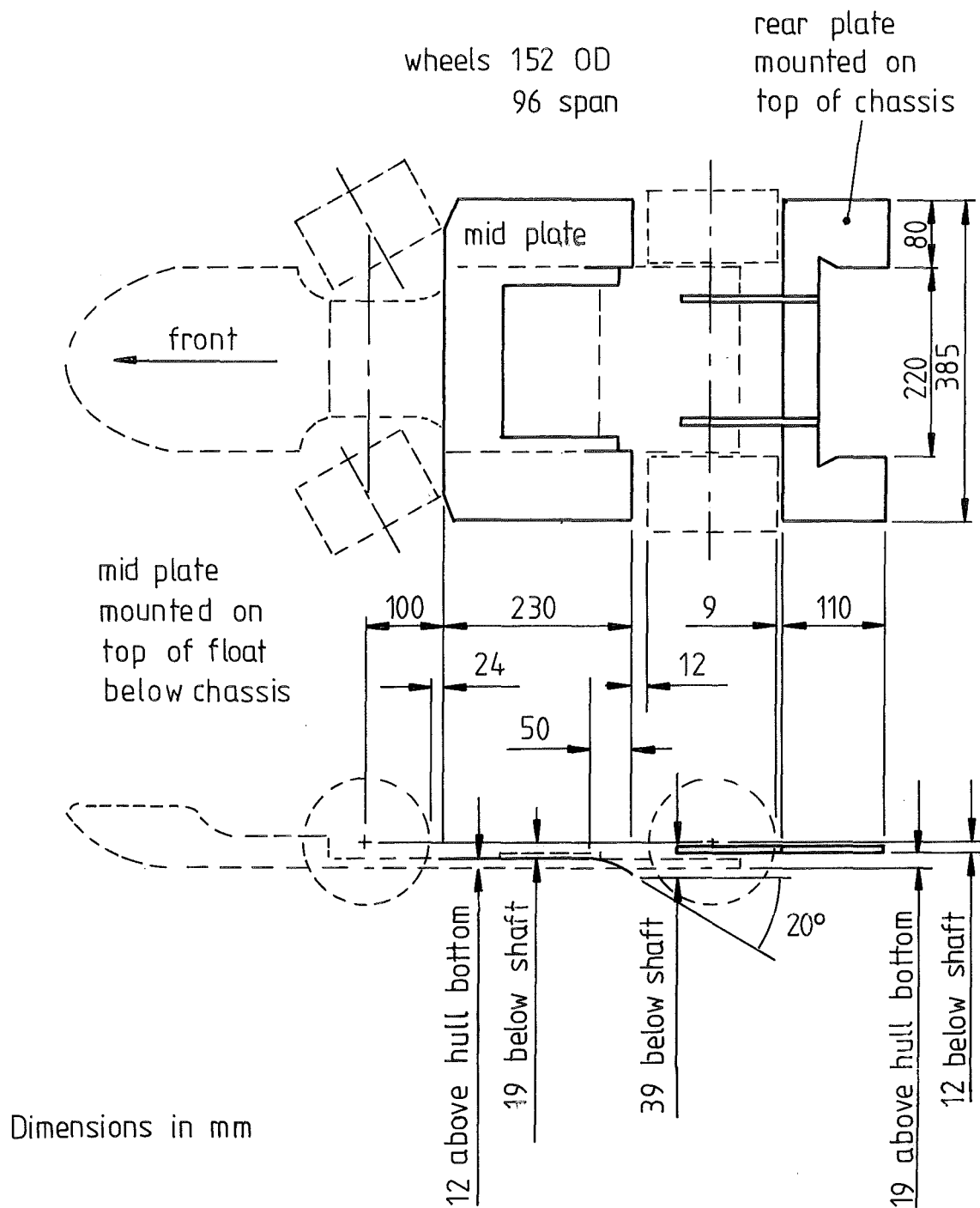


FIGURE 13-3 THE MID SECTION PLATE AND REAR PLATE AS USED ON THE MODEL LPW CRAFT (FLOAT DIMENSIONS IN FIG 13-2)

prevent lift-off on some occasions by holding the craft bow down (see section 12.6.3.3, point (4)). It is likely however that they would be an extra precaution against the fountain effect (Fig.12.17) should it occur in low speed operation, and they seem to be necessary for high speed operation to stop the craft's bouncing motion. The dimensions of those used on the model are given in Fig.13.3 and it is felt that they could be considerably smaller than this and still be effective, since their influence was always strong on the model's behaviour.

(6) Road vehicles used as prototype LPW craft would have a number of characteristics that were not present in the model craft. These could contribute to serious craft instabilities. The most notable of these are the suspension system and the presence of differentials in the transmission, neither of which were built in to the model. The effects of these systems on pre-lift-off performance and stability of the LPW craft cannot readily be foreseen and it remains for cautious prototype tests to clarify this area.

13.3.4 Hull Design

The design of the model hull was originally dictated by the twin demands of buoyancy, and providing clearance after lift-off. From the model tests a number of other requirements have come to light though to date little effort has been made to integrate them into an efficient, purpose-oriented hull. These requirements are as follows:

(1) The hull should be buoyant enough to float the craft, as well as have the reserves of buoyancy in the required places such as the bow. (See Fig.13.2(B).) It should have the capability of preventing the wheels from being readily immersed to the point where their thrust becomes negative.

(2) It should be capable of being fitted into a vehicle chassis without the loss of its integrity as a hull.

(3) It should be as close to flat-bottomed as possible (see (4) below) to allow the craft to lift it clear of the water. (This may not be completely necessary as there may be some advantage in keeping a keel or rudder in the water, this being arranged to be

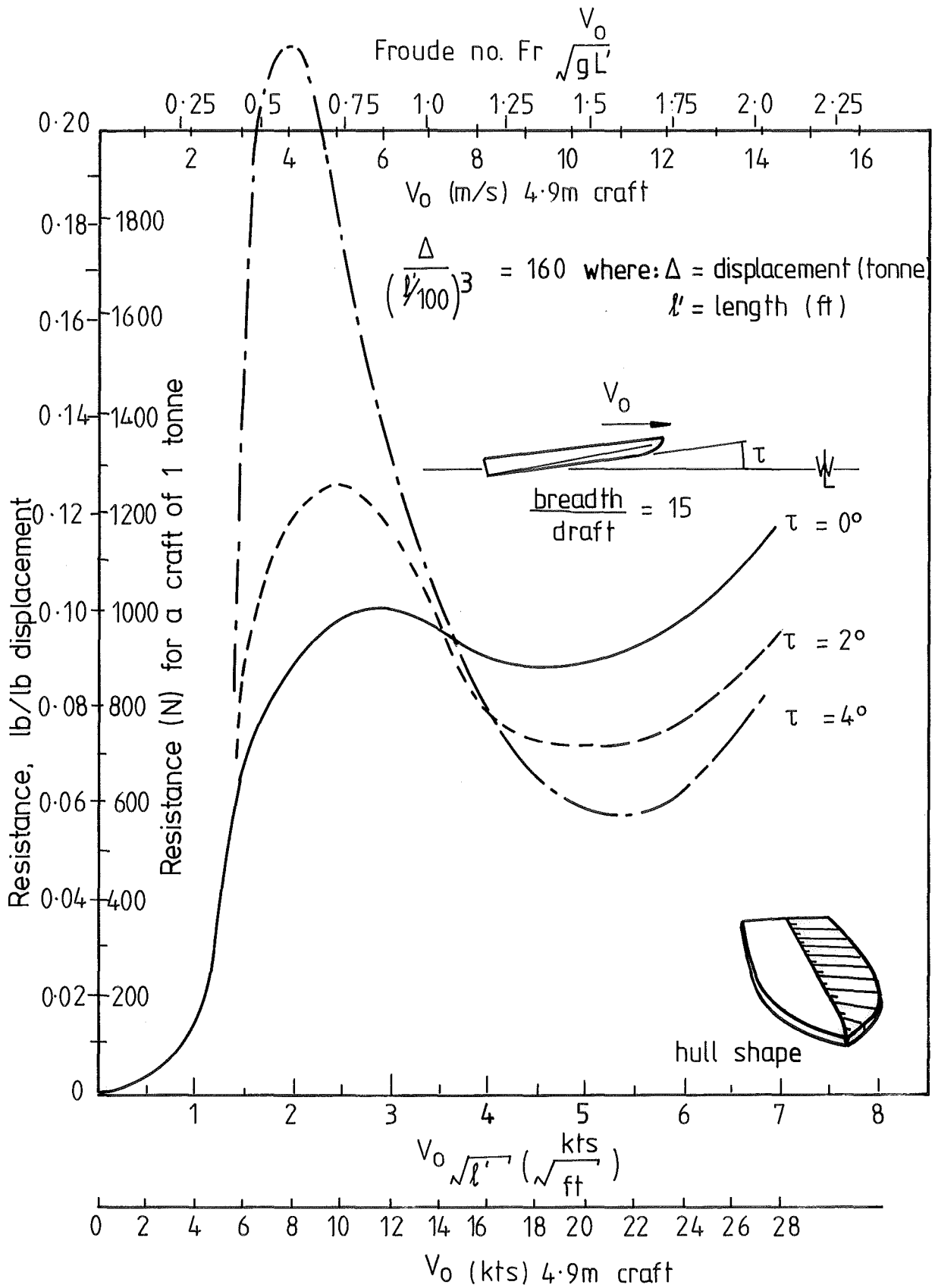


FIGURE 13.4 DRAG CURVES FOR A BROAD SHALLOW HULL
 DERIVED FROM EMB SERIES 50 1948

clear of the ground on land. This alternative, however, doesn't have the appeal of a craft which lifts its hull completely clear of the water.)

(4) The hull would probably need to be a planing design since the model craft experience showed that lift-off occurs in the craft planing mode and lift-off before these speeds is not expected to be the norm. A planing hull with a shallow V-bottom would have some stability advantages in the planing-planing mode of operation over a hull with a completely flat bottom.

(5) The hull should not roll easily at low speeds.

(6) It would be advantageous if curves of hull resistance against velocity were available, as these would assist in the lift-off calculations. This suggests hull designs from sources such as those tested in experimental towing tank series. Fig.13.4 gives resistance curves derived from the U.S. Experimental Model Basin results for V-Bottom boats, E.M.B. Series 50, 1948. These curves have been derived by the normal method of taking the resistance curves from model tests, subtracting model skin friction, determined from the model wetted area given in the tests, and a standard formula for skin friction, (1) to leave model residual drag. This residual drag has been scaled up, and the skin friction of the full-sized craft, based again on the wetted area and the standard formula, added to it. These curves apply to a hull of displacement to length ratio, $\Delta/(\lambda^3/100) = 160$, as shown in the diagram. Although the LPW craft would have such a ratio of over 200 while floating, once the wheels begin to lift, the effect would be to reduce this ratio to about 160, so that the curves shown would be relevant at craft lift-off as required. As noted earlier these curves would be expected to be affected by the presence of LPW's on the hull, but they nevertheless provide a starting point for calculations. Values on the scales have been calculated for a one tonne craft of 4.9 m length, as well as being given in their more usual dimensionless form.

(7) Hull shape, in contrast to the model hulls, would be more safely based upon craft with reasonable seakeeping qualities, such as the E.M.B. 50 shapes (Fig.13.4), though more modern tunnel hulls, flattened somewhat, may have some merits.

13.5 DESIGN FOR FLYING OPERATION

This area of the craft design assumes the craft hull to be lifted clear of the water, so that it is supported only by its wheels and is moving at a steady speed. The craft weight may be seen to be opposed by the LPW lift alone or the LPW lift along with a chosen amount of lift from spray and aerodynamic sources. Craft drag is balanced by LPW thrust. The major considerations in this area of the craft design are as follows:

- (1) Craft stability, trim and handling during flying operation.
- (2) LPW design for the conditions.
- (3) Determination of the most efficient or economical conditions of operation.
- (4) Determination of craft maximum speed and maximum power requirements.

While the first of these is treated separately in the next section, (13.5.1), the other three may be handled by a single process, described in section 13.5.2.

13.5.1 Stability Considerations for Flying Operation

This area is not well understood though a number of stability problems were brought to light by the flying operation of the model LPW craft. These were outlined earlier in sections 12.6.3.4 and 12.6.4 and may be summarised as follows:

- (1) Fore-and-aft galloping motion of the craft: this was effectively prevented by the addition of plates behind the rear wheels as can be seen in Figs.13.3 and 12.6.
- (2) A side-to-side wobble, which sometimes involved twisting of the chassis: this has not yet been dealt with on the model, though it could probably be prevented by making the chassis suitably stiff torsionally, or providing a larger moment of inertia around its fore-and-aft axis.
- (3) Lateral sliding which sometimes resulted in the model overturning at speed: this occurred when the model LPW's had flat

blades and seemed less likely to occur with the curved blades used (Number 17 in Table 12.22) since they had more immersion and provided greater traction. A second possible solution would be to extend the wheel discs beyond the blade tips to help prevent such slides, and a low centre of gravity position would make overturning less likely. This remains a potentially dangerous instability to be guarded against in any full-sized craft prototype tests, should the craft lift high in the water like the model in Fig.12.20.

(4) Steering geometry problems: apart from the simple damping of the steering system which was successful on the model, this remains an area for further investigation.

Apart from these areas of instability which showed up in the model flying operation there are a number of additional problems that may be foreseen if a standard road vehicle is adapted to use as a prototype craft:

(1) As was the case for the craft before lift-off (section 13.33 above) the vehicle suspension systems and the differentials may allow unexpected instabilities during flying operation.

(2) With a clutch, gear changes and brakes in a road vehicle the wheels can be subjected to decoupling from the engine, changes in torque, or rapid decelerations. As already noted in section 13.2.6 above, these may result in alterations to the longitudinal trim, or the hull being let down suddenly on the water surface. It is not clear how much these might be significant problems or whether they might be easily overcome.

From these comments it may be seen that the stability of any man-carrying, flying LPW craft adapted from a road vehicle, is an area which has yet to be thoroughly investigated, and care must be exercised in any prototype operation that dangerous instabilities are anticipated and avoided.

13.5.2 Design Procedure for Flying Operation

Calculation of the main LPW dimensions and operating conditions involves an iterative process. It is shown in Table 13.5 where equations are also given.

TABLE 13.5: THE LPW DESIGN PROCESS AFTER LIFT-OFF

(A) Fix craft weight; wheel diameter, D ; blade span, s ; blade chord, c ; blade angle, ϕ ; number of blades, B ; and cross-sectional area exposed to the air, A .

(B) Choose a velocity, V_o , above lift-off speed.

(C) Calculate craft drag from its air drag and spray drag.

$$4 \times \text{Thrust per LPW} = \text{Drag} = \frac{1}{2} \rho_{\text{air}} V_o^2 A C_D \quad (\text{See expr. (13.4)})$$

(D) From expression (13.5), $\frac{T}{L} = C_\beta \tan(\phi - \theta)$ determine θ and hence immersion depth, d .

(E) Using the lift or thrust equation (4.25) or (9.9) (also 13.7) solve for wheel revolutions, n , before cavity intrusion

$$\frac{\text{weight} \times g}{4} = L = \cos(\phi - \theta) (\pi n D s \sin \phi - V_o \sin(\phi - \theta)) \frac{\pi}{8} \rho c^2 s B n C_{Ll}$$

Using the lift or thrust equation after cavity intrusion, (4.27) again solve for wheel revolutions, n .

$$\frac{\text{weight} \times g}{4} = L = \cos(\phi - \theta) (\pi n D s \sin \phi - V_o \sin(\phi - \theta)) s \cdot d \cdot \rho \cdot V_o C_{2L}$$

Choose the larger of the two values for n and note whether it occurs before or after cavity intrusion. (This method avoids having to calculate cavity intrusion itself. See Appendices 5 and 6.)

Calculate the velocity ratio, $\frac{V_o}{V_t}$.

(F) Calculate the components of power in the power budget (expressions (4.43) and (9.4)). Add these to give total power, and multiply by power coefficient, C_p (expression (9.8)).

$$\text{Total input power, } P_i = C_p (P_T + P_{\text{loss}} + P_L + P_w + P_{\text{rot}})$$

$$\text{Calculate } \underline{\text{efficiency}}: \quad \eta = \frac{\text{Drag} \times V_o}{P_i}$$

The process from (C) to (F) may then be repeated for a different craft velocity, and repeated calculations of this sort build up a picture of craft performance and power consumption at the velocities of interest such as just after lift-off, cruising speed or expected maximum speed.

It may be seen that the coefficient equations have not been included in full in the expressions in Table 13.5. It is found however that the variable functions of the coefficient equations (see section 9.92) may be introduced into this scheme without altering the general procedure though it does become somewhat more complicated.

It will be seen from Table 13.5 that all the operating conditions for a given craft velocity may be calculated, and such results are underlined as they appear. By repeated use of this scheme for different LPW dimensions the three areas of design for flying operation mentioned above may be covered, namely: LPW design, determination of most efficient operating conditions and determination of craft maximum speed and power requirements.

13.6 COMPUTER PROGRAMME USED IN THIS DESIGN SCHEME

It is soon appreciated when working through the scheme shown in Table 13.5, especially if coefficients and variable functions are included, that the iterative calculation of any optimum set of conditions involves a profusion of tedious computations. For this reason the scheme of Table 13.5 was written out as a computer programme which included the variable functions and coefficient equations, and once operational, could rapidly produce sets of results from which optimum conditions and LPW dimensions could readily be determined. A full listing of this programme, 'LPWCRAFT' is contained in Appendix 7 and it will be found that the sections are labelled in the same way as the steps in the design scheme of Table 13.5. Some effort has gone into making this programme self-explanatory. An output listing from it is shown in Table 13.6 where it will be seen that each line represents results calculated at a different craft velocity (V_0). The following points may be noted:

TABLE 13.6: RESULTS FOR PROTOTYPE 1 TONNE SUZUKI 4WD VEHICLE, ASSUMING NO DRAG ADDITIONAL TO AIR DRAG.

VO	WT (KG)	X-AREA	CHORD	NO BL	ROW	ROA	DIA	SPAN	PHI	DRAGG	CONST	OPTION
2.0	1000.00	3.000	0.075	12	1000.0	1.200	0.700	0.600	60.00	0.00	0.00	1

PTOT	PLOST	PT	PROT	PWIND	PL	EFF	d/D	DEPTH (mm)	LIFT	CL	DRAG	CT	RPS	VO	VOVT	CIVOVVT	IFL
\$232637	0	11	\$180527	\$123442	993352	0.00	0.250	174	2452	0.06	1.44	0.05	106.34	2.00	0.009	0.88	2
\$184490	1	38	\$124876	2317731	568793	0.00	0.249	174	2452	0.07	3.24	0.06	60.89	3.00	0.022	0.88	2
2868603	2	92	1446996	584161	359249	0.00	0.249	174	2452	0.08	5.76	0.07	38.46	4.00	0.047	0.88	2
688826	3	180	189684	153915	230239	0.00	0.248	173	2452	0.10	9.00	0.09	24.66	5.00	0.092	0.88	2
234046	4	311	20651	34427	139644	0.00	0.247	173	2452	0.14	12.96	0.12	14.97	6.00	0.182	0.88	2
91786	4	493	1077	4458	70455	0.01	0.246	172	2452	0.24	17.64	0.21	7.57	7.00	0.420	0.88	2
52890	5	737	114	987	42230	0.01	0.244	170	2452	3.91	23.04	2.53	4.58	8.00	0.794	0.88	1
57328	9	1049	138	1238	45337	0.02	0.242	169	2452	3.38	29.16	2.19	4.94	9.00	0.828	0.88	1
61824	16	1440	164	1527	48372	0.02	0.240	168	2452	2.95	36.00	1.91	5.30	10.00	0.858	0.88	1
66398	25	1916	194	1857	51338	0.03	0.238	166	2452	2.60	43.56	1.69	5.66	11.00	0.884	0.87	1
75840	54	3163	264	2658	57059	0.04	0.234	163	2452	2.08	60.84	1.35	6.37	13.00	0.927	0.87	1
85748	105	4860	349	3670	62472	0.06	0.228	159	2452	1.71	81.00	1.10	7.10	15.00	0.961	0.86	1
96221	187	7074	450	4926	67544	0.07	0.222	155	2452	1.43	104.04	0.93	7.83	17.00	0.987	0.86	1
107325	313	9877	569	6461	72216	0.09	0.216	150	2452	1.22	129.96	0.79	8.57	19.00	1.008	0.85	1
119145	494	13335	707	8310	76438	0.11	0.208	145	2452	1.06	158.76	0.69	9.32	21.00	1.025	0.84	1
131760	746	17520	864	10514	80154	0.13	0.200	140	2452	0.94	190.44	0.61	10.08	23.00	1.038	0.83	1

THE WHEEL MAKES ITS TRANSITION TO PLANING AT 1.8m/s

FLAG MEANINGS: 1:-BEFORE, 2:-AFTER CAVITY INTRUSION, 10:-d/D<0.06 BEFORE CI.

LINE MISSED: LIFT VALUE CALCULATIONS ARE IN ERROR, (EXCEPT WHEN BLADE ANGLES > 85DEG.)

NOTATION:

CHORD	BLADE CHORD (M)	PLOST	POWER LOST IN GENERATING THRUST
CIVOVVT	VELOCITY RATIO AT CAVITY INTRUSION (CI)	PT	POWER USED IN PROPULSION=T*VO.
CL	LIFT COEFFICIENT	PROT	POWER ABSORBED IN ROTATING THE INDUCED MASS
CONST	INPUT VALUE OF CONST	PTOT	TOTAL POWER: ALL POWER COMPONENTS ADDED, AND MULTIPLIED BY THE POWER COEFFICIENT, CP.
CT	THRUST COEFFICIENT	PWIND	POWER ABSORBED IN ROTATIONAL AIR DRAG OF THE LPWS
d/D	IMMERSION RATIO: DEPTH/DIAMETER	ROA	DENSITY OF AIR: 1.2KG/M/M/M
DIA	LPW DIAMETER (M)	ROW	DENSITY OF WATER: 1000 KG/M/M/M
DRAG	CALCULATED CRAFT DRAG=THRUST	RPS	REVOLUTIONS PER SECOND OF THE LPW
DRAGG	INPUT VALUE OF (EXTRA) DRAG	SPAN	SPAN (OR LENGTH) OF THE LPW BLADES
EFF	PROPULSIVE EFFICIENCY: T*VO/POWER	VO	CRAFT SPEED IN m/s.
IFL	FLAG TO INDICATE WHETHER BEFORE OR AFTER CI (SEE ABOVE)	VOVT	VELOCITY RATIO: VO/VT, OR SPEED OF ADVANCE/RIM SPEED
LIFT	LIFT PER WHEEL (N), (ALSO A CALCULATION CHECK)	WT (KG)	CRAFT WEIGHT (KG), OR LIFT (N) FOR SINGLE WHEELS
NO BL	NUMBER OF BLADES ON THE LPW	X-AREA	CRAFT FRONTAL AREA, USED FOR AIR DRAG ESTIMATE
OPTION	THE INPUT VALUE OF OPT. (SEE THE PROGRAMME)	\$	THIS SYMBOL MEANS THE NUMBER IS GREATER THAN THE SPACE ALLOWED...OVERFLOW CONDITION.
PHI	THE BLADE ANGLE OF THE FLAT BLADED LPW		
PL	POWER USED FOR LIFT (WATTS)		

(1) Notation for the output is shown at the bottom.

(2) The LPW dimensions, craft weight, cross-sectional area and hull drag are shown first; these were read in by the programme as input conditions upon which the calculations were based.

(3) Total calculated power is shown in watts under 'PTOT'. This is the sum of all the components of power in the power budget, multiplied by the power coefficient C_p (discussed in section 9.8). The other components of the power budget are also shown.

(4) The calculations are based on the assumption that the craft has lifted off and is held at the immersion shown (under 'DEPTH') by the LPW's. This means that the wheel revolutions and the power required to generate the lift and thrust forces may, at low speeds, be well beyond the capabilities of a practical craft (see Fig.13.7 later). A real craft therefore would not be lifted off at these low speeds and higher speeds would have to be reached before lift-off could occur, when calculated power and installed power matched. This occurs for example when $V_o = 8$ m/s.

(5) To the right under 'IFL' the integer 1 means the calculations have been based on the pre-cavity intrusion theory and coefficients, while 2 indicates that the calculations used the post cavity intrusion theory and coefficients. (These were discussed in section 4.7.) The choice of which theory to use has been decided as shown in the programme scheme shown in Table 13.5 under (E).

(6) Cavity intrusion wheel revolutions has been calculated separately from the above method (as discussed in Appendix 5), and the velocity ratio at which it occurs, under the varying conditions of immersion, is recorded under 'CIVOVT'. It will be seen that the wheel velocity ratio under 'VOVT' at which the integer 'IFL' changes from 2 to 1 indicating the limit of cavity intrusion, does not exactly correspond with the cavity intrusion velocity ratio under 'CIVOUT', though the values do not differ greatly. This difference is a reflection upon the uncertainty of the force coefficients and the method used to calculate just when the conditions of cavity

intrusion will occur (discussed in sections 4.9.3 and 9.4.3.1 and Figs. 4.21, 4.23, 9.21, 9.25, 9.26). These two indicators of the onset of cavity intrusion are both printed out to show the region where it is most likely to occur.

(7) The 'LIFT' results indicate the lift force generated in newtons per wheel. This result is calculated at the end of the programme and is used as an internal check on the solution of the coefficient equations and the wheel revolutions iterations. If this value is multiplied up for four wheels, and the force does not equal the weight force of the craft, some programme error has occurred.

(8) The 'DRAG' is one quarter of the craft drag in newtons per wheel, as estimated from the air drag of the craft and any extra drag added in at the start under 'DRAGG' (in this case 'DRAGG' = 0). 'DRAG' is assumed equal to the thrust of each wheel. The use of the input 'DRAGG' allows any hull drag or spray drag to be used in the calculations by the programme under another option ('OPT' = 3).

(9) The values under 'CL' and 'CT' are the values calculated by the programme for the coefficient functions for lift and thrust respectively. As noted in section 4.8 the values of both of these before cavity intrusion (when 'IFL' = 1) may range to just over 4, while those after cavity intrusion ('IFL' = 2) range up to 0.25.

(10) The velocity ratio under 'VOVT' can be seen to rise above one. This is allowed by the present coefficient equations though it has not yet been observed (on the model craft) in practice. As noted in section 13.2.13 above, it is not clear whether such high values of velocity ratio are realistic.

(11) Propulsive efficiency values shown under 'EFF' can be seen to be low throughout this set of results. While calculated efficiencies up to 0.5 occur under some conditions the validity of these calculated results, based upon both force coefficients and the power coefficient is uncertain. Neither is this a very valuable result for a craft whose advantages lie in versatility rather than economy. It is included for interest. Its derivation was discussed in section 7.7.

(12) Under 'OPTION' the integer 1 indicates that for this output the results are for a four-wheeled craft with only air drag. Other options allow such things as calculations of the results for a single wheel, which may be used to compare the computer output with the flat-bladed data given in Appendix 4 (see Fig.9.51). The options are fully specified in the programme notation in Appendix 7.

13.6.1 Assumptions and Limitations of this Programme

This scheme and the computer programme 'LPWCRAFT' based on it both have a number of inherent limitations and assumptions. While many of these are simply the limitations of the impulse theory of Chapter 4 it is worth itemising them here in relation to this scheme. They are as follows:

(1) The forces have been assumed to have been generated impulsively at the moment of blade entry only. No consideration is given to what happens after blade entry. (See section 9.3.2.)

(2) The experimentally derived coefficients (section 9.9) have been assumed to apply only to the induced mass flow rate and treatment of them in the calculations neglects the fact that they may, in part, be associated with the velocity changes rather than the induced mass (see section 4.8).

(3) The coefficient equations and the variable functions were developed from the data of Appendix 4 centering upon the standard wheel, where they therefore apply most consistently. It is known that for extremes of chord and blade angle they do not apply so well but since these more extreme conditions are less likely to be encountered in practice they have not been further refined.

(4) The coefficient equations were primarily derived for an estimated centre of pressure position on the blade, (0.4 of the effective chord, c_{lim} , from the leading edge), but they are used in this scheme as if they applied to the blade tip. Although not examined in depth this assumption seems to be reasonable as noted in section 9.9.3 point (3).

(5) The power calculations have been based on the power budget and modified first by the power coefficient as described in

section 9.8, and then adjusted for diameter as discussed in section 9.4.4. The model craft dynamometer tests were not altogether conclusive in their attempt to determine the model craft power, which could have confirmed this way of calculating the power of the LPW craft. At this stage, then, based on the seeming accuracy of C_L and C_T , and the scatter found in Fig.9.45 for the power coefficient C_p , it may be reasonable to assume that actual power requirements would lie in the range +25% to -10% of the calculated power given by 'PTOT'.

(6) There are some discrepancies between the theoretical and actual results for the $\frac{T}{L}$ ratio, as shown in Fig.9.43. While the combination of variable functions resulting in the term 'CBTA...' in the programme (see also C_β in expression (13.5) section 13.2.5) may help to accommodate these differences, they have not yet been examined in detail; the results for the model craft, however, suggest the present approach cannot be much in error.

(7) All calculations are performed assuming the craft is moving at a steady speed.

(8) The LPW's have all been assumed to be immersed the same amount.

(9) All four LPW's have been assumed to be the same for a four-wheeled craft.

(10) The scheme does not work if the blade angle, ϕ , is greater than 90° , the coefficients were only developed for blade angles up to 90° .

(11) For blade angles between 85° and 90° all calculations assume cavity intrusion is occurring. This assumption is based on the observation that the lift force data for the blade angle $\phi = 90^\circ$ (see Appendix 4, wheel 6, $\phi = 90^\circ$) is zero or negative before cavity intrusion occurs.

(12) As noted above (section 13.6, point (6)) the cavity intrusion calculations are of limited accuracy, though the range of velocity ratios where it occurs may be judged from the two estimates given in the output in Table 13.6.

(13) As noted above (section 13.6, point (10)) there are uncertainties as to whether the velocity ratio can in fact be greater than one.

(14) Calculations for velocities greater than 5 m/s involve extrapolation from the experimental results.

(15) Similarly, calculations for wheel diameters greater than 0.38 m involve extrapolations.

(16) While the scheme is valid only for flat-bladed LPW's it may be used to estimate conditions for curved-bladed LPW's using the findings of Chapter 10, (section 10.4).

(17) Spray drag and hull drag, while unknown may be assumed, and read into the programme under 'DRAGG'. (This was performed for results in Table 12.23:)

(18) Similarly augmentation of the lift force by spray may be read into the programme by reducing the craft weight by the appropriate amount.

In spite of these limitations and assumptions the programme has been tested against the model LPW craft performance as discussed in section 12.8 and Table 12.23 where its results showed it to be a fair predictor of craft performance.

13.6.2 Design Optimisation Using This Programme

In the design of the LPW craft for flying operation there arise a number of factors which have to be traded off against one another. For this reason it is helpful to make repeated use of the programme 'LPWCRAFT' discussed above, for a variety of craft and LPW dimensions to discover the most acceptable craft parameters. In general the areas of interest will be:

- (1) Lift-off speed and power requirements.
- (2) Maximum speed and power requirements.
- (3) Speed for most economical operation in the flying condition, or minimum power operation.
- (4) Practical dimensional limitations to the LPW's.

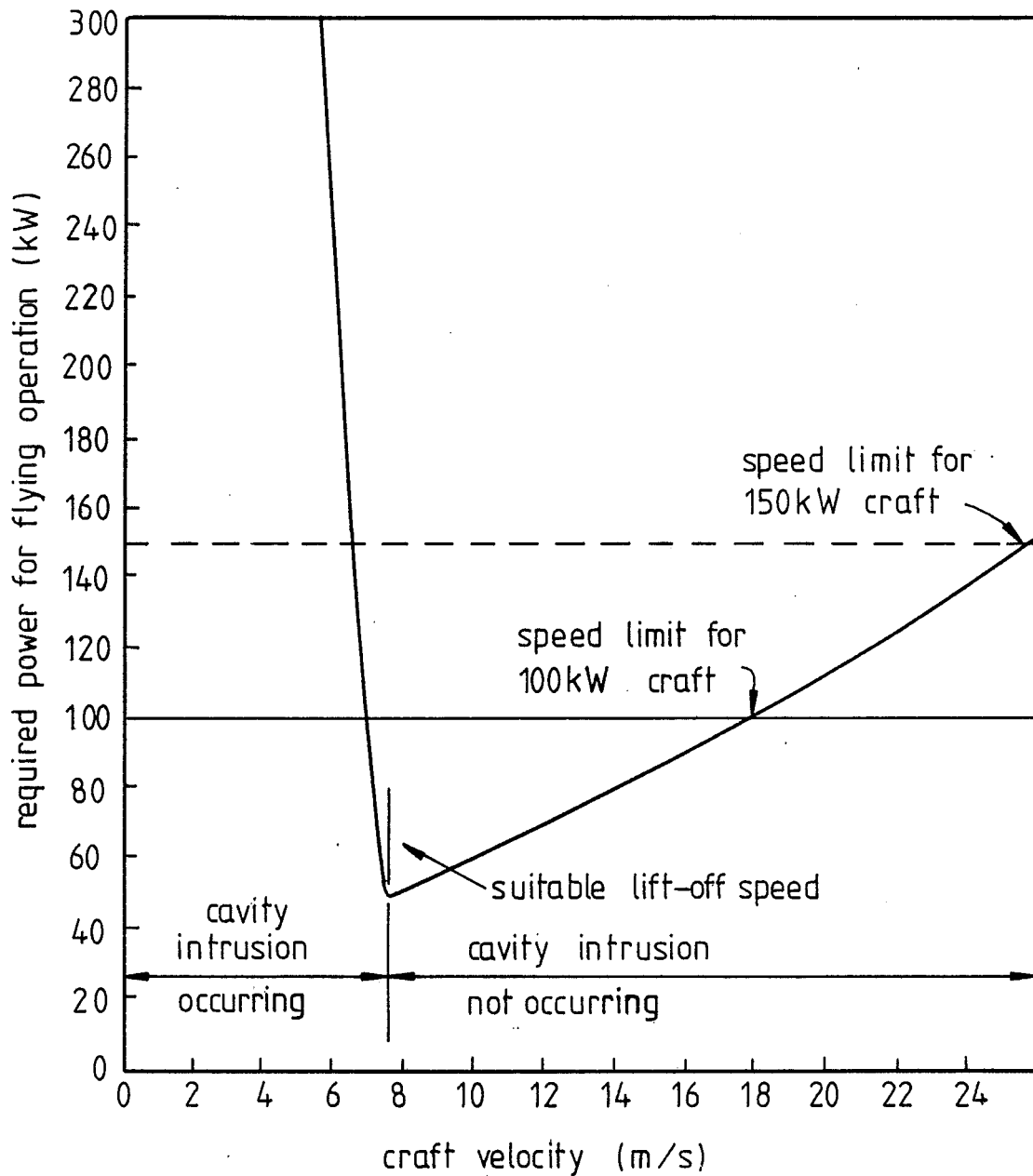


FIGURE 13.7: THE 1 TONNE CRAFT POWER vs SPEED CURVE ASSUMING AIR DRAG ONLY AND IGNORING HULL CLEARANCE CONSIDERATIONS. (DERIVED FROM TABLE 13.6)

These areas of interest are found to most often involve craft power and speed so that plots of these two conditions provide most of the necessary information. For example the power results under 'PTOT' of Table 13.6 above have been plotted against craft speed in Fig.13.7. The most dramatic feature of this plot is the change in the power curve at the onset of cavity intrusion. The very high power at low speeds does not indicate that the craft cannot operate below 7 m/s, but simply that it cannot operate in the flying condition below this speed. The horizontal line drawn through the plot at 100 kW represents the available craft power output. The intersection of this line with the power curve gives the minimum possible lift-off speed as being about 7 m/s with cavity intrusion occurring, and a maximum craft speed of 17.8 m/s. It is clear that for lift-off without cavity intrusion occurring craft speed would need to be about 7.5 m/s.

This curve also indicates that the most economical speed of operation for a flying craft is going to be just before cavity intrusion starts, right after lift-off. (That is, of course, if the hull is clear of the water at this speed.)

This power curve will vary in position and shape with changes in the LPW dimensions and craft conditions, and to illustrate how each variable alters the curve, Fig.13.8 (A) to (G) has been prepared. In each of the plots shown the curve of Fig.13.7 above has been reproduced for reference as the heavy solid line; the craft power limit of 100 kW has also been retained. Each of the other curves in each plot represents the power curve for a different value of the variable specified, while all other conditions remain constant. The following points are worthy of note:

(1) There are three ways in which the power curves may be altered:

- (a) Changes in lift-off speed and cavity intrusion.
- (b) Changes in maximum speed.
- (c) Changes in minimum power.

While some variables trade these changes off against each other, others alter one at a time. The appropriate choice of dimensional

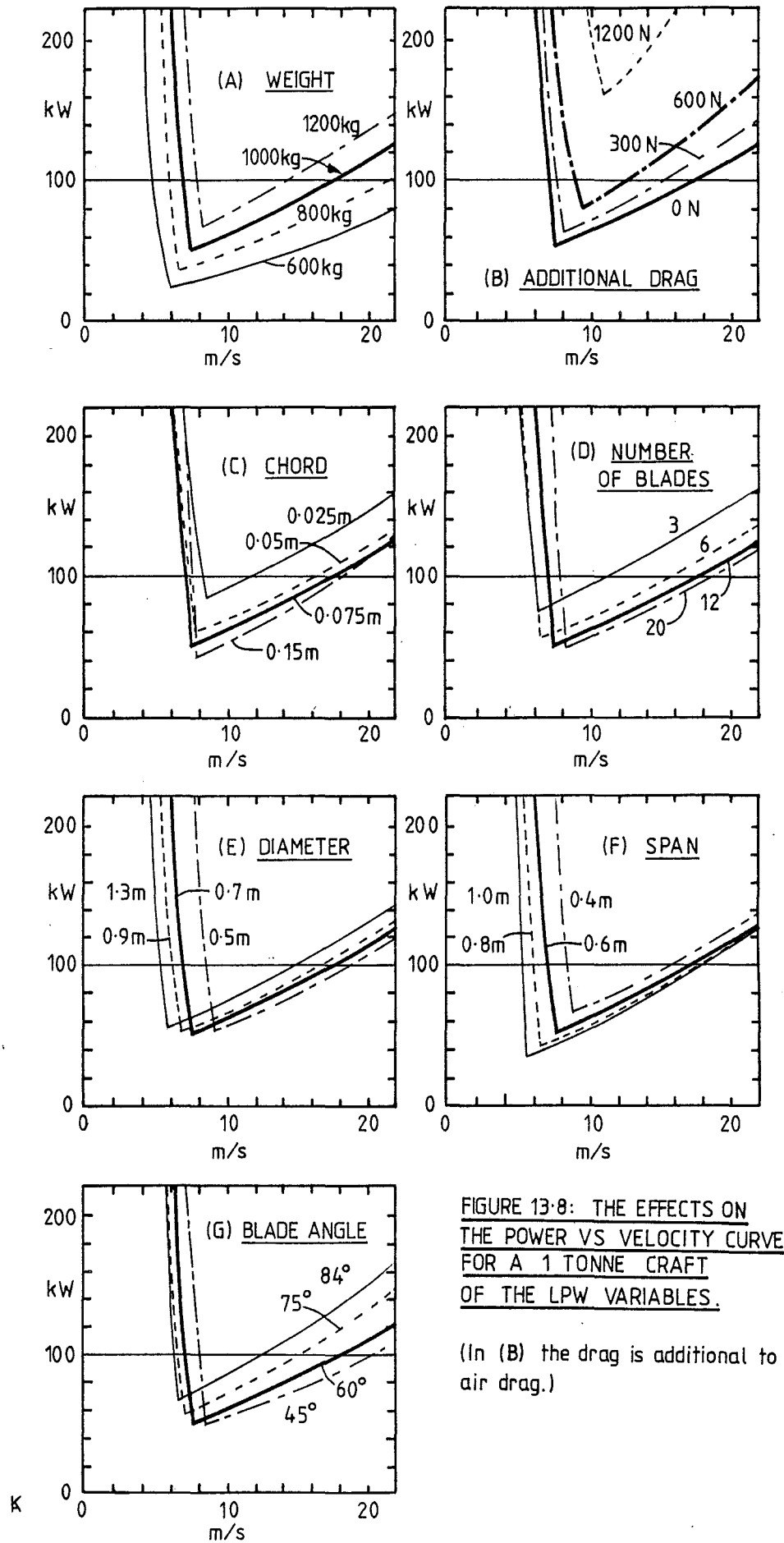


FIGURE 13.8: THE EFFECTS ON THE POWER VS VELOCITY CURVE FOR A 1 TONNE CRAFT OF THE LPW VARIABLES.

(In (B) the drag is additional to air drag.)

changes can improve the craft power consumption and speed characteristics.

(2) Craft weight has the greatest overall influence upon the power requirements. Weight saving is clearly advantageous; this is a reflection on the large component of power consumed in lift as indicated under 'PL' in Table 13.6.

(3) It is clear from point (2) above that spray augmentation of lift can help significantly in reducing craft power requirements - or in reducing lift-off speed and increasing maximum speed. For a practical 1 tonne craft this has been estimated as up to 100 kg at lift-off.

(4) Span variation, Fig.13.8(F), is notable for its large effect on lift-off speed and minimum power. These results, including of course the experimental coefficients C_L and C_T , are essentially consistent with the findings in the theory of Chapter 4 (see section 4.12).

(5) Evidence of the maximum speed limit (discussed in section 13.2.5) may be seen in Fig.13.8(B) where the curve of greatest drag at high speed rises steeply. It will reach some limiting value well beyond the craft speed capabilities in this case. For calculations relating to the model LPW craft, which was proportionally lighter, this maximum speed limit was much more in evidence.

(6) Fig.13.8(C) shows the effect of increased wheel windage losses, since at higher speeds the power curve for the largest chord (0.15 m) rises more steeply than the rest.

(7) The effect of decrease in diameter (Fig.13.(E)) is essentially to shift the curve to the right. Thus higher speeds may be achieved by smaller diameter wheels, at the expense of higher lift-off speeds. This result seems confusing since it is not immediately obvious why at a given velocity, say 12 m/s in Fig.13.8 (E), a smaller wheel should use less power than a larger one for the same size of craft. The explanation for this, is that the smaller wheel, rotating faster to provide the same forces, is operating nearer cavity intrusion than the larger wheel; this is also clear from the plot. But section 4.11.3 noted that the nearer a wheel

operated to the onset of cavity intrusion, the greater the induced mass flow rate per blade (\dot{m} in expression (4.16), section 4.5) and hence the lower the power required for lift, and lost to the wake for thrust as P_{lost} (Table 13.6 or section 9.8). Thus at 12 m/s in the figure the smaller wheel is operating more efficiently. For a given number of blades and a given power, then, a smaller diameter wheel will have a speed advantage over a larger diameter wheel. So for a small diameter wheel, if lift-off can be achieved, both cruising speed at minimum power, and maximum speed are higher than for those of a larger wheel; on the other hand a larger wheel may achieve lift-off at lower speeds. (Wheel diameter was further discussed in sections 9.4.4 and 9.92.)

Repeated use of the programme 'LPWCRAFT' and plots such as those of Fig.13.8 allow an iterative approach to an optimum design for a craft, and its LPW's. It should be pointed out however that the programme output (as shown in Table 13.6) also shows conditions other than the speed and power plotted in Figs.13.7 and 13.8. For example immersion and wheel revolutions are also given. From these the hull clearance and transmission ratios may be determined, and practical considerations such as a requirement for greater hull clearance may also be essential considerations in what will be an optimum design. The plots of Fig.13.8 do not show such things, and further plots may be required.

Of special note is the fact that the velocity ratio as calculated sometimes rises above one. This has already been discussed (section 13.2.13, 13.6, point (6) and 13.6.1, point (12)) and in practice it may be found that practical power requirements and wheel revolutions are greater than calculated under such circumstances. If this was the case the curves of Figs.13.7 and 13.8 would need to be altered.

13.6.3 Operational Power Curves and Flying Conditions

The use of the programme 'LPWCRAFT' and the results of Table 13.6 and Figs.13.7 and 13.8 have all assumed a constant speed, constant additional drag (under 'DRAGG') and a flying craft throughout the calculations. In the real case the drag would be different at each craft speed, depending on spray, and acceleration forces would be present. Lift augmentation would vary with the amount of

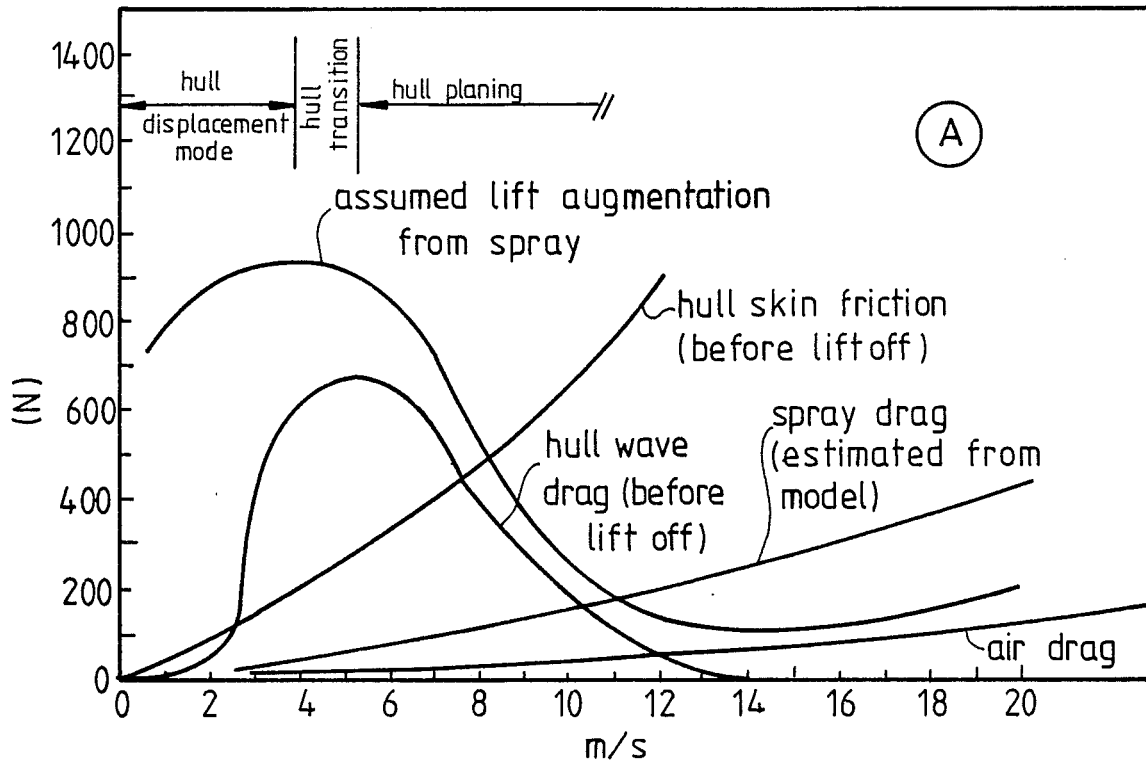
spray thrown up - it would be greater at lift-off than at high speed (compare Fig. 12.16 with 12.20).

Before lift-off, with the wheels in their planing mode the craft hull would provide drag approximately as shown above in Fig. 13.4, until lift-off was achieved. After lift-off the craft would accelerate rapidly possibly with the hull just skimming the water until the acceleration forces, spray drag and air drag could oppose the thrust sufficiently for the thrust to be great enough to decrease the immersion, lifting the hull well above the water (see section 13.2.7). Based on the experience with the model, the results of Table 12.23 and the sequence of events just described, it is possible to estimate the craft drag forces, and lift augmentation at each velocity over the expected range of craft velocities. These estimates are shown in Fig.13.9. As already noted, spray forces have not been measured, so that the spray drag and lift augmentation estimates are not at all conclusive; such estimates, however, allow a more realistic craft power curve to be produced than that on Fig.13.7.

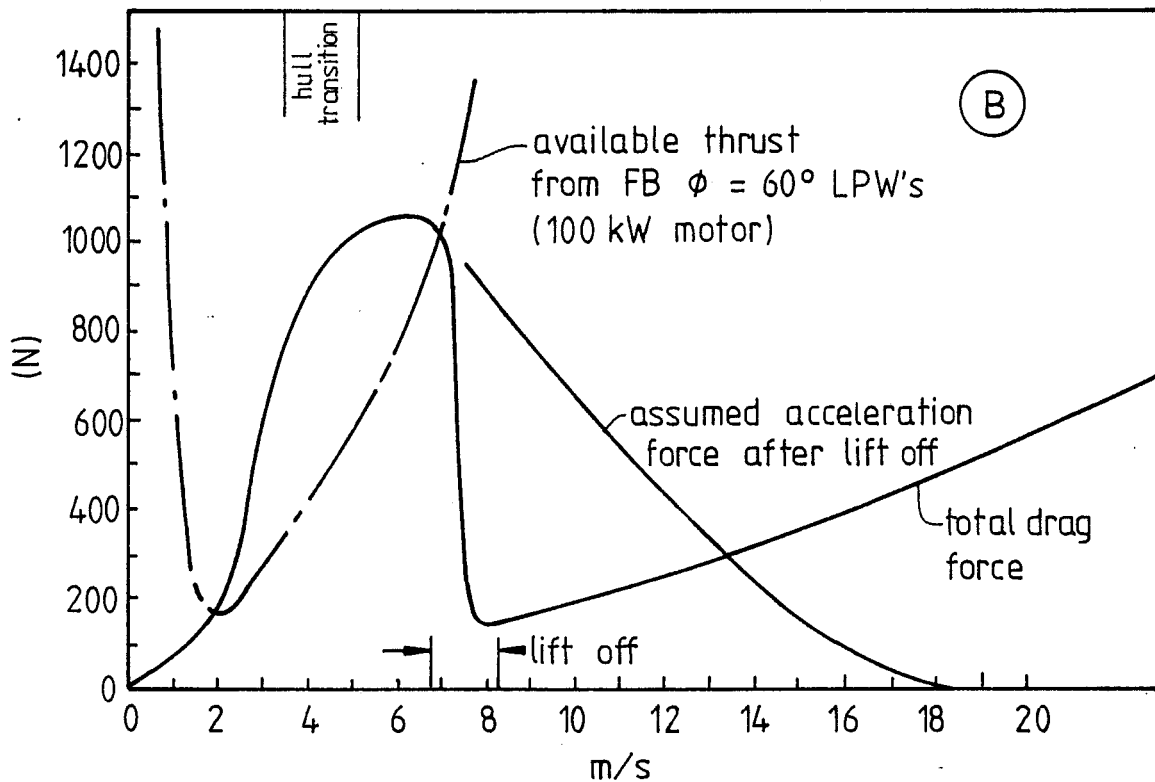
The programme 'LPWCRAFT' can be used to calculate the craft power for such varying conditions of lift and thrust, when it is run successively with the input conditions changed for each run. Each run produces a set of results calculated at a range of velocities like those of Table 13.6. The input conditions of drag and lift augmentation can then be matched with the calculations at the velocity to which they apply. Thus a series of computer runs can be used to compile a more realistic set of results than those of Fig.13.7 and Table 13.6. Such results are shown in Fig.13.9 and 13.10. Several points may be made:

(1) As designed, a 1 tonne craft will not be able to overcome its drag between 2 and 7 m/s, Fig.13.9(B). This sort of difficulty was experienced by the model craft (section 12.6.2). As was the case with the model this drag hump would probably be overcome if concave blades were to be used as intended.

(2) Also shown in Fig.13.10(A) is the immersion of the wheels. This will be seen to be little less than the maximum allowed immersion of 140 mm. (Greater immersion is prevented by the hull floatation.) Hull clearance above the water is never

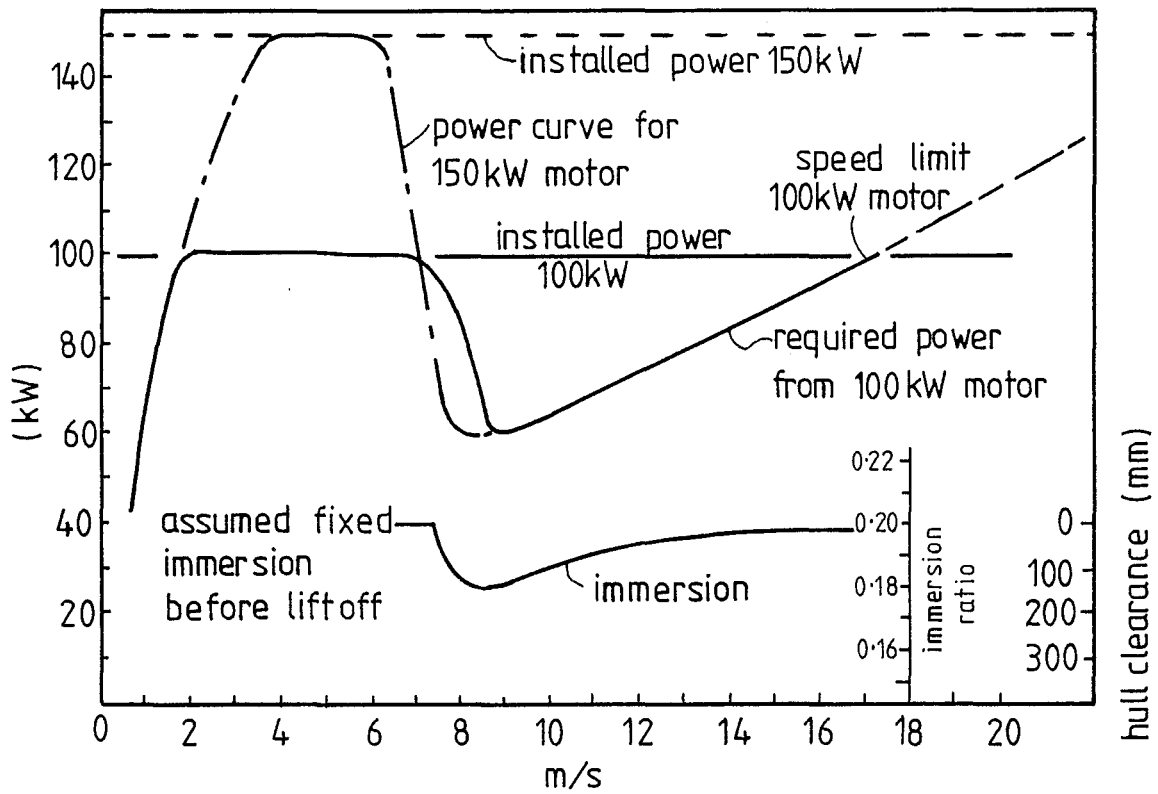


(a) COMPONENTS OF HULL DRAG & LIFT AUGUMENTATION vs CRAFT SPEED

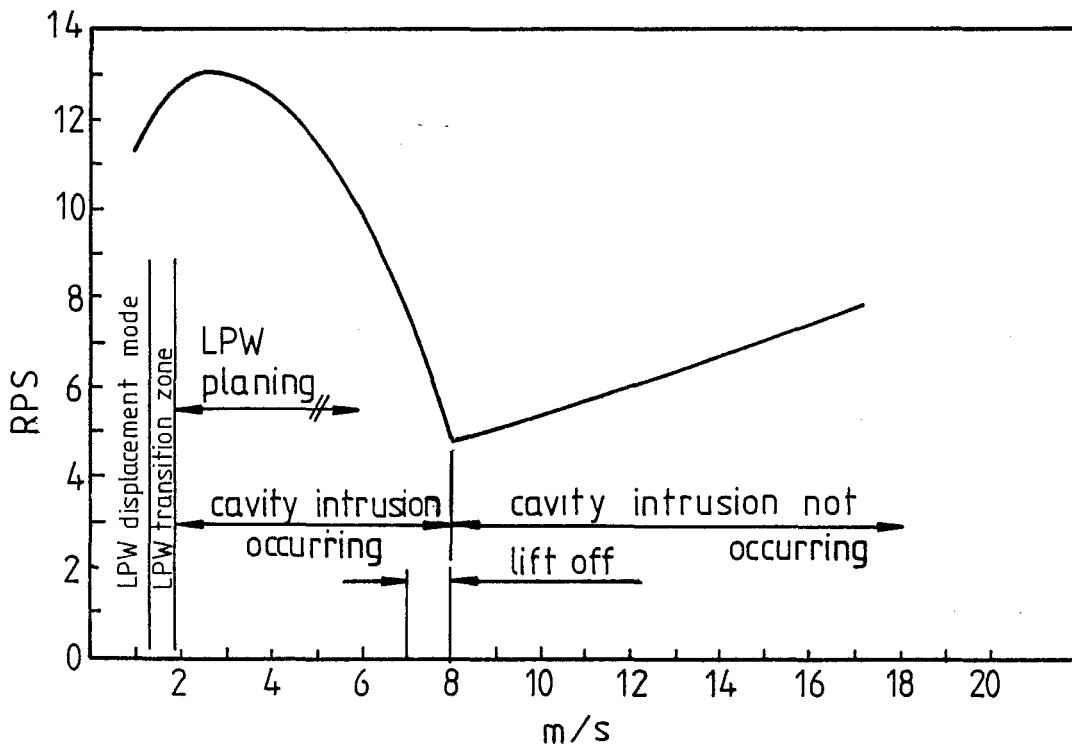


(b) TOTAL DRAG, ACCELERATION AND THRUST FORCES PRESENT

FIGURE 13.9 ESTIMATED OPERATING THRUST AND DRAG CONDITIONS FOR THE PROTOTYPE CRAFT.



(a) CALCULATED POWER & IMMERSION AGAINST CRAFT SPEED



(b) CALCULATED WHEEL REVOLUTIONS & WAKE CONDITIONS

FIGURE 13.10 CALCULATED OPERATING CONDITIONS FOR PROTOTYPE CRAFT DERIVED FROM PROGRAMME 'LPWCRAFT'

greater than 15 mm. This would hardly look like the flying condition for a 4.9 m craft, and would probably make it susceptible to porpoising instabilities as described in point (c), section 12.6.3.3. The model craft readily demonstrated much greater hull clearances (smaller wheel immersions) than this (see Table 12.23 and Fig.12.20). The reason for this small hull clearance (large immersion and large immersion angle, θ) for this full-sized craft lies in its small thrust to lift ratio (expression (13.1)) compared with that of the model, since the full-sized craft is proportionally much heavier than the model for its size (see Table 13.12 ahead). This weight is in excess of the scaled up weight of the model craft.

Since the craft as designed has a reasonable power to weight ratio when compared to other craft it would be of some value to design wheels which could hold the hull higher out of the water, thus avoiding the problems of a skimming hull. Little development along these lines has been undertaken since the model craft demonstrated adequate lift for its relatively light weight. At this stage, then, some suggestions to cope with this difficulty can be offered:

(a) If the blade angle, ϕ , is decreased the craft will sit higher in the water by expression (13.1) above. A small blade angle, however, presents difficulties at lower speeds and larger immersions where β ($=\phi-\theta$) can become negative, producing negative thrust, (see section 4.10.2).

(b) Variable blade angle, as discussed above in section 13.2.8 could overcome this difficulty.

(c) Hybrid wheels like those tried (superficially) on the model (number 10 in Fig.12.21 and Table 12.22) or like those of Fig.13.11 might be used. The purpose of such wheels would be to provide concave surfaces and high blade angles which produce large thrust forces, at the low velocity ratios (high wheel revolutions) which occur before lift-off, when large thrust forces are required. Then, after lift-off, they would present low blade angle surfaces which provide large lift forces at the high velocity ratios which occur after lift-off, when more lift than thrust is needed. The full potential of such wheels, however, has yet to be examined.

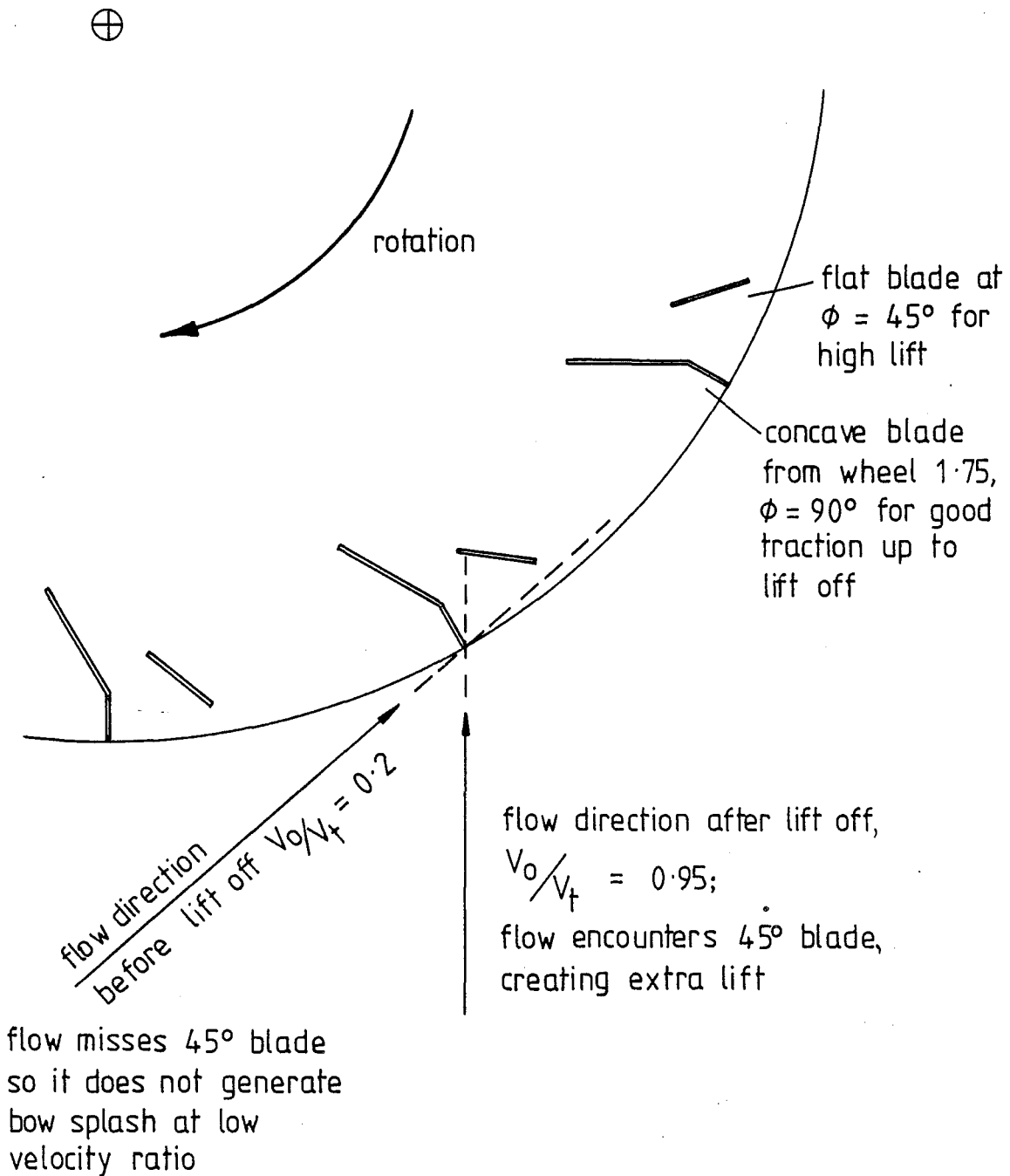


FIGURE 13.11: PROPOSED HYBRID LPW DESIGN FOR HIGH LIFT AND SMALL IMMERSIONS AFTER LIFT-OFF

(3) In the plot of total drag in Fig.13.9(B), a curve of the assumed acceleration force has been drawn. If this acceleration force is not used, the thrust force, in expression (13.1) for the lift to thrust ratio, becomes small immediately after lift-off and the craft sinks back on to the water surface. It will be apparent from this, that it is not possible for the craft, as designed, to maintain a flying condition at steady speeds below about 17 m/s since below this speed the drag is too small for the craft to be held aloft, and the acceleration force given is necessary to maintain the small hull clearance shown in Fig.13.10(A). In fact the total drag at a steady speed of 17 m/s is barely enough to maintain the flying condition, and only about 1 mm clearance results as shown in Fig.13.10(A).

It can be seen from the above, practical considerations that the full-sized craft, as designed, using simple flat-bladed LPW's is barely capable of demonstrating the concept of a craft supported on its wheels, and is unable to reach lift-off speeds because of its full drag. While concave blades would be expected to provide sufficient thrust to reach lift-off speeds they would not provide more lift after lift-off nor would they hold the craft higher in the water.

The craft design then is for a vehicle with about the minimum possible power to weight ratio with which lift-off can be achieved, with the present understanding of LPW operation. While there is still some room for improved performance at this power to weight ratio with a carefully designed hull, or high lift wheels, it is clear that decidedly better performances may be obtained with craft with greater power to weight ratios. Such craft, while relatively inefficient in terms of power consumption would more clearly demonstrate the LPW concept, using wheels already tested, running higher out of the water and demonstrating greater maximum speeds and lower lift-off speeds.

13.7 OUTLINE FOR THE DESIGN AND TESTING OF A FULL SIZED PROTOTYPE

The figures and calculations in this chapter have all been for a full-sized craft of one tonne and 100 kW power at the wheels, using flat-bladed LPW's. These calculations have centred around the idea that a Suzuki SJ410 four-wheel-drive vehicle (major dimensions shown in Table 13.12) could be converted for use as the first,

full-sized, prototype LPW craft. This would result in a craft dimensionally 4.6 times the size of the model LPW craft of Chapter 12. In terms of weight it would be heavy, about 2.5 times as heavy as if the model craft weight was multiplied by the cube of 4.6. This full-sized craft weight assumes that unnecessary panelling has been removed, and a hull and driver added to the vehicle with a kerb weight of 850 kg. This proportionally heavier craft presents some problems with immersion as noted above, but, as noted in point (2) in section 13.2.5 above it also has the doubtful advantage that the maximum speed limitation would not be a problem with a heavier craft. Other dimensions differ only a little from the scaling factor of 4.6, and these are shown in Table 13.12.

TABLE 13.12. Showing the comparisons between the model dimensions scaled up and the suggested prototype dimensions.

	MODEL DIMENSIONS	MODEL DIMENSIONS SCALED BY 4.6	SUZUKI SJ410
WHEEL DIAMETER	152 mm	700	~ 700
WHEELBASE mm	418	1923	2030
TRACK mm	320	1472	1242
WEIGHT	4 kg	390 kg	Kerb weight 850 kg Assume 1000 kg A.U.W.

Hull design has been assumed to be close to that of Fig.13.4 so that the drag curves of this figure may be used in lift-off calculations. Such calculations have usually assumed the hull to remain horizontal ($\tau = 0^\circ$) to avoid the large drag peaks at around 4 m/s.

The central performance prediction and LPW dimensions are those of Table 13.6 and Fig.13.7 and these have been put in the practical form with a drag force varying with speed in Figs.13.9 and 13.10.

If the speeds shown in these calculations were to be achieved a light motor of 100 kW would have to replace the smaller motor already in the vehicle. The installed power in these vehicles is rated at 33.5 kW. There is some merit in the idea of decreasing the minimum power required for lift-off in Figs.13.7 or 13.9 by any possible means indicated in Fig.13.8 so that this installed power could be used for an initial test run under the minimum power condition to verify the predictions of the calculations for a full-sized craft. The procedure would be to run the craft at the speed of minimum power, down a gently sloping beach into shallow, calm, water to ascertain whether it could maintain itself in the lifted-off condition as predicted. Such a test would provide experience before major engine changes and hull construction was undertaken.

The dimensions of the LPW's would be excessive under these circumstances and weight would be at a premium. For this test the hull might only be emergency floatation to stop the craft rolling or sinking should instabilities occur (as discussed in section 13.5.1 above). No shaped bow would be necessary though outrigger buoyancy might be used instead. Centre section and rear plates of some form would probably be an advantage for stability and lift augmentation.

If the installed power of the craft was insufficient, an intermediate test might involve turbocharging the motor.

Pending the experience and results of such a preliminary confirmatory test the more expensive engine changes and hull construction could be undertaken. Tests with the craft thus fitted out would involve the broad range tests necessary to ensure craft safety, usefulness and to confirm performance predictions. The criteria for such tests would arise from the results of the model tests of Chapter 12 and the findings of the preliminary tests described above.

While all the predictions and optimisation procedures have been based on the theory for flat-bladed LPW's, it is clear from the model tests (section 12.8 and section 10.6) that concave blades like those of wheel 1.75, $\phi = 90^\circ$ would in fact be used. These blades would alter the performance characteristics in ways that can

be deduced from the findings of section 10.4 and in general should give better than the predicted performance for flat-bladed LPW's as they did on the model. A cautious approach would be to use wheels with these concave blades but expect a performance no better than that predicted for flat-bladed LPW's.

13.7.1 Design of Practical LPW's

The LPW's, themselves, for a full-sized craft need to be robust enough to carry the craft weight on land, need to be easily attached and removed from the vehicle hubs, and need to be cheap to construct as well as being light in weight. The fact that some model craft blades bent indicated that each blade needs to be able to support about half the craft weight on its tip to cope with the loadings it will encounter while running on water. It is imagined that a light welded steel plate construction would be investigated for early tests.

In the long term, LPW's would need to be developed which would allow the craft to operate on roads, if its full amphibious capability is to be realised; metal wheels could not be used for this. Four basic approaches have been envisaged to this problem:

(1) LPW's made of metal could incorporate a central (?) rim where a conventional tyre might be mounted. This would have little effect in the water but having a larger circumference than the blade tips would provide support on land.

(2) Conventional wheels might be used, with a folding structure of blades mounted outboard of the hub. This folding-type LPW might be operable from the driver's seat.

(3) Separate road and water wheels could be carried by the vehicle much in the manner that spare wheels are carried, with chains already mounted on them, for mud and snow conditions. This would require wheel changes before and after water operation but may be the most practical method of use in many cases.

(4) Special ribbed tyres might be developed as sketched in Fig.13.13. Such purpose-built tyres would require careful investigation before their development because of the tendency for

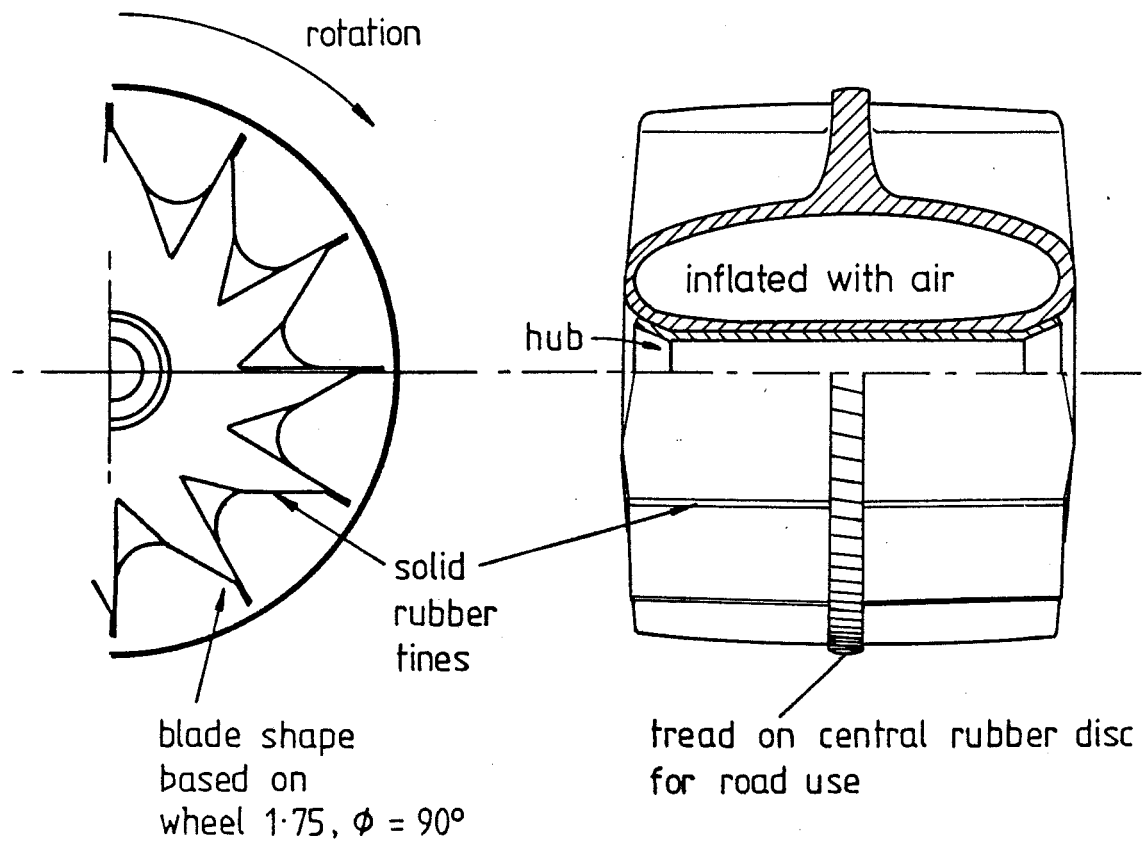


FIGURE 13.13: SUGGESTED RUBBER TYRE FOR A COMBINATION ROAD AND WATER LPW.

such shapes to produce the fountain effect discussed in section 11.2, point (2) and Fig.12.17. While tyres like this would be the ideal for the model craft for universal land and water use they would be unlikely to lift the full-sized craft high enough out of the water for adequate hull clearance (see section 13.6.3 above). Development along the lines of Fig.13.13, of hybrid wheels, like those of Fig.13.11, might be required for the land-water LPW for the full-sized craft.

13.8 TENTATIVE PERFORMANCE PREDICTIONS

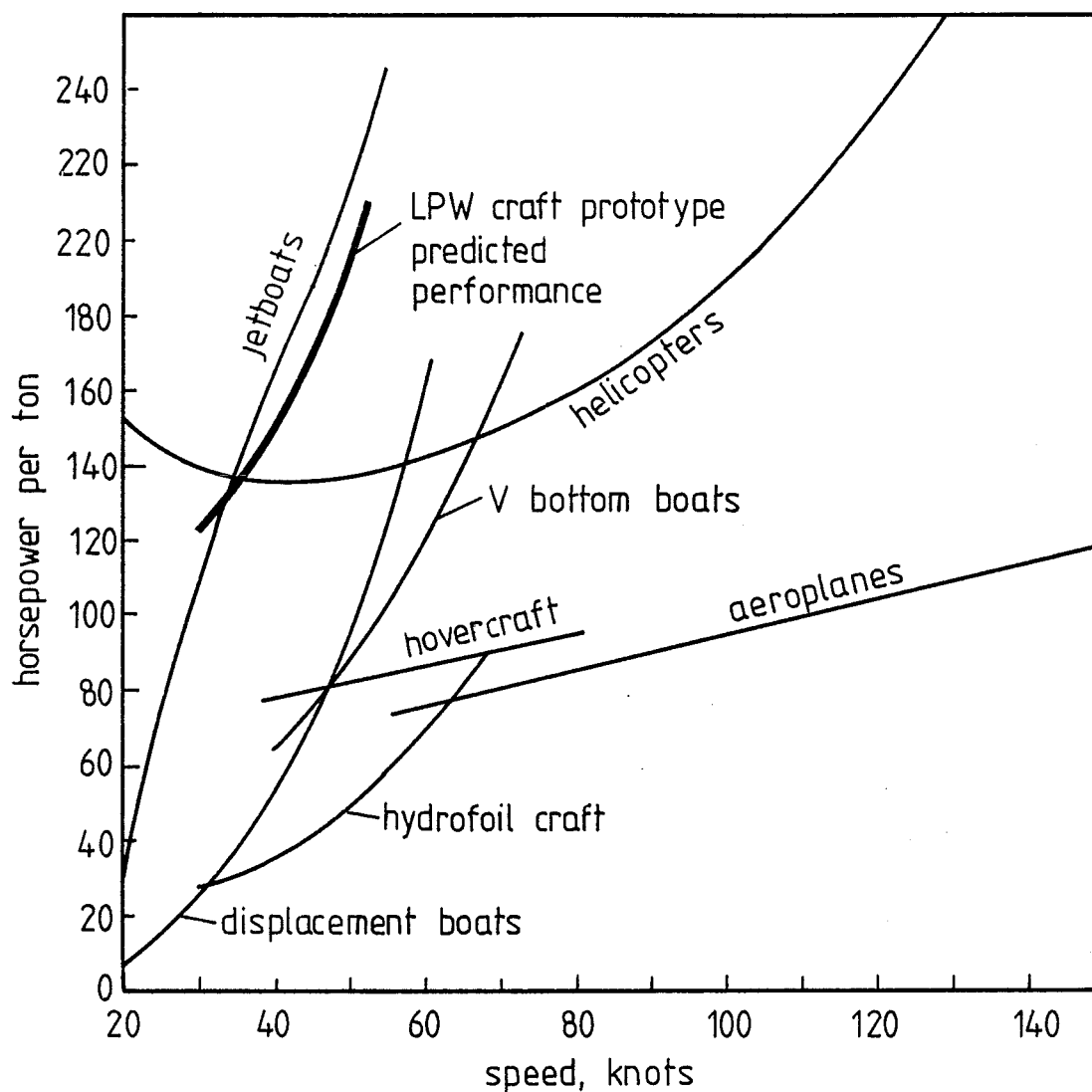
While uncertainties regarding the model craft power output made it difficult to get a conclusive assessment of the value of the programme 'LPWCRAFT' in predicting craft performance, it seems clear from the results of columns (e) and (h) of Table 12.23 that the most realistic predictions involved the addition of spray drag and lift augmentation to the calculations. Fig.12.25 placed such predictions close to the measured craft performance. The calculations for the full-sized craft of this chapter have therefore included estimates of spray drag and lift augmentation, so that their predictions of craft performance would be expected to be close to actual achievable craft performance. On this basis, it is possible to compare the LPW craft performance with those of other craft.

Two performance estimates have been made, the first assuming a 1 tonne craft with a 100 kW engine as used for the calculations in this chapter, and another assuming a 1 tonne craft with a 150 kW engine, which would more readily demonstrate the LPW concept with flat-bladed wheels as designed. Both these estimates were plotted earlier on Fig.12.25, where they can be seen to be placed in the racing craft category near to high powered jet boats and hydroplanes.

Another comparison on a different figure shown in Fig.13.14 emphasises the high power to weight ratio of the LPW craft as compared with other craft. This power to weight ratio, while large for a commercial craft is within the range of sport and specialist vehicles both for land and water use, and may well be improved upon with the employment of concave or hybrid blades on the LPW's.

13.9 CONCLUSIONS

This chapter has outlined the main features of LPW craft design and performance, and has come up with a set of design



sources: Hooke & Kermodie Fig 64
Hamilton Marine (jet unit manufacturers)

FIGURE 13·14 THE PREDICTED PERFORMANCE OF THE 1 TONNE LPW CRAFT ON A POWER TO WEIGHT RATIO PLOT.

procedures from which performance predictions may be made. From these, a tentative answer can be given to the fundamental question posed by the project: A full-sized LPW craft, while experiencing some difficulty with hull clearance with present LPW design is predicted as being capable of operating at speeds approaching those of high powered planing craft though using more power than most of these craft to achieve such speeds. Such a performance, while not putting the LPW craft into competition with the more efficient planing craft would be very respectable for a fully amphibious vehicle. It is to be expected that this performance could be improved upon with development, as these predictions centre mainly on the results from flat-bladed LPW's.

CHAPTER 14

CONCLUSIONS14.1 INTRODUCTION

Although the project aims in section 3.6 were to find out how well a lifting paddlewheel craft might operate, the work involved discoveries universal to all types of paddlewheels as well as results relating more specifically to LPW's, and findings concerning the LPW craft itself. The main findings of the project are here summarised in this order before remarks are made on the craft capabilities, its possible applications and recommendations for further work.

14.2 SUMMARY OF FINDINGS UNIVERSAL TO ALL TYPES OF PADDLEWHEELS

The following are results from the project which have clarified the performance of all types of paddlewheels:

(1) The wake of a paddlewheel or wheel in deep water was shown to be like that of any watercraft with the same speed and waterline length as the paddlewheel: wakes could be compared through a Froude Number based on waterline length. The wake of a paddlewheel can be determined from its speed and can be divided into static, displacement, transition and planing types.

(2) The mechanisms by which the paddlewheel forces were generated were seen to be different for low and high speed operation (or displacement and planing operation).

(3) Forces generated during displacement operation were usefully described by picturing the paddlewheel blades as generating drag forces during their passage through the water. These displacement forces were strongly affected by the wake formations, especially when the transition speeds were reached, when forces became small.

(4) In the planing mode of operation the forces were found to be generated at the point of blade entry rather than throughout their passage. They were best described as being generated by an impulsive momentum change in the induced mass of the entering paddlewheel blade, and the direction of the resultant force could be found from a vector treatment of the flow velocities.

(5) All paddlewheels in the planing mode of operation produced lift forces to a greater or lesser extent.

(6) Paddlewheels in the planing mode of operation generated maximum lift forces if the blade angle was near $\phi = 60^\circ$. They developed maximum thrust forces if the blade angle was near $\phi = 90^\circ$ (radial blades). Propulsive efficiency was greatest with blade angles near $\phi = 90^\circ$, and if the wheel generated lift it appeared to do so at the expense of propulsive efficiency and thrust.

(7) The twin phenomena of cavity intrusion and bowsplash were discovered in the planing mode, and they were shown to have significant effects on the generation of both lift and thrust forces. These effects were not unlike the stall of a wing in flight. They were successfully related to the wheel parameters of immersion depth, velocity ratio, blade chord, number of blades and blade angle.

(8) Doubt was thrown on the claims made that cylinder vehicles could rise and run on the water surface, as tests undertaken in this project showed the fountain effect caused by smooth wheels tended to pull them down at low speeds. A small possibility remains that they could be made to operate at high speeds if they could avoid this low speed phenomenon.

(9) The Rollercraft wheel was tested and found to provide lift and thrust forces. Its force performance through the transition zone was exceptional. Efficiency was low and the magnitudes of measured forces were widely different from measurements made by Kearsey.

(10) While the experimental measurements for this project were eventually undertaken by moving the wheel over still water, the considerations necessary for tests in flowing water were discussed. It was noted that critical flow with a Froude No. = 1 should be avoided; displacement type operation could be modelled only in deep subcritical flow with a Froude Number less than 1, and planing type operation might be modelled in either subcritical or supercritical flow.

14.3 SUMMARY OF FINDINGS RELATING SPECIFICALLY TO LPW'S

(1) The effects of the LPW variables were examined by experiment and were related in the impulse theory. These variables were: diameter, span chord, blade angle, blade shape, number of blades, immersion depth, wheel revolutions and speed of advance.

(2) Useful lift forces were generated by LPW's with the appropriate blade shape and blade angle.

(3) An analytical model of the forces of flat-bladed LPW's at planing speeds was developed, and with experimentally derived coefficients this was shown to be a useful predictive model. This has been called the impulse theory.

(4) A simple relationship derived from the impulse theory relates the lift and thrust forces, the blade angle and immersion angle:

$$\frac{T}{L} = \tan (\phi - \theta)$$

This has been found to be a useful analytical tool.

(5) Tests with curved-bladed LPW's were undertaken and although no comprehensive theory was developed to describe the results, the findings could be related systematically to the results of tests and theoretical predictions for flat blades. Concave blades were shown to give a superior performance to other types of blades in tank tests.

(6) Peak efficiencies for LPW's were not high and occurred at small immersions. Propulsive efficiencies of over 50% were measured at the conditions of velocity ratio that would be found in a craft in operation. There remains some uncertainty as to the attainable efficiencies at high speeds or at high velocity ratios for a practical craft.

14.4 SUMMARY OF FINDINGS FOR THE LPW CRAFT

The project aims were ambitious in that they posed a question that could, at best, only be partly answered by a project of this

sort. Nevertheless the work has been able to give preliminary answers, has found no reason to doubt the concept, and has provided some tools for analysis:

(1) The LPW craft has been shown to operate successfully in a model form, achieving speeds of up to 9 m/s over the water surface supported only by the dynamic forces generated by its wheels.

(2) The model craft tests to date have achieved the speeds of 9 m/s without much effort. This can be compared with model boats of the same power which regularly reach speeds of 14 m/s. It is believed that with perseverance a model LPW craft performance comparing favourably with that of model V-bottom boats could be achieved. This is assumed to be indicative of the speed capability of a full-sized craft.

(3) The model craft tests confirmed that the results of tank tests and theoretical predictions could be applied to the LPW craft. The best all round LPW's were found to have slightly concave blades: these showed good characteristics both in the tank tests and on the model craft.

(4) Experience with the model craft produced a wealth of information regarding craft stability, hull configuration and LPW design. This would be of importance in full-sized craft design.

(5) A computer programme based on the theory and experimental results was developed for use in the design of full-sized craft and the optimisation of their LPW dimensions. This was checked against the performance of the model craft and its value as a design tool thereby assessed.

(6) Predictions of the full-sized craft capabilities using this computer-based design indicate that it should be capable of over-water speeds equalling those of jet boats for the same installed power. While this predicted performance has yet to be achieved in practice, it is not necessarily the limit to the eventual capabilities of LPW craft. At present, however, it is the best answer that can be given by the project to its fundamental question of how well the LPW craft can operate over water.

14.5 CAPABILITIES AND LIMITATIONS OF THE LPW CRAFT

While there is still some way to go in fully developing the LPW craft and the LPW's themselves it is not inappropriate to speculate on some of the special capabilities that it might have (see also section 1.2):

(1) High speed over water capability which approaches that of planing craft with similar installed power and weight.

(2) All terrain overland capability not unlike that of four-wheel-drive land vehicles. This facility may be limited by the LPW craft requirement of a hull-shaped body and wide wheels, but may also be enhanced by the high installed power required for water operation.

(3) The craft may be used on roads probably to speeds approaching those of normal land vehicles.

(4) In water at low speeds it can provide a high thrust for towing purposes. (The model craft readily generated static thrusts equal to its own weight.)

(5) There is an untested possibility that the craft may be capable of operating at speed in soft mud or snow in the same manner as it operates in water.

(6) The wheels tend to roll over obstacles in the water rather than running into them. It is likely that the craft could operate successfully in shallow, shoal conditions.

(7) It would be expected that the craft could run from land to water and vice versa at speed and without any need to stop and make special adaptations.

(8) Transmission, hull and chassis design require no new technology beyond the technology of four-wheel-drive vehicles and planing hulls. In fact LPW's and floatation might be designed to bolt on to existing four-wheel-drive vehicles.

(9) The training of drivers would not seem to present a problem because of the craft's similarity to road vehicles.

This combination of facilities cannot readily be challenged by any present vehicle. The closest contenders are the hovercraft, which have poor traction and cannot be used on roads, and the LVHX-1 (see section 2.6.2) which, while handling waves well, is a specialised vehicle involving high technology.

As well as these possible advantages the LPW craft does have certain limitations. These are imagined to be:

(1) The LPW craft would not be expected to handle large waves well in its flying condition though this has not yet been examined in practice.

(2) The LPW craft generally requires large diameter or wide wheels which tend to be clumsy on land.

(3) At present it cannot be seen as a carrier of large loads: like the helicopter its advantage lies in its unique capabilities and speed.

(4) While it has generally been imagined that a wheeled craft on water would require less power than a planing craft, because its body would be clear of the surface, it seems that in the practical situation more power is required to produce the lift. In general this compensates for any savings that might otherwise be made.

(5) Power requirements for a useful water performance are large compared with those of normal road vehicles. This means that adaption of road vehicles into LPW craft would generally involve the installation of larger engines in standard vehicles.

(6) LPW's which are equally useful on land and water have yet to be evolved.

14.6 APPLICATIONS FOR THE LPW CRAFT

It is not possible to foresee all the special uses that the LPW craft might be suited though after the above discussion of its

probable capabilities and limitations some areas of application present themselves:

(1) Medical, mail and transport services to undeveloped areas where there may be few roads on land connected by rivers, lakes or swampland. River delta areas, or shallow braided rivers like the New Zealand South Island rivers might be especially negotiable by such a craft.

(2) Rescue services in areas where combinations of mudflats, land and water may deny access to many conventional craft. Auckland airport is one example of such an area.

(3) Rescue work in floods where land and water boundaries vary uncertainly, obstacles are floating in the water, and some roads might be accessible. Speed would be necessary in fast-moving currents.

(4) Arctic or Antarctic conditions where access might be required over snow, water or ice.

(5) Military landing operations or law enforcement patrols in sheltered coastal, and inland waterways where the high speed water capability, towing facility, roadability and cross-country ability might all be combined to advantage.

14.7 OTHER USES AND DEVELOPMENTS FOR THE LPW ITSELF

This project has, throughout, been biased towards the use of the lifting paddlewheel in an overwater four-wheel-drive craft. It may of course undergo developments and find other uses where its special characteristics make it useful in combination with other systems. Some ideas which have arisen during the course of the project are as follows:

(1) Free-wheeling undriven LPW's might be developed to provide lift. Such devices could be used as the front LPW's in a two-wheel-drive LPW vehicle.

(2) A motorcycle fitted with LPW's contains the elements of a specialised sports vehicle that would not be without challenge.

(3) The LPW might be used on hovercraft to provide traction on land and water. There is a possibility of setting the LPW on the end of an arm so that it always remained in contact with the water but carried its own weight while providing thrust.

(4) Propulsion and lift assistance might be provided for planing craft employing Beardsley's Surface Impulse Propulsion concept (see section 2.2.6) where the LPW could be placed across the stern of planing craft as envisaged by Wray and Starrett (see Fig.2.5).

(5) A snowmobile fitted out with a ski on the front and a lifting paddlewheel on the back instead of its track might make a combination snow and water craft.

14.8 RECOMMENDATIONS FOR FUTURE WORK

The work of this project has shown that the LPW concept is a feasible one. The first recommendation for further work is therefore that a full-sized craft be built as outlined in Chapter 13, and tested so that its capabilities may be thoroughly assessed. This would be seen to be the most productive next step, and could resolve many of the questions left unanswered in the project. Once such a step had been completed the project might well become a business venture rather than a research project.

Failing the construction of a full-sized craft or perhaps in conjunction with it there is much that may be continued on the project lines already started that could resolve unanswered questions. This smaller scale work divides into three areas where only the most useful areas of investigation are noted:

(A) Model LPW craft work

(1) Measure the power output of the model LPW craft as attempted and described in section 12.6.1.

(2) Improve the model performance to its limits to more carefully assess the computer design procedure.

(3) Find out how necessary the full bow is for stability, and compare a variety of mid-section and rear plates to determine their optimum performance parameters. (See sections 12.6.3.3, 12.6.3.4 and Fig.13.3.)

(B) Tank testing of LPW's

(1) Examine the flow around curved LPW blades in stroboscopic studies in the glass-sided tank. (See section 8.3.)

(2) Develop LPW's which combine the required properties of traction and small immersion that may be made into tyres for water and land use for full-sized craft. (See sections 13.7.1, 18.7.2 and Figs.13.10, 13.13.)

(3) Assess LPW performance at high speeds to determine the limits to propulsive efficiency at high velocity ratios. (See section 13.2.13.)

(C) Re-examination of Theoretical Work

(1) Ascertain why the impulse theory force coefficients vary linearly with wheel revolutions. (See sections 9.4.3, 9.9.2.)

(2) Find out how much the flat plate drag forces contribute to the impulsive blade forces in the wheel planing mode. (See section 9.3.2.)

(3) Develop a comprehensive theory which covers the performance of curved as well as flat LPW blades. (See section 4.9.3, point (5).)

14.9 CONCLUSION

One reason why wheels in water have not attracted much attention since the replacement of the paddlewheel with the screw propeller, is that the interaction between wheels and water is complex and not easily understood. Paddlewheel design, as far as it went, was based on little more than past experience. The difficulty in coming to a better understanding of this interaction had two aspects. Not only were there required vast amounts of data from large numbers of measurements to cover the range of variables of a paddlewheel, but there was also the need for a close examination of the results and the formulation of an adequate theoretical model

to provide a ready understanding of how the variables interacted. Thus one of the most important contributions of this project was the development of a theory, based on experimental results, describing high speed paddlewheel and lifting paddlewheel behaviour, which is able to predict with confidence the performance resulting from changes in any of the many variables involved in paddlewheels.

As well as this general contribution, the project has followed through with the development of a new specialised vehicle, taking it from the stage of an idea, through experimental work, the development of a theory of operation, and model tests, to the design specifications and performance predictions of a full-sized man-carrying craft. While there may still be speculation as to the full potential or best use of such a vehicle, there is now no doubt that it will be capable of driving at speed over a water surface supported only on its wheels.

REFERENCES

- ALEXANDER, K.V. Preliminary investigations of the lifting paddlewheel. Christchurch, University of Canterbury, 1976, 33 p. (A paper presented for the Templin Scroll Competition, Engineering School, 1976.)
- ALEXANDER, K.V. Further investigations of the lifting paddlewheel. Christchurch, University of Canterbury, 1977, 60 p. (Bachelor of Engineering Project Report No. 72/77.)
- BARNABY, K.C. Basic naval architecture. 6th ed. London, Hutchinson and Co.Ltd., 1969, 507 p.
- BATCHELOR, G.K. An introduction to fluid dynamics. Cambridge, Cambridge University Press, 1967, 615 p.
- BEARDSLEY, M.W. Surface Impulse Propulsion: a review and comment on future potential. Hovercraft and Hydrofoil, vol.12, no.9: 10-24, June 1973.
- BIRKHOFF, G. and ZARANTONELLO, E.H. Jets wakes and cavities. New York, Academic Press Inc., 1957, 353 p.
- BROADCASTING CORPORATION OF NEW ZEALAND "Animal Olympians", screened 11th November, 1980.
- CHUANG, S.L. Experiments on flat-bottom slamming. Journal of Ship Research, vol.10, no.1: 10-17, March 1966.
- ESDU Fluid forces and moments on flat plates. Engineering Sciences Data Item No.70015, October 1972, 17 p.

- DAVIDSON, K.S.M. and SUAREZ, A. Tests of twenty related models of V-bottom motor boats, E.M.B. series 50, for the David Taylor model basin. (Stevens Institute of Technology Report No. 170.) 1948, 103 p.
- FOX, U. Seamanlike sense in powercraft. London, P. Davies, 1968, 256 p.
- GREVILLE, T.N.E. Spline functions, interpolation, and numerical quadrature. In Ralston, A. and Wilf, H.S. Mathematical methods for digital computers, vol.II. New York, Wiley, 1967-68, 287 p.
- HAMILTON MARINE (Hydrojet unit manufacturers. Private communications)
- HELM, V.K. Study of a high-speed paddle wheel to propel shallow-draught inland vessels. Schiff und Hafen, 10: 688-703. 1967.
- HOOKE, C. and KERMODE, A.C. Hydrofoils. London, Pitman, 1967, 218 p.
- HOVERCRAFT AND HYDROFOIL New U.S. marine corps hydrofoil (LVHX1). Vol.4, no.2: 16-17, November 1964.
- HOVERCRAFT AND HYDROFOIL Lycoming's experience in amphibious hydrofoil activity (LVHX-1). Vol.4, no.5: 18-20. February, 1965.
- HOVERCRAFT AND HYDROFOIL People and projects. (Cylinder vehicle), Vol.6, no.10: 6-9, July 1967.
- HUGHES, C. and HUGHES, D. Teeming life of a rain forest. National Geographic Magazine, vol.163, no.1: 49-65, Jan. 1983.
- HUTCHINGS, I. Bouncing bombs of the second world war. New Scientist, vol.77, no.1092: 563-567, 2 March 1978.

- JOHNSON, D.E. and
HILBURN, J.L. Rapid practical design of active filters.
New York, John Wiley and Sons, Inc., 1975,
264 p.
- KEARSEY, J.A. On an amphibious surface craft utilising
flexible buoyant propellers. University
of Southampton, 1971. 193 p. (Thesis:
Ph.D: Engineering.)
- KEARSEY, J.A. The rollercraft. Hovercraft and hydrofoil,
vol.10, no.12: 14-25. September 1971.
- LAMB, H. Hydrodynamics. 6th ed. New York, Cambridge
University Press, 1953, 738 p.
- LIGHTHILL, M.J. Waves in fluids. Cambridge, University
Press, 1979. 504 p.
- LOGVINOVICH, G.V. Hydrodynamics of free-boundary flows.
Kiev, 1969. Translated from Russian by
Lederman, D. Jerusalem, IPST Press, 1972,
194 p.
- LOMBARDINI, P.C. and
FIDDERMAN, R. A new theory on propulsion of high speed
water craft and its application to the
hydroiler. Proceedings of the Seventh
International Congress of Applied Mechanics,
vol.2, part 2: 533-547, 1948.
- MASSEY, B.S. Mechanics of fluids. 2nd ed. London, Van
Nostrand Reinhold Co.Ltd., 1971, 508 p.
- PERRING, W.G.A. The porpoising of high-speed motor-boats.
Transactions of the Royal Institution of
Naval Architects, vol.75: 268-296, 1933.
- PRETTY, R.T. Jane's weapon systems 1979-1980, London,
Jane's Publishing Co.Ltd., 1980.
- ROBERTSON, J.M. Hydrodynamics in theory and application.
New Jersey, Prentice-Hall Inc., 1965, 652 p.

- SILVERLEAF, A. and
COOK, F.G.R. A comparison of some features of high-speed
marine craft. Hovercraft and Hydrofoil,
vol.8, no.7: 6-15, April, 1969.
- STREETER, V.L. Handbook of fluid dynamics. New York,
McGraw Hill Book Co., Inc., 1961, 1223 p.
- TAGGART, R. Marine propulsion, vol.I: A history of
propulsion development. Reed Research
report 1288. July 1957.
- TAGGART, R. Marine propulsion: principles and evolution.
Houston Texas. Gulf Publishing Co., 1969,
368 p.
- VOLPICH, H. and
BRIDGE, I.C. Paddle wheels, Pt I: Preliminary model
experiments. Paper no. 1193, Transactions
of the Institution of Shipbuilders and
Engineers of Scotland, vol.98:327-380,
February, 1955.
- VOLPICH, H. and
BRIDGE, I.C. Paddle wheels, Pt II: Systematic model
experiments. Paper no. 1208, Transactions
of the Institution of Shipbuilders and
Engineers of Scotland, vol.99: 467-510,
March, 1956.
- VOLPICH, H. and
BRIDGE, I.C. Paddle wheels, Pt IIa: Further model
experiments; Pt III: Ship/model correlation.
Paper no. 1222. Transactions of the
Institution of Shipbuilders and Engineers
of Scotland, vol.100: 505-550. February
1957.
- WAGNER, H. Landing of seaplanes. Zeitschrift für
Flugtechnik und Motorluftschiffahrt, vol.22,
no.1: 1-8, January 1931. Translated from
German in NACA technical memorandum no.622,
1931.

WAGNER, H.

Über Stofs- und Gleitvorgänge an der
Oberfläche von Flüssigkeiten. Zeitschrift
für Angewandte Mathematik und Mechanik,
vol.12, no.4: August 1932.

WRAY, G.A. and
STARRETT, J.A.

A model study of the hydrodynamic character-
istics of a series of paddle-wheel propulsive
devices for high-speed craft. (Davidson
Laboratory, Stevens Institute of Technology,
Report no. SIT-DL-70-1428.) 1970, 114 p.

WU, T.Y.

Inviscid cavity and wake flows. In Holt, M.
Basic developments in fluid dynamics, volume
2. New York, Academic Press Inc., 1968,
226 p.